

# BOOK OF ABSTRACTS

## 6<sup>th</sup> Euro-Asia Zeolite Conference

*Porous solids for the new societal challenges*



Alicante, Spain • January 19-22, 2025



**EAZC**  
2025

**6<sup>th</sup> Euro-Asia Zeolite Conference**  
Alicante (Spain), January 19-22, 2025



## ORGANIZED BY



## TECHNICAL SECRETARIAT

Viajes El Corte Inglés  
M.I.C.E. Murcia y Alicante  
Telf: (+34) 968 272 393  
Pl. Circular 4 - 30008 - Murcia  
[congresosA10@viajeseci.es](mailto:congresosA10@viajeseci.es)

**VIAJES El Corte Inglés**  
CONGRESOS



6<sup>th</sup> Euro-Asia Zeolite Conference  
Alicante (Spain), January 19-22, 2025



## PRESENTATION

The Spanish Zeolite Group, on behalf of the Spanish Catalysis Society, is proud to organize the **6<sup>th</sup> Euro-Asia Zeolite Conference - EAZC-2025**, to be held in the city of **Alicante**, southeastern Spain, from **January 19 to 22, 2025**.

The **Euro-Asia Zeolite Conference** is one of the most prestigious international congresses in the field of **zeolites and related nanostructured porous materials**. This biennial event, alternating between Asia and Europe, follows the success of previous editions held in Macau (2013), Nice (2015), Bali (2017), Taormina (2019), and Busan (2023).

**EAZC-2025** promises a comprehensive program featuring **4 Plenary Lectures, 4 Invited Keynotes**, an **Industrial Session**, and **170 Oral and Poster presentations**, alongside a **Commercial Exhibition**. Contributions will focus on crystalline microporous materials, both inorganic and hybrid (including MOFs), as well as mesoporous materials. Topics will encompass synthesis, characterization, and applications, with particular emphasis on catalytic applications in petrochemistry, energy, gas separations, fine chemicals, pharmaceuticals, and other advanced technological fields.

This conference will bring together leading experts, researchers, and professionals from around the globe to share knowledge, foster collaborations, and advance the field of zeolite science and technology. **EAZC-2025** promises not only cutting-edge presentations but also excellent networking opportunities, all set amidst the vibrant cultural backdrop of Spain's enchanting Mediterranean coast.



6<sup>th</sup> Euro-Asia Zeolite Conference  
Alicante (Spain), January 19-22, 2025



## ORGANIZING COMMITTEE

### Co-Chairs

Juana Frontela, *MOEVE*

Javier García-Martínez, *Universidad de Alicante*

### Co-ViceChairs

Zhongmin Liu, *Dalian Institute of Chemical Physics*

Fernando Rey, *Instituto de Tecnología Química (ITQ), UPV-CSIC*

### Secretaries

Teresa Blasco, *Instituto de Tecnología Química (ITQ), UPV-CSIC*

Carlos Márquez, *Instituto de Catálisis y Petroleoquímica (ICP), CSIC*

### Treasurers

Patricia Pizarro, *IMDEA Energía*

Manuel Moliner, *Instituto de Tecnología Química (ITQ), UPV-CSIC*

### Local Committee

Joaquín Silvestre, *Universidad de Alicante*

Susana Valencia, *Instituto de Tecnología Química (ITQ), UPV-CSIC*



## SCIENTIFIC COMMITTEE

### Coordinators

David Serrano, *IMDEA-Energía*

Joaquín Silvestre-Albero, *Universidad de Alicante*

Cristina Martínez, *Instituto de Tecnología Química (ITQ), UPV-CSIC*

Manuel Sánchez-Sánchez, *Instituto de Catálisis y Petroleoquímica (ICP), CSIC*

### International Advisory Board

Jiří Čejka (Czech Republic)

Xiaoxin Chen (China)

Minkee Choi (South Korea)

Avelino Corma (Spain)

Jorge Gascon (Saudi Arabia)

Girolamo Giordano (Italy)

Kinga Góra-Marek (Poland)

Martin Hartmann (Germany)

Suk Bong Hong (South Korea)

Zhongmin Liu (China)

Svetlana Mintova (France)

Eng-Poh Ng (Malaysia)

Junko Nomura Kondo (Japan)

Masaru Ogura (Japan)

Tatsuya Okubo (Japan)

Ana Palcic (Croatia)

Xiulian Pan (China)

Joaquín Pérez-Pariente (Spain)

Paolo Pescarmona (Netherlands)

Filipa Ribeiro (Portugal)

Raquel Simancas (Japan)

Alessandro Turrina (UK)

Valentin Valtchev (France)

Georgi Vayssilov (Bulgaria)

Chularat Wattanakit (Thailand)

Toshiyuki Yokoi (Japan)

Jihong Yu (China)

Natasa Zabukovec (Slovenia)



## VENUE

### HOTEL ALICANTE GOLF

Carrer Escultor José Gutierrez, 23

03540 Alicante

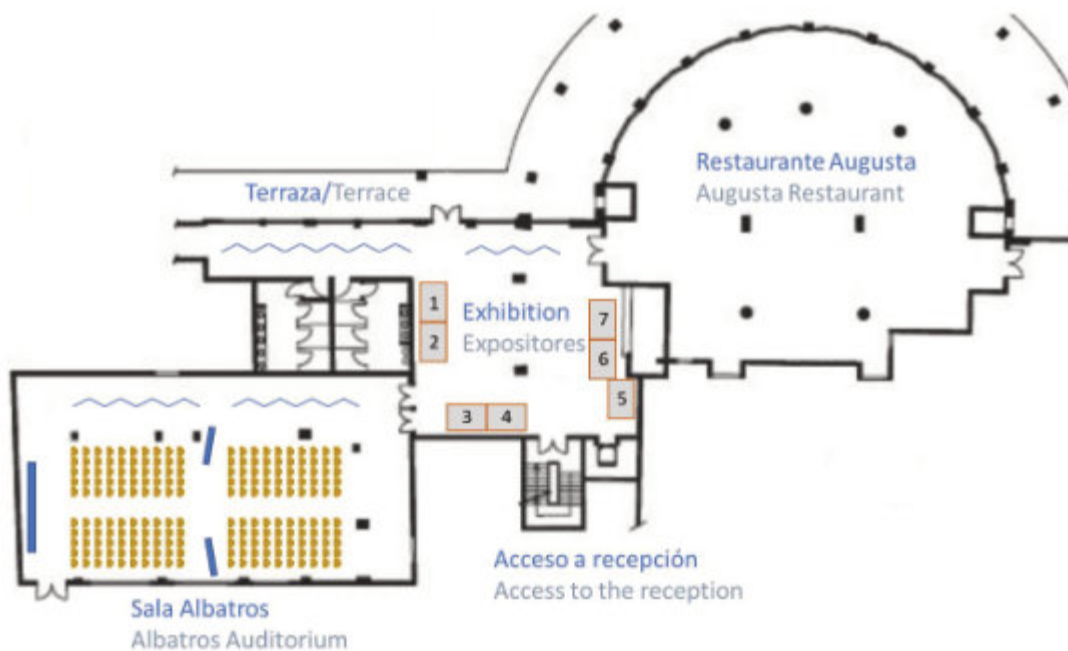
Tlf: +34 965235000

<https://www.hotelalicantegolf.com/>

Hotel Alicante Golf offers accommodation for conference attendees in a magnificent location, just 800 meters from San Juan Beach, and well-connected to the city center.

Session rooms, exhibitor booths, coffee area, and restaurant are all conveniently located close to each other.

### Conference floor plan





EAZC 2025

6<sup>th</sup> Euro-Asia Zeolite Conference  
Alicante (Spain), January 19-22, 2025



GOLD SPONSORS

**JM** Johnson Matthey  
Inspiring science, enhancing life

**ROYAL SOCIETY OF CHEMISTRY**

**TotalEnergies**

SILVER SPONSORS

**ifp** *Energies nouvelles*

**NanoMEGAS**  
Advanced Tools for electron diffraction

**TOPSOE**

COLLABORATORS

**STALI RSEQ**  
Sección Territorial de Alicante

**Alicante**  
City & Beach

EXHIBITORS

**Anton Paar**

**IBERFLUID**  
instruments

**mi micromeritics®**

**HIDEN**  
ISOHEMA

**Malvern Panalytical**  
a spectris company

**3P**  
INSTRUMENTS


**iesmat**

**NEURTEK**  
instruments

**MICROTRAC**  
PARTICLE CHARACTERIZATION



**PROGRAM OVERVIEW**

SUN 19			MON 20		
 <b>6<sup>th</sup> Euro-Asia Zeolite Conference</b> Alicante (Spain), January 19-22, 2025			8:40 - 9:00	Opening ceremony	
			9:00 - 9:50	Plenary lecture 2 Wakihara	
			9:50 - 10:10	Oral session 2	O07
			10:10 - 10:30		O08
			10:30 - 10:50	Coffee break	
			10:50 - 11:20	Keynote 1 · Palatinus	
			11:20 - 11:40	Oral session 3	O09
			11:40 - 12:00		O10
			12:00 - 12:20		O11
			12:20 - 12:40		O12
			12:40 - 13:00		O13
			13:00 - 14:30	Business Lunch	
			14:30 - 15:00	Industrial session	IS1
			15:00 - 15:30		IS2
15:30 - 16:00	IS3				
16:00 - 16:30	IS4				
16:30 - 16:50	Coffee break				
16:50 - 17:20	Keynote 2 · Wattanakit				
17:20 - 17:40	Oral session 4	O14			
17:40 - 18:00		O15			
18:00 - 18:20		O16			
18:20 - 19:00	EAZC Assembly				
18:00 - 18:20	Oral session 1	O01			
18:20 - 18:40		O02			
18:40 - 19:00		O03			
19:00 - 19:20		O04			
19:20 - 19:40		O05			
19:40 - 20:00		O06			
19:00 - 20:30	Poster session 1 P001 - P062 P129 - P135				
20:00 - 21:30	Welcome reception				
15:00 - 17:00	Registration				
17:00 - 17:50	Plenary lecture 1 Yu				





**PROGRAM OVERVIEW**

TUE 21			WED 22		
8:40 - 9:30	<b>Plenary lecture 3</b> Olsbye		8:40 - 9:30	<b>Plenary lecture 4</b> Rimer	
9:30 - 9:50	<b>Oral session 5</b>	O17	9:30 - 9:50	<b>Oral session 7</b>	O25
9:50 - 10:10		O18	9:50 - 10:10		O26
10:10 - 10:30		O19	10:10 - 10:30		O27
10:30 - 10:50	Coffee break		10:30 - 10:50	Coffee break	
10:50 - 11:20	<b>Keynote 3 · Calero</b>		10:50 - 11:20	<b>Keynote 4 · Choi</b>	
11:20 - 11:40	<b>Oral session 6</b>	O20	11:20 - 11:40	<b>Oral session 8</b>	O28
11:40 - 12:00		O21	11:40 - 12:00		O29
12:00 - 12:20		O22	12:00 - 12:20		O30
12:20 - 12:40		O23	12:20 - 12:40		O31
12:40 - 13:00		O24	12:40 - 13:00		O32
13:00 - 14:30	Business Lunch		13:00 - 14:30	Business Lunch	
14:30 - 16:00	<b>Poster session 2</b> P063 - P128		14:30 - 14:50	<b>Oral session 9</b>	O33
			14:50 - 15:10		O34
			15:10 - 15:30		O35
15:30 - 15:50	O36				
15:50 - 16:10	O37				
16:10 - 16:30	O38				
16:00 - 20:00	City tour		16:30 - 16:50	Closing remarks	
			Conference dinner		

**EAZC**  
**2025****6<sup>th</sup> Euro-Asia Zeolite Conference**  
Alicante (Spain), January 19-22, 2025**PROGRAM****SUNDAY JANUARY 19**

15:00 - 17:00	<b>REGISTRATION</b>
17:00 - 17:50	<b>PLENARY LECTURE 1</b> Advance in Zeolite Science: From Synthesis to Emerging Applications <b>Prof. Jihong Yu</b> Jilin University, China
18:00 - 20:00	<b>ORAL SESSION 1</b>
<a href="#">O01</a>	Pd-Containing Zeolite Catalysts And Their Reaction Mechanism For Indirect Oxidative Carbonylation Of Methanol To Dimethyl Carbonate <b>Chunzheng Wang</b> , Xinying Zhang, Junwei Wu, Hailing Guo, Svetlana Mintova
<a href="#">O02</a>	Effective Descriptors Correlating DME Carbonylation Reactivity With Zeolite Topology: A Study Of Brønsted Acid Sites In The Vicinity Of 8-MR Using DFT Calculations <b>Dong Jae Jeong</b> , Nam Jun Park, Wang Xu, Donggyu Lee, Jong Wook Bae, Won Bo Lee, Jong Hun Kang
<a href="#">O03</a>	CO <sub>2</sub> Hydrogenation To Hydrocarbons On The Zeolite-Mediate Bifunctional Catalysts <b>Sangho Chung</b> , Adrian Ramirez, Pierfrancesco Ticali, Edy Abou-hamad, Silvia Bordiga, Jorge Gascon, Javier Ruiz-Martinez
<a href="#">O04</a>	Structural Analysis Of Two ITQ-52 “as-Made” Zeolites With Different OSDA Molecule By 3D Electron Diffraction <b>Partha Pratim Das</b> , Juan I. Tirado, Jose L. Jorda, Lukas Palatinus, Sergi Plana-Ruiz, Jorge Simancas, Raquel Simancas, Stavros Nicolopoulos, Susana Valencia, Fernando Rey
<a href="#">O05</a>	Insights Into Crystallization Mechanism Of SAPO-34 Xiaosi Zhang, Miao Yang, <b>Peng Tian</b> , Zhongmin Liu
<a href="#">O06</a>	Electrochemical Tools For Record-Breaking Sn-Zeolite Synthesis: Mechanisms And Catalytic Application <b>Michiel Dusselier</b> , Gleb Ivanushkin, Aram Bugaev, Juan Martínez-Espín, Mostafa Torka Beydokhti
20:00 - 21:00	<b>WELCOME RECEPTION</b>

**MONDAY JANUARY 20**

8:40 - 9:00	<b>OPENING CEREMONY</b>
9:00 - 9:50	<b>PLENARY LECTURE 2</b> Tracking sub-nano-scale structural evolution in zeolite synthesis <b>Prof. Toru Wakihara</b> The University of Tokyo, Japan
9:50 - 10:30	<b>ORAL SESSION 2</b>
<a href="#">O07</a>	Metal-Exchanged Faujasites As Adsorbents For Carbon Dioxide – Computational Modeling Combined With Infrared Spectroscopic Study Hristiyan A. Aleksandrov, Nikola L. Drenchev, Martin Milenov, Petko St. Petkov, Konstantin I. Hadjiivanov, <b>Georgi N. Vayssilov</b>
<a href="#">O08</a>	Modelling Adsorption Isotherms In Aluminium-Substituted Zeolites Using Graph Neural Networks <b>Marko Petkovic</b> , José Manuel Vicent Luna, Vlado Menkovski, Sofía Calero
10:30 - 10:50	<b>COFFEE BREAK</b>


**EAZC 2025**
**6<sup>th</sup> Euro-Asia Zeolite Conference**  
 Alicante (Spain), January 19-22, 2025


10:50 - 11:20	<b>KEYNOTE LECTURE 1</b>
	Crystal structure determination from microcrystalline materials by 3D electron diffraction <b>Lukáš Palatinus</b> Institute of Physics of the Czech Academy of Sciences, Czech Republic
11:20 - 13:00	<b>ORAL SESSION 3</b>
<a href="#">O09</a>	Insights Into Dimethyl Ether Carbonylation Over Mordenite <b>Dong Fan</b> , Peng Tian, Zhongmin Liu
<a href="#">O10</a>	Boosted Production Of Aromatic Hydrocarbons Via Catalytic Co-Pyrolysis Of Lignocellulose And Light Alcohols Over N-ZSM-5 <b>Maurizio Pagano</b> , Jennifer Cueto, Javier Feroso, Inés Moreno, David Pedro Serrano
<a href="#">O11</a>	Correlation Of Zeolite Framework And Acidic Properties With Catalytic Activity And Regenerability In Methane And Shale Gas Dehydroaromatization <b>Jong Hun Kang</b> , Yangho Jeong, Eun Ji Choi, Yong Hyun Lim, Do Heui Kim
<a href="#">O12</a>	Zeolites in biogas VOC valorization: Acid-catalyzed D-limonene ethoxylation P. Bruno, E. Catizzone, F. Pietramale, <b>M. Migliori</b> , R. Mancuso, B. Gasbrielle, G. Giordano
<a href="#">O13</a>	Selective Catalysis Using Metal Nanoparticles Protected By A Zeolite Shell Jerrick Mielby, Dimitra Iltsiou, Gordon Zhuo, <b>Søren Kegnæs</b>
13:00 - 14:30	<b>BUSINESS LUNCH</b>
14:30 - 16:30	<b>INDUSTRIAL SESSION</b>
<a href="#">IS1</a>	One-step crude to chemicals refining technology: from catalyst design to pilot-plant operation Isa Al Aslani, Juan Manuel Colom, Mengmeng Cui, Arwa Alahmadi, Noah Mohammed, Salvador Salas, Anissa Bendjeriou-Sedjerari, Lujain Alfilfil, Isidoro Morales Osorio, Khalid Almajnouni, Pedro Castaño, <b>Jorge Gascon</b> King Abdullah University of Science and Technology (KAUST) and Aramco Research Center (ARC), Saudi Arabia
IS2	Title to be announced <b>Philip Llewellyn</b> TotalEnergies, France
<a href="#">IS3</a>	Development of Atomistic Simulator “Matlantis™” with Universal Neural Network Potential and its Application to Microporous Materials <b>Hideki Ono</b> ENEOS Corporation, Japan
<a href="#">IS4</a>	Catalyzing Chemistry Entrepreneurship <b>Javier García Martínez</b> Universidad de Alicante, Spain
16:30 - 16:50	<b>COFFEE BREAK</b>
16:50 - 17:20	<b>KEYNOTE LECTURE 2</b>
	State-of-the-art hierarchical zeolites for the catalytic conversion of bioethanol to fine chemicals and carbon-based materials <b>C. Wattanakit</b> , P. Chaipornchalerms, W. Nunthakitgason, A. Prasertsab, P. Iadrat, S. Tantisriyanurak, C. Rodaum Vidyasirimedhi Institute of Science and Technology, Thailand
17:20 - 18:20	<b>ORAL SESSION 4</b>
<a href="#">O14</a>	Reactions Kinetics Between Ingredients Affect The Structure Of Amorphous Aluminosilicates And The Crystallization Of Zeolites <b>Ching-Tien Chen</b> , Kenta Iyoki, Tatsuya Okubo, Toru Wakihara
<a href="#">O15</a>	Understanding Copper Sites In CHA By Continuous Rotation Electron Diffraction <b>Evgeniia Ikonnikova</b> , Michael Schmithorst, Bradley Chmelka, Tom Willhammar
<a href="#">O16</a>	Alcohol-To-Hydrocarbons Process – Operando FT-IR And UV-Vis Spectroscopic Studies Emphasise The Nature Of Coke Species Formed


**EAZC 2025**
**6<sup>th</sup> Euro-Asia Zeolite Conference**

Alicante (Spain), January 19-22, 2025



	<b>Karolina A. Tarach</b> , Anna Walczyk, Oliwia Rogala, Agata Kordek, Agata Olszewska, Kinga Góra-Marek Jagiellonian University, Kraków, Poland
18:20 - 19:00	<b>EAZC ASSEMBLY</b>
19:00 - 20:30	<b>POSTER SESSION 1</b>
<a href="#">P001</a>	Synthesis And Characterization Of Zeolite@ZIF-8 Composite By Various Methods As A Catalyst For Organic Reactions <b>Mojgan Zendehtdel</b> , Hadis Ghaedrahmat
<a href="#">P002</a>	Construct Core-Shell SSZ-13@Al <sub>2</sub> O <sub>3</sub> Architecture To Boost Pd-Catalyzed Passive NO <sub>x</sub> Adsorption Performance <b>Guoju Yang</b> , Xiaoxin Chen
<a href="#">P003</a>	Polypropylene Catalytic Upcycling In Bound Zeolite Catalysts <b>Kinga Gora-Marek</b> , Karolina A. Tarach, Oliwia Rogala, Louwanda Lakiss, Valentin Valtchev, Jean-Pierre Gilson
<a href="#">P004</a>	Recovering Hydrogen From SMR Using ITQ-12: A Simulation Approach <b>Ana Martin-Calvo</b> , Jeroen Van Heijst, Sofia Calero
<a href="#">P005</a>	Designing Zeolite-Encapsulated Metal Nanoparticles For Efficient CO <sub>2</sub> Conversion <b>Jerrick Mielby</b> , Gordon Zhuo, Emil Kowalewski, Dimitra Iltsiou, Søren Kegsnæs
<a href="#">P006</a>	Ultrasonic Monitoring Of The Synthesis Of Metal-Organic Framework <b>Rebecca Reber</b> , Louis Rupprecht, Marcus Fischer, Martin Hartmann
<a href="#">P007</a>	Computational Modeling Of Organic Structure-Directing Agents In SCM-14 And SCM-15 Germanosilicates <b>Stoyan Gramatikov</b> , Petko Petkov, Zhendong Wang, Weimin Yang, Georgi Vayssilov
<a href="#">P008</a>	Cation Induced Speciation Of Copper Species In The Mordeinite Zeolite Synthesis And Their Influence On The Selective Methane Oxidation To Methanol <b>Peter Njoroge</b>
<a href="#">P009</a>	Process Intensification At The Nanoscale: Embedding SiC In Zeolites For Energy-Efficient Catalysis Alexandre Ferreira Young, Julia Telles De Souza, Pedro Nothaft Romano, Javier García-Martinez, <b>João Monnerat Araújo Riberiro De Almeida</b>
<a href="#">P011</a>	Green Synthesis Approaches Towards The Preparation Of ZIF Compounds And Their Evaluation For CO <sub>2</sub> Sorption <b>Aljaž škrjanc</b> , Nataša Zabukovec Logar
<a href="#">P012</a>	Solventless Synthesis Of Zeolitic Imidazolate Frameworks At High Pressure And Temperature Marta Pérez-Miana, Álvaro Mayoral, <b>Joaquín Coronas</b>
<a href="#">P013</a>	In Search Of Energy-Efficient Materials For Atmospheric Water Harvesting <b>Haonuan Zhao</b> , Viktor yasnou, Remy Guillet-Nicolas, Valentin Valtchev
<a href="#">P014</a>	Catching A Zinc-Containing High-Silica Ferrierite Structure Through Mordeinite Interzeolite Conversion: Phase Selectivity In A Pool Of Newborn Structures <b>Mostafa Torka Beydokhti</b> , Gleb Ivanushkin, Ibrahim Khalil, Ahmed Sajid, Juna Bae, Thibaut Donckels, Dieter Plessers, Michiel Dusselier
<a href="#">P017</a>	Enhancing Plastic Waste Upcycling Efficiency Through Zeolite Confinement And Pore Diffusion <b>Joaquin Martinez-Ortigosa</b> , Saideep Singh, Nuria Ortuño, Vivek Polshettiwar, Javier Garcia-Martinez
<a href="#">P018</a>	Waste Reduction In Fine Chemical Synthesis Using Hierarchical Zeolites Mónica Judith Mendoza-Castro, Javier García-Martínez, <b>Noemi Linares</b>
<a href="#">P019</a>	Interzeolite Transformation Intermediates (ITIs): Superior Catalysts For The Conversion Of Bulky Molecules Mónica Judith Mendoza-Castro, <b>Noemi Linares</b> , Javier García-Martínez
<a href="#">P020</a>	Recyclable Synthesis Of SAPO-34 And Their Catalytic Applications: Utilizing Mother Liquid And Spent Industrial MTO Catalyst As Raw Sources <b>Quanyi Wang</b>
<a href="#">P021</a>	Adsorption Of Carbon Dioxide In Non-Löwenstein Zeolites <b>Juan José Gutiérrez-Sevillano</b> , Pablo Romero-Marimon, Sofía Calero
<a href="#">P022</a>	CDot@SiO <sub>2</sub> And CDot@TiO <sub>2</sub> As Superior Catalysis For The Photodegradation Of Cationic Dyes <b>Jorge Ivan Castro Castro</b> , Maria Rosell, Veronica Torregrosa Rivero, Andres Garzon Ruiz, Cristina Martín Álvarez, Javier Garcia Martinez, Noemi Linares, Elena Serrano
<a href="#">P023</a>	Engineering PtZn Nanoparticles Dispersed On Zeolite Composites As Bifunctional Catalyst For N-Butane Dehydroisomerization <b>Peeranat Chaipornchalem</b> , Watinee Nunthakitguson, Nattanida Thepphankulngarm, Supawadee Namuangruk, Chularat Wattanakit



<a href="#">P024</a>	Nickel-Decorated Carbon Nanotubes (CNTs) Derived From Bioethanol As Electrocatalysts For Featuring H <sub>2</sub> Production And Biorefinery <b>Watinee Nunthakitguson</b> , Peeranat Chaipornchalerm, Anousha sohail, Anawat Thivasasith, Chularat Wattanakit
<a href="#">P025</a>	Exploring The Interplay Between Properties And Catalytic Performance Of Partially Crystallized Zeolites <b>Nelcari Trinidad Ramírez-Marquez</b> , Joaquín Martínez-Ortigosa, Noemi Linares, Javier García-Martínez
<a href="#">P026</a>	Stabilization Of Carbon Dots By Embedding Them In Zeolites <b>David Fernández-Ortiz</b> , María Rosell, Cristina Martín, Elena Serrano, Noemi Linares, Javier García-Martínez
<a href="#">P027</a>	Designing The Novel Zn-URJC-11 Material For Hydrogen Adsorption Applications <b>Gisela Orcajo</b> , Pedro Leo, Jesús Tapiador, Elena García-Rojas, Isabel Aguayo, Felipe Gándara, Carmen Martos
<a href="#">P028</a>	Depillaring, An Effective Way To Prepare 2D Zeolites: Synthesis, Characterization, And Catalytic Evaluation <b>Aroldo José Romero-Anaya</b> , J Martínez-Ortigosa, Noemí Linares, Javier García
<a href="#">P029</a>	Cu-Zeolite Catalysts For CO <sub>2</sub> Conversion And Alcohol Synthesis <b>Dimitra Iltsiou</b> , Jerrik Mielby, Søren Kegnæs
<a href="#">P030</a>	Study Of Water And Ethanol Sorption In ZIFs For Heat Transformation Applications <b>Ciara Byrne</b> , Katja Vodlan, Amalija Golobic, Connor Hewson, Paul Iacomi, Nataša Zabukovec Loga
<a href="#">P031</a>	Mono Vs Bimetallic Pd-Fe/N-ZSM-5 Catalysts For The Conversion Of ELV Plastic Waste Into Dehalogenated Oil Via (Hydro)-Pyrolysis <b>Lidia Amodio</b> , Jennifer Cueto, Patricia Pizarro, David Pedro Serrano
<a href="#">P032</a>	Iridium-Encapsulated MWW-Type Zeolite Catalyst For The Hydrogenolysis Of Methylcyclopentane With Excess Methylcyclohexane <b>Satoshi Inagaki</b> , Yuki Maekawa, Keiju Tokita, Yoshihiro Kubota
<a href="#">P033</a>	Removal Of Polystyrene Nanoplastics From Aqueous Solution Using Zeolite Materials <b>Kinga Góra-Marek</b> , Karolina Tarach, Marta Marczak-Grzesik
<a href="#">P034</a>	How To Mitigate Pitfalls In The Characterization Of Zincosilicate Zeolites? <b>Gleb Ivanushkin</b> , Ibrahim Khalil, Mostafa Torka Beydokhti, Aram Bugaev, Juna Bae, Michiel Dusselier
<a href="#">P035</a>	Tailoring Pores Of AFN-Related Zeolites For Enhanced Separation Of CO <sub>2</sub> /N <sub>2</sub> Or CO <sub>2</sub> /CH <sub>4</sub> <b>Yining Yang</b>
<a href="#">P036</a>	Design And Synthesis Of Zeolite-Like Metal-Organic Frameworks Baobing Tang, Jiangtang Li, Xiaolong Luo, Shuang Wang, <b>Yunling Liu</b>
<a href="#">P037</a>	New Method For Creating Mesopores In Beta Zeolite Catalysts With Hot Liquid Water <b>Hana Jirglová</b>
<a href="#">P038</a>	From Waste To Resources: Control Over The Synthesis And Transformation Of LTA Into NaP Zeolites Through Non-Conventional Precursors <b>Rafael Carrizosa Muñoz</b> , Isabel Padilla Rodríguez, Maximina Romero Pérez, Aurora López Delgado
<a href="#">P039</a>	Sustainable Synthesis Of LTA Zeolite From Industrial Hazardous Waste: Research On SO <sub>2</sub> Adsorption Efficiency In Fixed Bed Applications <b>Rafael Carrizosa Muñoz</b> , Isabel Padilla Rodríguez, Claudia Barco Barona, Maximina Romero Pérez, Antonio Nieto-Márquez Ballesteros, Aurora López Delgado
<a href="#">P040</a>	Monitoring Zeolite Synthesis In Operando Conditions: Practical Insights And Use Cases Of Fed-Batch Reactors <b>Paola Herrero</b> , Amirhossein Javdani, Gleb Ivanushkin, Michiel Dusselier
<a href="#">P041</a>	Optimización De La Acidez De Materiales Mesoporosos Para Aplicaciones Catalíticas <b>Alicia De Diego De Amorím</b>
<a href="#">P043</a>	Investigating The Effect Of Extra-Framework Aluminum Species On (Hydro)Cracking Activity Of USY Zeolite <b>Sohrab Askarli</b>
<a href="#">P044</a>	Formation Of Active Oxygen Species Over Binuclear Fe(II) Species In Al-Rich *BEA Zeolite <b>Agnieszka Kornas</b> , Kinga Mlekodaj, Edyta Tabor, Dominik Kazimierz Wierzbicki, Radim Pilar, Hana Jirglova, Stepan Sklenak
<a href="#">P045</a>	YFI-Type Titanosilicate With Hierarchical Pore-Structure For Efficient Selective Oxidations <b>Shengxiang Zhang</b> , Satoshi Inagaki, Yoshihiro Kubota
<a href="#">P046</a>	Production Of Jet-Fuel Precursors From Volatile Fatty Acids Using TiO <sub>2</sub> Zeolitic Supported Catalysts <b>Adrián Lago Cambeiro</b> , Lorenzo Bertin, Gonzalo Martinez, Jacopo De Maron, Tomasso Tabanelli, Frabrizio Cavani, Cristina González Fernández (3,1), David Pedro Serrano, Inés Moreno
<a href="#">P047</a>	Investigation Of Zeolitic Aluminum By Low-Temperature Template Oxidation With Ozone <b>Julien Devos</b> , Michiel Dusselier
<a href="#">P048</a>	Carbon Dioxide Methanation Using Ni Catalysts Supported On Low-Cost Lynde Type A Zeolite Synthesized From Pretreated Iranian Coal Gangue <b>Soheil Bahraminia</b> , Mansoor Anbia



<a href="#">P049</a>	Optimizing The Physiochemical Properties Of Ni-Pt/MFI Zeolite Catalysts For The Hydrodeoxygenation Of Oleic Acid <b>Abdulla Alhendi</b> , Antigoni Margellou, Steve Hinder, Mark Baker, Kostas Triantafyllidis, Kyriaki Polychronopoulou, Maryam Khaleel
<a href="#">P050</a>	Cu-Oxo-Exchanged Mordenites Prepared By Activation Under He Or CO <sub>2</sub> : The Nature Of The Cu <sub>x</sub> O <sub>y</sub> Species Involved In The Methane Direct Oxidation To Methanol Determined By In Situ DRS-UV-Vis Analyses <b>Eliane Soares Da Silva</b> , João Emanuel Cabral Da Mata, Ernesto Antonio Urquieta-Gonzalez
<a href="#">P051</a>	Ultrafast Dealumination Of Beta Using A Continuous-Flow Reactor Ayano Minami, <b>Masanori Takemoto</b> , Yasuo Yonezawa, Zhendong Liu, Yutaka Yanaba, Chokkalingam Anand, Kenta Iyoki, Tsuneji Sano, Tatsuya Okubo, Toru Wakihara
<a href="#">P052</a>	Low-Silica Cu-CHA Zeolite Enriched With Al Pairs Transcribed From Silicoaluminophosphate Seed: Synthesis And Ammonia Selective Catalytic Reduction Performance <b>Wenfu Yan</b>
<a href="#">P053</a>	Understanding The Influence Of Aging Treatments On Properties Of Amorphous Precursors Towards Rational Synthesis Of CHA-Type Zeolite <b>Yukie Okada</b> , Yuki Sada, Hiroki Yamada, Koji Ohara, Masato Yoshioka, Tomoya Ishikawa, Tsuneji Sano, Tatsuya Okubo, Raquel Simancas, Toru Wakihara
<a href="#">P054</a>	Metal Exchanged Zeolites For Noble Gas Concentration <b>Sylvain Topin</b> , Gabriel Couchaux, Bruno Siberchicot, Fanny Hauquier, Tuel Alain, David Farrusseng
<a href="#">P055</a>	Effect Of The Recrystallization Process In The Catalytic Performance Of Micro-Mesoporous Zeolites On The Isomerization Of Methyl Oleate Jonathan Fabian Sierra-Cantor, Olinda Gimello, Luca Bernardi, Carlos-Alberto Gerrero-Fajardo, <b>Francesco Di Renzo</b> , Nathalie Tanchoux, Corine Gerardin
<a href="#">P056</a>	Synthesis Of Large-Pore Pure Silica Zeolites Using Phenyl-Containing Diquat OSDAs <b>Christian Wittee Lopes</b> , Addressa Vieira Hilário, Katia Bernardo-Gusmão
<a href="#">P057</a>	Enhancing Nucleation To Synthesize Al-Rich CHA Zeolites Under Ultra-Low OSDA Contents <b>Estefanía Bello-Jurado</b> , Isabel Millet, Leen Van Tendeloo, Frank Schütze, Peter N.r. Vennestrøm, Avelino Corma, Manuel Moliner
<a href="#">P058</a>	Seed-Assisted Synthesis Of Nanosized Zeolite P For Improved CO <sub>2</sub> Capture Kinetics <b>Jaouad Al Atrach</b> , Abdelhafid Aitblal, Abdallah Amedlous, Ying Xiong, Rémy Guillet-Nicolas, Valentin Valtchev
<a href="#">P059</a>	Seed-Assisted Synthesis Of LEV Zeolite: Exploring A Novel Adsorbent For CO <sub>2</sub> Capture And Gas Separation <b>Jaouad Al Atrach</b> , Abdallah Amedlous, Ying Xiong, Diogenes Honorato-Piva, Remy Guillet-Nicolas, Valentin Valtchev
<a href="#">P060</a>	Solvent-Free Synthesis Of Ti Isomorphously Substituted Beta Zeolite <b>Krissanapat - Yomthong</b> , Sorasak - Klinyod, Somlak - Ittisanronnachai, Chularat - Wattanakit
<a href="#">P061</a>	In-Situ EPR Study Of The Effect Of Sulfur Poisoning And Regeneration On Cu-CHA Catalysts <b>Thomas Krøier Rønne-Nielsen</b> , Qi Gao, Ton V. W. Janssens, Fei Wen, Peter N. R. Vennestrøm
<a href="#">P062</a>	Ru-MOFs As Catalysts For The Hydrogenation Of Dimethylurea To Methane <b>Itziar Arnaiz</b> , Carlos Márquez-álvarez, Enrique Álvarez-Catalá, Marcos Zubimendi, Joaquín Pérez-Pariente, Manuel Sánchez-Sánchez
<a href="#">P129</a>	Ethylene/ethane permeation behavior through Ag-Beta zeolite membrane <b>Y. Koshiishi</b> , M. Sakai, M. Matsukata
<a href="#">P130</a>	The Synthesis of Nanosized LEV Zeolite <b>Wenhua Fu</b> , Shengli Zhao, Tiezhu Zhang, Zhendong Wang
<a href="#">P131</a>	Operando Characterization of Zeolites via Reactive Neural Network Potentials I. Saha, D. Willimetz, D. Brako-Amofo, C. Bornes, A. Erlebach, L. Grajciar, <b>C.J. Heard</b>
<a href="#">P132</a>	Exploring Zeolite Crystal Size Effects in Palladium-Encapsulated Catalysts for the Selective Hydrogenation Reaction of Phenylacetylene <b>F.J. Escobar-Bedia</b> , A. Martínez Gomez-Aldaravi, C. Martínez, M. Moliner
<a href="#">P133</a>	Mixed Metal Oxide catalyst in tandem with zeolites as a highly selective Catalyst for CO <sub>2</sub> hydrogenation to Jet Fuel <b>P. Clayton</b> , R. Taylor
<a href="#">P134</a>	Design and investigation of superalkalis for CO <sub>2</sub> and N <sub>2</sub> molecules activation: first-principles studies N. Wiszowska, N. Rogoza, <b>C. Sikorska</b>
<a href="#">P135</a>	Design of Efficient Zeolite-Based Catalysts by Le Chatelier's Principle <b>Feng-Shou Xiao</b> , Liang Wang



TUESDAY JANUARY 21	
8:40 - 9:30	<b><a href="#">PLENARY LECTURE 3</a></b>
	A bottom-up approach to the design of next-generation zeolitic catalysts <b>Prof. Unni Olsbye</b> University of Oslo, Norway
9:30 - 10:30	<b>ORAL SESSION 5</b>
<a href="#">O17</a>	Toolkit for the Characterization of Nanoporous Zeolites and MOFs Using Gas Sorption <b>O. Maulik</b> , E. Turrini, K. Struckhoff
<a href="#">O18</a>	Tuning The Aluminum Distribution And Acidity Of ZSM-5 Zeolites Through Mineralizing Agents And Electrostatic Interactions Shadi Al-Nahari, Claudia Cammarano, Eddy Dib, Dominique Massiot, Vincent Sarou-Kanian, <b>Bruno Alonso</b>
<a href="#">O19</a>	Automated Transition State Finding In Zeolites Through High-Throughput Visual Screening <b>Pau Ferri Vicedo</b> , Alexander J. Hoffman, Avni Singhal, Rafael Gomez Bombarelli
10:30 - 10:50	<b>COFFEE BREAK</b>
10:50 - 11:20	<b><a href="#">KEYNOTE LECTURE 3</a></b>
	Inventing materials to meet today's energy and environmental challenges <b>Prof. Sofía Calero</b> Eindhoven University of Technology, The Netherlands
11:20 - 13:00	<b>ORAL SESSION 6</b>
<a href="#">O20</a>	Advancing Highly Selective Low-Temperature Ammonia Oxidation: Hydrophobic Silicalite-1 Shell Confining Silver Nanoparticles On Cu/ ZSM-5 Core <b>Xiaoxin Chen</b> , Guoju Yang
<a href="#">O21</a>	ZMQ-1: A Stable 28-Membered Ring Three-Dimensional Aluminosilicate Zeolite <b>Mohamamd Fahda</b> , Yiqing Sun, Lu Peng, Valentin Valtchev
<a href="#">O22</a>	On The Phase Selection In Zeolite Synthesis <b>Ana Palcic</b> , Sanja Bosnar, Mladenka Jurin, Nikola Jakupec
<a href="#">O23</a>	Zr-Based Metal-Organic Frameworks And SBA-15 Mesoporous Silica: A Synergistic Approach For Catalysis In The Production Of Bio-Jet Fuel María Sanz, <b>Pedro Leo</b> , Marta Paniagua, Gabriel Morales, Juan Antonio Melero
<a href="#">O24</a>	Molecular Recognition-Induced Structural Flexibility In ZIFs <b>Judit Farrando-Perez</b> , Carolina Carrillo-Carrión, Alexander Missyul, Joaquin Silvestre-Albero
13:00 - 14:30	<b>BUSINESS LUNCH</b>
14:30 - 16:00	<b>POSTER SESSION 2</b>
<a href="#">P063</a>	Emerging Co-Synthesis Of Dimethyl Oxalate And Dimethyl Carbonate Using Pd/Silicalite-1 Catalyst With Synergistic Interactions Of Pd And Silanols <b>Chunzheng Wang</b> , Rongyan Mei, Miao Li, Hailing Guo, Svetlana Mintova
<a href="#">P064</a>	Tuning The Adsorptive Characteristics Of MOFs Through Trans-Metalation: A Successful Strategy For Designing Selective Adsorbents For Aquas And Gas-Phase Applications <b>Fatemeh Nouroozi</b> , Hossein Kazemian
<a href="#">P065</a>	Hierarchical Zeolites Enable The Design Of Multifunctional Catalysts For Fatty Acids Hydrodeoxygenation To Alkanes <b>Shengzhe Ding</b> , Christopher Parlett, Xiaolei Fan
<a href="#">P066</a>	Highly Stable Subnanometric Pt Clusters In All Silica K-Doped Zeolites: Implications For The CO Oxidation Reaction <b>Benjamin Bohigues Vallet</b>
<a href="#">P067</a>	Effect Of Defect-Healing Treatment On Layered Silicate Precursors Toward Well-Defined, Cross-Linked Frameworks <b>Yoshiaki Ito</b> , Keiichiro Nayuki, Yukichi Sasaki, Toru Wakihara, Tatsuya Okubo, Kenta Iyoki
<a href="#">P068</a>	Ultrafast Laser Synthesis Of Silicalite-1 And Titanium-Silicalite-1 <b>Mehdi Hagverdiyev</b> , Meryem Merve Dogan, Serim Kayacan I?lday, Sezin Galioglu Ozaltug



<a href="#">P069</a>	Structural Modifications Of Pure Silica MEL Zeolite Studied By In-Situ X-Ray Diffraction During Adsorption Of Propane Alberto Barros, Silvia Martí, Miguel Palomino, José Luis Jordá, <b>Susana Valencia</b> , Fernando Rey
<a href="#">P070</a>	Machine Learning And High-Throughput Simulation Methods To Design Organic Structure-Directing Agents For Zeolites <b>Koki Muraoka</b> , Kota Oishi, Shusuke Ito, Akira Nakayama
<a href="#">P071</a>	End-Of-Life PV Panels As A Circular Economy Products In Synthesis Of Micro/Mesoporous Materials <b>Dorota Czarna-Juszkiewicz</b> , Piotr Kunecki, Lukasz Osuchowski, Tomasz Glowienko, Magdalena Wdowin
<a href="#">P072</a>	Rapid Synthesis Of Cu-Encapsulated Nanoparticles In ZSM-5 Zeolite For Enhanced Catalytic Conversion Of CO <sub>2</sub> To Methanol <b>Raquel Simancas</b> , Saeko Yamaguchi, Ryokuto Kanomata, Koki Awano, Suhei Yasuda, Hiroyasu Fujitsuka, Teruoki Tago, Toshiyuki Yokoi, Tatsuya Okubo, Toru Wakihara
<a href="#">P073</a>	Synthesis And Asymmetric Catalytic Activity Of The Chiral Zeolite GTM-4 Prepared From Benzylated Ephedrine Derivatives <b>Jaime Jurado-Sánchez</b> , Ramón De La Serna, Carlos Márquez-Alvarez, Joaquín Pérez-Pariente, Luis Gómez-Hortigüela
<a href="#">P074</a>	Synthesis Of Zeolites Coated 1D TiO <sub>2</sub> Nanotubes Arrays <b>Rosalba Passalacqua</b> , Alfredo Aloise, Alessia Marino, Nicola Di Nicola, Siglinda Perathoner, Gabriele Centi
<a href="#">P075</a>	Gold Nanoclusters Prepared From An Eighteenth Century Two-Phases Procedure Supported On Chiral Zeolitic Material GTM-4 For Liquid Phase Oxidation Of Cyclohexene With Molecular Oxygen <b>Paula Sánchez-Morena</b> , Álvaro Mayoral, Luis Gomez-Hortigüela, Joaquín Pérez-Pariente
<a href="#">P076</a>	Capturing Different Intermediate Phases During Zeolite Synthesis <b>Suk Bong Hong</b>
<a href="#">P077</a>	Synthesis, Characterization And Structural Determination By 3D Electron Diffraction Of The Extra-Large Pore Zeolite ITQ-70 <b>Juan Ignacio Tirado</b> , Andrés Sala, Antonio Bordes, Partha Pratim Das, Lukáš Palatinus, Stavros Nicolopoulos, Jose Luis Jordá, Alejandro Vidal-Moya, Teresa Blasco, Germán Sastre, Susana Valencia, Fernando Rey
<a href="#">P079</a>	Zeolites And MOFs As Easily-Tunable Macroligands Of Metal Catalysts For Organic Reactions <b>Antonio Leyva-Pérez</b> , Judit Oliver-Meseguer
<a href="#">P080</a>	Phase Selection And Framework Composition In Mixed-Cations Zeolite Synthesis Utilizing Hydrated Silicate Ionic Liquids (HSILs) <b>Anjul Rais</b> , Dries Vandenberghe, Nikolaus Doppelhammer, Christine Kirschhock, Eric Breynaert
<a href="#">P081</a>	Mechanism Of N <sub>2</sub> O Decomposition Catalysed By Cu-Exchanged Zeolites <b>Miguel Ródenas</b> , Mercedes Boronat, Reisel Millán
<a href="#">P082</a>	Post-Synthetic Structural Consolidation Of Sn-β: Enhancing Stability In The Continuous Production Of Methyl Lactate Jose Manuel Jimenez Martin, Stevie Hallen Lima, Alicia Garcia Sanchez, <b>Jose Iglesias Moran</b>
<a href="#">P083</a>	Mechanism Of Selective Oxidation Of Methane To Methanol Over A Pair Of α-Oxygens Formed By Dioxygen Splitting. DFT Study <b>Jiri Dedecek</b> , Stepan Sklenak, Mariia Lemishka, Hana Jirglova
<a href="#">P084</a>	On The Thermodynamics Of Adsorption Based Contaminant Removal: Pharmaceuticals And Hydrophobic Zeolites <b>Jakob Brauer</b> , Michael Fischer
<a href="#">P085</a>	TS-1@Co-PDA: A Bifunctional Catalyst For Synergistic Hydrogen Peroxide Generation And Oxidation Of Organic Molecules <b>Hedieh Sadat Tabatabaeizadeh</b> , Francesca Rosso, Francesca Bonino, Silvia Bordiga, Valentina Crocellà, Matteo Signorile
<a href="#">P086</a>	Insertion Of Active Sites In ZEO-3 Matrix: A Promising Catalyst For Partial Oxidation Of Bulky Molecules <b>Hedieh Sadat Tabatabaeizadeh</b> , Francesca Rosso, Francesca Bonino, Silvia Bordiga, Valentina Crocellà, Matteo Signorile
<a href="#">P087</a>	Comparison Of Physisorption And Chemosorption Integrated With Silica Gel For Direct Air Capture In Harsh Atmosphere Like Qatar <b>Yasser Mohamed Abdellatif</b> , Riham Sorkatti Abubakr, Raesh Muhammad, Ahmed Sodiq, Odi Fawwaz Alrebei, Tareq A. Al-Ansari, Abdulkarem I. Amhamed
<a href="#">P088</a>	Development Of Zeolite Adsorbent With Low Water Sensitivity For CO <sub>2</sub> Capture <b>Peidong Hu</b> , Ryusei Oishi, Hanlong Ya, Yasuo Yonezawa, Minoru Matsukura, Kenta Iyoki, Tatsuya Okubo, Toru Wakihara
<a href="#">P089</a>	Synthesis Of High-Silica ERI By Machine Learning Assisted OSDA Design <b>Yolanda Marcela Semanate Esquivel</b>





<a href="#">P090</a>	Alcohol-Assisted Synthesis Of ZSM-5 Zeolites Contributes To Enhanced BTX Production From Methanol <b>Qi Li</b> , Liang Zhao, Yong Wang, Peipei Xiao, Yuqin Sun, Toshiyuki Yokoi
<a href="#">P091</a>	Synthesis Of ZSM-5 From Natural Mordenite From Spain <b>Itziar Arnaiz</b> , Yaregal Awoke, Manuel Sánchez-Sánchez, Isabel Díaz
<a href="#">P092</a>	Crystallisation Kinetics Of ITQ-13: A Solid-State NMR Study <b>Matteo Tarchi</b> , Alejandro Vidal-Moya, Fernando Rey, Teresa Blasco
<a href="#">P093</a>	Ordered Mesoporous Carbons As Promising Electrocatalysts For The Selective Oxidation Of Lignin-Derived Molecules <b>Paolo Squillaci</b> , Donatella Chillè, Georgia Papanikolaou, Siglinda Perathoner, Gabriele Centi, Paola Lanzafame
<a href="#">P095</a>	Design Of Bi-Functional Ni-Zeolites For Ethylene Oligomerization: Controlling Zeolite Properties By One-Pot And Post-Synthetic Ni Incorporation <b>Christos Kantler</b>
<a href="#">P096</a>	LEU-2: A New Pure Silica Zeolite With 10-Ring Channels <b>Juna Bae</b> , Dieter Plessers, Lynne B. Mccusker, Michiel Dusselier
<a href="#">P097</a>	Zeolite-Catalyzed 1,2-Dibromination Of Cinnamates: A Green And Efficient Approach To $\alpha,\beta$ -Dibromohydrocinnamates Mladenka Jurin, <b>Ana Palcic</b>
<a href="#">P098</a>	Enhanced Hydrodeoxygenation Of M-Cresol Via Pt/HY Catalysts In Microwave-Assisted Systems: A Pathway To Efficient Bio-Oil Upgrading Caio B Souza, João Monnerat De Almeida, Javier Garcia Martinez, <b>Pedro Nothaft Romano</b>
<a href="#">P099</a>	Crystal Size And Morphology Control Of SAPO-40 Zeolite <b>Jie Du</b>
<a href="#">P100</a>	Neutron Total Scattering Unravels Pre-Zeolite Structures In Amorphous Aluminosilicate Gels Lara Gigli, Amine Morsli, Daniel T. Bowron, Silvia Imberti, Simona Quartieri, Abdelkader Bengueddach, <b>Francesco Di Renzo</b> , Rossella Arletti
<a href="#">P101</a>	Assessing The Effect Of Zeolites Structure Into Ethanol To Butanol Selective Conversion By Guerbet Reaction <b>Alessia Marino</b> , Emanuele Cocco, Rosalba Passalacqua, Armando Carlone, Marcello Crucianelli, Alfredo Aloise
<a href="#">P102</a>	Mobility Of Solvated Cu Cations In Cu-CHA Predicted By Machine Learning Accelerated Molecular Dynamics <b>Reisel Millan</b> , Mercedes Boronat
<a href="#">P103</a>	Application Of Zr-MOF And Ionic Liquids In SPEEK Membranes <b>Katiuscia Nobre Borba</b> , Caroline Troglio Ibanez, Leticia Zanchet, Leticia Trindade, Fernando Rey, Urbano Diaz, Katia Benardo Gusmão
<a href="#">P104</a>	Metal-Doped Hierarchical ZSM-5 Zeolites Towards More Stable Catalysts In The Aromatization Of Paraffins And Olefins In Plastic Pyrolysis Liquids <b>Marcelo E. Domine</b> , Roger Saúl Días Cevallos, Paola Rosa Frigols Arroyo, Alberto Fernández-Arroyo Naranjo
<a href="#">P105</a>	Binuclear Vanadium Species In Ferrierite Zeolite And Their Reactivity <b>Mariia Lemishka</b> , Jiri Dedecek, Kinga Mlekodaj, Dalibor Kaucky, Agnieszka Kornas, Edyta Tabor
<a href="#">P106</a>	Chirality in confined spaces. Study of the asymmetric catalytic reaction of GTM-4 with prochiral cis-stilbene oxide <b>Ramón De La Serna</b> , Jaime Jurado Sánchez, Joaquín Pérez Pariente, Luis Gómez-Hörtiguela
<a href="#">P107</a>	FT-IR And UV-Vis Spectroscopies Supported With MCR-ALS Analysis For Active Species Identification In Alcohol-To-Hydrocarbons Processes <b>Karolina A. Tarach</b> , Agata Kordek, Anna Walczyk, Agata Olszewska, Kinga Góra-Marek
<a href="#">P108</a>	Mixed Interzeolite Conversion Enabling Fast AEI Synthesis <b>Elena Brozzi</b> , Raquel Simancas, Toru Wakihara, Michiel Dusselier, Simon Kuhn
<a href="#">P109</a>	Finetuning The Adsorption Behavior Of SSZ-13 By The Addition Of Li During And After Synthesis <b>Sven Robijns</b> , Niels De Witte, Julien Devos, Tom R.c. Van Assche, Michiel Dusselier
<a href="#">P110</a>	In-Situ Investigation Of Water Harvesting By CAU-10-OH MOF: A 2-Steps Process <b>Gwilherm Nénert</b>
<a href="#">P111</a>	Adsorption Of Small Molecules On Zeolite SSZ-45 <b>Alberto Barros Pardo</b> , Jose Valero Jiménez, Fernando Rey García, Susana Valencia Valencia
<a href="#">P112</a>	Influence of Al distribution in transition-metal-free aluminosilicate Ferrierite zeolite on the performance of methane oxidation P. Xiao, H. Toyoda, K. Nakamura, Y. Wang, <b>Toshiyuki Yokoi</b>
<a href="#">P113</a>	Hierarchical MEL Type Materials with Intracrystalline Macropores: Syntheses and Characterization T Weissenberger, A. A. Machoke, B. Apeleo Zubiri, D. Drobek, E. Spiecker, M. Hartmann, <b>W. Schwieger</b>
<a href="#">P114</a>	Chlorate control in water phase by Pt-based zeolite catalysts <b>N. Benmebirouk-Pareja</b> , A. Plá-Hernández, A.E. Palomares



<a href="#">P115</a>	Morphological and Textural Changes in the Synthesis of Nanostructured ZSM-11 Zeolites <b>A. López Albero</b> , M. Alonso-Doncel, D.P. Serrano
<a href="#">P116</a>	ITQ-35: A new microporous germanate zeolite J.I. Tirado, <b>J. Valero</b> , P. Pratim Das, L. Palatinus, S. Nicolopoulos, J.L. Jordá, G. Sastre, A. Cantín, S. Valencia, F. Rey
<a href="#">P117</a>	Ni-based MOFs as CO <sub>2</sub> adsorbent in biogas: Effect of linker and its modification with ethylenediamine <b>Y.K. Krisnandy</b> , M.R. Ramdani, P. Andini, Rizkiyah, I. Abdullah
<a href="#">P118</a>	Investigation of Co behaviour encapsulated within the lamellar structure of hierarchical ZSM-5 zeolite <b>I. Khattrin</b> , I. Abdullah, A.J. Mccue, Y.K. Krisnandi
<a href="#">P119</a>	Enhancement of oil properties from plastic waste pyrolysis through zeolite-based (MCM and TNU) catalytic upgrading <b>A. Pinto</b> , L. Amodio, M. Kubů, J. Cueto, P. Eliášová, P. Pizarro, J. Čejka, D. P. Serrano
<a href="#">P120</a>	Bifunctional catalysts CuAl <sub>2</sub> O <sub>4</sub> /SAPO-34 for CO <sub>2</sub> hydrogenation to olefins <b>Abdelhakim Elmhamdi</b> , Khaleel Maryam
<a href="#">P122</a>	Production of jet fuel-ranged aromatic hydrocarbons through catalytic pyrolysis of lignocellulosic waste over metal-loaded HZSM-5 Haneul Shim, Bo Sung Kang, Jihyeon Seo, Yong Jun Choi, Hoesuk Yim, Sumin Pyo, <b>Young-Kwon Park</b>
<a href="#">P123</a>	Visualizing the Superiority of Binder-free Zeolite Catalyst for the Alkylation of Benzene with Ethylene <b>Duo Zheng Ma</b> , Eelco T. C. Vogt, Zhendong Wang, Bert M. Weckhuysen, Weimin Yang
<a href="#">P124</a>	Continuous flow CO <sub>2</sub> /CH <sub>4</sub> separation using MMU-1 and CHA zeolites <b>B. Tapping</b> , L. Tosheva, A. M. Doyle
<a href="#">P125</a>	SAPO Precursor and Multiple Template-Assisted Synthesis of Highly Acidic SAPO Molecular Sieves with Excellent NH <sub>3</sub> -SCR Activity of Their Cu-Exchanged Form <b>M. Yang</b> , Y. Wang, P. Tian and Z. Liu
<a href="#">P126</a>	A waste of time? The synthesis of Mg-doped Aluminophosphates from a waste source of magnesium <b>C. Crockett</b> , R. A. Taylor
<a href="#">P127</a>	Formation of Nanostructured Cu and Ni Si-MFI Zeolites for Bioethanol Upgrading <b>J. Bedward</b> , R. Taylor
<a href="#">P128</a>	Tuning the Cu/ZSM-5 properties as catalyst in the conversion of 2,3-Butanediol to butenes <b>Patricia Pizarro</b> , Adriana Souza, Sinay Turriziani, Mar Alonso-Doncel and David P. Serrano
16:00 - 20:00	<b>CITY TOUR</b>
20:00 - 22:00	<b>CONFERENCE DINNER</b>
<b>WEDNESDAY JANUARY 22</b>	
8:40 - 9:30	<b>PLENARY LECTURE 4</b>
	Elucidating and controlling zeolite crystallization for the design of advanced materials <b>Prof. Jeffrey D. Rimer</b> University of Houston, USA
9:30 - 10:30	<b>ORAL SESSION 7</b>
<a href="#">O25</a>	Interaction Of The Anticancer Drug 5-Fluorouracil With Brönsted And Lewis Acid Sites: Insights From Density Functional Theory <b>Michael Fischer</b>
<a href="#">O26</a>	Why Some Silica Zeolites Have Not Been Synthesized As Aluminosilicate? <b>German Sastre</b> , Ömer Faruk Altundal, Jose Valero, Susana Valencia, Fernando Rey, Maria Galvez, Frits Daeyaert
<a href="#">O27</a>	Enhanced Hydrocracking Efficiency And Catalyst Stability Through Structured Mesoporosity In Pt/HUSY Zeolites. Nilson De Paula, Holman Mesa, Joaquin Martinez-Ortigosa, João Monnerat De Almeida, Javier Garcia Martinez, <b>Pedro Nothaft Romano</b>
10:30 - 10:50	<b>COFFEE BREAK</b>



10:50 - 11:20	<b>KEYNOTE LECTURE 4</b>
	Replacing HCl with Zeolite-Based Solid Acid Catalysts in the Production of Polyurethane Intermediates <b>Minkee Choi</b> Korea Advanced Institute of Science and Technology, Republic of Korea
11:20 - 13:00	<b>ORAL SESSION 8</b>
<a href="#">O28</a>	Structural Insights And Exchange Dynamics Of Rare Earth Elements In Synthetic NH <sub>4</sub> -13X Zeolite <b>Francesco Colombo</b> , Riccardo Fantini, Mattia Sisti, Francesco Di Renzo, Giorgia Confalonieri, Gianluca Malavasi, Daniele Malferrari, Rossella Arletti
<a href="#">O29</a>	CO <sub>2</sub> Methanation Catalysed By NiO-CeO <sub>2</sub> Nanoparticles Supported On Beta-Zeolite <b>Iván Martínez-López</b> , Raquel Rodríguez-Bobada, Iris Martín-García, Arantxa Davó-Quifonero, Esteban Guillén-Bas, Dolores Lozano-Castelló, Agustín Bueno-López
<a href="#">O30</a>	MOR-Type Zeolite Membrane For Reverse Water Gas Shift Membrane Reactor <b>Motomu Sakai</b> , Kyoka Tanaka, Masahiko Matsukata
<a href="#">O31</a>	On The Origin Of Enantioselectivity In Chiral Zeolite Asymmetric Catalyst GTM-3: Host-Guest Transfer Of Chirality Ramón de La Serna, Jaime Jurado-Sánchez, Jian Li, Carlos Márquez-Álvarez, Joaquín Pérez-Pariente, <b>Luis Gómez-Hortigüela</b>
<a href="#">O32</a>	Magnesium Silicate MWW Molecular Sieve: An Efficient Basic Material Applied For Dry Reforming Of Methane And NO <sub>2</sub> Organic Sensor <b>Sungjoon Kweon</b> , Hyung-Ki Min, Yeong Don Park, Min Bum Park
13:00 - 14:30	<b>BUSINESS LUNCH</b>
14:30 - 16:30	<b>ORAL SESSION 9</b>
<a href="#">O33</a>	Ultrafast Encapsulation Of Bimetallic Nanoclusters Into Zeolites Tao Yu, Kai Jia, Yundong Wang, Jianhong Xu, <b>Zhendong Liu</b>
<a href="#">O34</a>	Rational Control Of Aluminum Distribution In Zeolites With Alternative Additives Boosts Catalytic Performance <b>Liang Zhao</b> , Yong Wang, Peipei Xiao, Qi Li, Hirota Toyoda, Toshiyuki Yokoi
<a href="#">O35</a>	Synthesis And Structural Analysis Of High-Silica ERI Zeolite With Spatially-Biased Al Distribution As A Promising NH <sub>3</sub> -SCR Catalyst <b>Jie Zhu</b> , Koki Muraoka, Takeshi Ohnishi, Yutaka Yanaba, Masaru Ogura, Akira Nakayama, Toru Wakihara, Zhendong Liu, Tatsuya Okubo
<a href="#">O36</a>	Determination Of Aluminum Distribution And Active Sites Location In Zeolite Based-Catalysts By Anomalous X-Ray Powder Diffraction <b>Przemyslaw Rzepka</b> , Kinga Mlekodaj, Edyta Tabor, Jirí Dedecek, Jeroen Van Bokhoven
<a href="#">O37</a>	How Water Impacts Zeolite Crystallization In Hydrated Silicate Ionic Liquids <b>Dries Vandenabeele</b> , Nikolaus Doppelhammer, Sambhu Radhakrishnan, Vinod C. Chandran, Anjul Rais, Christine Kirschhock, Eric Breynaert
<a href="#">O38</a>	Direct Submicron-Scale Imaging Of Al Distribution In Small-Pore Zeolites: Revealing Unique DeAl Behavior In Intracrystalline Architecture Of AFX <b>Yoshihiro Kamimura</b> , Tetsuya Kodaira, Akira Endo
16:30 - 16:50	<b>CLOSING REMARKS</b>

# PLENARY LECTURES

PL1 – PL4



## Advance in Zeolite Science: From Synthesis to Emerging Applications

Jihong Yu

<sup>1</sup>State Key Laboratory of Inorganic Synthesis and Preparative Chemistry, College of Chemistry, Jilin University, Changchun 130012, China

<sup>2</sup>International Center of Future Science, Jilin University, Changchun 130012, China

<sup>3</sup>College of Chemistry, Beijing Normal University, Beijing 100875, China

jihong@jlu.edu.cn

Zeolites as important catalysts and adsorbents are playing important roles in many sustainable processes involving energy-saving catalysis and environmentally benign adsorptive separation [1, 2]. In recent decade, significant progress has been achieved in zeolite synthesis, characterization techniques, theoretical studies and emerging applications, which brings zeolite science into a new era. With a deeper understanding of zeolite synthesis, increasing number of new zeolite structures, in particular those with stable extra-large pore structures, has been discovered based on template design and 1D/2D to 3D topological condensation strategies [3, 4]; hierarchical structures with hierarchical pores and heterostructures integrated with other porous materials (e.g., mesoporous materials, MOFs, COFs) can be constructed by kinetic control of crystallization and 3D printing techniques [5, 6]; zeolite fine structures such as framework Si/Al ratios, extra-framework cations, and intergrowth, etc., can be well modulated [7, 8]. Benefiting from the nanoconfinement effect, guest species like metallic active species and semiconductive species can be encapsulated within the channels/cavities to form host-guest synergistic catalytic systems via in situ and post synthesis strategies [9, 10]. These new zeolites and zeolite-based materials afford outstanding performance in various important catalytic reactions such as bulky molecular conversion, NH<sub>3</sub>-SCR, C1 conversion, propane dehydrogenation, hydrogen production, biomass conversion, and plastic degradation [11]. By fine tuning the pore structures, the extra-framework species, and synergism between sited protons and cations in zeolite, challenging separation, such as greenhouse gas separation and low carbon alkenes/alkanes separation can be achieved with high efficiency. Besides applications in catalysis and separation, zeolites are finding new applications in energy storage. For instance, ultrathin zeolite membranes can be utilized as solid electrolytes taking advantage of the low electron conductivity, high ion conductivity, and high chemical stability of zeolites [12]. In this presentation, I will showcase the advance in zeolite science from synthesis to application. The future studies in zeolite science will be focused on uncovering new zeolite materials with desired structures, advancing atomic-level in situ and operando characterization techniques and multi-scale simulations to elucidate formation and function mechanisms, harnessing artificial intelligence (AI) to discern the intricate relationships among synthesis, structure, and function of zeolitic materials to assist the rational synthesis of zeolite materials with desired functions, thus empowering zeolites in emerging applications contributing to the sustainable development in energy and environment.

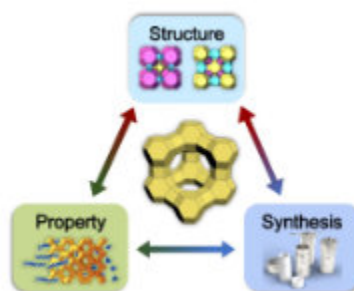


Figure 1. Uncovering the relationships among synthesis, structure, and function of zeolitic materials.

### References

- [1] Y. Li, L. Li, J. H. Yu, *Chem*, **3**, 928 (2017).
- [2] Y. Li, J. H. Yu, *Nat. Rev. Mater.* **6**, 1156 (2021).
- [3] J. Li, Z. Gao, Q. F. Lin, M. A. Cambor, F. J. Chen, J. H. Yu et al., *Science*, **379**, 283 (2023).
- [4] Z. Gao, H. Yu, F. J. Chen, J. Li, P. Wu, J. H. Yu, M. A. Cambor et al., *Nature*, **628**, 99 (2024).
- [5] G. R. Chen, B. Y. Buan, J. H. Yu et al., *Angew. Chem. Int. Ed.* **61**, e202200677 (2022).
- [6] Y. Z. Wei, J. H. Yu et al., *Adv. Mater.*, **36**, 2302912 (2024).
- [7] J. Y. Wang, M. Boronat, J. H. Yu et al., *Angew. Chem. Int. Ed.*, **59**, 17225 (2020).
- [8] J. F. Han, J. Y. Li, W. R. Zhao, D. H. Mei, J. H. Yu et al., *J. Am. Chem. Soc.*, **146**, 7605 (2024).
- [9] Z. Qu, G. He, T. Zhang, Q. M. Sun, D. H. Mei, J. H. Yu et al., *J. Am. Chem. Soc.*, **146**, 8939 (2024).
- [10] J. L. Li, Q. Zhang, J. H. Yu et al., *J. Am. Chem. Soc.*, **146**, 24358 (2024).
- [11] Q. Zhang, S. Q. Gao, J. H. Yu, *Chem. Rev.* **123**, 6039 (2023).
- [12] X. W. Chi, J. J. Xu, J. H. Yu et al., *Nature*, **592**, 551 (2021).

### Acknowledgments

We thank the National Natural Science Foundation of China (22288101), the National Key Research and Development Program of China (2021YFA1501202), and the '111 Center' (B17020) for supporting our work.



## Tracking sub-nano-scale structural evolution in zeolite synthesis

### T. Wakihara

Institute of Engineering Innovation, The University of Tokyo, 2-11-16 Yayoi, Bunkyo-ku, Tokyo 113-8656, Japan  
wakihara@chemsys.t.u-tokyo.ac.jp

Zeolites are artificially synthesized from silicon sources, aluminum sources, mineralizing agents and structure-directing agents in batch systems under hydrothermal conditions. To fulfill the wide industrial demands, efficient synthesis of zeolites with controllable crystallization kinetics is considered crucially important. It is believed that the amorphous aluminosilicate obtained by mixing raw materials first undergoes an induction stage, where its structure changes to a more stable amorphous state, and then a “crystal nucleus,” the smallest entity that can be recognized as a crystalline phase, is formed [1]. Thus, if the process of initial structural evolution of zeolites can be clarified and controlled, it will be possible to design and synthesize zeolites with controlled structure and composition in a rational manner. Furthermore, it is expected to make a significant contribution to the discovery of theoretical zeolites with unknown structure and composition. However, the multifaceted formation process of zeolites cannot be simply explained by the classical nucleation theory, in which monomers aggregate to reach a critical size. Furthermore, the aperiodic structure of the aluminosilicate precursor invalidates the conventional crystallographic characterization, and this amorphous-to-crystalline transition process is still a black box. Our group has employed the advanced high-energy X-ray total scattering (HEXTS) technique to track the sub-nano-scale structural evolution during the formation process of the zeolites [2-5]. In this talk, I will introduce the latest researches on the formation mechanism of zeolites using the HEXTS technique, especially in situ HEXTS technique, combined with pair distribution function (PDF) analysis.

### References

- [1] C.-T. Chen, K. Iyoki, Y. Yonezawa, T. Okubo, and T. Wakihara, *J.Phys.Chem.C*, **124**, 11516-11524 (2020).
- [2] C.-T. Chen, K. Iyoki, H. Yamada, S. Sukenaga, M. Ando, H. Shibata, K. Ohara, T. Wakihara, and T. Okubo, *J.Phys.Chem.C*, **123**, 20304-20313 (2019).
- [3] C.-T. Chen, K. Iyoki, P. Hu, H. Yamada, K. Ohara, S. Sukenaga, M. Ando, H. Shibata, T. Okubo, and T. Wakihara, *J. Am.Chem.Soc.*, **143**, 10986-10997 (2021).
- [4] H. Yamada, S. Tominaka, K. Ohara, Z. Liu, T. Okubo, and T. Wakihara, *J.Phys.Chem.C*, **123**, 28419-28426 (2019).
- [5] A. Minami, P. Hu, Y. Sada, H. Yamada, K. Ohara, Y. Yonezawa, Y. Sasaki, Y. Yanaba, M. Takemoto, Y. Yoshida, T. Okubo, and T. Wakihara, *J.Am.Chem.Soc.*, **144**, 23313-23320 (2022).



6<sup>th</sup> Euro-AsiaZeolite Conference  
Alicante (Spain), January 19-22, 2025



## A bottom-up approach to the design of next-generation zeolitic catalysts

### Unni Olsbye

*Dept. of Chemistry, University of Oslo, SemSælands vei 26, 0372 Oslo, Norway.*

*Email: unni.olsbye@kjemi.uio.no*

Zeolites and zeotypes constitute the second largest class of industrial catalysts. Their macroscopic selectivity relies on an intricate interplay of restricted diffusion and conversion of reactants and products. During the past decades, key mechanistic insight in industrially important reactions was achieved by combining kinetic and mechanistic studies, synthesis of materials with systematically modified properties, operando characterization techniques as well as static and dynamic DFT-based modelling.

In this lecture, focus will be set on studies aimed at decoupling diffusion and reaction kinetics, ultimately forming the basis of predictive models aimed at tailoring catalysts for next generation, renewable-based chemical industry.



## Elucidating and Controlling Zeolite Crystallization for the Design of Advanced Materials

J.D. Rimer

Department of Chemical and Biomolecular Engineering, University of Houston, 4226 Martin Building 1, Houston, TX 77204-4004 USA  
jrimer@central.uh.edu

Luther King Blvd., S222 Engineering

This talk will address recent progress in the understanding of zeolite growth mechanisms and how the knowledge gained from these studies can be used for the rational design of catalysts for diverse reactions of commercial significance. The complex pathways of zeolite crystallization make it difficult to control their physicochemical properties.<sup>1,2</sup> This talk will highlight several methods that can be used to tailor zeolite crystal size, morphology, and composition in ways that reduce diffusion limitations, tune acidity, and selectively control acid siting to enable the development of catalysts with superior performance compared to materials obtained by conventional synthesis routes. Examples include the use of seed-assisted syntheses and interzeolite transformations<sup>3</sup>, the design of core-shell and zoned materials<sup>4,5</sup>, self-pillared zeolites<sup>6</sup>, and a new class of zeolites referred to as finned materials that have been demonstrated for diverse structures.<sup>7</sup> Direct comparisons of ZSM-5 catalysts under identical reaction conditions using methanol to hydrocarbons as a benchmark reaction has revealed the presence of intrinsic defects in MFI-type materials related to several factors, including the nature of aluminum sites. Another subject that will be discussed in this talk is the replacement of aluminum with heteroatoms that can be integrated in both conventional and hierarchical zeolites to enhance catalyst performance.<sup>8</sup> Examples include the synthesis of finned zeolites using seeded growth to introduce fin-like protrusions with identical crystallographic registry as the interior crystal. Introduction of various heteroatoms (e.g., Ga, Ti) into zeolites is a strategy for tailoring zeolite acidity for a broad range of reactions, while these sites can also be used as sacrificial placeholders for post-synthesis removal as a means of defect engineering. Many of these approaches transform materials into pseudo-nanoparticles with improved mass transport and dramatically enhanced catalyst performance.

### References

1. Mallette, A.J., K. Shilpa, and J.D. Rimer, *The Current Understanding of Mechanistic Pathways in Zeolite Crystallization*. Chemical Reviews, 2024. **124**(6): p. 3416-3493.
2. Jain, R., A.J. Mallette, and J.D. Rimer, *Controlling Nucleation Pathways in Zeolite Crystallization: Seeding Conceptual Methodologies for Advanced Materials Design*. Journal of the American Chemical Society, 2021. **143**(51): p. 21446-21460.
3. Jain, R. and J.D. Rimer, *Seed-Assisted zeolite synthesis: The impact of seeding conditions and interzeolite transformations on crystal structure and morphology*. Microporous and Mesoporous Materials, 2020. **300**.
4. Le, T.T., K. Shilpa, C.S. Lee, S.M. Han, C. Weiland, S.R. Bare, P.J. Dauenhauer, and J.D. Rimer, *Core-shell and egg-shell zeolite catalysts for enhanced hydrocarbon processing*. Journal of Catalysis, 2022. **405**: p. 664-675.
5. Le, T.T., W. Qin, A. Agarwal, N. Nikolopoulos, D.L. Fu, M.D. Patton, C. Weiland, S.R. Bare, J.C. Palmer, B.M. Weckhuysen, and J.D. Rimer, *Elemental zoning enhances mass transport in zeolite catalysts for methanol to hydrocarbons*. Nature Catalysis, 2023. **6**(3): p. 254-+.
6. Jain, R., A. Chawla, N. Linares, J.G. Martinez, and J.D. Rimer, *Spontaneous Pillaring of Pentasil Zeolites*. Advanced Materials, 2021. **33**(22): p. 2100897.
7. Dai, H., Y.F. Shen, T.M. Yang, C.S. Lee, D.L. Fu, A. Agarwal, T.T. Le, M. Tsapatsis, J.C. Palmer, B.M. Weckhuysen, P.J. Dauenhauer, X.D. Zou, and J.D. Rimer, *Finned zeolite catalysts*. Nature Materials, 2020. **19**(10): p. 1074-+.
8. Abutalib, A., D. Parmar, J. Kim, and J.D. Rimer, *Pairing Ga/Al-Zeolites with tailored acidity as tandem catalysts for the conversion of alcohol to olefins*. Journal of Catalysis, 2024. **433**.



# KEYNOTE LECTURES

KN1 – KN4



## Crystal structure determination from microcrystalline materials by 3D electron diffraction

### L. Palatinus

*Institute of Physics of the Czech Academy of Sciences, Na Slovance 2, 182 00, Prague, Czechia  
palat@fzu.cz*

3D electron diffraction appeared suddenly as a meteor in the sky of crystallographic methods. Within ten years of its first publication in 2007, it evolved from a niche technique pursued by a few scientific groups to a developed and accepted method used by more and more chemistry, biochemistry, and material science institutions worldwide.

Compared with traditional X-ray diffraction techniques, 3D electron diffraction has a significant advantage in the size of crystals it can investigate. While for x-ray diffraction, single crystals need to have a lateral size of at least a few micrometres, more commonly over 10 micrometres, electron diffraction can investigate crystals as small as 10 nm in size. This is possible thanks to the strong Coulombic interaction between electrons and the atoms in the crystal. This interaction, however, is also the cause of the main challenge in electron diffraction – multiple scattering of electrons in the crystals. Due to this complication, processing electron diffraction data and accurately determining crystal structures from them is significantly more challenging than from x-ray diffraction.

Nevertheless, the development of data processing and structure refinement methods allowed us to surmount this problem, and more and more applications of 3D electron diffraction demonstrate the power of the method. The technique has proven especially useful in the field of framework materials. Modern synthetic methods produce more and more complex structures, very often only in the form of fine powders. The development of 3D ED methods, which allow the detailed analysis of even the most complex zeolites and other framework structures, has therefore marked a fundamental breakthrough in our ability to understand these materials.

The lecture will discuss the basic principles and challenges of the method, the solutions to these challenges, and illustrate the power of the technique on a range of applications.

### **Acknowledgments**

The research was supported by the Czech Science Foundation, project No. 21-05926X, and by MEYS CR, project Terafit, No. CZ.02.01.01/00/22\_008/0004594.



## State-of-the-art hierarchical zeolites for the catalytic conversion of bioethanol to fine chemicals and carbon-based materials

C. Wattanakit\*, P. Chaipornchaleram, W. Nunthakitguson, A. Prasertsab, P. Iadrat, S. Tantisriyanurak, C. Rodaum

Vidyasirimedhi Institute of Science and Technology (VISTEC), Rayong, 21210 THAILAND  
e-mail: chularat.w@vistec.ac.th

As the development of biorefinery is a vital issue, especially in catalysis communities, to date, several catalytic pathways have been involved, for example bioethanol dehydration to ethylene. In this context, we report the application of using various types of hierarchical zeolite nanosheets and metal-supported zeolites, for example, Ni supported on ZSM-5 nanosheets derived from layered double hydroxides (LDHs), for the catalytic upgrading of bioethanol to various high value-added chemicals, such as ethylene, acetaldehyde, and aromatics as well as carbon nanotubes (CNTs). In addition, the designed CNTs/zeolite composites have been further explored as a free-standing electrode as an electrocatalyst. To tackle the industrial challenges, we also illustrate the application of the designed hierarchical zeolite nanosheets in the bioethanol conversion on a pilot-plant scale.

Presently, the bioethanol upgrading to high value-added chemicals and materials has become a promising pathway for biorefinery. In this contribution, we illustrate the design of zeolites and zeolite composites with hierarchical structures, which have been used as catalysts for bioethanol upgrading<sup>1-7</sup>. Interestingly, the designed catalysts show outstanding physicochemical properties, particularly high surface area and porosity, suitable acidity, and thermal stability, eventually improving catalytic performances in bioethanol conversion to various chemicals and carbon materials. Apart from the isolated hierarchical zeolite, the binder-free hierarchical ZSM-5 monolith derived from zeolite@layered double hydroxides (LDH) composites significantly boosts ethylene yield up to 96% due to the synergistic effect of zeolites and LDHs<sup>1</sup>. To further demonstrate the real industrial application, we also exemplify the application of the synthesized hierarchical zeolite in bioethanol dehydration to ethylene on a pilot-plant scale.

Apart from ethylene as a desired product from bioethanol, we also illustrate the fabrication of qualified carbon nanotubes (CNTs) over hierarchical zeolites from bioethanol via ethylene as an intermediate. Typically, by using the traditional process for CNTs production from the direct conversion of ethanol, a significantly lower quality and yield of CNTs was obtained<sup>3-4</sup>. Indeed, even without the removal of a zeolite template, the obtained CNTs/zeolite composites can be utilized in a wide range of applications, such as catalysis and electrocatalysis<sup>3-4</sup>. These examples open up new perspectives on bioethanol upgrading using various types of hierarchical zeolites to produce fine chemicals and carbon materials. This work opens up new perspectives on bioethanol upgrading using various types of catalysts for the production of fine chemicals and carbon materials.

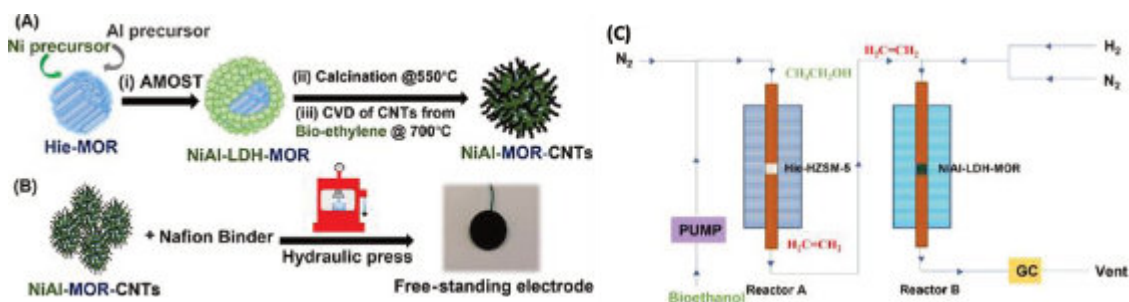


**Fig. 1.** Illustration of (A) the preparation step of the hybrid NiAl-MOR-CNTs composites, (B) fabrication of a free-standing electrode from the obtained composites, (C) dual reactor for ethanol to ethylene and CNTs production, respectively<sup>4</sup>.

### References

- [1] C. Rodaum, *C. et al.* Chem. Commun., 58 (2022), 9618-9621.
- [2] P. Pornsetmetakul, *et al.* ChemCatChem, 15 (2023), e202201387.
- [3] P. Iadrat, *et al.* ACS Applied Materials & Interfaces., 15 (2023), 36, 42854-42867.
- [4] S. Tantisriyanurak, *et al.* ACS Appl. Nano Mater., 6 (2023), 10, 8784–8794.
- [5] P. Iadrat, *et al.* Fuel, 338 (2023), 127208.
- [6] P. Iadrat, *et al.* ACS Appl. Mater. Interfaces, 13 (2021), 7, 8294-8305.
- [7] M. Ketkaew, *et al.* Chem. Commun., 56 (2020), 11394-11397.

### Acknowledgement

This work was financially supported by the Vidyasirimedhi Institute of Science and Technology (VISTEC) and the Program Management Unit for Human Resources & Institutional Development, Research, and Innovation.



## Inventing Materials to Meet Today's Energy and Environmental Challenges

### S. Calero

Department of Applied Physics and Science Education, Eindhoven University of Technology, Eindhoven, The Netherlands  
s.calero@tue.nl

In September 2000, we founded the Materials Modelling and Simulation (MSM) Group within the Department of Applied Physics at Eindhoven University of Technology. Our team harnesses high-performance computing to simulate materials with the potential to revolutionize renewable energy and green technologies. The MSM Group works in collaboration with the Eindhoven Institute for Renewable Energy (EIRES), the Institute for Complex and Molecular Systems (ICMS) and the Eindhoven Artificial Intelligence Systems Institute (EAISI). In this interdisciplinary environment, and in partnership with industry and experimental researchers, we develop and apply simulation and Deep Learning techniques in a multiscale framework, exploring complex materials and molecules from the atomic to the nanoscale. Our current research targets systems such as porous crystalline materials, advanced semiconductors, and hybrid nanomaterials.

One of our key strengths is bridging the gap between simulation and experimentation, enabling us to predict material behavior and guide experimental work towards optimal solutions. Much of our research is done in close collaboration with experimental groups in the field. Our force fields and methodologies allow us to investigate a wide range of materials and applications [1-4]. While we specialize in crystalline materials like zeolites and metal-organic frameworks (MOFs), we also work with more intricate structures such as perovskites, carbons, and 2D catalysts. These materials are applied in areas such as catalysis, enantioselectivity, adsorption/separation of molecules (e.g., water, alcohols, hydrocarbons, drugs, hydrogen, carbon oxides, nitrogen oxides), membrane development, and the production and purification of substances like ammonia, hydrogen, and formic acid [5-10]. In my presentation, I will provide an overview of our recent work in these areas, offering a platform for potential synergies and collaborations.

### References

- [1] D. Dubbeldam, S. Calero, D. E. Ellis and R. Q. Snurr, *Mol Simulation* 42 (2), 81-101 (2016)
- [2] S. Sharma, S. R. G. Balestra, R. Baur, U. Agarwal, E. Zuidema, M. S. Rigutto, S. Calero, T. J. H. Vlugt and D. Dubbeldam, *Molecular Simulation* 49 (9), 893-953, (2023)
- [3] Y. R., S Sharma, S. R. G. Balestra, Z. Li, S. Calero, T. J. H. Vlugt, R. Q. Snurr and D. Dubbeldam, *The Journal of Chemical Physics*, 161 (11) (2024)
- [4] M. Petković, J. M. Vicent-Luna, V. Menkovski and S. Calero, *ACS Applied Materials and Interfaces*, 16, 41, 56366–56375 (2024)
- [5] D. O. Wasik, J. M. Vicent-Luna, S. Rezaie, A. Luna-Triguero, T. J. H. Vlugt and S. Calero, *ACS Applied Materials and Interface* 16, 34, 45006–45019 (2024)
- [6] C. González-Galán, R. M. Madero-Castro, A. Luna-Triguero, J. M. Vicent-Luna and S. Calero, *Separation and Purification Technology*, 348, 127606, (2024)
- [7] J van Heijst, A Martin-Calvo and S Calero, *Separation and Purification Technology*, 350, 127895, (2024)
- [8] F. Stavarache, A. Luna-Triguero, S. Calero and J. M. Vicent-Luna, *Chemical Engineering Journal* 496, 153480 (2024)
- [9] E. Acuna-Yeomans, P. J. Goosen, J. J. Gutiérrez-Sevillano, D. Dubbeldam and S. Calero, *Journal of Materials Chemistry A* 12, 25233-25243 (2024)
- [10] R. M. Madero-Castro, A. Luna-Triguero, C. González-Galán, J. M. Vicent-Luna and S. Calero, *Journal of Materials Chemistry A* 12, 3434-3448, (2024)



## Replacing HCl with Zeolite-Based Solid Acid Catalysts in the Production of Polyurethane Intermediates

**Minkee Choi**

Department of Chemical and Biomolecular Engineering (BK21 Four), Korea Advanced Institute of Science and Technology (KAIST), Daejeon 34141, Republic of Korea  
mkchoi@kaist.ac.kr

Polyurethanes are industrially important thermoplastics widely used as foams, coatings, adhesives, sealants, elastomers, synthetic textiles, and optical lenses, with current global production accounting for approximately 6% of total polymer production. Methylenedianiline (MDA), a key intermediate in polyurethane production, has been industrially produced using a large amount of HCl as a homogeneous acid catalyst. However, the use of highly caustic HCl requires large capital investments to build corrosion-resistant reactor systems. The process also requires neutralization of the product with NaOH, which generates large amounts of problematic brine waste contaminated with aromatic amines. Since the 1970s, significant efforts have been devoted to developing green solid acid catalysts as a substitute for HCl in MDA production, but with limited success. All solid acid catalysts reported thus far still face challenges such as low activity, insufficient selectivity towards desired 4,4'-MDA isomer, and rapid deactivation.

In the present study [1], the reaction kinetics of various solid acid catalysts, including hierarchical/conventional zeolites (LTL, FAU, BEA, MOR, and MTW) and mesoporous aluminosilicates (ASA and Al-MCM-41), were rigorously investigated to understand the reaction mechanism and the structure-catalytic property relationship in MDA synthesis. Most notably, we demonstrate that hierarchical LTL zeolite exhibits unprecedentedly high catalytic activity, selectivity, and stability, making it a strong candidate for replacing commercially used HCl. Conventionally, LTL zeolite has been rarely studied in acid-catalyzed reactions involving bulky molecules due to its one-dimensional (1D) cage-like micropores, which can cause severe mass transfer limitation and are susceptible to fouling. We have discovered that the unique 1D cage-like micropores of LTL zeolite can offer exceptional advantages in selectively producing 4,4'-MDA and inhibiting catalyst deactivation, provided that the mass transfer limitation is alleviated by generating secondary mesopores. Due to hindered oligomer formation and fast mass transfer, the hierarchical LTL zeolite exhibited inappreciable deactivation in an industrially relevant continuous flow reactor. Thus, the hierarchical LTL zeolite demonstrates significant potential as an eco-friendly solid acid catalyst that can substitute HCl in industrial MDA production. Very recently, we have also developed a multi-stage process by combining the hierarchical LTL zeolite and other solid acid catalysts to further improve the 4,4'-MDA selectivity and co-produce polymeric MDAs, depending on the market situations.

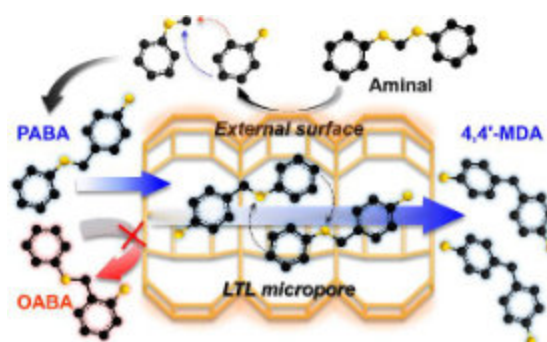


**Figure 1.** Schematic representation of the synthesis of polyurethane intermediate, 4,4'-methylenedianiline (4,4'-MDA), using hierarchical LTL zeolite as a catalyst. Meso-/microporous hierarchical LTL zeolite exhibits remarkable catalytic activity, selectivity, and stability in the conversion of aminal to 4,4'-MDA. External Brønsted acid sites convert aminal to aminobenzylaniline, whereas 1D cage-like micropores induces self-assembly of two linear para-aminobenzylaniline molecules and their bimolecular conversion into 4,4'-MDAs.

### References

- [1] S. Lee, Y. Park, Y. Baik, Y. Lee, M. Choi, *Angew. Chem. Int. Ed.*, **62**, e202304244 (2023).

# INDUSTRIAL SESSION

IS1 – IS4



## One-step crude to chemicals refining technology: from catalyst design to pilot-plant operation

**Isa Al Aslani<sup>a</sup>, Juan Manuel Colom<sup>a</sup>, Mengmeng Cui<sup>b</sup>, Arwa Alahmadi<sup>a</sup>, Noah Mohammed<sup>a</sup>, Salvador Salas<sup>a</sup>, Anissa Bendjeriou-Sedjerari<sup>a</sup>, Lujain Alfifil<sup>c</sup>, Isidoro Morales Osorio<sup>c</sup>, Khalid Almajnouni<sup>c</sup>, Pedro Castaño<sup>b,d</sup>, Jorge Gascon<sup>a,d\*</sup>**

<sup>a</sup> Advanced Catalytic Materials, KAUST Catalysis Center (KCC), King Abdullah University of Science and Technology (KAUST), Thuwal, 23955-6900, Saudi Arabia.

<sup>b</sup> Multiscale Reaction Engineering, KAUST Catalysis Center (KCC), King Abdullah University of Science and Technology (KAUST), Thuwal, 23955-6900, Saudi Arabia.

<sup>c</sup> Advanced Materials & Chemicals, Aramco Research Center (ARC), Thuwal, 23955-6900, Saudi Arabia.

<sup>d</sup> Chemical Engineering Program, Physical Science and Engineering (PSE) Division, King Abdullah University of Science and Technology (KAUST), Thuwal, 23955-6900, Saudi Arabia.

\* Corresponding author: [jorge.gascon@kaust.edu.sa](mailto:jorge.gascon@kaust.edu.sa)

The direct catalytic cracking from crude oil to chemicals is poised to potentially dominate the petrochemical industry shortly, promising reduced fuel consumption and increased production of light olefins and aromatics. We aim to simplify the refinery into a unique one-step conversion scheme, targeting the production of the most demanded petrochemicals. Using a bottom-up holistic approach, we design a catalytic crude oil-to-chemicals process by a combination of advanced catalysts, innovative reactor designs, and validated simulation strategies for system enhancement, intensification and scale up. Our formulated catalysts display improved physical, mechanical and heat-transport properties compared to commercial ones. In addition, the CFD simulation is used to further regulate the process, confirm the enhanced heat and mass transfer and support the operation of a pilot plant to handle 10L/day of crude oil. The pilot plant serves as a proof of concept, providing data for further scaling up to industrial levels.



## Development of Atomistic Simulator “Matlantis™” with Universal Neural Network Potential and its Application to Microporous Materials

H. Ono<sup>1</sup>

<sup>1</sup> ENEOS Corporation, 8, Chidoricho, Naka-ku, Yokohama, 231-0815 Japan  
ono.hideki@eneos.com

Zeolites are crystalline microporous materials widely used in industry. In addition to their traditional use as a catalyst for manufacturing fuels and chemicals from fossil resources, zeolites have recently attracted attention as materials for the adsorption and separation of carbon dioxide and for the catalysts for the conversion of carbon dioxide and biomass, as carbon neutrality is seen as a countermeasure against global warming. MOFs: Metal-Organic Frameworks, which have similarly ordered pores and a wider variety of chemical compositions than zeolites, are also being increasingly applied industrially.

The atomistic simulation based on first-principles calculations such as DFT is one of the most effective tools to promote further utilization of zeolites. For instance, studies have been conducted to explore the compatibility between zeolites and organic structure-directing agents (OSDAs) using experimental data from the literature and calculated data [1], whose results are valuable for the selective synthesis of desired zeolite species. While the use of first-principles calculation results as descriptors is effective for materials informatics-based zeolite research, the time cost of calculations can sometimes be a constraint. For another example, first-principles molecular dynamics is useful for reproducing the reaction of molecules in zeolites to know its mechanism, but it requires huge computer costs. To overcome these limitations in materials research in general, we co-developed the proprietary atomistic simulator “Matlantis™” [2] with Preferred Networks, which is overwhelmingly faster than conventional methods.

The developed simulator performs calculations more than 10,000 times faster while maintaining the same level of accuracy as DFT. It supports 96 elements from the periodic table, covering all elements occurring in nature. It can simulate the properties of any combination of atoms, including molecules and crystal systems, as well as unknown materials. It is based on a technique called neural network potential (NNP) which is a deep learning model learned results of a vast amount of DFT calculations. The developed NNP, named PFP [3] is characterized by a proprietary deep learning architecture and a wide variety of dataset. By using the PFP, it is possible to calculate the physical properties of materials with various chemical structures at high speed without high computational cost-theoretical calculations (Figure 1).

In this presentation, an overview of the developed atomistic simulator and its application to zeolites, MOFs, catalytic reactions, etc. will be presented.

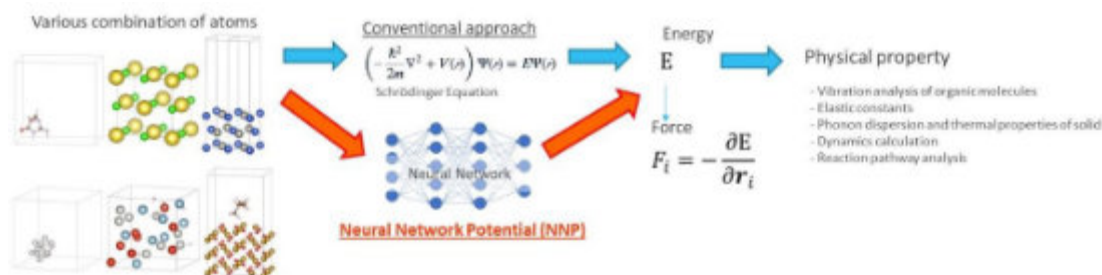


Figure 1. Schematic diagram of the calculation of physical properties using neural network potentials.

### References

- [1] D. Schwalbe-Koda, S. Kwon, C. Paris, E. Bello-Jurado, Z. Jensen, E. Olivetti, T. Willhammar, A. Corma, Y. Román-Leshkov, M. Moliner and R. Gómez-Bombarelli, *Science*, **374**, 308–315 (2021).
- [2] Matlantis (<https://matlantis.com/>), software as a service style material discovery tool.
- [3] S. Takamoto, C. Shinagawa, D. Motoki, K. Nakago, W. Li, I. Kurata, T. Watanabe, Y. Yayama, H. Iriguchi, Y. Asano, T. Onodera, T. Ishii, T. Kudo, H. Ono, R. Sawada, R. Ishitani, M. Ong, T. Yamaguchi, T. Kataoka, A. Hayashi, N. Charoenphakdee and T. Ibuka, *Nature Communications*, **13**, 2991 (2022).

### Acknowledgments

Matlantis™ was developed through joint research between Preferred Networks, Inc. and ENEOS Corporation, and is sold by Preferred Computational Chemistry, Inc. in software as a service style.





## Catalyzing Chemistry Entrepreneurship

**J. García-Martínez**

Molecular Nanotechnology Lab. Department of Inorganic Chemistry. Universidad de Alicante, Alicante CP03690, Spain  
[j.garcia@ua.es](mailto:j.garcia@ua.es)

Catalysis plays a critical role in chemistry, driving innovation in green chemistry and sustainability. Zeolites, in particular, are highly valuable catalysts due to their ability to selectively accelerate reactions while reducing our impact on the environment. Their applications range from petroleum refining to the production of high-value chemicals and biofuels, enabling the chemical industry to minimise environmental impact while maintaining economic growth.

In my presentation, I will discuss Rive Technology as a prime example of zeolite-based innovation and entrepreneurship. The company has pioneered advanced zeolite catalysts with improved pore structures that improve the efficiency of industrial processes such as oil refining. By enabling more sustainable energy production and reducing carbon emissions, Rive Technology's approach demonstrates how advanced zeolite technology is contributing to green chemistry solutions that have been brought to market, benefiting both the environment and the economy.

I will also mention the efforts we are making at IUPAC to promote chemistry entrepreneurship, particularly by launching an ambitious international project to provide educational resources on chemistry entrepreneurship [1]. At IUPAC, we are working to train, engage and inspire the new generation of young chemists who are capable of and committed to building a more sustainable future. Through this project, we are providing educators with useful and practical resources in our efforts to put the student at the centre of the learning process. [2-4].

I will also comment on an ongoing collaboration with Nature to produce a series of podcasts to help scientists start and grow successful businesses. [5] They provide useful tips and valuable information on how to translate scientific breakthroughs into commercial reality in a user-friendly way and free of charge.



**Figure 1.** Some useful resources related to chemistry entrepreneurship that will be discussed during the presentation, adapted from [5,7] and the website on the IUPAC project on Chemistry Entrepreneurship.

There is still a significant gap between academia and industry that needs to be bridged by bold entrepreneurs who are able to connect these two worlds and successfully commercialise the new and exciting research being carried out in universities. Entrepreneurship is another important part of the equation, taking discoveries from the lab to the marketplace is essential to implementing the solutions we need, and scientists have a key role to play here. [6,7]

### References

- [1] Chemistry Entrepreneurship, IUPAC Project 2023-012-2-022, [www.iupac.org/project/2023-012-2-022](http://www.iupac.org/project/2023-012-2-022)
- [2] E. Serrano Torregrosa, J. Garcia Martinez, The Chemical Element: Chemistry's Contributions to our Global Challenges, WILEY-VCH (2011)
- [3] F. Gomollón-Bel, J García-Martínez, Chemical solutions to the current polycrisis, *Angewandte Chemie* 135 (25), e202218975 (2023)
- [4] F. Gomollón-Bel, J García-Martínez, Emerging chemistry technologies for a better world, *Nature Chemistry* 14 (2), 113-114 (2022)
- [5] a) Beyond academia: debunking the industry–academia barrier myth, *Nature*, DOI:10.1038/d41586-022-00291-4 (2022), b) Business of science: Tips and tricks for a perfect pitch, *Nature*, DOI: 10.1038/d41586-021-01003-0 (2021)
- [6] J. Garcia Martinez, The Third Way: Becoming an Academic Entrepreneur, *Science Careers*, March 20, 2014
- [7] E. Li, J. Garcia Martinez, *Chemistry Entrepreneurship*, WILEY-VCH (2021)

# ORAL COMMUNICATIONS

001 – 038



## Pd-containing zeolite catalysts and their reaction mechanism for indirect oxidative carbonylation of methanol to dimethyl carbonate

C. Wang<sup>1,2\*</sup>, X. Zhang<sup>2</sup>, J. Wu<sup>1</sup>, H. Guo<sup>2</sup>, S. Mintova<sup>1,2\*</sup>

<sup>1</sup> Laboratoire Catalyse et Spectrochimie (LCS), Normandie Université, ENSICAEN, UNICAEN, CNRS, 6 boulevard Maréchal Juin, Caen 14050, France

<sup>2</sup> State Key Laboratory of Heavy Oil Processing, College of Chemistry and Chemical Engineering, China University of Petroleum (East China), Qingdao 266580, Shandong, China

chunzheng.wang@ensicaen.fr; svetlana.mintova@ensicaen.fr

### Introduction

C1 chemistry mainly addresses the transformations of one-carbon molecules including CO, CO<sub>2</sub>, CH<sub>3</sub>OH and CH<sub>4</sub>. C1 chemistry is becoming even more important due to the increasing need to produce valuable liquid fuels and chemicals, from alternative carbon resources such as natural gas, shale gas and CO<sub>2</sub> emissions. The indirect oxidative carbonylation of methanol to dimethyl carbonate (DMC) is a green and efficient process converting C1 feedstocks (CO and CH<sub>3</sub>OH) to C2 product [1-4].

High-pressure inorganic chemistry is one of the “Top Ten Emerging Technologies in Chemistry 2020” reported by the International Union of Pure and Applied Chemistry (IUPAC). The behavior of metal-containing zeolite catalysts under high pressure has not been systematically investigated. It is worthwhile to study whether the catalytic performance of metal-containing zeolite catalysts is dependent on the mechanical pressure, and if so, to what extent [5].

The structures of zeolites are not perfect, and the presence of silanols (Si–OH) significantly influences their thermal and chemical resistance as well as their performances in key areas such as catalysis, gas-liquid separations and ion exchange. Several techniques are available to heal the silanol defects in zeolites [3]. It is of vital importance to tune zeolite silanols and further investigate the interactions between silanols and metal species in the field of catalysis.

The goal of this work is to study the catalytic performance of Pd-containing zeolite catalyst in indirect oxidative carbonylation of methanol to dimethyl carbonate emphasizing on the reaction mechanism.

### Materials and Methods

The pure-silica silicalite-1 (S-1) zeolite was purchased from Nankai Catalyst Factory (China). The Pd/S-1 catalyst was prepared by a vacuum-assisted method according to the following procedure. 0.0106 g palladium acetate (Pd(CH<sub>3</sub>COO)<sub>2</sub>, 47.0 wt% Pd, Sinopharm Chemical Reagent Co., Ltd., China) was dissolved in 1.2 g toluene (C<sub>6</sub>H<sub>5</sub>CH<sub>3</sub>). S-1 zeolite was pre-dried at 110 °C for 12 h in a vacuum oven to remove the physically adsorbed water. 1.0 g S-1 zeolite was further pre-treated under vacuum for 2 h. Then, the resulting Pd(CH<sub>3</sub>COO)<sub>2</sub> solution was added dropwise into the pre-treated S-1 zeolite. After stirring for 2 h, the sample was dried at 60 °C for 8 h, and calcined for 2 h.

### Results and Discussion

Herein, the impact of the mechanical compression on the catalytic active sites of Pd/NaY catalysts responsible for the indirect oxidative carbonylation of methanol to dimethyl carbonate (DMC) has been disclosed [5]. The DMC selectivity of the catalysts was found to strongly depend on the mechanical-pressure applied, as the mechanical pressure controlled the ratio of Pd<sup>(2+δ)+</sup> and Pd<sup>δ+</sup> species (0 < δ ≤ 2) in the catalysts (Figure 1). The mono-dispersed Pd clusters (1.3 nm) in the Pd/NaY catalyst were obtained under mechanical treatment of 300 MPa. This catalyst showed high CO conversion of 89% and DMC selectivity of 83%, that maintained for at least 150 h. Combining experimental and density functional theory studies, we revealed that the Pd<sup>δ+</sup> rather than the Pd<sup>(2+δ)+</sup> species enhanced the adsorption of CO and CH<sub>3</sub>ONO reactants and inhibited the decomposition of CH<sub>3</sub>ONO reactant into byproducts, and thus enhanced the DMC selectivity. The mechanical pressure applied had a noticeable effect on the structural features of the metal-containing zeolite catalysts, but despite its importance, this aspect has been poorly considered in the heterogenous catalysis.

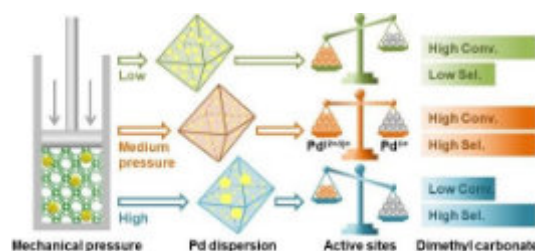


**Figure 1.** Schematic presentation of mechanical pressure-mediated Pd active sites in NaY zeolite catalysts for indirect oxidative carbonylation of methanol to dimethyl carbonate



In addition, an emerging synthetic route for the co-synthesis of dimethyl oxalate (DMO) and dimethyl carbonate (DMC) via the indirect oxidative carbonylation of  $\text{CH}_3\text{OH}$  is presented [3]. The promising co-synthesis process combines the advantages of two separate routes of DMO and DMC syntheses. Herein, palladium containing silicalite-1 zeolite (Pd/S-1) catalyst was first found to be highly active and stable for the co-synthesis of DMO and DMC (Figure 2). The catalytic performance strongly depended on the catalyst activation, as the heat treatment could tune the silanols around the Pd species on the silicalite-1 zeolite. The Pd/S-1 catalyst with abundant silanols exhibited a higher turnover frequency (TOF) of  $0.18 \text{ s}^{-1}$  and a lower apparent activation energy of  $51 \text{ kJ mol}^{-1}$  in comparison to the catalyst with low silanol sites ( $0.06 \text{ s}^{-1}$  and  $101 \text{ kJ mol}^{-1}$ ). The best performing catalyst had an average Pd nanoparticle size of 3.2 nm and Pd loading of 0.48 wt%. This catalyst showed a high CO conversion of 78% and DMO+DMC selectivity of 96%, maintaining high stability for at least 200 h. Furthermore, the synergistic interactions of silanols of silicalite-1 zeolite and Pd were confirmed, and were found to be responsible for enhanced activity. The silanols of S-1 zeolite played an essential role in forming the Pd active sites and had a very pronounced effect on the adsorption of CO reactant on the Pd species.

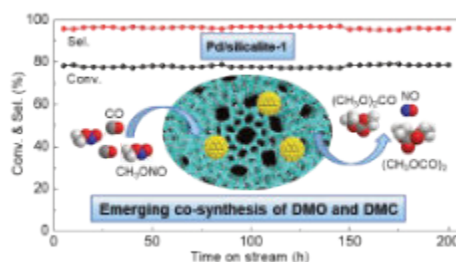


**Figure 2.** Schematic presentation of an emerging synthetic route for the co-synthesis of dimethyl oxalate and dimethyl carbonate.

*In situ* DRIFTS experiments combined with DFT calculations provide new information on the reaction mechanism of DMC synthesis using a NaY zeolite catalyst doped with 1.0 wt% Pd [4]. Two key reaction intermediates were captured by a series of steady-state, dynamic-pulse and time-resolved transient DRIFTS experiments, which were assigned to  $\text{CO}^*$  (\*, a surface site) and  $\text{COOCH}_3^*$  (Figure 3). It was found that the  $\text{CO}^*$  intermediate is predominant on the catalyst surface when the reaction reached steady-state. DFT results also showed that the insertion of  $\text{CH}_3\text{O}^*$  into  $\text{CO}^*$  had the highest energetic barrier of  $127.5 \text{ kJ mol}^{-1}$ . The results suggested that the rate-determining step of the DMC synthesis is the consumption of  $\text{CO}^*$ , i.e., the insertion of  $\text{OCH}_3^*$  into  $\text{CO}^*$  thus forming the  $\text{COOCH}_3^*$ . The Langmuir-Hinshelwood mechanism was thus proposed, including the fast formation of  $\text{CO}^*$ , and the rate-determining insertion of  $\text{OCH}_3^*$  into  $\text{CO}^*$  toward generation of  $\text{COOCH}_3^*$  to yield DMC.

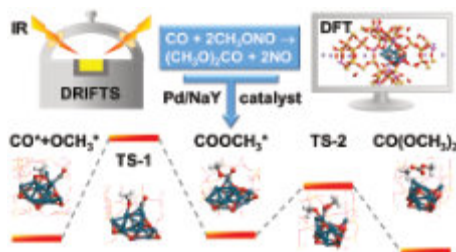


**Figure 3.** Schematic presentation of reaction mechanism of dimethyl carbonate synthesis on Pd/NaY catalyst

In summary, the novelty of our work can be summarized as follows: (1) a novel process of the indirect oxidative carbonylation of  $\text{CH}_3\text{OH}$  to co-synthesis DMO and DMC was proposed combining the advantages of the two separate routes of DMO and DMC syntheses. (2) highly active and stable Pd/S-1 catalyst was prepared and used on the co-synthesis of DMO and DMC for the first time. (3) the synergistic interactions between zeolite silanols and Pd species were confirmed. (4) the developed method of capturing the reaction intermediates can be applied to investigate other reactions such as the synthesis and transformation of methanol.

## References

- [1] K. Huang, S. Yuan, R. Mei, G. Yang, P. Bai, H. Guo, C. Wang, and S. Mintova, *Chin. J. Catal.*, **60**, 327-336 (2024).
- [2] C. Wang, X. Li, S. Yuan, L. Sun, P. Bai, L. Ling, H. Guo, and S. Mintova, *Catal. Rev.*, DOI: 10.1080/01614940.2024.2320165 (2024).
- [3] C. Wang, N. Xu, K. Huang, B. Liu, P. Zhang, G. Yang, H. Guo, P. Bai, and S. Mintova, *Chem. Eng. J.*, **466** 143136 (2023).
- [4] C. Wang, B. Liu, P. Liu, K. Huang, N. Xu, H. Guo, P. Bai, L. Ling, X. Liu, and S. Mintova, *J. Catal.*, **412** 30-41 (2022).
- [5] C. Wang, N. Xu, T. Liu, W. Xu, H. Guo, Y. Li, P. Bai, X. Wu, X. Gong, X. Liu, and S. Mintova, *J. Catal.*, **396** 269-280 (2021).

## Acknowledgments

This work was co-funded by European Union (ERC, ZEOLIGHT, 101054004), National Natural Science Foundation of China (22472204), National Key R&D Program of China (2022YFE0116000), and Sino-French International Research Network (IRN) "Zeolites".



# Effective Descriptors Correlating DME Carbonylation Reactivity with Zeolite Topology: A Study of Brønsted Acid Sites in the vicinity of 8-MR using DFT Calculations

D. J. Jeong<sup>1</sup>, N. J. Park<sup>1</sup>, W. Xu<sup>2</sup>, D. Lee<sup>1</sup>, J. W. Bae<sup>2</sup>, W. B. Lee<sup>1</sup>, J. H. Kang<sup>1,\*</sup>

<sup>1</sup> School of Chemical and Biological Engineering and the Institute of Chemical Processes, Seoul National University, Seoul 08826, Republic of Korea

<sup>2</sup> School of Chemical Engineering, Sungkyunkwan University, Suwon, South Korea

nuneteen@snu.ac.kr

\*jonghunkang@snu.ac.kr

## 1. Introduction

The carbonylation of dimethyl ether (DME) to methyl acetate (MA) is one of the key reactions for recycling waste syngas into valuable chemicals and renewable energy sources [1]. This process primarily occurs at Brønsted acid sites (BAS) on the 8-membered ring (8-MR) of zeolite, where the transition state of the adsorbed reactants ( $[\text{CH}_3\text{-CO}]^\ddagger$ ) is well stabilized [2, 3]. Although the importance of BAS and 8-MR structures in DME carbonylation has been established, few studies have systematically explored the geometric and energetic descriptors required for predicting reactivity in unknown 8-MR zeolites. In this work, we synthesized various zeolites (CHA, FER, LTA, ERI, AEI, and STI) which commonly have 8-MR structure and tested them for carbonylation reaction. To understand the relationship between structure and catalytic performance, all zeolites with various Si/Al ratios (within the range possible for synthesis) were subjected to catalytic tests in their H-forms. These zeolites were characterized using SEM, EDS, and XRD to confirm successful synthesis. The catalytic performance and acid properties of the samples were investigated using  $\text{NH}_3$ -TPD and Pyridine-IR. Based on the DFT results, we found that the energy landscapes of the reaction vary depending on where the surface methyl group (SMG) is located and to which zeolite topology it belongs. A pocket structure where two 8-MRs are connected consecutively, either directly or through small building units ( $\leq 6$ -MR), is the most influential structural feature affecting catalytic performance, followed by the activation barrier or methylation enthalpy of the effective Brønsted acid site.

## 2. Experimental

All zeolites examined were synthesized from widely-known representative protocols for each topology. Ion-exchange with ammonium nitrate ( $\text{NH}_4\text{NO}_3$ ) is adapted for all samples, followed by a calcination process to make them Proton form (H-Z). The DME carbonylation reaction was performed in stainless-steel tubular fixed-bed reactor (8.0 mm i.d.) under 2.0 MPa with 0.3 g of each catalyst. The loaded catalysts were pre-treated under  $\text{N}_2$  atmosphere (99.99 mol%) at 500 °C for 1 h to remove water and contaminants adsorbed on the catalyst surface. The catalytic reaction was performed for 30 hours or until catalyst was deactivated with introducing a flow of reactant gas with the composition of  $\text{DME}/\text{CO}/\text{N}_2 = 4.5/90/5.5$  (mol%) with adjustment to set gas hourly space velocity (GHSV) of  $2000 \text{ L}_{\text{cat}}\cdot\text{h}^{-1}$  at two different temperatures of 165 °C.

## 3. Results and Discussion

**Figure 1** shows the different reactivities for DME carbonylation reaction among the zeolite topologies. Most of the zeolites exhibit maximum reactivity within the Si/Al ratio range of 8–18. These findings are consistent with previous studies on the DME carbonylation reactivity of CHA [4] and FER [3], suggesting that the 8-MR structure plays a critical role in catalytic performance. While the MA generation rate is generally proportional to the acid site density, we calculated the turnover frequency (TOF) to provide a clearer assessment of the impact of the zeolite structure on catalytic performance. Additionally, ERI, AEI, and STI show similar reactivity with a comparable Si/Al ratio (5–10). This result suggests that while all samples share the 8-MR structure, their significantly different reactivities indicate the influence of additional geometric factors beyond the presence of 8-MR alone.

Over the past decade, significant efforts have been made to connect the obtained TOFs with DFT calculations for specific acid sites. Despite extensive analysis of energy parameters such as CO addition activation energy and methylation enthalpy, a direct linear correlation with TOF remains elusive. Instead, it appears that geometric factors, including the  $\angle\text{OCC}$  angle of the transition state ( $[\text{ZO}\cdots\text{CH}_3\cdots\text{CO}]^\ddagger$ ) and the effective volume for transient methyl group ( $\text{CH}_3\text{-}$ ) rearrangement, provide a more nuanced explanation for the variations in catalytic performance. A moderate correlation between the  $\angle\text{OCC}$  angle and reactivity was observed, with angles approaching 180° promoting CO addition. For instance, the  $\angle\text{OCC}$  angle of 170.1° at the T102 site in LTA suggests geometric hindrance, which may account for its reduced reactivity.

Once CO is added, a subsequent DME molecule donates a  $\text{CH}_3\text{O-}$  group to the acetyl intermediate ( $\text{Z-CH}_2\text{CO}$ ). This action regenerates the transient methyl group ( $\text{CH}_3\text{-}$ ), which then replaces the proton at the Brønsted acid site ( $\text{ZO-}$



H). The efficiency of this process improves when the space, or 'isovolume,' around the reaction site is more confined, allowing for smoother and quicker methyl group transfer. This step is more efficient when the isovolume of the partition is narrow. As shown in **Figure 2**, zeolites like MOR and FER have narrow isovolumes (Helium isovolume (HeV): 110.993 Å<sup>3</sup> and 88.047 Å<sup>3</sup>, respectively), facilitating the regeneration of the active methyl group and accelerating the carbonylation cycle. In contrast, pore-type zeolite (CHA, LTA, ERI, and AEI) has a larger isovolume than MOR and FER (200–250 Å<sup>3</sup>), periodically connected through 8-MR pores. The larger isovolume may result in less efficient rearrangement of the methyl group, affecting the overall reactivity of these zeolites.

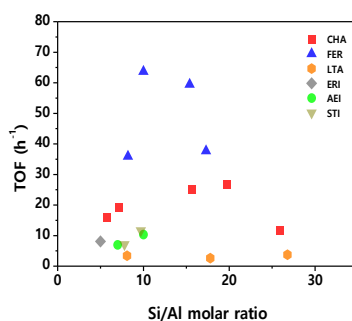


**Figure 1.** Turnover frequency of selected zeolites with various Si/Al ratios in DME carbonylation. All points represent the reactivity of each sample, averaged over 30–35 hours of testing within the Si/Al ratio range possible for synthesis. Reaction conditions: T = 165 °C, P = 2.0 MPa, space velocity = 2000 L/(kg<sub>cat</sub>·h). Feed gas composition: DME/CO/N<sub>2</sub> (mol %) = 4.5/90/5.5 for 40 hours.

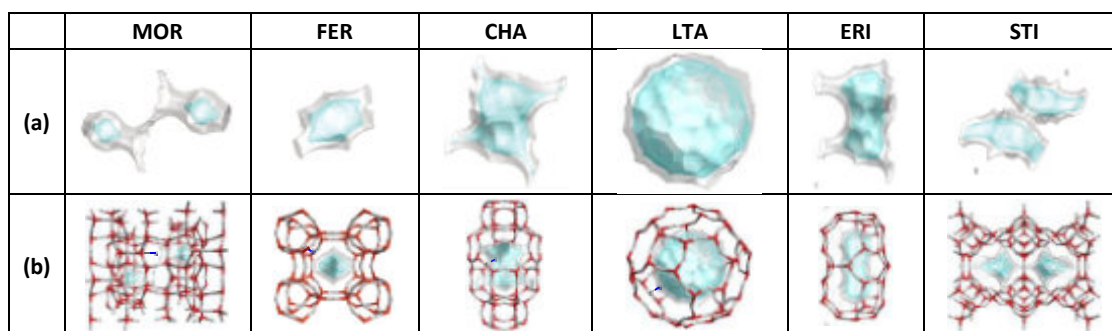


**Figure 2.** (a) Graphical data of isovolume where a probe molecule can diffuse into the zeolite framework considering the van der Waals radius of framework molecules and probe molecule. [Color] Gray: Helium isovolume region (Kinetic diameter of He: 260 pm), Cyan: Carbon monoxide isovolume region (Kinetic diameter of CO: 376 pm). (b) Considered framework partition of each zeolite. Especially 2-dimensional type zeolites (MOR, FER) have this particular partition in which the DME carbonylation reaction occurs predominantly. [Color] Light Gray: tetrahedral T site, Red: oxygen, Blue: Carbon (center atom of methyl group to derive  $d_{\min}$ ),  $d_{\min}$  is defined as minimum length from methyl group center carbon to CO molecule. This descriptor will be further explained in main presentation.

#### 4. Conclusions

To explain the varying DME carbonylation reactivity across different zeolite topologies, it is essential to consider not only the energy differences in the rate-determining step (RDS) and methylation process derived from DFT calculations, but also comprehensive crystallographic factors. Reactivity comparisons were conducted under CO-excess conditions and at relatively low temperatures to ensure thermodynamically favourable conditions. This approach account for the influence of the crystallographic features of each zeolite.

We propose several effective descriptors: the HeV value, which represents the efficiency of transient methyl group regeneration, and the  $\angle OCC$  angle of the transition state ( $[ZO\cdots CH_3\cdots CO]^\ddagger$ ), which offers further insight into catalytic performance due to representing how probable the acid site it is when it is added by CO. By carefully considering these descriptors, we can more accurately predict DME carbonylation reactivity for unknown 8-MR small-pore zeolite topologies, potentially expanding their application in industrial catalytic processes.

#### References

- [1] P. Cheung, A. Bhan, G. J. Sunley and E. Iglesia, *Angew. Chem. Int. Ed.*, **45**, 1617–1620 (2006).
- [2] D. B. Rasmussen, J. M. Chistensen, B. Temel, F. Studt, P. G. Moses, J. Rossmeisl, A. Riisager and A. D. Jensen, *Angew. Chem. Int. Ed.*, **54**, 7261–7264 (2015).
- [3] P. Feng, G. Zhang, X. Chen, K. Zang, X. Li and L. Xu, *Appl. Catal. A: Gen.*, **557**, 119–124 (2018).
- [4] M. Lusardi, T. T. Chen, M. Kale, J. H. Kang, M. Neurock and M. E. Davis, *ACS Catal.*, **10**, 842–851 (2020).



## CO<sub>2</sub> hydrogenation to hydrocarbons on the zeolite-mediate bifunctional catalysts

Sang-Ho Chung,<sup>1</sup> Adrian Ramirez,<sup>1</sup> Pierfrancesco Ticali,<sup>2</sup> Edy Abou-Hamad,<sup>3</sup> Silvia Bordiga, Jorge Gascon,<sup>1</sup> Javier Ruiz-Martinez<sup>1,\*</sup>

<sup>1</sup> KAUST Catalysis Center, King Abdullah University of Science and Technology, Thuwal, Saudi Arabia

<sup>2</sup> Department of Chemistry, NIS Center and INSTM Reference Center, University of Turin, Turin, Italy

<sup>3</sup> KAUST Core Labs, King Abdullah University of Science and Technology, Thuwal, Saudi Arabia

[sangho.chung@kaust.edu.sa](mailto:sangho.chung@kaust.edu.sa)

### 1. Introduction

Carbon capture, utilization and storage (CCUS) is receiving much attention to reduce CO<sub>2</sub> from atmosphere. One of the most promising CO<sub>2</sub> utilizations is catalytic hydrogenation (“CO<sub>2</sub> to chemicals and fuels”), to close CO<sub>2</sub> loop and achieve net zero emissions. More specifically, the use of cascade process is gaining strong momentum in heterogeneous catalysis, to produce chemical commodities in industrial scale [1]. Among various possible configurations, we previously demonstrated a bifunctional catalytic system for effective CO<sub>2</sub> conversion, using zinc-doped zirconia (ZnZrO<sub>2</sub>) and zeolites (SAPO-34, SAPO-18, RUB-13, and ZSM-5) [2]. In this work, to gain molecular-level understanding of the zeolite structure and the catalytic mechanism, we used <sup>13</sup>C-enriched CO<sub>2</sub> (<sup>13</sup>CO<sub>2</sub>) as reactant feed and applied multidimensional <sup>13</sup>C based solid-state nuclear magnetic resonance (ssNMR) with advanced magnetization transfer schemes.

### 2. Experimental

Herein, samples were prepared using fully enriched <sup>13</sup>CO<sub>2</sub> at experimental conditions (30 bar, 375 °C, H<sub>2</sub>:<sup>13</sup>CO<sub>2</sub> = 3, GHSV 10,000 mL·g<sup>-1</sup>·h<sup>-1</sup>). A dual-bed configuration was used [1], in order to be able to perform ssNMR studies on zeolites. All <sup>1</sup>H and <sup>13</sup>C related (both 1D and 2D) MAS ssNMR spectroscopic experiments were performed on Bruker AVANCE III spectrometer operating at 600 MHz using 3.2 mm MAS HXY probe and MAS frequency of 20 kHz. The 1D direct excitation (DE), <sup>1</sup>H-<sup>13</sup>C CP (cross-polarization), and INEPT (insensitive nuclei enhanced by polarization transfer) spectra were recorded using accumulation of 4 k scans. Two dimensional (2D) <sup>13</sup>C-<sup>13</sup>C spectra were recorded using <sup>13</sup>C-<sup>13</sup>C mixing, achieved through proton driven spin-diffusion (PDS) with phase-alternated-recoupling-irradiation-schemes (PARIS). To probe mobile and rigid molecules, 2D <sup>1</sup>H-<sup>13</sup>C INEPT-based heteronuclear correlation (HETCOR) and dipolar based <sup>1</sup>H-<sup>13</sup>C-<sup>1</sup>H HETCOR correlation spectra were obtained, respectively. A fixed 0.5 ms contact time was used for both <sup>1</sup>H-<sup>13</sup>C CP and <sup>13</sup>C-<sup>1</sup>H CP periods, suppressing background signals by an 8 kHz MISSISSIPPI block before the last CP period.

### 3. Results and Discussion

At the first catalyst layer, ZnZrO<sub>2</sub> could selectively convert CO<sub>2</sub> into methanol and CO under hydrogen atmosphere (selectivity to methanol and CO = ca. 25 and 75%, respectively) [2]. Next, at the second zeolite layer, the CO-rich methanol feed was converted into olefins and aromatics. To elucidate the molecular structure of trapped organic species, we performed ssNMR studies on the post-reacted zeolites, using a series of magnetization transfer schemes based on the mobility of trapped molecules. The 1D <sup>13</sup>C DE MAS ssNMR spectra show high amounts of aromatics-related species in spent SAPO-34 (**Fig.1**). By applying <sup>1</sup>H-<sup>13</sup>C CP magnetization transfer scheme, alkane species can be enhanced due to higher proton density around <sup>13</sup>C nuclei of interest (H/C ratio of alkane = ca. 1.7; aromatics = 1 (benzene), 1.25 (xylene), respectively). Most of the observed species in INEPT based pulse are confidently assigned as terminal alkyl groups from methylated aromatics or polyaromatics, i.e., most of the trapped aromatics are rigid aromatic species. The above results are further confirmed by applying 2D <sup>13</sup>C-<sup>13</sup>C and <sup>1</sup>H-<sup>13</sup>C-<sup>1</sup>H correlation spectra, which were achieved through (i) proton-driven spin diffusion using phase alternated recoupling irradiations schemes and (ii) proton detected CP-based hetero-nuclear correlation spectroscopy (double CP-HETCOR). For example, methylated aromatic species is readily observed at 135.2/20.0 and 131.3/19.9 (<sup>13</sup>C/<sup>13</sup>C), showing their correlation with <sup>1</sup>H at 7.2 ppm. According to the hydrocarbon pool mechanism [1,3], the C3 and C4 olefins are mostly produced by two competing cycles governed by olefinic and aromatic cycles. We observed the methylated poly-ene species as rigid compounds, showing <sup>13</sup>C and <sup>1</sup>H chemical shift ranges at 130–160 and 1–3 ppm, respectively. In spent SAPO-34, we could also observe the cross-peaks at 136.5/2.3 and 131.4/2.4 (<sup>13</sup>C/<sup>1</sup>H) ppm by 2D <sup>1</sup>H-<sup>13</sup>C CP-HETCOR, not by INEPT-HETCOR, indicating the presence of less-mobile methylated alkene species, which are presumably adsorbed in the zeolite micropores. Based on the results, we propose catalytic cycle on zeolites under CO-rich for methanol-to-hydrocarbons (MTH), especially the role of carbonylation of surface species to hydrocarbon pool species [3,4].

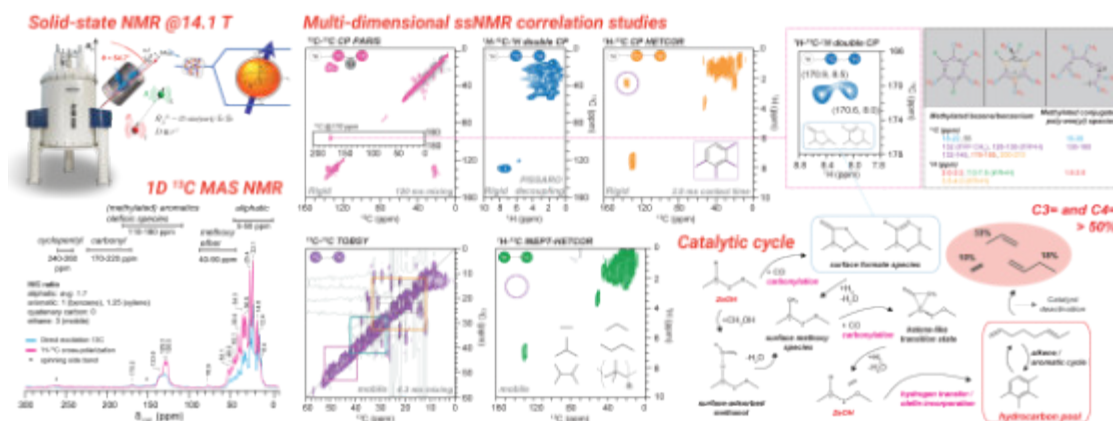


**Figure 1.** 1D and 2D <sup>13</sup>C DE, <sup>1</sup>H–<sup>13</sup>C CP, <sup>1</sup>H–<sup>13</sup>C INEPT ssNMR MAS spectra of a post-reacted zeolite (SAPO-34 as an example) after hydrogenation of fully isotope-enriched <sup>13</sup>CO<sub>2</sub> in the reactant feed and proposed mechanism for CO<sub>2</sub> rich methanol-to-hydrocarbons (MTH).

#### 4. Conclusions

In this work, we have focused on the characterization of a combined catalytic system for CO<sub>2</sub> hydrogenation into methanol on ZnZrO<sub>2</sub>, which can be further converted to hydrocarbons on zeolites. This system has shown to be highly active and selective for C<sub>3</sub> and C<sub>4</sub> hydrocarbons. By advanced ssNMR characterization, we report that carbonylation to surface methoxy species can play a key role, promoting the dual-cycle mechanism. The high selectivity to light olefins can be fine-tuned by zeolite topology as process descriptor.

#### References

- [1] A. Ramirez, X. Gong, M. Caglayan, S.A.F. Nastase, E. Abou-Hamad, L. Gevers, L. Cavallo, A. Chowdhury, J. Gascon, *Nat. Commun.*, **12**, 1–13, (2021).
- [2] P. Ticali, D. Salusso, R. Ahmad, C. Ahoba-Sam, A. Ramirez, G. Shterk, K.A. Lomachenko, E. Borfecchia, S. Morandi, L. Cavallo, J. Gascon, S. Bordiga, U. Olsbye, *Catal. Sci. Technol.*, **11**, 1249–1268, (2021)
- [3] A. Chowdhury, I. Yarulina, E. Abou-Hamad, A. Gurinov, J. Gascon, *Chem. Sci.*, **10**, 8946–8954, (2019).
- [4] P. Ticali, S. Morandi, G. Shterk, S. Ould-Chikh, A. Ramirez, J. Gascon, S. Chung, J. Ruiz-Martinez, S. Bordiga, *Appl. Catal. A Gen.*, **655**, 119100, (2023).

#### Acknowledgments

This project has received funding from the European Union's Horizon 2020 Research and Innovation Programme under grant agreement No. 837733. The authors are grateful to Dr. Christian Ahoba-Sam for the synthesis of the PdZn/ZrO<sub>2</sub> sample.





## Structural analysis of two ITQ-52 “as-made” zeolites with different OSDA molecule by 3D electron diffraction

**Partha P. Das,<sup>1</sup> Juan I. Tirado,<sup>2</sup> Jose L. Jorda,<sup>2</sup> Lukas Palatinus,<sup>3</sup> Sergi Plana-Ruiz,<sup>1,4</sup> Jorge Simancas,<sup>2</sup> Raquel Simancas,<sup>2,5</sup> Stavros Nicolopoulos,<sup>1</sup> Susana Valencia<sup>2</sup> and Fernando Rey.<sup>2</sup>**

<sup>1</sup> NanoMEGAS SPRL, Blvd Edmond Machtens 79, B-1080 Brussels, Belgium

<sup>2</sup> Instituto de Tecnología Química (UPV-CSIC), Universitat Politècnica de València-Consejo Superior de Investigaciones Científicas, Avenida de los Naranjos s/n, 46022, Valencia, Spain

<sup>3</sup> Institute of Physics of the Czech Academy of Sciences, v.v.i., Na Slovance 2, Prague 8 182 00, Czechia.

<sup>4</sup> Servei de Recursos Científics i Tècnics, Universitat Rovira i Virgili, Avinguda Països Catalans 26, Tarragona 43007, Catalonia, Spain

<sup>5</sup> Department of Chemical System Engineering, The University of Tokyo, 7-3-1 Hongo, Bunkyo-ku, Tokyo 113-8656, Japan

partha@nanomegas.com

A salient aspect of research in catalytic porous materials is the discovery of new properties through the inspection of crystalline structure using standard X-ray diffraction techniques such as single crystal X-ray diffraction (SCXRD) or powder X-ray diffraction (PXRD). Although these techniques remain main tools for structural characterization, there are challenges associated with them. For SCXRD, it is often difficult to grow crystals large enough for analysis. PXRD, on the other hand, can be very challenging due to severe peak overlapping. [1],[2]

In this work, we will present an example of the use of 3D Electron Diffraction (3DED) collected using a conventional Transmission Electron Microscope (TEM) to characterize zeolite crystals of just a few nanometers. [3] 3DED data can be collected either with continuous rotation (with or without beam precession) or by precession-assisted stepwise rotation of the crystal. The use of beam precession reduces dynamical effects and enables better integration of reflections, thereby increasing the likelihood of successful structure determination.[4] In the case of zeolite materials, due to their beam sensitivity, the accumulated electron dose on the crystal is critical for obtaining superior quality data for ab-initio structure solution. In the current work, we present two different data collection strategies: a) continuous rotation (without precession) and b) stepwise data acquisition in combination with beam precession (with beam blanking during crystal tilt and recentering of the crystal). These strategies demonstrate that by using careful data collection, one can achieve similar electron doses from both types of measurements, resulting in good quality results. Beam blanking during stepwise data acquisition can be implemented in most TEM columns. [5]

In this work, we have determined the structure of two synthetic zeolites with the ITQ-52 structure [6] (IFW framework type), where aminophosphonium and alkylphosphonium dications have been used as their respective organic structure-directing agents (OSDA). The obtained materials were named N-ITQ-52 and C-ITQ-52, with the difference being the substitution of the N atoms with C atoms in the OSDA. Both materials present similar monoclinic structures with space group I2/m. The unit cell parameters for N-ITQ-52, as obtained from PXRD refinement, are  $a = 17.48938(3)$  Å,  $b = 17.90101(3)$  Å,  $c = 12.32984(2)$  Å,  $\beta = 90.53220(10)^\circ$ . For C-ITQ-52, the parameters are  $a = 17.5050(6)$  Å,  $b = 17.9623(6)$  Å,  $c = 12.3602(4)$  Å,  $\beta = 90.6464(19)^\circ$ .

3DED data for the C-ITQ-52 sample was measured in NBD mode with continuous rotation of the crystal without beam precession, resulting in a total accumulated electron dose of  $1.836 \text{ e}/\text{Å}^2$ . Due to the smaller crystal size of N-ITQ-52 compared to C-ITQ-52, data was collected using stepwise rotation (step size  $1^\circ$ ) in combination with beam precession (precession angle  $1^\circ$ ). For the N-ITQ-52 sample, data from two different crystals were collected and merged to improve data completeness, with total accumulated electron doses of  $2.775 \text{ e}/\text{Å}^2$  for the first crystal and  $3.025 \text{ e}/\text{Å}^2$  for the second crystal. After intensity extraction from the 3DED data using PETS software, the zeolite framework structures were determined ab-initio for both cases. The position of OSDA was then determined using simulated annealing. In both cases, the OSDA molecules were found to occupy similar positions with a local symmetry of  $2/m$ . Following the determination of the structures from 3DED data, further Rietveld refinement was performed using JANA2020 software [Fig 1]. The refinement not only increased the accuracy in the location of the OSDAs, but also allowed to locate the boron atoms isomorphically replacing silicon in the framework structure. Although presenting almost identical structures and very similar placements for the organics, both materials present important differences in the location of the B atoms. This suggests that the different electron density distributions in both OSDAs are responsible of the different locations of the trivalent species on the zeolitic frameworks, with potential implications on the catalytic and adsorption properties of the materials.

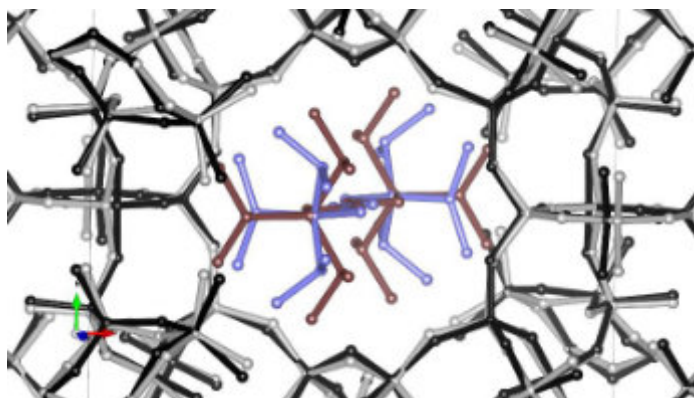


**Figure 1.** The comparison of the structures of N-ITQ-52 and C-ITQ-52, obtained through Rietveld refinement using PXRD data and viewed along the *c* axis, is as follows: Silicon and oxygen framework atoms from C-ITQ-52 are depicted as grey sticks, while those from N-ITQ-52 are shown as black sticks. The OSDA for N-ITQ-52 is represented in blue, and for C-ITQ-52, it is depicted in brown for clarity.

## References

- [1] P.J. Bereciartua et al., *Science*. Nov 24; 358(6366):1068-1071 (2017).
- [2] Z. Huang, T. Willhammar and X. Zou, *Chem. Sci.*, ,12, 1206-1219 (2021)
- [3] J. Simancas, R. Simancas, P.J. Bereciartua, J.L. Jordá, F. Rey, A. Corma, S. Nicolopoulos, P. P. Das, M. Gemmi, E. Mugnaioli, *J Am Chem Soc.* Aug 17; 138(32):10116-9 (2016).
- [4] E. Mugnaioli, T. Gorelik, U. Kolb, *Ultramicroscopy*, 109, 6, 758-765 (2009).
- [5] S. Kodjikian, H. Klein, *Ultramicroscopy*, 200, 1-19 (2019).
- [6] R. Simancas, J.L. Jordá, F. Rey, A. Corma, A. Cantín, I. Peral, C. Popescu. *J Am Chem Soc.* Mar 5;136(9): 3342-5 (2014).

## Acknowledgments

This research was supported by projects RTI2018-101784-B-I00 and SEV-2016-0683-18-3 and grant PRE2018-083623 from the Spanish government, and project PROMETEO/2021/077 from Generalitat Valenciana. Financial support by the Spanish Ministry of Science and Innovation (CEX2021-001230-S grant funded by MCIN/AEI/10.13039/501100011033) is gratefully acknowledged. Authors thank the Servicio de Microscopía Electrónica of the Universitat Politècnica de València for technical support.



## Insights into Crystallization mechanism of SAPO-34

X. Zhang, M. Yang, P. Tian<sup>1</sup> and Z. liu<sup>1</sup>

<sup>1</sup> National Engineering Research Center of Lower-Carbon Catalysis Technology, Dalian National Laboratory for Clean Energy, Dalian Institute of Chemical Physics, Chinese Academy of Sciences, Dalian 116023, China  
tianpeng@dicp.ac.cn

The Methanol-to-olefin (MTO) process represents a pivotal technology in the C1 chemistry industry, as it provides a non-petroleum route for producing bulk chemicals such as ethene and propene. SAPO-34, a silicoaluminophosphate molecular sieve with structure isomorphic to that of zeolite chabazite (CHA), is currently the most effective active component for MTO catalysts and attracts significant interest from both academia and industry. A deeper understanding of the crystallization mechanism of the SAPO-34 molecular sieve is crucial for guiding the rational design and synthesis of this catalytic material, leading to continuous improvement in catalytic efficiency.

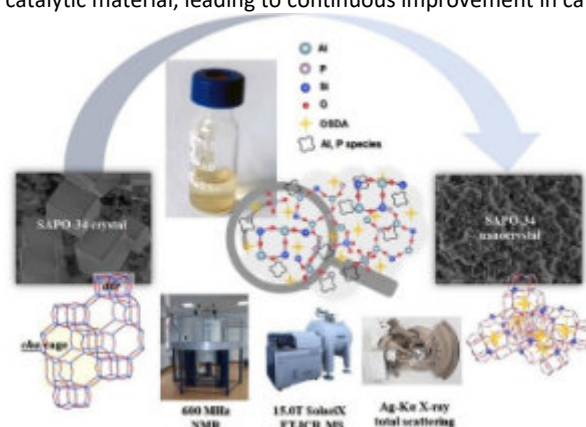


**Figure 1** The study of the crystallization of SAPO-34 based on a top-down synthesis system.

The present talk aims to share our recent understanding of the crystallization mechanism of SAPO-34, focusing on identifying the key active species involved in nucleation and elucidating the role of seeds in the crystallization process. To investigate the crystallization mechanism, a top-down synthesis system was employed (Figure 1). Small structural fragments, such as 4-/6-membered rings enriched with Si-O-Al bonds, were identified as the minimum structural units driving the crystallization of SAPO-34 [1]. The seed-assisted synthesis of SAPO-34 was systematically investigated using various seeds with different topologies, compositions, and morphologies [2]. Instead of CHA cage, double six-ring (d6r) units were revealed to be essential for the seeded crystallization of SAPO-34. This was exemplified by the seeded crystallization of SAPO-34, using SAPO-18, SAPO-35, and SAPO-56 as the hetero-seed. The solubility and provision of small fragments rich in d6r units were found to be key factors influencing the seeding effect during SAPO-34 crystallization. Based on our understanding of SAPO-34 crystallization, we have developed a metal-assisted *in situ* etching strategy to facilitate the synthesis of hollow, low-silica SAPO-34 with a pure CHA structure and inhibited CHA/AEI intergrowth [3]. This results in an elongated catalytic lifespan and ultra-high ethylene plus propylene selectivity (86.9 wt%, one of the highest values reported) in the MTO reaction.

These findings not only contribute to the fundamental understanding of SAPO-34 crystallization but also provide a roadmap for the development of more efficient catalysts by tailoring crystallization conditions. The metal-assisted *in situ* etching strategy opens up new possibilities for creating advanced SAPO-34 materials with enhanced physicochemical properties, leading to more sustainable and cost-effective production of light olefins.

### References

- [1] X. S. Zhang, M. Yang, L. Wang, J. F. Han, C. Y. Lou, S. T. Xu, Y. Y. Zhang, R. A. Wu, P. Tian; Z. M. Liu, *Chemistry-A European Journal*, **29** (2023), e202203886
- [2] X. S. Zhang, M. Yang, Y. Wang, C. Y. Lou, S. T. Xu, P. Tian; Z. M. Liu, *Inorganic Chemistry Frontiers*, **10** (2023), 3874-3883
- [3] X. S. Zhang, M. Yang, D. Fan, Y. Wang, C. Y. Lou, H. C. Hu, B. Li, P. Tian; Z. M. Liu, *Chemical Engineering Journal*, **489** (2024), 151101



## Electrochemical tools for record-breaking Sn-zeolite synthesis: mechanisms and catalytic application

M. Dusselier<sup>1</sup>, G. Ivanushkin<sup>1</sup>, A. Bugaev<sup>2</sup>, J. Martinez-Espin<sup>3</sup>, M. Torca Beydokhti<sup>1</sup>

<sup>1</sup> Center for Sustainable Catalysis and Engineering (CSCE), KU Leuven, 3001 Heverlee, Belgium

<sup>2</sup> Center for Photon Science, Paul Scherrer Institute, 5232 Villigen, Switzerland

<sup>3</sup> Biobased Chemicals R&D Topsoe A/S, 2800-Kgs. Lyngby, Denmark

michiel.dusselier@kuleuven.be

The incorporation of heteroatom nodes into zeolite frameworks is a challenging but rewarding pathway to superior materials for numerous applications. We recently invented a novel method for controlled heteroatom insertion by in-situ anodic release of a desired metal during hydrothermal zeolite synthesis which we label EAS (electro-assisted synthesis). The generic character of the technique and reactor was shown across 4 zeolite structures and 4 electrode metals and by offering access to a new mixed-metal zeolite. Timed and voltage-controlled metal release leads to tuned concentration profile of the heteroatom and in the end, a 10-fold increased incorporation for the most relevant stannosilicates (Sn-MFI/BEA/CHA) versus batch controls. One reason is the minimizing of the interference between tin and the zeolite crystallization but other clues have just emerged from an in-situ EXAFS study. The result of the method is that it effectively expands the synthesis space of stannosilicate zeolites. The focus in this talk will be the application of EAS to Sn-BEA, the first results of the EXAFS study (in situ during EAS during crystallization) and the application of that Sn-BEA in catalysis. The electro-made material with record tin content show higher productivities than their classic counterparts in lactate catalysis.

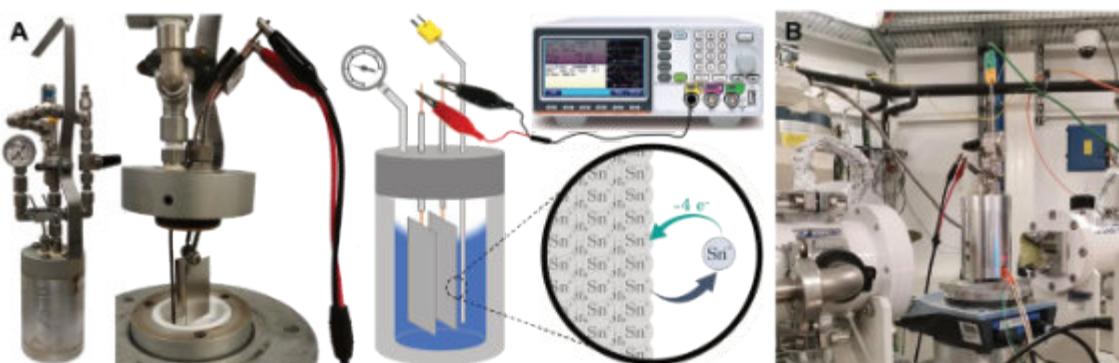


**Figure 1.** Electro-Assisted Synthesis (EAS) reactor showing Sn-release (A) and the adapted reactor allowing in situ EXAFS (B).

### Introduction

Zeolites are microporous materials that consist of connected silica and alumina tetrahedra. Introducing tetrahedral heteroatoms other than Al, such as B, Sn, Fe, Zn etc., enhances or modifies their (Lewis) acidity, creating a confined single atom catalyst [1]. As the development of biomass resources continues to advance, metal-incorporated zeolites are increasingly drawing attention as solid Lewis acids. These so-called zeotypes (e.g., Sn-BEA or Ti-MFI) and especially stannosilicates, have revolutionized biomass conversion and peroxide oxidations [2, 3].

Zeolite formation depends on both kinetics and thermodynamics, and the prevalence of one over the other can lead to different active site densities and distributions. Unfortunately, obtaining a targeted active site (heteroatom) density is never straightforward and the heteroatom metal content is often too low for zeotypes, yielding suboptimal catalytic performances. For instance, during the direct zeolite synthesis, isomorphous substitution heavily affects crystallization kinetics, prolonging synthesis time up to a large extent. On the other hand, post-synthetic modification techniques provides a shorter time, although their outcome relies a lot on the properties of the parent material [4].

Nowadays, attaining high metal loadings (>10 wt. %) in zeotype catalysts (e.g., Sn-BEA) is only possible through the post-synthetic approach, which is limited by the inherited properties of the parent zeolite. Here, using EAS, a modified hydrothermal synthesis procedure with Sn<sup>0</sup>-made electrodes [5], we were able to synthesize a series of Sn-MFI and Sn-BEA zeolites from the bottom up. We characterized the stannosilicates in full detail and tested the Sn-BEAs in catalysis. On top, we performed an EXAFS study in situ during the release process (Soleil-synchrotron France).

### Results and discussion

The EAS way of making heteroatom-containing zeolites was done in a novel flexible electrochemical reactor (Figure 1A). By performing anodic oxidation, which can be finely controlled by a voltage bias of immersed electrodes (made of different material), their area, the timing, and concentration of heteroatom precursors can be tuned in situ during a zeolite crystallization, opposed to only a starting concentration in classic batch synthesis. On top, one can play with



different waveforms (sine-square waves). The batch controls confirm the up to 10-fold higher Sn incorporation via EAS and we confirmed this chemical composition both by TEM EDX and by ICP-AES. For the Sn-BEA, the zeolite material possess the highest ever reported Si/Sn (final material) ratio of 14, a value that was never reported for hydrothermal bottom-up synthesis (some characterization: see Fig. 2).

Classic characterization of the product zeolites included: phase purity (PXRD, Figure 2), crystallinity, surface area, and micropore volume ( $N_2$ -physisorption), crystal size (SEM,TEM) and Lewis acidity (FT-IR of absorbed  $CD_3CN$ ).

Beyond the quite extensive characterization and the Sn content, mechanistically, it seems EAS allows the production of stannosilicates with record Sn incorporation by keeping tin concentration low and adjusting the release timing to avoid nucleation delays. Yet, in our effort to understand EAS at the molecular level and assess whether the released Sn species are uniquely active or different than in classic synthesis, we designed synchrotron capable reactors and measured EXAFS/XANES in situ (Fig. 1B). This very recently acquired data shows extremely interesting Sn speciation profiles in terms of oxidation state.

Finally, the evaluation of catalytic potential was done for the conversion of 1,3-dihydroxyacetone (DHA) to methyl lactate (ML) and we compared our Lewis acid superior materials to the widely described Sn-BEA-F made via the fluoride approach (and with less Sn) [6]. Our data suggest that Sn-BEA zeolite with the record Si/Sn 14 demonstrates 3-fold improved productivity after one hour of reaction versus the comparison sample (Sn-BEA-F). Based on the Arrhenius plot in a wide temperature range, very similar apparent activation energies were established (64 kJ/mol for both materials), which corresponds to the literature [7]. We have evidence that both samples undergo mass transport limitations: we surmise Sn-BEA-F has classic diffusion limitations occurring due to long-distance diffusion in the large crystals (10  $\mu m$ , Figure 2), while the extreme concentration of Lewis sites cannot be efficiently supplied by enough diffusing reactants in the small-crystal Sn-BEA Si/Sn 14 (200 nm, Figure 2).

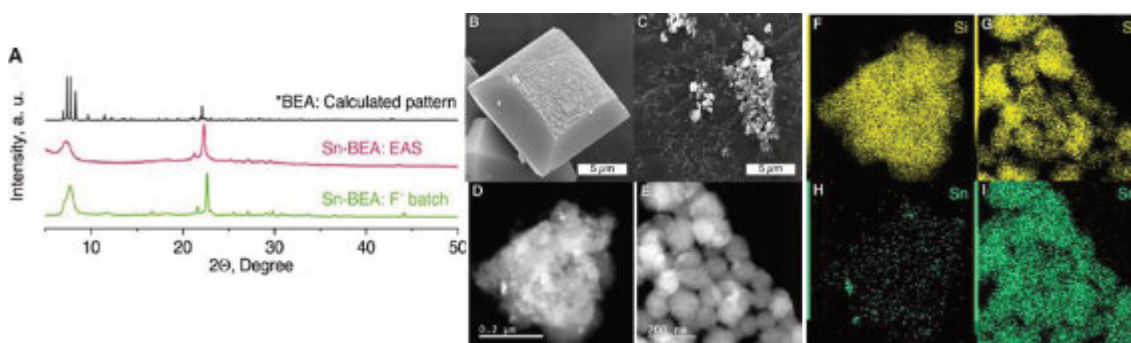


**Figure 2.** Comparison between fluoride-made and EAS-made Sn-BEA zeolites in (A) PXRD; (B and C) SEM imaging, and (D to I) TEM-EDS imaging. Image B, D, F and H are classic Fluoride-made zeolites; while C, E, G and I is EAS-made.

## References

- [1] A. Corma, A. Martinez, *Advanced Materials*, **7**, 137-144 (1995).
- [2] M. S. Holm, S. Saravanamurugan, E. Taarning, *Science*, **328**, 602-605 (2010).
- [3] W. R. Gunther, Y. Wang, Y. Ji, V. K. Michaelis, S. T. Hunt, R. G. Griffin, Y. Roman-Leshkov, *Nature Communications*, **3**, 1109 (2012).
- [4] J. Dijkmans, D. Gabriëls, M. Dusselier, F. de Clippel, P. Vanelderen, K. Houthoofd, A. Malfliet, Y. Pontikes, B. F. Sels, **15**, 2777-2785 (2013).
- [5] G. Ivanushkin, M. Dusselier, *Chemistry of Materials*, **35**, 5049-5058 (2023).
- [6] G. Ivanushkin, M. Torka Beydokhti, J. S. Martinez-Espin, M. Dusselier, *Chemistry of Materials*, **35**, 10216-10227 (2023).
- [7] Y. Liu, Y. Xiao, C. Xia, X. Yi, Y. Zhao, J. Yuan, K. Huang, B. Zhu, A. Zheng, M. Lin, X. Peng, *Journal of Catalysis*, **391**, 386-396 (2020).

## Acknowledgments

This research was sponsored by the European Research Council (ERC) in the form of ERC Starting Grant 948449: Z-EURECA: ZEolite synthesis in Unusual Reactors for Enhanced Catalysts (to MD). We acknowledge SOLEIL for provision of synchrotron radiation facilities and we would like to thank Dr. Emiliano Fonda for assistance in using beamline "SAMBA" (proposal number 20231908).



## Metal-exchanged faujasites as adsorbents for carbon dioxide – computational modeling combined with infrared spectroscopic study

H. A. Aleksandrov<sup>1</sup>, N. L. Drenchev<sup>2</sup>, M. Milenov<sup>1</sup>, P. St. Petkov<sup>1</sup>, K. I. Hadjiivanov<sup>2</sup>, G. N. Vayssilov<sup>1,\*</sup>

<sup>1</sup> Faculty of Chemistry and Pharmacy, University of Sofia, 1126 Sofia, Bulgaria

e-mail: gnv@chem.uni-sofia.bg

<sup>2</sup> Institute of General and Inorganic Chemistry, Bulgarian Academy of Sciences, Sofia 1113, Bulgaria

Due to their high specific surface area, controlled polarity of the framework and the presence of positively charged metal ions, alkaline and alkaline-earth exchanged zeolites are very suitable for CO<sub>2</sub> adsorbents for controlling carbon dioxide emissions and its sequestration. The selection of the appropriate materials is based on the knowledge of the adsorption mechanism and capacity, energetics of adsorption and desorption processes, competitiveness with other potential adsorbates, etc. To contribute to clarification of these questions, we report series of computational model studies of carbon dioxide sorption inside metal-exchanged zeolites with faujasite structure and formation of carbonates or hydrogen carbonates in their cavities.

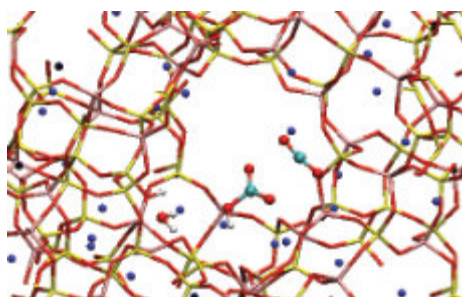


**Figure 1.** Snapshot from ab initio molecular dynamic simulation of model system in NaY zeolite.

The geometry optimization of carbon dioxide adsorption on NaY and CaX zeolites and the simulation of the corresponding vibrational frequencies were performed with periodic DFT method calculations with PBE exchange-correlation functional and D2 dispersion correction of Grimme, as implemented in VASP code.

For the ab initio molecular dynamic simulations of the different carbon dioxide containing species in NaY zeolite we used CP2K code with the same functional and D3 type dispersion correction.

As some of the most promising adsorbents we considered NaY, CaNaY or CaX zeolites with faujasite framework due to their high aluminium content leading to large number of alkaline/alkaline-earth cations, respectively. The structures of the adsorption complexes, the adsorption energies of CO<sub>2</sub> and their spectral features were determined by periodic quantum chemical calculations [1,2]. Both infrared spectroscopic studies and computational modelling showed that CaNaY zeolites possess a high CO<sub>2</sub> adsorption capacity at ambient temperature as both sodium and calcium cations act as adsorption centers. Each Ca<sup>2+</sup> site can attach two CO<sub>2</sub> molecules at relatively low partial pressure with binding energy of ca. 50 kJ/mol, and has the reserve potential to bind an additional molecule when the equilibrium pressure increases [1]. In CaX zeolite, with Si/Al ratio close to 1, our results suggested that up to three carbon dioxide ligands can be coordinated at each calcium cation as the average interaction energy decreases with the number of ligands, from 102 to 80 and 69 kJ/mol [2]. The dispersion component varies between 1/5 and 1/3 of the interaction energy. In presence of water the interaction energy of the carbon dioxide decreases to 54 kJ/mol and half of this energy is due to dispersion component.

In order to compare the computational results with real systems, we calculated vibrational frequencies of adsorbed CO<sub>2</sub> in all modelled complexes and compared to obtained values with experimental infrared spectra. The calculated frequencies of the complexes with one and two ligands in a model with one calcium cation, 2367 and 2371/2358 cm<sup>-1</sup>, respectively, fit well to the corresponding experimental values, 2364 and 2367/2354 cm<sup>-1</sup>. Changes in the vibrational frequencies in the mixed complexes with <sup>12</sup>CO<sub>2</sub> and <sup>13</sup>CO<sub>2</sub>, observed experimentally, are also well reproduced [1]. Interestingly, comparing the computational and experimental data for carbon dioxide adsorption on CaX zeolite, we concluded that the stretching band of adsorbed isotopically labelled <sup>13</sup>C<sup>16</sup>O<sup>18</sup>O molecule differs by 7 cm<sup>-1</sup>, depending on the side on which it is coordinated to the calcium cation - the complex in which the <sup>13</sup>C<sup>16</sup>O<sup>18</sup>O molecule is coordinated by its <sup>18</sup>O atom corresponds to the higher frequency band, at 2283, while the band at 2276 cm<sup>-1</sup> is due to the Ca<sup>2+</sup>-<sup>16</sup>O<sup>13</sup>C<sup>18</sup>O complex [2].

We also studied the most stable types of carbon dioxide containing species inside zeolite cavity. For this purpose we used ab initio molecular dynamic simulations of systems with two carbon dioxide and two water molecules in NaX zeolite as well various species formed by them – carbonic acids, hydrogen carbonates, carbonates, dicarbonic acid, and dicarbonate. This approach allows transformation of the species inside zeolite cavity. The most stable species inside zeolite cavity were carbonic acid and hydrogen carbonate, interacting with the basic oxygen centers of the zeolite framework and the charge-compensating sodium cations. They are by more than 30 kJ/mol per molecule more



**6<sup>th</sup> Euro-Asia Zeolite Conference**  
Alicante (Spain), January 19-22, 2025



stable that the separated water and carbon dioxide species. Carbonates are also disfavoured likely due to lower acidity of the hydrogen carbonates compared to bridging hydroxyl groups in zeolites, as recently shown [3].

#### References

- [1] N. L. Drenchev, E. Z. Ivanova, M. Y. Mihaylov, H. A. Aleksandrov, G. N. Vayssilov, and K. Hadjiivanov, *J. Phys. Chem. Lett.*, **14**, 1564-1569 (2023).
- [2] N. Drenchev, H. A. Aleksandrov, G. N. Vayssilov, B. Shivachev, and K. Hadjiivanov, *Separ. Purif. Technol.*, **349**, p.127662 (2024).
- [3] G. N. Vayssilov, H. A. Aleksandrov, E. Dib, I. M. Costa, N. Nesterenko, S. Mintova, *Micropor. Mesopor. Mater.*, **343**, p. 112144 (2022).

#### Acknowledgments

Computational resources are provided by the Nestum facility of Sofia Tech Park.



## Modelling Adsorption Isotherms in Aluminium-Substituted Zeolites using Graph Neural Networks

**M. Petkovic<sup>1</sup>, J.M. Vicent-Luna<sup>1</sup>, V. Menkovski<sup>2</sup>, S. Calero<sup>1</sup>**

<sup>1</sup> Department of Applied Physics and Science Education, Eindhoven University of Technology, 5612AZ Eindhoven, Netherlands

<sup>2</sup> Department of Mathematics and Computer Science, Eindhoven University of Technology, 5612AZ Eindhoven, Netherlands  
m.petkovic1@tue.nl

### Introduction

The adsorption performance of zeolites is not only influenced by the material's structural properties, such as topology, Si/Al ratio, Al distribution, and cation distribution, but also by operating conditions like temperature and pressure [1]. To fully characterize how a zeolite behaves under different conditions, it is essential to consider adsorption isotherms, which describe the relationship between the amount of adsorbate on the adsorbent and the pressure at constant temperature. Isotherms provide crucial insights into the efficiency and capacity of zeolites for CO<sub>2</sub> capture across a range of conditions, offering a more comprehensive understanding of their performance.

In this work, we extend the capabilities of our Equivariant Porous Crystal Networks (EPCN) model [2,3] to predict not only the heat of adsorption but also adsorption isotherms for different zeolite configurations. In addition, the model was extended to give insights regarding adsorption sites. By incorporating isotherm predictions, our model can now provide a more detailed and condition-dependent evaluation of zeolite performance. This addition enhances the model's utility for both forward and inverse design tasks, enabling the prediction of adsorption behaviour under various operating conditions and facilitating the optimization of zeolites for specific applications. The improved interpretability and predictive power of the model make it a valuable tool for advancing the design and application of zeolites in carbon capture technologies.

### Methods

To investigate the performance of the model in predicting CO<sub>2</sub> adsorption properties, we have considered four zeolite topologies with various pore types: MOR (large pore), MFI (medium pore/channels), ITW (small pore) and RHO (cage). To generate structures for each of the topologies, various algorithms [1] were used, which stochastically place aluminium atoms in all-silica versions of each zeolite. In total, 4992 structures were created with the MOR topology, 3296 for MFI, 1212 for RHO and 762 for ITW, with varying amounts and distributions of aluminium. For all zeolites, we calculated the heat of adsorption and Henry coefficient using Monte Carlo (MC) simulations with the Widom particle insertion method. For MOR and MFI, the adsorption isotherms were calculated using the Grand Canonical ensemble. All simulations were carried out using the RASPA software [4], while isotherms were fitted using the RUPTURA software [5]. Force field parameters from [1] were used, which account for structures not following the Löwenstein rule.

To model the adsorption properties, we used an extended version of the EPCN model. In this version, we predict each pores contribution to the various adsorption properties. As such, by inspecting the predictions for each pore, we can gather insights regarding their contribution to adsorption. In addition, we model the isotherm by predicting the loading of the zeolite given a pressure. Effectively, the model itself becomes the isotherm function, and can be evaluated at any pressure to obtain the full isotherm. By predicting the loading instead of the parameters of an isotherm equation (such as Langmuir-Freundlich), is more flexible and less restricted. For training, 90% of the structures for each topology were used, while the remaining 10% was used to evaluate the model.

### Results and Discussion

As can be seen in the parity plots in Figure 1, the model achieves a good performance in predicting the heat of adsorption and Henry coefficients of different zeolites. Overall, it achieves a Mean Absolute Error (MAE) of 1.28 and 0.10 for the heat of adsorption and Henry coefficient, respectively. The model struggles to predict structures with high values for the heat of adsorption, due to a lack of sufficient examples in the training set.

In addition, the model is also able to accurately model adsorption isotherms. We qualitatively investigated several MOR structures (Figure 2) and found that the model was able to accurately capture the varying shapes of adsorption isotherms. The model achieved MAEs of 0.05 and 0.04 for MOR and MFI, respectively. In comparison, predicting the average isotherm from the train set would yield an MAE of 0.15 for MOR and 0.14 for MFI, indicating that the model is able to accurately capture the differences in adsorption behaviour across different structures.



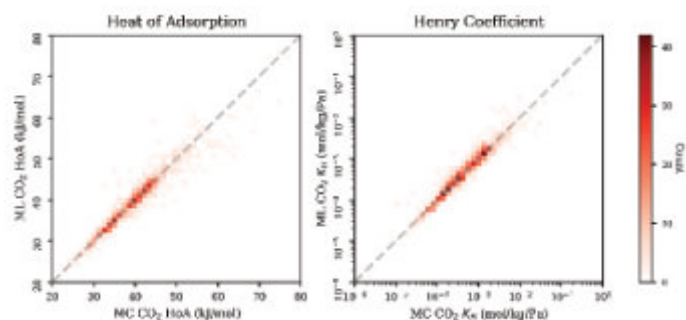


Figure 1. Parity plots for heat of adsorption and Henry coefficient prediction.

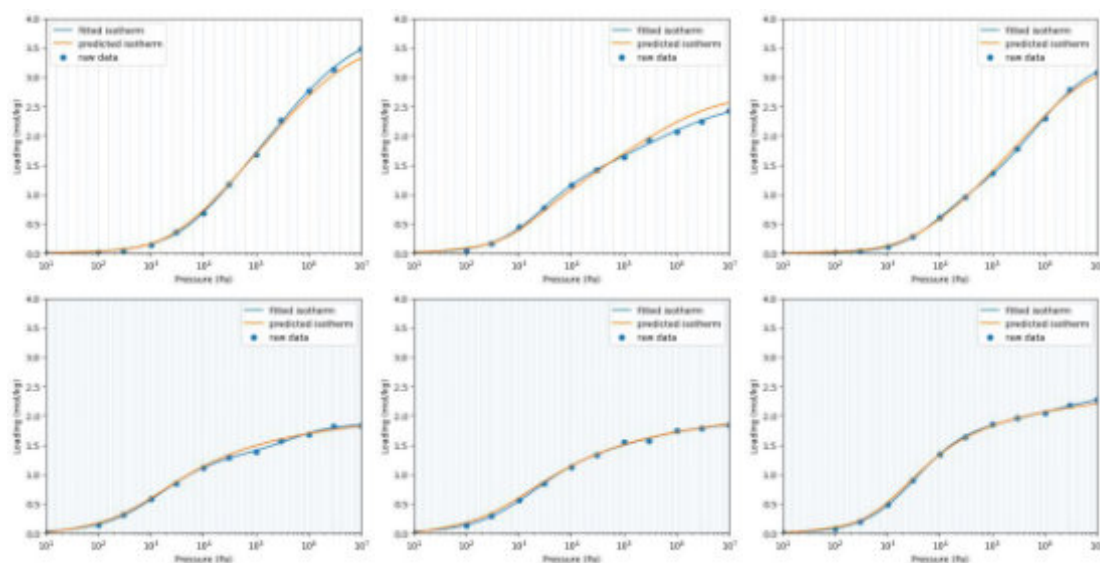


Figure 2. Simulated isotherms and predicted isotherms for different configurations of MOR (top row) and MFI (bottom row).

## Conclusion

We have extended the EPCN model to predict not only the heat of adsorption but also adsorption isotherms across various zeolite topologies, including MOR, MFI, ITW, and RHO. Our results demonstrate that the model accurately captures the distinct adsorption behaviours of these structures, offering a robust and flexible tool for predicting adsorption properties. Notably, the model excels in providing detailed insights into how different pore structures influence adsorption isotherms, which is crucial for optimizing zeolites for CO<sub>2</sub> capture under varying conditions. While the model performs well overall, it faces challenges in predicting high heats of adsorption, likely due to the limited representation of such cases in the training data. Addressing this in future research could further enhance the model's accuracy and applicability. The ability to directly predict adsorption loading without relying on predefined isotherm equations marks a significant advancement, making this model a valuable asset for the design and application of zeolites in carbon capture technologies.

## References

- [1] Romero-Marimon P., Gutiérrez-Sevillano J. J., Calero S. *Chem. Mater.* 5222-5231, **35** (2023)
- [2] Petković M., Romero-Marimon P., Menkovski V., Calero S. *International Symposium on Intelligent Data Analysis*, 129-140 (2024)
- [3] Petkovic M., Vicent-Luna J. M., Menkovski V., Calero S. *CoRR (arXiv)* (2024)
- [4] Dubbeldam D., Calero S., Ellis D. E., Snurr R. Q. *Mol. Simul.* 81-101, **42** (2016)
- [5] Sharma S., Balestra S. R., Baur R., Agarwal U., Zuidema E., Rigutto M. S., Dubbeldam D. *Mol. Simul.* 893-953, **49** (2023)



## Insights into Dimethyl Ether Carbonylation over Mordenite

D. Fan<sup>1</sup>, P. Tian<sup>1</sup> and Z. M. Liu<sup>1</sup>

<sup>1</sup> National Engineering Research Center of Lower-Carbon Catalysis Technology, Dalian National Laboratory for Clean Energy, Dalian Institute of Chemical Physics, Chinese Academy of Sciences, Dalian 116023, China  
fandong08@dicp.ac.cn

The increasing use of ethanol-blended fuels in transportation has spurred a pressing need for new and efficient methods to produce ethanol. Among these, dimethyl ether (DME) carbonylation has become a pivotal technique for transforming feedstocks such as coal, natural gas, and biomass into ethanol [1]. A milestone was reached in 2017 with the successful launch of a major coal-to-ethanol process capable of producing 100,000 tons of ethanol annually, wherein DME carbonylation constitutes the core chemical process. With its exceptional catalytic activity, mordenite has emerged as the foremost catalyst for DME carbonylation. The structure of mordenite featured the co-existence of two functional channels/cavities. Acidic sites within the 8-membered ring (8-MR) side pockets act as the genuine catalytic centers for DME carbonylation, whereas the 12-MR main channels are more susceptible to coking due to the formation of hydrocarbons from DME, resulting in rapid catalyst deactivation. The high catalytic activity of mordenite in DME carbonylation lies in the confined space of the 8-MR side pockets and consequently its unique transition-state selectivity. To further optimize the mordenite catalyst and achieve enhanced catalytic stability and activity, sustained efforts are warranted, focusing on enriching the acid sites within 8-MR side pockets, potentially via innovative synthesis and post-synthesis methods.

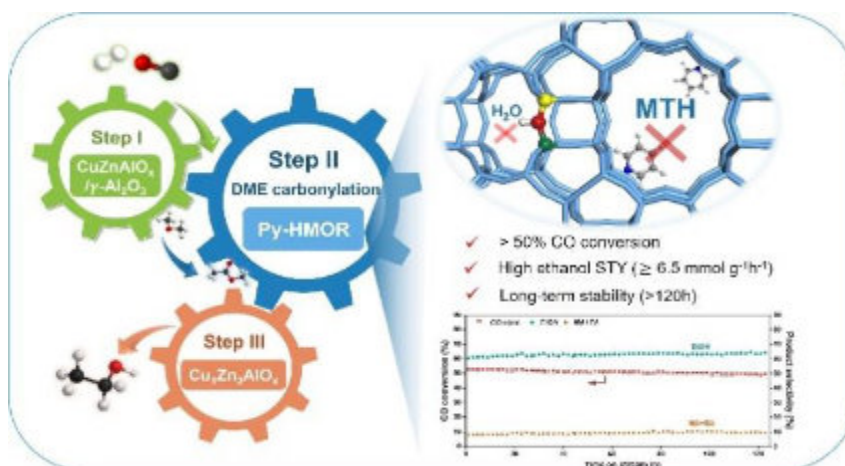


**Figure 1** Schematic illustration of the three-stage tandem catalytic system designed for the direct conversion of syngas to ethanol

This discussion focuses on sharing insights from recent studies aimed at enhancing our comprehension of DME carbonylation catalyzed by mordenite, as well as our endeavors to synthesize mordenite with superior DME carbonylation activity and stability. In 2020, our research team explored the interaction of pyridine with mordenite, revealing that pyridine can engage with the acid sites in the 8-MR side pockets, highlighting the topological flexibility inherent to the mordenite framework [2]. The selective exposure of acid sites in the 8-MR side pockets at elevated temperatures accounts for the good activity and stability of pyridine-modified mordenite. Moreover, we have discovered that diffusion properties, notably surface barriers, significantly impact DME carbonylation activity [3]. Building upon this understanding, we have successfully developed new mordenite catalysts with improved catalytic performance through targeted adjustments to their morphology [4] and acid properties [5]. A novel Cu-HMOR catalyst was engineered to sustain a catalytic lifetime exceeding 500 hours, facilitated by the co-feeding of hydrogen and the strategic deposition of *benign coke* [6]. Leveraging our optimized mordenite catalyst, we were also able to design a three-stage tandem catalytic system consisting of  $\text{CuZnAlO}_x/\gamma\text{-Al}_2\text{O}_3|\text{Py-HMOR}|\text{Cu,Zn,AlO}_x$ , enabling the direct conversion of syngas to ethanol with an impressive ethanol yield of up to  $6.5 \text{ mmol g}^{-1} \text{ h}^{-1}$  (Figure 1) [7].

These case studies not only provide valuable insights that can guide the design and engineering of advanced mordenite catalysts for DME carbonylation but also demonstrate the potential for developing more efficient and sustainable ethanol production processes.

### References

[1] A. Bhan; A. D. Allian; G. J. Sunley; D. J. Law; E. Iglesia, *J. Am. Chem. Soc.*, **129**, 4919-4924 (2007).



**6<sup>th</sup> Euro-Asia Zeolite Conference**  
Alicante (Spain), January 19-22, 2025



- [2] K. P. Cao; D. Fan; L. Y. Li; B. H. Fan; L. Y. Wang; D. L. Zhu; Q. Y. Wang; P. Tian; Z. M. Liu, *ACS Catal.*, **10**, 3372-3380 (2020).
- [3] K. P. Cao; D. Fan; M. B. Gao; B. H. Fan; N. Chen; L. Y. Wang; P. Tian; Z. M. Liu, *ACS Catal.*, **12**, 1-7 (2022).
- [4] K. P. Cao; W. Chen; D. Fan; Z. H. Jia; N. Chen; D. L. Zhu; S. T. Xu; A. M. Zheng, P. Tian; Z. M. Liu, *Chem. Eng. J.*, **487**, 150344 (2024)
- [5] N. Chen; J. Zhang; Y. T. Gu; W. N. Zhang; K. P. Cao; W. H. Cui; S. T. Xu; D. Fan; P. Tian; Z. M. Liu, *J. Mater. Chem. A*, **10**, 8334-8343 (2022).
- [6] D. Fan; N. Chen; S. Y. Han; L. Y. Li; N. Wang; W. H. Cui; Q. Y. Wang; P. Tian; Z. M. Liu, *ACS Appl. Mater. Interfaces*, **16**, 18745-18753 (2024)
- [7] S. Y. Han; D. Fan; N. Chen; W. H. Cui; L. H. He; P. Tian; Z. M. Liu, *ACS Catal.*, **13**, 10651-10660 (2023).

#### **Acknowledgments**

The authors acknowledge the funding by the National Natural Science Foundation of China (No. 22272173, 21991090, 21991091, and 22288101) and the Sino-French IRN (International Research Network).



## Boosted production of aromatic hydrocarbons via catalytic co-pyrolysis of lignocellulose and light alcohols over n-ZSM-5

M. Pagano<sup>1,2</sup>, J. Cueto<sup>1</sup>, J. Feroso<sup>1</sup>, I. Moreno<sup>1,2</sup>, D. P. Serrano<sup>1,2</sup>

<sup>1</sup> Thermochemical Processes Unit, IMDEA Energy, Avda. Ramón de la Sagra, 3, 28935, Móstoles, Madrid, España

<sup>2</sup> Environmental and Chemical Engineering Group, Rey Juan Carlos University, c/ Tulipán, s/n, 28933, Móstoles, Madrid, España

Maurizio.pagano@imdea.org

Catalytic pyrolysis of lignocellulose is a promising route to valorise forestry and agricultural residues and produce valuable hydrocarbons. Zeolites, due to their acidic and textural properties, are the most promising catalysts to produce aromatic hydrocarbons (AR) from both lignocellulose-derived furans and olefins [1, 2]. However, during conventional lignocellulose catalytic pyrolysis, the aromatization of furans results in a low yield of aromatic hydrocarbons, as secondary reactions can produce graphitic-coke precursors like benzofurans or lighter molecules through cracking, in addition to the scarce production of olefins. Moreover, other molecules different from benzofurans can hinder the catalytic activity of the zeolite and generate oxygenated-coke precursors. These molecules are primarily oxygenated aromatics generated from lignin decomposition such as phenyl ketones, methoxy/ethoxy benzenes, and lignin oligomers [3]. Hence, the process suffers from low hydrocarbon yield and short catalyst lifetime. Further understanding and optimization are needed to achieve the commercial feasibility of the process. Catalytic co-pyrolysis of lignocellulose with H-rich feedstocks is a promising strategy for the production of biofuels and chemicals, overcoming the issues derived from the low lignocellulose H/C ratio. Thus, the AR yield can be increased by using an external source of H-donors to favour Diels Alder condensation reactions with furans, creating a synergistic effect. Plastic residues, waste tires, and methane have been commonly used for the co-processing with lignocellulose [4], while the use of renewable liquids as co-feedstocks, such as bio-alcohols, has been less studied compared to solid residues.

In this work, an ex-situ reaction system, operating with continuous feeding modes, was used to explore the synergy between lignocellulose (3.5 g/h of oak tree biomass) and light alcohols (1.5 g/h of ethanol, 2-propanol, or 2-butanol). The reactor was divided into two independently heated zones: a thermal zone, where lignocellulose pyrolysis occurs, and a catalytic bed. The vapours produced from lignocellulose pyrolysis mix with the alcohol in the intermediary space between the two zones before entering the catalytic zone. A commercial nano-crystalline zeolite was used as catalyst (n-ZSM-5, Clariant) with a fixed load of 3 g. The physico-chemical properties of the catalyst are summarised in **Table 1**, showing it presents a relatively high external surface area due to its nano-crystalline nature.

The effect of different lignocellulose pyrolysis temperatures (350 and 500 °C) was also studied to maximize AR production and catalyst stability, while maintaining the catalytic bed temperature at 450 °C. To evaluate the synergistic effect between the lignocellulose and the alcohol, if any, the results obtained at 350/450 °C were compared to additive values calculated from the weighted sum of the individual catalytic pyrolysis of the feedstocks. Each experiment lasted for 4 h, with bio-oil and gas samples taken every hour. The bio-oil samples were analysed through GC-MS analysis (calibrated using internal standard method), while gas fraction composition was determined by micro-GC analysis. This approach allowed a detailed study of the deactivation of the n-ZSM-5 zeolite along the time on stream (TOS).

**Table 1.** Physico-chemical properties of the n-ZSM-5 catalyst.

Sample	Si/Al <sup>a</sup> mol	S <sub>BET</sub> <sup>b</sup> m <sup>2</sup> . g <sup>-1</sup>	S <sub>MICRO</sub> <sup>b,c</sup> m <sup>2</sup> . g <sup>-1</sup>	S <sub>EXT</sub> <sup>b,c</sup> m <sup>2</sup> . g <sup>-1</sup>	V <sub>TOT</sub> <sup>b,d</sup> cc/g	V <sub>MICRO</sub> <sup>b,c</sup> cc/g	C <sub>BRONSTED</sub> <sup>e</sup> mmol/g	C <sub>LEWIS</sub> <sup>e</sup> mmol/g
n-ZSM-5	50	412	284	128	0.538	0.177	0.252	0.034

<sup>a</sup> from ICP; <sup>b</sup> from Ar adsorption-desorption isotherm at 87 K; <sup>c</sup> Micropore surface area and volume calculated with NL-DFT method; <sup>d</sup> Total pore volume calculated at P/P<sub>0</sub>=0.98; <sup>e</sup> Determined from FTIR-pyridine adsorption after evacuation at 150 °C.

To understand the impact of lignocellulose pyrolysis temperature on AR yield and catalyst performance, a comparison between 350 °C and 500 °C as temperature for the thermal zone was conducted. The overall bio-oil yield increases from 13.75 to 20.70 wt% for Oak/EtOH and from 17.65 to 21.29 wt% for Oak/ButOH when the temperature increases. However, this is due mainly to the presence of highly substituted phenols and lignin oligomers since the estimated concentration of lignin-derived molecules in the vapour stream at 500 °C increases by 50% with respect to 350 °C [3]. These are highly reactive molecules that can generate coke through condensation and polymerization reactions, blocking the active sites of the n-ZSM-5 catalyst. As a result, the n-ZSM-5 deactivation rate is quite more pronounced when the lignocellulose pyrolysis temperature is raised from 350 to 500 °C, as shown in **Figure 1A** for the systems Oak/EtOH and Oak/ButOH. In contrast, only few phenols are detected in the bio-oil samples obtained at 350 °C (< 5% of total bio-oil).



On the other hand, the catalytic co-pyrolysis experiments performed at 350/450 °C resulted in overall bio-oil yields of 13.75, 14.19, and 17.65 wt% using oak with ethanol (EtOH), propanol (PrOH) and butanol (ButOH), respectively. The evolution of the AR yield along TOS is shown in **Figure 1B**. The AR yield is 27 and 57% higher than the additive values for PrOH and ButOH, respectively. This observation confirms the presence of a strong synergistic effect resulting from the interaction between lignocellulose-derived furans and the olefins produced through alcohol dehydration. The highest AR carbon yield is obtained using ButOH with a maximum value of c.a. 33 wt%, which is one of the best yields in comparison with those found in the literature for this type of process [5]. The catalytic bio-oil is highly concentrated in substituted monoaromatic compounds (> 95 wt%), with xylene and toluene accounting for more than 50 wt% of the total aromatic concentration. This high AR production is attributed to shape selectivity effects arising from the optimal micropore size of the n-ZSM-5 zeolite (about 5.5 Å).

On the contrary, no synergistic effect was observed when oak was co-processed with ethanol (EtOH), showing an AR yield very similar to the additive value for each time on stream. This finding can be related to the relatively low ethylene conversion (as indicated by its high concentration detected in the gas fraction) generated from EtOH dehydration due to its higher stability compared to the C3 and C4 olefins derived from PrOH and ButOH, respectively. Moreover, ethanol seems to tend to produce selectively benzofurans when interacting with lignocellulose vapours, reaching a yield higher than the additive value. This phenomenon can be also detrimental to the catalytic activity, as it facilitates the production of polyaromatics and coke.

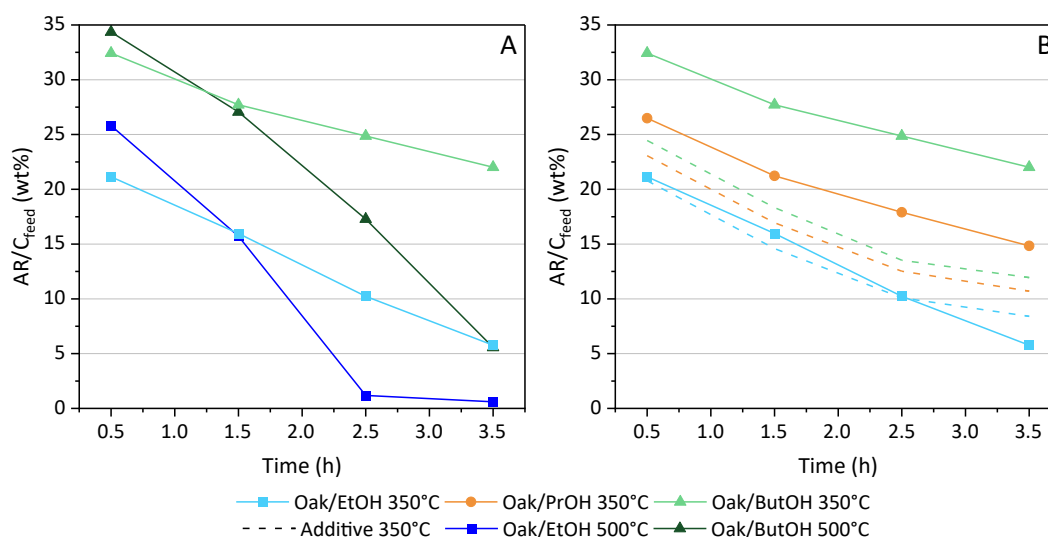


**Figure 1.** (B) AR carbon yield as a function of time on stream at 350/450°C compared to 500/450°C. (A) AR carbon yield as a function of time on stream compared to the additive values at 350/450°C. The first temperature refers to the lignocellulose pyrolysis, while the second one refers to the catalyst bed temperature.

In summary, both the nature of the co-processing alcohol and the temperature of the thermal pyrolysis zone have a significant impact over the total yield of AR and the zeolite lifetime during the catalytic co-pyrolysis process. The synergistic effect on AR yield, derived from co-processing, becomes more pronounced as the number of carbon atoms in the alcohol increases. On the other hand, the use of a relatively low temperature (350 °C) for the thermal pyrolysis zone minimizes the release of lignin derivatives and oligomers in the vapor stream, thereby preventing excessive coke formation and thus having a very positive effect on the catalyst lifetime.

## References

- [1] J. Liang, G. Shan, Y. Sun, *Renewable and Sustainable Energy Reviews*, **139**, 110707 (2021).
- [2] M. Inaba, K. Murata, M. Saito, I. Takahara, *Reaction Kinetics and Catalysis Letters*, **88**, 135-141 (2006).
- [3] M. Pagano, H. Hernando, J. Cueto, I. Moreno, D. P. Serrano, *Catalysis Today*, **426**, 114399 (2024).
- [4] M. Ahmed, N. Batalha, H. Mahmudul, G. Perkins, M. Koranova, *Bioresources Technology*, **310**, 123457 (2020).
- [5] Y. Zheng, J. Wang, D. Wang, Z. Zheng, *Application in Energy and Combustion Science*, **10**, 100061 (2022).

## Acknowledgments

The present work was financed by the Spanish Ministry of Science and Innovation (ADBIOCAP Project, PID2020-114740RB-C21).



## Correlation of Zeolite Framework and Acidic Properties with Catalytic Activity and Regenerability in Methane and Shale Gas Dehydroaromatization

Jong Hun Kang<sup>1,\*</sup>, Yangho Jeong<sup>1</sup>, Eun Ji Choi<sup>1</sup>, Yong Hyun Lim<sup>1,2</sup>, and Do Heui Kim<sup>1</sup>

<sup>1</sup> School of Chemical and Biological Engineering, Seoul National University, Seoul 08826, Republic of Korea

<sup>2</sup> Hanwha TotalEnergies Petrochemical Research Institute, Seosan-si, Chungcheongnam-do 31909, Republic of Korea

jonghunkang@snu.ac.kr

### Introduction

Light aromatics (benzene, toluene, and xylenes; BTX) are among the most essential base chemical products in the chemical industry. The dominant industrial technology for BTX production is naphtha reforming using multistage reactors, which requires complex reactor designs and is highly energy intensive as well. As a promising alternative, methane or shale gas, both abundant feedstocks, can be directly converted into BTX through methane dehydroaromatization (MDA) or shale-gas dehydroaromatization (SDA) reactions. In these reactions, 10-membered ring (10MR) zeolites loaded with Mo as active sites are utilized as catalysts. Various 10MR frameworks, such as MFI, MWW, TUN, and IMF, which provide shape selectivity for BTX, can be employed for this reaction. The Mo species anchored at the Al sites of the zeolite act as active Mo-carbide species, converting methane to BTX through hydrocarbon pool aromatization and shape selectivity induced by the confinement of the 10MR zeolite.

The regenerability and initial performance of Mo/zeolite catalysts in MDA and SDA reactions are closely related to coke formation. This is because the mechanism of coke formation during methane aromatization is fundamentally analogous to the mechanism of BTX production. Since coke formation is inevitable, regeneration cycles to remove the deposited coke are essential. Coke generated during MDA and SDA reactions can be classified into two types: soft coke, which combusts below 550 °C during the oxidative regeneration, and hard coke, which combusts at temperatures above 550 °C. Soft coke forms as polyaromatic species within the micropores, while hard coke deposits as graphitic structures on the external surfaces of the zeolite crystals (Figure 1(a)). Although coke can be removed through regeneration in an oxidative atmosphere, the active Mo species may be lost due to sublimation as MoO<sub>3</sub> or deactivated by irreversibly reacting with the framework Al sites to form inactive extraframework AlMoO<sub>x</sub> species. Therefore, the regeneration cycle must be conducted at mild temperatures below 550 °C to prevent Mo species deactivation, and the design of zeolites that can mitigate Mo deactivation is critical. Therefore, it becomes essential to suppress the formation of hard coke and to render the combustion temperature of deposited coke as low as possible. This study aims to propose an optimized zeolite design by examining the correlation between framework type, acid site distribution, and coke formation, based on various zeolite synthesis and post-synthetic treatment techniques for this process (Figure 1).

### Experimental

In this study, MCM-22 (MWW), TNU-9 (TUN), and ZSM-5 (MFI) zeolites were employed as model 10MR zeolites. MCM-22 was synthesized using hexamethyleneimine as the organic structure-directing agent (OSDA) and NaOH as the mineralizer, with the final Si/Al ratio within 8–25. [1] TNU-9 was synthesized with 1,4-bis(N-methylpyrrolidinium)butane as the OSDA and NaOH as the mineralizer, yielding a Si/Al ratio within 10–18. [2] ZSM-5 with a Si/Al ratio of 10–13 was purchased from Thermofisher Scientific and Albermale Co. ZSM-5 was post-treated using quaternary ammonium hydroxides (QAH) such as tetramethylammonium hydroxide (TMAOH), tetrapropylammonium hydroxide (TPAOH), and cetyltrimethylammonium hydroxide (CTAOH), as well as fluorosilicates like ammonium hexafluorosilicate (AHFS). [2] All as-made zeolites were calcined to remove the OSDA and converted into their proton form using ammonium nitrate. Ammonium molybdate hexahydrate was used as the precursor to load Mo species at 6 wt. % and 10 wt. % for MDA and SDA reactions, respectively.

The MDA and SDA reactions were conducted using lab-scale fixed-bed reactors. The MDA reaction was performed at 700 °C, with a feed of 90 vol. % methane (balanced with He) introduced at a flow rate of 10 mL/min. The SDA reaction was also conducted at 700 °C, with simulated shale gas consisting of 85 vol. % methane, 10 vol. % ethane, and 5 vol. % propane, fed at a corresponding flow rate. Each catalyst was pre-carburized using low concentrations of methane at a temperature near the reaction temperature (see Refs. [1] and [3] for details). The reaction products, BTX and light olefins (ethylene and propylene), were quantified in real-time using on-line GC-FID. Catalyst regeneration was performed after 15 hours of reaction by using 10 vol. % O<sub>2</sub> gas at 550 °C.

### Results and Discussions

In the MDA and SDA reactions, the apparent catalytic activity and coke formation behaviors are highly sensitive to various intrinsic properties of the employed zeolites, such as framework type, Si/Al ratio, spatial distribution of acid sites within crystals, and crystal morphology. Since the mechanisms of coke formation and BTX formation are fundamentally analogous, the selectivity for BTX and the behaviors of coke formation are ultimately determined by the micropore geometry of the 10MR zeolite used. Figure 1(b) shows the BTX yield during the MDA reaction at 700



°C for Mo-loaded catalysts (6 wt. %) using MCM-22, TNU-9, and ZSM-5 zeolites with similar Al content in the Si/Al range of 11–15. MCM-22 exhibited higher catalytic stability and BTX yield compared to the other two zeolites. As seen in the differential TGA profile of the spent catalysts (Figure 1(c)), this is primarily attributed to the superior ability of MCM-22 to form soft coke, likely due to the relatively higher specific micropore volume of MWW compared to MFI and TUN. Additionally, due to channel confinement, MCM-22 was more effective at suppressing the formation of the undesired product naphthalene during the MDA reaction compared to TUN and MFI (data not shown), suggesting that methane aromatization is controlled at the monoaromatic level. This trend was also observed in the corresponding SDA reactions (Figures 1(d) and 1(e)) [1], where the maximum BTX yield followed the order of MWW > TUN > MFI, strongly correlating with the proportion of coke that combusts at lower temperatures.

Another strategy to preferentially form coke with a lower combustion temperature from methane aromatization is to control the spatial distribution of Al-sites within the zeolite crystals. Mo-active sites preferentially anchor to framework Al sites within zeolites, where BTX and coke formation occur together. Unlike those within micropores, Mo-active sites located on the external surfaces of zeolites experience less spatial confinement, leading to the formation of surface graphitic hard coke, which is disadvantageous for regeneration since it requires removal at high temperatures over 600 °C. In one of our previous studies, we showed that treating ZSM-5 under hydrothermal conditions with QAHS, such as TMAOH, TPAOH, and CTAOH, reduced external acid site density and introduced surface mesoporosity, improving apparent activity and regenerability in the SDA reactions at 700 °C. [2] Extending this method, we introduced AHFS as a secondary post-treatment reagent, used in combination with TPAOH (Figure 1(f)), and observed a significant reduction in surface Al-site density in ZSM-5 (surface XPS Si/Al ~30; bulk ICP Si/Al ~16). ZSM-5 post-treated with both TPAOH and AHFS (ZAT) exhibited much better catalytic stability and regenerability in the SDA reaction compared to ZSM-5 treated with TPAOH alone (ZT) and pristine ZSM-5 (initial ICP Si/Al ~15) (see Figures 1(g) and 1(h)). A similar trend was observed in the MDA reaction, and it was confirmed that coke combustion temperatures could be lowered through post-synthetic modification of the zeolite.

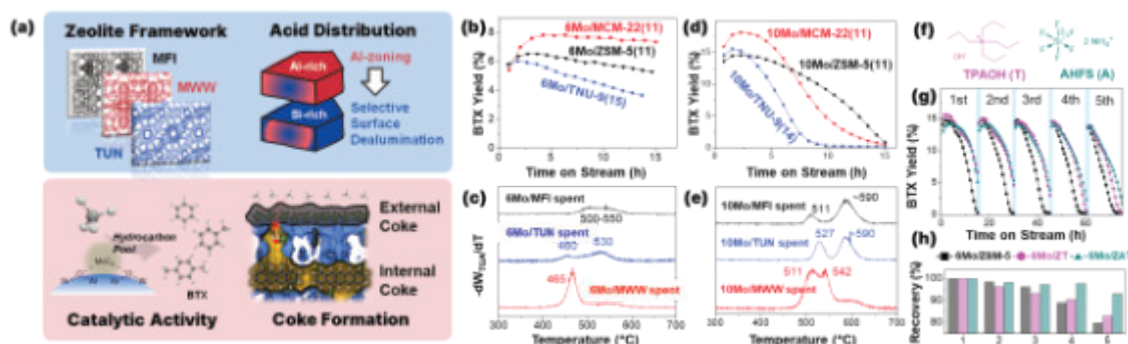


**Figure 1.** Structure of this work: (a) scope of this work encompassing the effects of zeolite framework types and acid site distribution on the catalytic activity and coke formation of MDA and SDA reactions. (b) time-on-stream BTX yields and (c) post-run catalysts DTG profiles from MDA reactions over 6 wt.% Mo zeolite catalysts at 700 °C. (d) time-on-stream BTX yields and (e) post-run catalysts DTG profiles from SDA reactions over 10 wt.% Mo zeolite catalysts at 700 °C. (f) Reagents used in the postsynthetic treatment of ZSM-5. (g) 5-cycle catalysis-regeneration of pristine and postsynthetically treated ZSM-5s in 700-°C SDA reactions. (h) Yield recoveries over 5 cycles of catalysis-regeneration.

## Conclusion

The intrinsic properties of zeolites, such as their frameworks and acidity, are critical factors in determining catalytic performance in the MDA and SDA reactions. From a framework perspective, MWW-type zeolites outperform MFI and TUN in terms of soft coke formation and naphthalene suppression, resulting in relatively higher BTX yield and catalytic stability. Although ZSM-5 shows lower BTX yield than MCM-22, its performance in both SDA and MDA reactions can be significantly enhanced through controlled synthesis methods and appropriate post-treatment using QAH or fluorosilicates. We believe that this work provides indispensable guidelines for designing optimal zeolite catalysts that achieve the highest BTX yield and regenerability in MDA and SDA reactions.

## References

- [1] E. J. Choi, Y. H. Lim, Y. Jeong, H. W. Ryu, J. Roh, D. H. Kim, J. H. Kang, *Catal. Today*, **425**, 114348 (2024).
- [2] S. B. Hong, H.-K. Min, C.-H. Shin, P. A. Cox, S. J. Warrender, P. A. Wright, *J. Am. Chem. Sci.*, **129**, 10870-10885 (2007).
- [3] Y. Jeong, Y. H. Lim, E. J. Choi, H. W. Ryu, J. Roh, S. Lee, M. Choi, D. H. Kim, J. H. Kang, *Chem. Eng. J.*, **482**, 148862 (2024).

## Acknowledgments

This research was financially supported by the C1 Gas Refinery Program through the National Research Foundation of Korea, funded by the Ministry of Science, ICT & Future Planning (2021M3D3A1A01022109), and the Carbon Neutral Industrial Strategic Technology Development Program funded by the Ministry of Trade, Industry & Energy of the Republic of Korea (RS-2023-00261088).



## Zeolites in biogas VOC valorization: Acid-catalyzed D-limonene ethoxylation

P. Bruno<sup>1,2</sup>, E. Catizzone<sup>1</sup>, F. Pietramale<sup>1,3</sup>, M. Migliori<sup>1</sup>, R. Mancuso<sup>4</sup>, B. Gabriele<sup>4</sup>, G. Giordano<sup>1</sup>

<sup>1</sup> CECaSP Laboratory, University of Calabria, Via P. Bucci 42/A, 87036, Rende (CS), Italy

<sup>2</sup> Chibiofaram, University of Messina, Viale F. Stagno D'Alcontres 31, 98165, Messina, Italy

<sup>3</sup> ENEA, Trisaia Research Center, 75026, Rotondella (MT), Italy

<sup>4</sup> LISOC Laboratory, University of Calabria, Via P. Bucci 12/C, 87036, Rende (CS), Italy

massimo.migliori@unical.it

The anaerobic digestion is a well-established industrial process for the conversion of organic waste into biogas. To obtain pure bio-methane, the gas that leaves the digester needs a purification step,<sup>1</sup> since it contains different pollutants, such as hydrogen sulfide, ammonia, siloxanes, water and volatile organic compounds (VOCs). The VOC fraction is mainly composed of *p*-cymene, an aromatic compound with NBP of 176 °C, and D-limonene, a terpene with NBP of 177 °C, used in pharmaceutical applications.<sup>2</sup> These two compounds are nearly impossible to separate via classic distillation due to their very close NBP values. A promising way to recover these compounds lays in the acid-catalyzed double bond alkoxylation reaction with bio-ethanol to convert D-limonene to a terpinyl ethyl ether, which exhibits a higher NBP than of the starting reagents, making the separation by distillation possible and the recover marketable.<sup>3</sup>

In this work, the liquid-phase ethoxylation was carried out under batch conditions using various zeolites as heterogeneous acid catalysts. BEA-, MFI- and MOR-type zeolites were successfully synthesized and fully characterized by means of XRD analysis, porosimetric analysis, *d*<sub>3</sub>-acetonitrile FT-IR, NH<sub>3</sub>-TPD, and SEM/EDX analysis. The performance of different zeolite frameworks were compared to gain new insights about the role of framework topology on catalyst activity. Reaction kinetic was obtained by studying the effect of temperature in the range 45 °C - 75 °C and initial D-Limonene concentration in the range 0.4% - 1.5% mol/mol. The effect of catalyst acid sites concentration was investigated by using Beta zeolites with different Lewis and Brønsted acid sites content and distribution. These samples were obtained by either changing the synthesis gel Si/Al ratio or by post-synthesis treatment, e.g. Na-ion exchange or heat treatment at high temperature (i.e. 700 °C). Product distribution determination was carried out by GC-MS spectrometry and NMR spectroscopy.

**Table 1. Physic chemical properties of the investigated catalysts**

Sample	Description	$S_{\text{BET}}/\text{m}^2 \text{ g}^{-1}$	Total Acidity / $\mu\text{mol g}^{-1}$
H-BEA-25	BEA-type sample with Si/Al <sub>gel</sub> =25 in acidic form	642	628
H-BEA-50	BEA-type sample with Si/Al <sub>gel</sub> =50 in acidic form	651	504
Na-BEA-550	BEA-type sample with Si/Al <sub>gel</sub> =25 calcined at 550 °C	690	290
Na-BEA-700	BEA-type sample with Si/Al <sub>gel</sub> =25 calcined at 700 °C	608	330
NaCl-BEA	BEA-type sample with Si/Al <sub>gel</sub> =25 ion-exchanged with sodium	663	120
H-MFI	MFI-type zeolite with Si/Al <sub>gel</sub> =25 in acidic form	445	569
H-MOR	MOR-type zeolite with Si/Al <sub>gel</sub> =25 in acidic form	531	966

The main physico-chemical properties of the analyzed samples are reported in Table 1, indicating that the adopted synthesis and post-synthesis procedures allowed to obtain BEA-type samples with different acidity, with no significant impact on BET surface area. Catalytic tests revealed that MFI zeolite is inactive for the investigated reaction under the adopted conditions, as it shows zero D-limonene conversion even at highest temperature and long contact time. MOR zeolite is partially active for the reaction as it shows low conversion values (i.e. < 10%) at 22 h of reaction and BEA zeolite is the most active, showing good conversion and selectivity under the investigated conditions. Therefore, the results indicate that the best configuration is a tri-dimensional 12 MR zeolite, such as BEA, among the investigated zeolite structures. The structure has then a strong impact on the catalysis of the reaction indicating an important effect of shape-selectivity. The effect of the main reaction parameters, that are, acid site concentration and temperature, on catalysis is reported for BEA-type zeolite in terms of limonene conversion in Figure 1.



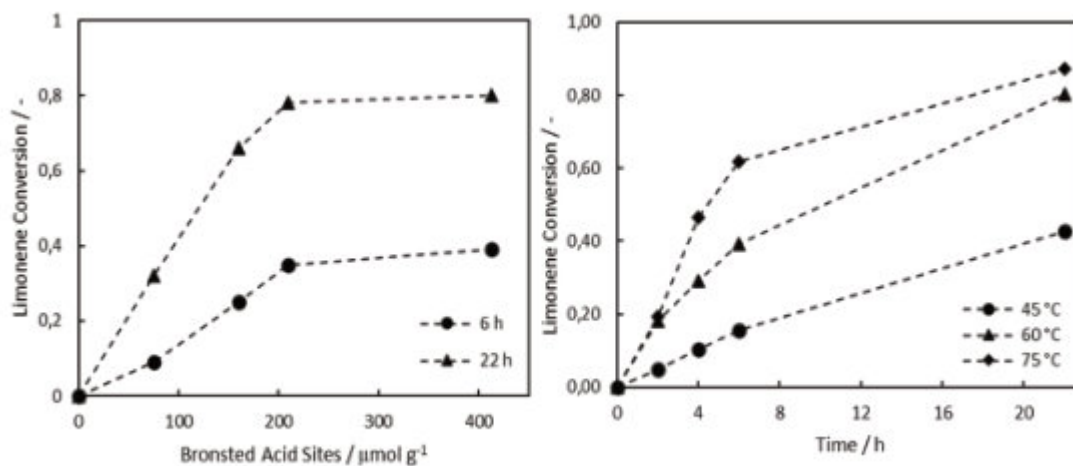


Figure 1. D-Limonene conversion: effect of Brønsted acid sites concentration (left) at 60°C, and effect of reaction temperature over H-BEA-25 sample (right)

Limonene conversion is promoted at higher temperature, with a selectivity towards  $\alpha$ -terpinyl ethyl ether above 65% up to 60°C. At 75°C and long reaction time, isomerization also reaction-significantly occurs and polyethers are formed, with selectivity towards the  $\alpha$ -terpinyl ethyl ether of about 45% after 22 h. Limonene conversion is also promoted by acid sites loading increase, but no benefits are observed for acid sites loading higher than 270  $\mu\text{mol}_{\text{acid sites}} \cdot \text{g}_{\text{limonene}}^{-1}$ , indicating that a high acid sites loading could promote the reverse reaction. Catalytic tests on real VOC mixtures revealed that the adopted catalysts are selective towards limonene conversion, while *p*-cymene, lacking the double bond, is clearly inert, thus indicating the high potentiality of the proposed catalytic process for biogas VOC condensate valorization. Kinetic evaluations allowed estimating kinetic parameters, such as reaction order and apparent activation energy.

## References

- [1] R. Zhao, J.T. Novak, and C. Douglas Goldsmith, *Waste Manag.*, **33**, 1207 (2013).
- [2] M.R. Thomsett et al., *Green Materials*, **4**, 115 (2016)
- [3] M. Stanculescu, M. Ikura, *J. Anal. Appl. Pyrolysis*, **75**, 217 (2006)



## Selective catalysis using metal nanoparticles protected by a zeolite shell

J. Mielby<sup>1</sup>, D. Itsiou<sup>1</sup>, G. Zhuo<sup>1</sup>, and S. Kegnæs<sup>1</sup>

<sup>1</sup> DTU Chemistry, the Technical University of Denmark, Kemitorvet 207, DK-2800 Kgs. Lyngby, Denmark  
skk@kemi.dtu.dk

In spite of the great technological, environmental, and economic interests, general methods for stabilizing metal nanoparticles against sintering are missing. However, for some specific systems, it has been achieved by optimizing the interaction of nanoparticles with a support material or by encapsulation of the metal particles [1-3]. However, these known catalytic systems are generally rather expensive and difficult to synthesize, and they cannot be produced on an industrial scale. Therefore, developing novel sintering stable heterogeneous nanoparticle catalysts, which find use in the chemical industry, is very important.

Recently, we have developed several different catalytic systems where metal nanoparticles are confined in different porous materials. [4-6] As an example, we have developed a novel concept for the synthesis of mesoporous zeolites with catalytically active metals, which are protected by a shell of microporous zeolite. [7] The approach, with a reactive core and a protective microporous shell, allows only selective small molecules to enter and react in the interior. This synthesis approach gives the opportunity to do selective catalysis on mixtures of molecules where only reactions with specific molecules are intended. Furthermore, the nanoparticles in the core are protected against sintering by the outer shell. The produced materials were tested in a range of different reactions, including selective hydrogenation reactions, methanation of CO<sub>2</sub> to methane, and conversion of methanol-to-hydrocarbons (MTH).

For instance, a mesoporous core of silicalite-1 or ZSM-5 zeolite was prepared using carbon as a hard template in a steam-assisted synthesis. Metal particles were supported on the mesoporous zeolite by incipient wetness impregnation. Finally, a protective shell of silicalite-1 was grown around the metal-containing mesoporous zeolite using a solvent-free synthesis.

The materials were characterized using X-ray powder diffraction, N<sub>2</sub> physisorption, X-ray photoelectron spectroscopy, transmission, and scanning electron microscopy. The materials were tested in different hydrogenation reactions to evaluate the protective shell's selectivity effect. To evaluate the stability effect of the protective shell on the nanoparticles, the materials were tested in methanation of CO<sub>2</sub> to methane and methanol-to-hydrocarbons (MTH) reaction.

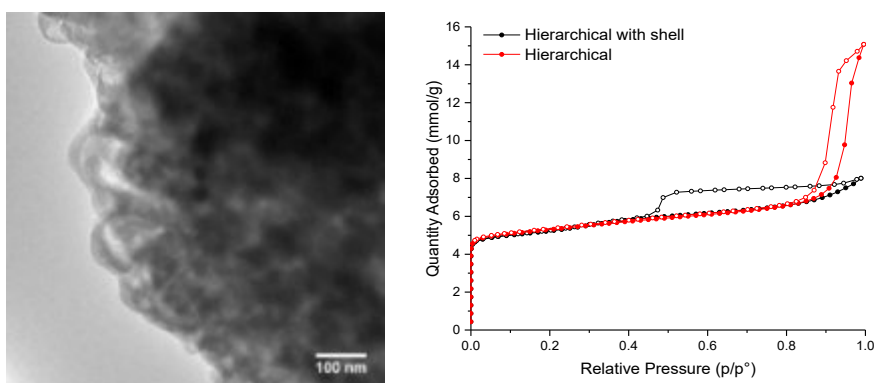


**Figure 1.** TEM image of hierarchical zeolite with shell (Left), physisorption isotherms of hierarchical zeolite and a hierarchical core zeolite with microporous shell (Right).

The transmission electron microscope image (Figure 1 left) shows an example of a shell formed around a porous metal-containing interior. The encapsulation of mesopores inside a microporous shell is also supported by the physisorption isotherms of hierarchical zeolite and hierarchical core zeolite with shell (Figure 1 right).

Catalytic tests show that the microporous shell provides the materials with selectivity for the molecules that can enter the microporous shell and reach the reactive core.

The zeolites produced were synthesized containing metals including Ni, Ru, Pd, Pt, etc. The materials were characterized by X-ray photoelectron spectroscopy (XPS). The XPS also confirms that only metal particles are trapped inside the zeolite. Additionally, the encapsulated nanoparticles were demonstrated to be highly active and selective



for the catalytic hydrogenation reactions. Zeolites containing other metals were produced and tested for different reactions. For instance, we have shown that nickel-encapsulated nanoparticles in zeolites are highly active and stable in the methanation of carbon dioxide to methane. Moreover, the materials obtained were characterized by various techniques, including SEM, TEM tomography, XRF, BET, and XRD.

In conclusion, we developed a new method to protect and encapsulate metal particles supported on a hierarchical zeolite with a microporous shell. The shell induced a selectivity for molecules that could diffuse and react in the catalytically active interior. The produced materials were tested in a range of different reactions and characterized with various techniques.

## References

- [1] P. M Arnal; M. Comotti; F. Schüth; *Angew. Chem. Int. Edit.*, 45, 8224 (2006).
- [2] Y. Dai Y.; et al., *Angew. Chem. Int. Ed.* 49, 1 (2010).
- [3] A. B. Laursen; et al., *Angew. Chem. Int. Ed.* 49, 3504 (2010)
- [4] J. O. Abildstrøm, M. Kegnæs, G. Hytoft, J. Mielby, S. Kegnæs, *Microporous Mesoporous Mater.* 2016, 225, 232.
- [5] J. Mielby; J.O Abildstrøm, F. Wang, T. Kasama, C. Weidenthaler, S. Kegnæs, *Angew. Chem.* 126, 1 (2014).
- [6] F. Goodarzi, L. Kang, F.R. Wang, F. Joensen, S. Kegnæs, J. Mielby, *ChemCatChem*, 10, 1566-1570 (2018).
- [7] K. H. Rasmussen, F. Goodarzi, D. B. Christensen, J. Mielby, S. Kegnæs, *ACS Appl. Nano Mater.* 2, 8083, (2019).

## Acknowledgments

The work is funded by the Independent Research Fund Denmark (Grant no. 3105-00207B).



## Reactions Kinetics Between Ingredients Affect the Structure of Amorphous Aluminosilicates and the Crystallization of Zeolites

Ching-Tien Chen<sup>1,2\*</sup>, Kenta Iyoki<sup>3</sup>, Tatsuya Okubo<sup>2</sup>, and Toru Wakihara<sup>2</sup>

<sup>1</sup> Department of Chemical Engineering, National Tsing Hua University, No. 101, Sec. 2, Kuan-Fu Rd., Hsinchu 30013, Taiwan (R.O.C.)

<sup>2</sup> Department of Chemical System Engineering, The University of Tokyo, 7-3-1 Hongo, Bunkyo-ku, Tokyo 113-8656, Japan

<sup>3</sup> Department of Environment Systems, The University of Tokyo, 5-1-5, Kashiwanoha, Kashiwa-shi, Chiba 277-8563, Japan

\*ctchen2@mx.nthu.edu.tw

### Introduction

Crystallization of zeolite represents a disorder-to-order transformation of the aluminosilicate matters, involving complex structural reorganizations through reactions such as dissolution, hydrolysis, and condensation during synthesis. Kinetics of these chemical reactions may depend on several factors, including temperature, agitation, and the composition of reactant mixture, which has been reported to change the crystallization rates, particle sizes, and topologies of zeolites. In this work, we showed that the form of Si reactant (i.e., in solid or solution states) significantly changes the crystallization behaviour of zeolite X (FAU), which is due to the formation of different amorphous structures at the beginning of synthesis. These results suggest controlling the structure of amorphous matter is the key to accelerate the crystallization of zeolites.

### Experimental Section

Fumed silica (Cab-O-Sil® M-5), sodium aluminate (NaAlO<sub>2</sub>), sodium hydroxide (NaOH), and water (H<sub>2</sub>O) were used as raw ingredients to prepare mixtures with the following composition: 1 Na<sub>2</sub>O/0.2 Al<sub>2</sub>O<sub>3</sub>/1 SiO<sub>2</sub>/50 H<sub>2</sub>O. Two different batches of mixture were prepared with different starting forms of Si source. The first batch (*fumed silica system*) represents the system using solid form Si as reactant, where fumed silica powder (1 SiO<sub>2</sub>) was added as it is to a transparent Al-containing solution (1 Na<sub>2</sub>O/0.2 Al<sub>2</sub>O<sub>3</sub>/50 H<sub>2</sub>O). The second batch (*silicate solution system*) represents the system using solution form Si as reactant, in which fumed silica was dissolved in a NaOH<sub>(aq)</sub> to form a transparent silicate solution (0.75 Na<sub>2</sub>O/1 SiO<sub>2</sub>/25 H<sub>2</sub>O), followed by the addition of an Al-containing solution (0.25 Na<sub>2</sub>O/0.2 Al<sub>2</sub>O<sub>3</sub>/25 H<sub>2</sub>O). These mixtures were then subjected to static hydrothermal synthesis at 80°C for desired time periods. The aluminosilicate matters collected at different times were analysed by an array of techniques, including XRD, solid-state NMR, ICP, Raman spectroscopy, and high-energy X-ray total scattering (synchrotron beamline BL04B2, SPring-8, Japan), to understand the structural evolution during the crystallization of zeolite X.

### Results and Discussion

Powder X-ray diffraction showed that under the designed composition of the mixture, both fumed silica and silicate solution systems produced zeolite X as crystalline products. The fumed silica system, however, showed a higher crystallization rate and smaller particle sizes of zeolite X compared to the silicate solution system (**Figure 1a**), suggesting a higher nucleation frequency of zeolite X in the fumed silica system. Pair distribution function (PDF) analysis revealed that the fumed silica system produced amorphous matters with symmetric Si-rich 6Rs after 1 h of hydrothermal treatment, and then symmetric Al-rich 6Rs became dominant after 3h of synthesis (**Figure 1b**). In addition, solid-state <sup>29</sup>Si NMR spectra indicated the formation of Al-rich aluminosilicate structures at 1 h in the fumed silica system; notably, these structures were in a chemical environment similar to that of crystalline zeolite X (**Figure 1c**). Since 4Rs and 6Rs construct the zeolite X framework, this suggests that within 1 h of synthesis, the fumed silica system produced uniform aluminosilicate structures containing plentiful Al-rich 4Rs and Si-rich 6Rs. We attributed this phenomenon to the gradual dissolution of fumed silica in the hot sodium aluminate solution, which allows, on the one hand, a condensation reaction environment with more Al and less Si species in the liquid phase and, on the other hand, an undissolved solid phase that contains relatively stable Si-rich structures (e.g., symmetric 6Rs). Consequently, the interaction between these rings facilitated the formation of *sod*-cages and, subsequently, the zeolite X framework.

In contrast, for the silicate solution system, a distorted aluminosilicate matrix was formed as soon as the silicate solution was mixed with the Al-containing solution due to a severe condensation reaction between the abundant active Si and Al species. The distorted structure exhibited high stability during the synthesis, which hindered the nucleation of zeolite X and led to a long crystallization process. To sum up, the comparative study between the fumed silica and silicate solution systems pointed out the significance of understanding the amorphous structure during zeolite synthesis, which enables researchers in this field to establish the relationship between synthesis parameters and the crystallization behaviour of zeolites.

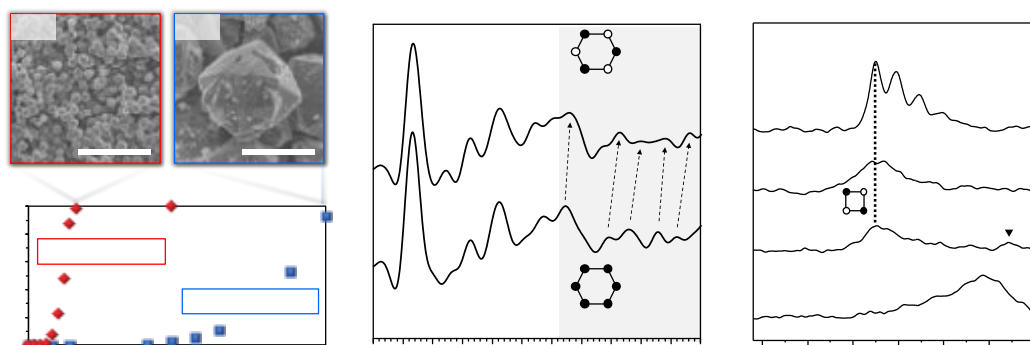


**Figure 1.** (a) Crystallization curves of zeolite X and the images of crystalline particles when different forms of Si reactant were used for the synthesis. (b) Pair distribution function calculated from HEXTS experiments for solid products collected from the fumed silica system at 1 and 3 h. (c) <sup>29</sup>Si solid-state NMR spectra of solid products collected from the fumed silica system at 0, 1, 3, and 8 h.

### References

[1] C.-T. Chen, K. Iyoki, P. Hu, H. Yamada, K. Ohara, S. Sukenaga, M. Ando, H. Shibata, T. Okubo, T. Wakihara, *J. Am. Chem. Soc.*, **143**, 10986-10997 (2021).

### Acknowledgments

This work was partially supported by NEDO Moonshot Project, JSPS KAKENHI Grant-in-Aid for Transformative Research Areas(A) (JP20A206/20H05880), and the Materials Processing Science project ("Materialize") of MEXT (JPMXP0219192801). C.-T.C. thanks the Japan–Taiwan Exchange Association for the scholarship during this work.



## Understanding Copper Sites In CHA By Continuous Rotation Electron Diffraction

E. Ikonnikova<sup>1</sup>, M. Schmithorst<sup>2</sup>, B. Chmelka<sup>2</sup>, T. Willhammar<sup>1</sup>

<sup>1</sup> Department of Materials and Environmental Chemistry, Stockholm University, 109 61 Stockholm, Sweden

<sup>2</sup> Department of Chemical Engineering, University of California, Santa Barbara, California 93106-5080, USA  
evgeniia.ikonnikova@mmk.su.se

Zeolites are nanoporous crystalline aluminosilicates of which there are approximately 250 different three-dimensional framework types. Many have technologically important properties, such as high catalytic activities and selectivities, high ion exchange capacities, and selective gas adsorption and separations, which are exploited in industrial applications. Different extra-framework cations, e.g., H<sup>+</sup>, Cu<sup>2+</sup>, or Pt<sup>2+</sup>, can be incorporated within the nanopores of zeolites to enhance their catalytic properties. Knowledge about the structures is essential to understand a material's properties. Zeolites are usually polycrystalline, with sub-micrometer sized crystals, which poses challenges using traditional crystallographic techniques such as single crystal X-ray diffraction. 3D electron diffraction (3DED) methods can overcome this limitation due to the strong interaction of electrons with matter by probing the electrostatic potential. Continuous rotation electron diffraction (cRED) enables the rapid and automated collection of 3D electron diffraction data.

In this study, we investigate copper sites in chabazite (CHA) zeolite by cRED. To examine the position of extra-framework cation species, four materials were studied: Cu-CHA, 4h-aged Cu-CHA, 16h-aged CHA and the acidic form, H-CHA, was used as a reference. Initially, cRED data was collected from sub-micrometer sized single-crystals at room temperature. Subsequently, the sample was dehydrated at 450°C under vacuum with a temperature ramp of 5°C/min, and data was collected again from the very same crystal. Dehydration was performed to exclude any uncertainty due to the possibility of water molecules occupying the same position as a copper ion. The refinement against cRED data shows a localized positive residual electrostatic potential peak in the difference Fourier map close to the 6-ring of Cu-CHA at a distance of ~2.6 Å, see Figure 1. The occupancy of the copper cation is approximately 15-18%. Herein, we demonstrate the power and feasibility of 3D electron diffraction analyses for obtaining information about extra-framework cation locations in a zeolite.

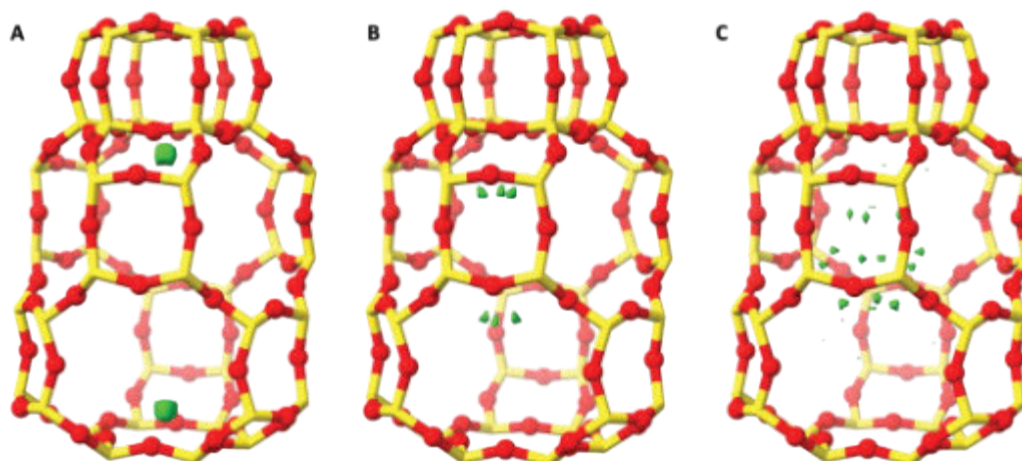


**Figure 1.** Comparison of positive electrostatic potential maps obtained at 5 $\sigma$ -level for (A) fresh Cu-CHA, (B) 4-h-aged Cu-CHA, (C) 16-h-aged Cu-CHA

### Acknowledgements

We acknowledge the Swedish Research Council for Sustainable Development, FORMAS 2022-01270 as well as the Knut & Alice Wallenberg Foundation



## Alcohol-to-hydrocarbons process – operando FT-IR and UV-vis spectroscopic studies emphasise the nature of coke species formed

K. A. Tarach\*, A. Walczyk, O. Rogala, A. Kordek, A. Olszewska, and K. Góra-Marek  
Faculty of Chemistry, Jagiellonian University in Kraków, Gronostajowa 2, 30-387 Krakow, Poland  
[karolina.tarach@uj.edu.pl](mailto:karolina.tarach@uj.edu.pl)

### Introduction

The ethanol and methanol conversion processes were performed over protonic SSZ-13 zeolite in advanced FT-IR and UV-vis *operando* spectroscopic studies with simultaneous mass spectrometry and gas chromatography analysis of products. The spectroscopic investigation provided information on species formed on the surface of catalysts, while mass spectrometry and gas chromatography methods identified the desorbed products. The studies were also supported by spectroscopic, chromatographic, and thermogravimetric analysis of coke species formed over the catalyst's surface during alcohol conversion.

### Results and Discussion

The UV-vis (Figure 1) and FT-IR (Figure 2) spectra were gathered during *operando* studies of ethanol conversion (WHSV = 14 or 7 h<sup>-1</sup>) over the HSSZ-13 sample at 325 °C. During the first minutes of ethanol conversion over studied HSSZ-13 zeolite, it might be anticipated that neutral olefinic and aromatic species will be formed (the bands below 220 nm and at 254 nm). Further, alkyl-substituted cyclopentenyl cations are formed (band at 300 nm); for instance, the tetramethyl(n-propyl)cyclopentenyl cation is identified on H-MOR at 303 nm<sup>1</sup>. The alkyl-substituted cyclopentenyl cations are then transformed into neutral aromatics (a band at 274 nm) and alkyl-substituted benzenium ions (bands at 330 and 357 nm). Simultaneously, the naphthalenes are formed (410 nm band). Thus, it is concluded that species represented by the 300 nm band are crucial for the hydrocarbon pool (HCP) mechanism driving the formation of propylene and higher hydrocarbons. The HCP primarily forms propylene and C<sub>4+</sub> products, while ethylene is expected to be created from ethanol dehydration<sup>2</sup>. The changes in the selectivity of catalysts are also observed as trace signals on the mass spectrum where the C<sub>4+</sub> (m/z = 55 and 56). The zeolite forms C<sub>4+</sub> hydrocarbons at the beginning of the reaction course.

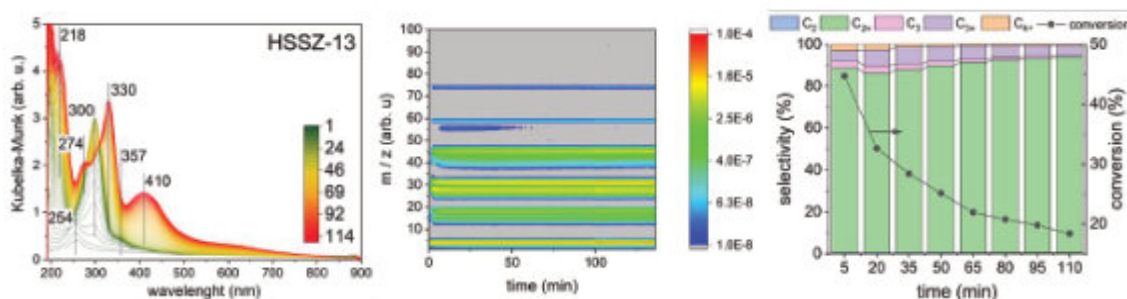


**Figure 1.** (Left) UV-vis spectra, (middle) mass spectrometry results and (right) gas chromatography selectivities and conversions collected during ethanol conversion over studied samples.

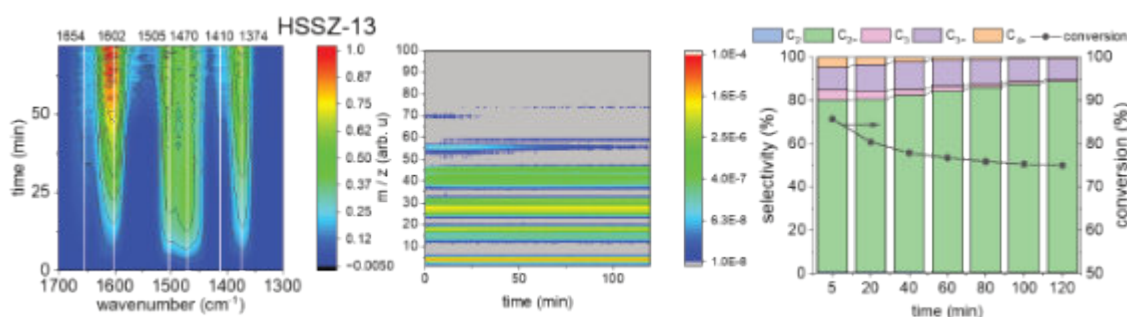


**Figure 2.** (Left) Top-down projection of FT-IR spectra, (middle) mass spectrometry results and (right) gas chromatography selectivities and conversions collected during ethanol conversion over HSSZ-13.

The FT-IR spectra (Figure 2) registered during ethanol conversion showed the extensive formation of species involved in HCP in chabazite cages. This is confirmed by the instant evolution of propylene and C<sub>4+</sub> hydrocarbons after contacting the HSSZ-13 catalyst with ethanol. The bands at 1602 and 1617 cm<sup>-1</sup> might be tentatively assigned to

aromatic species as highly methylated (ethylated) benzenium cations. The observed fragmentation ion of  $m/z = 70$  might originate from the divinyl ether formed over the acid sites of HSSZ-13 in trace amounts during the first 25 minutes of the reaction. The observed band at  $1505\text{ cm}^{-1}$  was identified in the methanol-to-hydrocarbon process as alkyl-substituted cyclopentenyl cations<sup>1,3</sup>. The GC-MS results (Figure 3) of extracted coke analysis demonstrate that a low feed amount ( $\text{WHSV} = 7\text{ h}^{-1}$ ) leads to the formation of more homogenous coke, with a dominant share of naphthalenes and alkyl-substituted naphthalenes. The coke species extracted from spent catalysts are more heterogeneous when the feed amount increases, resulting in a conversion drop. First, the higher relative share of alkyl-substituted naphthalenes is found in both catalysts. Similarly, tri- and tetraalkyl-substituted benzenes increase in relative content.

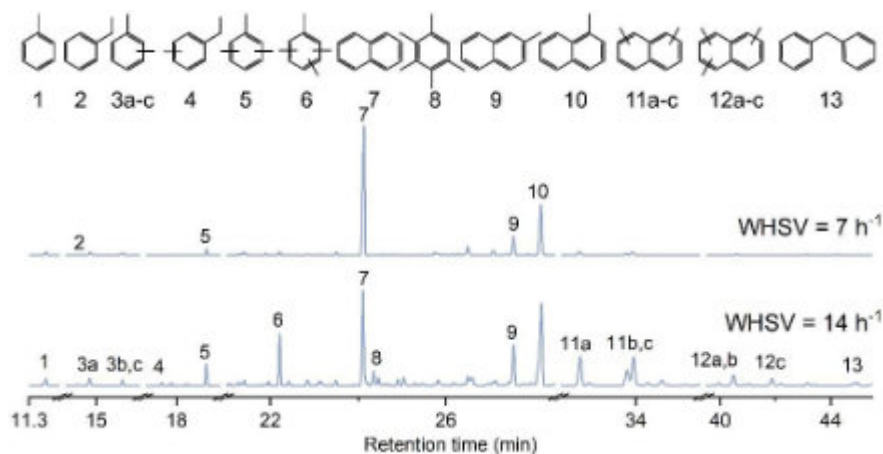


**Figure 3.** GC-MS analysis of coke extracted from spent catalysts after *operando* FT-IR ( $\text{WHSV} = 7\text{ h}^{-1}$ ) and UV-vis ( $\text{WHSV} = 14\text{ h}^{-1}$ ) studies.

#### Acknowledgement

The work was financed by Grant No 2020/37/B/ST4/01215 from the National Science Centre, Poland.

#### References

1. M.J. Wulfers, F.C. Jentoft, ACS Catalysis, 4 (2014) 3521-3532.
2. S. Zeng, W. Zhang, J. Li, S. Lin, S. Xu, Y. Wei, Z. Liu, Journal of Catalysis, 413 (2022) 517-526.
3. E.D. Hernandez, F.C. Jentoft, ACS Catalysis, 10 (2020) 5764-5782.





## Toolkit for the Characterization of Nanoporous Zeolites and MOFs Using Gas Sorption

**O. Maulik<sup>2</sup>, E. Turrini<sup>2</sup>, K. Struckhoff<sup>1</sup>**

<sup>1</sup> Anton Paar Quantatec, 1900 Corporate Dr., Boynton Beach, FL USA

<sup>2</sup> Anton Paar GmbH, Anton-Paar-Strasse 20, Graz, Austria

katie.struckhoff@anton-paar.com

Gas sorption is well-suited for the structural characterization of zeolites and MOFs because it assesses a wide range of pore sizes, spanning the entire micro- and mesopore size range. Determining properties such as surface area, pore size, and pore volume are critical to understand the material's structure and correlate that to applications. In addition to the structural characterization, gas sorption of vapors and gas sorption at high pressures can be used to evaluate a material under real application conditions. Here, a toolkit of recommended experimental and state-of-the-art data reduction methods for a comprehensive characterization of these nanoporous materials is proposed and includes:

Argon (87 K) adsorption: because of the polar nature of the nitrogen molecule, it is clear (and recommended by IUPAC) that polar materials, such as zeolites and MOFs, can only be accurately characterized using an adsorptive such as argon (87 K) [1-2].

NLDFT methods for pore size and volume distribution: NLDFT methods, which accurately describe the mechanism of adsorption and desorption and the pore geometry, are shown to be more accurate than classical methods such as SF or BJH and allow one to obtain a complete micro- and mesopore size distribution using one method [3].

Multi-temperature measurements: to understand the strength of the interaction between the gas of interest and the material, measurements can be performed at different temperatures simultaneously and the heat of adsorption can be calculated from the data.

Vapor sorption: applications of zeolites and MOFs may take place in humid applications. The water (or other vapors) sorption isotherms measured on these materials can indicate the stability of the material under these operating conditions.

High pressure sorption: for gas storage and separation applications, porous materials are excellent candidates as their properties can be tailored for certain gases at dedicated temperatures. High pressure gas sorption isotherms are measured to assess the material's behaviour under real conditions.

For each gas sorption tool, relevant examples of zeolites and MOFs will be shown and discussed.

### References

- [1] M. Thommes, K. Kaneko, A.V. Neimark, J.P. Olivier, F. Rodriguez-Reinoso, J. Rouquerol, and K.S.W. Singh, *Pure Appl. Chem.*, **87**, 1051 (2015)
- [2] K.A. Cychosz, R. Guillet-Nicolas, J. Garcia-Martinez, and M. Thommes, *Chem. Soc. Rev.*, **46**, 389 (2017)
- [3] J. Landers, G.Y. Gor, A.V. Neimark, *Coll. Surf. A*, **3**, 437 (2013)



## Tuning the aluminum distribution and acidity of ZSM-5 zeolites through mineralizing agents and electrostatic interactions

S. Al-Nahari<sup>1</sup>, C. Cammarano<sup>1</sup>, E. Dib<sup>2</sup>, D. Massiot<sup>2</sup>, V. Sarou-Kanian<sup>2</sup>, B. Alonso<sup>1</sup>

<sup>1</sup> ICGM, Université de Montpellier, CNRS, ENSCM, 34293 Montpellier cedex 5, France

<sup>2</sup> CNRS, CEMHTI UPR3079, Univ. Orléans, 45071 Orléans cedex 2, France

bruno.alonso@enscm.fr

Intensive research on improving the catalytic properties of zeolites is focused on modulating their acidity and the distribution of associated Al sites. Owing to the crucial role of acidity in heterogeneous catalysis, much effort is devoted to control the reactivity and selectivity of zeolites through the variation of Brønsted acid sites distribution [1,2].

During zeolite formation, the interplay between negative and positive charges in the growing framework has a considerable effect on the zeolite phase selectivity and stability. The charge distribution, and the related electrostatic interactions, are expected to determine the distribution of negatively charged aluminum tetrahedra in the frameworks of zeolites, responsible for Brønsted acidity. These charges are brought by (i) the forming elements sources (Si, Al), (ii) the organic or inorganic cations acting as structure directing agents (SDAs), and (iii) the mineralizing agents (F<sup>-</sup> or OH<sup>-</sup>) used in hydrothermal syntheses. In this sense, one of the current strategies to tune Al sites distribution is based on the variations in positively charged SDAs. For instance, this strategy has been proposed for ZSM-5, one of the widely used zeolites in industrial catalytic applications [3], following different approaches [4-9].

An alternative strategy, presented here, is to exploit the mineralizing agents as a possible means to tune Brønsted acid sites distribution [10]. When the amount of negatively charged Al tetrahedra in the zeolite is below that of the positive charges brought by the SDAs, the electrical neutrality is insured by negative charges coming from the mineralizing agents employed. It has been observed that using F<sup>-</sup> anions as mineralizing agents and varying the Si/Al molar ratio affect the Al sites distribution of ZSM-5 [11,12]. However, this behavior remained unexplained.

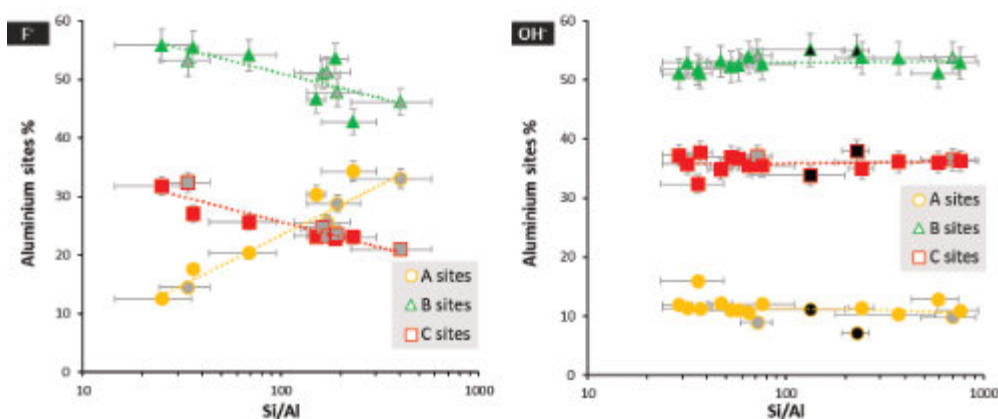


**Figure 1.** Variations in Al sites distributions probed by <sup>27</sup>Al NMR.

Herein, by studying a series of ZSM-5 zeolites over a broad range of Al content, we demonstrate how the nature of the mineralizing agent (F<sup>-</sup> or OH<sup>-</sup>) used in syntheses directly impacts Al sites distribution. The proportions of Al sites, probed by <sup>27</sup>Al 1D and 2D MQ-MAS NMR, depend on the Si/Al ratio for F<sup>-</sup>, but remain identical for OH<sup>-</sup> (from Si/Al=30 to 760, **Figure 1**). This leads to contrasting variations in weak and strong acidities probed by NH<sub>3</sub>-TPD. Such opposite effect of mineralizers is explained by the spatial location of negative charges and the resulting balance between short- and long-range electrostatic interactions. Preferential Al siting positions can be defined by strong short-range interactions between negatively charged framework areas and positively charged OSDA. This determines a distribution of Al sites that is identical at Si/Al close to 23 (one Al per OSDA) whatever the mineralizing anions. For higher Si/Al values, the other negative compensating charges might tune (F<sup>-</sup>) or not (silanols) the Al distribution. Our conclusion is supported by new solid-state <sup>1</sup>H and <sup>27</sup>Al NMR data obtained at various magnetic fields (up to 20 T) and MAS frequencies (up to 100 kHz). This understanding paves the way for additional and simple opportunities to control zeolites' acidity. Possible extensions of this work will also be presented.



## References

- [1] J. Dedecek, Z. Sobalik, and B. Wichterlova, *Catal. Rev.*, **54**, 135 (2012).
- [2] B.C. Knott, C.T. Nimlos, D.J. Robichaud, M.R. Nimlos, S. Kim, and R. Gounder, *ACS Catal.*, **8**, 770 (2018).
- [3] B. Yilmaz, and U. Müller, *Top. Catal.*, **52**, 888 (2009).
- [4] S. Sklenak, J. Dedecek, C.B. Li, B. Wichterlova, V. Gabova, M. Sierka, and J. Sauer, *Angew. Chem. Int. Ed.*, **46**, 7286 (2007).
- [5] J. Dedecek, V. Balgová, V. Pashkova, P. Klein, and B. Wichterlová, *Chem. Mater.*, **24**, 3231 (2012).
- [6] T. Yokoi, H. Mochizuki, S. Namba, J.N. Kondo, and T. Tatsumi, *J. Phys. Chem. C*, **119**, 15303 (2015).
- [7] T. Yokoi, H. Mochizuki, T. Biligetu, Y. Wang, and T. Tatsumi, *Chem. Lett.*, **46**, 798 (2017).
- [8] A. Chawla, R. Li, R. Jain, R.J. Clark, J.G. Sutjianto, J.C. Palmer, and J.D. Rimer, *Mol. Syst. Des. Eng.*, **3**, 159 (2018).
- [9] C.T. Nimlos, A.J. Hoffman, Y.G. Hur, B.J. Lee, J.R. Dilorio, D.D. Hibbitts, and R. Gounder, *Chem. Mater.*, **32**, 9277 (2020).
- [10] S. Al-Nahari, E. Dib, C. Cammarano, E. Saint-Germes, D. Massiot, V. Sarou-Kanian, and B. Alonso, *Angew. Chem. Int. Ed.*, **62**, e202217992 (2023).
- [11] O.H. Han, C.S. Kim, and S.B. Hong, *Angew. Chem. Int. Ed.*, **41**, 469 (2002).
- [12] E. Dib, T. Mineva, P. Gaveau, E. Véron, V. Sarou-Kanian, F. Fayon, and B. Alonso, *J. Phys. Chem. C*, **121**, 15831 (2017).

## Acknowledgments

The CNRS and the French National Research Agency (ANR) are acknowledged for financial support. The French research facility Infranalytics (FR-2054) is acknowledged for the access to a high magnetic field (20 T). We gratefully thank F. Fayon, P. Florian and P. Gaveau for their discussions and help in solid-state NMR. G. Delahay and C. Biolley are acknowledged for their implication in TPD analyses.



## Automated Transition State Finding in Zeolites through High-Throughput Visual Screening

P. Ferri-Vicedo<sup>1</sup>, A. J. Hoffman<sup>1</sup>, A. Singhal<sup>1</sup>, R. Gomez-Bombarelli<sup>1</sup>

<sup>1</sup> Massachusetts Institute of Technology, Department of Materials Science and Engineering, Cambridge, MA, 02139, USA  
paufv@mit.edu

The automation of chemical reaction discovery is a major challenge in computational chemistry. To identify thermodynamically and kinetically viable reactions, it is essential to understand the potential energy surface (PES), which involves pinpointing reactants, products, intermediates, and transition states (TSs). TS identification is critical for understanding reaction mechanisms but remains a computationally demanding task, especially for larger or more complex reaction networks. Traditional TS searches often rely on chemical intuition, making the process time-consuming and non-systematic. [1] Automated TS identification methods are broadly divided into single-ended and double-ended approaches. Single-ended methods explore unknown pathways without prior knowledge of the products, while double-ended approaches, which use information from both reactants and products, face limitations in multi-step reactions due to the exponential increase in complexity with additional intermediates. Recent advances have sought to automate this process for gas-phase reactions, addressing challenges such as the extensive conformational sampling required for flexible systems and the complexity of multi-step reactions. Automated approaches streamline the TS search process by combining graph-driven algorithms with quantum chemical calculations, allowing for efficient exploration of potential energy surfaces. Machine learning has further enhanced this process by predicting likely TS structures and guiding searches, particularly in complex catalytic systems where manual exploration is infeasible. However, TS identification becomes even more complex in solid structures like zeolites compared to gas-phase systems, that is why there has not been developed any TS automatization approach for heterogeneous catalysts yet. Zeolites are microporous materials composed of SiO<sub>4</sub> and AlO<sub>4</sub> tetrahedra, with uniform pore structures that enable selective adsorption and catalysis. The negative charges from aluminium, balanced by protons or cations, make zeolites highly effective solid acid catalysts, used in environmental applications such as gas purification and wastewater treatment. These systems pose computational challenges due to periodic boundary conditions, larger system sizes increase computational cost, and strong interactions between the TS and the solid catalyst, alter reaction pathways and energy landscapes, which complicate the PES and TS location.

In this study we developed a computational pipeline for automated TS finding in zeolites with high-throughput virtual screening that adapts vibrational modes from gas-phase TSs to periodic systems, enabling accurate modelling of catalytic processes in materials like zeolites with Density Functional Theory (DFT). This method ensures that gas-phase vibrational characteristics are appropriately transferred to solid-phase systems. The computational pipeline starts from a SMILES string to represent molecules, generating conformers with RDKit and optimizing them with GFN-xTB, followed by DFT refinement in ORCA. Then, reactions are explored using SMARTS for reactive site identification, and transition states are found through eigenvector-following methods. The negative vibrational mode from gas-phase transition states corresponding to the bond forming/breaking frequency is then translated to periodic systems by aligning geometries using a rotation matrix and singular value decomposition (SVD), ensuring proper alignment of vibrational displacements. In order to connect gas phase molecules to periodic crystal lattices, zeolite-minimum and transition-state structures were docked into the zeolite framework using the Voronoi Organic-Inorganic Docker (VOID) package. [2] In this case, a modified Monte Carlo algorithm was used in order to achieve more realistic reactivity poses. The modification introduced ensured that the docked cationic atom was positioned in a range of 2.5-3.5 Å from an active zeolite acid site allowing to run later periodic DFT simulations close to the most stable poses along zeolite channels and pores. Finally, the docked minimum structures and TS structures from the gas phase are refined at the DFT-D3 level inside the zeolite pores. For TS structures the DIMER method implemented in VASP was used with the guess mode vector imported from the gas phase and adapted to the crystal lattice to guide transition state searches in a solid-state environment.

Using this high-throughput pipeline we studied 136 gas-phase transition states (TSs) from various chemical reactions. For ethylbenzene transalkylation we identified 92 TS corresponding to all the possible combinations of ortho-, meta- and para-diethylbenzene (DEB) with benzene or another ortho-, meta-, para-diethylbenzene molecule. Regarding to alkene cracking, the formation of C8<sup>+</sup> and C9<sup>+</sup> species was studied with 1-butene, 2-butene, isobutene and 1-pentene reacting with 2-butyl, 3-methyl-2-butyl and 3-pentyl cations. In addition, hydrogen shift rearrangements along the C8<sup>+</sup> and C9<sup>+</sup> species were also studied forming a total of 22 TS. Finally, the ring contraction of cationic cycloalkanes with different methylation degrees and charge positioning was also studied through 22 TS. See Fig 1 for more detail.

The ethylbenzene transalkylation gas phase TS structures identified in the gas phase were docked into FAU (12x12x12), BOG (12x10), IWV (12x12) and UTL (14x12) zeolite topologies meanwhile the alkene cracking and ring contraction gas-phase TS structures were docked into the “big five” zeolite topologies, BEA (12x12x12), FAU (12x12x12), FER (10x8), MFI (10) and MOR (12x8). For each zeolite topology different aluminium positions were selected, the diverse positioning of the Al sites located either in the intersections or within the channels, allowed for

a comprehensive evaluation of how structural differences in the zeolite frameworks influence the identification of TSs and reaction outcomes. In total, this selection led to 1031 TS finding DIMER calculations launched through the automated high-throughput computational pipeline.

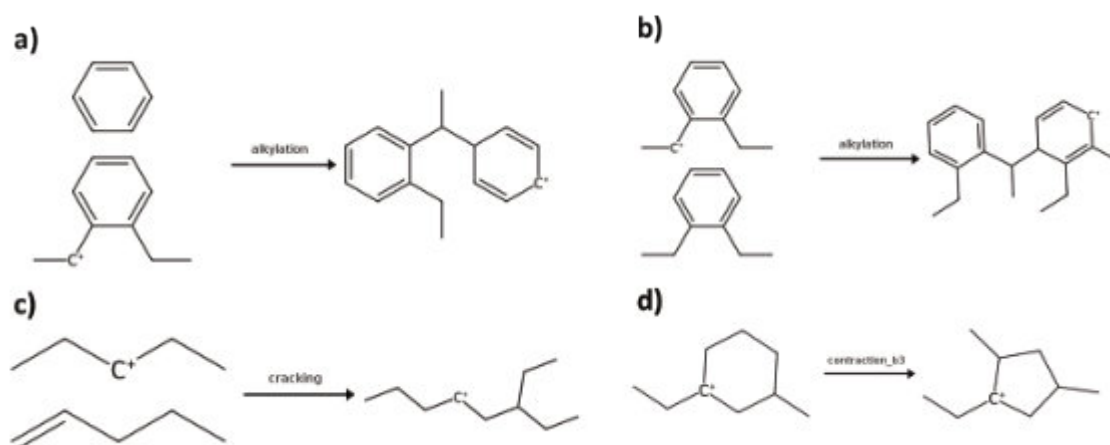


**Figure 1.** Reactions studied **a)** Diethylbenzene transalkylation **b)** Diethylbenzene disproportionation **c)** alkene cracking **d)** ring contraction.

Early results showcased a success ration slightly over 50% for TS identification in the diarylic reaction mechanism for ethylbenzene transalkylation. The activation energies ( $E_a$ ) obtained from the 291 TS identified allowed us to characterize full mechanistic pathways in different zeolites (see **Fig 2a**) achieving results comparable with prior studied for these reaction [3] were zeolites with broader channels and pores, UTL and FAU, are less effective in promoting transalkylation, DEB + Benzene yielding two ethylbenzene molecules (see **Fig 1a**), and hindering disproportionation, DEB + DEB yielding triethylbenzene as a product (see **Fig 1b**), than zeolites with narrower channels as BOG and IWV (see **Fig 2b**). [3] On top of these results, the use of high-throughput virtual screening has allowed to introduce all the possible isomer combinations of DEB which multiplies three times the previous results reported for just para-DEB transalkylation and nine times the ones for disproportionation where only para and para-DEB + meta-DEB isomers were studied.

Results for alkene cracking and ring contraction have not been processed yet with enough volume to withdraw relevant conclusions from them.

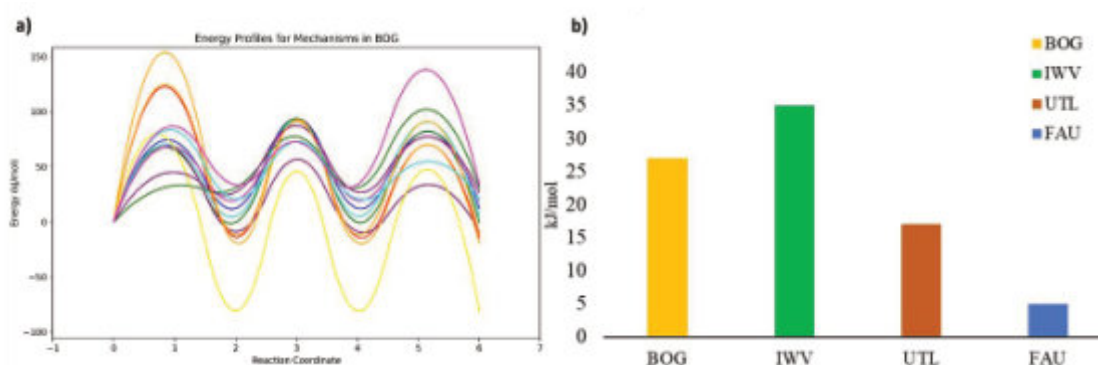


**Figure 2.** **a)** Reaction paths obtained for ... **b)** Average  $E_a$  increase for DEB disproportionation reaction vs DEB transalkylation in each topology.

## References

- [1] T. A. Young, J. J. Silcock, A. J. Sterling, and F. Duarte, "autodE: Automated calculation of reaction energy profiles—Application to organic and organometallic reactions," *Angew. Chem., Int. Ed.* 60, 4266 – 4274 (2021).
- [2] Daniel Schwalbe-Koda *et al.*, A priori control of zeolite phase competition and intergrowth with high-throughput simulations. *Science* 374, 308-315 (2021). DOI:10.1126/science.abh3350
- [3] Ferri, P., Li, C., Schwalbe-Koda, D. et al. Approaching enzymatic catalysis with zeolites or how to select one reaction mechanism competing with others. *Nat Commun* 14, 2878 (2023). <https://doi.org/10.1038/s41467-023-38544-z>



## Advancing highly selective low-temperature ammonia oxidation: Hydrophobic silicalite-1 shell confining silver nanoparticles on Cu/ZSM-5 core

Xiaoxin Chen<sup>1</sup>, Guoju Yang<sup>1</sup>

<sup>1</sup> State Key Laboratory of Inorganic Synthesis and Preparative Chemistry, College of Chemistry, Jilin University, 2699 Qianjin Street, Changchun 130012, P. R. China  
chenxiaoxin@jlu.edu.cn

The pungent gas NH<sub>3</sub> slipped from a reductant for the selective catalytic reduction of NO<sub>x</sub> poses environmental and human health concerns. Amongst the diverse treatment techniques developed to tackle NH<sub>3</sub> slip, the selective catalytic oxidation of NH<sub>3</sub> into benign nitrogen and water (NH<sub>3</sub>-SCO) is a highly promising process to eliminate gaseous ammonia, due to its technical and economic advantages. [1]

Zeolites possess superior hydrothermal stability, adjustable acidity/basicity, and excellent ion-exchange properties [2], which are more feasible for supporting metal species and thereafter are more suitable for high temperature or moisture reactions, e.g., the NH<sub>3</sub>-SCO reaction. Thus, zeolites have been widely applied to support metal species to regulate their stability, dispersion, as well as structural and electronic properties, thereby promoting their catalytic performance in NH<sub>3</sub>-SCO reactions [2-3]. The supported metal species generally fall into the categories of noble metals and transition metals. Transition metals exhibit robust N<sub>2</sub> selectivity but necessitate significantly higher operating temperatures (mostly higher than 300 °C). In contrast, noble metals generally display heightened activity at lower temperatures (~200 °C); however, their widespread use is limited by their high cost and relatively reduced N<sub>2</sub> selectivity. Of the various noble metals, Ag-based catalysts are of particular interest due to the semi-noble nature of Ag, which renders good catalytic activity at relatively low temperatures and is more cost-effective than noble metals-based catalysts (Pt, Au, etc.). However, the low selectivity toward N<sub>2</sub> has hindered the broader application of the Ag-based catalysts. Therefore, achieving high low-temperature activity and high N<sub>2</sub> selectivity in Ag-based catalysts is highly desirable.

In this work, a judiciously devised core-shell NH<sub>3</sub>-SCO catalyst featuring a Cu/ZSM-5 core enveloped by an Ag/silicalite-1 shell (Cu/ZSM-5@Ag/S-1) was rationally constructed [4]. Integrating the silicalite-1 shell effectively suppresses the migration of Ag into Cu/ZSM-5 core, conserving the active Cu<sup>2+</sup> sites for the catalytical conversion of byproducts NO<sub>x</sub>. Concurrently, the shell averts the formation of positively charged Ag species, facilitating the generation of abundant Ag<sub>0</sub> nanoparticles encapsulated in the S-1 shell. Comprehensive characterizations reveal abundant Ag<sub>0</sub> species within the core-shell Cu/ZSM-5@Ag/S-1 catalyst, boosting O<sub>2</sub> activation and NH<sub>3</sub> dehydrogenation and thereby contributing to superior low-temperature activity in NH<sub>3</sub>-SCO reactions. Furthermore, the hydrophobic S-1 shell effectively reinforces the hydrothermal stability of the core-shell Cu/ZSM-5@Ag/S-1. This work provides valuable insight into the design of bifunctional catalysts by constructing a core-shell structure zeolite.

### References

- [1] T. Lan, Y. Zhao, J. Deng, J. Zhang, L. Shi, D. Zhang, *Catal. Sci., Technol.* **10**, 5792–5810 (2020).
- [2] Z. Qiu, G. Yang, L. Li, S. Peng, M. Nan, J. Zhang, L. Li, Y. Hou, X. Chen, *Appl. Surf. Sci.*, **598**, 153856 (2022).
- [3] T. Zhang, H. Chang, Y. You, C. Shi, J. Li, *Environ. Sci. Technol.*, **52**, 4802–4808 (2018).
- [4] X. Chen, Z. Qiu, X. Wang, Y. Li, C. Hou, L. Li, J. Zhang, M. Nan, G. Yang, *Chem. Eng. J.*, **493**, 152605 (2024).

## ZMQ-1: A stable 28-membered ring three-dimensional aluminosilicate zeolite

M. Fahda,<sup>1</sup> Y. Sun,<sup>2</sup> P. Lu,<sup>2\*</sup> V. Valtchev<sup>1,2\*</sup>

<sup>1</sup> Laboratoire Catalyse et Spectrochimie (LCS), Normandie Université, ENSICAEN, UNICAEN, CNRS, Caen 14050, France

<sup>2</sup> The ZeoMat Group, Qingdao Institute of Bioenergy and Bioprocess Technology, CAS, Laoshan District, CN-266101 Qingdao, China

[mohammad.fahda@ensicaen.fr](mailto:mohammad.fahda@ensicaen.fr)

Since the introduction of zeolites for various industrial applications, the quest to bridge the gap between microporous and mesoporous materials has been ongoing. This is of paramount interest in expanding the functional limits of microporous materials to process bulky molecules whose kinetic diameters exceed the pore openings of 12-membered ring (12-MR) zeolites. The discovery of ordered mesoporous materials marked a significant step towards this goal; however, their amorphous nature, limited hydrothermal stability, and weak acidic strength have fallen short of industrial requirements [1]. While several extra-large pore zeolites have been identified, only two, ITQ-37 [2] and ITQ-43 [3], have achieved the 2 nm pore opening threshold to bridge the micro/mesoporous divide. However, these germanosilicate materials suffer from poor hydrothermal stability and insufficient aluminum content, limiting their industrial applicability. Herein, we report for the first time in zeolite history the discovery of a stable meso/microporous aluminosilicate zeolite, ZMQ-1 (Zeolitic Materials, Qingdao Institute of Bioenergy and Bioprocess Technology, No.1) [4,5]. This material features a fully connected three-dimensional framework with intersecting 28- and 10-membered ring channels, where the cross-sectional diameter of the 28-MR is 22.76 Å x 11.83 Å. In this work, we discuss the structural features and the investigation of the physicochemical properties of ZMQ-1, including *in situ* FTIR spectroscopy, solid-state NMR, and argon adsorption, among others. Furthermore, its catalytic performance in vacuum gas oil cracking is compared to other molecular sieve catalysts.

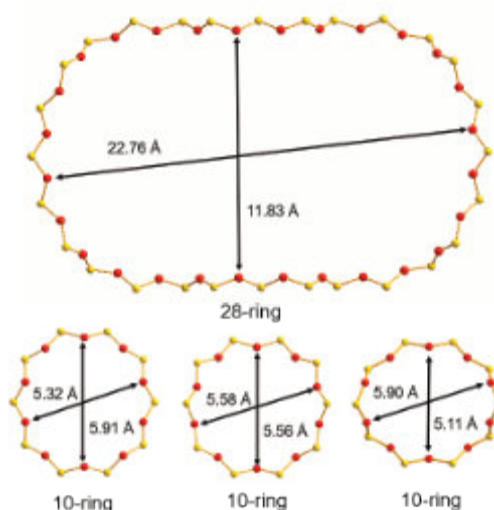


**Figure 1.** A schematic depiction of the 28- and 10-membered rings in ZMQ-1, along with their cross-sectional dimensions.

### References

- [1] Ciesla, U., & Schüth, F. (1999). Ordered mesoporous materials. *Microporous and mesoporous materials*, 27(2-3), 131-149.
- [2] Sun, J., Bonneau, C., Cantín, Á., Corma, A., Diaz-Cabanas, M.J., Moliner, M., Zhang, D., Li, M. and Zou, X., 2009. The ITQ-37 mesoporous chiral zeolite. *Nature*, 458(7242), pp.1154-1157.
- [3] Jiang, J., Jorda, J.L., Yu, J., Baumes, L.A., Mugnaioli, E., Diaz-Cabanas, M.J., Kolb, U. and Corma, A., 2011. Synthesis and structure determination of the hierarchical meso-microporous zeolite ITQ-43. *Science*, 333(6046), pp.1131-1134.
- [4] V. Valtchev, P. Lu, Y. Sun, Yang, Q. Lang, Novel silicate zeolite ZMQ-1 and application thereof, Luxembourg Patent Application LU508038, 2024
- [5] Lu, P., Xu, J., Sun, Y., Guillet-Nicolas, R., Willhammar, T., Fahda, M., Dib, E., Wang, Bo., Qin, Z., Xu, H., Liu, Z., Yu, H., Yang, X., Lang, Q., Mintova, S., Zou, X., & Valtchev, V. (2024). A stable zeolite with atomically ordered and interconnected mesopore channel. *Nature*, under revision



## On the phase selection in zeolite synthesis

**A. Palčić<sup>1\*</sup>, S. Bosnar<sup>1</sup>, M. Jurin<sup>1,2</sup>, N. Jakupec<sup>1</sup>**

<sup>1</sup> Laboratory for Synthesis of New Materials, Division of Materials Chemistry, Ruđer Bošković Institute, Bijenička cesta 54, 10000 Zagreb, Croatia

<sup>2</sup> Laboratory for Chemical Analytics, Institute for Anthropological Research, Gajeva ulica 32, 10000 Zagreb, Croatia  
ana.palcic@irb.hr

Although mechanochemistry is emerging as a green synthesis tool that provides unprecedented control over chemical, particularly organic, reactions, its application in zeolite synthesis typically involves hydrothermal treatment following the milling treatment. Indeed, introduction of mechanochemical methods in zeolite preparation processes offered novel opportunities in control over the material's properties and potentially reducing synthesis time. It has been demonstrated that ball milling alters the physicochemical properties of zeolites by changing their size, morphology, and crystallinity, often leading to the formation of an X-ray amorphous phase [1]. The time required for complete amorphization varies depending on the zeolite framework and cations present in the material's exchange sites. This knowledge has been applied to shorten zeolite synthesis times by using tribochemical treatment of crystal seeds and precursors [2]. Furthermore, combining bead milling and post-milling recrystallization has successfully produced highly crystalline nanosized zeolites [3]. Likewise, ball milling may facilitate the incorporation of heteroatoms into the zeolite lattice [4]. However, recent reports suggest that combining mechanochemistry with external heat sources can result in zeolite transformations, offering new prospects for designing zeolite materials [5].

This study investigates the effect of mechanochemical treatment on FAU- and HEU-type zeolite materials under different conditions, including variations in milling temperature and the use of certain amounts of water and seeds. A series of experiments were conducted using high-energy mixer mills at temperatures ranging from 90 °C to 130 °C, with and without the addition of seeds or water. *in situ* synchrotron X-ray diffraction and *ex situ* experiments revealed phase changes during milling, with new phases forming rather rapidly, sometimes within five minutes

The collected results highlight the impact of mechanochemical treatment on zeolite phase selectivity and the role of reaction temperature, seeds and water in modulating the reaction. Mechanochemistry proves to be an effective tool for producing a range of zeolite phases offering potential benefits for industrial applications. This study also presents the real-time monitoring of zeolite thermomechanochemical processes, providing valuable insights into zeolite formation pathways as well as guidelines for further application of mechanochemistry in zeolite processing.

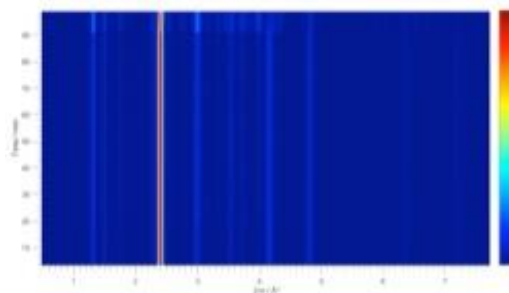


**Figure 1.** *in situ* synchrotron powder X-ray diffraction patterns taken during the milling of natural zeolite clinoptilolite with NaOH at 30 Hz, 110 °C for 90 minutes.

### References

- [1] C. Kosanović, A. Čižmek, B. Subotić, I. Šmit, M. Stubičar and A. Tonejc, *Zeolites*, **15**, 51 (1995).
- [2] V. Valtchev, S. Mintova, V. Dimov, A. Toneva and D. Radev, *Zeolites*, **15**, 193 (1995).
- [3] T. Wakihara, A. Ihara, S. Inagaki, J. Tatami, K. Sato, K. Komeya, T. Meguro, Y. Kubota and A. Nakahira, *Cryst. Growth Des.*, **11**, 6163 (2011).
- [4] K. Kanie, M. Sakaguchi, F. Muto, M. Horie, M. Nakaya, T. Yokoi and A. Muramatsu, *Sci. Technol. Adv. Mater.*, **19**, 545 (2018).
- [5] N. Jakupec, K.-J. Ardilla Fierro, V. Martinez, I. Halasz, J. Volavšek, G. Algara-Siller, M. Etter, V. Valtchev, K. Užarević and A. Palčić, *ACS Sust. Chem. Eng.*, **12**, 5220 (2024).

### Acknowledgments

Croatian Science Foundation is acknowledged for funding this research, project ID: UIP-2019-04-4977.





## Zr-based Metal-Organic Frameworks and SBA-15 mesoporous silica: a synergistic approach for catalysis in the production of bio-jet fuel

M. Sanz<sup>1</sup>, P. Leo<sup>1</sup>, M. Paniagua<sup>1</sup>, G. Morales<sup>1,2</sup>, J. A. Melero<sup>1,2</sup>

<sup>1</sup> Chemical and Environmental Engineering Group (GIQA), Universidad Rey Juan Carlos, C/ Tulipán s/n, 28933, Móstoles, Spain.

<sup>2</sup> Instituto de Investigación de Tecnologías para la Sostenibilidad (ITPS) Universidad Rey Juan Carlos, C/ Tulipán s/n, 28933, Móstoles, Spain.

pedro.leo@urjc.es

The chemical conversion of biomass-derived platform molecules like furfural or levulinic acid into molecules suitable for the production of Sustainable Aviation Fuel (SAF) is receiving increasing attention [1]. In order to obtain the components of a typical Jet A1 fuel blend from these platform molecules, it is necessary to perform C-C coupling reactions followed by hydrodeoxygenation (HDO) to achieve the proper jet-fuel range hydrocarbons. In this context, this work explores the first step of C-chain enlargement via aldol condensation between furfural and methyl isobutyl ketone (MIBK) to produce the corresponding C11 oxygenated adduct (herein denoted as FuMe), displaying a carbon-chain length adequate for jet-fuel formulation after a subsequent HDO process.

As catalyst for the aldol condensation, the use of Zr-modified MOF supported on mesoporous SBA-15 silica is proposed, since this kind of Zr-MOFs have been previously reported as highly efficient for this reaction, both in terms of activity and selectivity [2]. However, the small pore size and poor reusability of crystalline MOF materials limit their application to process bulky molecules like the C11 jet-fuel precursor herein considered. To overcome these drawbacks and enhance the catalytic activity, we present several Zr-MOF phases supported on mesoporous SBA-15 silica, synthesised following the *in-situ* method described by Rojas-Buzo et al [3]. In this strategy, a high dispersion of highly active Zr species can be achieved, potentially improving the catalytic activity as well as the stability of the active sites of the Zr-MOF phases.

Characterization and analytical approaches demonstrate that the catalytic performances of the prepared Zr-MOF/silica hybrid materials are superior to the corresponding free crystalline Zr-MOFs in the aldol condensation of furfural and MIBK to obtain FuMe, resulting not only in higher condensation activity but also in superior selectivity to the desired adduct (see Fig.1a vs Fig.1 b).

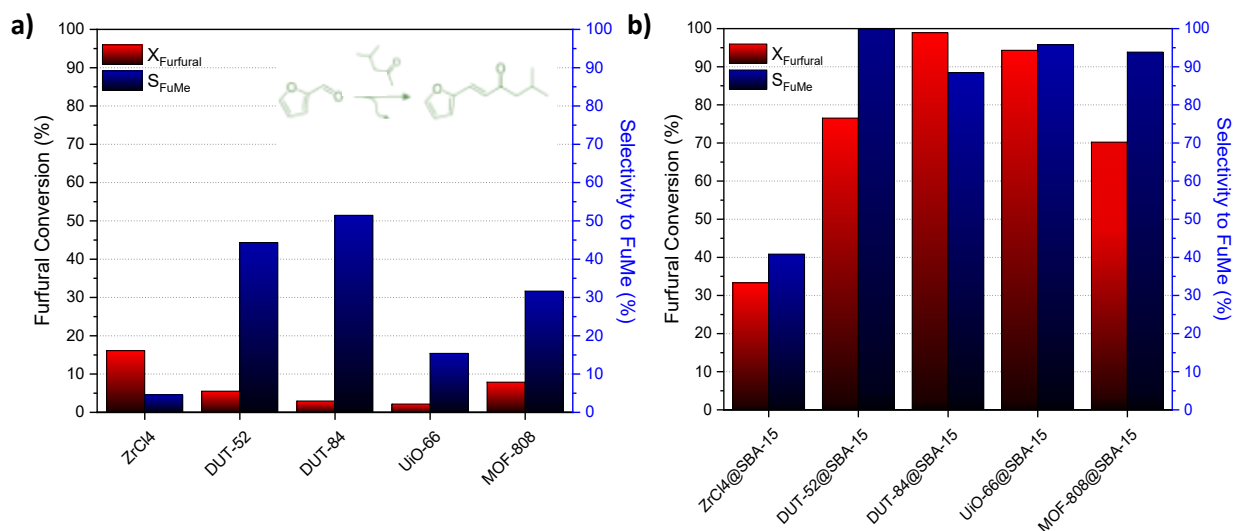


**Figure 1:** Catalytic performance of pure unsupported Zr-MOFs (a) and SBA-15-supported Zr-MOFs (b). Reaction conditions: 130 °C, 4 hours, FUR:Zr mass ratio = 75:1, MIBK:FUR ratio (mol/mol) = 4:1.

The impressive improvement in the catalytic behaviour is ascribed to a synergistic surface effect between the Zr active phase and the support, together with a high dispersion of the metal all over the silica surface. The remarkable textural properties typical of the SBA-15 silica support enable hybrid catalysts with high surface areas and large mesopore volumes (as shown in Table 1).

In addition to demonstrating enhanced catalytic activity, the synthesised materials have also exhibited improved stability during subsequent condensation processes.



**Table 1.** Physicochemical properties of parent silica, unsupported MOFs and SBA-15-supported Zr-MOFs.

Catalyst	Zr (wt%)	S <sub>BET</sub> (m <sup>2</sup> ·g <sup>-1</sup> )	S <sub>micropore</sub> (m <sup>2</sup> ·g <sup>-1</sup> )	S <sub>external</sub> (m <sup>2</sup> ·g <sup>-1</sup> )	V <sub>p</sub> (cm <sup>3</sup> ·g <sup>-1</sup> )
SBA-15	-	751	85	666	1.03
ZrCl <sub>4</sub> @SBA-15	7.11	539	73	466	0.79
DUT-52	27.9	1,471	1,324	147	0.61
DUT-52@SBA-15	5.7	573	109	464	0.76
DUT-84	35.0	549	436	113	0.26
DUT-84@SBA-15	6.1	553	68	485	0.77
UIO-66	32.9	1,324	1,216	108	0.53
UIO-66@SBA-15	4.1	727	134	593	1.02
MOF 808	44.8	1,036	888	148	0.74
MOF808@SBA-15	4.9	664	216	448	0.86

### References

- [1] M. Wang, R. Dewil, K. Maniatis, J. Wheeldon, T. Tan, J. Baeyens, Y. Fang, *Prog. Energ. Comb. Sci.*, **74**, 31-49 (2019).  
 [2] D. De la Flor, C. López-Aguado, M. Paniagua, G. Morales, R. Mariscal, J.A. Melero, *J. Catal*, **401**, 27–39 (2021).  
 [3] S. Rojas-Buzo, P. García-García, A. Corma, *Green Chem.*, **20**, 3081-3091 (2018).

### Acknowledgements

Financial support from the Spanish Ministry of Science and Innovation, through the project SAFADCAT (PID2021–122334OB-I00) is kindly acknowledged.



## Molecular Recognition-Induced Structural Flexibility in ZIFs

J. Farrando-Perez<sup>1</sup>, C. Carrillo-Carrión<sup>2</sup>, A. Missyl<sup>3</sup>, J. Silvestre-Albero<sup>1</sup>

<sup>1</sup> Advanced Materials Laboratory, Inorganic Chemistry Department, University of Alicante, Alicante, Spain

<sup>2</sup> Institute of Chemical Research (IIQ), CSIC-University of Seville, 41092 Seville, Spain

<sup>3</sup> CELLS-ALBA Synchrotron, Cerdanyola del Vallés, Spain

Joaquin.silvestre@ua.es

Removal of chemical contaminants (POP, CEC, PFOAs, etc.) in wastewater and air streams requires the design of novel adsorbents able to selectively retain/concentrate these pollutants with a high adsorption capacity. Activated carbons, zeolites, silicas, and metal-organic frameworks (MOFs) are among the most frequently used adsorbents to this end. Application of MOF materials offer significant advantages, e.g., porous structure and surface chemistry can be tailored to match specific applications, rendering them as highly versatile tools for adsorption processes.

Zeolitic imidazolate frameworks (ZIFs), a sub-class of MOFs, are characterized by a high specific surface area, a hydrophobic porous structure, a high chemical and thermal stability and, more importantly, a unique structural flexibility [1]. These structural changes/transformations upon an external stimulus (e.g., gas adsorption, heat treatment, high-pressure), include gate-opening phenomena, phase-to-phase transitions, breathing effects, and so on [2,3]. Interestingly, the nature of these phenomena highly depends on the nature of the imidazolate linker, including the presence of functional groups, i.e., depends on the competition between strong non-bonding interactions, which favor the formation of highly dense structures, and bonding interactions, which favor the formation of a high symmetry, low-density crystal structures. Furthermore, these intracrystalline interactions can be altered/modified, depending on the nature of the adsorbate molecules, thus opening the gate to unexplored adsorption phenomena in gas and liquid-phase processes. In this communication we will summarize some examples of structural changes in ZIFs (**Figure 1**), their sensitivity to the nature of the probe, and how the knowledge of the associated mechanism can be used to design porous materials able to outperform in a wide variety of applications

from gas storage/separation, to mechanical energy storage and liquid-phase selective separation processes [4,5].

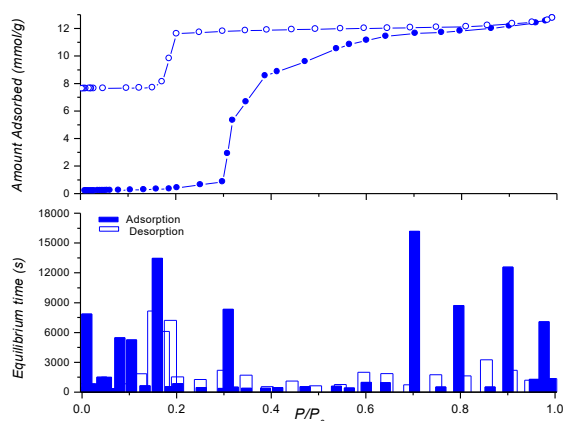


**Fig. 1.** N<sub>2</sub> adsorption/desorption isotherm for ZIF-7 at 77K (upper panel). Time requested to reach equilibrium for each of the adsorption and desorption points (lower panel).

### References

- [1] R.P. Lively, M.E. Dose, J.A. Thompson, B.A. McCool, R.R. Chance, W.J. Koros, *Chem. Commun.*, **2011**, 47, 8667.
- [2] M.E. Casco, Y.Q. Cheng, L.L. Daemen, D. Fairen-Jimenez, E.V. Ramos-Fernandez, A.J. Ramirez-Cuesta, J. Silvestre-Albero, *Chem. Commun.*, **2016**, 52, 3639.
- [3] J. Gandara-Loe, A. Missyl, F. Fauth, L.L. Daemen, Y.Q. Cheng, A. Ramirez-Cuesta, P.I. Ravikovitch, J. Silvestre-Albero, *J. Mater. Chem. A*, **2019**, 7, 14552.
- [4] J. Gandara-Loe, R. Bueno-Perez, A. Missyl, D. Fairen-Jimenez, J. Silvestre-Albero, *ACS Appl. Nano Mater.*, **2021**, 4, 3519.
- [5] E. Amayuelas, J. Farrando-Perez, A. Missyl, Y. Grosu, J. Silvestre-Albero, C. Carrillo-Carrión, *ACS Appl. Mater. Interf.*, **2024**, 16, 46374.

### Acknowledgements:

The authors acknowledge financial support from the MINECO (Projects PID2022-142960OB-C21 and PCI2020-111968/ERANET-M/3D-Photocat), Conselleria de Innovación, Universidades, Ciencia y Sociedad Digital (Project CIPROM/2021/022) and European Union: Horizon Europe (project MOST-H<sub>2</sub>; Grant agreement no. 101058547).



## Interaction of the anticancer drug 5-fluorouracil with Brönsted and Lewis acid sites: Insights from density functional theory

M. Fischer<sup>1</sup>

<sup>1</sup> Crystallography & Geomaterials Research, Faculty of Geosciences, University of Bremen, 28359 Bremen, Germany

<sup>2</sup> Bremen Center for Computational Materials Science and MAPEX Center for Materials and Processes, University of Bremen, 28359 Bremen, Germany

michael.fischer@uni-bremen.de

The interaction of zeolites with functional organic molecules, such as pharmaceuticals and personal care products (PPCPs), is not only of fundamental interest. Besides, a good understanding of these interactions may also pave the way towards new applications of zeolites in environmental remediation and healthcare. For example, high-silica zeolites have been proposed for the removal of PPCPs from wastewaters [1], and different types of zeolites have been investigated as carrier materials for drug delivery applications [2]. The anticancer drug 5-fluorouracil ( $C_4H_3FN_2O_2$ , IUPAC name 5-fluoro-1*H*-pyrimidine-2,4-dione, abbreviated 5-FU) is one of several molecules for which the potential usefulness of zeolites as host materials has been studied in a drug delivery context [3,4]. For example, Datt et al. investigated the adsorption of 5-FU in faujasite-type (FAU-type) zeolites having different Si/Al ratios as well as their release behaviour [3]. An analysis of the 5-FU@FAU composites using infrared (IR) and NMR spectroscopy pointed towards a preferential adsorption of 5-FU at the Lewis acidic extra-framework aluminium (EFAL) sites, however, no direct insights into the interaction could be obtained experimentally.

In this contribution, dispersion-corrected density functional theory (DFT) calculations are employed to investigate the interaction of 5-FU with different types of acid sites in FAU-type zeolites. To begin with, the adsorption of 5-FU in FAU models containing different local arrangements of framework protons (Brönsted acid sites) was considered [5]. It was observed that a simultaneous interaction of 5-FU with more than one framework proton (“multi-site” interaction, **Figure 1a**) results in a significant stabilisation of the adsorbed molecule compared to scenarios in which 5-FU interacts only with a single proton. While DFT-based ab initio molecular dynamics (AIMD) simulations confirmed the stability of these adsorption complexes in the absence of water (at room temperature), the presence of water molecules in the vicinity resulted in a displacement of 5-FU away from the acid sites during the AIMD simulation. This finding indicates that the exposure of 5-FU-loaded FAU samples to humidity could be a suitable strategy to trigger the release of the drug, for example, in the human body. DFT-predicted IR spectra of models in which 5-FU interacts with framework protons showed significant deviations from experimental spectra reported by Datt et al. [3], in accordance with their finding that the interaction with framework protons is not the dominant process in the experimentally studied samples.

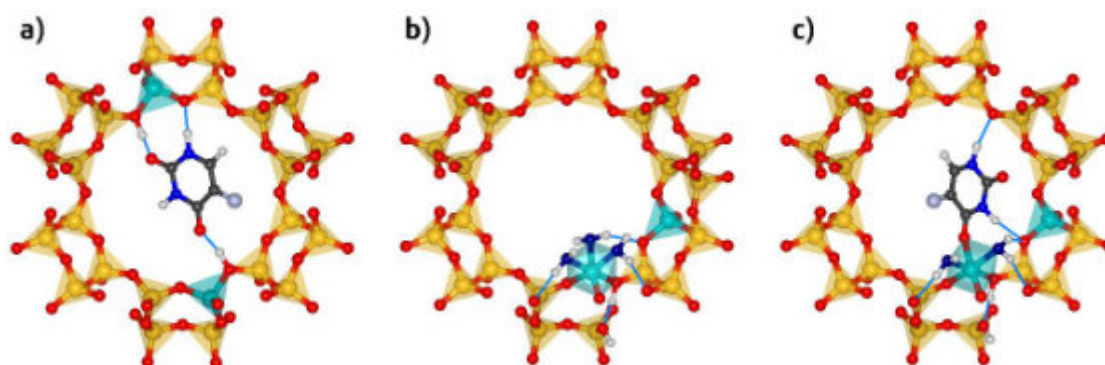


**Figure 1.** a) Typical adsorption complex of 5-FU in protonated FAU, b) model of framework-associated extra-framework aluminium site in FAU, c) adsorption complex of 5-FU interacting with EFAL site in FAU. Shown structures are DFT-optimised. For clarity, only the environment of one 12-membered ring is shown.

To compare the interaction of 5-FU (or any other guest molecules) with framework protons and with EFAL sites, a realistic atomistic model of the octahedrally coordinated EFAL sites is a first prerequisite. Such a model was constructed for FAU, using a recent DFT study of framework-associated octahedral EFAL sites in zeolites as starting point (**Figure 1b**) [6]. The stability of the local environment was studied with AIMD simulations, and it was found that one of the three  $H_2O$  molecules detaches from the Al site over the course of the simulation, resulting in the formation of trigonal-bipyramidal Al. However, the octahedrally coordinated environment can be stabilised by introducing additional water molecules that are hydrogen-bonded to the Al-coordinated  $H_2O$  molecules. In the next step, one of



the Al-coordinated H<sub>2</sub>O molecules was replaced by 5-FU, considering different possible positions and orientations. For the lowest-energy configuration, shown in **Figure 1 c**, the calculated adsorption energy  $E_{\text{ads}}$  amounts to  $-119$  kJ/mol, being considerably less negative than adsorption energies obtained for 5-FU interacting with Brønsted acid sites ( $E_{\text{ads}} = -144$  kJ/mol and  $-189$  kJ/mol for interaction with one and two protons in the same twelve-membered ring [5]). Despite the apparently weaker interaction, 5-FU remained firmly bonded to the EFAL site over the course of AIMD simulations, whereas one of the Al-coordinated water molecules was removed, again leading to trigonal-bipyramidal coordination. At the moment, extensive AIMD simulations are performed to investigate whether the octahedral EFAL site with a coordinated 5-FU molecule is stabilised by additional water molecules. Furthermore, DFT-based predictions of the vibrational spectra will be made in order to elucidate whether the coordination of 5-FU to EFAL sites causes characteristic shifts of certain vibrational modes. The resulting spectra will be compared to the available experimental data [3].

Altogether, this contribution highlights how state-of-the-art computational chemistry methods can provide atomic-level insights into the interaction of relatively complex organic guest molecules with different types of acid sites in zeolites. Due to significant advances in the modelling of EFAL sites that have been made in the past few years, it is now possible to investigate these complex local environments with electronic structure methods. By combining AIMD simulations, which give access to the dynamic behaviour on the picosecond timescale, with an inclusion of co-adsorbed water molecules in the model, it is possible to create reasonably realistic conditions that should be representative for real-world adsorption phenomena.

## References

- [1] N. Jiang, R. Shang, S. G. J. Heijman, and L. C. Rietveld, *Water Res.* **144**, 145 (2018).
- [2] S. Mintova, M. Jaber, and V. Valtchev, *Chem. Soc. Rev.* **44**, 7207 (2015).
- [3] A. Datt, E. A. Burns, N. A. Dhuna, and S. C. Larsen, *Microporous Mesoporous Mater.* **167**, 182 (2013).
- [4] N. Vilaça, A. R. Bertão, E. A. Prasetyanto, S. Granja, M. Costa, R. Fernandes, F. Figueiredo, A. M. Fonseca, L. De Cola, F. Baltazar, and I. C. Neves, *Mater. Sci. Eng. C* **120**, 111721 (2021).
- [5] M. Fischer, *CrystEngComm* **26**, 3795 (2024).
- [6] M. Jin, M. Ravi, C. Lei, C. J. Heard, F. Brivio, Z. Tošner, L. Grajciar, J. A. van Bokhoven, and P. Nachtigall, *Angew. Chem. Int. Ed.* **62**, e202306183 (2023).

## Acknowledgments

Funding by the German Research Foundation through a Heisenberg grant (project number 455871835) is gratefully acknowledged.



## Why some silica zeolites have not been synthesized as aluminosilicate?

Ömer F. Altundal<sup>1</sup>, Frits Daeyaert<sup>2</sup>, Maria Galvez<sup>3</sup>, Jose Valero<sup>1</sup>, Susana Valencia<sup>1</sup>, Fernando Rey<sup>1</sup>, German Sastre<sup>1</sup>

<sup>1</sup> Instituto de Tecnología Química UPV-CSIC, Universidad Politécnica de Valencia, Valencia, Spain

<sup>2</sup> Synopsidenovodesign, Beerse, Belgium

<sup>3</sup> Faculty of Pharmacy and Food Sciences, Universidad de Valencia, Valencia, Spain

[gsastre@itq.upv.es](mailto:gsastre@itq.upv.es)

Originally discovered as aluminosilicate minerals in 1756, approximately 60 zeolite polymorphs of natural origin are known to date, with composition  $M_n^{n+}Al_xSi_{1-x}O_2$  ( $x=n-a$ ), M being an inorganic cation ( $Na^+$ ,  $K^+$ ,  $Mg^{2+}$ ,  $Ca^{2+}$ ) located in the micropore and close to the Al of the crystal lattice. It was not until 1862 when for the first time a zeolite was obtained by laboratory synthesis by the hydrothermal method, from a silica-alumina gel in a basic medium, at a temperature of 140-200 °C, and autoclaved under autogenous pressure. In 1960 Barrer replaced the inorganic cations by organic cations, typically quaternary nitrogen molecules, called organic structure directing agents (OSDAs). Since then the number of known zeolites rapidly increased to more than 200 known today [1].

Not all chemical compositions are possible; from the 99 aluminosilicate zeolites only 35 have also been obtained as pure silica. On the other hand, 36 zeolites that do not exist commonly as aluminosilicates have been repeatedly obtained as pure silica [2]. Apart from the synthesis gel composition, the major synthesis variable is the OSDA used. Other variables (time, pH, stirring, temperature) are also important. There are few studies able to rationalize the most favorable chemical compositions for each structure. Our recent study allows us to propose an explanation [3].

The OSDB database contains bibliographic information on which organic cations have been used for the synthesis of each zeolite. SSZ-35 (STF) has been obtained only at very high Si/Al ratio using 32 OSDAs, most of which are located in the Pareto front of energy vs. volume (Figure 1). Following the Pareto front, 121 other OSDAs were suggested that, according to the literature, give 19 zeolites that are competitors to STF [4].

Using our specific software, zeoTSDa, based on interatomic potentials, geometry optimization and Monte Carlo, we obtained the energy and atomic positions of the zeolite+'organic cation' unit cell corresponding to the maximum (optimal) number of organic cations that fit in the micropore, for the 20×121 selected combinations. With the energy values obtained and the recent definition of 'synthesis energy' [3], we obtain an energy value whose minimum, for each organic cation, indicates which zeolite would be obtained in the synthesis using silica/alumina gel. The results show that with these 121 organic cations, from the list of 20 competing zeolites, there are only three favorable aluminosilicate zeolites (AEI, CHA, BEA), while none of the other 17 competing zeolites are stable.

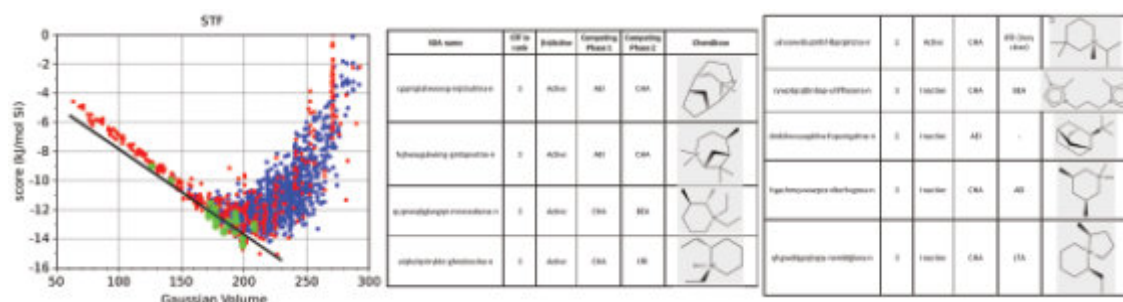


**Figure 1.** Left: plot of zeo-OSDA van der Waals energy versus OSDA volume for STF zeolite using a database of OSDAs. Middle and right: score (using 'synthesis energy') of more favourable aluminosilicate zeolites for a selected list of OSDAs, all of them good candidates to obtain silica STF, but none of them a good candidate to obtain AlSi STF.

### References

- [1] A. F. Masters, T. Maschmeyer; Zeolites – From curiosity to cornerstone; Microporous Mesoporous Mater. **2011**, 142, 423–438. <http://dx.doi.org/10.1016/j.micromeso.2010.12.026>
- [2] AST, ATS, BEC, CDO, CFI, CSV, DOH, DON, EEI, EWO, GON, IFR, IFY, IHW, IMF, ISV, ITH, ITW, IWR, JZT, MEP, MTF, MTN, NSI, OKO, PCR, RFE, RRO, RTE, RWR, SFE, SFF, SGT, STF, STT, STW, VET.
- [3] O. F. Altundal, S. Leon, G. Sastre; Different Zeolite Phases Obtained with the Same Organic Structure Directing Agent in the Presence and Absence of Aluminum: The Directing Role of Aluminum in the Synthesis of Zeolites; J. Phys. Chem. C **2023**, 127, 10797–10805. <https://dx.doi.org/10.1021/acs.jpcc.3c01567>
- [4] AEI, BEA, BEC, CHA, DDR, DOH, EUO, IFR, ITE, LTA, MEL, MFI, MOR, MTW, NON, RTH, SFF, SGT, STF, STO.

### Acknowledgments

We thank MICIN of Spain for funding and also ASIC-UPV and CTI-CSIC for computational facilities.



## Enhanced Hydrocracking Efficiency and Catalyst Stability through Structured Mesoporosity in Pt/HUSY zeolites

N.F.L. de Paula<sup>1</sup>, H.M. Mesa<sup>1</sup>, J.M. Ortigosa<sup>2</sup>, J.M.A.R. de Almeida<sup>1</sup>, J. Garcia-Martinez<sup>2</sup>, P.N. Romano<sup>3</sup>

<sup>1</sup> Instituto de Química, Universidade Federal do Rio de Janeiro, Av. Athos da Silveira Ramos, 149, Rio de Janeiro, Brazil 21941-909

<sup>2</sup> Laboratorio de Nanotecnología Molecular, Departamento de Química Inorgánica, Universidad de Alicante, 03690, Alicante, Spain

<sup>3</sup> Campus Duque de Caxias, Universidade Federal do Rio de Janeiro, Rodovia Washington Luiz, 19593, Rio de Janeiro, Brazil, 25240-005.

pedro.romano@caxias.ufrrj.br

### Motivation

Enhancing the diffusion efficiency of reacting molecules within catalyst particles is a significant industrial challenge, particularly for zeolites with their well-defined crystalline structures. Some reacting species encounter severe diffusion limitations due to their size exceeding the pore or channel openings in the crystal matrix [1]. A well-known solution to this problem is the steaming process, which generates mesopores with undefined extents in the catalyst particle, thereby alleviating intracrystalline mass transport limitations [2]. Another effective approach is the surfactant-templating method. This highly adaptable technique creates specific intracrystalline mesoporosity in zeolites and has proven exceptionally effective in precisely regulating the amount of mesoporosity and the dimensions of the mesopores. It maintains the primary characteristics of the original zeolite, such as crystallinity, acidity, and hydrothermal stability, leading to a high degree of interconnectivity and significantly facilitating the inward and outward diffusion of large molecules [3,4].

In this study, we evaluate the benefits of organized and interconnected mesopore arrangements in surfactant-templated zeolites for hexadecane cracking. A commercial pre-steamed faujasite (CBV780\_Parent) was used as the base material. Two derivatives were produced using cetyltrimethylammonium bromide (CTAB) as a surfactant for two different treatment times: 3 hours (CBV780\_3hrs) and 20 hours (CBV780\_20hrs). Subsequently, all the materials were impregnated with platinum to achieve a 1% wt. loading and tested accordingly.

### Results and Discussion

Table 1 presents the main physicochemical properties of the prepared catalysts. The surfactant-templated materials showed no significant changes in Si/Al ratios or Brønsted acid site (BAS) density, as determined by temperature-programmed desorption of isopropylamine and infrared spectroscopy of pyridine. The differences observed between the values appear to stem from methodological considerations, with no discernible trend linked to the surfactant modifications. However, a substantial increase in mesopore volume at the expense of micropore volume was observed, as expected due to the surfactant treatment. Notably, the mesopore volume of the Pt/CBV780\_20hrs catalyst increased by approximately 2.5-fold compared to the base material, while other physicochemical properties remained virtually unchanged. The Pt particle size, its distribution and the metal-per-acid-site ratio remained consistent across all catalyst supports, ensuring uniform hydrogenation performance in all samples, without affecting the overall reaction kinetics.

**Table 1:** Physicochemical properties of non-treated and surfactant treated USY.

Catalyst	Si/Al <sup>a</sup>	BAS Density (μmol/g <sub>cat</sub> ) <sup>b</sup>		Pore Volume (cm <sup>3</sup> /g) <sup>d</sup>		d <sub>Pt CO</sub> (nm) <sup>e</sup>	Pt Dispersion (%) <sup>e</sup>	n <sub>Pt</sub> /n <sub>BAS</sub>	Coke Deposited after reaction <sup>f</sup>	k <sub>d</sub> (X <sub>hexadecane</sub> 10 <sup>-3</sup> h <sup>-1</sup> )
		IPA-TPD <sup>b</sup>	FTIR-Py <sup>c</sup>	V <sub>micro</sub>	V <sub>meso</sub> <sup>*</sup>					
Pt/CBV780_Parent	40.0	106	140	0.24	0.23	8.2	13.8	0.067	2.6%	3.0
Pt/CBV780_3hrs	37.0	100	133	0.21	0.33	8.9	12.7	0.065	4.5%	2.7
Pt/CBV780_20hrs	37.9	99	147	0.18	0.58	8.9	12.8	0.066	4.1%	1.4

<sup>a</sup> Estimated with energy dispersive X-ray spectroscopy (EDS).

<sup>b</sup> Brønsted acid site density calculated through isopropyl amine temperature programmed desorption method.

<sup>c</sup> Determined by Pyridine FTIR.

<sup>d</sup> Pore volumes obtained using nitrogen adsorption technique and NL-DFT method.

<sup>e</sup> Determined by CO chemisorption.

<sup>f</sup> Calculated based on thermogravimetry tests with post-reaction catalysts.

\* V<sub>meso</sub> was estimated from 2 to 20 nm only using the NL-DFT method.

The implications of such changes in textural properties are demonstrated in the catalyst activity in different temperatures as shown in Figure 1a. The Pt/CBV780\_20hrs sample presented approximately full conversion of hexadecane at 350 °C outperforming the Pt/CBV780\_Parent catalyst. Such improvement not only impacted hexadecane conversion but also the Pt/CBV780\_20hrs material presented higher selectivity to liquid products and a



significant improvement in the jet fuel fraction when compared at isoconversion with the other materials (Figure 1b and 1c).

Additionally, the surfactant-templated zeolites exhibited improved stability under reaction conditions over a three-day period on stream (Figure 1d). To quantitatively compare the stability of these materials, a deactivation constant ( $k_d$ ) was calculated for each sample (Table 1). Notably, all surfactant-templated materials exhibited lower deactivation constants compared to the parent material. The Pt/CBV780\_20hrs catalyst showed a deactivation constant of less than half that of the Pt/CBV780\_Parent ( $1.4$  vs.  $3.0 \times 10^{-3} \cdot \text{h}^{-1}$ , respectively), which can be related to the higher mesoporosity presented by this material.

Despite exhibiting improved stability, both surfactant-treated catalysts showed a slightly higher amounts of coke deposits compared to the parent catalyst (Table 1, Figures 1e and 1f) but no significant trend to be correlated to the treatment time. Thermogravimetry tests indicated that the coke content consisted primarily of lighter carbonaceous species, rather than the bulky compounds typically observed in cracking catalysts (Figure 1f). Even though, the highly interconnected mesoporosity in these materials seem to prevent deactivation due to the enhanced pore accessibility and consequent egression of the deactivation precursors.

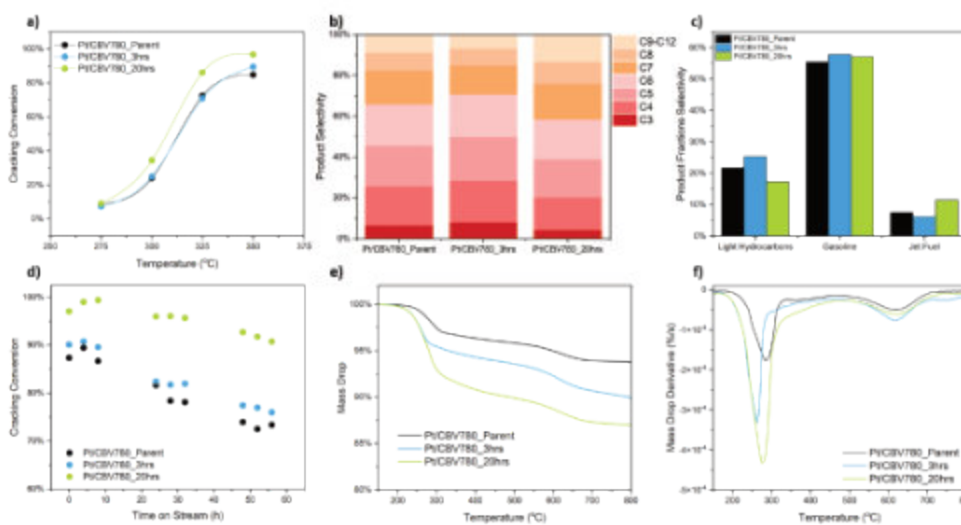


**Figure 1.** **a)** Cracking yield of hexadecane at different reaction temperatures on 1%(wt/wt) platinum non-treated and treated zeolites. **b)** Products selectivity at isoconversion ( $\sim 85\%$ ) for the Pt/CBV780\_Parent, Pt/CBV780\_3hrs, and Pt/CBV780\_20hrs zeolites. **c)** Products fraction distribution at isoconversion for the Pt/CBV780\_Parent, Pt/CBV780\_3hrs, and Pt/CBV780\_20hrs zeolites. **d)** Cracking yield evolution over 3 days onstream ( $350^\circ\text{C}$ ,  $0.03 \text{ mL hexadecane/min}$  reactant feeding,  $20 \text{ bar of H}_2$ ). **e)** Thermogravimetry analysis of the post-reaction catalysts after the 3-days stability test. **f)** Respective mass derivative of the thermogravimetry tests for the three studied zeolite samples.

## Conclusions

The introduction of well-defined intracrystalline mesoporosity into Pt/HUSY zeolites through surfactant-templating has led to substantial improvements in hydrocracking efficiency and catalyst stability. The Pt/CBV780\_20hrs catalyst, with its highly interconnected mesoporous structure, achieved near-complete conversion of hexadecane at  $350^\circ\text{C}$ , showing its higher activity compared with the Pt/CBV780\_Parent.

Additionally, the introduced mesoporosity led to remarkably improved catalyst stability, as indicated by lower deactivation constants ( $1.4$  vs.  $3.0 \times 10^{-3} \cdot \text{h}^{-1}$ ) over extended reaction periods, despite increased coke formation. These findings underscore the potential of surfactant-templated zeolites in addressing the challenges of diffusion limitations and deactivation in industrial catalytic processes. The ability to precisely control mesopore dimensions while maintaining the intrinsic properties of zeolites opens new avenues for designing highly efficient and durable catalysts for various hydrocarbon transformations as well as tuning operational cracking parameters to meet product specifications.

## References

- [1] R. C. Runnebaum and J. Maginn, *The Journal of Physical Chemistry B*, **101**, 6394-6408 (1997).
- [2] H. Qu, Y. Ma, B. Li, and L. Wang, *Emergent Materials*, **3**, 381-405 (2020).
- [3] M.J. Mendoza-Castro, E. Serrano, N. Linares, and J. García-Martínez, *Advanced Materials Interfaces*, **8**, 2001388 (2021).
- [4] A. Sachse, A. Grau-Atienza, E. O. Jardim, N. Linares, M. Thommes, and J. García-Martínez, *Crystal Growth & Design*, **17**, 4289-4305 (2017).





## Structural Insights and Exchange Dynamics of Rare Earth Elements in Synthetic NH<sub>4</sub>-13X Zeolite

F. Colombo<sup>1</sup>, R. Fantini<sup>1</sup>, M. Sisti<sup>1</sup>, F. Di Renzo<sup>2</sup>, G. Confalonieri<sup>3</sup>, G. Malavasi<sup>1</sup>, D. Malferrari<sup>1</sup> and R. Arletti<sup>1</sup>

<sup>1</sup>Dipartimento di Scienze Chimiche e Geologiche, Università degli Studi di Modena e Reggio Emilia, Modena, Italy

<sup>2</sup>ICGM, University of Montpellier, CNRS, ENSCM, Place Eugène Bataillon, 34095 Montpellier, France

<sup>3</sup>Dipartimento di Scienze della Terra, Università degli Studi di Roma "La Sapienza" - Piazzale Aldo Moro 5, 00185 Roma  
francesco.colombo@unimore.it

Rare Earth Elements (REEs) are part of the list of the so called Critical Raw Materials (CRMs) for the European Union since 2011, the first year in which a list of materials of high importance was drawn up. A specific material is considered a CRM based on two parameters: Economic Importance (EI) and Supply Risk (SR). EI and SR values for REEs have been high since the last 13 years, meaning that these elements remain important for end-use applications, not having the possibility of being substituted with other materials. REEs are divided in two groups: Heavy Rare Earth Elements (HREEs), used in applications related to their optical properties such as laser dopants and radiography; and Light Rare Earth Elements (LREEs), more abundant in the earth crust than HREEs, used in a wide range of applications such as catalysis, metallurgy, glass polishing, magnets and others. The risk of a disruption in their supply chain is especially high, given that 85% of LREEs and the whole amount of HREEs needed are imported from China [1]. In the recent "Regulation (EU) 2024/1252 of the European Parliament and of the Council", is stated the importance of the adoption and implementation of national programmes containing measures designed to increase the collection, sorting and processing of wastes with relevant CRMs recovery potential, with a view to increase the use of secondary critical raw materials [2]. An important step in the production of secondary raw materials, and particularly REEs, is the separation of these elements from other elements and from each other. Different wastes have been proven to be rich in REEs, especially WEEE (waste from electrical and electronic equipment), but their recovery is still long from being exploited. This study is part of a wide project aimed at the exploitation of the cation exchange property of zeolite for the recovery of REEs from wastes. In this contribution we will present results of experiments aimed at the evaluation of the exchange capacity and selectivity of synthetic 13X zeolite towards four different REEs with concentrations mimicking the ones obtained from a two-step leaching of spent fluorescent lamps [3]. In a recent work a NH<sub>4</sub> exchanged 13X zeolite was put in contact with four different mono-elemental solutions: Ce 0.03M, La 0.04M, Eu 0.006M and Y 0.17M. Three different solid/liquid ratios (g/ml) of 1/10, 1/50 and 1/100 were tested for each solution. Further NH<sub>4</sub> exchanges were performed to recover REEs from the zeolites so obtained. All the powders obtained were analysed by SEM-EDS, TG and EA, while only the solution after the first exchange were analysed by ICP-OES. The most representative samples for each REE before and after the recovery were analysed by XRPD (ID22 – ESRF) to obtain structural information. Following the interesting results obtained from mono-elemental exchanges [4], selectivity tests were performed on solutions containing coupled REE elements (Ce + La, Eu + Y). For the Ce+La solution s/l ratios (g/ml) of 1/10, 1/50 and 1/100 were tested, while for the Eu+Y solution s/l ratios (g/ml) of 1/10, 1/20 and 1/50 were tested. Further NH<sub>4</sub> exchanges were performed to recover REEs. Both solids and solutions were analysed after the exchanges as previously described. Selected Ce-exchanged samples obtained after both mono- and bi-elemental solutions exchanges were analysed to obtain both EXAFS and XANES spectra (BM08 – ESRF), necessary to evaluate the oxidation state of Ce (III or IV) and to better understand the interaction of Ce with the zeolite framework, other cations, and water. The results obtained from the mono-elemental exchanges showed that different Rare Earths show different exchange behaviours. In particular Y, despite being the most concentrated REE in the starting solution, reached exchange values clearly lower than those obtained for Ce and La, that instead gave very similar results. Eu concentration in the starting solution was too low compared to the other REEs to give enough information on the adsorption behaviour. The structural characterization of the Ce and La exchanged zeolite confirmed that the exchanged cations occupy the same crystallographic positions, with similar occupancies, thus reflecting and confirming the almost identical behaviour highlighted from the exchange dynamic. Site I' and II\* (named after Frising et al. are the two sites involved in the Ce and La exchanges, in line with what was observed by various authors in past works [5]. Different observations can be done for Y. From the structural analysis it turned out that the sites involved are different from the ones of Ce and La, as well as the interaction of the cation with the zeolite framework and extra framework H<sub>2</sub>O molecules. Y shares a cation site with Ce and La (site I') but it is also exchanged in site IV, a less stable site in which Y is bonded with water molecules and not to the zeolite framework. This fact supports the idea that Y is more soluble and tends to stay in the solutions, and thus in more hydrated sites, leading to a lower overall exchange. Some information was also obtained for Eu, despite the zeolite not being saturated, that showed a behaviour more similar to Ce and La rather than to Y. Bi-elemental exchange results support the mono-elemental exchange evidences indicating that Ce and La behaviours are almost identical, while in the case of Eu and Y, the exchange is strictly controlled by the concentration of the REEs in the starting solution, with Y being exchanged over Eu in every s/l ratio tested. XAS data, in support of XRPD data are still under investigation.

### References



- [1] Directorate-General for Internal Market, I., Grohol, M. & Veeh, C. Study on the Critical Raw Materials for the EU 2023: Final Report. (Publications Office of the European Union, LU, 2023).
- [2] Regulation (EU) 2024/1252. Regulation (EU) 2024/1252 of the European Parliament and of the Council of 11 April 2024 Establishing a Framework for Ensuring a Secure and Sustainable Supply of Critical Raw Materials and Amending Regulations (EU) No 168/2013, (EU) 2018/858, (EU) 2018/1724 and (EU) 2019/1020. (2024).
- [3] Eduafo, P. M., Strauss, M. L. & Mishra, B. Experimental investigation of recycling rare earth metals from waste fluorescent lamp phosphors. in vols 15-19-March-2015 253–259 (2015).
- [4] Colombo, F. et al. An insight into REEs recovery from spent fluorescent lamps: Evaluation of the affinity of an NH<sub>4</sub>-13X zeolite towards Ce, La, Eu and Y. Waste Manag. 175, 339–347 (2024).
- [5] Frising, T. & Leflaive, P. Extraframework cation distributions in X and Y faujasite zeolites: A review. Microporous Mesoporous Mater. 114, 27–63 (2008).



## CO<sub>2</sub> methanation catalysed by NiO-CeO<sub>2</sub> nanoparticles supported on beta-zeolite

I. Martínez-López<sup>1</sup>, R. Rodríguez-Bobada<sup>1</sup>, I. Martín-García<sup>1</sup>, A. Davó-Quiñonero<sup>1</sup>, E. Guillén-Bas<sup>1</sup>, D. Lozano-Castelló<sup>1</sup>, A. Bueno-López<sup>1</sup>

<sup>1</sup> Department of Inorganic Chemistry, Science Faculty, University of Alicante, Apdo. 99, 03080 Alicante, Spain.  
[ivan.martinez1@ua.es](mailto:ivan.martinez1@ua.es)

### Introduction

Greenhouse gas emissions have experienced an exponential growth in the last decades, mainly in form of CO<sub>2</sub> from fossil fuels combustion, deforestation and industrial processes [1]. The development of greener and more efficient catalytic systems remains a significant challenge considering this situation.

Among the different practices, the use of Dual Function Materials (DFMs) has achieved a great attention for CO<sub>2</sub> capture and conversion. These materials are constituted by active phases, typically transition metals, supported on inorganic solids (commonly, alkali or alkali-doped metal oxides and metal carbonates) that show a synergetic effect between adsorption and activity, improving their overall catalytic performance when compared with analogue conventional catalysts [2-6].

### Experimental

This work was focused on the development of novel DFMs based on NiO-CeO<sub>2</sub> (NiCe) nanoparticles supported on beta-zeolite (Z) and their application in CO<sub>2</sub> methanation. Combining the inversed microemulsion (for NiCe synthesis) and solvothermal methods (for zeolite synthesis), an array of five catalysts were synthesised. Namely: **(1)** ZS 10% NiCe; **(2)** ZI 10% NiCe; **(3)** ZI 20% NiCe; **(4)** ZI 20% NiCe + 5% Mg and **(5)** ZI 20% + 15% Mg.

**(1)** ZS 10% NiCe. During the synthesis of beta-zeolite (Z), the necessary amount of active phase (NiCe) was added to the synthesis gel to obtain a catalyst with a NiCe content of 10 wt%.

**(2)** ZI 10% NiCe; **(3)** ZI 20% NiCe. These catalysts were prepared by impregnation-calcination. The beta-zeolite (Z) was impregnated with an ethanolic dispersion of NiCe (10-20 wt%). Next, the solid was dried at 80 °C and calcined at 500 °C for 1 h.

**(4)** ZI 20% NiCe + 5% Mg; **(5)** ZI 20% NiCe + 15% Mg. Following the same impregnation-calcination method, the ZI 20% NiCe was impregnated with a solution of MgCO<sub>3</sub> (5-15 wt%) in water and nitric acid, followed by a heat treatment at 120 °C and calcination at 500 °C for 1h.

### Results and discussion

The XRD patterns (not shown) of the catalysts confirm that the presence of NiCe and MgO does not affect the crystalline structure of the beta-zeolite, and that it has a crystal size of 14 ± 2 nm in all cases (Table 1, column 1).

The N<sub>2</sub> physisorption isotherms (not shown) reveal a high microporosity of the materials and show Type IV isotherms characteristic of the presence of mesopores in the solid. On the other hand, the CO<sub>2</sub> isotherms reveal that the presence of MgO in the material increases its adsorption capacity. The physical properties extracted from the N<sub>2</sub> and CO<sub>2</sub> physisorption isotherms (Table 1, columns 2-5), show that all the catalysts present surface areas with values between 370 to 471 m<sup>2</sup>/g (Table 1, column 2). On the other hand, the non-existence of significant differences between the V<sub>DR</sub> values of the N<sub>2</sub> and CO<sub>2</sub> isotherms (Table 1, columns 3 and 4), confirm a high narrow microporosity in all the synthesised materials, having a micropore volume of 0.19 ± 0.04 cm<sup>3</sup>/g.

**Table 1.** Textural properties of NiCe/Z catalysts.

Sample	d <sub>DRX</sub> (nm) <sup>a</sup>	BET (m <sup>2</sup> /g)	V <sub>N<sub>2</sub></sub> (cm <sup>3</sup> /g) <sup>b</sup>	V <sub>CO<sub>2</sub></sub> (cm <sup>3</sup> /g) <sup>b</sup>	V <sub>TOTAL</sub> (cm <sup>3</sup> /g)
Z	15	448	0.22	0.21	0.61
ZI 10% NiCe	15	455	0.23	0.20	0.54
ZS 10% NiCe	16	471	0.22	0.21	0.33
ZI 20% NiCe	13	399	0.20	0.22	0.50
ZI 20% NiCe + 5% Mg	13	441	0.21	0.19	0.36
ZI 20% NiCe + 15% Mg	12	371	0.19	0.15	0.39

<sup>a</sup> Crystal size of the beta zeolite calculated with Scherrer at 22.5°. <sup>b</sup> Volume determined by Dubinin-Radushkevich.



The catalytic experiments evidence that the catalyst obtained by means of impregnation-calcination procedure and 20% of active phase loading (ZI 20% NiCe) presents the best CO<sub>2</sub> conversion in Figure 1 (left), with 100% of selectivity in CH<sub>4</sub> formation and carbon-neutral balances (not shown for brevity). On the other hand, a slight negative effect of MgO in the catalytic performance was only observed above 300 °C (Figure 1, right), when compared to counterpart Mg-free sample, confirming the good performance of the zeolite-containing materials.

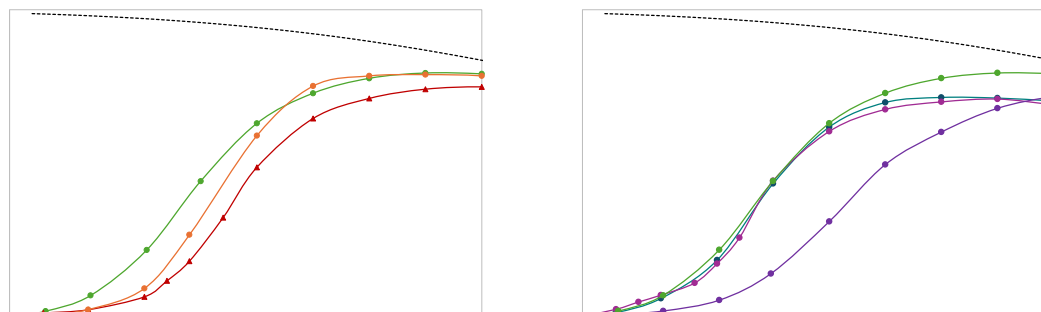


**Figure 1.** CO<sub>2</sub> conversion profiles. Experimental conditions: 1 g of catalyst (200 mg of active phase); Total gas flow 200 mL/min; 10% CO<sub>2</sub>, 40% H<sub>2</sub> and 50% N<sub>2</sub>. Pre-treatment: 50% H<sub>2</sub>/N<sub>2</sub> at 400 °C/1 h.

TGA experiments reveal that the zeolite does not have an impact in the chemisorption of CO<sub>2</sub> showing 0.40 mg of CO<sub>2</sub>/mg sample of CO<sub>2</sub> physisorption. Nevertheless, CO<sub>2</sub> chemisorption was observed with NiCe and MgO. The active phase (NiCe) captures 0.13 mg CO<sub>2</sub>/mg NiCe and, in the presence of 15% MgO, the capacity moderately increases to 0.15 mg CO<sub>2</sub>/ mg NiCe. While ZI 20% NiCe + 15% Mg, multiplies its CO<sub>2</sub> retention capacity four times, capturing a total of 0.56 mg CO<sub>2</sub>/mg NiCe, evidencing a synergistic effect between the beta-zeolite, the active phase and the MgO.

Among the five catalysts, ZI 20% NiCe was the most effective for the CO<sub>2</sub> methanation. Meanwhile, ZI 20% NiCe + 15% Mg showed the highest adsorption capacity. Then, both were selected as interesting catalysts to continue working with them.

## Conclusions

Amid the DFMs described in this work, those prepared by impregnation-calcination and with 20% active phase are the most efficient in the methanation of CO<sub>2</sub>. On the other hand, this study shows that the presence of MgO slightly affect the catalytic activity of the active phase and has a beneficial impact on the CO<sub>2</sub> chemisorption of these materials. Nevertheless, more experiments are needed to confirm the role of MgO in these DFMs.

The characterisation of the materials shows a highly microporous structure with good surface areas. However, more experimental work is required to postulate the reaction mechanism and correlate the data obtained with the nature of the materials. Nonetheless, our results show that DFMs based on NiO-CeO<sub>2</sub>/ beta-zeolite are an attractive option to achieve a good performance in CO<sub>2</sub> methanation in an efficient, versatile and greener way.

## References

- [1] IPCC, in Climate Change 2023: Synthesis Report. Contribution of Working Groups I, II and III to the Sixth Assessment Report of the Intergovernmental Panel on Climate Change, H. Lee and J. Romero (eds.) Geneva, 35 (2023).
- [2] I.S. Omodolor, H.O. Otor, J.A. Andonegui, B.J. Allen, A.C. Alba-Rubio, *Ind. Eng. Chem. Res.*, **59**, 17612 (2020).
- [3] J. Chen, Y. Xu, P. Liao, H. Wang, H. Zhou, *Carbon Capture Sci. Technol.*, **4**, 100052 (2022).
- [4] A. Quindimil, U. De-La-Torre, B. Pereda, J.A. González-Marcos, J. R. González-Velasco, *Appl. Catal. B: Environ.*, **238**, 393 (2018).
- [5] M. C. Bacariza, M. Maleval, I. Graça, J. M. Lopes, C. Henriques, *Microporous Mesoporous Mater.*, **274** (2019) 102.
- [6] W. Gac, W. Zawadzki, G. Słowik, M. Kuśmiercz, S. Dzwigaj, *Appl. Surf. Sci.*, **564**, 150421 (2021).

## Acknowledgments

The authors thank the financial support of the Project PID2022-139552OB-C22 by MICIU/AEI/10.13039/501100011033, FEDER,UE; TED2021-129216B-I00 and PDC2022-133839-C22 by MICIU/AEI /10.13039/501100011033 and Next Generation EU/PRTR; MFA/2022/036 by MCIN NextGeneration EU (PRTR-C17.I1) and by Generalitat Valenciana; CIPROM/2021/74 by Generalitat Valenciana; INVEST/2022/431 by MTES and Next Generation EU/PRTR. RYC2021-034791-I by MICIU/AEI.



## MOR-type zeolite membrane for reverse water gas shift membrane reactor

**M. Sakai<sup>1\*</sup>, K. Tanaka<sup>1</sup>, M. Matsukata<sup>1,2,3</sup>**

<sup>1</sup> Department of Applied Chemistry, Faculty of Science and Engineering, Waseda University, Shinjuku 162-0041, Japan

<sup>2</sup> Research Organization for Nano & Life Innovation, Waseda University, Shinjuku 162-0041, Japan

<sup>3</sup> Research Institute for Science and Engineering, Shinjuku 169-8555, Japan

\*saka.moto@aoni.waseda.jp

Membrane reactor with MOR-type zeolite membrane for reverse water gas shift was developed. Reverse water gas shift was carried out at 623 K at atmospheric pressure with MOR membrane for dehydration. Selective removal of water vapor from the reaction system enhanced CO yield and reached approximately 48 %, exceeding an equilibrium yield (18%) under the reaction conditions. The simulation study about the effect of dehydration membranes had good agreement with the experimental results.

### Introduction

Reverse water gas shift (RWGS) (eq. 1) is a promising technology for CO<sub>2</sub> utilization.



RWGS is a reversible and endothermic reaction; thus, a high reaction temperature is needed to achieve a high CO yield. For example, CO yield at 1073 K is finally achieved at 50 and 75 % with the feed composition of CO<sub>2</sub>:H<sub>2</sub> = 1:1 and 1:3, respectively. However, such high reaction temperature often causes the deterioration of both a catalyst and a reactor.

A membrane reactor is a key technology for overcoming the equilibrium constraint [1]. In this study, MOR-type zeolite was used as a dehydration membrane to enhance RWGS.

### Experimental and simulation method

CuO/ZnO/γ-Al<sub>2</sub>O<sub>3</sub> was used as a catalyst for RWGS. The catalyst was prepared according to the literature [2]. It was pre-treated at 623 K for 1 h in the H<sub>2</sub> stream for activation before use.

MOR-type zeolite membrane was prepared on an outer surface of tubular support by a secondary growth method. A porous α-alumina tube with an outer diameter of 12 mm, inner diameter of 9.0 mm, and length of 90 mm was used as a support. Seeded support prepared by a dip-coating method was grown at 453 K for 6 h in a synthesis solution having a molar composition of 10Na<sub>2</sub>O: 0.15Al<sub>2</sub>O<sub>3</sub>: 36SiO<sub>2</sub>: 960H<sub>2</sub>O.

A mixture of CO<sub>2</sub> and H<sub>2</sub> was fed to a catalyst bed around a tubular membrane. The composition of feed gas was adjusted as CO<sub>2</sub>:H<sub>2</sub> = 1:1 or 1:3. Reaction temperature and pressure were fixed at 623 K and 100 kPa. An inside support was swept by flowing N<sub>2</sub> to remove permeated molecules. Figure 1 depicts the photograph and schematic diagram of a membrane module. In this study, three reactors connected in series were used.

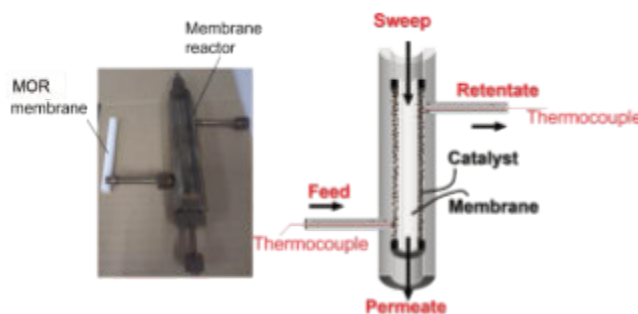


Figure 1. A photograph and schematic diagram of a membrane module.

A material balance was calculated in the tubular membrane reactor which is modeled as continuous stirred tank reactors (CSTR) and membrane modules placed in alternate shifts. One membrane module is divided into 10,000 CSTRs and 10,000 membrane modules with infinitesimal volume. The outlet of the first CSTR is connected to the inlet of the first membrane module, and the retentate of the membrane module is sent as the feed of the next CSTR. The composition of the exit of each CSTR is calculated by a reaction rate equation. In addition, mass transfer between the feed and permeate sides is calculated in a membrane module.

### Results and discussion



Figure 2 shows the results of membrane reactor tests and simulation studies. Rhombic symbols show the experimental CO yield at the exits of three reactors in series. Solid and dashed lines represent the simulated CO yield and equilibrium yield.

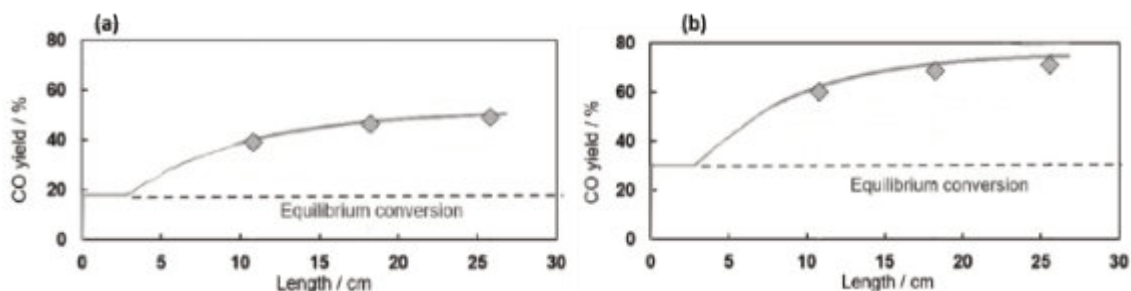


**Figure 2.** Results of membrane reactor tests at 623 K with feed gas of (a) CO<sub>2</sub>:H<sub>2</sub>=1:1 and (b) CO<sub>2</sub>:H<sub>2</sub>=1:3. ◊, Experimental results; Solid line, Simulation results.

The reaction progressed beyond the equilibrium conversion in a conventional reactor by dehydration by MOR membrane.

From an equimolar mixture of CO<sub>2</sub> and H<sub>2</sub>, the CO yield at the equilibrium at 623 K was 18.0%. In the membrane reactor, CO yields at the exit of the first, second, and third reactors were 38.7, 45.2, and 48.5 %, respectively. These values were more than two times larger than the equilibrium conversion, indicating that RWGS was successfully enhanced by a dehydration membrane reactor.

A similar trend was observed with the feed gas of CO<sub>2</sub>:H<sub>2</sub>=1:3. CO yield by membrane reactors overwhelmed the equilibrium conversion of 30.1 %. The yield reached 59.2, 68.0, and 70.5 % at the exit of each reactor in series. In addition, these experimental results were in good agreement with the results from the simulation study.

The CO yields in the membrane reactor (48.5 and 70.5%) were counterparts of the equilibrium yields at 1050 K and 1000 K in the conventional reactor without membrane; i.e. membrane reactor contributed to lowering the reaction temperature by approximately 400 K in these conditions.

## References

- [1] M. Sakai, K. Tanaka, and M. Matsukata, *Membranes*, **12**, 1272 (2022).
- [2] M. Kakihana and M. Yoshimura, *Bull. Chem. Soc. Jpn.*, **72**, 1427 (1999).



## On the origin of enantioselectivity in chiral zeolite asymmetric catalyst GTM-3: host-guest transfer of chirality

R. de la Serna,<sup>1</sup> J. Jurado-Sánchez,<sup>1</sup> J. Li,<sup>2</sup> C. Márquez-Álvarez,<sup>1</sup> J. Pérez-Pariente<sup>1</sup> and L. Gómez-Hortigüela<sup>1,\*</sup>

<sup>1</sup> Instituto de Catálisis y Petroleoquímica, Consejo Superior de Investigaciones Científicas (ICP-CSIC), c/ Marie Curie 2, 28049 Madrid, Spain.

<sup>2</sup> State Key Laboratory of Coordination Chemistry, School of Chemistry and Chemical Engineering, Nanjing University, 210023, Nanjing, China

Email: [lhortiguela@icp.csic.es](mailto:lhortiguela@icp.csic.es)

We have recently discovered a new class of extra-large pore chiral zeolite asymmetric catalysts based on the -ITV germanosilicate framework (GTM-3 and GTM-4) that are able to perform enantioselective operations during catalytic processes, reaching notably high enantiomeric excess values up to 60 %.<sup>1-3</sup> Their unique combination of extra-large pores, chiral confinement and ease of preparation using natural alkaloids as chiral precursors makes them very attractive catalytic materials to be used in industrial processes involving chiral molecules. Because of their novelty, understanding how these microporous materials transfer their chirality from their framework into molecular guest entities during a catalytic reaction is crucial in order to spread the scope for the catalytic enantioselective production of chiral compounds of interest. With this aim, we have carried out an extensive experimental and computational study about the catalytic activity of antipode GTM-3 catalysts, prepared from both enantiomers ((1*S*,2*S*) and (1*R*,2*R*)) of the organic structure-directing agent *N,N*-ethyl-methyl-pseudoephedrinium (EMPS), during the ring-opening of *trans*-stilbene oxide with 1-butanol, reaction that was found to meet the best chiral host-guest match among different alcohols.<sup>4</sup> *Trans*-stilbene oxide (TSO) is a chiral reactant that displays two enantiomeric forms, (*R,R*) and (*S,S*). The major products of the acid-catalyzed ring-opening of TSO with 1-butanol are i) the *unlike* 2-butoxy-1,2-diphenylethanol products, with (*R,S*) and (*S,R*) configurations (the first refers to the configuration of the hydroxyl-containing C, and the second to the butoxy-containing C) from (*R,R*) and (*S,S*)-TSO reactants via an  $S_N2$  route (with inversion of configuration), respectively, and ii) the *like* products, which are obtained via a  $S_N1$  route, with retention of configuration [(*R,R*) and (*S,S*)-2-butoxy-1,2-diphenylethanol from (*R,R*) and (*S,S*)-TSO, respectively]. Additionally, diphenylacetaldehyde (DPA) resulting from *Meinwald* rearrangement of TSO is also formed as secondary product from the  $S_N1$  route, as well as others derived from this.

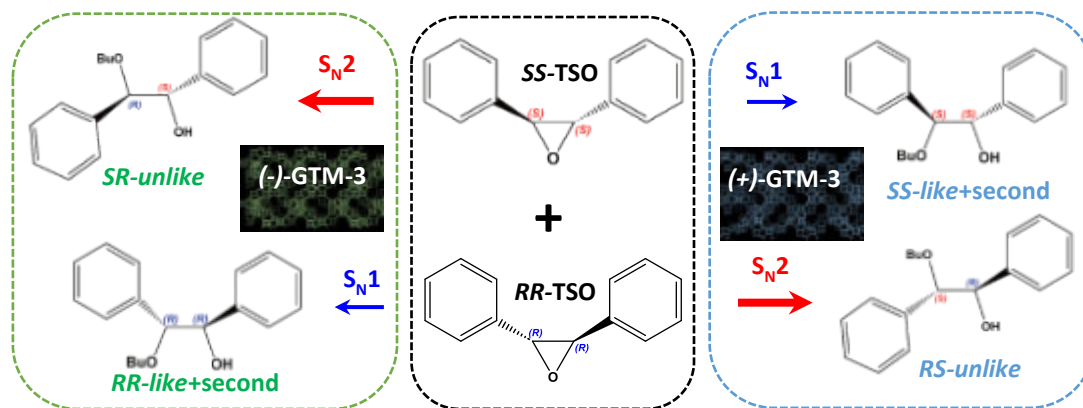
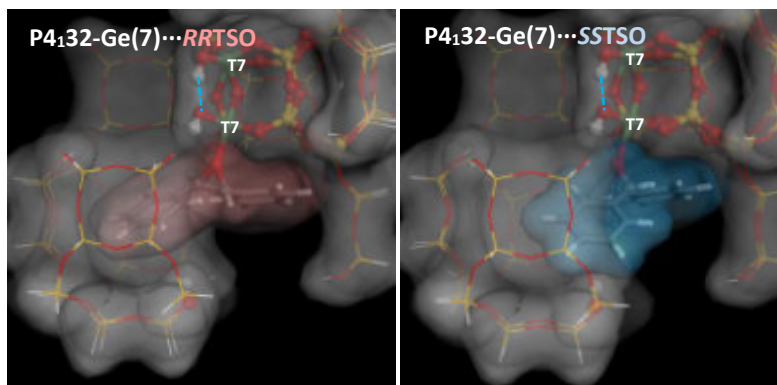


Figure 1. Prevalence of  $S_N2$  and  $S_N1$  routes to give the chiral products from racemic TSO using (-)-GTM-3 and (+)-GTM-3 catalysts.

The experimental catalytic study using GTM-3 as catalyst unraveled a surprising behavior: these chiral catalysts promote the transformation of one enantiomer of TSO in the corresponding *unlike* product (with inversion of configuration of the attacked C) via an  $S_N2$  mechanism (red arrows in Figure 1), and at the same time the transformation of the other enantiomer of TSO via an  $S_N1$ -like mechanism into the *like* (with retention of configuration) and secondary products (diphenylacetaldehyde via *Meinwald* rearrangement and derived products) (blue arrows). Of course, antipode (+)- and (-)-GTM-3 catalysts, prepared from (1*S*,2*S*) and (1*R*,2*R*) enantiomers of EMPS, respectively, gave mirror-image catalytic behaviors, with the former favoring the formation of (*RS*)-*unlike* (via  $S_N2$ ) and (*SS*)-*like* (via  $S_N1$ ) products (Figure 1-right, dashed blue rectangle), and the opposite for the latter (Figure 1-left, dashed green rectangle).

A subsequent computational study based on DFT+D methods was performed in order to gain insights on the origin of the enantioselectivity observed for these asymmetric heterogeneous catalysts, using a model of the  $P4_132$  enantiomeric polymorph. The results suggest a potential explanation for this catalytic behavior: TSO enantiomers bind on the Ge(T7) interrupted positions within  $d4r$  units in order to become pre-activated (Figure 2). Such TSO...Ge



**Figure 2.** Structure of the Ge(T7)···TSO complexes ( $P4_132$ ) with  $RR$ -TSO (left) and  $SS$ -TSO (right); Connolly surfaces are displayed to highlight the host-guest match.

complexes distort the Ge environment so that a new intraframework H-bond is developed between the two interrupted T7OH adjacent positions characteristic of this framework (dashed blue lines). Importantly, the absolute configuration of TSO enantiomers involves a rather different orientation of TSO on these complexes, with the oxirane ring of each enantiomer displaying perpendicular arrangements (Figure 2). Calculations suggest that each enantiomer of TSO then

follows a different reaction pathway, one favoring the  $S_N2$  route by addition of butanol from the opposite side to form the *unlike*-products, while the different orientation of the antipode enantiomer disfavors such  $S_N2$  route mainly by steric repulsions along the final H-transfer reaction. Our computational study suggests that the strong enantioselectivity of GTM-3 catalysts for this reaction is a result of a synergetic effect connected to the singular characteristics of the chiral -ITV framework: the host-guest transfer of chirality is associated to the particular orientation adopted by the chiral reactants within the chiral nanospace provided by the -ITV framework, similarly to what occurs with enzymes, and such preferential orientation is determined by the asymmetric cavities where the catalytic reaction takes place, by the particular features of the Ge active sites in adjacent T7 interrupted positions, and by the presence of several framework OH groups in the nearby nanospace that interact with guest species.

**Table 1.** 3D-ED Determination of absolute configuration of GTM-3 crystals.

Sample	SDA	Number of crystals			Enrichment
		analyzed	$P4_132$	$P4_332$	
$(+)$ -GTM-3	(1 <i>S</i> ,2 <i>S</i> )-EMPS	15	2	13	13/87
$(-)$ -GTM-3	(1 <i>R</i> ,2 <i>R</i> )-EMPS	13	10	3	77/23

The combination of the experimental catalytic results and the reaction mechanism proposed from our computational study suggests that  $(+)$ -GTM-3 catalysts prepared from the (1*S*,2*S*) enantiomer of EMPS organic agent should be enriched in the  $P4_332$

enantiomeric space group of the -ITV framework, and  $(-)$ -GTM-3 prepared from the (1*R*,2*R*) enantiomer in the  $P4_132$  enantiomeric polymorph. Interestingly, resolution of the absolute configuration of GTM-3 materials from *state-of-the-art* 3D-Electron Diffraction methods<sup>5</sup> has been finally accomplished and confirm the predicted assignment (Table 1), where 13 out of 15 analyzed crystals of  $(+)$ -GTM-3 were assigned to  $P4_332$  polymorph, and 10 out of 13 crystals of  $(-)$ -GTM-3 crystals to the antipode  $P4_132$  polymorph, giving an average 82 % enantio-enrichment in the corresponding chiral polymorph by each enantiomer of the EMPS organic agent. Interestingly, structure-solution of the location of the chiral EMPS organic structure-directing agents within each -ITV polymorph indicates that the transfer of chirality from the molecular component to the zeolite polymorph during crystallization is governed by the development of strong H-bonds between the molecular hydroxyl group of the organic chiral agent and the interrupted T(7)OH framework positions, what has been confirmed by FTIR spectroscopic studies.

## References

- [1] R. de la Serna, D. Nieto, R. Sainz, B. Bernardo-Maestro, Á. Mayoral, C. Márquez-Álvarez, J. Pérez-Pariente, and L. Gómez-Hortigüela, *J. Am. Chem. Soc.* **144**, 8249 (2022).
- [2] R. de la Serna, I. Arnaiz, C. Márquez-Álvarez, J. Pérez-Pariente, and L. Gómez-Hortigüela, *Chem. Commun.* **58**, 13083 (2022).
- [3] R. de la Serna, J. Jurado-Sánchez, C. Márquez-Álvarez, J. Pérez-Pariente, and L. Gómez-Hortigüela, *Microporous Mesoporous Mater.* **371**, 113083 (2024).
- [4] R. de la Serna, J. Pérez-Pariente, and L. Gómez-Hortigüela, *Catal. Today* **426**, 114389 (2024).
- [5] P. B. Klar, Y. Krysiak, H. Xu, G. Steciuk, J. Cho, X. Zou, and L. Palatinus, *Nat. Chem.* **15**, 848 (2023).

## Acknowledgments

This work has been partially financed by the Spanish State Research Agency (Agencia Española de Investigación, AEI, MCIN/AEI/10.13039/501100011033) and the European Regional Development Fund (Fondo Europeo de Desarrollo Regional, FEDER) through the Projects PID2019-107968RB-I00 and PID2022-138481NB-I00. RS acknowledges MCIN for predoctoral grant (PRE2020-095946). This work is also part of the Project PDC2022-133681-I00, funded by MCIN/AEI/10.13039/501100011033 and by the European Union "NextGenerationEU"/PRTR. We acknowledge Centro Técnico de Informática (CSIC) for running the calculations. The synchrotron data were collected at the MSPD beamline at ALBA Synchrotron with the collaboration of ALBA staff; M. A. Cambor and Z. Rei Gao are acknowledged for collecting the synchrotron SPXRD data.





## Magnesium silicate MWW molecular sieve: An efficient basic material applied for dry reforming of methane and NO<sub>2</sub> organic sensor

S. Kweon<sup>1</sup>, H.-K. Min<sup>2</sup>, Y. D. Park<sup>1</sup>, M. B. Park<sup>1</sup>

<sup>1</sup> Department of Energy and Chemical Engineering, Incheon National University, Incheon 22012, Korea

<sup>2</sup> Hydrogen & C1 Gas Research Center, Korea Research Institute of Chemical Technology, Daejeon 34114, Korea

sjkweon@inu.ac.kr

Expanding the zeolite application has led to synthesis of newly isomorphic heteroatom-tuned zeolitic materials known as metallosilicates. These materials have garnered attracted considerable attention in modern energy and environmental applications due to their unique acidic-basic properties and inherent zeolitic structural properties [1]. While bottom-up synthesis for metallosilicates can embed stable and uniform metal species within framework, it is challenging because of the unfavourable formation of M(OH)<sub>x</sub> and M-O bond lengths and angles where M is the metal atom in framework. To address these challenges, we developed a direct hydrothermal treatment of a borosilicate MWW zeolitic precursor (B-MWW(P)) with various metal precursor solutions. This method produced three- and two-dimensional (3D and 2D) MWW-type cobalt (Co), nickel (Ni), and zinc (Zn)-containing zeolitic materials (Co-, Ni-, and Zn-DMLs) [2-4]. In this study, we prepared 3D and 2D MWW magnesium silicates (Mg-DML-x, where x is 100–180 °C) under the developed single-step hydrothermal treatment. We then applied Mg-DML as a basic support and adsorbent for the dry reforming of methane (DRM) and organic field effect transistor (OFET)-based gas sensor, respectively.

The homogenized mixture containing B-MWW(P) and 1.0 M magnesium(II) nitrate hexahydrate solution (1g/50 mL) was heated at 100–160 °C for 4 d under 100 rpm in a Teflon-lined stainless autoclave to obtain Mg-DML-x (x = 100–180 °C). As-made Mg-DML-x samples were calcined at 550 °C for 8 h to eliminate the organic compounds. Ni impregnation on Mg-DML-x supports was carried out by the incipient wetness impregnation with a nickel concentration of 5 wt.% relative to Mg-DML-x to prepare Ni/Mg-DML-x catalysts. Meanwhile, P3HT blended with Mg-DML-100–160 solutions were spin-cast on HMDS-modified SiO<sub>2</sub>/Si substrates, which produced P3HT/Mg-DML-x blended film. Subsequently, thermal evaporation of Au electrodes on resulting P3HT/Mg-DML-x film was used to prepare OFET gas sensor. The resulting catalysts and OFET gas sensors were analyzed using various characterization tools, and were evaluated in DRM reaction at 700 °C with 60,000 and 90,000 cm<sup>3</sup> g<sub>cat</sub><sup>-1</sup> h<sup>-1</sup> GHSV using GC-TCD as well as in gas sensing tests for NO<sub>2</sub>, SO<sub>2</sub>, and CO<sub>2</sub> at 0 to 100 ppm in gas-sensor tester and semiconductor analyzer.

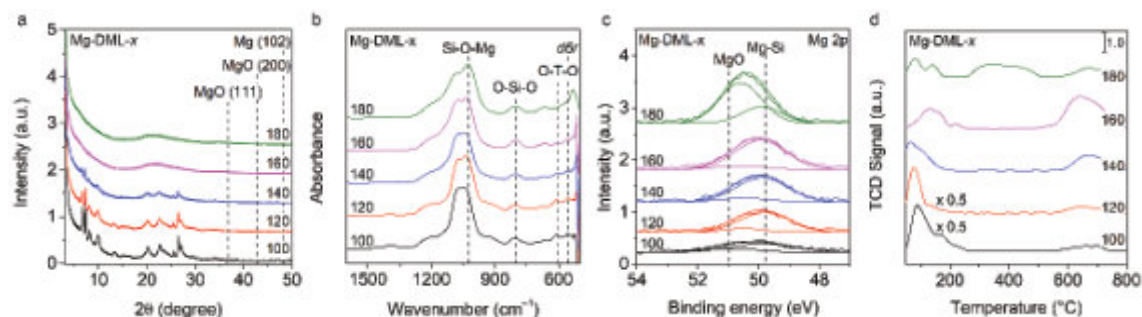


**Figure 1.** (a) Powder XRD patterns, (b) normalized IR spectra in the structural region, (c) Mg 2p XPS, and (d) CO<sub>2</sub> TPD profiles of Mg-DML-x (x = 100–180 °C).

Powder XRD patterns of Mg-DML-x exhibited a gradual decrease in typical MWW X-ray peaks due to the disordering MWW layers via further delamination at higher hydrothermal temperatures (Figure 1a). This was also evidenced by TGA/DTA showing a decrease of organic contents, and an increase in external surface areas as calculated from N<sub>2</sub> sorption isotherm (not shown). Normalized IR spectra of Mg-DML-x revealed that, while characteristic MWW peaks at 550 and 611 cm<sup>-1</sup> appeared up to Mg-DML-160, these peaks were absent in Mg-DML-180 (Figure 1b). This indicates that MWW framework was almost degraded at the high hydrothermal temperature (180 °C). Additionally, intensities of IR peaks for Si-O-Mg at 1026 cm<sup>-1</sup> were enhanced with rising hydrothermal temperatures due to growing Mg contents (1.1–3.7 wt.%). Notably, Mg-DML-160 showed the highest intensity of framework Mg species at 49.9 eV, whereas Mg-DML-180 exhibited a dominant proportion of MgO at 50.7 eV, which is more stable Mg species at a such high temperature (Figure 1c). Figure 1d shows the CO<sub>2</sub> TPD profiles of Mg-DML-x (x = 100–180 °C) in the range of 30–800 °C. All Mg-DML-x displayed the CO<sub>2</sub> desorption peaks at approximately 200 °C, which can be attributed to weak basic sites likely originating from lattice oxygen in the framework. Particularly, the CO<sub>2</sub> desorption peaks above 600 °C, assignable to strong basic sites gradually increased up to Mg-DML-160. However, Mg-DML-180 had a higher concentration of intermediate basic sites compared to the others. This difference can be attributed to the different predominant chemical states of Mg: Framework Mg for Mg-DML-100–160 and MgO for Mg-DML-180.



Ni impregnated Ni/Mg-DML- $x$  ( $x = 100$ – $180$  °C) catalysts were prepared for DRM. Each structural features of Ni/Mg-DML- $x$ , i.e., 3D to 2D MWW, were preserved after Ni impregnation (Figure 2a). Ni 2p<sub>3/2</sub> XPS spectra also exhibited the dominant Ni 2p XPS peaks assigned to NiO species for all Ni/Mg-DML- $x$  owing to the incipient wetness impregnation method (Figure 2b). Especially, the H<sub>2</sub> consumption peaks moved to higher temperatures up to Ni/Mg-DML-160 as observed in H<sub>2</sub> TPR (Figure 2c), due to the stronger basicity stemming from increasing framework Mg species (Figure 1c and 1d). In contrast, Ni/Mg-DML-180 showed the H<sub>2</sub> reduction peak at lower temperature compared to Ni/Mg-DML-160 owing to its weaker basicity. Based on H<sub>2</sub> chemisorption, Ni/Mg-DML-160 demonstrated the smallest Ni size (20 nm) among Ni/Mg-DML- $x$  catalysts, which are attributed to the strongest metal-support interaction resulting from the strongest basicity (not shown). When these Ni/Mg-DML- $x$  catalysts were applied to DRM reaction, Ni/Mg-DML-160 showed the highest initial conversions of CH<sub>4</sub> and CO<sub>2</sub> (70 and 75%, respectively) as well as the lowest content of coke (4 wt.%) among the Ni catalysts studied here (Figure 2d–f). This performance is attributed to Lewis basic framework Mg sites, which facilitate high dispersion of Ni species and the CO<sub>2</sub> chemisorption that can oxidize the coke species in reaction. In contrast, Ni/Mg-DML-180 showed the lower DRM activities and higher deactivation rate due to the decrease of Lewis basicity. Under the harsher DRM conditions (700 °C and 90,000 cm<sup>3</sup> g<sub>cat</sub><sup>-1</sup> h<sup>-1</sup> GHSV), Ni/Mg-DML-160 still showed the excellent catalyst durability (10% and 11% for deactivation rates of CH<sub>4</sub> and CO<sub>2</sub>, not shown). Furthermore, this catalyst showed the excellent stability (<5% of deactivation rates of CH<sub>4</sub> and CO<sub>2</sub>) with ca. 60 wt.% of coke in DRM reaction even after 100 h owing to its 2D MWW structure.

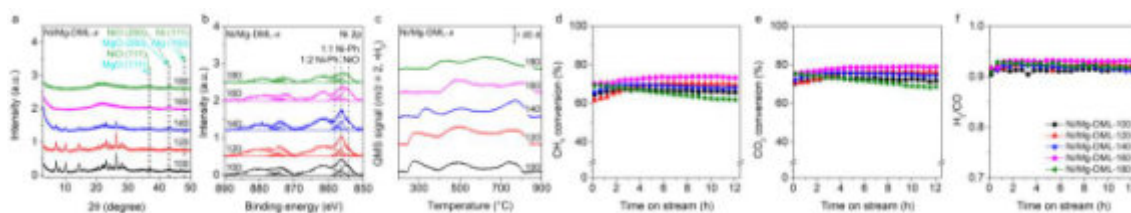


**Figure 2.** (a) Powder XRD patterns, (b) Ni 2p XPS, (c) H<sub>2</sub>-TPR, (d) CH<sub>4</sub> conversion, (e) CO<sub>2</sub> conversion, and (f) H<sub>2</sub>/CO ratio as a function of TOS at 700 °C and 60,000 cm<sup>3</sup> g<sub>cat</sub><sup>-1</sup> h<sup>-1</sup> GHSV for 12 h of Ni/Mg-DML- $x$  catalysts ( $x = 100$ – $180$  °C).

Furthermore, we prepared P3HT/Mg-DML- $x$  ( $x = 100$ – $160$  °C) blended films for use in OFET-based gas sensor. SEM images of the P3HT/Mg-DML- $x$  blended films showed the well dispersed aggregates of Mg-DML- $x$  with 4–5 μm in size within the polymer matrix (Figure 3a). The Mg contents of the P3HT/Mg-DML- $x$  blended film was comparable to Mg-DML- $x$  as determined by SEM-EDS, indicating that the framework Mg were well maintained even after the fabrication procedure. UV-Vis absorption spectra of P3HT/Mg-DML- $x$  blended films exhibited the similar A<sub>0,0</sub>/A<sub>0,1</sub> peak ratio (ca. 0.7) and thickness (25–30 nm) compared to pristine P3HT, indicating that the high dispersion of blended Mg-DML- $x$  in the P3HT/Mg-DML- $x$  films, which did not affect the crystallinity of P3HT (Figure 3b). After then, we fabricated OFET gas sensor based on bottom-gated P3HT/Mg-DML- $x$ . As p-type FETs, P3HT/Mg-DML- $x$  films demonstrated improved field-effect mobility compared to pristine P3HT, likely due to the framework Mg and/or Si of Mg-DML- $x$  acting as electron acceptors. Particularly, the gas sensing performance toward NO<sub>2</sub> in terms of responsivity, response and recovery rates, generally improved as increasing the hydrothermal temperatures for Mg-DML- $x$  synthesis (Figure 3c). This enhancement can be attributed to the Lewis basic Mg sites to efficiently attract Lewis acidic NO<sub>2</sub> gas and the 2D MWW property that allows more Mg sites to be exposed to NO<sub>2</sub>. When comparing various gases, i.e., NO<sub>2</sub>, SO<sub>2</sub>, and CO<sub>2</sub>, over these hybrid OFET gas sensors, NO<sub>2</sub> was demonstrated to be the most selectively detected gas for P3HT/Mg-DML- $x$  based gas sensor (Figure 3d and 3e), likely due to a stronger electron-withdrawing characteristic compared to SO<sub>2</sub> and CO<sub>2</sub>. In conclusion, as these above-mentioned research results demonstrated, it can be suggested that Mg-DML- $x$  can be effectively utilized as both basic and 2D MWW support and adsorbent for various applications.

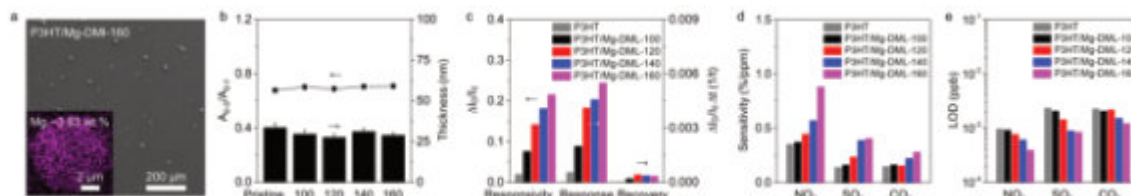


**Figure 3.** (a) SEM-EDS image of P3HT/Mg-DML-160 blended film, (b) Crystallinity and thickness were calculated from the 0–1 peak of the films, (c) Gas-sensing parameters of gas sensors upon 10ppm NO<sub>2</sub> gas. (d) Sensitivity, and (e) limit of the detection value of sensor devices for various gases.

## References

- [1] Q. Wu, C. Xu, L. Zhu, X. Meng, and F.-S. Xiao, *Catal. Today*, **390–391**, 2–11 (2022).
- [2] H.-K. Min, S. Kweon, Y. W. Kim, H. An, D. Jo, E. D. Park, C.-H. Shin, M. B. Park, *Appl. Catal. B*, **298**, 120627 (2021).
- [3] H.-K. Min, S. Kweon, Y. W. Kim, S. Oh, H. An, Y. Cho, H. Min, D. Jo, J. F. Kim, C.-H. Shin, S. B. Kang, M. B. Park, *Green Chem.*, **23**, 9489–9501 (2021).
- [4] S. Lee, S. W. Byun, S. Kweon, H. Shin, H.-K. Min, M. B. Park, S. B. Kang, *Appl. Catal. B*, **340**, 123264 (2024).



## Ultrafast Encapsulation of Bimetallic Nanoclusters into Zeolites

Tao Yu, Kai Jia, Yundong Wang, Jianhong Xu, **Zhendong Liu\***

State Key Laboratory of Chemical Engineering, Department of Chemical Engineering, Tsinghua University, Haidian District, Beijing 100084, China

liuzd@tsinghua.edu.cn

Bimetallic nanoclusters are superior to the corresponding monometallic counterparts for their unique geometric and electronic structures;<sup>[1]</sup> and, encapsulating them into zeolites can further incorporate merits of the porous host to create highly active and remarkably stable catalysts.<sup>[2]</sup> Yet, it is a daunting challenge to enclose bimetallic nanoclusters into the nanospace of zeolites as well as tune their structural features.<sup>[3]</sup> We herein present a universal methodology that leads to the ultrafast, *in situ* encapsulation of bimetallic nanoclusters in the course of zeolite crystallization. The efficiency and applicability of this method was verified by spontaneously confining a variety of bimetallic nanoclusters, including PtNi, PtCo and PtZn – all with tunable compositions, during the ultrafast synthesis of silicalite-1 in a few minutes (**Figure 1**). Focusing on PtNi@silicalite-1 as a typical case, detailed characterizations reveal that there exists a gradient distribution of the two metal entities within the zeolite and that their interactions are tunable with the composition. The silicalite-1 zeolite encapsulated with 1.2 wt% Pt and 1.0 wt% Ni nanoclusters show a notably high activity and excellent stability in the preferential oxidation of carbon monoxide. The utilization of ultrafast encapsulation as a general strategy demonstrates promising potential for synthesizing zeolite-supported bimetallic nanoclusters, which are characterized by distinctive structural attributes and enhanced catalytic capabilities, thereby offering opportunities for practical applications in catalysis.

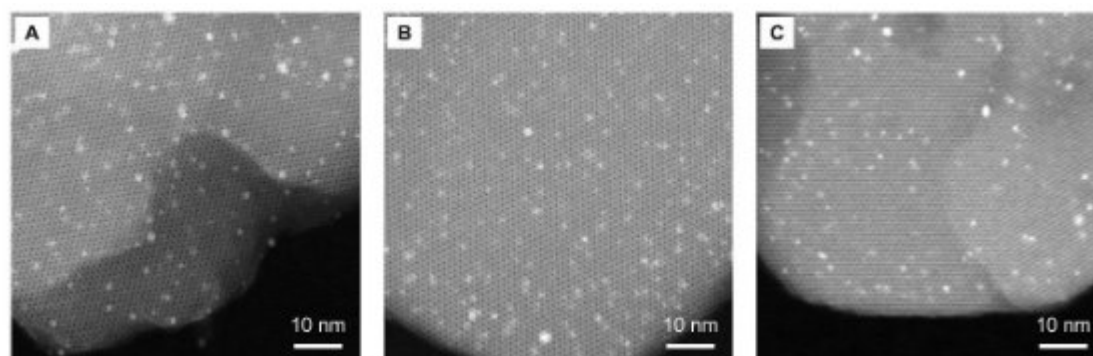


**Figure 1.** Ultrafast encapsulation of bimetallic nanoclusters into a silicalite-1 zeolite. A – C, Cs-corrected STEM images of silicalite-1 zeolites encapsulated with PtNi, PtCo and PtZn bimetallic nanoclusters, respectively. All the bimetallic-nanoclusters-encapsulated zeolites were synthesized for only 5 min at 210 °C.

### References

- [1] Liu, L.; Corma, A. Bimetallic Sites for Catalysis: From Binuclear Metal Sites to Bimetallic Nanoclusters and Nanoparticles. *Chemical Reviews* **2023**, *123* (8), 4855-4933.
- [2] Zhang, Q.; Gao, S.; Yu, J. Metal Sites in Zeolites: Synthesis, Characterization, and Catalysis. *Chemical Reviews* **2023**, *123* (9), 6039-6106.
- [3] Yu, T.; Wang, Y.; Xu, J.; Liu, Z. A generalized strategy for the ultrafast encapsulation of metal oxide nanoclusters into zeolites. *Reaction Chemistry & Engineering* **2024**, *9* (6), 1532-1540.

### Acknowledgments

This work was supported in part by National Natural Science Foundation of China (grant no.: 22278237), State Key Laboratory of Chemical Engineering (grant no.: SKL-CHE-22T04) and Tsinghua University (a start-up fund to Z.L.).



## Rational Control of Aluminum Distribution in Zeolites with Alternative Additives Boosts Catalytic Performance

L. Zhao<sup>1</sup>, Y. Wang<sup>1,2</sup>, P. Xiao<sup>1</sup>, Q. Li<sup>1</sup>, H. Toyoda<sup>1</sup>, T. Yokoi<sup>1,2</sup>

<sup>1</sup> Institute of Innovative Research, Tokyo Institute of Technology, 4259 Nagatsuta, Midori-ku, Yokohama 226-8501, Japan

<sup>2</sup> iPEACE223 Inc., Konwa Building, Tsukiji, Chuo-ku, Tokyo, 1-12-22, Japan

zhao.l.ae@m.titech.ac.jp

### Abstract

The acid sites distribution in the framework of zeolite plays a pivotal role in the catalytic reactions. This study aims to tune the Bronsted sites (Al sites) based on the variations of electrostatic interaction with the negatively charged  $[AlO_4]^-$  in the MFI-type zeolite framework. The strategy is to employ distinct additives accompanied by typical template of TPAOH. It was found that the various electronic environment brought by organic, inorganic or mineralizing agents in the synthetic gel compositions leads to different existing form of tetrapropylammonium (TPA) cations. The proportion of ion-paired TPA cations increased with the order of pentaerythritol (PET) < cetyltrimethylammonium bromide (CTAB) < urea <  $NH_4F$  as additives. This observation indicates that the role of structure-directing agent (SDA) has been influenced and maybe lead to different interaction or distance between Al-N during synthesis process, which is expected to determine the distribution of tetrahedra  $[AlO_4]^-$  in the framework. The change in the Al distribution has been demonstrated by NMR and Co-UV-vis techniques, in which  $NH_4F$  leads to more single Al in the framework preferentially located in the channels. Besides, the activity of various zeolites in the methanol-to-olefin (MTO) reaction has also been impacted,  $NH_4F$  contributes to boosted catalytic stability and products selectivity. This study provides a promising strategy to modulate the Al distribution in high-silica (Si/Al>100) zeolite framework, while reducing the cost of organic templating agents.

### Introduction

The MFI-type aluminosilicate zeolite (ZSM-5), which has generally been synthesized with TPA cations as the template, has been widely used as a solid acid catalyst in many petrochemical catalytic processes. The distribution of Al atoms in the zeolite framework has been recognized as an important factor in activity and selectivity, because it profoundly affects the accessibility of molecules to acid sites and the spatial constraints of the reaction field in the pores. It has been reported that the distance between N atoms in TPA cations and Al atoms is controlled by different binding energies, offering a strategy to adjust the distribution of Al in zeolites [1]. By weakening the interaction of TPA with Al through the addition of other substances, Al atoms can be positioned at channels, away from the influence of TPA. For instance, our group has explored the use of Na cations to alter Al distribution and recently combined neutral PET with TPA to further manipulate Al positioning [2-3]. These results suggest that the structural directing effect (electronic effect) of TPA cations can be influenced by external additives. To gain a more comprehensive understanding of this mechanism and provide broader insights, we extended our research to include other common additives. This study thus presents a thorough discussion on the use of various additives and strategies to reduce the reliance on traditional TPA templates. By redefining the role of TPA, we propose new approaches for the design of zeolite catalysts and the enhancement of catalytic performance.

### Synthesis of various ZSM-5 zeolites

Various ZSM-5 samples synthesized with TPAOH and different additives including PET, urea,  $NH_4F$ , CTAB were labeled as Z5-PET, Z5-Urea, Z5- $NH_4F$ , Z5-CTAB. The gel composition is 1  $SiO_2$ :0.005  $Al_2O_3$ : 0.1 additive:0.15 TPAOH:0.25 NaOH:60  $H_2O$ :5 wt.% silicate-1, Besides the control zeolite is synthesized with only TPAOH, the TPAOH/Si is 0.25 and labeled as Z5-TPA. The mother gel was crystallized at 443 K for 3 days. All synthesized samples were filtered, washed with deionized water, and dried. The organic components were removed by calcination at 823 K for 6 h.  $NH_4^+$ -exchanged ZSM-5 samples were obtained by stirring in a 2.5 M  $NH_4NO_3$  solution at 353 K for 24 h, which was subsequently converted to H-type ZSM-5 by calcination at 823 K for 6 h. Unless otherwise stated, H-type samples were used for the characterization and reactions in this study.

### Results and discussion

The ZSM-5 synthesized with different additives exhibited similar Si/Al ratios (around 100), and XRD analysis showed that all zeolites had improved crystallinity compared to Z5-TPA, even with reduced TPA usage. Moreover, the crystal size and morphology of the zeolites remained largely unchanged. Elemental analysis of the as-made samples revealed that, except for the Z5-CTAB sample, which retained a small amount of residual CTAB, the organic species present in the other samples consisted solely of TPA, consistent with the results from  $^{13}C$  NMR. Thermogravimetric analysis (TGA) showed that the TPA species in the as-made samples varied (Figure 1a). Two distinct degradation temperatures for TPA cations were observed: one for ion-paired TPA at a lower degradation temperature and another for

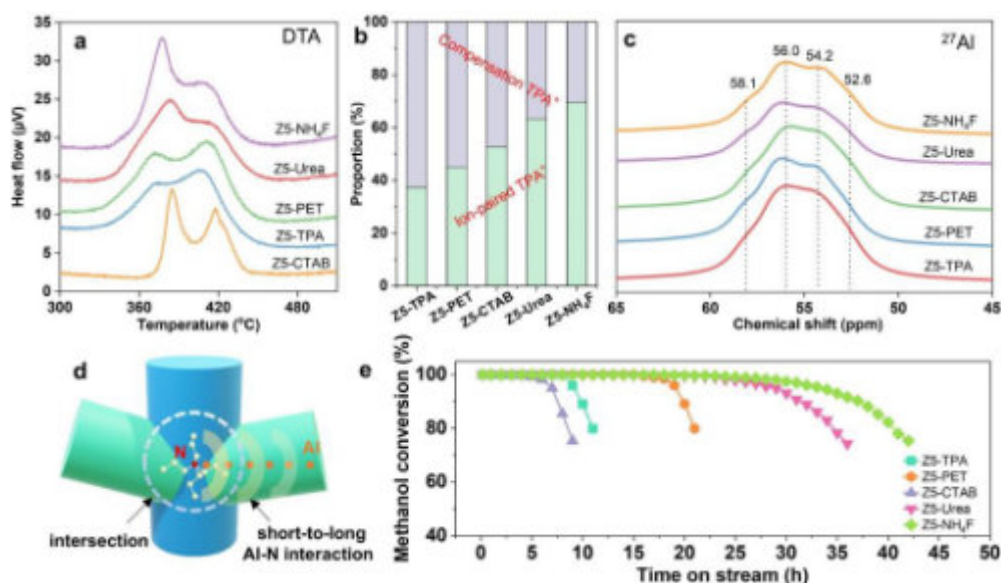


**Figure 1.** (a) DTA results of as-made samples; (b) Proportion of different TPA form based on DTA results; (c) <sup>27</sup>Al NMR results of various samples; (d) Proposed Al-N interaction catalysts, 450 °C, WHSV=5.5 h<sup>-1</sup>; (e) Catalytic performance in MTO reaction. Reaction conditions: 50 mg catalysts, 450 °C, WHSV=5.5 h<sup>-1</sup>.

compensation TPA linked to tetrahedral [AlO<sub>4</sub>]<sup>-</sup> at a higher temperature. Several additives were found to increase the peak corresponding to ion-paired TPA, with the Z5-NH<sub>4</sub>F sample showing the highest peak (Figure 1b), indicating that NH<sub>4</sub>F altered directing effect of TPA. The <sup>27</sup>Al NMR results showed that the Z5-NH<sub>4</sub>F sample had the highest peak at a chemical shift of 58 ppm (Figure 1c), indicating that more Al sites in this sample were located in the channels rather than at the intersections. Additionally, UV-vis analysis of Co ion-exchanged samples demonstrated a significant increase in the amount of isolated Al, suggesting that the distribution of Al in the samples was influenced by the additives, leading to Al being located away from TPA (N atoms) at the intersections, with Al distribution varying according to the additives used (Figure 1d). Future research will focus on using DFT simulations to calculate the changes in binding energies at different Al-N distances induced by various additives, and determining the specific tetrahedral sites corresponding to these Al-N distances using MQMAS techniques. In methanol-to-olefins catalytic reactions, the order of catalytic lifetime improvement for the samples was Z5-NH<sub>4</sub>F < Z5-Urea < Z5-PET, with the Z5-CTAB sample showing no improvement in lifetime. This could be due to some CTAB acting as a co-OSDA, causing Al to be distributed on the external surface of the catalyst, which increased coke formation and degraded the catalytic activity.

## Conclusion

This study demonstrates the critical influence of various additives on the structural and catalytic properties of ZSM-5 zeolites synthesized with TPAOH as the primary template. By systematically introducing organic, inorganic, and mineralizing agents, we successfully modulated the electronic environment within the synthetic gel, leading to distinct changes in the form of TPA cations and the distribution of tetrahedral [AlO<sub>4</sub>]<sup>-</sup> sites in the zeolite framework. This research provides a new strategy for controlling Al site distribution in high-silica zeolites while reducing reliance on organic templates like TPA. The findings offer valuable insights into the design of zeolite catalysts with optimized acid site distribution, which can significantly improve catalytic efficiency in industrial processes. Future investigations will focus on further elucidating the Al-N interactions through DFT simulations and advanced spectroscopic techniques, enabling the development of tailored catalysts with enhanced performance in various catalytic applications.

## References

- [1] C. T. Nimlos, et. al *Chem. Mater.*, **32**, 9277–9298 (2022).
- [2] T. Yokoi, et. al. *J. Phys. Chem. C.*, **119**, 15303–15315 (2015).
- [3] L. Zhao et.al. *ACS Appl. Mater. Interfaces*, **16**, 14, 17701–17714 (2024).



## Synthesis and Structural Analysis of High-Silica ERI Zeolite with Spatially-Biased Al Distribution as a Promising NH<sub>3</sub>-SCR Catalyst

J. Zhu<sup>1</sup>, K. Muraoka<sup>\*1</sup>, T. Ohnishi<sup>2</sup>, Y. Yanaba<sup>2</sup>, M. Ogura<sup>2</sup>, A. Nakayama<sup>1</sup>, T. Wakihara<sup>\*1,3</sup>, Z. Liu<sup>\*1,3,4</sup>, T. Okubo<sup>1</sup>

<sup>1</sup> Department of Chemical System Engineering, The University of Tokyo, 7-3-1 Hongo, Bunkyo-ku, Tokyo 113-8656, Japan

<sup>2</sup> Institute of Industrial Science, The University of Tokyo, 4-6-1 Komaba, Meguro-ku, Tokyo, 153-8505, Japan

<sup>3</sup> Institute of Engineering Innovation, The University of Tokyo, 2-11-16 Yayoi, Bunkyo-ku, Tokyo 113-8656, Japan

<sup>4</sup> State Key Laboratory of Chemical Engineering, Department of Chemical Engineering, Tsinghua University, Haidian District, Beijing 100084, China

jiezhu@mit.edu

Selective catalytic reduction of NO<sub>x</sub> with ammonia (NH<sub>3</sub>-SCR) over metal-exchanged zeolite catalysts has been developed as one of the most effective technologies for the mitigation of NO<sub>x</sub>.<sup>[1]</sup> In particular, small-pore zeolites have received considerable attention due to their high hydrothermal stability and long-lasting performance in the NH<sub>3</sub>-SCR reaction.<sup>[2,3]</sup> The synthesis of high-silica zeolites usually involves the addition of complicated organic structure-directing agents (OSDAs) or even the presence of fluoride (F<sup>-</sup>) media, which imposes high costs and safety concerns in obtaining high-silica SCR catalysts. Erionite (ERI) zeolite has recently attracted significant interest for its potential application in NH<sub>3</sub>-SCR reaction;<sup>[4]</sup> however, achieving a high Si/Al ratio (>7) in ERI zeolites using a simple OSDA while preserving their structural integrity remains a challenge.

In this work, we report the synthesis of high-silica ERI zeolite with tunable Si/Al ratios using a single OSDA. Three ERI zeolites with different Si/Al ratios (4.6, 6.4 and 9.1) can be prepared via an ultrafast route by using either ordinary amorphous silica and alumina sources or faujasite (FAU) as starting material.<sup>[5]</sup> The solid-state <sup>29</sup>Si MAS NMR spectroscopic study in combination with a computational simulation allowed us to figure out the atomic configurations of the Al species in the ERI zeolites with different Si/Al ratios. The results revealed that ERI-9.1 (where the number indicates the Si/Al ratio) exhibited a spatially-biased Al occupancy at T1 site, probably due to the higher fraction of the residual K<sup>+</sup> cations in the *can* cages, which could preferably direct the Al insertion into the T1 site. On the contrary, the Al occupancy at the two T sites in ERI-4.6 and ERI-6.4 was found close to the theoretical ratio between the multiplicity of the two T sites, suggesting a relatively random Al distribution in the two samples.

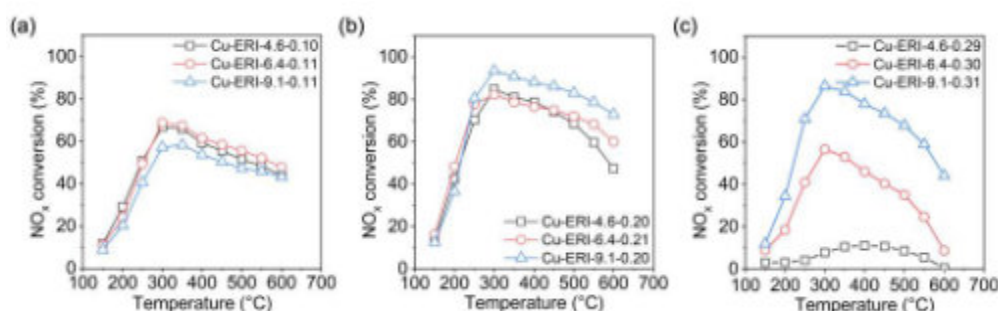


**Figure 1.** NH<sub>3</sub>-SCR activity of hydrothermally aged Cu-ERI zeolites with different Si/Al ratios but the same Cu/Al ratios. (a) Cu/Al=0.10; (b) Cu/Al=0.20; (c) Cu/Al=0.30.

The synthesis of ERI zeolite with a high Si/Al ratio offers a chance to explore this small-pore zeolite as a potential NH<sub>3</sub>-SCR catalyst. The three ERI zeolites were ion-exchanged into corresponding copper-form ones of different Cu/Al ratios, and the resultant Cu-ERI catalysts were labelled as Cu-ERI-x-y, where x and y represent the Si/Al ratio and the Cu/Al ratio, respectively. After hydrothermal aging at 800 °C for 5 hours, Cu-ERI-9.1 maintained its crystallinity and exhibited higher NO<sub>x</sub> conversion rates across a range of temperatures (Figure 1), particularly at higher copper loadings (Cu/Al=0.20 and 0.30). This performance was markedly better than that of Cu-ERI-4.6 and Cu-ERI-6.4, demonstrating that a higher Si/Al ratio enhances both the hydrothermal stability and catalytic activity of the material.<sup>[5]</sup>

This study demonstrates that high-silica ERI-9.1 zeolite, characterized by a spatially-biased Al distribution, exhibits improved hydrothermal stability and NH<sub>3</sub>-SCR activity. The synthesis of ERI zeolites with tunable Si/Al ratios and the comprehensive analysis into their structural characteristics will deepen our understandings into the ERI zeolite and unlock its potential in industrial applications.

### References

- [1] P. Granger, and V. I. Parvulescu, *Chem. Rev.* **111**, 3155 (2011).
- [2] T. Ryu, N. H. Ahn, S. Seo, J. Cho, H. Kim, D. Jo, G. T. Park, P. S. Kim, C. H. Kim, E. L. Bruce, P. A. Wright, I.-S. Nam, and S. B. Hong, *Angew. Chem. Int. Ed.* **56**, 3256 (2017).
- [3] J. Kim, S. J. Cho, and D. H. Kim, *ACS Catal.* **7**, 6070 (2017).
- [4] J. Zhu, Z. Liu, L. Xu, T. Ohnishi, Y. Yanaba, M. Ogura, T. Wakihara, and T. Okubo, *J. Catal.* **391**, 346 (2020).
- [5] J. Zhu, K. Muraoka, T. Ohnishi, Y. Yanaba, M. Ogura, A. Nakayama, T. Wakihara, Z. Liu, and T. Okubo, *Adv. Sci.* **11**, 2307674 (2024).

## Determination of aluminum distribution and active sites location in zeolite based-catalysts by anomalous X-ray powder diffraction

P. Rzepka<sup>1,2\*</sup>, K. Mlekodaj<sup>1</sup>, E. Tabor<sup>1</sup>, J. Dědeček<sup>1</sup>, J. A. van Bokhoven<sup>2</sup>

<sup>1</sup> J. Heyrovský Institute of Physical Chemistry of the CAS, Dolejškova 2155/3, 182 23 Prague 8, Czech Republic

<sup>2</sup> Institute for Chemical and Bioengineering, ETH Zurich, Vladimir-Prelog-Weg 1-5 / 10, 8093, Zürich, Switzerland

przemyslaw.rzepka@jh-inst.cas.cz

The organization of aluminum (Al) atoms in zeolites, along with their topology, is a critical parameter defining the presence and behavior of catalytically active centers. Al atoms introduce a negative charge in the zeolitic lattice, which needs to be balanced by extra-framework counter-ions serving as active sites, including acid (protons) and redox (transition metal ions) sites. In Si-rich zeolites (Si/Al > 10), Al atoms can be present as single Al atoms, Al pairs, and close Al atoms. Single Al atoms can stabilize monovalent species, while Al pairs, arranged in Al-(SiO<sub>2</sub>)<sub>2</sub>-Al sequences, are balanced by bare divalent cations or provide proton proximity in acid sites. When close Al atoms are present, Al-(SiO<sub>2</sub>)<sub>3</sub>-Al sequences can accommodate complexes of divalent cations. It has been shown that the distribution of Al atoms in the structure of zeolite ZSM-5 reflects their catalytic performance in propane oligomerization. The sample with a high fraction of Al pairs is more active due to the repulsive forces of alkoxides stabilized on Al pairs, which control the rates of adsorption and desorption, formation of intermediates, and product release. The location of Al atoms in Si-rich zeolites is not random and can be influenced by synthesis conditions. This provides a robust tool for customizing the zeolite structure, determining the prevalent type of desired active centers, and thus fine-tuning its catalytic properties.

Discriminating aluminum from silicon in the zeolite framework and recognizing T-site dependent reactivity of zeolites is a long-standing question in zeolite science. There is currently no general method that can directly identify which T sites in a zeolite framework structure are occupied by aluminum. Aluminum substitution for silicon is usually only partial (typical zeolite catalysts have Si:Al ratios larger than 5) and the scattering power of these two elements is very similar. Until now, the organization of Al atoms in zeolites has been investigated using well-proven methods based on UV-Vis and FTIR of Co-containing zeolites, chemical analysis, and <sup>27</sup>Al and <sup>29</sup>Si MAS NMR studies, which are all short-range probes and can report only on the local environment around the aluminum positions. Therefore, we have developed anomalous X-ray powder diffraction (AXRD) methodology across the Al K-edge (1.56 keV), where the aluminum scattering factor changes significantly while that of silicon remains unchanged. These changes in the scattering power highlight aluminum in the structure. In contrast to spectroscopic methods, AXRD can collect information on the long-range structural order of Al:Si distribution and consequently unambiguously pinpoint aluminum's positions in the framework structure. Because the diffraction limit at 1.56 keV corresponds to a d-spacing of only 3.98 Å, data from a conventional measurement were combined with those at energies near the X-ray absorption edge to quantify the aluminum concentration at all T sites in the refined zeolite structure.

The H-ZSM-5 zeolite studied here has a framework structure with 12 T-atoms in the Pnma unit cell and comprises a 3D network of intersecting 10-ring straight and sinusoidal channels. Two samples with similar Si/Al molar ratios of 18 and 15, but differing in the concentrations of Al pairs (9% and 82%, respectively), were determined using Co(II) as a probe molecule. Spectroscopic studies have identified typical sites for divalent cobalt cations at the elongated 6-rings formed from two-folded 5-rings ( $\alpha$  site) and at the 5- or deformed 6-rings ( $\beta$  site). The  $\alpha$  and  $\beta$  sites in highly exchanged ZSM-5 are suggested to be located at the walls of the straight and sinusoidal channels, respectively. The minor boat-shaped  $\gamma$  site formed from the 5- and 6-rings is speculated to be in the sinusoidal channel. Our pioneering AXRD studies assigned precise ordering of Al atoms to particular T-atom positions. It was shown that the aluminum pairs up at adjacent T8 atoms located at the intersection of the straight and sinusoidal channels, matching the definition of the  $\beta$  site. Additionally, the  $\beta$  site can form between T4 and T10 or T4 and T11 atoms in the 5-ring, which is isolated from large-pore voids. The Al pair at T8 and T11, with underlying silicon at T3, establishes siting for the  $\alpha$  site. The aluminum ordering corroborates well with the refined positions of three Co atoms found at the determined  $\alpha$  and  $\beta$  sites.

These findings show that the definition of cationic sites coined by spectroscopic studies is correct; however, their situation in the long-range periodic structure remains elusive. We believe that AXRD at the Al K-edge may be the right technique to reevaluate other zeolite framework structures hosting Al-paired distributions.

[1] Dědeček, J., Tabor, E., Sklenak, S. (2019). *ChemSusChem*. **12** (3), 556-576.

[2] Bernauer, M., Tabor, E., Pashkova, V., Kaucký, D., Sobalík, Z., Wichterlová, B., Dedecek, J. (2016). *J. Catal.* **344**, 157-172.

[3] Tabor, E., Bernauer, M., Wichterlová, B., Dedecek, J. (2019). *Catal. Sci. Technol.* **9** (16), 4262-4275.

[4] Pinar, A. B., Rzepka, P., Knorpp, A. J., McCusker, L. B., Baerlocher, C., Huthwelker, T., Van Bokhoven, J. A. (2021). *J. Am. Chem. Soc.* **143** (43), 17926-17930.

[5] Baerlocher, C.; McCusker, L. B. Database of zeolite structures; <http://www.iza-structure.org/databases/> (accessed 2024-07-31).

# How water impacts zeolite crystallization in Hydrated Silicate Ionic Liquids

Dries Vandenabeele, Nikolaus Doppelhammer, Sambhu Radhakrishnan, C. Vinod Chandran, Anjul Rais, Christine Kirschhock, Eric Breynaert

Zeolite crystallization in Hydrated Silicate Ionic Liquids (HSILs) offers significant advantages over traditional gel-based methods for studying zeolite formation [1,2]. HSILs can be described as molten alkali silicates in which aluminate can dissolve, to form over 15 distinct zeolite structures [3]. The homogeneous nature of HSILs eliminates concentration gradients that typically occur near gel(-like) particles in conventional systems [2]. These gradients can heavily influence crystallization processes, yet they are difficult to quantify. In addition, HSILs enable the precise study of individual parameters without the interference of complex cross-correlations that usually arise during the aging phase of zeolite formation.

Previous research has demonstrated the critical role of water in the crystallization of zeolites. Water availability not only controls whether porous or dense materials are formed, but it also affects the final Si/Al ratio of the product [3,4]. Since zeolite formation is also significantly influenced by kinetic factors, this study expands on earlier findings by conducting a detailed kinetic analysis of the crystallization process [1]. In this study, we monitor zeolite formation using a combination of in situ static  $^{27}\text{Al}$  NMR and conductivity measurements obtained through Differential Impedance Spectroscopy (DIS). The system we investigated forms synthetic pollucite using the composition:  $0.5 \text{ SiO}_2 - 0.03 \text{ Al}(\text{OH})_3 - 1 \text{ CsOH} - X \text{ H}_2\text{O}$ . NMR is used to track the aluminum content in the liquid phase, while conductivity monitors the number of chemical bonds formed during crystallization.

Water has a profound impact on crystallization behavior. Increasing the amount of water not only influences the rate of crystallization but also alters the crystallization profile. Specifically, the process shifts from a symmetric sigmoidal curve to a two-step profile. Additionally, dilution prolongs the induction phase while sharpening the growth phase. The two-step profile is due to the formation of an intermediate side phase known as aluminite, which eventually dissolves. Since aluminite does not share any structural or compositional resemblance to the final zeolite product, we believe it does not act as a precursor phase. Additional XRD analysis, turbidity measurements, yield analysis, and  $^{29}\text{Si}$  NMR show that shifting growth and induction times can be related to a shifting supersaturation ratio, which influences the silicate solubility, the nucleation and growth rates, the grain size, and the overall solid yield.

When considering these findings in the context of thermodynamic phase selection criteria, it becomes clear that water content plays a crucial role in determining the pathway and outcome of crystallization. By controlling water content, it is possible to fine-tune crystallization behavior, offering valuable insights for future crystal engineering strategies.

## References:

[1] Vandenabeele, Dries, et al. "Can the combination of in situ differential impedance spectroscopy and  $^{27}\text{Al}$  NMR detect incongruent zeolite crystallization?" *Microporous and Mesoporous Materials* 374 (2024): 113141. [2] Pellens, Nick, et al. "Nucleation of Porous Crystals from Ion-Paired Prenucleation Clusters." *Chemistry of Materials* 34.16 (2022): 7139-7149. [3] Asselman, Karel, et al. "Ion-pairs in aluminosilicate-alkali synthesis liquids determine the aluminum content and topology of crystallizing zeolites." *Chemistry of Materials* 34.16 (2022): 7150-7158. [4] Asselman, Karel, et al. "Does water enable porosity in aluminosilicate zeolites? Porous frameworks versus dense minerals." *Crystal Growth & Design* 23.5 (2023): 3338-3348.





## Direct submicron-scale imaging of Al distribution in small-pore zeolites: Revealing unique deAl behavior in intracrystalline architecture of AFX

Y. Kamimura<sup>1</sup>, T. Kodaira<sup>1</sup>, and A. Endo<sup>1</sup>

<sup>1</sup> National Institute of Advanced Industrial Science and Technology (AIST), 1-1-1 Higashi, Tsukuba, Ibaraki 305-8565, Japan  
yoshihiro-kamimura@aist.go.jp

### Introduction

Recent development on the dealumination of small pore zeolites with the aid of occluded organic structure-directing agent (OSDA) has realized to control bulk silicon to aluminium (Si/Al) ratios with well-preserved framework. Despite being useful strategy to tune the Si/Al ratios of the small-pore zeolites toward desired properties, its dealumination process especially at the intermediate stage has not been fully clarified yet. This is because several intricate events occur parallelly during the dealumination of zeolites, which makes difficult to acquire the comprehensive understanding of the detailed scenarios in the sequential dealumination process. For this reason, we have performed the direct submicron-scale imaging of Al distribution related with its structural change in the intracrystalline architecture of dealuminated small-pore zeolites using integrated techniques of high-resolution low-accelerating voltage field-emission scanning electron microscope (FE-SEM) and energy-dispersive X-ray spectroscopy (EDS) elemental mapping. Both top-surface and cross-sectional FE-SEM observations and EDS elemental mapping have revealed the unique features in its dealumination behavior of corresponding small-pore zeolites, which were strictly governed by the presence or absence of OSDA. Further information on the detailed dealumination behavior by linking findings with a series of statistical analyses will be disclosed and discussed in the presentation.

### Experimental

Aluminosilicate AFX zeolite (also recognized as SSZ-16) was selected as an example for the dealumination of small-pore zeolites in this study. Parent AFX (Si/Al<sub>EDS</sub>=3.5) was synthesized according to the previous literature with using DABCO-C<sub>4</sub>-Diquat-Br<sub>2</sub> as an OSDA [1]. Obtained AFX was subjected to the dealumination treatment based on the pore-opening migration process (POMP) [2]. This treatment was realized by the acid leaching of zeolite in the presence of OSDA occluded in the *aft* cage of AFX-type framework. Similar acid leaching of AFX in the absence of OSDA (obtained after calcination) was also performed for the comparison. Direct imaging of top-surface and cross-sectional structure in the series of AFX zeolite particles was performed using low-accelerating voltage FE-SEM. The Al distribution on the cross-sectional structure at the same observation area by FE-SEM was acquired using the EDS elemental mapping. Cross-section of AFX zeolite particles was prepared by the argon (Ar) broad ion beam (BIB) milling operated under mild, less damaging conditions. The discussion is not only made based on the local observation related to cross-sectional structure and its Al distribution, but also statistical analyses including powder X-ray diffraction (PXRD), Ar physisorption from low pressure region ( $P/P_0 > 10^{-8}$ ), solid-state nuclear magnetic resonance (NMR), thermogravimetric analysis (TG-DTA), and chemical analysis were conducted to correlate with the detailed structural features.

### Results and discussion

Fig. 1a and c show the top-surface images for parent AFX in as-made (with OSDA) and calcined forms (without OSDA). Both parent AFX zeolites exhibited pencil-like morphology with a particle size of 1-3  $\mu\text{m}$ , and calcination of parent AFX gave no distinctive change on its appearance. After the acid treatment, AFX with OSDA showed rough surface with several cracks (Fig. 1b), while AFX without OSDA exhibited smooth surface and no cracks were observed (Fig. 1d). To understand the change in intracrystalline architecture of AFX particles minutely, FE-SEM and EDS elemental mapping on the cross-sectional structure (sliced parallelly along with *c*-axis) were performed. Fig. 2a and c show cross-sectional FE-SEM and EDS elemental mapping images for the parent AFX with or without OSDA, where both AFX displayed smooth surface in secondary electron (SE) images, and uniform distribution of Al and Si elements was observed by EDS. For the case of acid treated AFX with OSDA (Fig. 2b), formation of cracks was observed inside of the AFX particle in the SE image. EDS analysis at the same viewing position showed non-uniform distribution of Al element. Here, dark contrast seen in the Al distribution resembled to the shape of cracks formed in the AFX particle, while bright contrast in the Si distribution was observed at the same viewing position. In the case of acid treated AFX without OSDA (Fig. 1d), SE image showed smooth surface, and no cracks was observed. When EDS was applied at the same

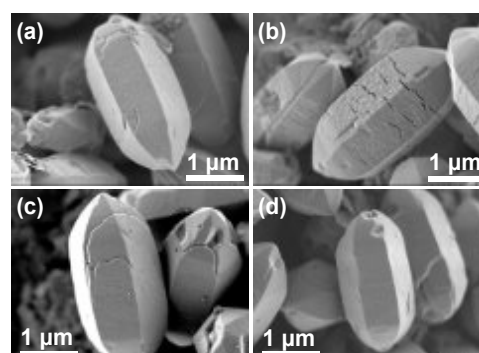


**Figure 1.** Top-surface FE-SEM images for (a) parent AFX (with OSDA), (b) acid treated AFX with OSDA, (c) parent AFX in calcined form (without OSDA), and (d) acid treated AFX without OSDA.

viewing position, there is non-uniform distribution in both Al and Si elements. Here, Al element with high concentration located inner part of the particle, and Al mapping signal at outer part of the particle was less pronounced as compared to the inner part. Also, the distribution of Si element was inverted to the distribution of the Al element. Average Si/Al ratios evaluated by the EDS ( $\text{Si}/\text{Al}_{\text{EDS}}$ ) at the viewing areas showed a following trend: Parent AFX ( $\text{Si}/\text{Al}_{\text{EDS}} = 3.5\text{-}3.7$ ) < acid treated AFX with OSDA ( $\text{Si}/\text{Al}_{\text{EDS}} = 4.3$ ) < acid treated AFX without OSDA ( $\text{Si}/\text{Al}_{\text{EDS}} = 11.6$ ). The local  $\text{Si}/\text{Al}_{\text{EDS}}$  ratios for both acid treated AFX particles differed from the average  $\text{Si}/\text{Al}_{\text{EDS}}$ . In the acid treated AFX with OSDA, cracks showed higher  $\text{Si}/\text{Al}_{\text{EDS}} = 6.3\text{-}6.6$  as compared to the smooth surface region having uniform Al distribution ( $\text{Si}/\text{Al}_{\text{EDS}} = 3.4$ ). Local  $\text{Si}/\text{Al}_{\text{EDS}}$  ratios for the AFX without OSDA exhibited higher  $\text{Si}/\text{Al}_{\text{EDS}} = 48.2$  at outside of the particle while inside remained as Al-rich having  $\text{Si}/\text{Al}_{\text{EDS}} = 3.3$ . The  $\text{Si}/\text{Al}_{\text{EDS}}$  ratio at the Al-rich region in both acid treated AFX particles were similar to the  $\text{Si}/\text{Al}_{\text{EDS}}$  ratio of the parent AFX samples. PXRD patterns and baseline profile extracted from them indicated that AFX framework after acid treatment retained but there is a gradual increase of amorphous matter when the OSDA is present. In contrast, framework was no longer maintained (mainly amorphous matter) when the OSDA is absent. Also lattice constants for the acid leached AFX with the OSDA showed large expansion in the **a**- and **b**-axes and shrinkage in the **c** axis. Ar physisorption of the acid leached AFX (calcined prior to the physisorption measurement) showed that micropore structure was maintained when the OSDA is present, while almost 90 % of micropore was lost in the case when the OSDA is absent. Moreover, Ar physisorption uptake at low pressure region ( $P/P_0 > 10^{-8}$ ) showed gradual shift to high pressure region after acid leaching of AFX with the OSDA, which indicates that there is micropore widening due to ejection of Al atoms from the framework. TG-DTA of the parent AFX in as-made form showed that *ca.* 1 OSDA molecule occluded in the unit cell of AFX, which indicates that the OSDA inhibits the acid intrusion, but acid can enter through 8R where no OSDA is occluded. Based on the obtained results, following possible dealumination processes are proposed. Presence of OSDA stabilizes the AFX framework during the acid treatment, which resulted in the partial ejection of Al with retaining its framework to give moderate increase in the  $\text{Si}/\text{Al}_{\text{EDS}}$  ratio. Acid leaching preferentially starts from the outside of the AFX particle (where no OSDA is occluded) accompanied with the formation of the cracks due to the expansion and shrinkage of the lattice constants. Further acid intrusion occurs from the crack and continues irregularly to remove Al species from intruded pathways. The acid treatment of AFX without the OSDA ejects the Al from the framework and transforms to an amorphous matter by the framework collapse at an early stage. At a later stage of the acid treatment, dealuminated species were removed from the particles, which resulted in the remaining of Si-rich species having extremely higher  $\text{Si}/\text{Al}_{\text{EDS}}$  ratio.

### Conclusion

Direct submicron-scale imaging of small-pore zeolite by cross-sectional FE-SEM combined with EDS allows us to visualize the intracrystalline structure with distribution of Al and Si elements in the zeolite particles. It is found that stability of the AFX framework is strictly depends on the presence of OSDA occluded in the *aft* cage. Acid treatment of AFX with or without OSDA affects its microporous framework, and also gives a significant change in the intracrystalline structure and Al distribution under submicron scale. More details in the dealumination process specifically at the intermediate stage will be discussed in the presentation, where we would like to provide insights how does Al distribution in a submicron scale relates to the dealumination behavior as well as change in the structural features of AFX zeolite particles.

### References

- [1] H. Yamada, T. Iida, Z. Liu, Y. Naraki, K. Ohara, S. Kohara, T. Okubo, and T. Wakihara, *Cryst. Growth Des.*, 16, 3389 (2016).
- [2] T. Yoshioka, K. Iyoki, Y. Hotta, Y. Kamimura, H. Yamada, Q. Han, T. Kato, C.A.J. Fisher, Z. Liu, R. Ohnishi, Y. Yanaba, K. Ohara, Y. Sasaki, A. Endo, T. Takewaki, T. Sano, T. Okubo, T. Wakihara, *Sci. Adv.*, 8, eabo3093 (2022).

### Acknowledgments

This work was supported by a Moonshot Project from the New Energy and Industrial Technology Development Organization (NEDO) funding agency, Japan.

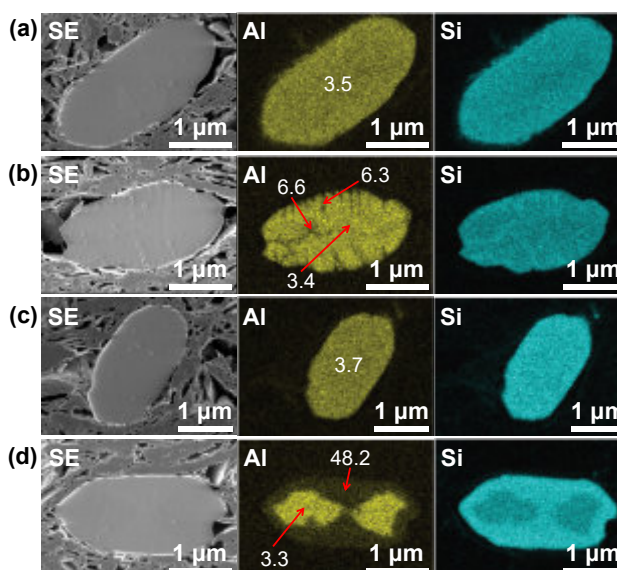


**Figure 2.** Cross-sectional FE-SEM (secondary electron, SE) and EDS elemental mapping (Al and Si) images for (a) parent AFX (with OSDA), (b) acid treated AFX with organic pore-filler, (c) parent AFX in calcined form (without OSDA), and (d) acid treated AFX without OSDA. Numbers shown in the Al mapping images indicate local  $\text{Si}/\text{Al}_{\text{EDS}}$  evaluated by EDS.

# POSTER COMMUNICATIONS

P001 – P135



## Synthesis and characterization of zeolite@ZIF-8 composite by various methods as a catalyst for organic reactions

M. Zendehdela<sup>1</sup>, H. Ghaedrahmat<sup>1</sup>, MY. Masoomi<sup>1</sup>

<sup>1</sup> Department of Chemistry, Faculty of Science, Arak University, Arak 38156-8-8349, Iran.  
m-zendehdela@araku.ac.ir and mojganzendehdela@yahoo.com

Zeolite imidazolate frameworks (ZIFs) are composited with zeolite (NaP and NaY) using ship-in-bottle and sol-gel methods through two different approaches. Two synthesized nanocatalysts showed that ZIF-8 composite with zeolite can stabilize its structure as a catalyst in acidic environment. The prepared Zeolite@ZIF-8 nanocomposites were characterized by FT-IR, XRD, SEM, BET, MAP, TGA, NH<sub>3</sub>-TPD and ICP analyses. The synthesized composites were used as catalysts for the Aldol condensation of 2-X and 4-X benzaldehyde derivatives, esterification reaction of acetic acid with four different alcohols and the transesterification reaction of animal fats, vegetable oils and waste oils. The obtained results show that the efficiency of the esterification reaction for both catalytic composites is 98.5% and 94.3%, respectively, and 78.1% for the transesterification reaction. The results show that Zeolite@ZIF-8 composite catalyst bring about 91.4% for and Aldol condensation reaction.

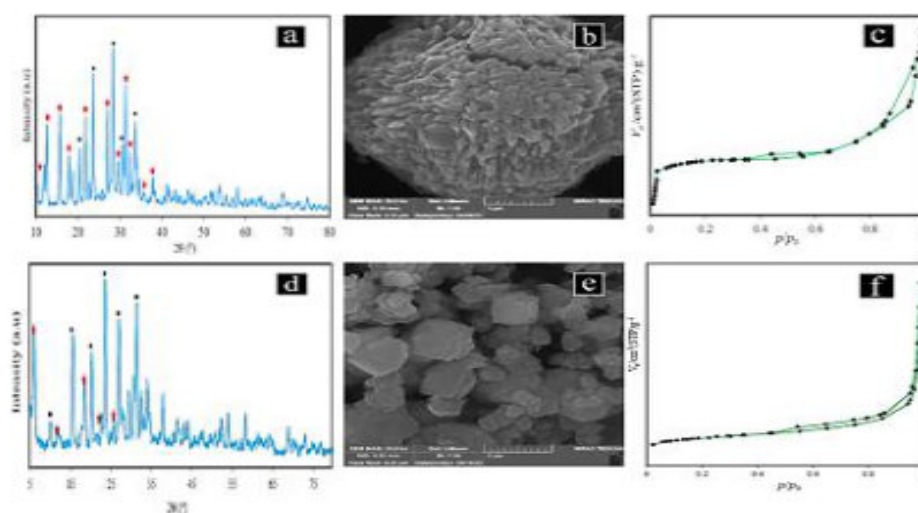


**Figure 1.** A number of analysis related to synthetic nanocatalysts: (a) XRD pattern nanocatalysts ZIF-8/NaP, (b) FESEM morphology nanocatalysts ZIF-8/NaP, (c) The nitrogen absorption–desorption isotherms nanocatalysts ZIF-8/NaP, (d) XRD pattern nanocatalysts ZIF-8/NaY, (e) FESEM morphology nanocatalysts ZIF-8/NaY, (f) The nitrogen absorption–desorption isotherms nanocatalysts ZIF-8/NaY

**Table 1.** Organic reactions carried out with synthetic catalysts under optimal conditions

Entry	reactions	Catalyst	Catalyst amount (mg)	Time (h)	Temperature(°C)	Yield (%)
1	Esterification	ZIF-8/NaP	150	5	115	94.3
2		ZIF-8/NaY	150	5	115	98.5
3	Aldol condensation	ZIF-8/NaP	60	16	room temperature	91.3
4		ZIF-8/NaY	30	16	room temperature	91.4
5	Transesterification	ZIF-8/NaY	200	5	80	78.1

### References

- [1] H. Ghaedrahmat, MY. Masoomi, M. Zendehdela, "Synthesize and characterization of ZIF-8/NaP zeolite composites as a stable acid-base catalyst for organic reactions," *Polyhedron*, vol. 15, p. 116372, 2023.
- [2] H. Ghaedrahmat, MY. Masoomi, M. Zendehdela, "Synthesis and characterization of NaY@ ZIF-8 composite by the ship-in-bottle method as a catalyst for esterification and transesterification reactions," *Biofuels, Bioproducts and Biorefining*, 2024.
- [3] H. Ghaedrahmat, MY. Masoomi, M. Zendehdela, "Synthesis and Characterization of Faujasite/ZIF-8 Composite by One-Pot Method, Used as a Catalyst for Esterification and Aldol Condensation Reaction," *Catalysis Surveys from Asia*, vol. 28, p. 58-73, 2024.



## Construct core-shell SSZ-13@Al<sub>2</sub>O<sub>3</sub> architecture to boost Pd-Catalyzed passive NO<sub>x</sub> adsorption performance

Guoju Yang<sup>1</sup>, Xiaoxin Chen<sup>1</sup>

<sup>1</sup> State Key Laboratory of Inorganic Synthesis and Preparative Chemistry, College of Chemistry, Jilin University, 2699 Qianjin Street, Changchun 130012, P. R. China

[yanggj@jlu.edu.cn](mailto:yanggj@jlu.edu.cn)

Nitrogen oxides (NO<sub>x</sub>) emitted from vehicle exhaust pose a significant threat to air quality and human health. While selective catalytic reduction of NO<sub>x</sub> with NH<sub>3</sub> (NH<sub>3</sub>-SCR) has proven to be effective above 200°C, substantial NO<sub>x</sub> emissions occur during the cold-start period at temperatures below 200°C. To address this issue, a passive NO<sub>x</sub> adsorber (PNA) is proposed as a complementary technology to the NH<sub>3</sub>-SCR catalyst. The PNA traps NO<sub>x</sub> at low temperatures and releases it when the SCR catalyst becomes active [1].

Numerous efforts have been dedicated to improving the performance of PNA materials. According to different supports, PNA materials can be divided into two parts: one is metal-supported oxides, and the other is metal-modified zeolites. The potential of γ-Al<sub>2</sub>O<sub>3</sub>, ZrO<sub>2</sub>/CeO<sub>2</sub> supported Pt or Pd materials was exploited for low-temperature PNA applications, the high desorption temperature, and the stability of metal oxide supports [2]. In comparison, Pd-based zeolites (Pd/zeolites) exhibited superior NO<sub>x</sub> adsorption efficiency and capacity for low-temperature NO adsorption, due to their unique porous structure and good thermal/hydrothermal stability of zeolites. Moreover, Pd/zeolites demonstrated excellent hydrothermal stability and poisoning resistance [3]. It is noteworthy that the framework structure of the zeolite (i.e. **CHA**, **MFI**, or **BEA**) affects the PNA performance of the Pd/zeolite materials [4]. The isolated Pd<sup>2+</sup> sites (Pd<sup>2+</sup> and [Pd(OH)]<sup>+</sup>) can be stabilized in the small pore of zeolites, which prevents the formation of bulky PdO during hydrothermal aging. Thus, Pd/SSZ-13 exhibited the highest hydrothermal stability among the Pd/SSZ-13, Pd/ZSM-5, and Pd/Beta with similar Si/Al ratios. The SSZ-13 support with a low Si/Al ratio possesses a higher concentration of ion exchange sites, which promotes the formation of more active Pd species and contributes to excellent PNA performance. However, severe hydrothermal aging may cause dealumination and subsequent agglomeration of large PdO particles in Al-rich SSZ-13, resulting in the inevitable deactivation of Pd/SSZ-13. Therefore, it is necessary to develop PNA materials with highly dispersive Pd<sup>2+</sup> species and superior stability.

In this work, a Pd-based core-shell material consisting of SSZ-13 core and γ-Al<sub>2</sub>O<sub>3</sub> shell (Pd/(SSZ-13@Al<sub>2</sub>O<sub>3</sub>)) was constructed as support for NO<sub>x</sub> adsorption [5]. The physicochemical properties of prepared Pd-based SSZ-13 zeolites were systematically characterized using techniques such as N<sub>2</sub> physisorption, STEM-EDX, <sup>27</sup>Al MAS NMR, NH<sub>3</sub>-TPD, XPS, and H<sub>2</sub>-TPR. The preparation of Pd/(SSZ-13@Al<sub>2</sub>O<sub>3</sub>) under high-temperature calcination conditions is beneficial to the dispersion of Pd species and the generation of more active Pd species. The core-shell structured material facilitated the dispersal and stabilization of the active Pd<sup>2+</sup> species. Compared to Pd/SSZ-13, Pd/(SSZ-13@Al<sub>2</sub>O<sub>3</sub>) showed significantly improved NO<sub>x</sub> storage capacity, moderate desorption temperature, excellent hydrothermal aging stability, and resistance to phosphorus poisoning. This study provides a design concept for preparing Pd-based zeolites with high tolerance and high stability for cold-start application.

### References

- [1] H.W. Zhao, A.J. Hill, L. Ma, A. Bhat, G. Jing, J.W. Schwank, *Catal. Sci. Technol.*, **11**, 5986–6000 (2021).
- [2] Y.Y. Ji, S.L. Bai, M. Crocker, *Appl. Catal. B Environ.*, **170–171**, 283–292 (2015).
- [3] H.-Y. Chen, J.E. Collier, D.X. Liu, L. Mantarosie, D. Durán-Martín, V. Novák, R. R. Rajaram, D. Thompsett, *Catal. Lett.*, **146**, 1706–1711 (2016).
- [4] J. Lee, Y. Ryou, S. Hwang, Y. Kim, S.J. Cho, H. Lee, C.H. Kim, D.H. Kim, *Catal. Sci. Technol.*, **9**, 163–173 (2019).
- [5] G. Yang, X. Chen, M. Nan, In preparation.

## Polypropylene catalytic upcycling in bound zeolite catalysts

Kinga Góra-Marek<sup>1\*</sup>, Karolina A. Tarach<sup>1</sup>, Oliwia Rogala<sup>1,2</sup>, Louwanda Lakiss<sup>3</sup>, Valentin Valtchev<sup>3</sup>, Jean-Pierre Gilson<sup>3</sup>

<sup>1</sup>Faculty of Chemistry, Jagiellonian University in Kraków, Gronostajowa 2, Kraków, Poland

<sup>2</sup>Doctoral School of Exact and Natural Sciences, Jagiellonian University in Krakow, Łojasiewicza 11, 30-348 Krakow, Poland

<sup>3</sup>Laboratoire Catalyse et Spectrochimie (LCS), Normandie University, Caen, France

\* kinga.gora-marek@uj.edu.pl

The relationship between zeolite properties and their catalytic performance in polyolefin (PO) conversion in higher value (petro)chemicals and transportation fuels is still well-researched, mainly focusing on the impact of acid site density and pore structure on catalytic performances (activity, selectivity, stability). However, most academic research on zeolitic catalysts is performed on pure powders, even though they are always formed into various shapes using binders in commercial applications. A better understanding of the relation between catalyst properties and catalytic performances is required to fine-tune the design of higher-performance catalysts in the chemical upcycling of waste PO.

This study proves the necessity for a deeper understanding of shaped catalysts and the importance of the impact of the binder and active phase interaction on their physicochemical properties and catalytic performance. We carried out the operando spectroscopic analysis of zeolites Y (LZY-64, CBV-712 and CBY760) and their bound counterparts of tailored acid properties ( $\gamma$ -Al<sub>2</sub>O<sub>3</sub> as a binder) for catalytic cracking of polypropylene. The catalytic cracking polypropylene (PP) performance was assessed in TG- and IR-GC&MS *operando* studies. Two-dimensional correlation analysis (2D COS IR) was applied to conclude the PP cracking and the subsequent coke combustion on a catalytically active surface. The work revealed that the strength and accessibility of BAS in shaped ultrastabilised zeolites could be regulated by alumina binder content. Rather than pure zeolites, as generally believed, it is found that the shaped zeolites with 50% alumina binder very effectively catalysed PP cracking. For extrudates, there is a noticeable shift in the distribution of products towards lighter hydrocarbons. This change in selectivity is very advantageous because it offsets the effect of the increase in cracking temperature induced by the reduced amount of zeolite in extrudates.

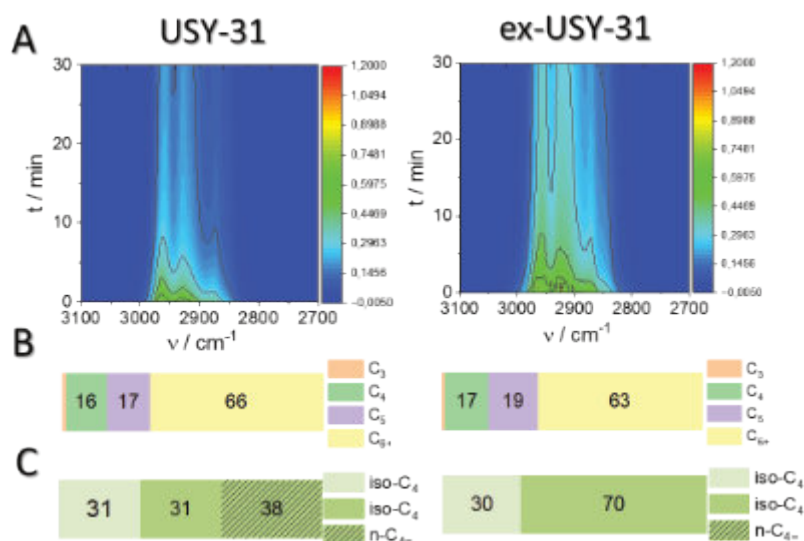


**Figure 1.** (A) Top-projection of the IR spectra presenting erosion of C–H stretching band intensity within 30 min of PP cracking on zeolites Y-2.5, USY-6 and USY-31. (B) Product distribution from the catalytic PP cracking. (C) Cracking products distribution in C<sub>4</sub> fraction: paraffinic (light green), olefinic (dark green), branched (filled), and linear (hatched).

**Acknowledgement:** The work was financed by Grant No. 2021/43/B/ST4/00307 from the National Science Centre, Poland.



## Recovering Hydrogen from SMR using ITQ-12: A Simulation Approach

A. Martin-Calvo<sup>1</sup>, J. van Heijst<sup>2</sup>, S. Calero<sup>2</sup>

<sup>1</sup> Center for Nanoscience and Sustainable Technologies (CNATS), Universidad Pablo de Olavide, Seville, Spain

<sup>2</sup> Department of Applied Physics, Eindhoven University of Technology, Eindhoven, The Netherlands  
amarcal@upo.es

Hydrogen is a promising future fuel due to its convenient storage properties and lack of harmful emissions. A popular industrial method for producing hydrogen from natural gas is Steam Methane Reforming (SMR), especially suitable in the early stages of the hydrogen economy. SMR involves multiple steps including methane purification, reforming with water to produce hydrogen, and a water-gas shift reaction to convert carbon monoxide to carbon dioxide and hydrogen. Despite its advantages, SMR faces challenges such as economic viability, cost reduction, and hydrogen recovery efficiency. Improving hydrogen capture from SMR involves the use of porous materials like zeolites, which are thermally stable and cost-effective compared to alternatives like metal organic frameworks (MOFs). [1]

This work investigates the potential use of the ITQ-12 zeolite in a pressure swing adsorption (PSA) process to obtain purified hydrogen from the SMR product stream using molecular simulations. We focus on separating the primary components of the SMR product stream, hydrogen and carbon dioxide, while also briefly addressing the separation of hydrogen from the full mixture including methane, carbon monoxide, and nitrogen. Molecular simulations were conducted using RASPA [2] to evaluate the mixture adsorption isotherms of carbon dioxide and hydrogen in ITQ-12 at industrially relevant conditions (311 K and  $16 \cdot 10^5$  Pa). Breakthrough curves obtained with RUPTURA [3] were analysed to assess ITQ-12's performance in separating hydrogen from carbon dioxide in a PSA process. Various parameters, including column length and gas feed velocity, were adjusted to optimize the separation process. The adsorption behaviour of the full mixture was also studied to evaluate ITQ-12's overall effectiveness. (Figure 1)

The simulation results reveal that ITQ-12 exhibits high selectivity for carbon dioxide over hydrogen, particularly at pressures relevant to industrial operations. Breakthrough curves showed significant differences in retention times, with hydrogen exiting the column quickly while carbon dioxide remained adsorbed for longer periods. This suggests ITQ-12's potential effectiveness in hydrogen-carbon dioxide separation via PSA. However, separating hydrogen from other components such as carbon monoxide and nitrogen proved less efficient due to similar retention times. Longer column lengths were found to enhance separation efficiency for the full mixture, indicating ITQ-12 could be used alongside other techniques for optimal results. These findings suggest ITQ-12 zeolite could significantly enhance the viability of hydrogen production from SMR by improving separation efficiency. Its high selectivity for carbon dioxide and potential for optimizing column length and gas feed velocity highlight practical applications in industrial settings. [4]

In conclusion, ITQ-12 shows promise for effective hydrogen recovery from SMR. Its high selectivity for carbon dioxide and favourable breakthrough behaviour make it a strong candidate for industrial use. Future research should be addressed exploring experimental conditions more thoroughly, and optimizing the operational parameters to fully exploit the potential of ITQ-12 in hydrogen production.

### References

- [1] N. Hajjaji, *et al.*, Energy Policy. **42**, 392-399 (2012).
- [2] D. Dubbeldam, *et al.*, Mol. Simul., **42**, 81-101 (2015).
- [3] S. Sharma, *et al.*, Mol. Simul., **49**, 893-953 (2023).
- [4] J. van Heijst, *et al.*, Sep. Purif. Technol., **350**, 127895 (2024).

### Acknowledgments

We are grateful to C3UPO for the HPC support. A. Martin-Calvo thanks the Spanish "Ministerio de Ciencia, Innovación y Universidades" (IJC2019-042207-I).

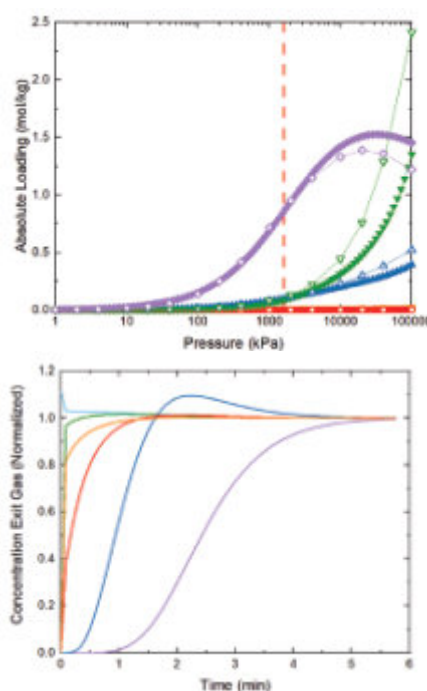


**Figure 1.** Adsorption isotherms (top) at 311 K (full-RASPA vs empty-RUPTURA) and breakthrough curves (bottom) for column length of 0.3 m and gas feed velocity equals 0.1 m/s from the full mixture. Color coding corresponds to CO<sub>2</sub> (purple), H<sub>2</sub> (green), CH<sub>4</sub> (methane), CO (red), and N<sub>2</sub> (orange).



## Designing Zeolite-Encapsulated Metal Nanoparticles for Efficient CO<sub>2</sub> Conversion

J. Mielby<sup>1</sup>, G. Zhuo<sup>1</sup>, E. Kowalewski<sup>1</sup>, D. Iltsiou<sup>1</sup>, and S. Kegnæs<sup>1</sup>

<sup>1</sup> DTU Chemistry, the Technical University of Denmark, Kemitorvet 207, DK-2800 Kgs. Lyngby, Denmark  
jjmie@kemi.dtu.dk

With the worldwide efforts to keep the global temperature increase well below 2°C, there is a critical need for new and efficient processes to utilize CO<sub>2</sub>. For example, CO<sub>2</sub> and H<sub>2</sub> may be converted into CO and H<sub>2</sub>O by the reverse water-gas shift reaction (RWGS). CO finds extensive use in syngas (CO+H<sub>2</sub>), which is an essential industrial feedstock for producing a range of chemicals and liquid transportation fuels. Although the RWGS reaction is considered an individual process, it is also an intermediate step in several other processes that involve CO<sub>2</sub> hydrogenation, including CO<sub>2</sub> methanation (the Sabatier reaction).[1] From a green and sustainable perspective, CO<sub>2</sub> methanation offers an attractive opportunity for upgrading biogas produced by anaerobic digestion of biomass or wastewater sludge, which often contains high amounts of CO<sub>2</sub>. However, because of the thermodynamics and the complicated reaction pathways, achieving a high selectivity towards the desired product (CO, CH<sub>4</sub>, or CH<sub>3</sub>OH) still poses a significant technical challenge.[2]

Another challenge is that the catalytic activity of supported metal nanoparticles is often related to their small size and high fraction of surface exposed atoms. Unfortunately, such nanoparticles are often prone to sintering, a thermal deactivation caused by Ostwald ripening or particle migration and coalescence. One strategy to overcome this challenge is to encapsulate the small and active metal nanoparticles inside the microporous framework of a zeolite.

This work compares two new methods to encapsulate Ni nanoparticles inside MFI-type zeolites (Silicalite-1, S1). In the first method, the zeolite is modified by a selective recrystallization process that creates intra-particle voids and mesopores, facilitating the formation of small and dispersed Ni nanoparticles upon simple impregnation.[3] In the second method, inspired by Yu and co-workers [4], a stable Ni ethylenediamine complex is added directly to the zeolite gel before the hydrothermal crystallization. Figure 1 shows a TEM image of a reference sample prepared by simple impregnation compared to the as-prepared catalysts. Although all three preparation methods result in catalysts with the same chemical composition, the metal nanoparticles' dispersion and exact location remarkably affect the catalytic activity and selectivity for CO<sub>2</sub> hydrogenation. Therefore, our results demonstrate the importance of considering not only the size of the Ni nanoparticles and the nature of the support material but also the three-dimensional distribution and the structure of the Ni-support interfacial sites.

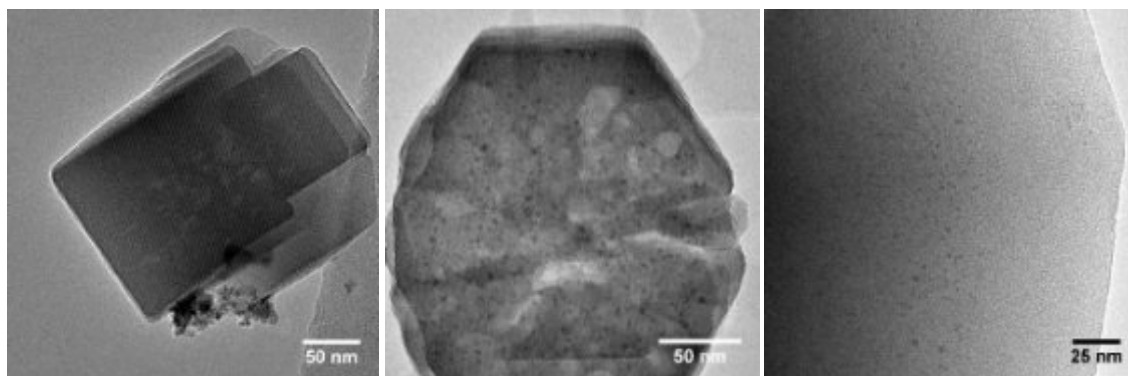


**Figure 1.** TEM images of A) Ni/S1 prepared by simple incipient wetness impregnation, B) Ni@m-S1 prepared by incipient wetness impregnation of a mesoporous zeolite modified by selective recrystallization, and C) Ni@S1 prepared by direct hydrothermal synthesis with [Ni(en)<sub>2</sub>](NO<sub>3</sub>)<sub>2</sub> in the gel.

### References

- [1] M. Kock, E. Kowalewski, D. Iltsiou, J. Mielby and S. Kegnæs, *ChemCatChem*, **16**, e202301447 (2024).
- [2] L-X. Wang, L. Wang, and F-S. Xiao, *Chem. Sci.*, **44**, 14660 (2021).
- [3] F. Goodarzi, L. Kang, F. R. Wang, F. Joensen, S. Kegnæs, and J. Mielby, *ChemCatChem*, **10**, 1566-1570 (2018).
- [4] N. Wang, Q. Sun, R. Bai, X. Li, G. Guo, and J. Yu, *J. Am. Chem. Soc.*, **183**, 7484-7487 (2016).

### Acknowledgments

The work is funded by the Independent Research Fund Denmark (Grant no. 3105-00207B).





## Ultrasonic Monitoring of the Synthesis of Metal-Organic Framework

**R. Reber, L. Rupprecht, M. Fischer, M. Hartmann**

Erlangen Center for Interface Research and Catalysis, Friedrich-Alexander-Universität Erlangen-Nürnberg  
Egerlandstraße 3, 92058 Erlangen, Germany  
rebecca.reber@fau.de

### Introduction

The synthesis of metal-organic frameworks (MOFs) remains a complex challenge in the field of porous materials. Current models suggest the formation of pre-nucleation building units (PNBUs) as critical intermediates, which are “the minimum assembly of atoms, ions or molecules which, by condensation of the group with others (identical or different) give rise to the final solid” [1]. The nature of these PNBUs is widely discussed, but detailed insights are still rare. Recent studies have proposed the formation of  $[Al(H_2O)_4(HBDC)]^{2+}$  PNBUs in the synthesis of MIL-53 [2]. For ZIF-8 as one of the extensively researched metal-organic frameworks, however, the formation mechanisms is not yet fully understood. While Venna et al. advocate a solution and solid mediated mechanism [3], Cravillon suggests prenucleation clusters as well as nanoparticles [4]. To enhance understanding of the mechanism of MOF syntheses, in-situ ultrasonic monitoring has emerged as a valuable tool that allows obtaining additional insights, which are easily missed by ex-situ characterization of isolated samples from the synthesis mixture. In addition to the robustness and non-destructiveness, the high temporal resolution is a significant advantage of this method [5].

### Experimental Section

In this study, ultrasonic monitoring was employed in order to track the formation of ZIFs (zeolitic imidazolate frameworks). ZIF-8 was synthesized using zinc nitrate hexahydrate, 2-methylimidazole and deionized water. Through varying the molar ratio of the linker and the solvent, the particle size was varied.

The setup and exemplary ultrasound-signal is depicted in **Figure 1**. In the pulse echo method, the transducer sends a pulse into the synthesis mixture, which gets reflected on the opposing surface of the reaction vessel. The transducer also records the reflected echo. The US attenuation and the US velocity can be measured at the same time. The US velocity results from the runtime of the echo and changes with the density change of the reaction mixture during the synthesis through the particle formation. The second information, the US attenuation, depends on the dampening of the US signal, when the US waves interact with the solid particles. The attenuation depends on the elastic properties of the solid and the reaction system.

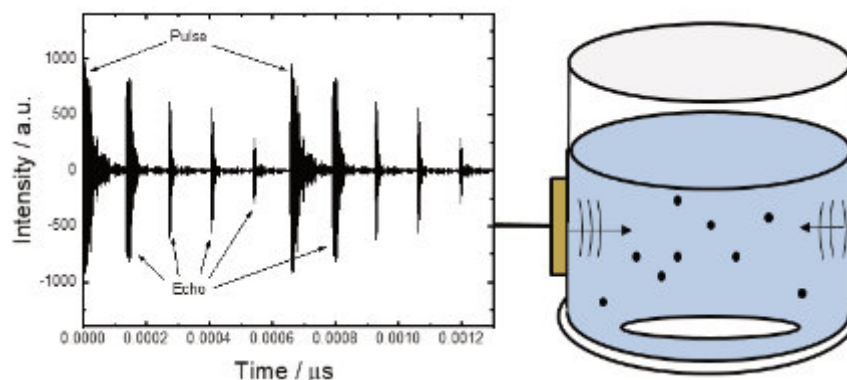


**Figure 1.** Set-up for insitu US-Monitoring with exemplary US-Signal

### Results and Discussion

In Figure 2, an exemplary measurement of the ultrasound attenuation and velocity of a ZIF-8 synthesis with a molar ratio of 1  $Zn^{2+}$ : 40 2-mim: 1400  $H_2O$  is shown. The attenuation increases sharply in the beginning of the synthesis and decreases then again until a plateau is reached. The ultrasound velocity increases from the beginning of the synthesis until the end of the measurement. Notably, a knee in the velocity is visible in the moment, in which the attenuation decreases again. The ultrasound velocity in solids is faster than in liquids, therefore the sharp increase can be correlated with the particle formation. To prevent further formation and growth of the particles during the workup procedure, the syntheses was quenched by adding acetic acid in the initial phases of the synthesis. In **Figure 3** the powder x-ray diffraction patterns of syntheses with different 2-mim:  $Zn^{2+}$  ratios are shown.

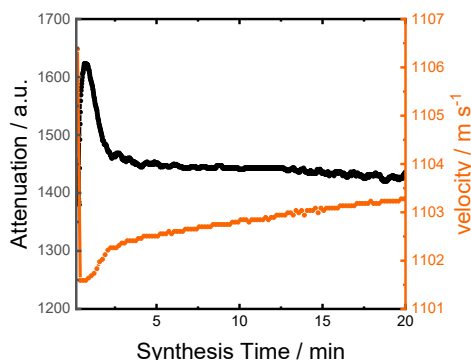


Figure 2. Ultrasound attenuation and velocity of a ZIF-8 synthesis with 1 Zn<sup>2+</sup>:40 2-mim:1400 H<sub>2</sub>O

The quenched products indicate clearly that already in the first seconds a solid product is formed. The diffraction patterns show that first another phase, namely ZIF-L, is formed. Correlating with the ultrasound signals, this results confirm that the rapid increase of the velocity in the beginning is due to formation of ZIF-L, which then later converts into ZIF-8. The phase change is visible in the ultrasonic signal through a slower increase in the velocity and a decrease in the ultrasound attenuation.

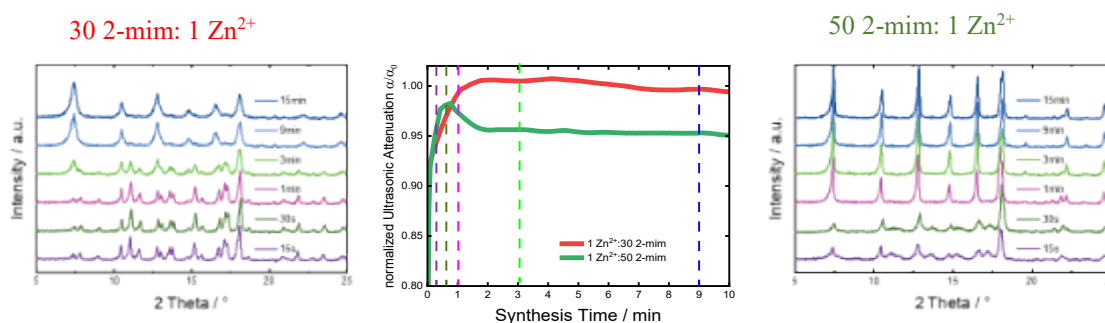


Figure 3. Powder X-ray diffraction patterns of the product obtained after quenching the syntheses mixture after different synthesis times.

In conclusion, ultrasonic monitoring is a valuable technique for investigating the complex synthesis of ZIFs and other molecular sieves. Using the pulse echo method, the ultrasound velocity and the ultrasound attenuation provide deep insights of the particle formation in the synthesis. In the rapid nanoparticle synthesis of ZIF-8 in an aqueous system, our observations revealed the initial formation of a secondary phase, ZIF-L, which subsequently transforms into ZIF-8 after several minutes. This study demonstrates that ultrasonic monitoring can significantly enhance the understanding of synthesis parameters and mechanisms, thereby contributing to the optimization of large-scale MOF production.

## References

- [1] G. Férey, *Journal of Solid State Chemistry*, **152**, 37-48 (2000).
- [2] H. Embrechts, M. Kriesten, M. Ermer, W. Peukert, M. Hartmann, M. Distaso, *Crystl. Growth Des.* **20**, 2631–3649 (2020).
- [3] S. Venna, J. Jasinski, M. Carreon, *Journal of American Chemical Society*, **132**, 18030-18033 (2010).
- [4] J. Cravillon, C. Schröder, R. Nayuk, J. Gummel, K. Huber, M. Wiebcke, *Angewandte Chemie*, **123**, 8217-8221 (2011).
- [5] M. Ermer, R. Reber, H. Baser, M. Fischer, W. Schwieger, M. Hartmann, *Crystl. Growth Des.*, **23**, 5355-5367 (2023).

## Acknowledgments

We thank the German Research Foundation for funding (Project Number: 445323933).



## Computational modeling of organic structure-directing agents in SCM-14 and SCM-15 germanosilicates

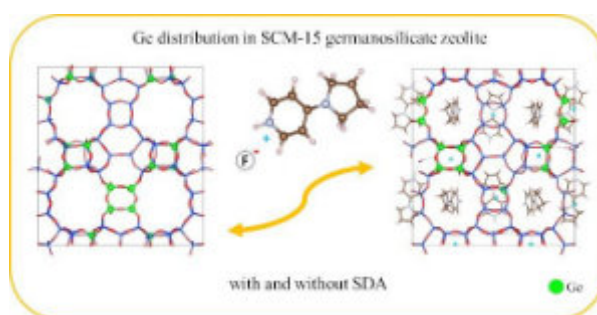
Stoyan P. Gramatikov,<sup>1</sup> Petko St. Petkov,<sup>1</sup> Zhendong Wang,<sup>2</sup> Weimin Yang,<sup>2</sup> and Georgi N. Vayssilov<sup>1</sup>

<sup>1</sup> Faculty of Chemistry and Pharmacy, University of Sofia, 1126 Sofia, Bulgaria

<sup>2</sup> State Key Laboratory of Green Chemical Engineering and Industrial Catalysis; Sinopec Shanghai Research Institute of Petrochemical Technology Co., Ltd., 1658 North Pudong Rd., Pudong, Shanghai 201208, China

\* ohspg@chem.uni-sofia.bg

We report results for different distributions of germanium ions in the double-four membered rings, D4Rs, of SCM-14 and SCM-15 germanosilicate structures and the influence of the organic structure-directing agents (OSDA), on this distribution based on quantum chemical modelling with geometry optimization and ab initio molecular dynamic simulations, aiMD. The calculations suggest strong influence of the OSDA on the germanium distribution in the zeolite frameworks, in particular for SCM-15, and highlight differences between two germanosilicates due to their specific channel systems and the amount of the OSDA per unit cell.



### Introduction

The incorporation of germanium centers in zeolite frameworks is found to facilitate the formation of small building units, such as D4Rs, which opened the way for synthesis of various novel zeolite frameworks via direct synthesis or post-synthetic modifications [1,2]. A key component in the synthesis of new types of germanosilicates are OSDA, which affects the topology of the synthesized zeolite framework. In the present work we study the preference for germanium distribution within the D4Rs of SCM-14 and SCM-15 zeolites [3,4] and the OSDA influence on this distribution based on calculated relative energies of various modelled structures.

### Computational method

For our simulations we employed completely periodic model structures. We used density functional theory method with the exchange-correlation functional of Perdew-Burke-Ernzerhof with the additional empirical dispersion correction. Structural optimization was performed with VASP package [5] using PAW pseudopotentials. The ab initio molecular dynamics calculations were performed with an NVT ensemble at 300 K using CP2K/Quickstep package [6] with combined method (GPW) and Goedecker-Teter-Hutter pseudopotentials. The germanium content of the modelled structures, corresponds to that of the experimentally synthesized materials.

### Results and Discussion

When we modelled zeolite frameworks without OSDA in their channels, the calculated relative energies for both SCM-14 and SCM-15 suggest that the germanium ions prefer clustering together and forming D4Rs populated entirely with Ge heteroatoms, while part of the D4Rs contain only Si at T-atoms. In the most energetically unfavorable models, the Ge heteroatoms are distributed among all the D4Rs. There is a qualitative trend, although not a quantitative correlation, that the most stable structures have large number Ge-O-Ge linkages.

In the as-synthesized models we introduced the OSDA, 4-pyrrolidinopyridine.HF (4-pyrrolidinopyridine protonated by HF), in the zeolite channels using the data from the CIF files of original papers [3,4]. As expected, the most favorable location of the fluoride anions is in the D4Rs, containing germanium T-atoms, while if they are outside the D4Rs or in D4Rs composed by silicon T-atoms, the structure is strongly destabilized. For SCM-14 zeolite the OSDA stabilizes the structure but the stability order of the models with different germanium distribution is preserved as found for the bare frameworks [7]. However, for the whole set of modelled structures there is no clear correlation between the stability of the structure without OSDA and the stability of the same structure with OSDA. The reason for this is that the variations of the calculated energy for stabilization due to the presence of OSDA, 255 kJ/mol, are higher than the variations in the relative energies of the zeolite due to different germanium distribution, 144 kJ/mol.



The aiMD simulations have shown substantial mobility of the OSDA in the channels of SCM-14 germanosilicate. Independent on its initial orientation, after the simulations in all structures the OSDA is positioned almost perpendicular to the large 12-ring channels of SCM-14. The structures obtained from the dynamic simulation are more stable by 157 to 331 kJ/mol than the structures obtained by initial geometry optimization. Interestingly, part of this stabilization is due to changes of the zeolite framework itself by 66 to 94 kJ/mol.

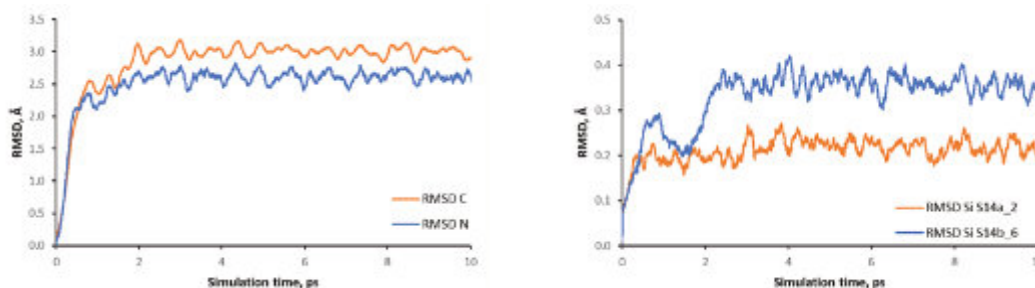


**Figure 1.** Calculated averaged root mean square deviation of the positions of the carbon and nitrogen atoms in OSDA with the simulation time (left) and the calculated root mean square deviation of the positions of the silicon centers in one of the SCM-14 models (right).

The simulations of various orientations of the OSDA in the pores of SCM-15 zeolite, however, show different stability order than found for the bare framework [8,9]. In presence of OSDA in SCM-15 channels the most stable models are those with germanium ions evenly spread among the all D4Rs with smaller number of Ge-O-Ge contacts. In addition, as-synthesized models with the same distribution of germanium but with different orientation of the template have significantly different stability. Thus, the stabilization energies due to the presence of the template with specific orientation, which accounts for the template-framework interactions and locations of the fluoride anions, may be a thermodynamic factor that influences not only the formation of the specific framework type, but also the Ge distribution in the zeolite framework during the synthesis. The relative stability of bare structures with different germanium distribution is of minor importance.

## Conclusion

The general conclusion for both germanosilicate structures is that the stabilization due to the presence of the OSDA and their orientation is thermodynamic factor directing both the formation of specific framework type and germanium distribution in the framework during the synthesis, while the relative stability of bare structures with different germanium distribution is of minor importance. This interplay between the two energy contributions results in different energy preference for the germanium distribution among the D4Rs in the as-synthesized forms of SCM-14 and SCM-15 zeolites due to their specific channel systems – for SCM-14 the favorable structures are those with clustered germanium ions, featuring high number of Ge-O-Ge links, while for SCM-15 the presence of OSDA favors structures with germanium ions distributed among all D4Rs. Thus, even for zeolites with the same chemical composition and OSDA, the characteristics of their framework lead to different energetic preference for germanium distribution.

## References

- [1] J. Li, A. Corma, and J. Yu, *Chem. Soc. Rev.*, 44 (2015) 7112–7127.
- [2] P. Eliášová, M. Opanasenko, P.S. Wheatley, M. Shamzhy, M. Mazur, P. Nachtigall, W.J. Roth, R.E. Morris, and J. Čejka, *Chem. Soc. Rev.*, 44 (2015), 7177-7206.
- [3] Y. Luo, S. Smeets, F. Peng, A.S. Etman, Z. Wang, J. Sun, and W. Yang, *Chem. Eur. J.*, 23 (2017) 16829–16834.
- [4] Y. Luo, S. Smeets, Z. Wang, J. Sun, and W. Yang, *Chem. Eur. J.*, 25 (2019) 2184–2188.
- [5] G. Kresse and J. Hafner, *Phys. Rev. B*, 49 (1994) 14251-14269.
- [6] J.V. Vondele, M. Krack, F. Mohamed, M. Parrinello, T. Chassaing and J. Hutter, *Comput. Phys. Commun.*, 167 (2005) 103–128.
- [7] S.P. Gramatikov, P.St. Petkov, and G.N. Vayssilov, *Inorg. Chem. Front.*, 9 (2022) 3747-3757.
- [8] S.P. Gramatikov, P.St. Petkov, Zh. Wang, Y. Weimin and G.N. Vayssilov, *Nanomaterials*, 14 (2024) 159.
- [9] S.P. Gramatikov, P.St. Petkov, Zh. Wang, Y. Weimin and G.N. Vayssilov, *Front. Chem. Sci. Eng.*, 18(5) (2024) 58.

## Cation induced speciation of Copper species in the Mordenite Zeolite Synthesis and their influence on the Selective Methane Oxidation to Methanol.

Peter Njoroge<sup>1</sup>, Unni Olsbye<sup>1</sup>, Sebastian Prodinge<sup>1\*</sup>

<sup>1</sup>Center for Materials Science and Nanotechnology (SMN), Department of Chemistry, University of Oslo, 1033 Blindern, 0315 Oslo, Norway

\*Corresponding author: Sebastian.prodinge@smn.uio.no

The capability of copper zeolites to selectively oxidize light alkenes is well established. The inclusion of copper into the zeolite framework comes from trying to mimic methanotrophic enzymes (e.g., pMMO) found in nature, where Cu and Fe single-atom sites can facilitate the C-H bond activation of methane under ambient conditions and in the presence of oxygen. Among the different zeolite topologies screened in literature, mordenite (MOR) emerges with the highest activity towards the methane-to-methanol (MTM) reaction. MOR is classified as a large pore zeolite with straight 12-ring channels ( $7.0 \times 6.5 \text{ \AA}$ ) and compressed 8-ring channels ( $5.7 \times 2.6 \text{ \AA}$ ) parallel to each other in the *c* direction.

These two channels are interconnected by a highly tortuous perpendicular channel made of regular 8-rings, known as the side pocket. The MOR has four unique T-sites that can be occupied by Al in the framework. It is also known that MOR can exist as both small-pore and large-pore. Knorpp *et al.* reported a connection between small- and large-pore MOR and its activity towards the MTM reaction and saw that the large-pore variant had a higher methanol yield. Previous studies by Pappas *et al.* indicate that a di-copper-oxo species, possible in the 12-ring channel and the side pocket of the mordenite are the active species that can oxidize the methane in the MTM reaction, with Prodinge *et al.* claiming that species accessible *via* the 12-ring channel are more active for activating methane. *in situ* X-ray spectroscopy on Cu-MOR during heating to 500 °C in either oxygen or inert suggested two different framework coordinated Cu[II]-species.

These studies suggest that there is a relationship between the structure of the MOR and the type of copper species formed and its activity towards the methane to methanol reaction and we believe if understood can be used to improve activity of the MOR towards MTM reaction.

In this work, in-house mordenite was synthesized with different amounts of sodium and potassium as mineralizing agents, subsequently exchanged with varying amounts of copper, and tested for the activity towards the activation of light alkanes. Advanced spectroscopic techniques, together with reaction tests, were employed to investigate the correlation between large- versus small-pore mordenite and their effect on the formation of different active copper sites for the activation of methane. Lastly, DFT calculations were performed to investigate the effects of different aluminum positions in the MOR framework.

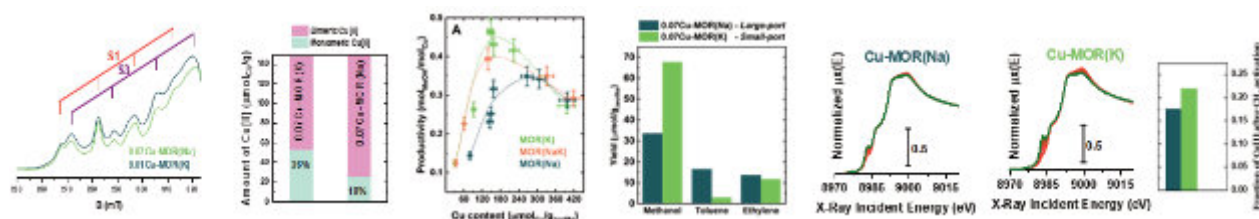


Figure 1: a) EPR shows difference in copper species between the samples. b) Comparing copper content vs productivity. c) Probing the methoxy location using different extraction molecules. d) XAS showing similar copper changes during in situ measurements.

We see that there are differences in the copper species formed in each sample according to Fig.1. (a) which results in difference in productivity as seen in Fig.1. (b) across the samples in different copper loadings with K-MOR showing highest productivity while as seen in Fig.1.(c) XAS shows that despite both samples forming Cu(I) after methane activation K-MOR forms more Cu(I) species which supports the reason that we have K-MOR being more active.

The use of different cations during synthesis of MOR,  $K^+$  and  $Na^+$  in this case leads to the formation of MOR that have different copper species and can inherently improve the activity of the MOR towards methane to methanol reaction.



## Process Intensification at the Nanoscale: Embedding SiC in Zeolites for Energy-Efficient Catalysis

A.F. Young<sup>1</sup>, J.T. de Souza<sup>1</sup>, P.N. Romano<sup>1</sup>, J. García-Martínez<sup>2</sup> and J.M.A.R. de Almeida<sup>1</sup>

<sup>1</sup> Laboratório de Intensificação de Processos e Catalise (LIPCAT), Universidade Federal do Rio de Janeiro, Rua Sydney Martins Gomes dos Santos, 13 Parque Tecnológico, Cidade Universitária, Rio de Janeiro, Brazil, 21941-859.

<sup>2</sup> Laboratorio de Nanotecnología Molecular, Departamento de Química Inorgánica, Universidad de Alicante, 03690, Alicante, Spain  
j.monnerat@iq.ufrj.br

### Motivation

Building on strategies to improve both the MW absorbing capacity and textural properties of novel catalytic systems, here we report a step forward in the integration of the MW absorber and the catalytic phase consisting of embedding SiC nanoparticles in FER zeolite crystals (FER@SiC) with improved heating properties by synthesising the zeolite in the presence of SiC nanoparticles, resulting in a hybrid material consisting of FER crystals with SiC nanoparticles inside. [1]

### Results and Discussion

All materials used in this study consist of highly crystalline ferrierite (FER), confirmed by X-ray diffraction (Figure 1a), with no other crystalline phases except added SiC. The hybrid FER@SiC shows FER's XRD pattern plus SiC peaks. Scanning electron microscopy (SEM) images of FER (Figure 1g), FER@SiC (Figure 1h), and FER/SiC (Figure 1k) reveal that FER's plate-like morphology is unchanged by SiC nanoparticles (Figure 1j). Transmission electron microscopy (TEM) images show embedded SiC in FER@SiC (Figure 1i) and separate phases in FER/SiC (Figure 1l). The former consists of SiC particles embedded in the zeolite, while the latter has the two phases, i.e. the zeolite and the SiC, clearly separated. [2]

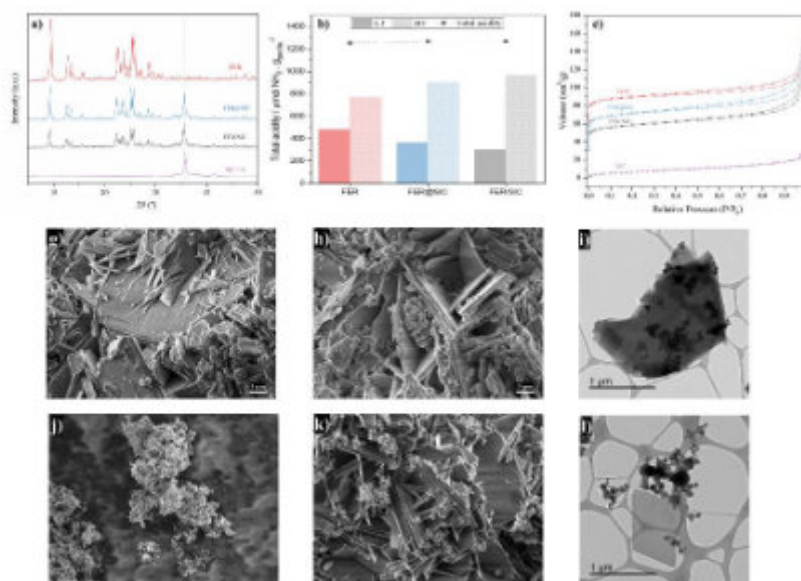


**Figure 1.** Characterisations of the catalysts. a) XRD patterns, b) NH<sub>3</sub>-TPD, c) Total acidity per gram of, d) N<sub>2</sub> physisorption isotherms at 77 K, e) <sup>29</sup>Si NMR and f) <sup>27</sup>Al NMR for FER, FER@SiC, FER/SiC, and SiC samples. SEM images of g) FER, h) FER@SiC, j) SiC and k) FER/SiC along with TEM images of i) FER@SiC and l) FER/SiC.

NH<sub>3</sub>-TPD analysis (Table 1, Figure 1b) confirms that FER's total acidity remains unchanged with SiC, with only a minor shift in acidity strength. Textural characterization (Table 1, Figure 1c) shows comparable properties for FER and FER@SiC when normalized for zeolite content (33 wt%), indicating no significant pore blocking by SiC. Micropore volumes for both the physical mixture and the embedded material are similar and typical of FER topology. [3]

Elemental analysis via atomic absorption spectroscopy (Table 1) shows a one-third higher Si/Al ratio in FER@SiC, attributed to added SiC. <sup>29</sup>Si and <sup>27</sup>Al NMR (Table 1) confirm identical framework Si/Al values for FER and FER@SiC, indicating no structural modification due to SiC and further supporting the suggestion that there is no modification of the zeolitic structure upon the addition of SiC.

Structural, morphological, and acidity characterizations show that the zeolite in FER@SiC and FER/SiC is identical to pure FER. However, catalytic activity in the Friedel-Crafts alkylation of mesitylene with benzyl alcohol differs notably, especially under MW irradiation (Figure 2). FER and FER@SiC exhibit similar conversion rates under conventional heating, with FER@SiC performing 6% better. Under MW heating, FER@SiC shows a 2.5-fold increase in catalytic



activity compared to FER due to SiC's MW absorbing properties. FER@SiC and FER/SiC behave similarly under conventional heating but differ under MW heating; FER@SiC shows a 2.2-fold improvement due to intimate contact between SiC and FER, enhancing the initial reaction rate (Figure 2c).

**Table 1.** Textural and acidic properties of synthesized materials and SiC.

Catalyst	S <sub>BET</sub> (m <sup>2</sup> /g <sub>cat</sub> )	S <sub>BET</sub> (m <sup>2</sup> /g <sub>zeolite</sub> )	V <sub>mic</sub> <sup>[a]</sup> (cm <sup>3</sup> /g <sub>cat</sub> )	V <sub>mic</sub> <sup>[a]</sup> (cm <sup>3</sup> /g <sub>zeolite</sub> )	V <sub>meso</sub> <sup>[a]</sup> (cm <sup>3</sup> /g <sub>cat</sub> )	Total acidity (μmol/g <sub>zeolite</sub> )	Si/Al <sup>[b]</sup>	Framework Si/Al <sup>[c]</sup>
FER	356	356	0.14	0.14	0.02	1254	8.2	10.7
FER@SiC	277	415	0.09	0.14	0.04	1268	12.9	10.9
FER/SiC	225	337	0.09	0.14	0.04	1349	14.5	10.1
SiC	30	-	< 0.01	-	0.04	190	-	-

[a] micro- and mesopore volumes calculated through NLDFT. [b] bulk Si/Al obtained through Atomic Absorption Spectrometry. [c] framework Si/Al obtained through <sup>29</sup>Si and <sup>27</sup>Al NMR.

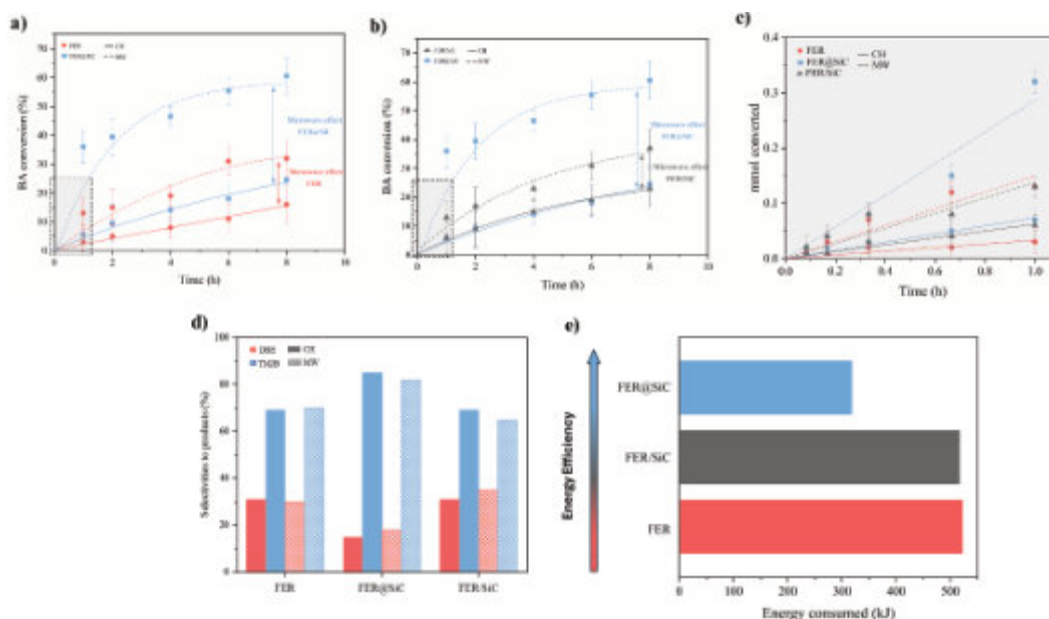


**Figure 2.** Conversion profiles of BA over times for a) FER and FER@SiC, b) FER/SiC, FER@SiC, and c) amount of BA converted at short times for all three materials. d) Selectivities towards dibenzyl ether (DBE) and 1,3,5-trimethyl-2-benzylbenzene (TM2B) under both conventional (solid) and microwave heating (lines) for FER, FER@SiC, and FER/SiC at an isoconversion of 15%. e) Energy consumed in microwave reactor for each catalyst at 15% benzyl alcohol isoconversion

No change in selectivity is observed for any system under either heating method, though FER@SiC slightly improves alkylation product yield due to its micro- and mesoporous structure (Figure 2d). Figure 2e shows FER@SiC requires only 60% of the energy to achieve 15% conversion, highlighting the importance of close contact between the heating element (SiC) and the catalytic phase (FER). This demonstrates that simply blending MW absorbing materials is ineffective, and the improved performance of FER@SiC is due to the intimate contact between SiC and FER.

## Conclusion

By simply incorporating SiC nanoparticles into FER zeolite crystals during their synthesis, we were able to achieve a remarkable 2.5-fold increase in catalytic activity in the Friedel-Crafts alkylation of mesitylene with benzyl alcohol under microwave heating over the SiC-free system, and a similar improvement in the case of the physical mixture. Our findings underscore the critical role of the intimate contact between the heating medium (SiC) and the catalytic phase (FER zeolite) in facilitating effective microwave-assisted catalysis, as evidenced by the superior conversion rate, close to 2.2-fold, and a remarkable reduction in energy consumption, exceeding 40%, when comparing the FER zeolite and the physical mixture between FER and SiC (FER/SiC).

## References

- [1] A.F. Young, J.T.d. Souza, P.N. Romano, J. García-Martínez, J.M.A.R.d. Almeida, Electronic copy available at: <https://ssrn.com/abstract=4863056>, (2024).
- [2] F. Kishimoto, T. Yoshioka, R. Ishibashi, H. Yamada, K. Muraoka, H. Taniguchi, T. Wakihara, K. Takanebe, Science Advances, 9 (2023) eadi1744.
- [3] Y. Li, D. Ma, W. Fu, C. Liu, Y. Wang, Z. Wang, W. Yang, RSC Adv, 12 (2022) 14183-14189.

## Green Synthesis approaches towards the preparation of ZIF compounds and their evaluation for CO<sub>2</sub> sorption

A. Škrjanc<sup>1,2\*</sup>, N. Zabukovec Logar<sup>1,2</sup>

<sup>1</sup> National Institute of Chemistry, Hajdrihova 19, SI-1001 Ljubljana, Slovenia

<sup>2</sup> Faculty of Science, University of Nova Gorica, Vipavska 13, SI-5000 Nova Gorica, Slovenia  
aljz.skrjanc@ki.si

Zeolitic imidazolate frameworks (ZIFs), a subgroup of MOFs, have in recent years been extensively studied for sorption applications, also CO<sub>2</sub>, due to their commonly superior stability and kinetics for vapour/gas adsorption if compared to carboxylate-based MOFs. While extensively studied, an overview of articles shows that most research is limited to a limited set group of frameworks, with ZIF-8 being used in more than half of ZIF papers. While ZIF-8 has successfully been prepared in water and even in solvent-free conditions, the rest of the ZIFs synthesis still heavily rely on solvothermal synthesis with formamide based solvent systems and synthesis times upwards of 5 days. Even in the case of ZIF-8, while greener synthesis approaches are available, dimethylformamide (DMF) synthesis is still used in the cases tested for CO<sub>2</sub> capture, mainly due to the increased CO<sub>2</sub> uptake resulting from the synergistic contribution of the remaining DMF solvent in the pores.

The goal of this work was to develop green synthesis approaches, both solvothermal<sup>1</sup> and mechanochemical<sup>2</sup> (Figure 1), for known ZIFs and then to extend the scope towards preparation of new ZIF materials<sup>3</sup>.

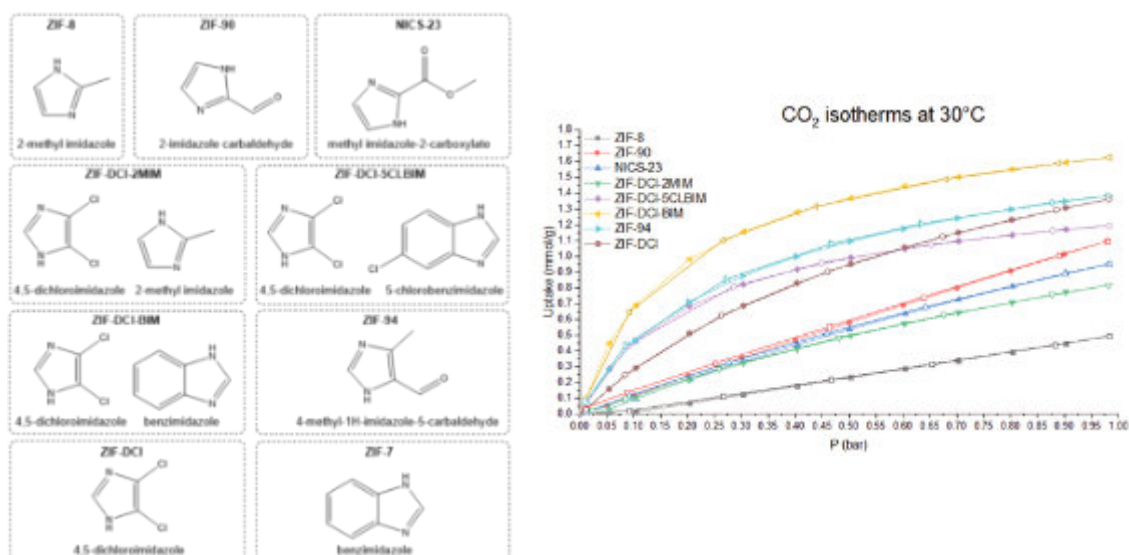


**Figure 1.** List of Mechanochemically prepared ZIFs and their CO<sub>2</sub> isotherms.

The CO<sub>2</sub> isotherms of the prepared materials were collected to determine the carbon capture potential of studied ZIFs and to recognize the most promising directions for future research for ZIFs for CO<sub>2</sub> capture. Of all the examined samples, the ZIFs with SOD topology and with imidazolate linkers functionalized at C4 and C5 atoms in the imidazolate ring demonstrated the highest affinity for CO<sub>2</sub> as evident by a transition from linear adsorption isotherms.

On the other hand the green solvothermal and/or mechanochemical syntheses proved to be suitable alternatives for preparation of porous materials with comparable sorption properties.

Most notable was the development of approaches towards preparation of ZIFs with metals that prefer octahedral coordination (Figure 2), thus preparing the first two pure nickel zeolitic frameworks NICS-21 (RHO) and NICS-22 (SOD)<sup>3</sup>. The two nickel frameworks, aside from having high potential as water (NICS-21) and CO<sub>2</sub> (NICS-22) sorbents, were also tested for heterogenous organocatalysis in the Suzuki-Miyaura cross-coupling reaction. Both were active, but only NICS-21 showed recyclability, thus allowing for easy purification of the obtained products without having to worry about dissolved nickel complexes.



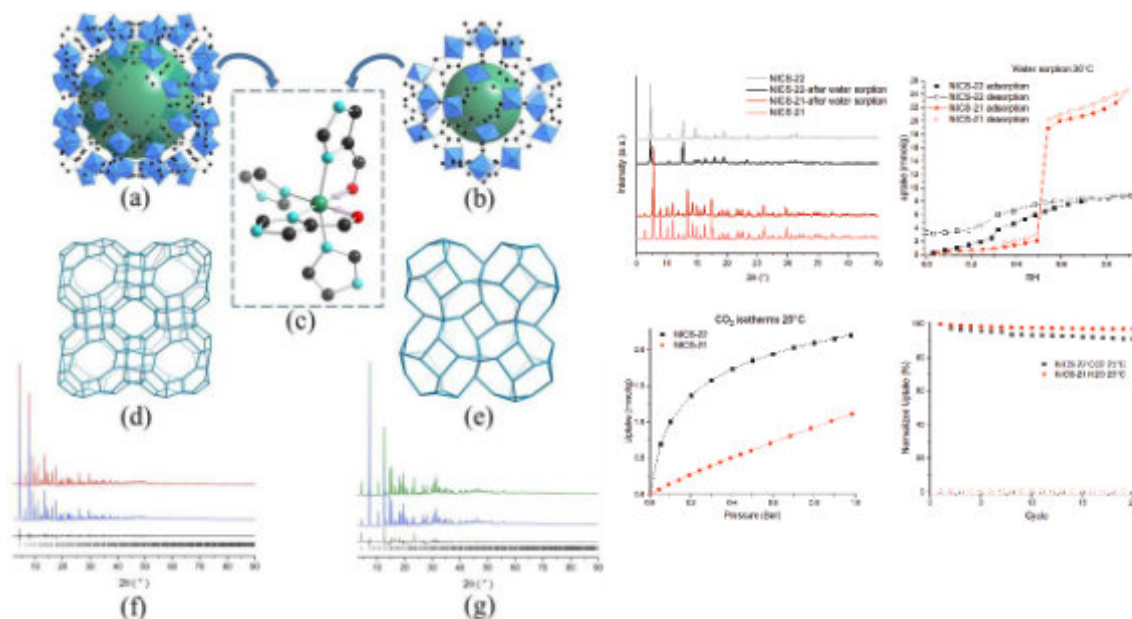


**Figure 2.** Nickel based ZIFs structures with RHO and SOD topology. Sorption and stability data for NICS-21 and NICS-22: PXRD of samples after water sorption, water sorption isotherms, CO<sub>2</sub> sorption isotherms, NICS-21 H<sub>2</sub>O and NICS-22 CO<sub>2</sub> cycling test.

## References

- [1] A. Škrjanc, C. Byrne and N. Zabukovec Logar, *Molecules*, 2021, **26**, 1573.
- [2] M. Švegovec, A. Škrjanc, A. Krajnc and N. Z. Logar, *Cryst. Growth Des.*, 2023, **23**, 3754–3760.
- [3] A. Škrjanc, D. Jankovič, A. Meden, M. Mazaj, E. S. Grape, M. Gazvoda, N. Zabukovec Logar, A. Škrjanc, M. Mazaj, N. Zabukovec Logar, D. Jankovič, A. Meden, M. Gazvoda and E. S. Grape, *Small*, 2023, 2305258.

## Acknowledgments

We would like to thank Mojca Opresnik for SEM/EDX measurements and Edi Kranjc for XRD measurements. Matjaž Mazaj, Amalija Golobič, Anton Meden and Marta Počkaj for structure analyses. We thank Dr Felix Hennersdorf from Rigaku Europe SE for providing the opportunity for diffraction measurements of NICS-22 on the electron diffractometer XtaLAB Synergy-ED with the Hypix3000-ED detector. We would also like to thank Erik Svensson Grape for his help with ED of NICS-21.



## Solventless synthesis of zeolitic imidazolate frameworks at high pressure and temperature

M. Pérez-Miana<sup>1,2</sup>, A. Mayoral<sup>1</sup>, J. Coronas<sup>1,2</sup>

<sup>1</sup>Instituto de Nanociencia y Materiales de Aragón (INMA), CSIC-Universidad de Zaragoza, Zaragoza, 50018, Spain

<sup>2</sup>Chemical and Environmental Engineering Department, Universidad de Zaragoza, Zaragoza, 50018, Spain  
coronas@unizar.es

Due to their crystallinity, microporosity and organic-inorganic character, metal-organic frameworks (MOFs) combine in a unique solid material some of the best properties of zeolites (crystalline inorganic porous materials) and polymers. Because of their exceptional properties, MOFs find application in several fields like those of catalysis, adsorption, membranes, composites, medicine, etc. MOFs can be prepared by several procedures related to solvothermal synthesis, use of microwave irradiation, mechanochemistry, etc. MOFs can be roughly divided into carboxylate type MOFs and imidazolates (zeolitic imidazolate frameworks, ZIFs). Recently, we have developed the solventless synthesis of ZIF-8 which we want to extend to other ZIFs by applying high pressure (up to 600 MPa) and moderate to high temperatures (up to 145 °C) [1, 2]. Interestingly, the high pressure methodology has also been applied to the encapsulation of drugs (e.g. caffeine, kojic acid) into MOFs [3].

As an example of results, Table 1 shows the solventless synthesis of ZIF-8 at high temperature and pressure, with yields referred to the limiting reactant of ca. 70% and BET specific surface areas (SSA) of up to 480 m<sup>2</sup>/g (as compared to the 1730 m<sup>2</sup>/g of the ZIF-8 achieved in the conventional solvent based synthesis). The low value of BET SSA was due to the fact that the non-converted reactants (including the Zn source of ZnO) were not separated from the solventless reaction products. The solid state reaction was favoured by the presence of a minimum amount of NH<sub>4</sub>NO<sub>3</sub> (5-40 mg in 0.6 gram of the 2-methylimidazole-HmIm/ZnO mixture), favouring the deprotonation of the ligand and the reaction of ZnO [4]. However, this salt, at its higher levels, provoked the occurrence of ZIF-L (in mixture with ZIF-8) which upon conversion into ZIF-8 by contact with either methanol or ethanol [5] produced ZIF-8 powders with up to 947 m<sup>2</sup>/g.

**Table 1.** Solventless synthesis of ZIF-8 at high pressure and temperature.

Temperature (°C)	Pressure (MPa)	NH <sub>4</sub> NO <sub>3</sub> (mg)	HmIm/Zn	Yield (%)	BET SSA (m <sup>2</sup> /g)
110	150	5	2	62.3	129
110	150	15	2	67.0	480
110	150	15	2.5	70.3	328
110	150	15	3.0	72.1	275

In conclusion, this work demonstrates that the combination of high pressure and high temperature can give rise to the solventless synthesis of ZIFs. These ZIFs are in principle ZIF-8 and ZIF-L but also other interesting ZIFs are currently under study and characterization.

### References

- [1] L. Paseta, G. Potier, S. Sorribas, J. Coronas, ACS Sustainable Chem. Eng. **4**, 3780 (2016).
- [2] M. Perez-Miana, J.U. Resendiz-Ordóñez, J. Coronas, Microporous Mesoporous Mater. **328**, 111487 (2021).
- [3] R. Monteagudo-Olivan, L. Paseta, G. Potier, P. López-Ram-de-Viu, J. Coronas, Eur. J. Inorg. Chem. **29** (2019).
- [4] S. Tanaka, K. Kida, T. Nagaoka, T. Ota, Y. Miyake, Chem. Commun. **49**, 7884 (2013).
- [5] Z. Low, J. Yao, Q. Liu, M. He, Z. Wang, A. Suresh, J. Bellare, H. Wang, Cryst. Growth Des. **14**, 6589 (2014).

### Acknowledgments

This research acknowledges grant PID2022-138582OB-I00 funded by Spanish Agencia Estatal de Investigación and Ministerio de Ciencia e Innovación and by "ERDF a way of making Europe". Financial support from the Aragón Government, T68-23R and M. P.-M. PhD grants, is also gratefully acknowledged.



## In search of energy-efficient materials for atmospheric water harvesting

H. ZHAO<sup>1,2</sup>, V. Yasnou<sup>1</sup>, R. Guillet-Nicolas<sup>1</sup>, V. Valtchev<sup>1\*</sup>

<sup>1</sup> Laboratoire Catalyse et Spectrochimie, Normandie University, ENSICAEN, UNICAEN, CNRS, F-14050 Caen, France.

<sup>2</sup> The ZeoMat Group, Qingdao Institute of Bioenergy and Bioprocess Technologies, CAS, Laoshan District, CN-266101 Qingdao, China.

E-mail: haonuan.zhao@ensicaen.fr

The availability and utilization of freshwater are critical for human health, economics, and ecosystem stability. However, the growing mismatch between human demand and available freshwater resources results in severe water scarcity. According to the United Nations Sustainable Development Goals, freshwater scarcity is the sixth most urgent issue among the current global “poly-crises” [1]. Developing feasible strategies to alleviate the water crisis is pressing for the whole globe.

Atmospheric water is considered an alternative resource since it accounts for up to 13% of the current water resources and corresponds to ~13,000 km<sup>3</sup> of water. Thus, the atmospheric water harvesting (AWH) strategy is under development as a promising solution. The conventional method to harvest moisture in AWH is based on classical air-conditioning technology. It collects the condensate by cooling the ambient air below its dewpoint. The huge energy consumption and dependency on high local humidity significantly hinder this method's practical application. Some desiccant materials could selectively extract local humidity from the air and substantially improve the current state of the art [2-3].

Sorbent materials are the core of sorption-based AWH systems. Prospect materials should meet 5 criteria to enable reliable and energy-saving water production: high water capacity, rapid kinetics, facile regeneration, robust cycling stability, and low-cost. The most promising candidates mainly include zeolites, zeolitic materials, and metal-organic frameworks (MOFs).

Originating from the extra framework cations, zeolites possess a strong affinity to water molecule, which is defined as high hydrophilicity. This strong link brings zeolites quick water capture and holding capability while causing them a tricky regeneration process, in general, over 200°C is needed. The following huge energy consumption is a prohibitive shortfall. Alternatively, MOFs emerged as a better choice from an energy-efficiency point of view. Due to the tunable metal species and ligands in MOFs, less than 100°C is enough to break the H-bond formed between the water molecule and MOF structure. Unfortunately, MOFs are now disputed over several facts of the quantity production, price, long-term hydrothermal stability, and toxicity in water-related applications. It is very difficult to realize industry implementation before solving all these issues well. Hence, some aluminophosphate molecule sieves (AIPOs) without extra framework cations attract our attention. Crystalline AIPOs are typically built up from strict AlO<sub>4</sub> and PO<sub>4</sub> tetrahedra alternation through corner-sharing. They possess electroneutral and open frameworks. The unique feature of AIPOs is highly likely to retain or even enhance zeolites' superior water absorption capacity while significantly mitigating its excessive hydrophilicity. Theoretically, it could be possible to identify an AIPO that combines the advantages of both zeolites and MOFs, as a competitive sorbent candidate for AWH [3].

Targeting this purpose, we systematically screen and assess diverse vapor sorbents including zeolites, AIPOs, and MOFs in this work. Through a comparative study of water capacity, water adsorption isotherms, sorption kinetics, regeneration energy cost, and temperature request, an AIPO with AEI framework topology (AIPO-18) stands out. AIPO-18 shows a special S-shaped water adsorption isotherm. Around 70% of uptake quantity happens in a very narrow relative humidity range (10%-13%). This is an excellent point for AWH since only a small swing of temperature or humidity could induce a great amount of water vapor release and sorbent regeneration. The thermogravimetric analysis gives a more intuitive result: AIPO-18 is almost completely regenerated below 70°C, and costs only 0.27 Wh/g for the regeneration, even comparable to some MOFs. Moreover, high-temperature *in situ* XRD analyses state AIPO-18 has robust structural hydrothermal stability, which is one of the reasons for its great performance during cycling tests. The breakthrough results also indicate the generalization of AIPO-18 in different climate conditions. Above all, here we propose AIPO-18 as a potential candidate for developing energy-saving atmospheric water harvest technology to extract fresh water from “dry” air.

Detailed information and an in-depth discussion will be delivered during the presentation.

### References

- [1] P. H. Gleick, and H. Cooley, *Annual Review of Environment and Resources Freshwater Scarcity*, **46**, 319-348 (2021).
- [2] X. Zhou, H. Lu, F. Zhao, and G. Yu, *ACS Materials Letters*, **2**, 671-684 (2020).
- [3] H. Zhao, X. Yang, R. Guillet-Nicolas, V. Yasnou, and V. Valtchev, *Microporous and Mesoporous Materials*, **369**, 113043 (2024).



## Catching a zinc-containing high-silica Ferrierite structure through Mordenite interzeolite conversion: phase selectivity in a pool of newborn structures

Mostafa Torka Beydokhti<sup>1</sup>, Dr. Gleb Ivanushkin<sup>1</sup>, Dr. Ibrahim Khalil<sup>1</sup>, Ahmed Sajid<sup>1</sup>, Dr. Juna Bae<sup>1</sup>, Thibault Donckels<sup>1</sup>, Dr. Dieter Plessers<sup>1</sup>, Prof. Michiel Dusselier<sup>1</sup>

<sup>1</sup> Center for Sustainable Catalysis and Engineering, Faculty of Bioscience Engineering, B-3000, Leuven, Belgium  
mostafa.torkabeydokhti@kuleuven.be

According to our group's recent findings in interzeolite conversion (IZC) [1-4], a controlled dissolution kinetic of parents by a conscious selection of pH, alkali or alkaline metals, OSDA (Organic Structure Directing Agent), other heteroatoms and/or synthesis modifiers, as well as temperature and time, paves the way for discovering zeolites with prodigious properties that are either hard or impossible to obtain via amorphous precursors pathway (Regardless of structure and lattice similarity between parents and daughters). Up to now, extensive works and studies have been performed to elaborate on the roles of Al in IZC including incongruent dissolution of parents, locally heterogeneous nucleation via solid nanoparts, interaction with OSDA and alkali/alkaline cations, crystallization, and growth [3, 4]. Meanwhile, there is still a comparative lack of research on the effects of other heteroatoms and even inorganic modifiers than Al in IZC especially zinc as not more than 15 frameworks have been synthesized with incorporated Zn [1, 5].

Taking advantage of the fast dissolution of pre-crystalline sources for a parent's composition-manipulated T-atoms adding, IZC can overcome kinetic hurdles toward unprecedented phases. Here, we provide new insights into the gap of zinc heteroatom influence on the kinetic of an IZC system. Selective dissolution of the parent in the presence of ZnO and influenced complexly by other precursors enables us to catch a high-silica FER phase, which is challenging to reach from a one-pot synthesis in OH media, through IZC of silicious MOR.

Figure 1 shows the phase diagram resulting from the IZC of MOR (Si/Al=100) at 160 °C for 88 h under static conditions with the following molar composition: 1 Si: 1/x ZnO: 0.6 1,4Diaminobutane: y NaOH: 1/100 Al: z H<sub>2</sub>O. Substantial phase variation reveals close competition due to changes in ingredient composition, especially ZnO. Close energetic states of appeared structures and their similarity can set the stage for such a competitive phase selection. Moreover, a non-selective OSDA and ISDA (In-organic Structure Directing Agent), Na and Zn, can cause mixture growth of products. So, an exact selection of precursor types and concentrations, which will initially affect the MOR dissolution as the rate-determining step in an IZC, is crucial for achieving kinetically desired phases.

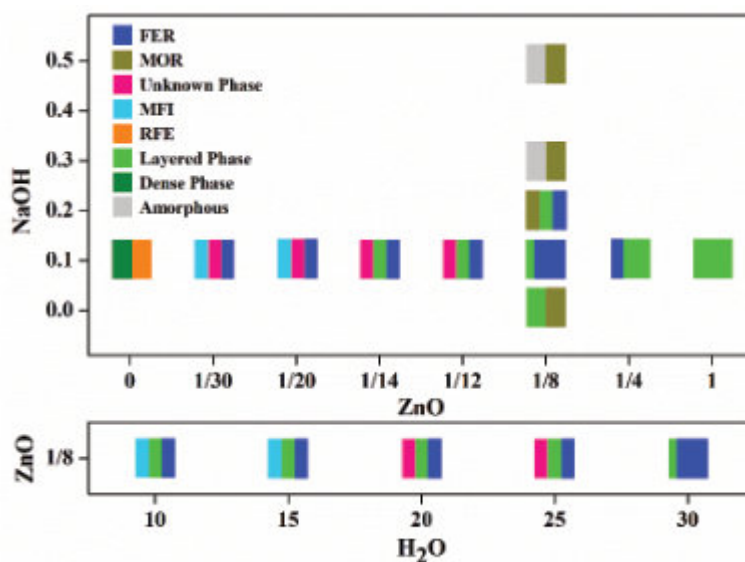


**Figure 1.** Phase selectivity diagram for IZC of MOR. For each set of synthesizes, one variable has been changed. The phases were determined using PXRD measurements, while for a mix of FER and Layered phases which have been quantified using PXRD analysis of corresponding pure phases, the other points are qualitative illustrations acquired using detected phases in PXRD spectra. For the ZnO and NaOH composition changes, the water was adjusted at z=30 (upper plot) and for the water composition variation the NaOH was fixed at y=0.1 (lower plot).

Accordingly, a FER zeolite can be attained through the IZC of MOR in a narrow region of compositions assisted with ZnO. Table 1 shows the textural and compositional properties of obtained FER from IZC of a high-silica MOR (Si/Al=160) and acid-washed samples in two different conditions (FER<sub>AW1</sub> and FER<sub>AW2</sub>) compared to a commercial FER structure with a Si/Al ratio of 40 (FER<sub>40</sub>). Structural characterizations prove defect engineering achieved from a mild



post-treatment can tune composition and properties ranging from an unprecedented Zn-containing FER with a Si/Zn ratio of 36 to a siliceous FER with a Si/Al ratio of 170. The extent of acid washing can regulate the framework-coordinated Zn species toward a Lewis acidic catalyst and an almost non-acidic high-silica counterpart.

**Table 1.** Compositional and textural properties of FER and acid-washed FER in two conditions achieved from ICP-OES, nitrogen physisorption, and FT-IR spectroscopy. Solid yield was calculated based on weight loss in TGA.

	Si/Al	Si/Zn	Surface area (m <sup>2</sup> /g)	Internal Surface area (m <sup>2</sup> /g)	Total pore volume (cm <sup>3</sup> /g)	Micropore volume (cm <sup>3</sup> /g)	BAS (μmol e/g)	LAS (μmol e/g)	Solid yield (wt%)
FER	163	8.6	284	209	0.13	0.08	4	30	92
FER <sub>AW1</sub>	175	36	360	256	0.16	0.10	14	105	68
FER <sub>AW2</sub>	172	700	394	258	0.19	0.10	4	8	65
Commercial FER <sub>40</sub>	40	-	368	282	0.15	0.11	148	3	-

It has been challenging to exactly resolve the zinc position and environment due to the nature of zinc and producing different species inside or outside the zeolite matrix. We used multiple techniques to obtain a clear picture of zinc speciation in the FER samples. According to TEM/STEM, UV-Vis-DRS, and FT-IR analysis, the Zn is not in a pure framework or extra-framework position. TEM images show that FER<sub>AW1</sub> comprises ultra-fine ZnO particles (under 5nm) dispersed on the surface. Moreover, the UV-Vis-DRS technique shows that not only is Zn present as ZnO on the external surface but also serves as an extra-framework species inside the pores. However, the pyridine FT-IR spectroscopy reveals the Lewis acidity of zinc-containing FER samples derived from 23 mole% of incorporated Zn.

Thanks to the IZC advantages (smaller particle size, nanoplates with thickness of 10-100 nm) and a simple post-treatment step (defect engineering, Zn species regulation, increasing external surface area and mesoporosity), the final materials are excellent candidates for catalysis and also adsorption. We examined the activity of post-treated FER samples in the CO<sub>2</sub> hydrogenation to hydrocarbons reaction.

In similar (but crucially different) conditions we also found a new zeolite and to finish the talk, we will lift a little bit of the curtain on this new topology discovered in our lab [6].

## References

- [1] Devos. J, Shah. M. A, Dusselier. M, RSC Adv., 11 (42), 26188–26210 (2021).
- [2] Bae. J, Dusselier. M, Chem. Commun., 59 (7), 852–867 (2023).
- [3] Robijns. S, Devos. J, Donckels. T, de Oliveira-Silva. R, De Witte. N, Sakellariou. D, Van Assche. T. R. C, Dusselier. M, Cryst. Growth Des., 23 (1), 289–299 (2023).
- [4] Devos. J, Robijns. S, Van Goethem. C, Khalil. I, Dusselier. M, Chem. Mater., 33 (7), 2516–2531 (2021).
- [5] Mazzei, Irene. R, Durham University, 2022, <http://etheses.dur.ac.uk/14552/>.
- [6] Dusselier. M, Bae. J, Plessers. D and coworkers and collaborators. In preparation.



## Enhancing Plastic Waste Upcycling Efficiency through Zeolite Confinement and Pore Diffusion

J. Martínez-Ortigosa<sup>\*,1,2</sup>, S. Singh<sup>3</sup>, Nuria Ortuño<sup>4</sup>, Vivek Polshettiwar<sup>3</sup>, Javier García-Martínez<sup>2</sup>

<sup>1</sup>Instituto de Tecnología Química, Universitat Politècnica de València – Consejo Superior de Investigaciones Científicas (UPV-CSIC), Avda. de los Naranjos s/n, 46022 Valencia, Spain

<sup>2</sup>Laboratorio de Nanotecnología Molecular, Departamento de Química Inorgánica, Universidad de Alicante, Ctra. San Vicente-Alicante s/n, 03690, Alicante, Spain

<sup>3</sup>Department of Chemical Sciences, Tata Institute of Fundamental Research, Mumbai, 40005 India

<sup>4</sup>University Institute of Chemical Process Engineering, University of Alicante, Carretera de San Vicente del Raspeig, s/n, 03690 Alicante, Spain

e-mail: joaquin.martinezortigosa@ua.es

The burgeoning environmental impact of plastic waste poses a significant challenge to ecosystems and human health. The extensive production and disposal of non-degradable plastic items have led to the build-up of plastic wastes in both aquatic environments and landfills affecting wildlife and, through the food chain, human health. [1] This crisis necessitates urgent and innovative solutions, among which plastic waste upcycling emerges as a promising strategy. In this context, zeolite-based catalysts have garnered significant attention due to their strong acidity, porous structures, high surface area, and thermal stability. Despite their potential, existing zeolite-based catalysts face several challenges that limit their widespread application in plastic waste upcycling. [1] One of the primary issues is the efficient diffusion of plastic polymer chain into the zeolite pores because of the size and complexity of plastic polymers. In this sense, introducing mesoporosity in zeolites seems promising to address problems faced in microporous zeolites. Among them, the surfactant templating technique has proved to be an efficient way to introduce well-defined, tunable, and highly interconnected mesopores in FAU-type zeolite, while maintaining the key properties of conventional zeolites, i.e., crystalline structure, hydrothermal stability, and strong acidity. However, the confinement effects within the zeolite structure, crucial for catalytic activity, are not fully understood and optimized in the context of plastic waste upcycling with different branching, and different types. [2-3]

This work addresses these critical challenges by exploring innovative strategies to modulate the confinement and pore diffusion properties of zeolites which perform at very low temperatures (<280 °C) where the thermal cracking is completely avoided. Through a comprehensive study, we enhanced the efficiency of FAU-type zeolite catalysts in plastic waste upcycling, paving the way for more sustainable and economically viable waste management solutions. To do so, CBV720 and surfactant templated CBV720 (M720) have been washed with either citric acid or ammonium hexafluorosilicate (NH<sub>4</sub>SiF<sub>6</sub>), in order to modify their acidic properties, and the catalysts have been tested for the polyethylene (PE) catalytic cracking by using three different PEs: HDPE, LDPE, and LLDPE.

The materials prepared were analysed by a multi-technique approach by employing: XRD, UV-Vis Raman, N<sub>2</sub> Isotherms, TEM and acidity measurements (NH<sub>3</sub>-TPD and Py-FTIR). The catalytic tests were done by following the degradation temperature of the different plastics (mixed or not with a catalyst) by thermogravimetric analysis. The product distribution analysis of the catalytic experiments was studied in a tubular gas-flow reactor and analysing both the gas fraction and the non-volatile products by GC-MS.

The characterization of the materials revealed that the zeolitic structure was well-preserved after the mesoporosity introduction or the washing treatments with citric acid or NH<sub>4</sub>SiF<sub>6</sub> as observed by Raman or XRD. The development of mesoporosity was confirmed by N<sub>2</sub> isotherms and was also observed by TEM analysis, moreover it was fully maintained after the washing treatments. The nature and quantity of Al in the catalysts, and thus the acidic properties, was altered by the washing treatments: 1) citric acid did not modify the total Si/Al but in the mesoporous zeolites decreased the extraframework Al; and, 2) the NH<sub>4</sub>SiF<sub>6</sub> treatment significantly altered the total Si/Al moving from Si/Al ~15 of the parent zeolite to around Si/Al ~40 in the modified materials. The acidic properties, studied by NH<sub>3</sub>-TPD and Py-DRIFT showed that the introduction of mesoporosity did not alter the total acidity but the accessibility to the Brønsted acid sites was improved due to a higher Brønsted/Lewis (B/L) ratio compared with the parent zeolite. The modified materials revealed that the washing treatment with NH<sub>4</sub>SiF<sub>6</sub> dramatically decrease the total acidity of the materials and the washing treatment with citric acid slightly decrease the total acidity compared with the former zeolites but the B/L ratio was even higher pointing a better accessibility to the Brønsted sites after the treatment.

In general, the results of the degradation of the PEs showed that the tested materials decreased, between 50 °C and 200 °C, **Figure 1a**, the degradation temperature of the all three polymers. The general behaviour was that the commercial, the surfactant templated zeolites and the washed materials with citric acid showed good behaviour for the cracking of the three different polymers. Deeping into the cracking ability of the catalysts, we found that for the HDPE or LLDPE no differences were observed either for the mesoporous or microporous zeolites, however, when the materials faced the LPDE polymer, the presence of mesopores clearly helped and decreased the degradation temperature -30 °C over the microporous zeolite, **Figure 1b**, and almost 200 °C from the thermal experiment.



Our results indicate that even though the acidity of the surfactant-templated zeolites is slightly lower than that of the commercial microporous zeolite, the ratio Bronsted/Lewis acidity, which is higher in the mesoporous zeolites, plays a major role in the LDPE cracking ability and thus is improved due to the existence of mesoporosity.

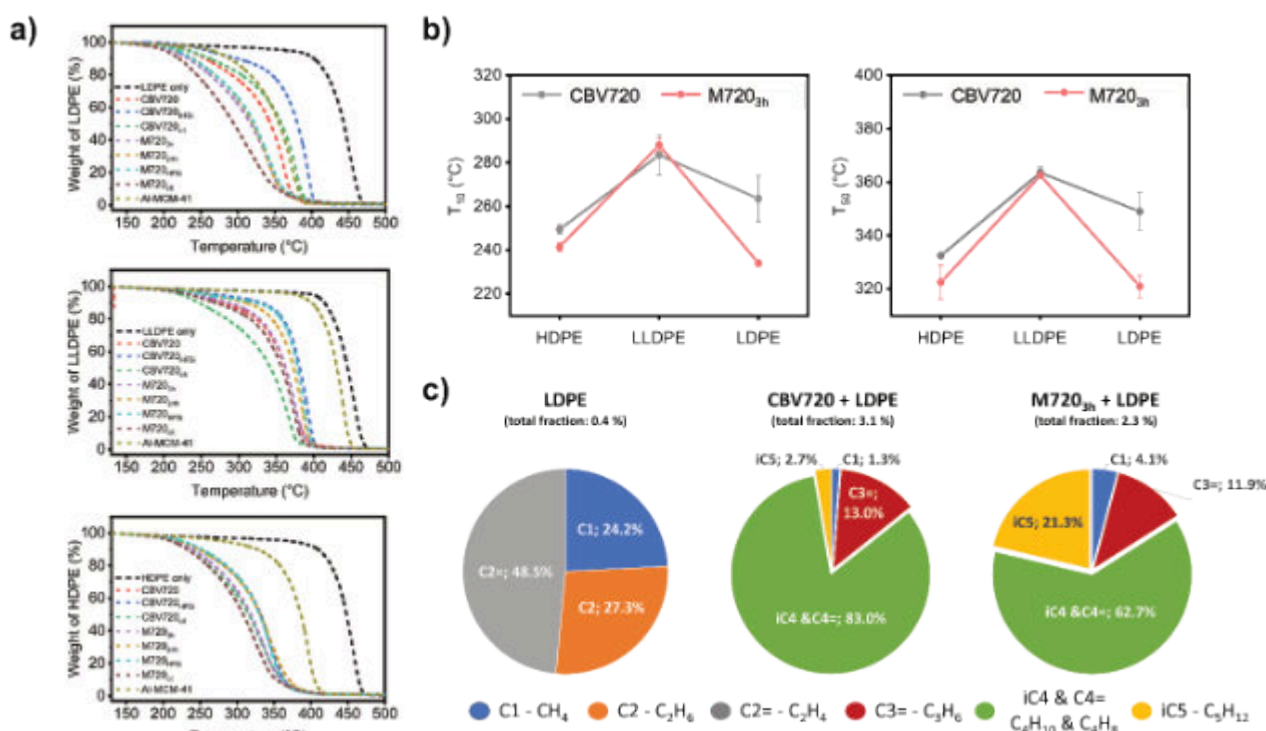


**Figure 1.** a) TGA curves of all catalysts prepared and the three polymers studied, b) T<sub>10</sub> (10% degradation) and T<sub>50</sub> (50% degradation) of the CBV720 and M720 facing the three PEs and b) gas fraction product distribution after LDPE cracking.

The product distribution (PD), **Figure 1c**, analysis showed a totally different selectivity without catalyst and using zeolites and, the most promising results is that the mesoporous zeolite showed a very similar PD, compared with the microporous zeolite, manifesting that the zeolitic microcrystalline structure it is still well retained after the post-synthetic treatments. It is important to note that in the gas fraction there was more C5 product in the mesoporous zeolite related with the shorter long-path for the hydrocarbons to release the zeolitic crystals. Additionally, the mesoporous zeolite was tested for the degradation of a wide variety of real and commercial plastics and the M720 showed good cracking ability facing polymers coming from plastic bottles, milk packages and electric wires. In summary, as shown in the model study with pure HDPE, LDPE or LLDPE, FAU-type zeolites and their mesoporous versions are good candidates for degrading some everyday plastics.

In conclusion, our mesoporous zeolites showed improved textural and accessibility properties, without significantly altering the crystalline structure, which was crucial for the cracking ability of the PEs, especially LDPE, demonstrating enhanced plastic degradation with mesoporous zeolites compared to conventional zeolites.

## References

- [1] U. Khalil, Z. Liu, C. Peng, N. Hikichi, T. Wakihara, J. García-Martínez, T. Okubo, S. Bhattacharya, *Chemical Engineering*, **412**, 128566 (2021).
- [2] J. García-Martínez and K. Li (editors), *Mesoporous Zeolites: Preparation, Characterization and Applications*, Wiley-VCH, Weinheim (2015).
- [3] A. Sasche and J. García-Martínez, *Chemistry of Materials*, **29**, 3827 (2017).

## Acknowledgments

This study forms part of the Advanced Materials program (MFA/2022/059) and was supported by MCIN with funding from European Union NextGenerationEU (PRTR-C17.11) and by Generalitat Valenciana. We acknowledge the funding support of the Department of Atomic Energy, Government of India, project no. 12-R&D-TFR-RTI4003 and grant PID2022-137364OB-I00 funded by MCIN/AEI/10.13039/501100011033. J.M-O acknowledges the financial support from the European Union – NextGeneration EU through the Universitat Politècnica de València, Ministerio de Universidades, Plan de Recuperación, Transformación y Resiliencia for the Margarita Salas grant.



## Waste Reduction in Fine Chemical Synthesis Using Hierarchical Zeolites

M. J. Mendoza-Castro<sup>1</sup>, J. García Martínez<sup>1,\*</sup>, N. Linares<sup>1,\*</sup>

<sup>1</sup> Laboratorio de Nanotecnología Molecular, Departamento de Química Inorgánica, Universidad de Alicante, Ctra. San Vicente-Alicante s/n, 03690 Alicante, Spain  
Noemi.linares@ua.es

The development of intracrystalline mesoporosity within zeolites has been a long-standing goal in catalysis as it greatly contributes to alleviating the diffusion limitations of these widely used microporous materials. [1] In the last years, our group has described the surfactant-templating in zeolites, which allows for the introduction of tailored mesoporosity within a given zeolite, while broadly preserving its key properties such as strong acidity, crystallinity, and hydrothermal stability (Figure 1).

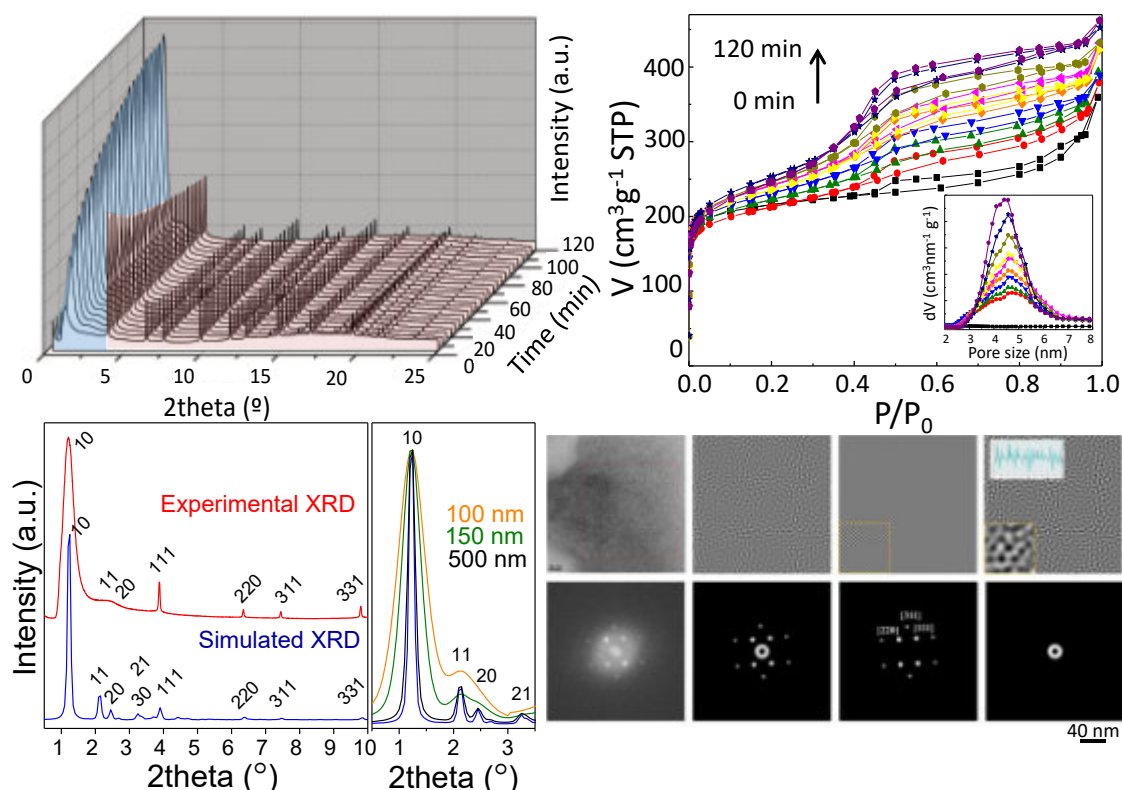


**Figure 1.** Textural and structural characterization of the surfactant-templating process in FAU zeolite.

This communication presents an overview of how the application of new materials in the transformation of bulky molecules allows for the development of more environmentally friendly procedures. The use of these more accessible heterogeneous catalysts has enabled the removal of organic solvents in various fine chemistry processes. On one hand, zeolites prepared with surfactants in its acidic form show excellent activity in the solvent-free production of steroid analogues and indole-based structures (Figure 2a). The commercial USY zeolite is a very active acid catalyst for these reactions, as confirmed by using smaller analogues (Figure 2b); however, the diffusional problems associated to the transformation/production of the bulky intermediates greatly limits its use. The presence of intracrystalline mesoporosity introduced by surfactants yields not only enhanced performance, but also better recyclability and lower pore blocking due to undesired products to the catalysts, emerging as a very attractive option both in terms of catalytic performance and lifetime for the synthesis of important pharmaceutical intermediates.





On the other hand, surfactant-templated zeolites have been also evaluated as basic catalysts in the multicomponent synthesis of a 2-amino-chromene derivative (Figure 2c), a bulky molecule with different pharmacological applications. Under solvent-free conditions, K- and Cs-ion-exchanged mesoporous zeolites show up to 2.5-fold increase in yield over commercial microporous ion-exchanged USY zeolites. Furthermore, when compared against a mesoporous ion-exchanged Al-MCM-41, mesoporous zeolites yield a 200-fold increase in TON (Figure 2d), highlighting the importance, not only of the mesoporosity but also of strong basicity.

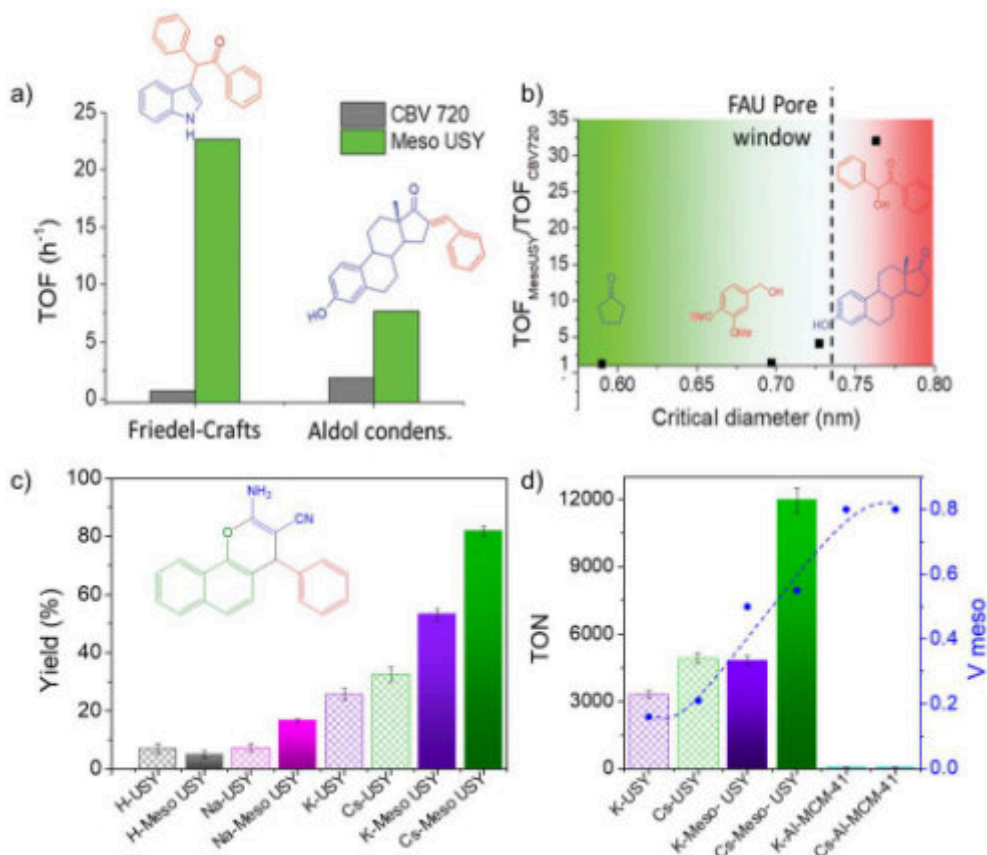


**Figure 2.** a-b) Friedel-Crafts alkylation and Aldol condensation under solvent-free conditions using bulky reagents. C-d) Multicomponent synthesis of a bulky chromene derivative.

Finally, the use of solvent-free synthesis in combination with the excellent performances, allowed us to drastically reduce the amount of wastes produced in these processes, yielding E-factors (kg waste / kg product) more than 10 times lower than similar processes already reported. In conclusion, surfactant-templated hierarchical USY zeolites featuring well-defined mesoporosity and easily accessible catalytic sites represent an attractive option for the sustainable synthesis of bulky molecules.

## References

- [1] M. Mendoza-Castro, E. Serrano, N. Linares, J. García-Martínez, *Adv. Mater. Interfaces.* 8 (2021) 2001388.
- [2] N. Linares, F. G. Cirujano, D. E. De Vos, J. García-Martínez, *Chem. Commun.*, 55 (2019) 12869.
- [3] M. Mendoza-Castro, N. Linares, J. García-Martínez, *Catalysis Today* 419 (2023) 114152.

## Acknowledgments

Thanks are due to the European Commission for funding through the H2020-MSCA-RISE-2019 program (Ref. ZEOBIOCHEM – 872102) and Spanish MCIN (Ref. PID2021–1287610B-C21). This study forms part of the Advanced Materials programme and was supported by MCIN with funding from European Union NextGenerationEU (PRTR-C17.11) and by Generalitat Valenciana.



## Interzeolite Transformation Intermediates (ITIs): Superior Catalysts for the Conversion of Bulky Molecules

M. J. Mendoza-Castro<sup>1</sup>, N. Linares<sup>1,\*</sup>, J. García Martínez<sup>1,\*</sup>

<sup>1</sup> Laboratorio de Nanotecnología Molecular, Departamento de Química Inorgánica, Universidad de Alicante, Ctra. San Vicente-Alicante s/n, 03690 Alicante, Spain.

Email: noemi.linares@ua.es

A new family of X-ray amorphous zeolites with unique structural properties was prepared by partial zeolite interconversion. [1,2] These ITIs (Interzeolite Transformation Intermediates) are composed of zeolitic building units, and display both enhanced accessibility and strong acidity. A key advantage of this method is that the properties of the solids can be adjusted by simply interrupting the interconversion of different times. We have evaluated the potential of these materials as superior catalysts for the conversion of bulky molecules for a number of reactions including Friedel–Crafts alkylations, the Claisen–Schmidt condensations, and the cracking of plastics.

We realized this strategy for two different interconversions and various synthetic approaches. In a first case, the partial interconversion from FAU into BEA was studied by using a combination of TEOH (the typical structure directing agent for this transformation) and/or CTAB (a cationic surfactant), which determines the kinetics of the transformation and the textural properties evolution, Figure 1a-d. The use of the quaternary ammonium surfactant develops well-defined mesoporosity in the intermediates. By stopping the interconversion at different times, we were able to produce Interzeolite Transformation Intermediates (ITIs) showing optimized catalytic performance. The synthesized materials were tested in different reactions such as, the Friedel–Crafts alkylation of indole with benzhydrol, the Claisen–Schmidt condensation of benzaldehyde and hydroxyacetophenone, and the cracking of polystyrene, demonstrating their broad applicability, Figure 1e-f, respectively.

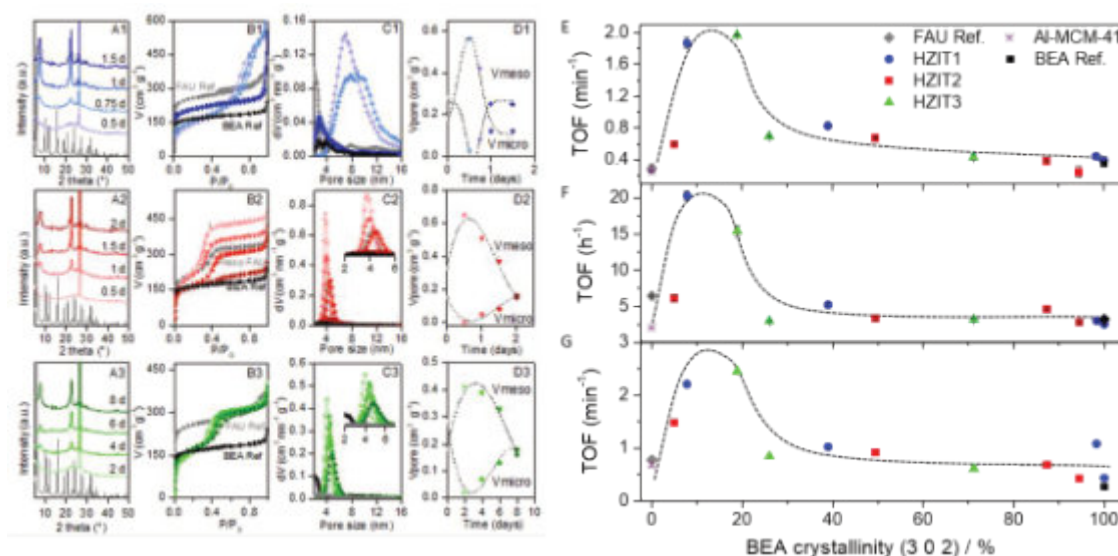


**Figure 1.** a) Structural and b-d) textural characterization of the interzeolite transformation from FAU to BEA zeolite. Catalytic performance (TOF) of the ITI materials for the e) Friedel–Crafts alkylation of indole with benzhydrol, (f) Claisen–Schmidt condensation of benzaldehyde and hydroxyacetophenone, and (g) polystyrene cracking.

In a second case, the interzeolite transformation of FAU into MFI was carried out by using a long-chain quaternary amine as both a structure-directing agent and porogen, and interrupting the transformation at various times. By this approach, we have produced superior hybrid catalysts, which structure is made of building units of different zeolites types (Figure 2). The catalytic performance can be optimized by simply stopping the interconversion at various times. To assess the potential of the hybrid zeolites to convert bulky molecules, they were tested for the catalytic cracking of 1,3,5-triisopropylbenzene (TiPBz), Figure 3. The hybrid catalysts made of FAU and MFI units show a 5-fold increase in selectivity towards the desired product, 1,3-diisopropylbenzene, compared to the commercial FAU and a 7-fold increase in conversion at constant selectivity compared to MFI zeolite. Furthermore, these intermediates always yield lower amounts of the two unwanted over-cracked products (cumene and benzene) than FAU and MFI zeolites at the same conversion.

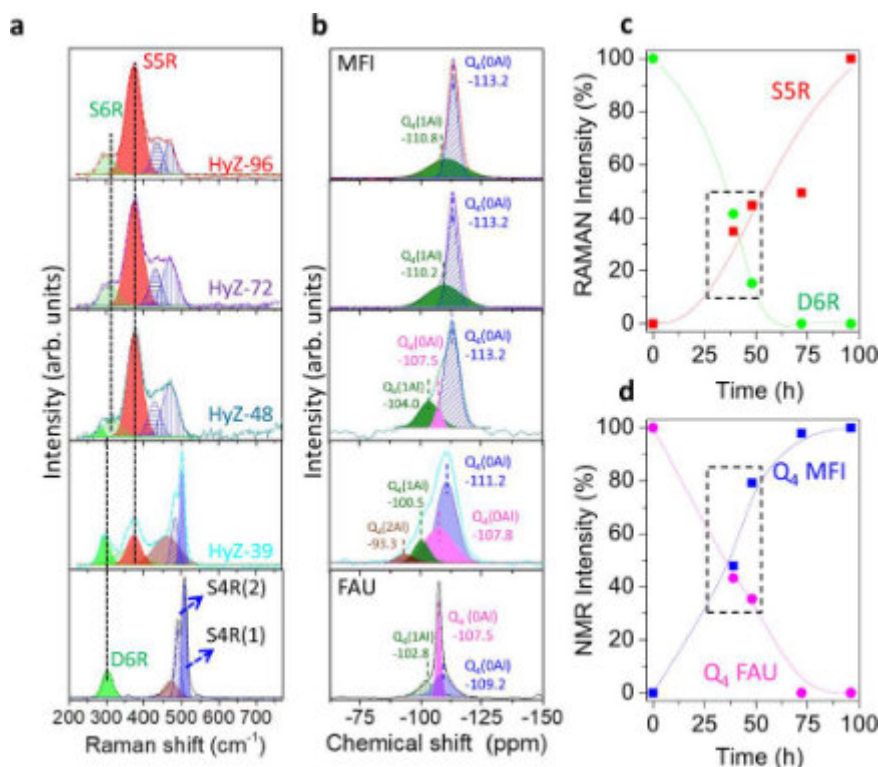


**Figure 2.** a) UV-Raman and b)  $^{29}\text{Si}$  NMR spectra of the hybrid zeolites. Evolution of the percentage of c) UV-Raman intensity and d) the Q4 intensity in the  $^{29}\text{Si}$  NMR.

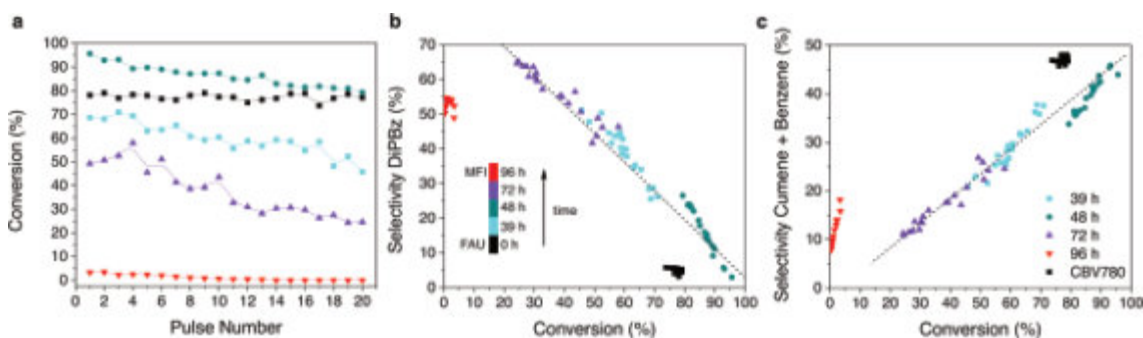


**Figure 3.** a) Conversion in the catalytic cracking of TiPBz. Evolution of the selectivity for b) 1,3-diisopropylbenzene and c) cumene and benzene.

In conclusion, the partial interzeolite transformation strategy allows to finely tuned both the physicochemical properties and, therefore, the catalytic performance of the hierarchical catalysts by simply stopping the interzeolite transformation at different times. This creates countless opportunities for the development of new hierarchical catalysts (ITIs) with optimized properties and superior catalytic performance for those reactions in which zeolites present significant diffusion limitations.

## References

- [1] M. J. Mendoza-Castro, E. De Oliveira-Jardim, N.T. Ramírez-Marquez, C. A. Trujillo, N. Linares, J.García-Martínez, *J. Am. Chem. Soc.*, **144**(11) 5163–5171 (2022)
- [2] M. J. Mendoza-Castro, Z. Qie, X. Fan, N. Linares, J.García-Martínez, *Nature Commun.*, **14**, 1256 (2023).

## Acknowledgments

Thanks are due to the European Commission for funding through the H2020-MSCA-RISE-2019 program (Ref. ZEOBIOCHEM – 872102) and Spanish MCIN (Ref. PID2021–128761OB-C21). This study forms part of the Advanced Materials programme and was supported by MCIN with funding from European Union NextGenerationEU (PRTR-C17.I1) and by Generalitat Valenciana.



## Recyclable synthesis of SAPO-34 and their catalytic applications: utilizing mother liquid and spent industrial MTO catalyst as raw sources

Quanyi Wang, Peng Tian and Zhongmin Liu

National Engineering Research Center of Lower-Carbon Catalysis Technology, Dalian National Laboratory for Clean Energy, Dalian Institute of Chemical Physics, Chinese Academy of Sciences, Dalian 116023, China  
[gywang@dicp.ac.cn](mailto:gywang@dicp.ac.cn)

The methanol-to-olefin (MTO) process is a pivotal technology in the C1 chemistry industry, as it provides a non-petrol route for the production of ethene and propene. A SAPO-34 molecular sieve with the isomorphous structure of zeolite chabazite (CHA) is hitherto the most effective component for MTO catalysts and has been attracting significant interest from both academia and industry. The CHA structure of SAPO-34 is fabricated by the ordered arrangements of double 6-membered rings, forming barrel-like nanocages featuring 8-membered ring openings. This special structure provides an ideal “incubation cradle” for the development of polymethylbenzene species, the authentic active center for the MTO reaction. Commercial MTO utility with an olefin production capacity of 600 000 tons was first commissioned in 2010. Since then, an emerging MTO industry has been booming in China with the olefin production capacity reaching 17 million tons per annum.

Hitherto, the corresponding consumption of SAPO-34 based catalysts has now increased up to 10000 tons per year. The rapid deactivation of MTO catalysts allows for the production of a large amount of waste catalysts. However, the spent industrial MTO catalysts are classified as hazardous waste, which requires special disposal to avoid its potential threats to the environment. Furthermore, SAPO-34 is conventionally synthesized via a hydrothermal route. One drawback associated with the hydrothermal production of SAPO-34 is the co-production of large quantities of mother liquid, similarly regarded as industrial waste and demanding expensive disposals to meet environmental regulations.

In fact, the dry basis of industrial MTO catalyst and the mother liquid is mainly composed of silica, alumina and phosphorus oxide, which can provide all three inorganic sources required for the synthesis of SAPO-34 molecular sieves. In addition, the structure of SAPO-34 may be partially maintained in the spent catalyst and the mother liquid, which can play as seeds and would be beneficial for the crystallization of SAPO-34. The discharge of the spent MTO catalyst and the mother liquid not only results in a waste of unreacted raw resources but also intrigues serious environmental problems. Therefore, it is highly valuable to develop an effective method to convert the mother liquid and the spent MTO catalysts into an efficient SAPO-34 catalyst.

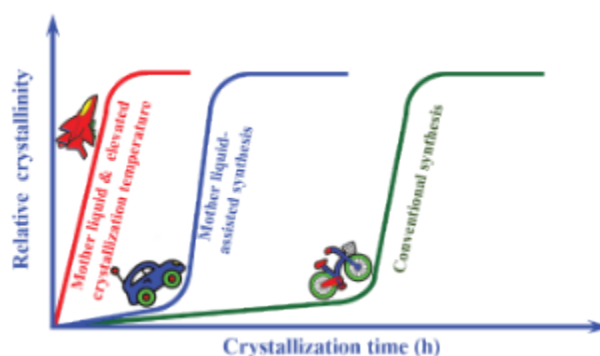


Figure 1 Schematic illustration of crystallization speed comparison under different synthesis conditions

In the first part<sup>[1]</sup> of our research, an eco-friendly approach with the utilization of the recycled mother liquid was reported for the synthesis of SAPO-34. The developed system can allow an elevated crystallization temperature, leading to fast synthesis of SAPO-34 within 1–3 h and with reduced silica content. Both the product phase and crystallization kinetics were demonstrated to be significantly dependent on the crystallization temperature and the dosage of the mother liquid. The rapidly synthesized low-silica SAPO-34 was well characterized and its MTO catalytic performance was evaluated.

In the second part<sup>[2]</sup> of our research, the spent industrial MTO catalyst was utilized as raw material to explore the synthesis of SAPO-34 and their catalytic applications. Two amines with different sizes including diethylamine (DEA) and tetraethylammonium hydroxide (TEAOH) were employed as the synthesis templates. It was found that the Si/Al/P sources in spent MTO catalyst have high reactivity and SAPO-34 with varied Si contents can be synthesized in high crystallinity. Low-silica SAPO-34 exhibits good catalytic performance in the MTO reaction. More importantly, compared with SAPO-34-TEAOH, SAPO-34-DEA shows excellent catalytic performance in the methanol ammoniation reaction with high selectivity to methylamine (MMA) and dimethylamine (DMA) due to its higher acid concentration



and larger crystal size. After hydrothermal treatment of SAPO-34-DEA at 800 °C, although the methanol conversion shows a decrease (~25% drop), the MMA plus DMA selectivity in three methylamines increases to as high as 94%.

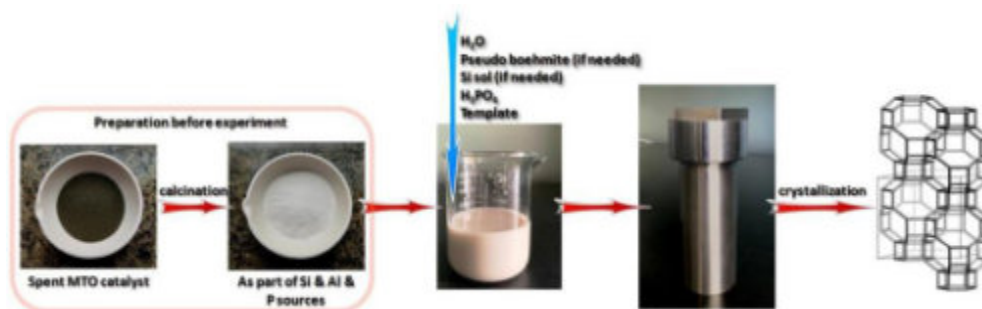


Figure 2 Schematic procedure for SAPO-34 synthesis using spent industrial MTO catalyst as raw sources

These present studies could provide valuable insights that can guide the controlled synthesis of SAPO-34 through recyclable utilization of mother liquid and spent industrial MTO catalyst as raw sources, which would facilitate their rational disposal and the development of MTO industrial process.

### References

- [1] Xiaoxia Zou, Dong Fan, Xiaosi Zhang, Caiyi Lou, Miao Yang, Shutao Xu, Quanyi Wang, Peng Tian, Zhongmin Liu, A rapid and eco-friendly approach for the synthesis of low-silica SAPO-34 with excellent MTO catalytic performance, *Chemical Communications*, 2024, 60, 4805
- [2] Zhao Liu, Quanyi Wang, Shiping Liu, Miao Yang, Dong Fan, Dali Zhu, Peng Tian, Zhongmin Liu, Synthesis of SAPO-34 by utilizing spent industrial MTO catalyst and their catalytic applications, *Materials Today Sustainability*, 2023, 21, 100302

### Acknowledgments

The authors acknowledge the funding by the National Natural Science Foundation of China (No. 22171259, 22272173, 21991090, 21991091, and 22288101) and the AIS&T Program of Yulin Branch, Dalian National Laboratory for Clean Energy, CAS (DNL-YL A202206). The authors are grateful for the funding from the Sino-French IRN (International Research Network).



## Adsorption of Carbon Dioxide in Non-Löwenstein Zeolites

J. J. Gutiérrez-Sevillano<sup>1</sup>, P. Romero-Marimon<sup>2</sup>, S. Calero<sup>2</sup>,

<sup>1</sup> Center for Nanoscience and Sustainable Technologies (CNATS), University Pablo de Olavide, Ctra. Utrera km. 1, 41013 Seville, Spain

<sup>2</sup> Department of Applied Physics and Science Education, Eindhoven University of Technology, 5612AZ Eindhoven, Netherlands  
jjgutierrez@upo.es

**1. Introduction.** The adsorption performance of zeolites depends on the operating conditions. The temperature, pressure, and moisture content seem to be the most relevant factors in the adsorption of carbon dioxide[1]. The adsorption efficiency is also strongly dependent on the structural properties of the zeolite. In fact, different topologies might perform differently with different adsorbates, depending on their size and polarity. Besides, for a given topology, multiple Si/Al ratios and distributions of the aluminum atoms can also lead to different results [2,3]. The substitution of Si atoms with Al atoms leads to a negative net charge in the framework, which needs to be compensated by introducing extraframework cations. The cation distribution is highly dependent on the positions of the aluminum substitutions and has an impact on the interactions between the zeolite and the adsorbates. There is a balance between the strength of the framework-adsorbate interactions and the availability of space and it is not clear which Si/Al ratio leads to a better performance and which is the optimal distribution of the Al atoms. The so-called Löwenstein's rule, introduced for the first time in 1954, prohibits the bonding between two Al atoms through a single oxygen (Al-O-Al) and has been traditionally supported by many experimental studies. Nevertheless, a solid theory on the instability of the Al-O-Al linkage is still missing, and some recent studies have found violations of this rule [4,5]. The main goal of this work is to study the influence of different aluminum distributions in the adsorption properties of zeolites. In particular, the effect of the non-Löwenstein bonds.

**2. Methods.** Three zeolites have been used to consider a different topology for each pore size: MOR (large pore), MFI (medium pore), and ITW (small pore). MOR-type zeolites have an orthorhombic unit cell with one-dimensional channels along the *c* axis, which we call main channels or C-channels. We implemented a series of algorithms to generate zeolite structures stochastically, where the aluminum distributions are sampled from different probability distributions allowing us to accurately obtain structures with a certain number of non-Löwenstein bonds. The strength of the interactions between the CO<sub>2</sub> molecules and the zeolites were studied via the heat of adsorption. To calculate the heat of adsorption, we performed Monte Carlo simulations using the Widom particle insertion method. Additional Monte Carlo simulations in the Grand Canonical Monte Carlo ensemble were performed to obtain adsorption isotherms. All simulations were performed with the RASPA software.[6]

**3. Results and Discussion.** For each topology we considered different Si/Al ratios and we analyzed the effect of (a) the Si/Al ratio and (b) the aluminum distribution on the adsorption properties. As we include in our study structures non holding the Löwenstein's rule, we first developed a set of charges compatible with models for "regular" zeolites. Then the effect of the Al distribution in three zeolites (MFI, MOR, and ITW) was study. We obtained adsorption isotherms for multiple configurations and calculated the heat of adsorption for each of them. Additionally, the preferential adsorption sites for carbon dioxide were analyzed for each topology.

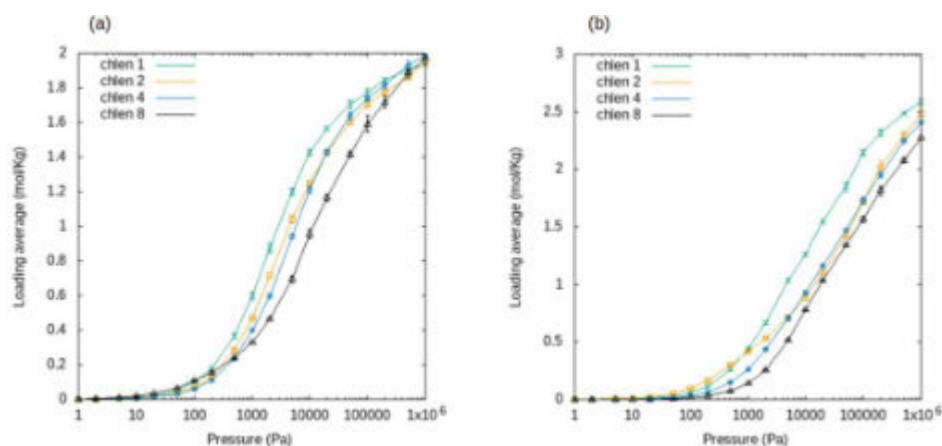


**Figure 1.** CO<sub>2</sub> adsorption isotherms for (a) MFI and (b) MOR. In both cases, all the structures contain 8 Al substitutions, which are distributed in chains of equal length (chlen).

On figure 1, the adsorption isotherm of CO<sub>2</sub> in MFI and MOR is shown for different distribution of 8 Al-substitution. As can be observed, the distribution of the aluminium chains has influence in the range of mid-high pressure for MFI, while in the MOR, it also affects to the maximum adsorption. In the MOR topology we also found that the T position



of the substitution modify the adsorption sites for carbon dioxide and varying the heat of adsorption, as can be seen on figure 2.

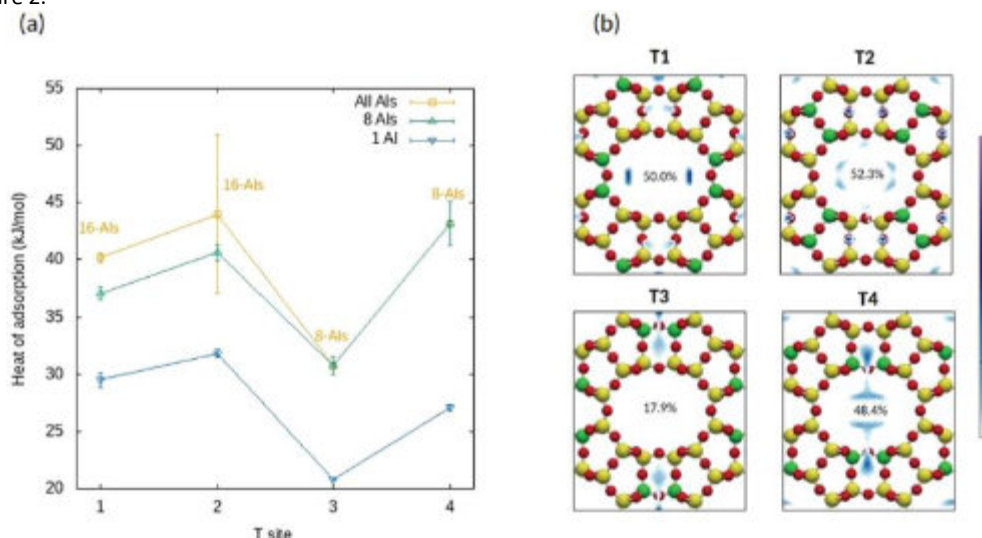


**Figure 1.** (a) Heat of adsorption as a function of the T position in MOR for different number of aluminum substitutions. (b) Adsorption sites of the sodium cations in the 4 MOR frameworks where all equivalent positions contain aluminum atoms. The percentages correspond to the amount of sodium cations confined in the main channel.

**4. Conclusions.** We proposed a new set of charges for zeolites that generalize a transferable force field which accounts for non-Löwenstein linkages to study carbon dioxide adsorption in zeolites. We found that in MFI the heat of adsorption depends mainly on the number of Al atoms and the amount of non-Löwenstein bonds does not significantly affect this magnitude. For MOR zeolites, the influence of the number of non-Löwenstein linkages was notable, as in general when this is higher the Al atoms are more clusterized. This leads to a reduction of the interactions between the framework and the adsorbate. Structures contained consecutive Al-O-Al linkages, but not clustered, exhibit a very high heat of adsorption as compared to other structures with the same number of Al atoms. In the ITW topology for the higher Si/Al ratios tested, a small preference for the maximal entropy structures was observed.

## References

- [1] Bonenfant, D.; Kharoune, M.; Niquette, P.; Mimeault, M.; Hausler, R. *Sci. Technol. Adv. Mater.* 013007, **9** (2008)
- [2] Yang, C.; Janda, A.; Bell, A.; Lin, L. *J. Phys. Chem. C* 9397-9410, **122** (2018)
- [3] Choi, H.; Jo, D.; Hong, S. *Chem. Eng. J.* 137100, **446** (2022)
- [4] Fletcher, R.; Ling, S.; Slater, B.. *Chem. Sci.* 7483-7491, **8** (2017)
- [5] Heard, C.; Grajciar, L.; Nachtigall, P.. *Chem. Sci.* 5705-5711, **10** (2019)
- [6] Dubbeldam, D.; Calero, S.; Ellis, D.; Snurr, *Mol. Simul.* 81-101, **42** (2016)

## Acknowledgments

J.J.G.S thanks to the Spanish Ministerio de Ciencia e Innovacion for its financial support (CNS2022- 136163)



## CDot@SiO<sub>2</sub> and CDot@TiO<sub>2</sub> as superior catalysis for the photodegradation of cationic dyes

J. Castro<sup>1,\*</sup>, M. Rosell<sup>2</sup>, V. Torregrosa-Rivero<sup>1</sup>, A. Garzón-Ruiz<sup>2</sup>, C. Martín<sup>2</sup>, J. García-Martínez<sup>1</sup>, N. Linares<sup>1</sup>, E. Serrano<sup>1</sup>

<sup>1</sup> Laboratorio de Nanotecnología Molecular, Dpto. Química Inorgánica, Universidad de Alicante, Carretera Alicante-S. Vicente s/n, 03690 Alicante (Spain). \* Presenting author: [Jorgeivan.castro@ua.es](mailto:Jorgeivan.castro@ua.es)

<sup>2</sup> FOTOAIR, Dpto. Química-Física, Facultad de Farmacia, Universidad de Castilla-La Mancha. C/José María Sánchez Ibañez s/n, 02071 Albacete (Spain)

Carbon dots (CDots) have remarkable physicochemical properties such as small size, photoluminescence, photostability, low toxicity, diversity of preparation methods, and low cost [1,2]. However, important aspects of their photochemistry remain elusive because the relationship between their optical and structural properties is still largely unknown. In this context, the present work aims to elucidate the relationship between the physical properties of CDots and their structure, where the latter is closely related to the synthesis conditions.

A variety of CDs (carbon dots) were synthesized using different organic precursors, including biomass-based compounds like cellulose derivatives, amino acids, and benzene derivatives with hydroxyl, carboxylic, and amine functional groups. The synthesis involved hydrothermal treatment at 180-200 °C with water as the solvent, followed by dialysis using a 500 Da membrane. This method produced luminescent CDs with 3-20% quantum yields, varying with the precursor. Adjusting the carbon source and synthesis conditions can control the graphitization degree of the carbon core and the surface functional groups. The carbon core primarily dictates emission for CDs made from cellulose derivatives, which the surface groups can enhance (Figure 1).

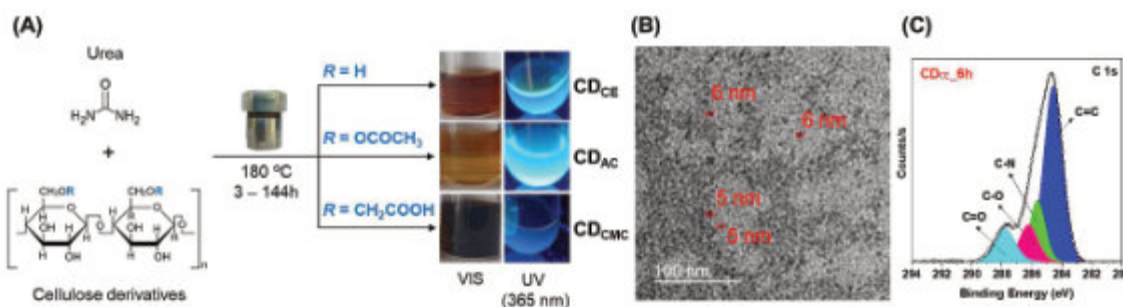


**Figure 1.** (A) Schematic illustration of the hydrothermal synthesis of N-doped CDots by solvothermal decomposition of urea and three different cellulose derivatives in water: cellulose (CE), acetate cellulose (AC) and carboxymethylcellulose (CMC). (B) Representative TEM image of dialyzed CD<sub>CE</sub> after 6h of hydrothermal treatment at 180 °C. (C) XPS in the C1s region of dialyzed CD<sub>CE</sub> after 6h of hydrothermal treatment at 180 °C [3].

Another challenge is that CDs often undergo aggregated-induced luminescence quenching (ACQ), which results from  $\pi$ - $\pi$  interactions of CDs graphitized cores, excessive resonance energy transfer, and interparticle coupled surface areas, which limits the luminous efficiency and the photocatalytic activity. In this sense, hybrids based on the incorporation of CDs into titania and silica materials represent promising candidates for acting as a confining matrix to overcome the limitations of the CDs in terms of their aggregate-induced luminescence quenching, excessive resonance energy transfer and coupled surface areas between particles, as well as their efficacy under ultraviolet light.

In the present work, a series of silica- and titania-based nanohybrid materials were synthesized by (i) incorporating CDs both during the synthesis of the inorganic matrix and (ii) by impregnating the previously synthesized inorganic matrices. In the case of silica, a gel was formed without surfactant, obtaining a stable emissive material. This material incorporates species of carbon dots of tyrosine into the silica network (figure 2). The resulting Carbon dot-silica gels are particularly noteworthy because their behavior at room temperature mimics the emission properties of pure carbon dot in solution, whether at room temperature or in a rigid, frozen matrix. On the other hand, gas adsorption shows a type IV isotherm for carbon dots incorporated in silica. Furthermore, it probably indicates that incorporating CDs in this matrix mostly fills the pores present in the matrix, decreasing the matrix surface area.



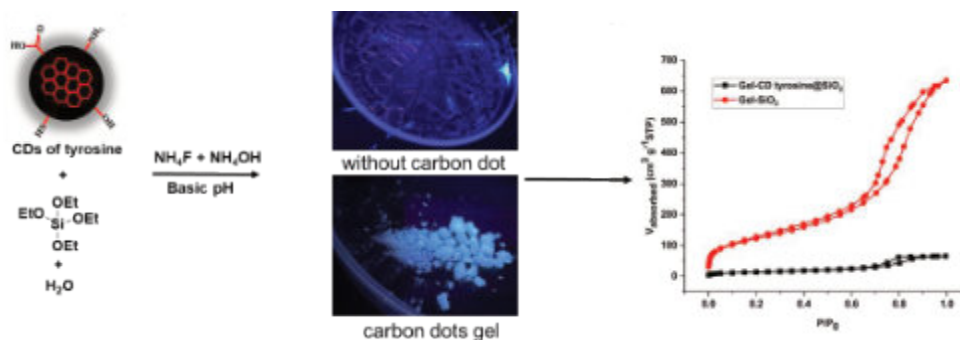


**Figure 2.** Schematic representation of the preparation of luminescent mesoporous hybrid CD of tyrosine inside a silica matrix to form a gel. Picture of the gel (down) with its respective target (bottom). Nitrogen adsorption/desorption isotherms at 77 K

TiO<sub>2</sub> nanoparticles have limited use in large-scale wastewater treatment for degrading organic compounds due to issues like recombination of photogenerated electron holes, isolation difficulties in aqueous solutions, and dependence on UV light. In this regard, the photocatalytic activity of hybrids was tested on industrial dyes like rhodamine 6G and methylene blue under visible light from a mercury lamp and commercial LEDs. Results showed that incorporating CDs into the TiO<sub>2</sub>\_Phen hybrid reduces charge carrier recombination, likely due to electronic injection from the N-Ti bond and synergy between the titania matrix and carbon dots, which lowers the band gap from 2.83 eV to 2.45 eV (Figure 3A). Consequently, the CDs@TiO<sub>2</sub>\_Phen hybrid exhibited five times higher photocatalytic efficiency on methylene blue under white LED irradiation than TiO<sub>2</sub>\_Phen, with pseudo-order constants of 31.6 and 6.1 x10<sup>3</sup>, respectively (Figure 3D and 3E).

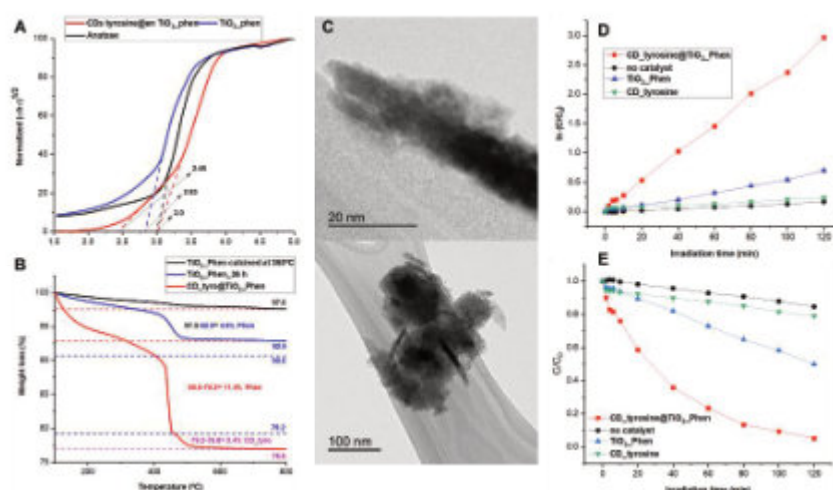


**Figure 3.** (A) Tauc plot of the transformed Kubelka–Munk function versus the energy of light absorbed; (B) TG curves; (C) TEM micrographs at two different magnifications of CDs tyrosine@TiO<sub>2</sub>\_Phen; (D) and (E) Rh6G photodegradation reaction using the hybrid CDs tyrosine@TiO<sub>2</sub>\_Phen as a photocatalyst

#### References

- Liu, J.; Li, R.; Yang, B. Carbon Dots: A New Type of Carbon-Based Nanomaterial with Wide Applications. *ACS Cent. Sci.* **2020**, *6*, 2179–2195.
- He, L.; Zhang, H.; Fan, H.; Jiang, X.; Zhao, W.; Xiang, G.Q. Carbon-Dot-Based Dual-Emission Silica Nanoparticles as a Ratiometric Fluorescent Probe for Vanadium (V) Detection in Mineral Water Samples. *Spectrochim. Acta Part A Mol. Biomol. Spectrosc.* **2018**, *189*, 51–56.
- Rosell, M.; Torregrosa-Rivero, V.; Herrera-Ochoa, D.; García-Martínez, J.; Garzón-Ruiz, A.; Serrano, E.; Martín Álvarez, C. Unlocking the Potential of Different Types of Biomass-derived Carbon Dots as Fluorescence Lifetime Imaging Probes. *ChemPhotoChem* **2024**, *202400133*, doi:10.1002/cptc.202400133.

#### Acknowledgments

The authors thank the MICIN/AEI projects refs. PID2021-1287610B-C21 and PID2021-1287610A-C22 were funded by MICIN/AEI/10.13039/501100011033 and FEDER, UE, by FEDER/ UE. The authors also thank CNS2022-136052, which was funded by MICIN/AEI/10.13039/501100011033 by “European Union NextGenerationEU/PRTR. This project has also received funding from the Generalitat Valenciana under project ref. AICO/2021/132. This research was also supported by SBPLY/21/180501/000127, funded by JCCM and the EU through “Fondo Europeo de Desarrollo Regional” (FEDER).



## Engineering PtZn Nanoparticles Dispersed on Zeolite Composites as Bifunctional Catalyst for *n*-Butane Dehydroisomerization

P. Chaipornchalerm<sup>1</sup>, W. Nunthakitguson<sup>1</sup>, N. Thepphankulgarm<sup>1</sup>, S. Namuangruk<sup>2</sup>, C. Wattanakit<sup>1</sup>

<sup>1</sup> Department of Chemical and Biomolecular Engineering, School of Energy Science and Engineering, Vidyasirimedhi Institute of Science and Technology, Rayong, 21210, Thailand.

<sup>2</sup> National Nanotechnology Center, National Science and Technology Development Agency, Pathum Thani 12120, Thailand.  
peeranat.c\_s20@vistec.ac.th

*n*-Butane dehydroisomerization (BDHISO) has emerged as an efficient and environmentally friendly alternative to traditional petrochemical processes such as steam cracking and fluid catalytic cracking for producing isobutene, eventually offering high isobutene selectivity without greenhouse gas emissions. Although several studies have reported that Pt nanoparticle-supported acidic zeolite catalysts exhibit high catalytic activity for the BDHISO process, the related catalysts face challenges such as metal sintering and excessive acidity, resulting in low isobutene yield and poor durability [1]. To address these limitations, we have successfully fabricated PtZn alloy nanoparticles dispersed on various zeolite composites, combining a core of parent zeolites (FER, MOR, and ZSM-5) with a shell of hierarchical silicalite-1 nanosheets (SN1), as bifunctional catalysts for the BDHISO reaction. The synthesis of these zeolite composites involved the recrystallization of the core zeolite followed by the growth of SN1 on the core zeolite surface [2]. The morphology of the synthesized composites revealed full coverage of SN1 nanocrystals on the outermost surface of the core zeolite (Figure 1), with ultra-small PtZn nanoparticles highly dispersed on the SN1 phase. Compared to the direct impregnation of PtZn species on pristine zeolites, the NH<sub>3</sub>-TPD profiles and FTIR spectra of pyridine adsorption over PtZn supported on zeolite composites revealed significantly weakened Brønsted acid sites. Among these composites, the PtZn-FER/SN1 composite exhibited the highest isobutene yield of 16.2%, attributed to the suitable channel size of the ferrierite framework, which allows isobutene to diffuse out and suppresses side reactions, as shown in Figure 2. In contrast, the PtZn-ZSM-5/SN1 and PtZn-MOR/SN1 composites, which possess larger pore sizes, promoted oligomerization and aromatization, resulting in lower isobutene yields. Moreover, the synergistic effect of additional zinc species into Pt nanoparticles making alloys, which prevent platinum sintering and alter its electronic properties [3], along with the weakened Brønsted acidity of the parent zeolite and the enhanced metal dispersion due to the presence of SN1 [4-5], enhanced the catalytic performance and durability. This work illustrates a new strategy on fabricating zeolite composites as the bifunctional catalysts to achieve high isobutene yield in BDHISO process.

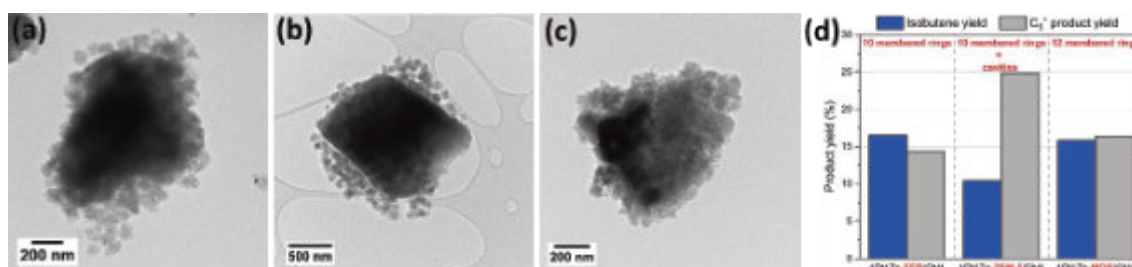


**Figure 1.** (a-c) TEM images of various synthesized zeolite composites (a) FER/SN1 composite, (b) ZSM-5/SN1 composite, and (c) MOR/SN1 composite. (d) The comparison of product yield over the 1Pt1Zn-FER/SN1, the 1Pt1Zn-ZSM-5/SN1, and the 1Pt1Zn-MOR/SN1, at TOS of 2 hours (The reaction conditions: feed molar ratio C<sub>4</sub>H<sub>10</sub>:N<sub>2</sub> of 1:9, WHSV of 1.74 hr<sup>-1</sup>, and operating temperature of 550 °C.). Reproduced from ref. [6]. Copyright 2023 American Chemistry Society.

### References

- [1] G.D. Pirngruber, K. Seshan, and J.A. Lercher, *Journal of Catalysis*, **190** (2), 338-351 (2000).
- [2] T. Imyen, W. Wannapakdee, S. Ittisanronnachai, T. Witoon, and C. Wattanakit, *Nanoscale Advances*, **2**, 4437-4449 (2020).
- [3] C. Rodaum, P. Chaipornchalerm, W. Nunthakitguson, A. Thivasasith, T. Maihom, T. Atitthep, P. Kidkhunthod, C. Uthayopas, S. Nutanong, S. Thongratkaew, K. Faungnawakij, and C. Wattanakit, *Fuel*, **325**, 124833 (2022).
- [4] P. Chaipornchalerm, W. Nunthakitguson, P. Mano, P. Kidkhunthod, A. Montoya, S. Namuangruk, and C. Wattanakit, *ACS Applied Materials & Interfaces*, **16** (26), 33590-33600 (2024).
- [5] P. Chaipornchalerm, A. Prasertsab, W. Prasanseang, and C. Wattanakit, *Energy & Fuels*, **Article ASAP**, DOI: 10.1021/acs.energyfuels.4c02069
- [6] P. Chaipornchalerm, W. Nunthakitguson, N. Thepphankulgarm, S. Namuangruk, and C. Wattanakit, *Industrial & Engineering Chemistry Research*, **62** (43), 17513-17526 (2023).



**6<sup>th</sup> Euro-Asia Zeolite Conference**  
Alicante (Spain), January 19-22, 2025



### **Acknowledgments**

This project is funded by the National Research Council of Thailand (NRCT) and the Vidyasirimedhi Institute of Science and Technology (VISTEC) under grant number N42A660307. Additionally, financial support for this research is scholared by the National Science and Technology Development Agency (NSTDA). Further funding has been received from the NSRF through the Program Management Unit for Human Resources & Institutional Development, Research, and Innovation under grant number B42G670029.



## Nickel-decorated carbon nanotubes (CNTs) derived from bioethanol as electrocatalysts for featuring H<sub>2</sub> production and biorefinery

W. Nunthakitguson, P. Chaipornchalem, A. Sohail, A. Thivasasith, and C. Wattanakit

Department of Chemical and Biomolecular Engineering, School of Energy Science and Engineering, Vidyasirimedhi Institute of Science and Technology, Rayong, 21210, Thailand.

E-mail :Watinee.n\_s21@vistec.ac.th

The utilization of biomass for producing fuels and chemicals is a rapidly advancing field due to the finite nature of fossil fuels and the urgent threat of global warming. Among the valuable byproducts of biomass conversion, bioethanol stands out as a prominent commodity, chemically derived from the fermentation of sugarcane or energy-rich crops like corn. While ethanol is produced in large quantities as an alternative or supplement to fuels derived from crude oil, its production remains costly. A promising approach is the conversion of bioethanol into high-value substances, such as carbon nanotubes (CNTs) emerging as a versatile material for various technologies, including chemical and biological sensing, thermal management, polymer nanocomposites, and black coatings for space applications, due to their high aspect ratio, chemical stability, and electronic and optical properties.

CNTs are traditionally manufactured using arc discharge, laser ablation, and chemical vapor deposition (CVD) techniques. Among these, thermal CVD is particularly favored for its low cost and ease of control under basic operating conditions. This process typically involves decomposing carbon sources over a catalyst composed of well-dispersed transition metal nanoparticles (e.g., Fe, Ni, Co) on a solid substrate. The dispersion of metal nanoparticles is crucial in determining the quality of CNTs. Zeolite, with its large surface area, well-defined porous structure, and high porosity, is considered an ideal solid material for supporting metal species. Therefore, combining bioethanol dehydration using an acidic zeolite catalyst with CCVD of catalytic metal species supported on zeolites can produce uniform CNTs with excellent quality and yield.<sup>[1,2]</sup>

This study introduces a novel method for producing CNTs from bioethanol using a two-stage process. First, bioethanol is dehydrated into ethylene over ZSM-5 zeolite. Subsequently, these carbon species are converted into CNTs using the CCVD procedure. The study examines the effects of Ni nanoparticles supported on conventional and hierarchical ZSM-5 zeolites (5wt.%NiCON-ZSM-5 and 5wt.%NiHie-ZSM-5) used as templates for synthesizing CNTs with varying properties. This research presents the innovative concept of utilizing bioethanol to produce high-value CNTs using metal-supported hierarchical zeolite catalysts.

Ni nanoparticles supported on CON-ZSM-5 and Hie-ZSM-5 were developed via the impregnation method. Among these catalysts, the 5wt% NiHie-ZSM-5 catalyst demonstrated the highest activity for CNT synthesis at 700°C. The resulting CNTs, produced using the 5wt% Ni-Hie-ZSM-5 catalyst, exhibited remarkable characteristics, including a diameter size of 13.0±5.2 nm, a CNT yield of 21.8%, and an I<sub>D</sub>/I<sub>G</sub> ratio of 0.62, indicative of their exceptional quality. Furthermore, the synthesized CNTs underwent electrochemical performance evaluation, with the fabricated Ni-CNT electrodes applied as electrocatalysts for efficient HMF oxidation and hydrogen generation. The kinetic curves of HMF electrooxidation over Ni-CNTs at a constant potential of 1.45 V were obtained, revealing that HMF oxidation occurs via HMFCa as an intermediate, which can then be converted to FFCA. Notably, after two hours of reaction, FDCA selectivity dramatically increased to 95%, with 100% HMF conversion. Simultaneously, the initial modest hydrogen production rate of 21 μmol.cm<sup>-2</sup> increased substantially to 150 μmol.cm<sup>-2</sup> when the reaction time was extended to two hours.<sup>[3,4]</sup> Additionally, the electrolysis system designed for the electrochemical oxidation of furfural demonstrated outstanding performance, achieving 98.2% furfural conversion to 2-furoic acid (2-FA) and hydrogen production of 84 μmol cm<sup>-2</sup> at an optimal voltage of 1.45 V as depicted in Figure 1d. This study presents a rational design of a highly efficient electrocatalyst for an electrochemical process that simultaneously converts biomass-derived compounds into chemicals and produces clean hydrogen.

**Table 1** the characteristics of CNTs grown over the various catalysts at 700 °C .<sup>[5]</sup>

Sample	CNTs yield (%) <sup>a</sup>	Outer Diameter (nm) <sup>b</sup>	Inner Diameter (nm) <sup>b</sup>	Number of walls <sup>b</sup>	I <sub>D</sub> /I <sub>G</sub> <sup>c</sup>
NiCONZSM-5-CNTs	10.4	26.2 ± 2.51	14.2±3.4	25-37	1.12
NiHieZSM-5-CNTs	21.8	13.0±5.2	9.4±3.4	10-22	0.62

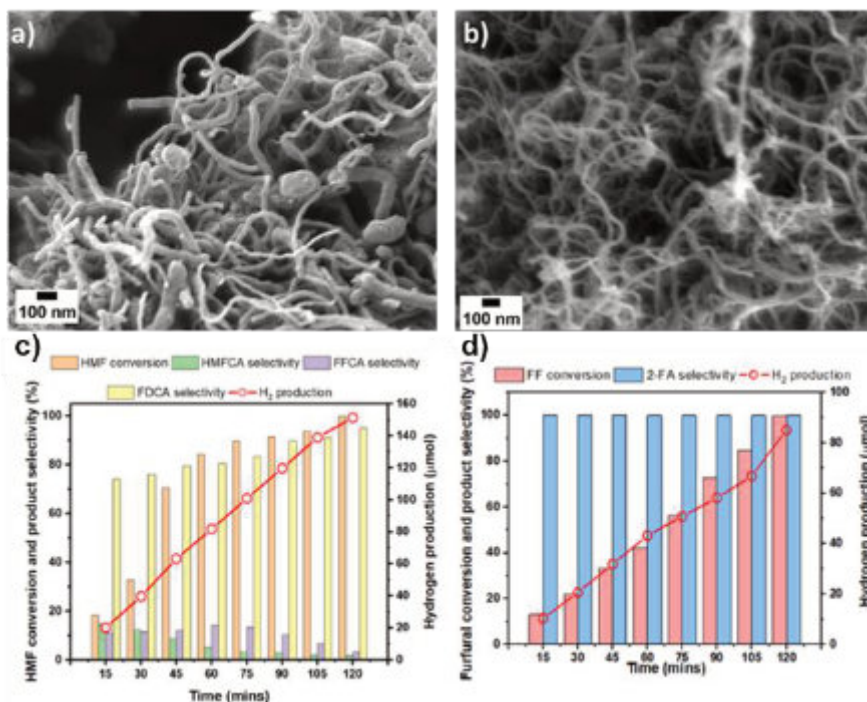


**Figure 1** SEM image of (a) NiCONZSM-5-CNTs, and (b) NiHieZSM-5-CNTs and kinetic study over NiCNTs/NF at 1.45 V for both anodic and cathodic compartments: (c) electrooxidation of HMF and (d) hydrogen evolution reaction (HER) in KOH as a supporting electrolyte.<sup>[5]</sup>

#### References

- [1] C. Rodaum, S. Klynyod, W. Nunthakitguson, P. Chaipornchalerm, N. Liwatthanakul, P. Iadrat and C. Wattanakit, *Chemical Communications*, **58**, 9618-9621 (2022).
- [2] A. Thivasasith, C. Rodaum, W. Nunthakitguson, S. Assavapanumat and C. Wattanakit, *Chemical Carbon Trends*, **7**, 100158 (2022)
- [3] Y. Xie, Z. Zhou, N. Yang, and G. Zhao., *Advanced Functional Materials*, **31**, 2102886 (2021).
- [4] W. Liu, J. L. Dang, Z. Xu, H. Q. Yu, S. Jin, and G. W. Huber, *ACS Catalysis*, **8**, 5533-5541 (2018).
- [5] W. Nunthakitguson, P. Chaipornchalerm, A. Sohail, A. Thivasasith, and C. Wattanakit (Manuscript in revision)

#### Acknowledgments

This project is funded by the National Research Council of Thailand and Vidyasirimedhi Institute of Science and Technology (N42A660307), the National Science and Technology Development Agency (NSTDA), the Thailand Science Research and Innovation (TSRI, grant FRB670026/0457), and the Program Management Unit for Human Resources & Institutional Development, Research and Innovation (grant number: B42G670029).



## Exploring the Interplay between Properties and Catalytic Performance of Partially Crystallized Zeolites

Nelcari-Trinidad Ramírez-Marquez<sup>1</sup>, Joaquín Martínez-Ortigosa<sup>1,2</sup>, Noemi Linares<sup>1</sup>, Javier García-Martínez<sup>1</sup>

<sup>1</sup>Laboratorio de Nanotecnología Molecular, Departamento de Química Inorgánica, Universidad de Alicante, Ctra. San Vicente-Alicante s/n, 03690, Alicante, Spain

<sup>2</sup>Instituto de Tecnología Química, Universitat Politècnica de València – Consejo Superior de Investigaciones Científicas (UPV-CSIC), Avda. de los Naranjos s/n, 46022 Valencia, Spain  
nelcarit.ramirez@ua.es

### Abstract

In this study, we explore the partial crystallisation of zeolites as a way to prepare superior catalysts for the conversion of bulky molecules. Specifically, we have collected both the solids and liquids of partially crystallised MFI and FAU zeolites. In the case of the liquid phase, we precipitated the species present in solution to obtain solids. These intermediates contain SBU and CBU of these two zeolites with different degrees of local order. We used UV-Raman spectroscopy, nitrogen adsorption and Friedel-Crafts alkylation of indole with *o*-xylene to study the interplay between the key properties of these materials and their catalytic performance. Our results show that materials obtained by precipitation of the soluble species present during the crystallisation of MFI and FAU exhibit superior catalytic performance than both the pristine zeolites and the solids obtained directly from the partial crystallisation of these zeolites. These findings open up new possibilities for the preparation of superior catalysts for the conversion of bulky molecules.

### Introduction

Recent work has shown that low crystallinity zeolitic materials featuring large surface areas, and strong acidity are able to efficiently convert bulky molecules. This has been attributed to enhanced accessibility to the active sites (Lewis and/or Bronsted), as large molecules can not enter the narrow microporosity of conventional zeolites [2]. The strong acidity is likely due to the presence of zeolite structural units, such as secondary building units (SBU) and composite building units (CBU), within an amorphous phase. [3] These materials lack long-range order beyond a few crystalline units but offer greater accessibility to the active sites. Herein, we present two different methods to prepare such catalytic materials: (i) by interrupting the zeolite synthesis process before complete crystallization, and (ii) by the precipitation of the zeolite fragments present in the liquid phase of this partial crystallization. We realised this approach for two different zeolite phases, namely, MFI and FAU structures.

### Materials and methods

MFI zeolite was synthesized using gels with a molar composition of 100 SiO<sub>2</sub>:2.5 Al<sub>2</sub>O<sub>3</sub>:4 NaOH:20 TPAOH:2500 H<sub>2</sub>O. Sodium hydroxide and sodium aluminate were first dissolved in deionized water (DI) and mixed for 15 min by mechanical stirring. The OSDA, TPAOH (1 M aqueous solution), was then added and the mixture was stirred for an additional hour. Finally, the silicon source, TEOS, was introduced into the solution. The FAU phase was synthesized using gels with a molar composition of 12 SiO<sub>2</sub>:1 Al<sub>2</sub>O<sub>3</sub>:5 NaOH:160 H<sub>2</sub>O. Sodium hydroxide and sodium aluminate were first dissolved in DI and mixed for 2 h by mechanical stirring. The silica source, LUDOX AS-40 (Sigma Aldrich), was then added to the solution. MFI gels were aged for 3 h and FAU gels for 24 h with orbital rotation at 90 rpm.

The gels for the MFI phase were subsequently transferred into Teflon-lined reactors with a stainless-steel jacket and heated in an oven at 125 °C for different times (1, 2, 3, 6, and 48 h). For the FAU phase, the gels were heated at 100 °C for 4, 18, 27, 48, and 96 h. After each specified heating period, the liquid phase was separated from the solid phase; the solution was precipitated into solids using a solution of 0.33 M CTAB and 2.00 M NH<sub>4</sub>Cl. All the samples were calcined at 550 °C for 5 h.

### Results and discussion

In the presented work, zeolitic materials based on zeolite structural subunits (SBU/CBU) of the MFI and FAU phases within an amorphous matrix were prepared using two methods: (i) interruption of the zeolite synthesis process and (ii) precipitation of the post-synthesis solutions. Furthermore, two different approaches were used for the precipitation; first, by treating the liquid phase of the partial crystallization with cetyltrimethylammonium bromide (CTAB), and, the second, by using a combination of CTAB with ammonium chloride (NH<sub>4</sub>Cl). The latter producing higher yield to solids.

The isotherms of all materials are shown in Figure 1. While the partially crystallized samples do not show any significant adsorption, the precipitated solids display type IV isotherms, characteristic of mesoporous materials, confirming that these materials possess significant mesoporosity. This supports the hypothesis of an amorphous matrix embedding SBUs/CBUs, features a large surface area and pore volume typical of mesoporous materials. This mesoporosity enhances the material's ability to convert or absorb bulky molecules.

The presence of SBUs/CBUs was confirmed by Raman spectroscopy (Figure 1). Amorphous materials typically show broad, less-defined Raman bands, whereas crystalline materials exhibit sharp, distinct peaks. [2,4] In the precipitated solids, in



addition to the SBUs/CBUs, there is likely to be material that lacks this local order, which does not have a long-range ordered structure but still contains the essential building blocks of the zeolite framework. This amorphous matrix can serve as a reservoir of precursor materials that can crystallise into the zeolite structure under appropriate conditions.

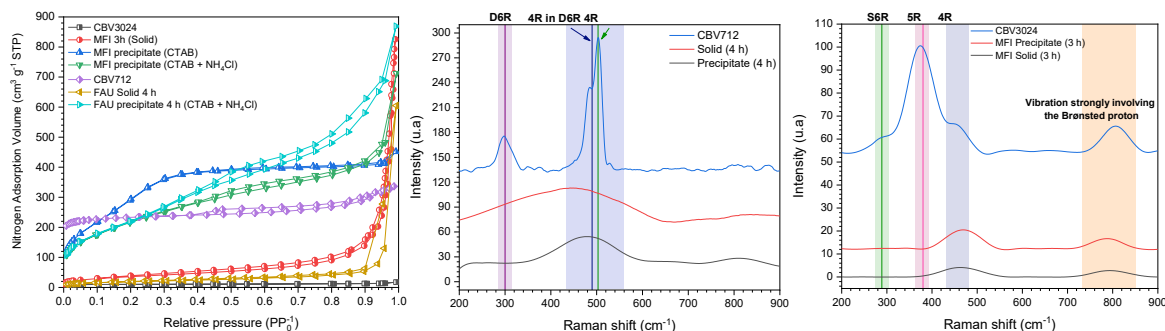


**Figure 1.** (left) Isotherms of nitrogen adsorption at 77 K over the partial crystalline solids and the precipitates from MFI and FAU gels. UV-Raman spectra of the partial crystalline solids and the precipitates of (center) MFI and (right) FAU.

Figure 2 shows that the mesoporous zeolitic materials present improved catalytic activity when compared with fully crystalline commercial zeolites (FAU - CBV712 and MFI - CBV3024E\*). In all cases, Friedel-Crafts alkylation catalytic activity tests were carried out with two different test molecules, *o*-xylene and indole. [5] It is worth noting that, the mesoporous materials precipitated from the post-synthesis solutions show better catalytic activity than the solids obtained by partial crystallisation.

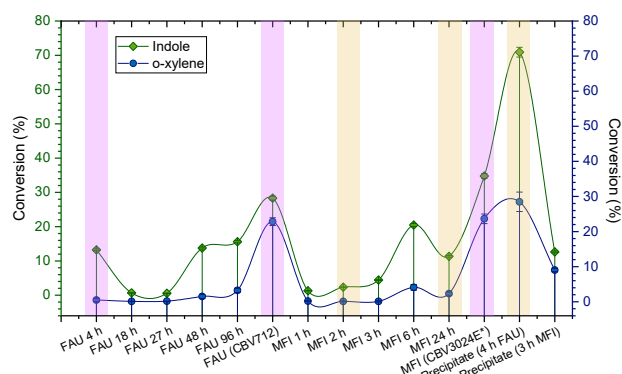
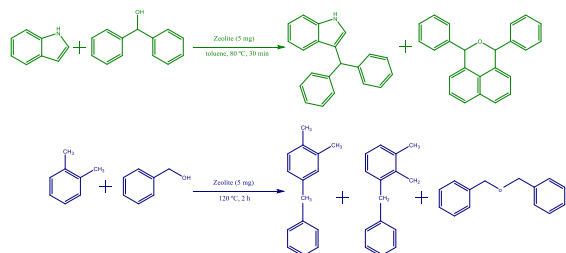


**Figure 2.** Conversion for Friedel-Crafts alkylation reaction of MFI and FAU materials with two test molecules (*o*-xylene and indole).

These results show that the combination of zeolitic local order, strong acidity and mesoporosity - enables for the conversion of bulky molecules.

## Conclusions

In this study we show partial zeolite crystallization can be used to prepare superior catalysts for the conversion of bulky molecules. These materials are comprised of zeolitic SBU and CBU, and offer improved accessibility to active sites. The two synthesis methods explored—1) collecting the solids of the zeolite partial interconversion and 2) precipitation of the soluble species present in that partial crystallization. The latter method yields materials with large mesoporosity, and superior catalytic performance as compared to those produced by partial crystallization. These results underscore the importance of controlling crystallization pathways to optimize zeolite properties for catalytic applications.

## References

- [1] Adam J. Mallette, Kumari Shilpa, and Jeffrey D. Rimer, *Chem. Rev.* 2024, 124, 6, 3416–3493.
- [2] M. J. Mendoza-Castro, E. De Oliveira-Jardim, N-T. Ramírez-Marquez, C-A. Trujillo, N. Linares, J. García-Martínez, *J. Am. Chem. Soc.*, 2022, 144, 5163 - 5171.
- [3] M. J. Mendoza-Castro, Z. Qie, X. Fan, N. Linares, J. García-Martínez, *Nature Commun.*, **14**, 1256 (2023).
- [4] Prantika Bhattacharjee and Utpal Bora., *ACS Omega* 2019, 4, 11770–11776T.
- [5] N. Linares, F. G. Cirujano, D. E. De Vos, J. García-Martínez. *Chem. Commun.*, 2019, 55, 12869.

## Acknowledgments

This study forms part of the Advanced Materials programme and was supported by MCIN with funding from European Union NextGenerationEU (PRTR-C17.11) and by Generalitat Valenciana. J.M-O acknowledges the financial support from the European Union – NextGeneration EU through the Universitat Politècnica de València, Ministerio de Universidades, Plan de Recuperación, Transformación y Resiliencia for the Margarita Salas grant.



## Stabilization Of Carbon Dots By Embedding Them In Zeolites

**D. Fernández-Ortiz<sup>1</sup>, M. Rosell<sup>2</sup>, C. Martín<sup>2</sup>, E. Serrano<sup>1</sup>, N. Linares<sup>1</sup>, J. García-Martínez<sup>1</sup>**

<sup>1</sup> Inorganic Chemistry Department. University of Alicante. Ctra. San Vicente del Raspeig, s/n, 03690 San Vicente del Raspeig  
[david.fernandez@ua.es](mailto:david.fernandez@ua.es)

<sup>2</sup> Physical Chemistry Department. University of Castilla-la Mancha. Avda. Dr. José María Sánchez Ibáñez, s/n, 02071 Albacete

Carbon dots (Cdots) have emerged as a novel class of fluorescence material with excellent optical and electronical properties making them suitable for a myriad of different applications [1]. However, when used in suspension they can easily undergo to aggregated-induced luminescence quenching, which limits the luminous efficiency and the photocatalytic activity. So, one of the solutions to enhance their stability during application is their stabilization in porous materials [2]. When embedded into the pores and channels of zeolites, these particles can display a tuneable fluorescence and phosphorescence emission, presumably due to the confinement effect of the pores of the zeolite [3], thus making the composites Zeolite@Cdots very promising materials in photochemistry and photophysics.

On the other hand, amino acids are very interesting raw materials to synthesize Cdots because they are small molecules that act both as carbon and nitrogen source [4]. Arginine is one of the positively charged (or basic) Aas at pH = 7 and has been reported as a nitrogen dopant agent in a typical hydrothermal synthesis of citric acid based Cdots [5]. However, the incorporation of these molecules into zeolites aiming to obtain Cdots@zeolite composites has not been explored yet.

In this study, Cdots@Zeolite composites have been synthesized using commercial faujasite (CBV720) and arginine as carbon and nitrogen source by two different approaches: partial carbonization of the arginine in the pores of the zeolite and in situ generation of Cdots in the acidic sites by hydrothermal treatment, as depicts Fig. 1.

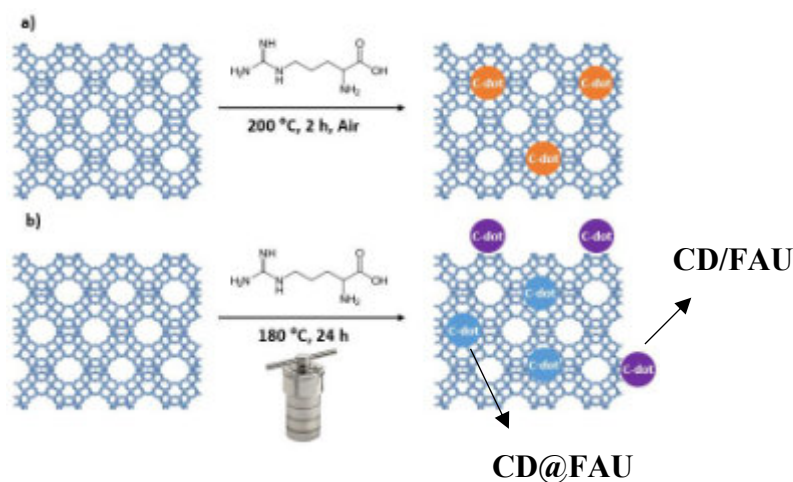


**Figure 1.** – Scheme of synthetic approach for a) arginine-based carbon dots by partial carbonization in the pores of faujasite and b) arginine-based carbon dots by in situ generation in the acidic sites of the zeolite by hydrothermal treatment.

The resulting composite materials have been characterized by UV-Vis spectroscopy, TEM, TGA, among other techniques, and its photoluminescent behaviour has been studied by absorption, emission and excitation fluorescence spectroscopy. For comparison purposes, we have synthesized and characterized arginine-based Cdots suspensions by a hydrothermal method to elucidate its photoluminescent behaviour prior to embedding the Cdots into the faujasite zeolite. Then, we have studied the composite materials prepared by two synthetic methodologies aforementioned.

The optical properties of the Cdots were investigated by UV-Visible absorption and fluorescence emission spectroscopies (Fig. 2a,b). The UV-Visible spectrum (Fig. 2a, red) shows a main band at ~280 nm and a low intense one at ~320 nm. The first transition is related to the  $\pi-\pi^*$  (e. g., C=C) occurring in the Cdots core network, while the second one can be assigned to the  $n-\pi^*$  transitions from the core  $sp^2$  to the surface functional groups. Regarding the fluorescence emission, a band centred at ~420 nm is observed (Fig. 2b, red), which can be related to the emission originated from the conjugated  $\pi$ -domains in the carbonaceous core (~440 nm). The hybrid materials present different optical properties depending on the synthetic approach. While no fluorescence peak was found in the materials prepared by carbonization, two differentiated emission peaks (at 425 nm and 480 nm) were observed for the Cdots generated by the in situ approach, which can be attributed to the generation of two populations of Cdots by this method. First, some Cdots with a similar behaviour than the suspensions, which can be explained by a lower interaction with the faujasite structure. This surface Cdots (CD/FAU) present a similar purple fluorescence emission





than the solution (Fig. 2b). A stronger stabilization of the Cdots, which can be generated in the internal pores of the faujasite (CD@FAU), gives rise to more stable particles, producing a red-shift in their emission, probably due this increment in the zeolite-Cdot interaction. In addition, a shift to longer fluorescence lifetimes can be observed for the Cdots synthesized by the hydrothermal method (Fig. 2c). These results confirm the hypothesis about the stabilizing effect of the zeolitic matrix.

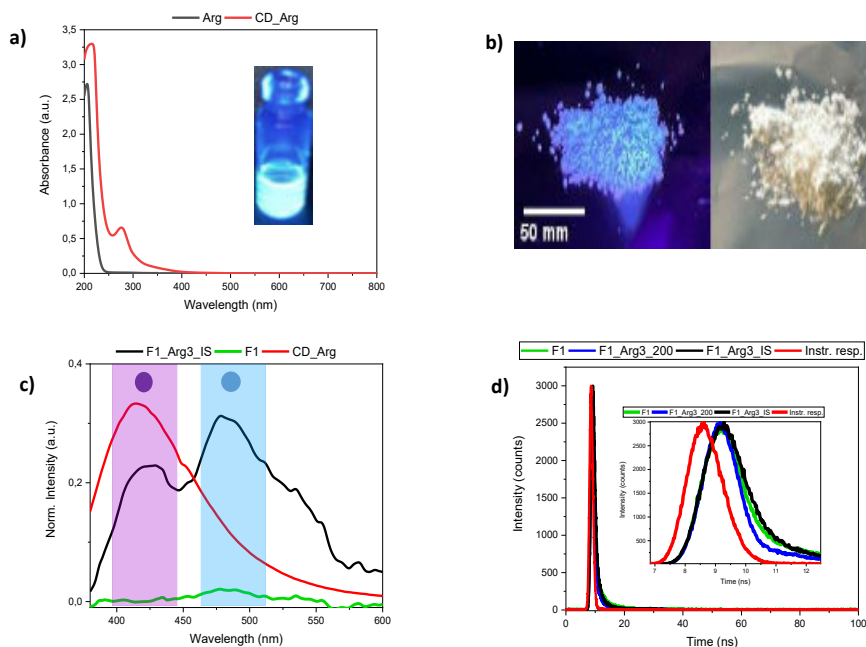


**Figure 2.** – a) UV-Vis absorption spectra of arginine and arginine-derived Cdots synthesized by hydrothermal method at 180 °C for 24 hours. The image embedded depicts the fluorescence of the Cdots suspension when irradiated at 365 nm. b) Cdots embedded into faujasite by in situ approach when irradiated at 365 nm (left) and with no specific wavelength irradiation (right). c) Emission spectra of Cdots prepared from arginine by hydrothermal method at 180 °C for 24 hours (red), CBV720 (green) and Cdots generated by in situ approach in faujasite (black) with a 330 nm excitation wavelength. d) Fluorescence lifetimes recorded with a 368 nm laser of Cdots suspension from arginine prepared by hydrothermal method (red), CBV720 (green) and Cdots generated by in situ approach in faujasite (black) and Cdots synthesized by carbonization in the pores of the faujasite (blue). The red spectrum depicts the response time of the instrument (no sample experiment).

In conclusion, the preparation of arginine-derived Cdots embedded in FAU by hydrothermal treatment greatly stabilizes the Cdots most likely due to the confinement effect of the pores and the high interaction between the zeolitic matrix and the Cdots, resulting in a red-shift of their fluorescence emission and extended lifetimes, making these composites very interesting materials for its use in optoelectronic devices. More studies are needed to evaluate the distribution and location of the different populations of Cdots.

## References

- [1] V. Torregrosa-Rivero, M. Rosell, D. Herrera-Ochoa, A. Garzón-Ruiz, J. García-Martínez, E. Serrano and C. Martín, *ChemPhotoChem*, e202400133 (2024)
- [2] M. Liu, Z. Wang, J. Gong, X. Meng, Z. Yan, D. Guo, X. Feng, T. Zhang, X. Li and P. Li, *Ceram. Int.*, **50**, 9125 (2024).
- [3] S. Zhong, B. Wang, X. Yin, W. Ma, J. Zhang and J. Li, *Nano Res.*, **15**, 9454 (2022).
- [4] X. Chen, M. Yu, P. Li, C. Xu, S. Zhang, Y. Wang and X. Xing, *ACS Biomater. Sci. Eng.*, **9**, 5548 (2023).
- [5] K.G. Nguyen, M. Huš, I-A. Baragau, J. Bowen, T. Heil, A. Nicolaev, L.E. Abramiuc, A. Sapelkin, M.T. Sajjad and S. Kellici, *Small*, **20**, 2310587 (2024)

## Acknowledgments

The authors thank the MICIN/AEI projects refs. PID2021-128761OB-- C21 and PID2021-128761OA-C22 funded by MCIN/AEI/10.13039/501100011033 and FEDER, UE, by FEDER/ UE. The authors also thank CNS2022-136052 funded by MCIN/AEI/10.13039/501100011033 by "European Union NextGenerationEU/PRTR. This project has also received funding from the Generalitat Valenciana under project ref. AICO/2021/132. This research was also supported by SBPLY/21/180501/000127, funded by JCCM and the EU through "Fondo Europeo de Desarrollo Regional" (FEDER).



## Designing the novel Zn-URJC-11 material for hydrogen adsorption applications

G. Orcajo<sup>1</sup>, P. Leo<sup>1</sup>, J. Tapiador<sup>1</sup>, E. García-Rojas<sup>1</sup>, I. Aguayo<sup>1</sup>, F. Gándara<sup>2</sup>, C. Martos<sup>1</sup>

<sup>1</sup> Chemical and Environmental Engineering Group. ESCET, Rey Juan Carlos University, C/Tulipán s/n 28933 Móstoles, Spain.

<sup>2</sup> Department of New Architectures in Materials Chemistry, ICMM-CSIC, Sor Juana Inés de la Cruz 3, Cantoblanco, Madrid, Spain.  
gisela.orcajo@urjc.es

The production, handling, and storage of energy have become priorities in the contemporary world. Currently, oil, coal, and natural gas account for more than 70% of energy consumption, according to the International Energy Agency [1]. The considerable environmental impact generated by the use of fossil fuels, as well as the continuous increase in their prices and the dependence on oil-producing countries, necessitate the development of new global, clean, and sustainable energy sources. The potential of hydrogen as a fuel source for the future is becoming increasingly acknowledged by the scientific and expert community. It has a higher energy density than fossil fuels and does not produce any direct greenhouse gas emissions. The objective of a hydrogen-based economy by 2050, with a focus on the production of hydrogen using sustainable energy sources [2], is consistent with the growing interest in hydrogen. However, effective storage options in transportation sector are currently impeding the growth of the hydrogen industry. Porous solid adsorbents show promise in this regard. The US Department of Energy has set ambitious targets for the storage of hydrogen by 2025 and favors materials with high volumetric and gravimetric capabilities[3].

In the context of environmental concerns, metal-organic frameworks (MOFs) have been identified as a promising candidate for the development of next-generation hydrogen storage systems [4]. This phenomenon can be attributed to the unique potential of these materials to integrate diverse components and functionalities. Furthermore, the inherent complexity and heterogeneity of these materials often manifest in unexpected qualities that transcend the mere sum of their constituent parts (organic and metallic) [5].

The objective of this research is to develop a new zinc-based metal-organic framework (MOF) material to effectively adsorb the hydrogen at moderate pressure. In particular, this new crystalline material is constituted by zinc(II) and 5,5'-(1H-1,2,3-triazol-1,4-diyl)diisophthalic acid ( $H_4L_1$ ) as a ligand. While this ligand is not currently available on the commercial market, it exhibits a great potential, since it has a tetratopic nature that allows the formation of highly stable structures, it contains a triazole group that enhances the electronic density within the MOF cavities, thereby increasing the  $H_2$  adsorption capacity.

Following an investigation of the synthesis variables, the new material Zn-URJC-11 was attained, for which the crystal structure was elucidated by single-crystal X-ray diffraction (Figure 1), showing an accessible volume of 38%. This novel MOF structure crystallizes in the single-crystal space group  $P2_1/c$  and the unit cell was found to be 18.098, 20.307, and 20.137 Å along the crystallographic axes  $a$ ,  $b$ , and  $c$ , respectively. Additionally, the angles  $\alpha$ ,  $\beta$ , and  $\gamma$  were determined to be 90°, 90°, and 111.355°, respectively.

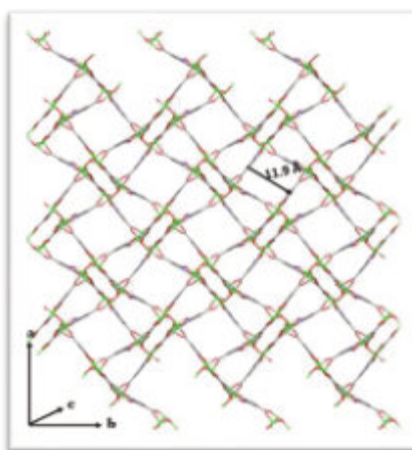


Figure 1. 3D structure of the new material Zn-URJC-11.

The new MOF structure has been subjected to a complete physico-chemical characterization (not shown), which revealed a thermal stability up to 300 °C, as indicated by the thermogravimetric analysis. Additionally, it exhibited intriguing textural properties, including a specific surface area of 707 m<sup>2</sup>/g and a pore volume of 0.47 cm<sup>3</sup>/g. The Ar adsorption isotherm at 87K of this material is of the type I and IV variety, corresponding to a micropores (8.5 Å) and



mesoporous structures (42 Å), rendering it a highly promising material for adsorption applications since this hierarchical structure.

The material was test in hydrogen adsorption analysis at various pressure and temperature conditions. Figure 2 illustrates the hydrogen adsorption isotherms in a gravimetric and volumetric basis at room temperature (298 K). The storage capacity achieved at room temperature and high pressure (170 bar) is considerable, reaching a gravimetric adsorption value of approximately 1% by mass. This value is higher than those achieved by other MOFs with higher specific surface areas, such as MOF-5 ( $V_p = 1.18 \text{ cm}^3 \cdot \text{g}^{-1}$ ;  $S_{\text{BET}} = 2296 \text{ m}^2 \cdot \text{g}^{-1}$ ) and PCN-5 ( $V_p = 1.18 \text{ cm}^3 \cdot \text{g}^{-1}$ ;  $S_{\text{BET}} = 2095 \text{ m}^2 \cdot \text{g}^{-1}$ ), which exhibits gravimetric hydrogen adsorption capacities of 0.25 and 0.19 mass percent, respectively [6]. The interaction strength between the MOF structure and hydrogen molecules was estimated by the adsorption enthalpy, which was  $-11.9 \text{ KJ} \cdot \text{mol}^{-1}$  at low coverage, indicating a high value that could be attributed to the presence of preferential hydrogen adsorption sites related to exposed metal sites.

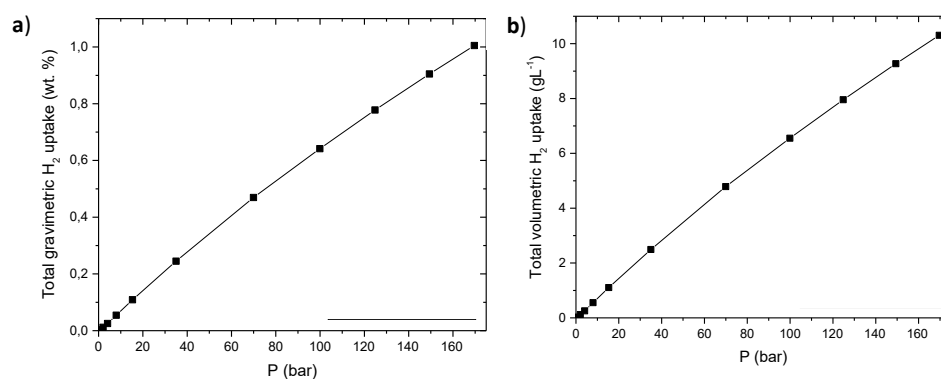


**Figure 2.** Isotherms of hydrogen adsorption on gravimetric basis (a) and storage volume density (b) at 298 K of the Zn-URJC-11 material.

## References

- [1] International Energy Agency, *World Energy Outlook 2023*, Enhanced Reader, (2023).
- [2] B.C. Tashie-Lewis and S.G. Nnabuike, *Chemical Engineering Journal Advances*, **8**, 100172 (2021).
- [3] C. Grady, S. McWhorter, M. Sulic, S.J. Sprik, M.J. Thornton, K.P. Brooks and D.A. Tamburello, *Int J Hydrogen Energy*, **47**, 29847 (2022).
- [4] Z.A. Sandhu, M.A. Raza, N.S. Awwad, H.A. Ibrahim, U. Farwa, S. Ashraf, A. Dildar, E. Fatima, S. Ashraf and F. Ali, *Mater Adv*, **5**, 30 (2024).
- [5] M. Viciano-Chumillas, X. Liu, A. Leyva-Pérez, D. Armentano, J. Ferrando-Soria and E. Pardo, *Coord Chem Rev*, **451**, 214273 (2022).
- [6] T.K.P. Myunghyun Paik Suh and Hye Jeong Park, *Chem Rev*, **112**, 782 (2012).

## Acknowledgments

The authors gratefully acknowledge the financial support of Spanish Ministry of Science and Innovation to the ECOCAT Project (PID2022-136321OA-C22).



## Depillaring, an effective way to prepare 2D zeolites: Synthesis, characterization, and catalytic evaluation

**A.J. Romero-Anaya<sup>1</sup>, J. Martínez-Ortigosa<sup>1,2</sup>, N. Linares-Pérez<sup>1</sup>, J. García-Martínez<sup>1</sup>.**

<sup>1</sup>Laboratorio de Nanotecnología Molecular, Departamento de Química Inorgánica, Universidad de Alicante, Ctra. San Vicente-Alicante s/n, 03690, Alicante, Spain

<sup>2</sup>Instituto de Tecnología Química, Universitat Politècnica de València – Consejo Superior de Investigaciones Científicas (UPV-CSIC), Avda. de los Naranjos s/n, 46022 Valencia, Spain.

[ajromero@ua.es](mailto:ajromero@ua.es)

**Abstract:** In this work, we introduce an innovative method for preparing 2D zeolitic nanomaterials from self-pillared structures through a depillaring process. This simple technique allows for addressing some of the main challenges and costs associated with traditional methods for the production of 2D zeolites. More specifically, unlike the use of complex di-cationic organic structure-directing agents (OSDAs) for 2D structure preparation, our approach utilizes OSDA-free MFI-type self-pillared structures, followed by depillaring. Specifically, this is done using ammonium fluoride and ammonium bifluoride to selectively dissolve the intersection points of nanosheets in the self-pillared structures to yield 2D nanozeoles. These materials were tested for Friedel-Crafts (benzylation of o-xylene with Benzyl Alcohol (BA)) and the Methanol To Olefins (MTO) reactions, where our 2D zeolitic materials demonstrated higher conversions than both the parent self-pillared zeolite and a commercial zeolite, proving the enhanced diffusion properties of these 2D zeolites and the effectiveness of our method.

**Motivation:** The synthesis of 2D materials can be achieved through various physical and chemical methods, such as mechanical exfoliation and/or ultrasonic-assisted liquid phase exfoliation [1], ion intercalation and hydrothermal synthesis [2], or Chemical Vapor Deposition (CVD) [3], with properties varying significantly based on the preparation conditions. Our study aims to understand the formation of 2D zeolitic materials by depillaring self-pillared structures [4,5] using ammonium fluoride and ammonium bifluoride solutions [6], which will presumably attack the joints between the sheets as they have more defects and therefore are more reactive than the sheets themselves [6]. We have investigated and optimized the use of various fluoride species to selectively dissolve the intersection points of the self-pillared structures to obtain 2D materials. These have been thoroughly characterized and tested in two chemical transformation involving bulky molecules to investigate the improved diffusional properties of our 2D zeolites prepared by depillaring.

**Preparation of 2D zeolites by depillaring of self-pillared MFI:** As previously reported [5] the self-pillared zeolites (SPP) were prepared by seed induced growth. Briefly, about 10 % by mass of zeolite seeds is suspended in a solution of sodium aluminate dissolved in sodium hydroxide to which a source of silicon (LUDOX AS-40) is added ( $18\text{SiO}_2:3.42\text{Na}_2\text{O}:\text{Al}_2\text{O}_3:324\text{H}_2\text{O}$ ), and after 24 hours of aging, this mixture is subjected to hydrothermal treatment at 150 °C for 72 h. The washed and dried (110 °C) samples are then calcined (550 °C) to get the self-pillared structure. To obtain the 2D nanomaterials, they were treated for 60 min with a 40 wt.%  $\text{NH}_4\text{F}$  solution (SPP- $\text{NH}_4\text{F}$ ) or  $\text{NH}_4\text{HF}_2$  solution (SPP- $\text{NH}_4\text{HF}_2$ ) with lower concentration due to the high presence of fluoride anions. All the samples have been characterized by x-ray diffraction (DRX), microscopy (SEM and TEM) and Selected Area Electron Diffraction (SAED), Pair Distribution Function (PDF), and Nuclear Magnetic Resonance ( $^{27}\text{Al}$ -NMR). In the Friedel-Crafts alkylation of BA the catalyst was mixed with 455  $\mu\text{l}$  of o-xylene and 30  $\mu\text{l}$  of benzyl-alcohol and stirred (400 rpm) at 120 °C for 120 min. In the MTO reaction, the catalyst preheated to 550 °C is established with the reaction temperature at 350 °C and the methanol was introduced into a fixed-bed U-shaped quartz reactor by bubbling 30 mL/min of nitrogen through a saturator set at 30 °C. The reactor effluent was analyzed using an online gas chromatograph.

**Evidences of the formation of 2D zeolites with preserved crystalline structure:** The XRD patterns of the depillared samples, SPP- $\text{NH}_4\text{F}$  y SPP- $\text{NH}_4\text{FH}_2$  (see Figure 1a) retain all the peaks characteristic of the MFI structure confirming the preservation of this crystalline topology in the 2D nanosheets. The spectra  $^{27}\text{Al}$ -NMR show (Figure 1b) a very intense resonance band at 54 ppm corresponding to tetra-coordinated aluminum (Al(IV)) in the framework of the materials and two weak resonance bands at 0 ppm and 30 ppm due to the hexa- and pentacoordinated aluminum (Al(VI) and Al(V)) in the extra-framework of the SPP sample. The treatment with fluoride ions reduce the amount of Al(VI) and Al(V) in the samples, probably due to the removal of amorphous phases. The PDF analysis carried out using synchrotron radiation (Figure 1c) has shown that the peaks corresponding to the closest distances Si-O (1.62 Å), O-O (2.63 Å) and Si-Si (3.12 Å) remain essentially unchanged and are characteristic of siliceous zeolites. This confirms the presence of the basic (Si,Al) $_4$  tetrahedral building blocks in the SPP structures and the nanomaterials after the treatment with fluorides. In addition, TEM images in Figure 1d show the self-pillared structures obtained, resembling a house of cards, and the evolution over time with the fluorides treatment until 2D nanomaterials are obtained (Figure 1e). Similarly, The SAED image of the SPP- $\text{NH}_4\text{HF}_2$  sample demonstrates a well-ordered crystalline structure, characterized by sharp and well-defined diffraction spots characteristics of the MFI structures. These results show that under our conditions, fluoride solutions dissolve the interconnections of self-pillared structures, allowing for the proper separation of 2D materials. This process enables the isolation of 2D zeolites, which are initially interconnected in a house-of-cards-like arrangement.

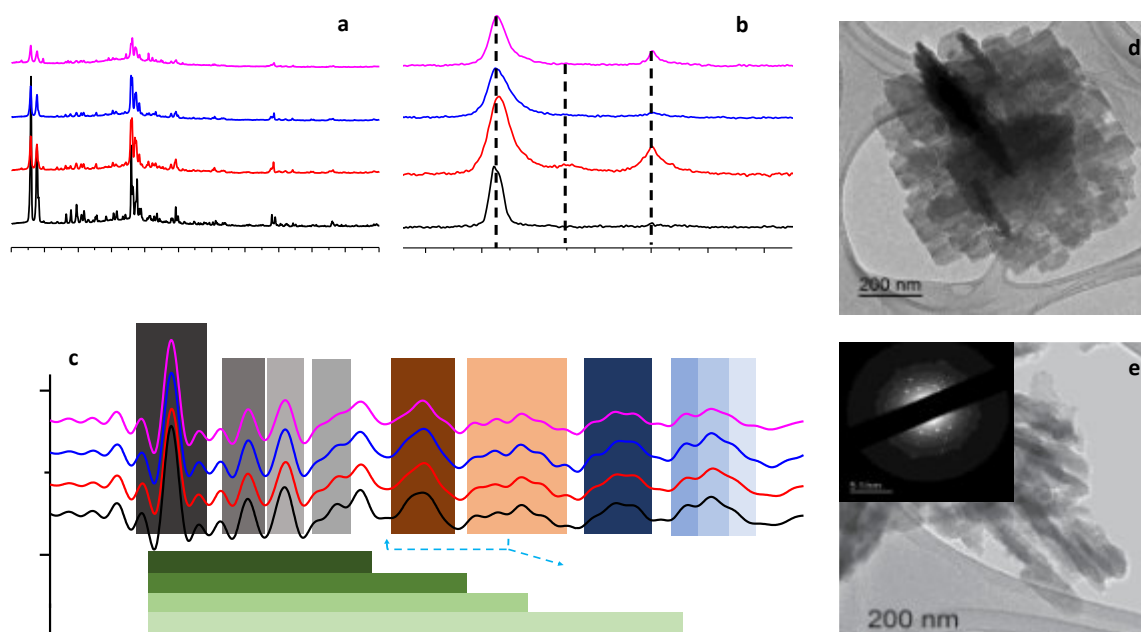


**Figure 1.** (a) XRD, (b)  $^{27}\text{NMR}$ , (c) PDFs of the samples SPP, SPP-NH<sub>4</sub>F, SPP-NH<sub>4</sub>HF<sub>2</sub> and the commercial zeolite CBV8014, and TEM images of the (d) SPP, (e) SPP-NH<sub>4</sub>HF<sub>2</sub>. The inset in figure 1e shows the SAED images.

**Superior catalytic performance: Increased conversion for the production of bulky molecules:** The activity of the 2D nanomaterials was tested in the conversion of some model molecules in well-known reactions, such as the Friedel-Crafts reaction. SPP-NH<sub>4</sub>HF<sub>2</sub> and SPP-NH<sub>4</sub>F samples achieve higher conversion values for both reactions than the precursor (the SPP sample). These findings indicate that SPP-NH<sub>4</sub>HF<sub>2</sub> and SPP-NH<sub>4</sub>F are superior catalysts for the treatment of bulky molecules compared to the original self-pillared structures. The enhanced performance of the fluoride treated samples can be related to the improving of the diffusion of bulky molecules in MFI by producing 2D nanosheets of this zeolites by depillaring of the precursor SSP, offering a promising alternative to existing commercial catalysts.

In addition, the samples have also been tested in the MTO reaction, a well-established and extensively studied reaction, to investigate the improved diffusional properties of our 2D zeolites. In preliminary studies, the obtained conversion in the MTO reaction using our catalysts are shown in Figure 2. After four hours of reaction, the conversion rates obtained for the SPP-NH<sub>4</sub>HF<sub>2</sub> and SPP-NH<sub>4</sub>F samples are higher compared to the precursor SPP. These results highlight the potential of our 2D materials in both the Friedel-Crafts and MTO reactions.

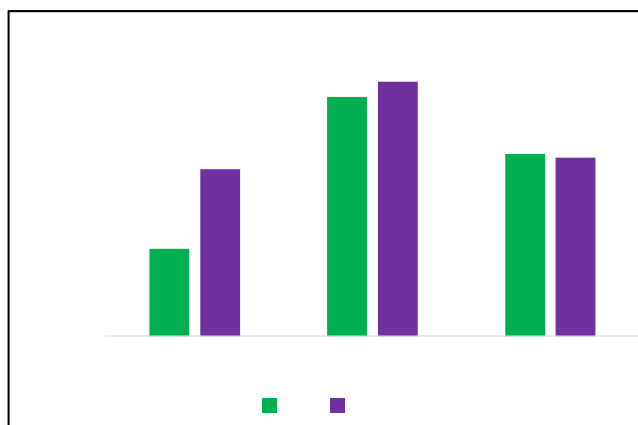


**Figure 2.** Conversion obtained in Benzylation of o-xylene with benzyl alcohol and MTO reaction

#### References:

- [1] Y. Liu, R. Li. *Ultrason. Sonochem.* **63**,104923 (2020)
- [2] J. Přečh, P. Pizarro, D. P. Serrano, J. Čejka. *Chem. Soc. Rev.* **47**, 8263-8306 (2018)
- [3] Z. Cai, B. Liu, X. Zou, H.M. Cheng. *Chem. Rev.* **118**, 13, 6091–6133 (2018)
- [4] Y. Ma, X. Tang, J. Hu, Y. Ma, W. Chen, Z. Liu, S. Han, C. Xu, Q. Wu, A. Zheng, L. Zhu, X. J. *Am. Chem. Soc.* **144**, 6270–6277 (2022)
- [5] R. Jain, A. Chawla, N. Linares, J. García Martínez, J.D. Rimer. *Adv. Mater.* **33**, 22, 2100897 (2021)
- [6] V. Babić, L. Tang, Z. Qin, L. Hafiz, J.P. Gilson, V. Valtchev. *Adv. Mater. Interfaces*, **8**, 2000348 (2020)

#### Acknowledgments

This study forms part of the Advanced Materials programme and was supported by MCIN with funding from European Union NextGenerationEU (PRTR-C17.I1) and by Generalitat Valenciana. J. Martínez-Ortigosa acknowledges the financial support from the European Union – NextGeneration EU through the Universitat Politècnica de València, Ministerio de Universidades, Plan de Recuperación, Transformación y Resiliencia for the Margarita Salas grant.



## Cu-zeolite catalysts for CO<sub>2</sub> conversion and alcohol synthesis

D. Iltsiou<sup>1</sup>, J. Mielby<sup>1</sup>, S. Kegnæs<sup>1</sup>

<sup>1</sup> Department of Chemistry - Technical University of Denmark Kemitorvet Building 207, 2800 Kgs. Lyngby, Denmark  
dimilt@kemi.dtu.dk

The carbon circular economy provides solutions to address the high levels of CO<sub>2</sub> in the atmosphere by researching ways to store, use, and remove it. As an inexpensive, abundant, non-toxic, renewable carbon source, the use of CO<sub>2</sub> has received great interest in many areas. Lately, the focus of researchers is the production of fuels and high-value-added chemicals such as alcohol products, throughout the hydrogenation of CO<sub>2</sub>. Among alcohol products, ethanol attracts great attention due to its notable energy density and current engine knowledge. However, the conversion of CO<sub>2</sub> to ethanol has been difficult due to the presence on the catalyst of various functional groups and the high energy barrier of the C-C coupling [1]. Therefore, the development of novel, stable, heterogeneous nanoparticle catalysts for the selective production of ethanol directly from CO<sub>2</sub> is of great importance.

Zeolites are the most widely used industrial heterogeneous catalysts. They are classified as aluminosilicate materials with intracrystalline pores and cavities of molecular dimensions. The catalytically active sites in zeolite micropores can be acid sites that result from the charge compensation of the framework with protons, which is necessary when, e.g., Al<sup>3+</sup> substitutes Si<sup>4+</sup> in the framework. Alternatively, it can also be redox active sites resulting when the charge compensation is done with redox-active ions such as Cu(II) rather than with protons [2]. Here, we report the synthesis and encapsulation of the Gmelinite (GME) zeolite framework with Cu nanoparticles, achieved through the interzeolite transformation of Cu-FAU (Figure 1). The Cu-based GME catalysts were used in flow reactor experiments at 100-350 °C and various CO<sub>2</sub>/H<sub>2</sub> ratios and pressures in order to optimize the selectivity to ethanol. We have shown that the structure of the GME framework has a great influence on the catalytic activity. All the obtained catalysts were characterized using IR, XRD, BET, TEM, SEM, UV-VIS and XAS [3]. Moreover, Figure 1 illustrates the experimental setup used for the CO<sub>2</sub> hydrogenation.

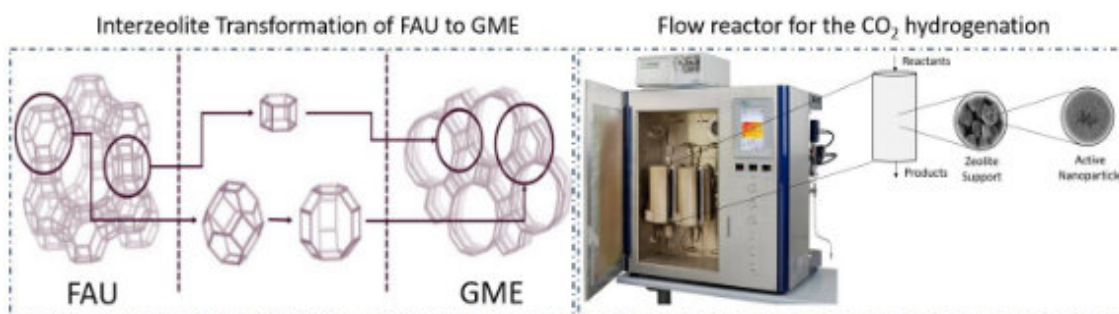


Figure 1. Overview of themes discussed in this abstract.

### References

- [1] D. Xu, Y. Wang, M. Ding, X. Hong, G. Liu, S. C. E. Tsang, *Chem*, **7**(4), 849-881 (2021).
- [2] K. H. Rasmussen, F. Goodarzi, D. B. Christensen, J. Mielby, S. Kegnæs, *Acs Applied Nano Materials*, **2**(12), 8083-8091 (2019).
- [3] D. Iltsiou, T. Nielsen, J. Mielby, S. Kegnæs, (2024), submitted.



## Study of Water and Ethanol Sorption in ZIFs for Heat Transformation Applications

C. Byrne<sup>1,2</sup>, K. Vodlan<sup>3</sup>, A. Golobič<sup>3</sup>, C. Hewson<sup>4</sup>, P. Iacomi<sup>4</sup>, N. Zabukovec Logar<sup>1,2</sup>

<sup>1</sup> National Institute of Chemistry, 1000 Ljubljana, Slovenia

<sup>2</sup> University of Nova Gorica, 5000 Nova Gorica, Slovenia

<sup>3</sup> University of Ljubljana, 1000 Ljubljana, Slovenia

<sup>4</sup> Surface Measurement Systems, London, HA0 4PE, United Kingdom

ciara.byrne@ki.si

The growing demand for heating and cooling energy is increasingly significant due to the continuously rising population. As heating and cooling energy accounts for up to 50% of global final energy consumption, there is a heightened interest in eco-friendly methods to optimize heat supply and demand. One promising solution is thermal energy storage (TES), which leverages reversible chemical reactions and/or sorption processes involving gases in solids or liquids. This method has the major benefit of minimal heat loss while achieving a significantly higher energy storage density. Sorption-based thermal energy storage can be explored using traditional adsorbents like zeolites or innovative ones like metal-organic frameworks (MOFs). [1-3] One subgroup of MOFs are Zeolitic imidazolate frameworks (ZIFs), which consists of transition metal ions (such as Zn and Co) and imidazolate linkers. ZIFs have a structure similar to zeolites, with metal ions replacing silicon/aluminum and imidazolate linkers replacing oxygen atoms. They are highly stable and, due to their ordered porous structures and potential to form glass-like monoliths, ZIFs have been suggested as supports for adsorptive separation applications. [4] Despite their potential, there are few reports on optimizing ZIFs for heat storage applications, with most studies focusing on water as the working fluid. However, using ethanol instead of water offers some advantages, e.g. ethanol as an adsorbate may be beneficial for lower temperature applications compared to water. [5-7]

The large-scale application of ZIFs is hindered by the lack of low-cost mass production methods and sustainable synthesis routes to reduce the environmental impact of ZIF preparation. [8] Most stable ZIFs are produced via solvothermal synthesis, which requires high temperatures and can take 72 hours or more, often using large amounts of N,N-dimethylformamide (DMF). As DMF is toxic and carcinogenic, significant efforts have been made to incorporate greener solvents into the ZIF synthesis process to reduce environmental impact. [9] Additionally, the search for a DMF replacement has intensified following the EU's stringent restrictions and partial bans on DMF use implemented in 2023 [COMMISSION REGULATION (EU) 2021/2030 of 19 November 2021].

The goal of our study is to examine a series of ZIFs as possible adsorbents for heat transformation applications with water or ethanol as working fluids. The two main criteria for the materials selection was the pore entrance size and the pore/cage capacity of a particular ZIF. It is worth noting that reported data for these criteria are based on static measurements and subject to possible variations due to synthesis conditions, activation method, sorption-driven flexibility, etc. Five ZIFs with large pore entrance size and pore capacities, determined by the type of topology and presence of more or less bulky linker functional groups (Figure 1), were selected (ZIF-8, ZIF-71, ZIF-76, ZIF-90 and ZIF-93) Additionally, two ZIFs with small pore entrance size and pore capacities were studied for comparison purposes (ZIF-62 and ZIF-74).

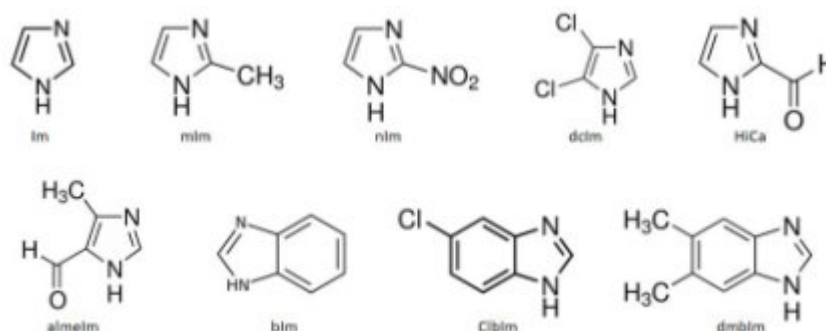


**Figure 1.** Linkers for ZIF-8 (mIm), ZIF-62 (Im and blm), ZIF-71 (dclm), ZIF-74 (nIm and dmbIm), ZIF-76 (ClIm and Im), ZIF-90 (HiCa) and ZIF-93 (almIm).

The ZIFs were first synthesized as per previously published methods and fully structurally investigated (using PXRD, TGA, N<sub>2</sub> physisorption, SEM). The five ZIFs (ZIF-8, ZIF-71, ZIF-76, ZIF-90 and ZIF-93) were selected for further studies, including optimization of synthesis methods, which were completed *via* green synthesis methods (*i.e.* using greener solvents, reducing the synthesis time, removed the activation step, using precipitation method at room temperature and/or with ball milling). In all cases, we found that the optimized green synthesis samples preformed the same or



even better than the original DMF-based samples, considering specific surface areas, the ease of activation procedures, etc..

The evaluation of selected ZIFs as adsorbents by water/ethanol adsorption and DCS measurements revealed that ethanol sorption generally occurs at lower relative pressures, if compared to water. Furthermore, the presence of hydrophobic functional groups in ZIFs significantly reduces the water uptake, but not the ethanol uptake. DSC results revealed that the desorption enthalpies for ZIF-ethanol pair are lower than for ZIF-water pairs. Stability and cycling tests revealed that the sorption performance is not affected by several cycles of ethanol sorption, while with water some ZIF structures can suffer partial degradation. Considering stability and sorption performance, we found that ZIF-93 was the most promising material for both working fluids (Figure 2).

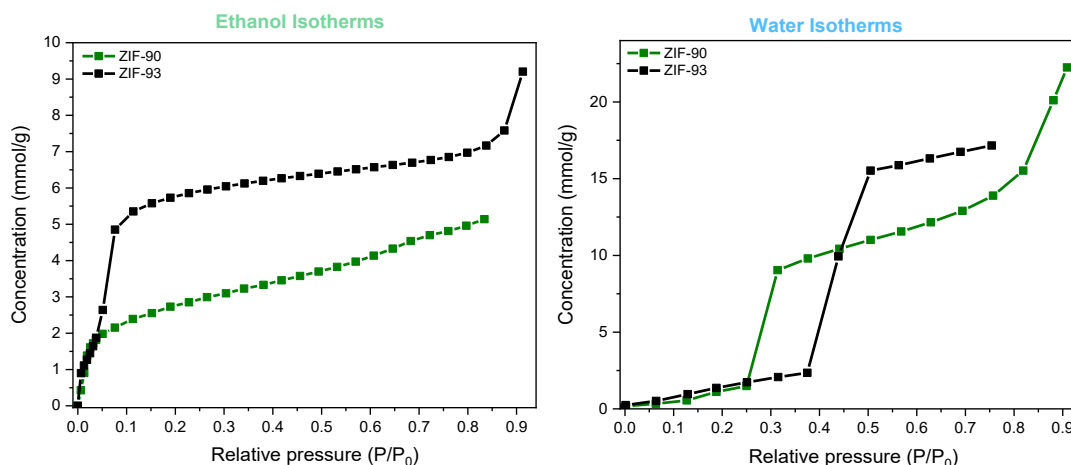


Figure 2. Ethanol (left) and water (right) isotherms for ZIF-90 and ZIF-93 which were obtained at 25°C.

## References

- [1] S. K. Henninger, S. J. Ernst, L. Gordeeva, P. Bendix, D. Fröhlich, A. D. Grekova, L. Bonaccorsi, Y. Aristov and J. Jaenchen, *Renewable Energy*, **110**, 59-68 (2017)
- [2] A. Ristić and N. Z. Logar, *Nanomaterials*, **9**, 27 (2019)
- [3] A. Krajnc, J. Varlec, M. Mazaj, A. Raistić, N. Z. Logar and G. Mali, *Advanced Energy Materials*, **7**, 1601815 (2017)
- [4] C. Zhou, L. Longley, A. Krajnc, G. J. Smales, A. Qiao, I. Erucar, C. M. Doherty, A. W. Thornton, A. J. Hill, C. W. Ashling, O. T. Qazvini, S. J. Lee, P. A. Chater, N. J. Terrill, A. J. Smith, Y. Yue, G. Mali, D. A. Keen, S. G. Telfer and T. D. Bennett, *Nature Communications*, **9**, 5042 (2018)
- [5] M. F. De Lange, B. L. Van Velzen, C. P. Ottevanger, K. J. F. M. Verouden, L. C. Lin, T. J. H. Vlugt, J. Gascon and F. Kapteijn, *Langmuir*, **31**, 12783-12796 (2015)
- [6] H. Wu, F. Salles and J. Zajac, *Molecules*, **24**, 945 (2019)
- [7] B. R. Pimentel, M. L. Jue, E. K. Zhou, R. J. Verploegh, J. Leisen, D. S. Sholl and R. P. Lively, *Journal of Physical Chemistry C*, **123**, 12862 (2019)
- [8] H. Li, W. Chen, B. Liu, M. Yang, Z. Huang, C. Sun, C. Deng, D. Cao, G. Chen, M. Shahsavari, P. M. Jahani, I. Sheikhshoae, S. Tajik, A. A. Afshar, M. B. Askari, P. Salarizadeh, A. Di Bartolomeo and H. Beitollahi, *Materials (Basel)*, **8**, 775 (2022)
- [9] A. Škrjanc, C. Byrne and N. Zabukovec Logar, *Molecules*, **26**, 1573 (2021)

## Acknowledgments

The authors would like to thank Mojca Opresnik for SEM imaging and Edi Kranjc for PXRD measurements.





## Mono vs Bimetallic Pd-Fe/n-ZSM-5 catalysts for the conversion of ELV plastic waste into dehalogenated oil via (Hydro)-Pyrolysis

L. Amodio<sup>1,2</sup>, J. Cueto<sup>2</sup>, P. Pizarro<sup>1,2</sup>, D.P. Serrano<sup>1,2</sup>

<sup>1</sup> Thermochemical Processes Unit, IMDEA Energy, Avda. Ramón de la Sagra 3, 28935, Móstoles, Madrid, Spain

<sup>2</sup> Chemical and Environmental Engineering Group, Rey Juan Carlos University, Móstoles, Madrid, Spain

lidia.amodio@imdea.org

The recovery and recycling of plastic waste from End-of-Life Vehicles (ELV) is a significant environmental challenge. Currently, only about 19% of ELV plastics are recycled [1]. Modern low-emission vehicles use lightweight materials, batteries, and electronics, but vehicles reaching the end of their lifespan are currently not managed in the most efficient manner, leading to resource wastage and environmental pollution. Among the challenges hindering the recovery of plastics from the ELV sector, a major obstacle is the high level of heterogeneity, which arises not only from the use of a wide range of polymers but also from the presence of heteroatoms, such as oxygen, nitrogen, but especially halogens coming from PVC or additives. The latter are used to improve plastic performances and can release harmful substances into the surrounding soil when chlorinated materials are disposed of in landfills or generate dioxins and furans when heated or incinerated. Therefore, it is crucial to develop effective strategies for managing these materials in a way that minimizes environmental impact and maximizes resource recovery. In recent years, pyrolysis and hydrolysis have gained special relevance as alternatives for the processing of plastic waste [2]. Pyrolysis consists in the thermal decomposition of materials at elevated temperatures in an inert atmosphere, which can break down complex plastic polymers into simpler compounds. Hydrolysis, on the other hand, involves the addition of hydrogen during the pyrolysis process. This can further reduce the formation of unwanted by-products and enhance chlorine elimination from liquid product promoting dehalogenation reactions.

Taking advantage that zeolites, and in particular the MFI topology, are primary components in the design of successful catalysts for cracking and hydrotreatment processes [3], this work is focused on the development of ZSM-5-based catalysts for the valorization of a real plastic waste from ELV into high quality oils, comparing its performance under both catalytic pyrolysis and hydrolysis conditions. The intrinsic acidity of the zeolite, ideal to promote reactions such as cracking, isomerization and aromatization, is complemented by the incorporation of additional active phases able to dehalogenate and upgrade the pyrolysis vapors. The objective is to obtain oils with minimum halogen (Cl) content and properties adequate to be fed into refinery processes. For that purpose, the synergistic effect of a bimetallic catalyst consisting of Palladium (Pd, 1 wt%) and Iron oxide (Fe<sub>2</sub>O<sub>3</sub>, 5 wt%) was investigated. In the case of Pd, it is known to be active towards hydrodehalogenation (HDH) reactions, whereas iron oxide can act as a halogen trap, as demonstrated in previous works [4,5].

The pyrolysis and hydrolysis experiments were conducted in a discontinuous up-flow fixed bed reactor under moderate pressure (6 bar), as described in a previous study [4]. Eight grams of the ELV sample were heated to 550°C at a heating rate of 10°C/min, while the catalytic bed was maintained at 450°C, with a catalyst-to-feed ratio of 0.4. The raw plastic and fresh catalysts characterization are summarized in Table 1. The incorporation of both metals into the zeolite slightly reduces the total pore volume, whereas the changes in surface areas are minimal and can be attributed mainly to the addition of 5-6% of non-porous metallic phases rather than to any significant pore blocking.

Table 1. Raw Plastic and catalysts characterization.

Polymer composition:					Proximate analysis (wt%):			Catalyst properties:							
ABS, PVC, PA, PP, PE, PMMA, PS, PET, PUR, PC					Volatile matter	Fixed carbon	Ash	Sample	S <sub>BET</sub> [m <sup>2</sup> /g]	S <sub>EXT</sub> [m <sup>2</sup> /g]	Total Volume [cm <sup>3</sup> /g]				
					76.4	9.6	14.0								
Ultimate analysis (wt%):					Halogen content (ppm)			Fe <sub>2</sub> O <sub>3</sub> / n-ZSM-5	395	122	0.473				
C	H	N	S	O	Cl							Pd/ n-ZSM-5	406	127	0.493
77.2	8.9	4.6	0.8	12.5	4092										

Non-catalytic (NC) pyrolysis and hydrolysis at 1 and 6 bar assays were also performed to be used as reference. Regarding the product distribution, the primary product obtained from both pyrolysis and hydrolysis was the oil fraction, accounting for about 50 wt.% of the total product (Figure 1A). The presence of catalysts slightly reduced the oil fraction yield, favouring the formation of gas and coke which never overcame 13 and 3 wt.% yields, respectively. This can be attributed to the strong acidic nature of the ZSM-5 zeolite, which promote cracking reactions that break down larger hydrocarbon molecules into smaller gaseous compounds and solid coke. The solid residue (char), which was accumulated in the thermal zone of the reaction system, constituted the second major product with a yield of approximately 38 wt.% (of which about 36 wt.% is inorganic as it contains the ashes present in the ELV plastic waste). The char fraction could potentially be utilized for energy recovery or as a raw material for other industrial applications.

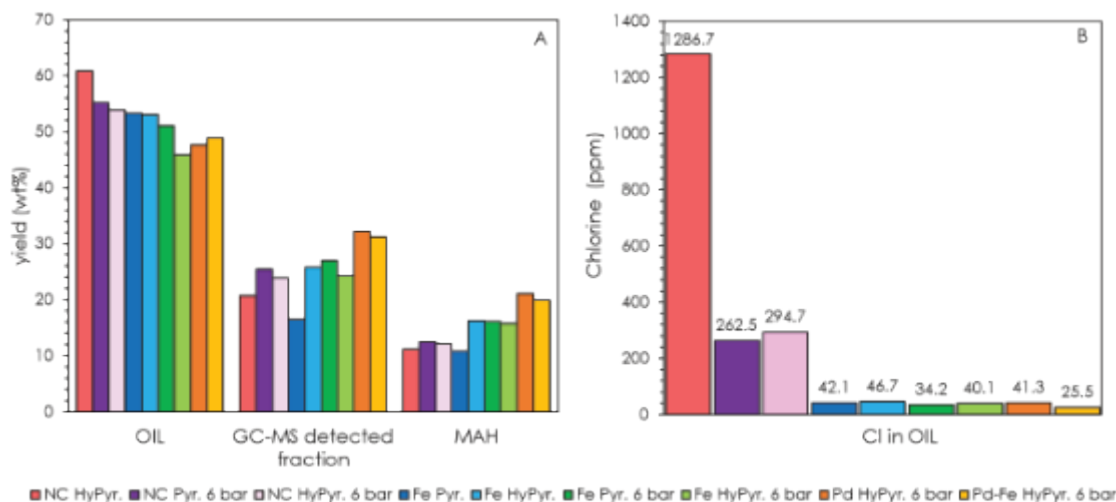


**Figure 1.** Yields of oil, oil GC-MS detected fraction and monoaromatic hydrocarbons (A) and oil Cl content (B) obtained in pyrolysis and hydropyrolysis experiments of the ELV plastic waste.

Oil GC-MS analysis revealed a complex mixture of components, indicating the breakdown of the plastic polymers into simpler compounds, mainly monoaromatic hydrocarbons (around 12 wt.% yield in the NC pyrolysis reaction, Figure 1A) followed by aliphatic compounds (paraffins, olefins and cyclic hydrocarbons). This fact underscores the potential of these processes to convert ELV plastic residues into valuable chemical feedstocks. Furthermore, the GC-MS results showed a significant increase in the yield of monoaromatic compounds for the catalytic reactions. Particularly, in the hydropyrolysis configuration with the Pd-based catalysts the yield of monoaromatics exceeded 20 wt.%, with a significant increase also in the overall yield of GC-MS detected species. These results indicate a more intensive cracking of heavier compounds and, therefore, an enhanced value of the produced oil. Likewise, a moderate increase of pressure (from 1 to 6 bar) seems to promote the elimination of nitrogenated compounds. Thus, in the test with the bimetallic catalyst and hydropyrolysis at 6 bar, it was obtained the lowest yield of nitrogenated compounds, which decrease from 5 wt.% in the thermal pyrolysis reaction down to 2wt.%.

Regarding the oil halogen content, it can be appreciated in Figure 1B that a remarkable decrease (from 1287 to 295 ppm of Cl) occurs when increasing the pressure up to 6 bar. Likewise, a strong reduction in the oil Cl content is denoted for the catalytic tests in comparison with the non-catalytic ones under both pyrolysis and hydropyrolysis conditions. The most effective oil dehalogenation was achieved using the hydropyrolysis configuration with a Pd-Fe/n-ZSM-5 catalyst under a hydrogen atmosphere at 6 bar pressure. This configuration resulted in a liquid fraction with minimal halogen content (25.5 ppm), highlighting the efficiency of the bimetallic catalyst system to promote dehalogenation reactions and evidencing a synergistic effect between iron oxide and palladium. The char also played a crucial role in halogen elimination, acting as a highly effective halogen trap with about 76% of the total chlorine content of the starting sample being retained in the char.

In conclusion, the combination of hydropyrolysis at 6 bar with a bimetallic Pd-Fe/n-ZSM-5 catalyst for the conversion of ELV plastic waste leads to a relevant improvement in the quality of the liquid product by promoting its dehalogenation, reducing the presence of nitrogenated and heavy compounds and increasing the production of valuable monoaromatic hydrocarbons. Thus, this process maximizes the recovery of valuable components in the oil fraction and reduces the environmental impact by efficiently trapping halogens.

## References

- [1] <https://plasticseurope.org/knowledge-hub/the-circular-economy-for-plastics-a-european-analysis-2024/>
- [2] F. Ardolino, G.F. Cardamone and U. Arena, *Waste Management*, **135**, 347-359 (2021).
- [3] S.S. Mabaleha, A. Delo, P. Kalita, *Renewable and Sustainable Energy Reviews*, **203**, 114789 (2024).
- [4] L. Amodio, J. López, A. Souza, J. Cueto, H. Hernando, P. Pizarro, D. Serrano, *Journal of Hazardous Materials*, **465**, 133357 (2024).
- [5] J. López, L. Amodio, M. Alonso-Doncel, J. Cueto, H. Hernando, M. Mazur, J. Cejka, P. Pizarro, D. Serrano, *Journal of Environmental Engineering*, **12**, 111790 (2024).

## Acknowledgments

The authors gratefully acknowledge the financial support from project I+D+i TED2021-130820B-C22 (CIRPLACAR) funded by MCIN/AEI /10.13039/501100011033 and by the European Union NextGenerationEU/ PRTR



## Iridium-encapsulated MWW-type zeolite catalyst for the hydrogenolysis of methylcyclopentane with excess methylcyclohexane

Satoshi Inagaki<sup>1</sup>, Yuki Maekawa<sup>1</sup>, Keiju Tokita<sup>1</sup>, and Yoshihiro Kubota<sup>1</sup>

<sup>1</sup> Division of Materials Science and Chemical Engineering, Yokohama National University, 79-5, Tokiwadai, Hodogaya-ku, Yokohama 240-8501, Japan

inagaki-satoshi-zr@ynu.ac.jp

The successful preparation of MWW-type zeolite encapsulating iridium clusters in the micropores through H<sub>2</sub> treatment at 400 °C due to reduction of Ir<sup>n+</sup> into Ir<sup>0</sup> species followed by the hydrogenolysis of organic structure-directing agents with the aid of Ir<sup>0</sup> catalyst was achieved. This Ir/MWW catalyst exhibited excellent shape selectivity in the selective hydrogenolysis of methylcyclopentane in the presence of excess methylcyclohexane.

### Introduction

Liquid organic hydrogen carrier (LOHC) system is an important potential method for the storage and transportation of H<sub>2</sub> produced from renewable energy sources. Methylcyclohexane (MCH) is a very good candidate of LOHC because it can be stored and transported in the liquid phase at ambient temperature and pressure [1,2]. During the catalytic hydrogenation of toluene with H<sub>2</sub>, MCH is partially isomerized to undesirable five-membered-ring compounds, such as ethylcyclopentane (ECP) and dimethylcyclopentanes (DMCPs). Accumulation of such compounds in the LOHC system reduces the hydrogen storage efficiency of the carrier, so the purification of the MCH is necessary before reuse.

Computational studies based on density functional theory (DFT), which are powerful tools for gaining a better understanding of the elementary steps of complex reaction networks, are utilized to explore the ring-opening mechanism of MCP [4]. The possible reaction mechanism for the hydrogenolysis of MCP is proposed as multiple dehydrogenation steps prior to the endocyclic cleavage as follows: first, dehydrogenation of MCP to an  $\alpha,\alpha,\beta$ -tetra-adsorbed cyclic intermediate or an  $\alpha,\alpha,\beta$ -tri-adsorbed cyclic intermediate with a methyl substituent at the  $\beta$  position; then, endocyclic C–C bond cleavage; and finally, hydrogenation to produce hexane isomers [4,5]. In DFT calculations, all of four metal catalyst are active for the ring-opening reaction of MCP, with the activity following the trend, Ir  $\approx$  Rh > Pt > Pd [4].

Recently, we have disclosed that Ir/SiO<sub>2</sub> catalyst efficiently works for the selective hydrogenolysis of methylcyclopentane (MCP), which is a model of the five-membered-ring compounds, in the presence of excess MCH at a relatively low temperature of 200 °C [5]. The different reactivities of MCP and MCH in this catalyst system can be explained by the relatively high strain energy and formation enthalpy of MCP compared to the more stable MCH [3]. It is expected that nano-sized Ir catalyst encapsulated within zeolitic micropores could exhibit “shape-selectivity” for MCP to MCH. In this study, we have attempted the hydrothermal synthesis of pure-silica MWW precursor occluding Ir<sup>n+</sup> followed by direct H<sub>2</sub> treatment to give MWW-type zeolite containing with highly dispersed Ir species. Furthermore, we have evaluated the catalytic performance of the prepared Ir/MWW catalyst for the hydrogenolysis of MCP with excess MCH [5].

### Experimental

The synthesis of Ir-containing MWW layered precursor was conducted using *N,N,N*-trimethyl-1-adamantanonium hydroxide (TMAda<sup>+</sup>OH<sup>-</sup>) and hexamethylenimine (HMI) as organic structure-directing agents (OSDAs) according to the previous reports [5,6]. After the hydrothermal synthesis at 150 °C for 7 days under 20-rpm rotation, the obtained mixture was filtered and rinsed with distilled water, and then the recovered solid was dried in an oven at 80 °C overnight to obtain a white powder, Ir<sup>n+</sup>/MWW(P).

Ir<sup>n+</sup>/MWW(P) was treated under H<sub>2</sub> flow to promote the hydrogenolysis of OSDA catalyzed by Ir. The sample was reduced by H<sub>2</sub> treatment at 400 °C for 5 h. This sample is designated as Ir/MWW\_H<sub>2</sub>. Independently, Ir<sup>n+</sup>/MWW(P) was calcined in a muffle furnace at 560 °C for 8 h to remove organic components to give a grey powder, Ir/MWW\_cal. The calcined sample was reduced by H<sub>2</sub> treatment at 400 °C for 5 h to give Ir/MWW\_cal\_H<sub>2</sub>.

The prepared samples were characterized by using powder XRD, ICP-AES, TG-DTA, CHN elemental analysis, H<sub>2</sub>-TPR, XPS and high-resolution TEM.

Selective hydrogenolysis of MCP diluted with MCH was performed in a fixed-bed reactor equipped with an electric furnace. Prior to the reaction, the catalyst (200 mg) was treated at 400 °C for 1 h under H<sub>2</sub> flow. MCP and MCH were diluted with H<sub>2</sub> flow (40 cm<sup>3</sup> (N.T.P.) min<sup>-1</sup>) to give a H<sub>2</sub>:MCP:MCH ratio of 30:0.1:0.9, which was fed into the reactor with the catalyst at 200 °C. In this reaction, C<sub>6</sub> paraffins (*n*-hexane, 2-MP, and 3-MP) and C<sub>1</sub>–C<sub>5</sub> paraffins were regarded as products from MCP, whereas C<sub>7</sub> paraffins, such as *n*-heptane, 2-methylhexane (2-MH), 3-methylhexane (3-MH), and toluene were regarded as products from MCH.

### Results and discussion

The layered precursor of MWW-type zeolite, MWW(P), can be hydrothermally synthesized from a synthetic mixture containing with TMAda<sup>+</sup> and HMI as OSDAs, as proven by the powder XRD. It is noted that adding IrCl<sub>3</sub> and



ethylenediamine into the synthetic mixture can give MMW(P) phase without any impurities. From the results of ICP-AES and TGA, the Ir content of the as-made sample was  $46.6 \mu\text{mol} (\text{g-SiO}_2)^{-1}$ , while the input Ir content was  $52.0 \mu\text{mol} (\text{g-SiO}_2)^{-1}$ .

When  $\text{Ir}^{n+}/\text{MWW}(\text{P})$  was calcined at  $560 \text{ }^\circ\text{C}$  to remove OSDAs followed by  $\text{H}_2$  treatment at  $400 \text{ }^\circ\text{C}$ , Ir species in  $\text{Ir}/\text{MWW\_cal\_H}_2$  was very large, of which the size was ca.  $15 \text{ nm}$  estimated by CO chemisorption, and  $6.1 \pm 5.2 \text{ nm}$  by TEM. This is due to sintering of  $\text{IrO}_x$  species during calcination. To avoid sintering of Ir species, the thermal treatment of  $\text{Ir}^{n+}/\text{MWW}(\text{P})$  under  $\text{H}_2$  flow at  $400 \text{ }^\circ\text{C}$  was conducted. In the case of  $\text{Ir}/\text{MWW\_H}_2$ , the size of Ir particles was ca.  $0.9 \text{ nm}$  estimated by CO chemisorption. In the high-resolution TEM, very tiny Ir clusters were highly dispersed in MWW-type zeolite, especially some of them seemed to be the atomic size.

The cationic  $\text{Ir}^{n+}$  in of  $\text{Ir}^{n+}/\text{MWW}(\text{P})$  was reduced to metallic  $\text{Ir}^0$  during  $\text{H}_2$  treatment, as confirmed by the XPS analysis. From a  $\text{H}_2$ -TPR profile of  $\text{Ir}^{n+}/\text{MWW}(\text{P})$ , the hydrogenolysis of organic SDA molecules progressed with the aid of  $\text{Ir}^0$  catalyst, which formed during  $\text{H}_2$  treatment. The micropore volume of  $\text{Ir}/\text{MWW\_H}_2$  was  $0.12 \text{ cm}^3 \text{ g}^{-1}$ , which is very close to that of  $\text{MWW\_cal}$  ( $0.15 \text{ cm}^3 \text{ g}^{-1}$ ), indicating that most of OSDA molecules occluded in the micropores was eliminated during  $\text{H}_2$  treatment at  $400 \text{ }^\circ\text{C}$ .

Table 1 lists the results of the catalytic hydrogenolysis of MCP in the presence of excess MCH over  $\text{Ir}/\text{SiO}_2$  and  $\text{Ir}/\text{MWW}$  samples. All the catalysts exhibited catalytic activity in the hydrogenolysis of MCP at  $200 \text{ }^\circ\text{C}$ , while the product yields of toluene and ring-opening products derived from MCH was very low. Focusing on the ratio ( $R$ ) of the MCP conversion over MCH conversion after 5 min of the time on stream (see Table 1), the  $R$  of  $\text{Ir}(\text{imp.})/\text{MWW}$  was 21.0 and comparable to the  $R$  of  $\text{Ir}/\text{SiO}_2$  (22.6) which was prepared by impregnation method using non-porous silica particles as a catalyst support [3]. Since Ir particles in  $\text{Ir}(\text{imp.})/\text{MWW}$  were predominantly located on the external surface, as like  $\text{Ir}/\text{SiO}_2$ , both MCP and MCH competitively react on the external Ir sites. It is noted that the  $R$  of  $\text{Ir}/\text{MWW\_H}_2$  was very high (28.0), implying that the hydrogenolysis of MCP preferentially progress with avoiding the catalytic reaction of MCH. Because relatively small MCP molecules can access very tiny Ir clusters within the 10-ring micropores in  $\text{Ir}/\text{MWW\_H}_2$ , while the size of MCH molecule is too large to enter the 10-ring channels. In other words, the 10-ring window of MWW efficiently acts as “molecular sieve” for the selective hydrogenolysis of MCP with excess MCH.  $\text{Ir}/\text{MWW\_cal\_H}_2$  showed both lower MCP conversion (3.1%) and lower  $R$  value (11.6), because there were extremely large Ir particles ( $15.0 \text{ nm}$ ) on the external surface of MWW-type zeolite.

Table 1 Catalytic hydrogenolysis of MCP in the presence of excess MCH at  $200 \text{ }^\circ\text{C}$

Catalyst	Ir content ( $\mu\text{mol g}^{-1}$ )	Ir particle size (nm)		Conversion (%)		MCP conversion /MCH conversion
		CO chemisorption	TEM	MCP	MCH	
$\text{Ir}/\text{MWW\_H}_2$	46.6	0.9	0.3–0.8	15.1	0.54	28.0
$\text{Ir}/\text{MWW\_cal\_H}_2$	46.6	15.0	0.9–11.3	3.1	0.27	11.6
$\text{Ir}(\text{imp.})/\text{MWW}$	56.0	2.0	–	16.2	0.77	21.0
$\text{Ir}/\text{SiO}_2$	56.0	3.2	1.0–2.1	33.6	1.48	22.6

## Conclusion

The prepared catalyst,  $\text{Ir}/\text{MWW\_H}_2$ , showed higher activity and selectivity for the hydrogenolysis of MCP at  $200 \text{ }^\circ\text{C}$  in the presence of excess MCH. This catalyst could address the issue of accumulating five-membered ring products, such as ECP and DMCPs, in the MCH-toluene system by removing impurities through selective hydrogenolysis to improve the energy carrier efficiency of the system. Furthermore, the catalyst preparation technique developed in this study can be used to prepare highly dispersed clusters of precious metals, including Pt, Pd, Rh, and Ru, inside the micropores of the zeolites for hydrogenolysis and hydrogenation/dehydrogenation.

## References

- [1] S. Hodoshima, H. Arai, S. Takaiwa, Y. Saito, *Int. J. Hydrogen Energy*, **28**, 1255 (2003).
- [2] Y. Okada, E. Sasaki, E. Watanabe, S. Hyodo, H. Nishijima, *Int. J. Hydrogen Energy*, **31**, 1348 (2006).
- [3] S. Inagaki, Y. Maekawa, Y. Orui, R. Wakatsuki, Y. Nishi, N. Hiyoshi, Y. Kubota, *J. Jpn. Petroleum Inst.*, **66**, 57 (2023).
- [4] Z.-J. Zhao, L.V. Moskaleva, N. Rösch, *ACS Catal.*, **3**, 196 (2013).
- [5] Y. Maekawa, K. Tokita, R. Wakatsuki, Y. Nishi, K. Yoshida, Y. Kubota, S. Inagaki, *Micropor. Mesopor. Mater.*, **379**, 113264 (2024).
- [6] L. Liu, M. Lopez-Haro, D.M. Meira, P. Concepcion, J.J. Calvino, A. Corma, *Angew. Chem. Int. Ed.*, **59**, 15695 (2020).

## Acknowledgments

This work was supported by Mukai Science and Technology Foundation. We thank Dr. Kaname Yoshida (Japan Fine Ceramics Center) for technical assistance of high-resolution TEM observation.

## Removal of polystyrene nanoplastics from aqueous solution using zeolite materials

Kinga Góra-Marek<sup>1</sup>, Karolina A. Tarach<sup>1</sup>, Marta Marczak-Grzesik<sup>1,\*</sup>

<sup>1</sup>Faculty of Chemistry, Jagiellonian University in Kraków, Gronostajowa 2, Kraków, Poland

\* marta.marczak-grzesik@uj.edu.pl

### Introduction

Microplastics (MPs) and nanoplastics (NPs) are assumed to be emerging toxic pollutants due to their unique persistent physicochemical attributes, chemical stability, and nonbiodegradable nature. Owing to their possible toxicological impacts (not only on aquatic biota but also on humans), scientific communities are developing innovative technologies to remove microplastics and nanoplastics from polluted waters. Continued research and collaboration across scientific, industrial, and governmental sectors are crucial to mitigate the effects of nanoplastics and protect environmental and public health<sup>1-3</sup>.

Various technologies, including adsorption, coagulation, photocatalysis, bioremediation, and filtration, have been developed and employed to eliminate microplastics and nanoplastics. Recently, adsorption technology has received great interest in capturing microplastics and nanoplastics and achieving excellent removal performance. Promising sorbent materials for nanoplastics are zeolites. They have attracted significant interest among researchers seeking solutions to the problem of nano- and microplastics in aquatic environments<sup>4</sup>. Zeolites are microporous, aluminosilicate minerals commonly used as adsorbents and catalysts due to their high surface area, large pore volume, and unique ion-exchange properties<sup>2,3</sup>.

In this study, various zeolites and their capacity for removing microplastics such as polystyrene (PS) from water were tested.

### Materials and Methods

Fluorescent polystyrene nanoplastics with micron size (PSNPs) with an average diameter of 0.2  $\mu\text{m}$ , 2% w/v was used for the studies. The fluorescent PSNP stock solution was diluted using deionised water and then treated with an ultrasonic device for 10 min to obtain the desired PS concentrations (100, 200 mg/L). For the studies the commercially available zeolite were selected: H-SDUSY (CBV 760, Si/Al=31, BET 720  $\text{m}^2/\text{g}$ ), H-Beta (980HOA, Si/Al=250, BET 500  $\text{m}^2/\text{g}$ ), X (13X, Si/Al=1.3, BET 310  $\text{m}^2/\text{g}$ ), desilicated zeolite Beta (CP814C, Si/Al=19, BET 710  $\text{m}^2/\text{g}$ ), and clinoptilolite. Desilication of zeolite Beta was carried out with 0.2M NaOH at 65°C, for 10 min, then an ion-exchange procedure with 0.5 M  $\text{NH}_4\text{NO}_3$  solution for 30 min at 65°C was performed three times to provide the ammonium form of the sample.

In the adsorption process, the zeolites (with different masses: 25, 50, 100, and 500 mg) and PSNP solutions (with different concentrations: 100 and 200 mg/L, 10 mL) were added to a conical glass flask and placed on a magnetic stirrer with a speed of 500 rpm for 20 min. The solutions were then filtered, and the zeolites were left to dry at room temperature. After the sorption process, the amounts of nanoplastic in water and zeolites were analysed quantitatively using IR and UV-vis spectroscopies and thermogravimetric analysis.

### Results and Discussion

In this work, the effect of the zeolite structures on PSNP removal in an aqueous solution was studied. Using zeolite H-SDUSY in amounts ranging from 25 to 500 g/L, the adsorption ratio of PSNPs increased from 76.5 to 90.6% for PSNP solution with 100 mg/L and 78.9 to 82.8% for PSNP solution with 200 mg/L. This very efficient adsorption of PSNPs could be attributed to the least limited mass transfer of PSNPs in this highly mesoporous zeolite. The opposite effect was obtained for purely microporous zeolite H-Beta. The adsorption ratio of PSNPs by H-Beta (980HOA) decreased from 35 to 17.5% (for PSNP solution with 100 mg/L) and 43.5 to 18.4% (for PSNP solution with 200 mg/L), when the PSNPs dose increased from 50 to 500 g/L. The highest adsorption rate (92.3 and 93.7% suitable for concentrations PSNP of 100 and 200 mg/L) of PSNPs in an aqueous solution was observed for clinoptilolite at a dosage of 25 g/L. Desilicated and calcined zeolite Beta (CP814C) proved ineffective in removing PSMP. The adsorption ratio of PSNPs by H-SDUSY fluctuated between 2.9% and 49.8%, ranging from 25 to 500 g/L. Similarly, in the case of zeolite 13X - the adsorption ratio of PSNPs increased from 15.3% to 50.8%.

Acknowledgement: The work was financed by Grant No. 2021/43/B/ST4/00307 from the National Science Centre, Poland.

### References

1. Tan X. et al., *Water Research*. **2023**, 230, 119526.
2. Ahmed R. et al., *Chemosphere*. **2022**, 293, 133557.
3. Syberg, K., Almroth, B.C., Fernandez, M.O. et al., *Micropl.&Nanopl* **2024**, 4, 14.
4. Ranasinghe M. et al., *Analytical Chemistry*. **2024**, 96, 11734-11741.



## How to mitigate pitfalls in the characterization of zincosilicate zeolites?

**Gleb Ivanushkin<sup>1</sup>, Ibrahim Khalil<sup>1</sup>, Mostafa Torka Beydokhti<sup>1</sup>, Aram Bugaev<sup>2</sup>, Juna Bae<sup>1</sup>, Michiel Dusselier<sup>1</sup>**

<sup>1</sup> Center for Sustainable Catalysis and Engineering CSCE, KU Leuven, Faculty of Bioscience Engineering, B-3000 Leuven, Belgium

<sup>2</sup> Paul Scherrer Institute, 5232 Villigen, Switzerland

gleb.ivanushkin@kuleuven.be

Heteroatom substitution in various silicates is a general way to introduce functionality to materials, rendering them useful in broader applications [1]. More closely, modification of siliceous zeolites – microporous crystalline materials, which consist of a silicon-based matrix built by multiple tetrahedrally-coordinated (T-) atoms connected through oxygen bridges, forming a solid carcass – can yield a wide range of industrially-valuable materials [2]. Recently, the presence of zinc species into zeolites has received quite a bit of attention from the scientific community independently from the preparation procedure. Among many publications, activity of zinc-containing materials was recognized in the following areas of research: ion exchange, alkanes dehydrogenation, aromatization cracking, biomass conversion, and CO<sub>2</sub> adsorption [3-5].

Due to high pH, the hydrothermal synthesis of zincosilicates is inevitably coupled with formation of zinc hydroxide and/or oxide species, arising from basic media conditions. Precipitation of the heteroatom (oxide or hydroxide form) from synthesis solutions leads to poor incorporation, but this can be partially eliminated by a careful design of the preparation procedure [3], by stabilization of zinc particles with various ligands [6], or by Electro-Assisted Synthesis (EAS) [7,8]. However, lab-scale characterization of produced zincosilicate materials, allowing to resolve zinc positioning in the zeolite lattice, is limited to ion exchange capacity tests and/or UV-vis measurements.

In this contribution, Zn-incorporated zeolites with MFI structure were synthesized via classic hydrothermal batch and EAS methodologies at two key temperatures, providing different levels of zinc incorporation into the zeolite lattice. We further benchmarked these materials with a series of Zn-impregnated pure siliceous MFI zeolites. Seeking a solid confirmation of isomorphous substitution, the prepared Zn-MFI and ZnO/Si-MFI were characterized using a set of characterization methods, such as PXRD, N<sub>2</sub> physisorption, TGA, DF TEM EDS and divalent cation exchange capacity. From these conventional analysis techniques we could already make an intermediate conclusions about metal positioning of the metal. For instance, the ion exchange method stands out from the list of performed conventional characterization, being straightforward in use and (quite) reliable in interpretation along with other results, simultaneously suggesting both zinc stability to leaching and divalent cation capacity available due to the framework zinc sites (Table 1).

**Table 1.** Ion-exchange performance of Zn-containing MFI zeolites.

Synthesis type and EAS specifics		Temp., °C	Si/Zn before ion exchange	Si/Zn after ion exchange	Loss of Zn atoms, %	K/2Zn	Ni/Zn	
Impregnated		(160)	19	20 ± 1	5	0.06	0.01	
			38	41 ± 1	10	0.06	0.01	
			88	97 ± 1	10	0.09	0.02	
			218	222 ± 3	1	0.12	0.02	
Batch	*with NaOH	90	25	42 ± 5	39	0.19	0.73	
			11	19	39	—	0.87	
		160	23	27 ± 1	14	0.07	0.03	
EAS		90	Sine, 0.4 V <sub>pp</sub>	57	92	37	—	0.20
			Sine, 0.8 V <sub>pp</sub>	46 ± 1	74 ± 12	37	0.26	0.38
			Sine, 1.6 V <sub>pp</sub>	74	78	5	—	0.05
			Sine, 3.2 V <sub>pp</sub>	59	60	3	—	0.05
			Sine, 6.4 V <sub>pp</sub>	68	77	11	—	0.10
		Square, 0.8 V <sub>pp</sub>	58	78	26	—	0.27	
		160	Sine, 0.8 V <sub>pp</sub>	21	28 ± 2	24	0.23	0.18



In addition, the identification and estimation of the amount incorporated Zn were explored with a set of spectroscopic techniques, such as UV-vis, FT-IR (also using CD<sub>3</sub>CN and Pyridine as probe molecules), and XAS. For FT-IR spectroscopy in particular, by following the evolution of the IR vibrational peaks in three different wavenumber regions, we believe that this analysis could provide a necessary hint in the metal position resolution. Moreover, the FT-IR investigation approach was further broadened toward another Zn-containing framework – Zn-BEA (CIT-6), confirming our analysis. Finally, from the XAS perspective, two types of Zn<sup>II</sup> species were rigidly distinguished in the studied series of samples [9].

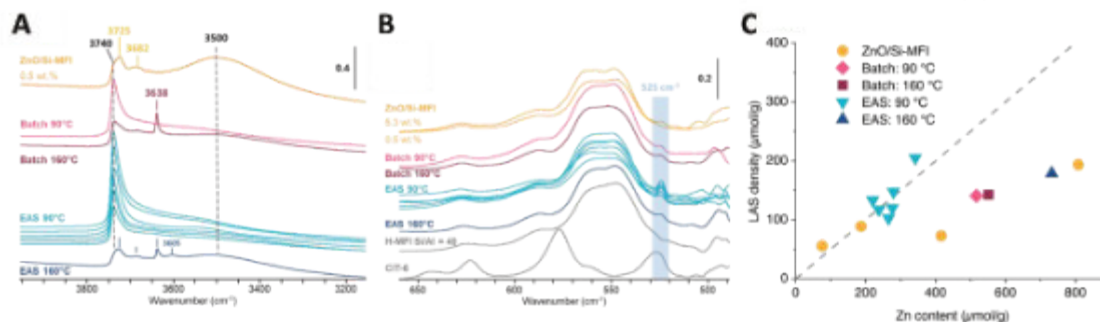


**Figure 1.** (A) FT-IR spectra in the stretching OH vibration zone for Zn containing samples from different synthesis methods after their in-situ activation at 400 °C, (B) KBr FT-IR spectra for the fingerprint zone for Zn containing samples from different synthesis methods in comparison to H-MFI and CIT-6. The sample powder was diluted with KBr (in a ratio of 1/100). (C) Correlation between the Zn-LAS density quantified by pyridine probe adsorption (after desorption at 150 °C) and the Zn content in the different Zn-containing zeolites. The dashed line in (C) is a visual representation of the function  $y = 0.5x$  which corresponds to 50 % of Zn incorporation.

## References

- [1] Y. Li, L. Li, J. Yu, *Chem*, 3, 6, 928-949, (2017).
- [2] M. Dusselier, M.E. Davis, *Chem Rev*, 118, 5265–5329, (2018).
- [3] N. Koike, K. Iyoki, S.H. Keoh, W. Chaikittisilp, T. Okubo, *Chemistry - A European Journal*, 24, 808–812, (2018).
- [4] D. Zhao, X. Tian, D.E. Doronkin, S. Han, V.A. Kondratenko, J.D. Grunwaldt, A. Perechodjuk, T.H. Vuong, J. Rabeah, R. Eckelt, U. Rodemerck, D. Linke, G. Jiang, H. Jiao, E. V. Kondratenko, *Nature*, 599, (2021).
- [5] D. Fu, Y. Park, M.E. Davis, *Angewandte Chemie International Edition*, 61, (2022).
- [6] X. Su, Z.P. Hu, J. Han, Y. Jia, S. Xu, J. Zhang, D. Fan, Y. Wei, Z. Liu, *Microporous and Mesoporous Materials*, 348, (2023).
- [7] G. Ivanushkin, M. Dusselier, *Chemistry of Materials*, 35, 5049–5058, (2023).
- [8] G. Ivanushkin, M. Torka Beydokhti, J.S. Martinez-Espin, M. Dusselier, *Chemistry of Materials*, 35, (2023).
- [9] G. Ivanushkin, I. Khalil, M. Torka Beydokhti, A. Bugaev, J. Bae, T. Donckels, M. Dusselier, *Microporous and Mesoporous Materials*, *Submitted*, (2024).

## Acknowledgments

GI, MT and MD thank the European Research Council (ERC) for funding (ERC Starting Grant 948449 named Z-EURECA). IK and JB thank postdoctoral funding from FWO Grants (12A3M24N and 12E6923N, respectfully). Three patent applications have been filed for the Electro-Assisted zeolite Synthesis invention (EP22196233, EP22196236, EP22196238) on the method, apparatus and heteroatom-rich zeolites. The TEM-EDS in this research was supported by the FWO infrastructure projects (AKUL13/19 and I000920N).



## Tailoring pores of AFN-related zeolites for enhanced separation of CO<sub>2</sub>/N<sub>2</sub> or CO<sub>2</sub>/CH<sub>4</sub>

Y. N. Yang and J. Y. Li\*

State Key Laboratory of Inorganic Synthesis and Preparative Chemistry, College of Chemistry, Jilin University, Changchun 130012, P. R. China.

lijiyang@jlu.edu.cn

Carbon dioxide (CO<sub>2</sub>), a well-known green-house gas, is the main product of fossil fuel combustion, which poses great environmental hazards. Separating CO<sub>2</sub> from the flue (mainly CO<sub>2</sub>/N<sub>2</sub> separation) is considered the most promising method to reduce CO<sub>2</sub> emissions and solve environmental problem. At the same time, the presence of CO<sub>2</sub> in natural gas can corrode pipelines during transportation, thus separating CO<sub>2</sub> from methane (CH<sub>4</sub>) has also received widespread attention.

Zeolites are a class of crystalline microporous silicates or aluminosilicates. Due to the excellent thermal stability and well-defined pores (< 2nm), zeolites are widely used in adsorption of industrially gas [1-2]. Particularly, the uniform aperture size of pores endow zeolites unique molecular sieving effect, in which small molecules can be diffused while other large competitors are excluded, exhibiting superiority in gas separation. As for CO<sub>2</sub>, CH<sub>4</sub> and N<sub>2</sub>, their kinetic diameters are of 3.3 Å, 3.8 Å and 3.6 Å, respectively. Thus, the small-pore zeolites with 8-ring windows (aperture size < 4.0 Å) are promising candidates for separation of these small gas molecules. Considering very small difference in kinetic diameters of CO<sub>2</sub>, CH<sub>4</sub> and N<sub>2</sub>, the slight difference in aperture sizes may have an impact on the gas selectivity. Therefore, the precise tuning of aperture sizes is vital to achieve the ideal selectivity, but still remains challenge due to the limited available small-pore zeolites in industry.

In this work, SAPO-14 zeolite with AFN topology featuring by different 8-ring windows in three-dimension directions has been synthesized and studied in the separation of CO<sub>2</sub>/N<sub>2</sub> or CO<sub>2</sub>/CH<sub>4</sub>. Aiming to further adjust pores and channels of the adsorbents, S-1 composite zeolite was synthesized in the synthesis system of SAPO-14 using SAPO-34 as the crystal seed. Similarly, S-X was prepared using a seeds-assisted method, and SAPO-34 and SAPO-14 were mechanically mixed as S-M as comparison samples. S-1 maintains high CO<sub>2</sub> storage capacity and excellent selectivity.

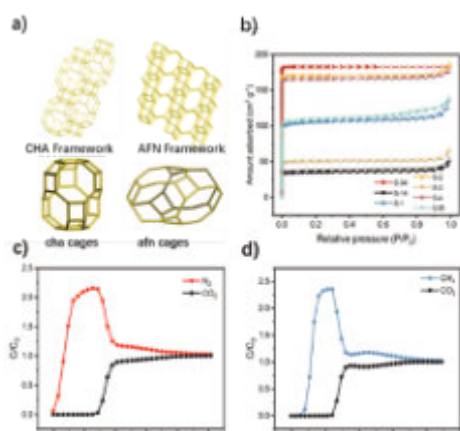


Figure 1. Zeolite structure

Table 1. Gas adsorptions (cm<sup>3</sup> g<sup>-1</sup>) and IAST separations (CO<sub>2</sub>/CH<sub>4</sub>:2/98 CO<sub>2</sub>/N<sub>2</sub>:15/85) at 298 K and 1.0 bar.

Sample	N <sub>2</sub>	CO <sub>2</sub>	CH <sub>4</sub>	α(CO <sub>2</sub> /CH <sub>4</sub> )	α(CO <sub>2</sub> /N <sub>2</sub> )
S-34	4.10	60.27	11.26	11.49	31.53
S-14	2.27	37.26	5.78	22.18	54.36
S-1	2.53	47.24	7.72	21.61	68.64
S-4	3.23	54.07	8.11	20.04	49.22
S-M	3.10	41.94	6.49	19.44	33.39

Figure 1 and Table 1 indicate that SAPO-34 zeolite has a high CO<sub>2</sub> adsorption capacity due to its inherent topological structure, while SAPO-14 zeolite has good CO<sub>2</sub> separation performance for N<sub>2</sub> and CH<sub>4</sub>. N<sub>2</sub> desorption-adsorption isotherms (Figure 1b) indicate that the composite strategy can adjust the pore characteristics and pore size of zeolite, thereby significantly improving gas selectivity. In addition,

the small crystal size and small number of mesopores of composite zeolites also contribute to gas diffusion, which can be used for gas separation. As a result, SAPO-14/SAPO-34 zeolites (S-1) exhibit the comprehensive performance of high CO<sub>2</sub> capacity of SAPO-34 and good selectivity of SAPO-14 due to their appropriate pore structure. At 298 K, the CO<sub>2</sub> capacity of S-1 composite is 47.24 cm<sup>3</sup> g<sup>-1</sup>, giving a high gas selectivity for CO<sub>2</sub>/N<sub>2</sub>. The highly-efficiency and good reproducibility in gas separation are verified by the binary breakthrough experiments (Figure 1c,d). Considering the diverse zeolite structures, we speculate that more composite zeolites with tailoring pores could be prepared by optimizing synthesis methods, and pre-designing and selecting zeolite candidates. The composite zeolites should have great potentials in industrial gas separation.

### References

- [1] R. B. Bai, X. W. Song, W. F. Yan, J. H. Yu, National Science Review, 9 (2022) nwac064
- [2] Y. C. Chai, W. L. Dai, G. J. Wu, N. J. Guan, L. D. Li, Accounts of Chemical Research, 54 (2021) 2894-2904.

### Acknowledgments

This work was supported by the National Key Research and Development Program of China (grant no. 2023YFA1507700) and the 111 Project (B17020).





## Design and synthesis of zeolite-like metal-organic frameworks

B. B. Tang, J. T. Li, X. L. Luo, S. Wang, Y. L. Liu\*

State Key Laboratory of Inorganic Synthesis and Preparative Chemistry, College of Chemistry, Jilin University, Changchun 130012, P. R. China.

yunling@jlu.edu.cn

Zeolite-like metal-organic frameworks (ZMOFs) are a unique subclass of metal-organic frameworks (MOFs) distinguished by their zeolite-like underlying topologies. These distinctive structural features offer significant potential for applications in gas adsorption and separation. However, constructing novel ZMOFs with underlying zeolite topologies remains an ongoing challenge in reticular chemistry [1]. We have used various synthesis strategies, including the use of elaborate secondary building units (SBUs) or supermolecular building blocks (SBBs) including metal-organic squares (MOSs), metal-organic cubes (MOCs) and metal-organic one-dimensional chains. Rationally in the near past, we introduced and explored MOSs as a four-membered ring (4MR) SBU, the most abundant SBU in conventional zeolites with over 80 zeolite structures based on 4MR, for the construction of zeolite-like supramolecular assemblies (ZSAs) [2-4]. Noticeably to access readily functional 4MR MOSs, we employed imidazolecarboxylate-like ligands as bridging linkers due to their potential to present peripheral uncoordinated oxygen centers when chelated to a metal ion in N, O-bis(monodentate) fashion, and bis(monodentate) diamines as capping ligands. It is conceivable that the deliberately exposed amino groups on the terminal ligands provide additional hydrogen bonding sites on the periphery of molecular building blocks. The sole hydrogen bond donor can form predictable and controlled N-H...O hydrogen bonds with the carboxyl oxygen on the ligand, which acts as the only hydrogen bond acceptor, thus facilitating the directional assembly of the ZSA. Indeed, we successfully synthesized ZSA-1 with GIS topology via hydrothermal reaction and ZSA-2 with RHO topology through solvothermal reaction. The variation in topologies resulting from different reaction conditions highlights the potential for obtaining novel MOS materials by adjusting the ratio of water to organic solvent in the reaction medium. Guided by this concept, we synthesized a new type of MOS and two novel ZMOFs with MER and ABW topologies by tuning the water/DMF ratio in the solvent. Additionally, through functional modifications of organic ligands, we successfully introduced a series of functional groups that allowed precise control over pore size and performance, leading to outstanding gas adsorption and separation capabilities for these materials [5].

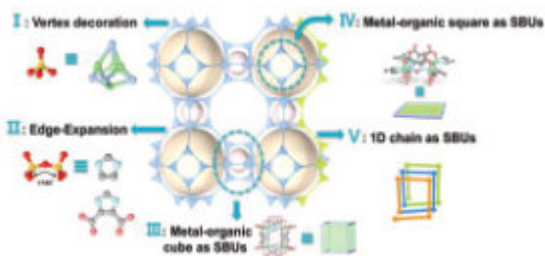


Figure 1. Design and synthesis of zeolite-like metal-organic frameworks through diversified strategies.

Table 1. ZMOFs synthesized using multiple synthesis strategies

Sample	Synthesis strategy	Topology
ZSA-1	SBBs	GIS
ZSA-2	SBBs	RHO
ZSA-3–ZSA-9	SBBs	GIS
ZSA-10	SBBs	MER
ZSA-11	SBBs	ABW
JLU-Liu23	MBBs	UNJ

### References

- [1] M. Eddaoudi, D. F. Sava, J. F. Eubank, K. Adil, V. Guillerm, *Chem. Soc. Rev.*, **44**, 228 (2015).
- [2] S. Wang, T. T. Zhao, G. H. Li, N. J. Guan, L. Wojtas, Q. S. Huo, M. Eddaoudi, Y. L. Liu, *J. Am. Chem. Soc.*, **132**, 18038 (2010).
- [3] X. L. Luo, Y. Cao, T. Wang, G. H. Li, J. T. Li, Y. G. Yang, Z. X. Xu, J. Zhang, Q. S. Huo, Y. L. Liu, M. Eddaoudi, *J. Am. Chem. Soc.*, **138**, 786 (2016).
- [4] J. T. Li, L. Kan, J. Y. Li, Y. L. Liu, M. Eddaoudi, *Angew. Chem. Int. Ed.*, **59**, 19659 (2020).
- [5] J. T. Li, C. Dai, Y. Cao, X. D. Sun, G. H. Li, Q. S. Huo, Y. L. Liu, *J. Mater. Chem. A*, **5**, 21429 (2017).

### Acknowledgments

This work was supported by the National Natural Science Foundation of China (No. 22171100 and U23A20360) and the '111 Center' (B17020).



## New method for creating mesopores in beta zeolite catalysts with hot liquid water

H. Jirglová<sup>1</sup>, E. Tabor<sup>1</sup>, S. Stiborová<sup>2</sup>, J. Dědeček<sup>1</sup>, K. Mlekodaj<sup>1</sup>, P. Klein<sup>1</sup>, V. Tokarová<sup>2</sup>

<sup>1</sup> J. Heyrovský Institute of Physical Chemistry of the CAS, Dolejškova 3/2155, 182 23 Prague, Czech Republic

<sup>2</sup> ORLEN UniCRE a.s., Revoluční 1521/84, 400 01 Ústí nad Labem, Czech Republic

hana.jirglova@jh-inst.cas.cz

### Introduction

Catalytic conversion of biomass and waste materials into platform compounds require the development of active, selective, and stable catalysts that effectively operate in a wide range of liquid-phase reactions. Crystalline microporous aluminosilicates, zeolites are well known as excellent catalysts in refinery and petrochemical processes. However, it was recently shown that zeolites can be considered as promising catalysts for biomass-related reactions [1,2], the main drawback of their application came from transport restrains of large molecules in the microporous channel system of these catalysts. Nevertheless, this obstacle can be overcome by the creation of mesopores in the zeolite crystals. For the mesoporization of zeolites both synthetic and post-synthetic approaches were developed. However, both methods of creating mesoporous zeolites have negative effect on the environment, as they require template removal or involve extensive energy and chemicals usage for desilication or dealumination in post-synthesis treatment. Thus, we were focused on the development of eco-friendly mesoporization method of zeolite based on hot liquid water treatment (HLWT). In this work, we present, simple and environmentally friendly method for the formation of mesopores in \*BEA, which play a crucial role in transport of biomass-based reactants. In the study, <sup>29</sup>Si and <sup>27</sup>Al MAS NMR spectroscopy was employed to uncover the mechanism of mesoporization of studied \*BEA zeolites.

### Results and Discussion

Three H-\*BEA zeolites with Si/Al molar ratio 12, 13 and 19 (denoted as B12, B13, and B19 respectively) were used for the study of the influence of HLWT on their porosity. B13 and B19 samples were commercially supplied (Zeolyst International), in contrast the sample B12, was prepared in the laboratory using template free method described elsewhere [3]. Employment of the samples with similar Si/Al molar ratio obtained using various protocols could help to determine the role of preparation method on the mesoporization mechanism. Parent B12, B13, and B19 zeolites were treated in hot liquid water at 95°C and 180°C for 24h under autogenic pressure to assess hydrothermal stability [4]. After treatment samples were characterized by the combination of XRD, SEM, nitrogen physisorption, FTIR, and <sup>27</sup>Al and <sup>29</sup>Si MAS NMR. XRD and SEM results revealed that the HLWT treatment preserves both \*BEA crystallinity (see Fig.1) and crystal size in all studied samples. Mesopore formation was analyzed using nitrogen physisorption evaluated by NLDFT method. Table 1 gathered the changes in the volume of mesopores in B12, B13, and B19 samples after 24 h HLWT at 95°C and 180 °C.

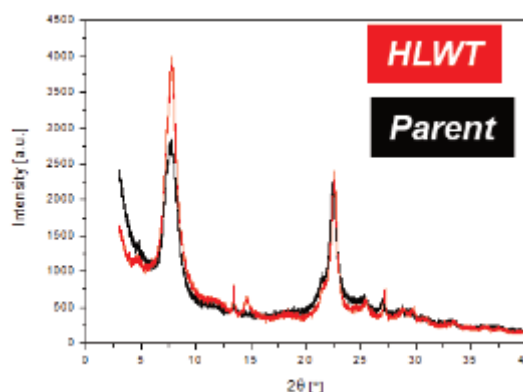


**Figure 1** XRD patterns of B17 zeolite. Black curves corresponds to zeolite before treatment in HLW at 250°C, red after treatment.

**Table 1.** Volume of mesopores in B12, B13, and B19 samples before HTLW treatment and after 24 h HTLW at 95 and 180 °C.

Sample	Mesopores volume, cm <sup>3</sup> /g		
	parent	HLWT at 95 °C for 24h	HLWT at 180°C for 24h
B12	0.489	0.548	0.299
B13	0.670	0.711	0.549
B19	0.190	0.222	0.201

Results presented in Table 1 showed that employment of HWT at 95°C led to increasing of mesopores in all studied \*BEA zeolites. In contrary, treatment at 180 °C decreased the mesopore volume of B12 and B13 and in B19 the small increase of pore volume is observed.



The FTIR study of adsorbed  $d_3$ -acetonitrile on B12, B13, and B19 (before and after HLWT) showed that both Brønsted and Al-Lewis sites were preserved upon HLWT and they are accessible for this probe molecule. Moreover, it was shown that extra-framework Al atoms (25 % of all Al atoms) present in the parent B12, B13, and B19 zeolite were fully removed by HLW treatment. Thus, all observed Al-Lewis sites correspond to the framework Al-Lewis sites. The concentration of Al atoms obtained from FTIR study agrees with the chemical analysis.

Multinuclear  $^{27}\text{Al}$  and  $^{29}\text{Si}$  MAS NMR study of B12, B13, and B19 were employed to analyze the mechanism of the mesopore formation in \*BEA zeolite during HLW. Obtained NMR results confirmed that the first step in the mesopores formation is extraction of extra-framework Al atoms from the channel system. Then leaching of framework Al atoms of \*BEA matrix occurred, this is reflected in the formation of the new type of extra-framework Al species. Next, leaching of Si atoms from the zeolite proceeds, which is not accompanied by the formation of observable extra-framework Si species in the zeolite channel system. Simultaneously, newly formed extra-framework Al species are extracted from the zeolite. Resulting material represent zeolite with channel system free of extra-framework Al and Si species with Si/Al similar to that of the parent zeolite.

Reported procedure of \*BEA zeolites mesoporization using hot liquid water treatment represents one step simple and environmentally friendly (no acids and bases are required) approach to increase mesopores in the zeolite and thus, increasing the accessibility of the active sites embedded in zeolites for larger molecules. Moreover, acid properties (type of acid sites and their concentration) of the parent zeolite are preserved. Moreover, multinuclear NMR study results suggests that this approach is versatile and tunable.

#### References

- [1] P. A. Jacobs, M. Dusselier, B. F. Sells, *Angew. Chem. Int. Ed.*, **53**, 8621 (2014).
- [2] D. Kubicka, I. Kubickova, J. Cejka, *Catal. Rev.*, **55**, 1 (2013).
- [3] K. Mlekodaj, J. E. Olszowka, V. Tokarova, E. Tabor, A. Kasperek, J. Novakova, G. Stavova, O. Gonsiorova, L. Peliskova, J. Brus, R. Pilar, P. Klein, J. Dedecek, *Molecules*, **25**, 15, 3434 (2020).
- [4]. V. Tokarova, S. Stiborova, P. Belecký, J. Dedecek, K. Mlekodaj, *Czech patent application* PV 2023-500 (2023).



## From waste to resources: control over the synthesis and transformation of LTA into NaP zeolites through non-conventional precursors

R. Carrizosa<sup>1</sup>, I. Padilla<sup>1</sup>, M. Romero<sup>1</sup> and A. López-Delgado<sup>1</sup>

<sup>1</sup> Eduardo Torroja Institute for Construction Sciences, IETcc-CSIC. C/ Serrano Galvache, 4, 28033 Madrid, Spain.

[rafael.carrizosa@ietcc.csic.es](mailto:rafael.carrizosa@ietcc.csic.es); [alopezdelgado@ietcc.csic.es](mailto:alopezdelgado@ietcc.csic.es)

Zeolites are low-density crystalline microporous aluminosilicates with a distinctive arrangement of cavities and channels of very specific dimensions. Their three-dimensional structure consists of interconnected tetrahedral lattices of [SiO<sub>4</sub>] and [AlO<sub>4</sub>] linked by oxygen atoms. The micropores of zeolites have a molecular size that confers them with adsorption, catalytic and ion exchange properties of utmost importance both in the industrial chemical field and in the study of new applications associated with green chemistry, lithium-ion batteries, pollutant removal, photovoltaic cells, medicine, gas sensors, animal feed, microreactors, membranes, and construction materials [1].

One of the most widely used zeolite in terms of volume and value is Linde Type A zeolite (LTA or zeolite A) with the general formula Na<sub>12</sub>[(Al<sub>2</sub>O<sub>3</sub>)<sub>12</sub>(SiO<sub>2</sub>)<sub>12</sub>].27H<sub>2</sub>O. On the market, LTA zeolite is mainly employed as a detergent additive. Its high cation exchange capacity allows for the removal of calcium and magnesium ions in a short contact time, thereby reducing water hardness. In addition, the possibility to synthesise zeolite A with a consistent morphology that does not damage textile materials during washing, make it an essential inorganic material for society, with production reaching 73% of total synthetic zeolite market [2].

On the other hand, zeolite P, with general formula Na<sub>6</sub>[(Al<sub>2</sub>O<sub>3</sub>)<sub>6</sub>(SiO<sub>2</sub>)<sub>10</sub>].15H<sub>2</sub>O, belongs to the GIS topological structure and, as in the case of zeolite A, zeolite P shows a high cation exchange capacity, especially for calcium. To date, NaP zeolite has shown high performance in the removal of molecules from gases and liquids, in the treatment of toxic and/or radioactive species from aqueous effluents, and as a water softener in the production of environmentally friendly detergents [3].

Today, there is a growing interest in the research of zeolites based on non-conventional raw materials. Waste-based precursors with a high Si and Al content are a potentially viable and holistic alternative that minimizes landfilling, reduces natural resources exploitation, and mitigates their impact on the environment. In this context, the management of salt slag from the aluminium industry is a worldwide problem. The amount of salt slag resulting from the recovery of secondary aluminium, can vary between 30% and 60% of the metal produced, which along with its hazardousness means that action must be taken on the sustainable management of this waste [4]. On the other hand, diatomaceous earth is a fine sedimentary rock of biogenic origin, consisting mainly of amorphous silica (SiO<sub>2</sub>). It is used as an adjuvant for beer filtration. Diatoms are essential in the brewing industry to remove any turbidity and to clean yeast and other micro-organisms from beer. In addition, they also reduce the iron content of beer, which increases its lifespan without affecting its colour and flavour [5]. When diatomaceous earth has fulfilled its filtering and adsorbing function, it is discarded and stored in landfills.

In search of more integral and eco-friendly solutions to waste management, the valorisation of aluminium salt slag and diatom waste for sustainable zeolite production has been studied. Aluminium salt slag provides the aluminium source, while diatoms provides the silicon needed to complete the stoichiometry of zeolites.

In this way, the controlled synthesis of LTA and NaP zeolites from non-conventional precursors consisting of aluminium salt slag and diatomaceous waste has been accomplished. The synthesis has been carried out by means of a "one pot" hydrothermal process, which incorporates all the wastes without any prior phase dissolution or extraction process. In the case of diatoms, the integration of SiO<sub>2</sub> into the zeolitic structure is favoured by its highly amorphous nature and low content of crystalline SiO<sub>2</sub> phases such as quartz and cristobalite. The influence of temperature, reaction time, and NaOH concentration on the formation of zeolite from salt slag and diatoms has been studied to obtain pure LTA or NaP zeolites or as mixtures with the desired proportions as these conditions are varied.

It was observed that the formation of NaP zeolite occurs at 90 °C, with reaction times longer than 6 h and NaOH concentration higher than 0.6 M. These conditions entail a turning point for the transformation of a LTA zeolite into a NaP zeolite, and a possible mechanism for this transformation has been proposed based on the experimental results. Morphological, structural, textural and chemical characterization of the zeolites obtained have been also carried out.

Figure 1 shows a SEM image of the material obtained by reaction of salt slag and diatoms at 90 °C for 24h, and 1 M NaOH solution, where cubic-shaped crystals characteristic of a zeolitic structure of LTA type are observed embedded within the distinctive "cauliflower" microstructure of NaP zeolite.

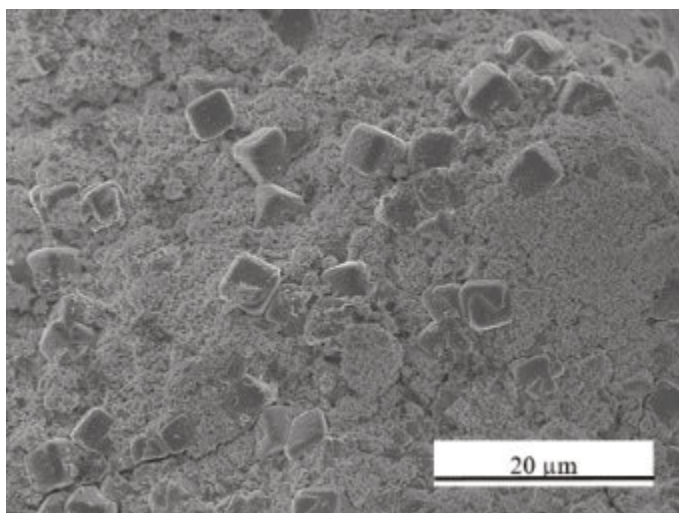


**Figure 1.** SEM micrograph of zeolitic material developed from salt slag and diatoms at 90 °C for 24h, and [NaOH] 1 M.

### References

- [1] K. Margeta, B. Vojnovi, N. Zabukovec Logar, *Recent Pat Nanotechnol*, **5**, 89–99 (2011)
- [2] J. Antúnez-García, D. H. Galván, V. Petranovskii, F. N. Murrieta-Rico, et al. *Comput Mater Sci*, **196** (2021)
- [3] I. O. Ali, S. M. El-Sheikh, T. M. Salama, M. F. Bakr, et al. *Sci China Mater*, **58**, 621–633 (2015)
- [4] I. Padilla, M. Romero, S. López-Andrés, A. López-Delgado, *Sustainability*, **14** (2022)
- [5] J. Seckbach, R. Gordon, *Diatoms: Fundamentals and Applications*, Wiley & Sons (2019)



## Sustainable synthesis of LTA zeolite from industrial hazardous waste: research on SO<sub>2</sub> adsorption efficiency in fixed bed applications

R. Carrizosa<sup>1</sup>, I. Padilla<sup>1</sup>, C. Barco<sup>2</sup>, M. Romero<sup>1</sup>, A. Nieto-Márquez<sup>2</sup> and A. López-Delgado<sup>1</sup>

<sup>1</sup> Eduardo Torroja Institute for Construction Sciences, IETcc-CSIC. C/ Serrano Galvache, 4, 28033 Madrid, Spain.

<sup>2</sup> School of Engineering and Industrial Design, Polytechnic University of Madrid (ETSIDI-UPM). Ronda de Valencia, 3, 28012 Madrid, Spain

[rafael.carrizosa@ietcc.csic.es](mailto:rafael.carrizosa@ietcc.csic.es); [antonio.nieto@upm.es](mailto:antonio.nieto@upm.es); [alopezdelgado@ietcc.csic.es](mailto:alopezdelgado@ietcc.csic.es)

There is growing concern about air pollution and its impact on human health, as it significantly shortens life expectancy worldwide. In recent years, SO<sub>2</sub>, one of the major pollutants that are emitted during the combustion of fossil fuels and the incineration of solid waste, has been found to be widespread in the atmosphere. The increase in SO<sub>2</sub> emissions will lead to a 1.01 % additional mortality risk through the breathing system. Moreover, acid rain caused by deposition of sulphate acids can be harmful to aquatic and terrestrial ecosystems, plants and animals [1]. As a consequence of the accumulation of SO<sub>2</sub> in the atmosphere and the resulting damage caused by acid rain, the concentration of SO<sub>2</sub> in flue gas that is discharged into the atmosphere is currently restricted by federal and state agencies. Mitigation measures may involve significant alterations to existing combustion processes, redesign of equipment and implementation of new technologies to reduce pollutants. In the case of SO<sub>2</sub>, the techniques employed in industry for its removal are mainly based on adsorption or chemical reactions. The abatement of SO<sub>2</sub> emissions by means of different types of adsorbents is of great importance. There are about fifteen different processes that can be applied to remove sulphur dioxide from flue gas generated in combustion operations. In general, these processes are classified into two main groups: wet and dry processes [2].

Zeolite-based technologies for flue gas desulphurisation, which rely on SO<sub>2</sub> adsorption and the catalytic conversion of SO<sub>2</sub> to sulphuric acid have been explored and applied. The SO<sub>2</sub> adsorption capacity of zeolites is attributed to their texture and surface chemical properties, allowing for the design of tailor-made porous materials that provide optimal capture of the pollutant [3]. Zeolites are of significant commercial interest because of their unique properties, including ion exchange, molecular sieving and catalytic abilities. They are a key class of microporous solids used in heterogeneous catalysis, adsorption, gas detachment and ion exchange operations. Zeolites possess excellent physicochemical properties, such as low density with remarkable porosity and permeability, substantial surface area, large volume of molecular cavities and channellings pathways due to their distinctive crystalline structure. They also show a high degree of hydration and substantial physical strength. Compared to metal oxides, SO<sub>2</sub> adsorption on zeolites is less intricate and can be regenerated for multiple cycles once the pores are filled with the pollutant [2].

The stockpiling and management of hazardous industrial waste is another major concern. Some wastes, such as aluminium salt slag, can react with moisture in the environment to form toxic or flammable gases. Others, with high levels of toxic metals, can pollute nearby soil and water, posing serious health and environmental risk. The ultimate solution for managing such waste lies in its valorisation, transforming a hazardous waste with high management cost into materials that are currently in high demand by society. Wastes such as aluminium salt slag, fly ash, paper sludge, kaolin waste, windshield waste, or rice husk ash can serve as precursors in the sustainable synthesis of zeolites. Many of these wastes are a source of aluminium or silicon that can be employed to synthesise specific porous structures.

The zeolitization process from waste involves four stages: Al and Si dissolution, geopolymer formation, crystalline structure nucleation and zeolite crystal growth. Furthermore, the main parameters influencing synthesis are the available contents of Si and Al, temperature, pressure, alkalinity and liquid/solid ratio [4]. The optimisation of these variables enables the development of tailor-made molecular sieves specifically designed to target and remove particular pollutants.

The purpose of this work is to study the efficient adsorption of SO<sub>2</sub> on a Linde-type A (LTA) zeolite synthesised from non-conventional raw materials that include aluminium salt slag and rice husk ash [5]. For comparison, a commercial adsorbent currently used in industry for flue gas purification has also been tested. The studies of kinetics and adsorption isotherms will be used to design a fixed bed reactor where this process can be scaled up.

Figure 1, shows the XRD patterns of the waste-based LTA zeolite and a commercial adsorbent that contains portlandite, calcite and dolomite phases.

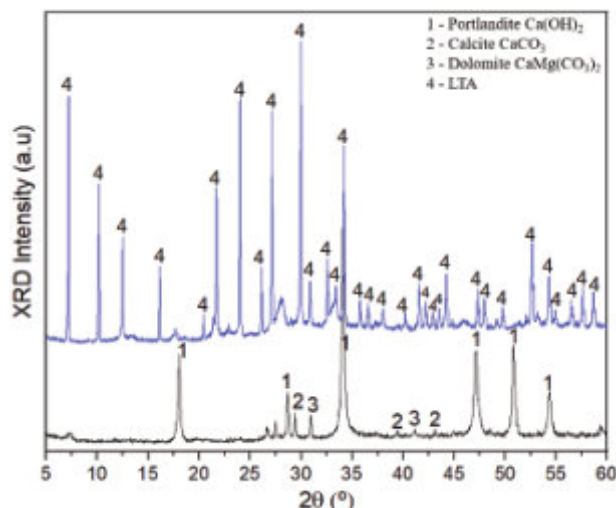


**Figure 1.** XRD patterns of the waste-based LTA zeolite (blue) and a commercial adsorbent (black).

SO<sub>2</sub> adsorption experiments were carried out at 105 °C to simulate the real temperature conditions that may exist in a fume extraction chimney. It was observed that increasing the temperature can compromise the adsorption process. Adsorption of SO<sub>2</sub> was monitored by thermogravimetry, by maintaining a constant temperature and subjecting the adsorbent (LTA zeolite or commercial adsorbent) to a constant concentration of pollutant ranging from 1x10<sup>3</sup> to 1x10<sup>4</sup> ppm.

As time goes by, the adsorption of SO<sub>2</sub> increases, until reaching an equilibrium stage, where the pores are saturated and no additional pollutant can be adsorbed. From this result, SO<sub>2</sub> maximum adsorption capacity of 59.1 mg/g was obtained on the synthesised LTA zeolite at pollutant concentration of 1x10<sup>4</sup> ppm, while for the commercial adsorbent a maximum adsorption capacity of 40.1 mg/g was reached at the same inlet concentration. The kinetic analysis of the uptake curve fitted better to a pseudo-second order model for the two adsorbents. Regarding the equilibrium, the Freundlich model provides the best fit for the LTA zeolite while the Langmuir model fits better for the commercial adsorbent. The experimental data, together with the corresponding fit, are shown in Figure 2.

Equilibrium and kinetic results were applied with the Thomas model to pre-design a fixed bed adsorption column.

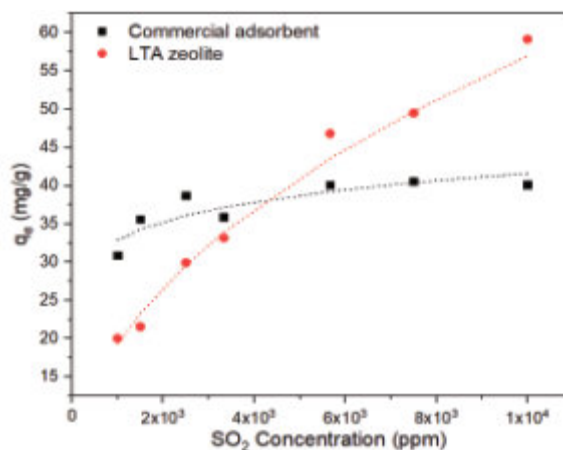


**Figure 2.** SO<sub>2</sub> adsorption isotherms at 105 °C and atmospheric pressure.

## References

- [1] Y. Guo, L. Zhu, X. Wang, X. Qiu, et al. *Science of the Total Environment*, **831** (2022).
- [2] A. Demirbas, *Energy Sources, Part A: Recovery, Utilization and Environmental Effects*, **28**, 1329-1335 (2006).
- [3] Y. Zhu, J. Gao, Y. Li, F. Sun, et al. *J Taiwan Inst Chem Eng*, **43**, 112–119 (2012).
- [4] R. Sánchez-Hernández, A. López-Delgado, I. Padilla, R. Galindo, et al. *Microporous and Mesoporous Materials*, **226**, 267-277 (2016).
- [5] M.T. Ritter, I. Padilla, M.A. Lobo-Recio, M. Romero, A. López-Delgado. Submitted to *Materials*, (2024)



## MONITORING ZEOLITE SYNTHESIS IN *OPERANDO* CONDITIONS: PRACTICAL INSIGHTS AND USE CASES OF FED-BATCH REACTORS

P. Herrero<sup>1</sup>, A. Javdani<sup>1</sup>, G. Ivanushkin<sup>1</sup>, M. Dusselier<sup>1</sup>

<sup>1</sup> Center for Sustainable Catalysis and Engineering (CSCE), KU Leuven, 3001 Heverlee, Belgium  
michiel.dusselier@kuleuven.be

Nowadays the demand for the production of zeolites is increasing due to their wide applications in the fields of industrial catalysis, ion exchange, and adsorption [1]. Multiple efforts have been explored to break the boundaries commonly associated with the synthesis of microporous materials, for instance, major accomplishments usually cover ingredient-based solutions. Among these, the kinetically-driven interzeolite conversion [2] has been employed to shorten synthesis time and obtain frameworks that were hardly achievable due to thermodynamical constraints of the crystallization pathway. Accordingly, since conventional zeolite synthesis often faces limitations, new methods must be developed. Recently, among many interesting approaches, the design and construction of novel nonconventional reactors is gaining attention. These reactors could directly affect the reaction kinetics or alter the physical environment, which leads to obtain final product with different properties. [3]

While, due to the restricted nature of batch reactors the interactions, intermediates and/or mid-synthesis concentration changes cannot be accessed directly, the basic idea of Fed-batch (FB, Fig.1a) reactors is to resolve these limitations by a direct impact on concentration profiles and interactions among compounds, utilizing timed and gradual ingredient feeding during synthesis. In addition, operating the FB reactor's sampling feature, samples could be extracted at operational temperature and pressure along with the synthesis, giving a more accurate picture of crucial crystallization events.

FB reactors can be used for better understanding of the zeolite synthesis parameters evolution such as, temperature, pressure and pH, *in-situ/ex-situ* monitoring (Fig.1b). As a result, an efficient way will be described for building crystallization S-curves from one synthesis only, eliminating inconsistency of experimental results, which arises from running multiple parallel batches or synthesis quenching (i.e., cooling/heating cycles). Having a more accurate picture of zeolite formation will help design systems to synthesize zeolites with modified properties.

In our project, we focus on developing active tools that, contrary to the “black box” of the classic batch approach, facilitate fine-tuned zeolite synthesis, which would allow to add new reagents along the crystallization timeline and simultaneously obtain a better control over the physical environment of the synthesis, including the option to monitor and sample. This will lead to a better understanding of the unknown interactions and gradients, which can determine the kinetics and outcome of zeolite synthesis.

A few cases will be presented of the use of these reactors, one in controlling Sn and Zn content in zeotype synthesis and one on monitoring interzeolite conversion of FAU-to-CHA. [4]

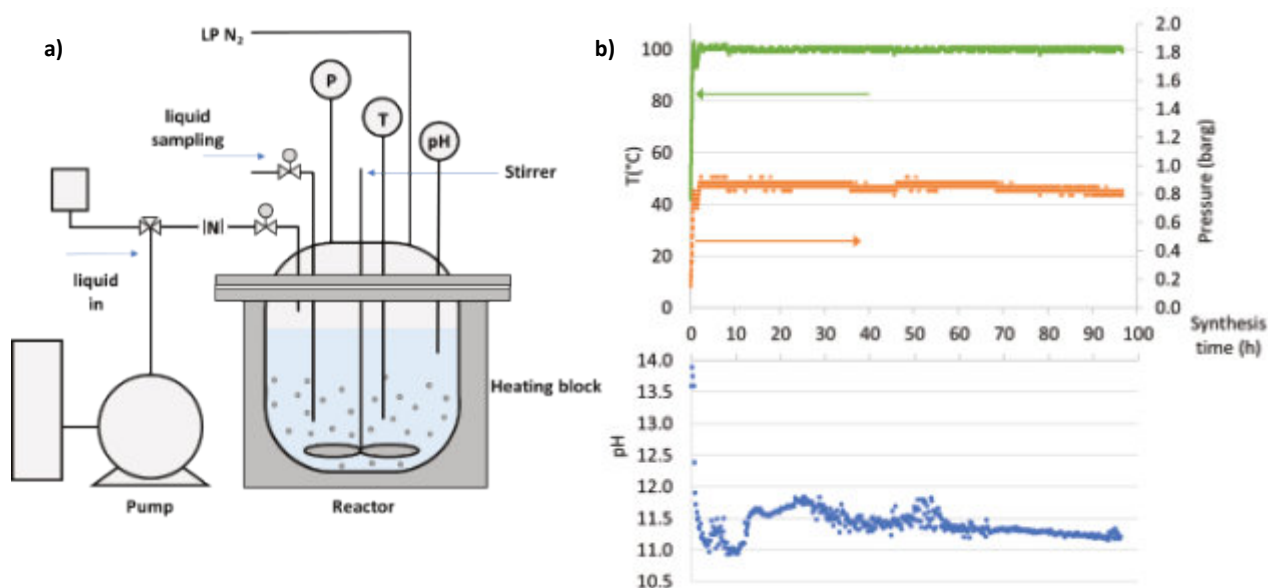


Figure 1 a) Scheme of a Fed-batch system. b) Temperature, pressure and pH profiles along CHA synthesis time





## References

- [1] W. Vermeiren, JP. Gilson, “Impact of Zeolites on the Petroleum and Petrochemical Industry”, *Top. Cat.*, Vol. 52, pp. 1131–1161, 2009, doi:10.1007/s11244-009-9271-8.
- [2] J. Devos, S. Robijns, C. Van Goethem, I. Khalil, and M. Dusselier, “Interzeolite Conversion and the Role of Aluminum: Toward Generic Principles of Acid Site Genesis and Distributions in ZSM-5 and SSZ-13”, *Chem. Mat.*, Vol. 33 (7), pp. 2516–2531, 2021, doi: 10.1021/acs.chemmater.0c04832
- [3] A. Deneyer, Q. Ke, J. Devos, and M. Dusselier, “Zeolite Synthesis under Nonconventional Conditions: Reagents, Reactors, and Modi Operandi,” *Chem. Mater*, Vol. 32, pp. 4884–4919, 2020, doi:10.1021/acs.chemmater.9b04741
- [4] A. Javdani, G. Ivanushkin, A. Deneyer, and M. Dusselier, “Monitoring and controlling zeolite synthesis via reactor-based solutions: A Fed-batch strategy,” *Submitted*, 2024.



## Optimization of the Acidity of Mesoporous Materials for Catalytic Applications

**A. de Diego de Amorím<sup>1,2</sup>, M. Romero Vázquez<sup>2</sup>, S. Armenise<sup>2</sup>.**

*1 University of Alcalá de Henares, Ctra Madrid-Barcelona, 33,600 .28805 Alcalá de Henares (Madrid).*

*2. Innovation Center Cepsa, Av.Punto Com, 1, 28805, Alcalá de Henares, Madrid.*

*aliciadediegodeamorim@gmail.com*

This study focuses on optimizing the acidity of mesoporous materials, specifically mesocellular foams (MCF) and ordered SBA-15 silicas, through sulfonic group functionalization. The primary objective is to assess the effectiveness of these materials as acid catalysts in hydroxyalkylation and carbon-carbon condensation reactions of furanic compounds, with the aim of enhancing biofuel production.

To achieve this goal, two distinct synthesis methods were employed: in-situ sulfonation and ex-situ sulfonation. In both methods, MPTMS (3-mercaptopropyl)trimethoxysilane was used as the sulfonating agent, applied in various molar ratios relative to the silicon in the support (Si). The in-situ method incorporates sulfonation during the catalyst synthesis, while the ex-situ method applies sulfonation to an already synthesized support.

The results obtained through a series of characterization techniques provide detailed insight into how these modifications affect both the acidic properties and the textural characteristics of the materials. To evaluate these properties, nitrogen (N<sub>2</sub>) adsorption/desorption isotherms were used to determine the textural characteristics, while the SBA-15 structure was analysed using low-angle X-ray diffraction. The elemental chemical composition was analysed using X-ray fluorescence, and a CHNS elemental analysis was performed to evaluate the carbon, hydrogen, sulfur, and nitrogen contents, as well as the sulfonation efficiency. Additionally, thermogravimetric analyses in a nitrogen atmosphere and potentiometric titrations were conducted to analyse the acidity of the materials.

**Tabla 1.** Textural Properties and Acidity of Sulfonated MCF and SBA-15 Materials.

Catalyst	Theoretical Si/MPTMS	N <sub>2</sub> Adsorption/Desorption								Acidic titration
		Surface Area, m <sup>2</sup> /g		Pore Volume, m <sup>3</sup> /g			Pore size, nm		Eq H <sup>+</sup> /kg	
		BET	S <sub>meso</sub>	S <sub>micro</sub>	V <sub>t</sub>	V <sub>meso</sub>	V <sub>micro</sub>	BJH <sub>ads</sub>		BJH <sub>des</sub>
MCF	-	733	677	56	1,76	1,74	0,02	11	8	-
MCF-S <sub>ex-situ</sub>	4,0	458	440	18	1,1	1,09	0,01	10	6	1,40
MCF-S <sub>in-situ</sub>	5,0	664	538	126	1,16	1,11	0,05	9	4	1,10
SBA-15	-	559	492	67	1,05	1,03	0,02	7	6	-
SBA-15-S <sub>ex-situ</sub>	4,0	489	453	36	0,94	0,93	0,01	7	6	0,92
SBA-15-S <sub>in-situ</sub>	4,0	572	572	-	1,36	1,36	-	9	8	1,04

In the context of ex-situ sulfonation, the functionalization of MCF with MPTMS resulted in a significant reduction in surface area and pore volume, as evidenced in Table 1. This decrease is attributed to the filling of pores by the sulfonic groups, leading to a shift in pore size distribution towards smaller dimensions and a reduction in adsorption capacity [1-2]. Conversely, in-situ sulfonation exhibited different behavior. Although a reduction in surface area was also observed, as shown in Table 1, this decrease was less pronounced than in the ex-situ case and was accompanied by an increase in micropore area and volume, suggesting a better dispersion of sulfonic groups. The pore size distribution was narrower, indicating more precise control in the formation of smaller pores.

For the ex-situ sulfonated SBA-15 samples, the structural ordering was confirmed by low-angle XRD (data not shown), reflecting a uniform distribution of mesoporous pores (see Table 1). Despite an increase in sulfur concentration, the textural properties did not vary significantly, likely due to surface saturation and limited incorporation of MPTMS. On the other hand, in-situ sulfonated SBA-15 samples showed a significant reduction in XRD peak intensity, indicating a considerable loss of ordering and structural alteration due to the steric hindrance of MPTMS, which disrupts pore regularity.

Regarding acidity, a proportional increase with MPTMS concentration was observed in both cases. However, like MCF, the acid capacity of the ex-situ SBA-15 showed signs of surface saturation, limiting the increase in acidity at higher concentrations. In contrast, in-situ sulfonation resulted in a more pronounced increase in acidity with MPTMS



concentration, reflecting a more complete and efficient oxidation, despite partial condensation due to residuals that limit the accessibility of the oxidizing agent.

TGA data, shown in Figure 1, reveal the presence of two or three mass loss peaks, depending on the synthesis method used. For ex-situ synthesis of both MCF and SBA-15, three distinct peaks are observed: the first at 100°C, associated with the decomposition of water; the second at 350°C, corresponding to the decomposition of thiol groups; and the third at 500°C, related to the decomposition of sulfonic groups. These peaks indicate incomplete oxidation of MPTMS, likely due to the limited accessibility of the oxidizing agent within the pores of the support.

In contrast, in-situ sulfonation of the two materials shows a different behavior, as depicted in Figure 1. Here, two decomposition peaks are observed: one related to water loss and the other to the decomposition of sulfonic groups. This pattern suggests a complete oxidation of MPTMS, facilitated by improved diffusion of H<sub>2</sub>O<sub>2</sub> through the material's channels during synthesis [1].

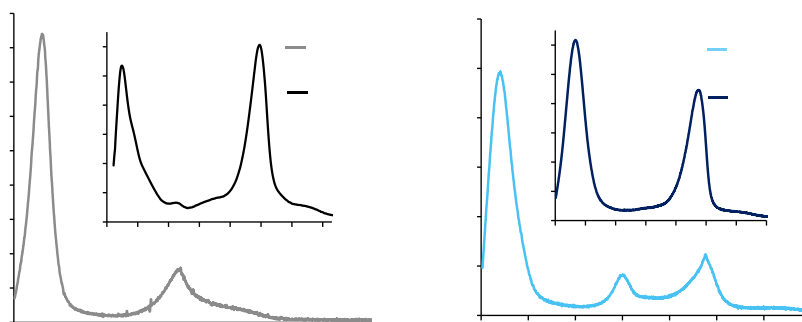


**Figura 1.** Thermogravimetric Analysis (TGA). a) Ex-situ sulfonated MCF. b) In-situ sulfonated MCF. c) Ex-situ sulfonated SBA-15. d) In-situ sulfonated SBA-15.

In conclusion, ex-situ sulfonation for MCF and SBA-15 results in a significant reduction in surface area and pore volume, along with incomplete oxidation of thiol groups, which limits the achievable acidity. In contrast, in-situ sulfonation allows for higher acidity and more complete oxidation, although it may induce some distortions in the porous structure. The choice between these methods should balance the improvement in acidity with the preservation of the mesoporous structure, tailored to the specific requirements of each catalytic application.

#### References:

- [1] Stawicka, K.; Trejda, M.; Ziolk, M. The Production of Biofuels Additives on Sulphonated MCF Materials Modified with Nb and Ta - Towards Efficient Solid Catalysts of Esterification. *Appl Catal A Gen*, **2013**, *467*, 325–334. <https://doi.org/10.1016/j.apcata.2013.07.036>.
- [2] Li, H.; Gui, Z.; Yang, S.; Qi, Z.; Saravanamurugan, S.; Riisager, A. Catalytic Tandem Reaction for the Production of Jet and Diesel Fuel Range Alkanes. *Energy Technology*, **2018**, *6* (6), 1060–1066. <https://doi.org/10.1002/ente.201700637>
- [3] Karaki, M.; Karout, A.; Toufaily, J.; Rataboul, F.; Essayem, N.; Lebeau, B. Synthesis and Characterization of Acidic Ordered Mesoporous Organosilica SBA-15: Application to the Hydrolysis of Cellobiose and Insight into the Stability of the Acidic Functions. *J Catal*, **2013**, *305*, 204–216. <https://doi.org/10.1016/j.jcat.2013.04.024>.



## Investigating the effect of extra-framework aluminum species on (hydro)cracking activity of USY zeolite

S. Askarli<sup>1</sup>, I. Mukhambetov<sup>1</sup>, S. Chung<sup>1</sup>, J. Ruiz-Martínez<sup>1</sup>

<sup>1</sup> Catalysis, Nanomaterials, and Spectroscopy group, Physical Science and Engineering Division, King Abdullah University of Science and Technology, 23955, Thuwal, Saudi Arabia  
sohrab.askarli@kaust.edu.sa

**Introduction.** Extraframework aluminum (EFAl) species generated from hydrothermal treatment (steaming) have been observed to influence the acidity of zeolites [1]. While it has been reported that the presence of these species alters the concentration and strength of Brønsted acid sites (BASs), their impact on hydrocracking – a critical process for producing fuels from heavy petroleum fractions [2] and biomass conversion [3] – requires further investigation.

**Materials and Methods.** Metal component of bifunctional hydrocracking catalyst – 1% Pt/Al<sub>2</sub>O<sub>3</sub> was prepared by incipient wetness impregnation method. Commercially available USY zeolites with SiO<sub>2</sub>/Al<sub>2</sub>O<sub>3</sub> ratios (SAR) of 5, 12, and 30 underwent steaming at 600 °C until they exhibited catalytic activity similar to that of the reference sample ZY60 in hydrocracking of hexadecane and were labeled by their SAR and respective steaming times in hours (e.g., ZY5S7, ZY12S8, and ZY30S4). Acidity of the samples were quantified by Fourier-transform infrared (FTIR) spectroscopy of pyridine adsorption/desorption (Py-FTIR). Intrinsic activity of BAS was addressed by turnover frequency (TOF). The influence of EFAl in proximity to BAS was characterized by solid-state MAS NMR spectroscopy (Bruker 900 MHz wide-bore magnet with AVANCE-III console). The 1D <sup>27</sup>Al direct excitation spectrum was recorded using a <sup>27</sup>Al π/6 hard pulse with a field strength of 170 kHz and 2D <sup>1</sup>H–<sup>27</sup>Al cross-polarization frequency switched Lee-Goldburg heteronuclear correlation (CP FSLG HETCOR) was achieved 3.5 ms contact time at MAS frequency of 20 kHz.

**Results and Discussion.** In our approach, USY zeolites with different SAR were steamed until all of them showed a similar catalytic performance in the hydrocracking of n-hexadecane. This treatment led the samples to have similar BAS content with varying EFAl content. Investigating acidity of the samples, we notice that the total number of BAS obtained by Py-FTIR is directly related to hydrocracking activity (Fig. 1a). On the other hand, although samples have different EFAl number, they have similar TOF (Fig. 1b) in hydrocracking reaction suggesting that catalytic performance in hydrocracking is not influenced by the EFAl species, rather it is solely dependent on the concentration of the BAS.

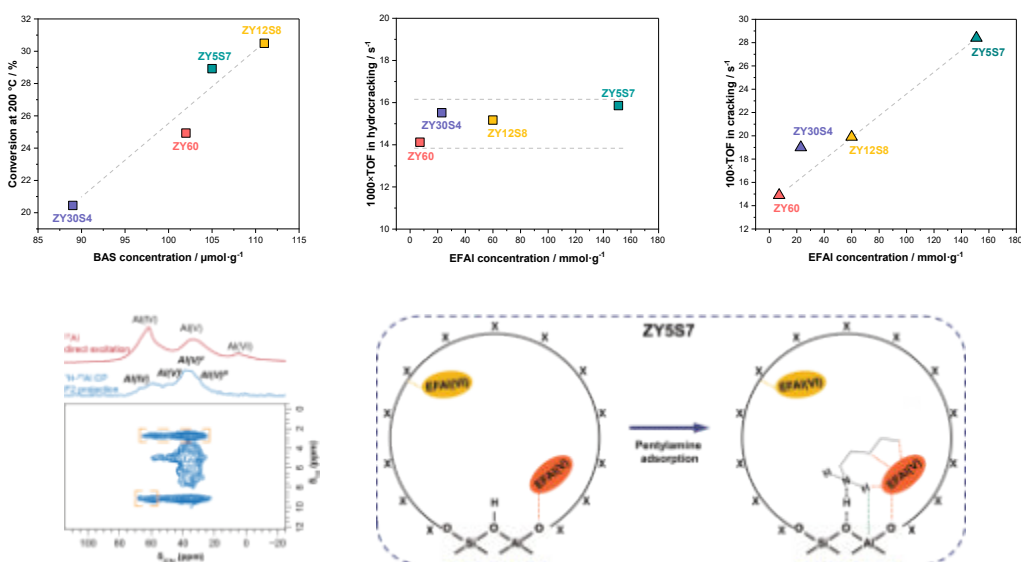


**Figure 1.** (a) Conversion of n-hexadecane at 200 °C plotted against total BAS number by Py-FTIR; TOF of the catalysts in (b) hydrocracking of n-hexadecane and (c) cracking of n-hexane against total number of EFAl sites; (d) <sup>1</sup>H–<sup>27</sup>Al CP FSLG HETCOR NMR results; (e) scheme of interaction of pentylamine protons with Al sites of the sample ZY5S7.

The intrinsic activity of zeolites was also characterized by cracking of n-hexane. High reaction temperature, low partial pressure of n-hexane were applied to ensure that reaction occurred under monomolecular cracking mechanism. In contrast with the hydrocracking reactions, it is observed that TOF results align well with catalytic testing outcomes in



hexane cracking (Fig. 1c). This correlation leads to the conclusion that unlike hydrocracking, the cracking reaction is influenced by the EFAl species located nearby BAS.

The proximity of BAS and EFAl species was investigated through  $^1\text{H}$ - $^{27}\text{Al}$  CP HETCOR NMR spectroscopy of adsorbed pentylamine on reference and most active steamed sample. Results of NMR experiments (Fig. 1d) revealed co-interaction of tetrahedral Al (framework) and pentahedral Al sites with the protons of pentylamine (Fig. 1e) which suggests that EFAl(V) species in close proximity to the Brønsted acid sites. This confirms that the proximity of those two species are influencing cracking reactions but are irrelevant in ideal hydrocracking tests.

## References

- [1] L. Kubelkova, S. Beran, A. Malecka, and V. M. Mastikhin, *Zeolites*, **9** (1), 12-17 (1989).
- [2] J. Weitkamp, *ChemCatChem*, **4** (3), 292-306 (2012).
- [3] K. Murata, Y. Liu, M. Inaba, and I. Takahara, *Catal. Letters*, **140**, 8-13 (2010).



## Formation of active oxygen species over binuclear Fe(II) species in Al-rich \*BEA zeolite

A. Kornas<sup>1</sup>, K. Mlekodaj<sup>1</sup>, E. Tabor<sup>1</sup>, D. K. Wierzbicki<sup>2,3</sup>, R. Pilař<sup>1</sup>, H. Jirglová<sup>1</sup>, S. Sklenák<sup>1</sup>, J. Dědeček<sup>1,4</sup>

<sup>1</sup> J. Heyrovský Institute of Physical Chemistry CAS, Dolejškova 2155/3, 182 23 Prague, Czech Republic

<sup>2</sup> Brookhaven National Laboratory, Upton, NY, 11973, USA

<sup>3</sup> Paul Scherrer Institute, Forschungsstrasse 111, 5232 Villigen PSI, Switzerland

<sup>4</sup> METTOC, Nyklickova 40, CZ15800 Prague, Czech Republic

agnieszka.kornas@jh-inst.cas.cz

### Introduction

A recent study showed that binuclear Fe(II) sites in zeolite of FER topology exhibit the unique ability to split molecular oxygen with the formation of  $\alpha$ -oxygen species [1]. Formed  $\alpha$ -oxygen possesses an outstanding activity in the oxidation of CH<sub>4</sub> already at ambient temperature. Moreover, the products of this reaction were detected in the gas stream without an additional extraction step [2]. According to the current state of the art, to form binuclear sites in the zeolitic matrix, a high population of closely located Al atoms (Al pairs), which stabilize divalent cations, is required, as well as an axial geometry of two the cationic sites distanced by  $\sim 7\text{Å}$  [2,3]. The DFT study predicted that iron cations can form binuclear centers in wide-pore \*BEA [3]. Here, we present the first experimental confirmation of the formation of binuclear iron centers in the Al-rich zeolite matrix of \*BEA topology.

### Experimental

DFT calculations (VASP program), including molecular dynamics, were used to verify the possibility of O<sub>2</sub> splitting over iron centers in zeolite beta. Al-rich \*BEA sample (Si/Al 4.5) was synthesized with the template-free procedure [4]. Fe(II) was introduced to the zeolitic matrix (Fe/Al 0.05) through the impregnation method with an acetylacetonate solution of FeCl<sub>3</sub>/<sup>57</sup>FeCl<sub>3</sub>. To confirm the typical structural parameters for zeolite \*BEA and the exclusive presence of framework Al atoms, X-ray diffraction analysis (XRD) and Nuclear Magnetic Resonance spectroscopy (NMR) were used. Mössbauer and XAS spectroscopies were applied to study the speciation and redox properties of iron sites after the evacuation of the zeolite at 450 °C, interaction with O<sub>2</sub>, and subsequent reaction with CH<sub>4</sub> (as a testing reaction) at 220 °C. Analysis of the products of methane oxidation was carried out with FTIR spectroscopy of the gas phase. The catalytic activity of the sample in CH<sub>4</sub> oxidation was performed at various oxidation times and temperatures in three consecutive redox cycles with mass spectrometry detection of the reaction products.

### Results and discussion

**Table 1.** Mössbauer parameters of iron species in evacuated and with O<sub>2</sub> Al-rich <sup>57</sup>Fe-\*BEA.

<sup>57</sup> Fe-*BEA	IS [mm/s]	QS [mm/s]	Rel. [%]	Fe species
3 h @ 450 °C	0.81	1.09	24	Fe(II) <sub>β</sub>
	1.20	2.10	18	Fe(II) <sub>α</sub>
	0.80	0.60	58	Fe(II) <sub>β</sub>
+ O <sub>2</sub> @ 220 °C	0.37	2.70	6	Fe(III)
	0.90	2.70	35	Fe(II) <sub>α</sub>
	0.41	1.00	59	Fe(IV)=O

Obtained XRD patterns proved that synthesized material exhibits reflexes typical for well-developed \*BEA without impurities. Only one symmetric signal with a shift around 58 ppm in the <sup>27</sup>Al MAS NMR spectrum confirms the exclusive presence of tetrahedrally coordinated Al atoms in an oxygen environment.

Mössbauer's studies of the evacuated Fe-beta (**Table 1**) confirmed the presence of atomically dispersed Fe(II) cations. The doublet, visible in the Mössbauer spectrum of evacuated Fe-\*BEA with the isomer shift (IS) values higher than 0.7 mm/s, confirms the presence of divalent iron. Moreover, the majority of Fe sites (82 %) are characterized by the value of quadrupole splitting (QS)  $\leq 1$ . Interaction of the sample with O<sub>2</sub> leads to the

formation of a subspectrum with Mössbauer parameters characteristic for alpha-O [5]. The in-situ XAS results align with those obtained in Mössbauer spectroscopy and confirm the change of the oxidation state and the geometry of the iron sites embedded in the zeolite matrix. Activity tests revealed the presence of oxidation products, methanol, and CO<sub>2</sub> directly in the gas stream at 220 °C. The stability of the catalyst was confirmed in three consecutive redox cycles. The results of the spectroscopic study and activity tests confirmed the formation of  $\alpha$ -O from O<sub>2</sub> over binuclear Fe(II) centers in the \*BEA zeolite. This contribution presents the first evidence that the formation of binuclear centers is not restricted solely to zeolites of the FER topology.



## References

- [1] K. Mlekodaj, M. Lemishka, A. Kornas, D. K. Wierzbicki, J. E. Olszowka, H. Jirglova, J. Dedecek, E. Tabor, *ACS Catalysis*, **13**, 3345 (2023)
- [2] E. Tabor, J. Dedecek, K. Mlekodaj, Z. Sobalik, P. C. Andrikopoulos, S. Sklenak, *Science Advances*, **6**, eaaz9776 (2020)
- [3] E. Tabor, M. Lemishka, J. E. Olszowka, K. Mlekodaj, J. Dedecek, P. C. Andrikopoulos, S. Sklenak, *ACS Catalysis*, **11**, 2340 (2021)
- [4] R. Pilar, J. Moravkova, G. Sadovska, S. Sklenak, L. Brabec, J. Pastvova, P. Sazama, *Microporous and Mesoporous Materials*, **333**, 111726 (2022)
- [5] B. E. R. Snyder, P. Vanelderen, M. L. Bols, S. D. Hallaert, L. H. Bottger, L. Ungur, K. Pierloot, R. A. Schoonheydt, B. F. Sels, E. I. Solomon, *Nature*, **536**, 317 (2016)

## Acknowledgments

Optional section. – Calibri 8 pt justified



## YFI-type titanosilicate with hierarchical pore-structure for efficient selective oxidations

S. Zhang<sup>1</sup>, S. Inagaki<sup>1</sup>, Y. Kubota<sup>1,\*</sup>

<sup>1</sup> Division of Materials Science and Chemical Engineering, Yokohama National University, 79-5 Tokiwadai, Hodogaya-ku, Yokohama 240-8501, Japan  
kubota-yoshihiro-sr@ynu.ac.jp

Hierarchical titanosilicate catalyst [Ti]-YNU-5\_h was prepared from large-pore YFI-type zeolite after stepwise post-synthesis treatments. Mesopores were successfully generated by desilication, which introduced the hierarchical pore-structure in the YFI framework. Ti-incorporation was carried out by vapor-phase TiCl<sub>4</sub> treatment. The novel catalyst showed excellent catalytic performance for cycloalkene epoxidations using hydrogen peroxide as an oxidant.

### Introduction

Microporous titanosilicates, with tetra-coordinated Ti species in highly crystalline zeolite framework, are a class of unique heterogeneous catalysts for the green and sustainable oxidation using hydrogen peroxide as an oxidant [1,2]. In recent years, titanosilicates with multidimensional large-pore such as [Ti]-MCM-68 and [Ti]-beta have been found to be good catalysts for selective oxidation reactions [3,4]. The large-pore zeolite YNU-5 with novel YFI framework has been first synthesized by our research group [5]. Figure 1 shows the schematic illustration including the pore-structure of YFI framework. The framework has been found stable and further stabilized via Si-migration [6]. [Ti]-YNU-5 is expected to be a new type of titanosilicate catalyst due to its unique pore-structure [7]. However, the diffusion constraints tend to be the main concern in epoxidation of cycloalkenes over microporous titanosilicate catalysts including the [Ti]-YNU-5. In detail, mass transport of substrates with a size equivalent to a 12-membered ring micropore diameter to and from the active sites located within the micropores of conventional zeolite is slow. To overcome this problem, introducing hierarchical pore-structure and nanoparticulation can be considered as effective strategies. Because of the narrow synthesis window of YFI, the simple and low-cost post-synthesis methods like desilication [8] have more advantages than direct synthesis methods by various templates and nanoparticulation. Furthermore, desilication has been proved to be effective strategy to create hierarchical pore-structure in YFI [9].

In this work, we focused on the preparation of hierarchical YFI-type titanosilicate denoted as [Ti]-YNU-5\_h by stepwise post-synthesis treatments for the purpose of improving its catalytic performance for epoxidation of cycloalkenes.

### Experimental

To obtain hierarchical titanosilicate [Ti]-YNU-5\_h, zeolite [Al]-YNU-5 was hydrothermally synthesized using dimethyldipropylammonium (Me<sub>2</sub>Pr<sub>2</sub>N<sup>+</sup>) and FAU-type zeolite as an organic structure-directing agent (OSDA) and a starting material, respectively [5,6]. The typical mixture gel with a molar composition of 0.275 SiO<sub>2</sub> (from FAU) – 0.725 SiO<sub>2</sub> (from colloidal silica) – 0.025 Al<sub>2</sub>O<sub>3</sub> (from FAU) – 0.17 Me<sub>2</sub>Pr<sub>2</sub>N<sup>+</sup>OH<sup>-</sup> – 0.15 NaOH – 0.15 KOH – 7.5 H<sub>2</sub>O was crystallized at 160°C for 96 hours. As-synthesized sample was calcined at 550°C for 6 h to remove the OSDA. Then the calcined sample was desilicated by base-treatment, deeply dealuminated by acid-treatment (twice), treated with vapor-phase TiCl<sub>4</sub> at 600°C for incorporating Ti into framework, and thermally treated at 650°C for 6 h. [Ti]-YNU-5 without hierarchical pore-structure was obtained by omitting only the base-treatment in the above method. TS-1, [Ti]-MCM-68 and [Ti]-beta were used for comparison.

Epoxidation reaction was carried out by stirring a mixture of cycloalkene (cyclohexene or *cis*-cyclooctene), 30 wt% H<sub>2</sub>O<sub>2</sub>(aq), catalyst, and solvent (MeCN) in a glass pressure tube at 60°C for 120 min. The reaction mixture was analyzed by GC (FID). The amount of remaining H<sub>2</sub>O<sub>2</sub> was quantified by titration using aqueous Ce(SO<sub>4</sub>)<sub>2</sub> solution.

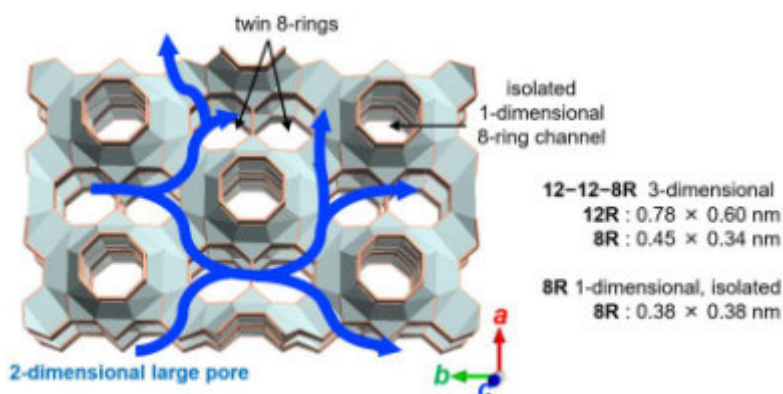


Figure 1. The schematic illustration emphasizing the pore-structure of the YFI





## Results and Discussion

Powder XRD revealed that all prepared samples retained the **YFI** framework. The nitrogen adsorption-desorption isotherms of the samples are shown in Figure 2. Base-treated YNU-5 and [Ti]-YNU-5<sub>h</sub> exhibited significant hysteresis loops, indicating the presence of mesopores within a certain range. The adsorption branch of the samples was type-I(b), suggesting that micropores were intact or slightly expanded. In the DR/UV-vis spectrum of [Ti]-YNU-5<sub>h</sub>, a peak assignable to the tetra-coordinated Ti(OSi)<sub>4</sub> species of the closed site was observed near 210 nm.

Figure 3 shows the results of cyclohexene epoxidation and *cis*-cyclooctene epoxidation. Compared with the non-hierarchical [Ti]-YNU-5 and other conventional titanasilicate catalysts, the use of [Ti]-YNU-5<sub>h</sub> catalyst gave the desired epoxide products in higher yields and also increased turnover number of the Ti active sites. It is worth noting that in the epoxidation of cyclooctene over [Ti]-YNU-5<sub>h</sub>, yield of cyclooctene oxide and turnover number were obviously increased, which were much higher than other titanasilicate catalysts.

## Conclusion

Hierarchical **YFI**-type titanasilicate [Ti]-YNU-5<sub>h</sub> was successfully prepared through stepwise post-synthesis treatments. [Ti]-YNU-5<sub>h</sub> exhibited superior catalytic performance over conventional titanosilicates and non-hierarchical [Ti]-YNU-5 in the epoxidation of cycloalkenes. This can be attributed to the introduced hierarchical pore-structure by desilication, which effectively improved the diffusion of substrates from the liquid phase to the Ti active sites in the 12-ring micropore channels of the **YFI** framework.

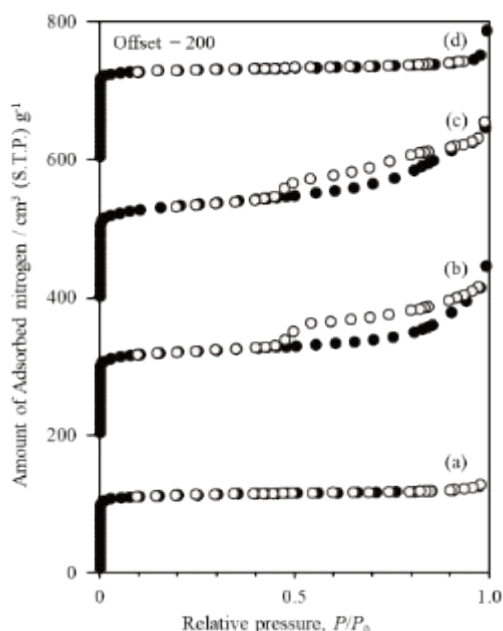


**Figure 2.** Nitrogen adsorption-desorption isotherms ( $-196^{\circ}\text{C}$ ) of (a) calcined YNU-5, (b) base-treated YNU-5, (c) [Ti]-YNU-5<sub>h</sub> derived from sample (b), and (d) [Ti]-YNU-5 derived from sample (a).

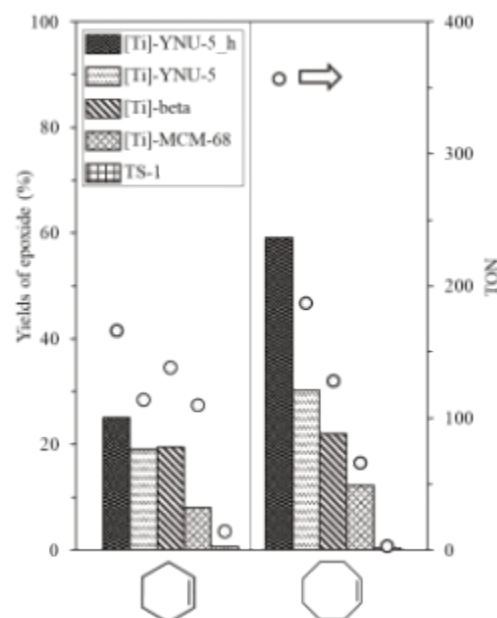


**Figure 3.** Yields of epoxide and turnover numbers for the epoxidations of cyclohexene and *cis*-cyclooctene over various titanasilicate catalysts.

## References

- [1] B. Notari, *Adv. Catal.*, **41**, 253 (1996).
- [2] T. Tatsumi, *Curr. Opin. Solid State Mater. Sci.*, **2**, 76 (1997).
- [3] S. Inagaki, Y. Tsuboi, M. Sasaki, K. Mamiya, S. Park, Y. Kubota, *Green Chem.*, **18**, 735 (2016).
- [4] S. Inagaki, M. Takeyama, K. Asanuma, Y. Yokose, S. Zhang, T. Okuda, K. Nakamura, Y. Nishi, Y. Kubota, *Micropor. Mesopor. Mater.*, **346**, 112323 (2022).
- [5] N. Nakazawa, T. Ikeda, N. Hiyoshi, Y. Yoshida, Q. Han, S. Inagaki, Y. Kubota, *J. Am. Chem. Soc.*, **139**, 7989 (2017).
- [6] N. Nakazawa, Y. Yoshida, S. Inagaki, Y. Kubota, *Micropor. Mesopor. Mater.*, **280**, 66 (2019).
- [7] S. Zhang, K. Asanuma, S. Inagaki, Y. Kubota, *Chem. Lett.*, **53**, upae130 (2024).
- [8] M. Ogura, S. Shinomiya, J. Tateno, Y. Nara, M. Nomura, E. Kikuchi, M. Matsukata, *Appl. Catal., A*, **219**, 33 (2001).
- [9] Q. Liu, R. Sugimoto, S. Inagaki, Y. Kubota, *Chem. Lett.*, **50**, 1725 (2021).



## Production of jet-fuel precursors from volatile fatty acids using TiO<sub>2</sub> zeolitic supported catalysts

**A. Lago<sup>1,2</sup>, L. Bertin<sup>3</sup>, G.A. Martinez<sup>3</sup>, J. De Maron<sup>4</sup>, T. Tabanelli<sup>4</sup>, F. Cavani<sup>4</sup>, C. González-Fernández<sup>2,5,6</sup>, D.P. Serrano<sup>1,7</sup>, I. Moreno<sup>1,7</sup>**

<sup>1</sup>Thermochemical Processes Unit, IMDEA Energy, Avda. Ramón de la Sagra 3, 28935, Móstoles, Madrid, Spain.

<sup>2</sup>Biotechnology Processes Unit, IMDEA Energy, Avda. Ramón de la Sagra 3, 28935, Móstoles, Madrid, Spain.

<sup>3</sup>Department of Civil, Chemical, Environmental and Materials Engineering (DICAM), University of Bologna, Via Terracini 28, 40131 Bologna, Italy.

<sup>4</sup>Department of Industrial Chemistry "Toso Montanari" and Center for Chemical Catalysis-C3, Università di Bologna, Viale del Risorgimento 4, 40136 Bologna, Italy

<sup>5</sup>Department of Chemical Engineering and Environmental Technology, School of Industrial Engineering, University of Valladolid, Dr. Mergelina, s/n, Valladolid, 47011, Spain

<sup>6</sup>Institute of Sustainable Processes, Dr. Mergelina, s/n, Valladolid, 47011, Spain

<sup>7</sup>Chemical and Environmental Engineering Group, ESCET, Rey Juan Carlos University, 28933, Móstoles, Madrid, Spain

[adrian.lago@imdea.org](mailto:adrian.lago@imdea.org)

In recent years, the use of air transport has increased steadily. Between 2005 and 2019, the number of flights from airports in the European Union increased by 15% and the distance flown almost doubled, resulting in a significant increase in CO<sub>2</sub> emissions from the aviation sector, which increased by around 34% [1]. To achieve the decarbonization of the aviation sector, the European Commission has proposed a mandate requiring aviation fuels to contain at least 63% Sustainable Aviation Fuel (SAF) by 2050 [1].

Anaerobic digestion (AD) has proven to be an effective technology for recovering high value products from organic wastes such as agricultural and forestry residues, municipal solid waste, wastewater sludge, etc. By manipulating the operating conditions of the process, an effluent rich in volatile fatty acids (VFAs) including acetic, butyric and hexanoic acids can be produced. These VFAs are considered platform molecules for the production of renewable jet fuels. To meet the key operational property specifications, such as freezing point, viscosity and flash point, SAF must consist predominantly of linear alkanes with a carbon chain length between 8 and 15 carbon, centred around C<sub>11</sub> [2]. VFAs can be converted to n-alkanes by ketonization followed by a hydrodeoxygenation process of the resulting ketones. While ketonization has been extensively studied for short-chain VFAs such as acetic and propionic acids, it has been less investigated for longer-chain VFAs such as butyric and hexanoic acids [3]. Metal oxide catalysts, such as TiO<sub>2</sub>, ZrO<sub>2</sub>, and CeO<sub>2</sub>, have been the most widely used for this reaction due to their amphoteric nature, which provides both acidic and basic Lewis sites. However, these oxides have low specific surface areas, which can limit their catalytic performance [4]. Therefore, their deposition on porous supports could be of great interest. In this context, the ketonization of long-chain VFAs, especially hexanoic acid (HA), over multifunctional catalysts based on TiO<sub>2</sub> supported on different zeolitic materials has been studied in this work.

Firstly, a screening of different zeolites with moderate acidity ( $[\text{Si}/\text{Al}]_{\text{MOL}} \sim 40$ ) was performed to identify the support that best promotes the production of 6-undecanone by means of synthetic hexanoic acid ketonization. For this purpose, TiO<sub>2</sub> was supported on different commercial zeolites: a ZSM-5 nanocrystalline zeolite (n-ZSM-5, Clariant), a beta zeolite (H-B, Clariant), and a USY zeolite (Zeolyst) with an active phase loading of 15 wt%. As a reference, a pure commercial TiO<sub>2</sub> (Aeroxide P25, Aldrich) was also tested using the same amount of sample as that loaded on the zeolitic catalysts. The ketonization experiments were carried out in a fixed bed reactor with a contact time of 0.5 s at a temperature of 375 °C and a total time of stream (TOS) of 5 h. In addition, catalytic ketonization experiments were performed with the bare zeolites. The hexanoic acid conversions, 6-undecanone selectivities and C-molar yields are shown in Figure 1 A, B and C, respectively.

Commercial TiO<sub>2</sub> exhibited 100% selectivity towards the target product (6-undecanone), but low conversion (~ 15%), leading to a low carbon yield of this compound. Higher conversions were obtained using the bare zeolites as catalysts during the first two hours of TOS, although these values decrease rapidly over the reaction time, indicating a significant catalyst deactivation. Moreover, the selectivity towards 6-undecanone with the parent zeolites was very limited, producing mainly aromatic hydrocarbons (toluene, xylenes and C<sub>9</sub>-branched aromatics) and gases. This effect was attributed to the presence of Brønsted acid sites on the raw supports that catalyze the aromatization of ketone and/or hexanoic acid and cracking reactions. These Brønsted acid sites seem to be deactivated along the TOS, favouring the production of 6-undecanone. This effect was especially marked in the case of ZSM-5 zeolite.

The incorporation of TiO<sub>2</sub> as active phase attenuated the Brønsted acidity of the zeolite and increased the Lewis acidity of the resulting catalysts, improving, in all cases, the production of 6-undecanone compared to the raw supports. In addition, the deactivation rate was much lower for TiO<sub>2</sub> supported materials. Interestingly, the use as supports of these zeolitic materials also exceeded the catalytic activity of the commercial TiO<sub>2</sub> sample, revealing that a better dispersion of the active phase favours both conversion and selectivity towards the target product. Among



these catalysts, the highest 6-undecanone production was obtained over  $\text{TiO}_2/\text{H}\beta$ , showing a relatively high conversion, around 55 %, with a selectivity above 70 %.

Considering the remarkable catalytic behaviour of  $\text{TiO}_2/\text{H}\beta$ , ketonization was tested with hexanoic acid produced in a real anaerobic digestion process. This stream is mostly composed of hexanoic acid (91.5 wt%) and minor proportions of butyric (5.8 wt%) and valeric acids (1.6 wt%), previously separated from water by the procedure described elsewhere [5]. To optimize the production of 6-undecanone, the reaction temperature was increased from 375 to 400 °C using a TOS of 18 h (Fig. 1D). Under these conditions, the conversion of hexanoic acid increased to 90 %, slightly decreasing to 80 % along TOS, while the selectivity remained almost constant at values of 65 %, after 2 h of TOS. In addition, a small proportion of 5-nonanone (selectivity ~6%) was observed, derived from the cross-ketonization of hexanoic and butyric acids. These results denoted a high tolerance against deactivation of the  $\text{TiO}_2/\text{H}\beta$  catalyst, resulting in a constant C-molar yield of 6-undecanone.

In summary, it can be concluded that  $\text{TiO}_2$  deposition on zeolitic supports had beneficial effects for the production of 6-undecanone from hexanoic acid, sharply improving both the conversion and yield of the targeted product when compared to pure  $\text{TiO}_2$ . Among the catalysts tested,  $\text{TiO}_2/\text{H}\beta$  showed the best catalytic performance and high potential for ketonization of VFAs derived from real biological streams.

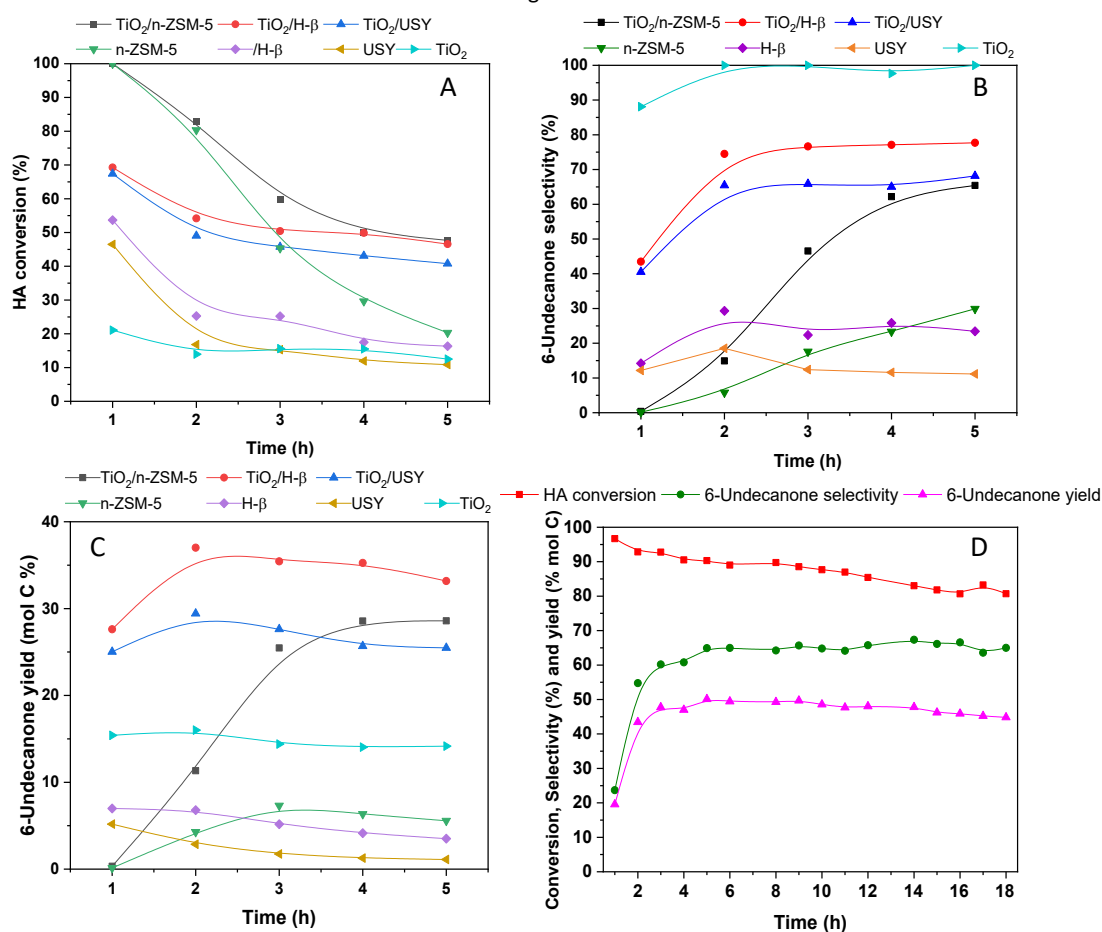


**Figure 1.** Commercial hexanoic acid ketonization over  $\text{TiO}_2/\text{zeolitic}$  catalysts: A) hexanoic acid conversion, B) selectivity towards 6-undecanone and C) 6-undecanone yield and D) Biological hexanoic acid ketonization over  $\text{TiO}_2/\text{H}\beta$  catalyst

## References

- [1] European Union Aviation Safety Agency, European Aviation Environmental Report 2022.
- [2] J. H. Miller, G.R. Hafenstine, H. H. Nguyen, and D. R. Vardon *Ind. Eng. Chem. Res.* 61 (2022) 2997–3010.
- [3] B. Boekaerts, B.F. Sels, *Appl. Catal. B Environ.* 283 (2021) 119607.
- [4] Q. Yu, Y. Guo, X. Wu, Z. Yang, H. Wang, Q. Ge, X. Zhu, *ACS Sustain. Chem. Eng.* 9 (2021) 7982–7992.
- [5] V. D'Ambrosio, G. Martinez, E. Jones, L. Bertin, C. Pastore, *Sep. Purif. Technol.* 309 (2023) 123100.

## Acknowledgments

Grant PRE2020-094485 funded by MICIU/AEI/10.13039/501100011033 and by “ESF Investing in your future”. J. De Maron, T. Tabanelli and F. Cavani acknowledge funding from the European Commission, NextGenerationEU – Piano Nazionale di Ripresa e Resilienza (PNRR) - Ministero dell’Università e della Ricerca (MUR); (project number PE\_00000021).



## Investigation of zeolitic Aluminum by Low-Temperature Template Oxidation with Ozone

**J. Devos, M. Dusselier**

Center for Sustainable Catalysis and Engineering (CSCE), KU Leuven, Celestijnenlaan 200F, B-3001 Leuven, Belgium.  
julien.devos@kuleuven.be

### INTRODUCTION

In this work,[1] we focus on the role of the thermal activation on zeolitic acid site and its local arrangement. Zeolites are versatile materials not only in crystal lattice, but also due to the variety of acidic features given the presence of defect sites, amorphous fractions, acidic silanols, external surface, etc... The acidic features sites can be tuned from selection of synthetic conditions and the consecutive (hydro-)thermal activation it is subjected to. Ozonation enables template (organic structure directing agent) oxidation at low temperatures (100-200 °C), and thus effectively a very wide thermal activation range for acidity tuning, previously inaccessible for OSDA-containing high Si zeolites. Ozonation allows acidity tuning within the first/most step of `activation`, which makes it a straightforward novel strategy to functionalize zeolites to application. Furthermore, it allows for an OSDA-deconvoluted study of acid site evolution in high Si materials.

### EXPERIMENTAL

Zeolites (SSZ-13; CHA) are synthesized using hydrothermal crystallization methods, in line with earlier work [2-3] using batch composition: 1Si:0.0667Al:0.35SSDA<sup>+</sup>:0.35OH<sup>-</sup>:15H<sub>2</sub>O. Crystalline CHA resulting from synthesis is labelled 'n/μ-CHA[Si/Al<sub>B</sub>]' The prefix n- or μ- is used reflecting two different synthesis methods yielding either nanosized (n-) or microsized (μ-) crystals. Either conventional `muffle oven` calcination (≥500 °C, i.e. high temperature activation) or low-temperature `ozonation` is applied on the investigated materials (at 175 °C). An optimized `ozonation` method is applied according to our earlier work [4]: as-made SSZ-13 (CHA; 250-500mg) is placed in a porcelain disk (`boat`) in shallow bed configuration. The oven is heated to 175°C and ~90 μg O<sub>3</sub>/ml of oxygen is flown at 90 ml/min for 24 h. Detemplation was verified using elemental (CN) analysis, TGA, P-XRD and N<sub>2</sub> physisorption and the materials were further analyzed via ICP-AES, P-XRD, SS NMR, ex-situ FT-IR (after activation) and in-situ FT-IR (activation inside the cell, with CO probing) and finally aqueous Co<sup>II</sup>-exchange (DCC) for acid site (Al) distribution estimations.

### RESULTS & DISCUSSION

Well-defined SSZ-13 (CHA) was synthesized with control over the chemical and textural properties. Both nanosized n-CHA[15] and microsized μ-CHA[15] were subjected to thermal activation, either via ozonation (at 175 °C) or to classic muffle oven calcination at several temperatures (200-750 °C). Ex-situ acidity measurements including <sup>27</sup>Al MAS NMR and FT-IR spectroscopy draw a picture on the evolution of Al speciation upon the incremental temperature activation. The thermal activation of ozonated zeolites was mimicked successfully in-situ by adding a portion (10Torr) of water to the FT-IR cell. The in-situ spectra match the ex-situ FTIR experiments and allow for CO probing at incremental activation temperatures from 300 to 650 °C. Figure 1 shows ex-situ <sup>27</sup>Al NMR and in-situ CO-probed FTIR data versus its maximum activation temperature. From the analysis of IR-bands and CO-related shifts, an overall sequence of events is proposed for the thermal evolution of acid sites, involving silanol condensation, high Brønsted acid site (BAS) depletion and a limited extent of Lewis acid site (LAS) formation. The same order of events is found for μ-CHA[15], although the temperature required for these changes are slightly higher (less than 50 °C higher), suggesting that the smaller n-CHA[15] is more prone to (framework Al) degradation.

Co<sup>2+</sup> cation exchange is used to probe acid site proximity and Al speciation. We found out that the extent of Co<sup>2+</sup> exchange (or DCC, divalent cation capacity) is strongly dependent on the applied (maximal) activation temperature. Figure 1 demonstrates a strong dependence of DCC on activation temperature of n-CHA[15] (pink stars), especially in the range of typical calcination temperatures (550-600 °C). Figure 1 also shows very strong correlation between DCC and strong framework BAS descriptors such as tetrahedral Al (4Al<sub>NMR</sub>) and FTIR (ν(OH---CO)<sub>BAS</sub>) above 500 °C. The decrease in BAS is not replenished by an equivalent amount of LAS, suggesting that majority of acid (Al) functions is just depleted upon thermal activation.

At temperatures below 500 °C (i.e. pivotal value), the strong BAS contributions have seemingly constant values, suggesting no change in (strong) BAS until reaching this temperature. Nonetheless, DCC (pink) is decreasing in this temperature range. The latter suggests the interaction between exchanged cobalt and defective sites (`transitory Al`), cfr. the work of Lee *et al.*[5] In contrast to n-CHA[15], μ-CHA[15] shows a very low DCC in all cases (Co/Al >0.05). Hence, synthetic conditions still remain the main cause of DCC alterations. Also note that record high `DCC` found after ozonation treatment is generic. Record high DCC and similar DCC-temperature trends were also found for other ozonated zeolitic materials such as BEA and MFI.

High multivalent cation exchange capacity suggests that ozonated materials are promising candidates for several applications. For example, as host materials for metal-zeolite catalysts (redox chemistry), given the high exchange



capacity, or for post-synthetic treatments such as 'metal healing'. Furthermore, we demonstrated the value of ozonated materials in low-temperature catalysis applications. Ozonated MFI[40] was used as dehydration catalyst in a tandem with ZnZrOx (performing CO<sub>2</sub> hydrogenation to methanol first) and proved to yield DME much more selectively than conventionally calcined zeolites.

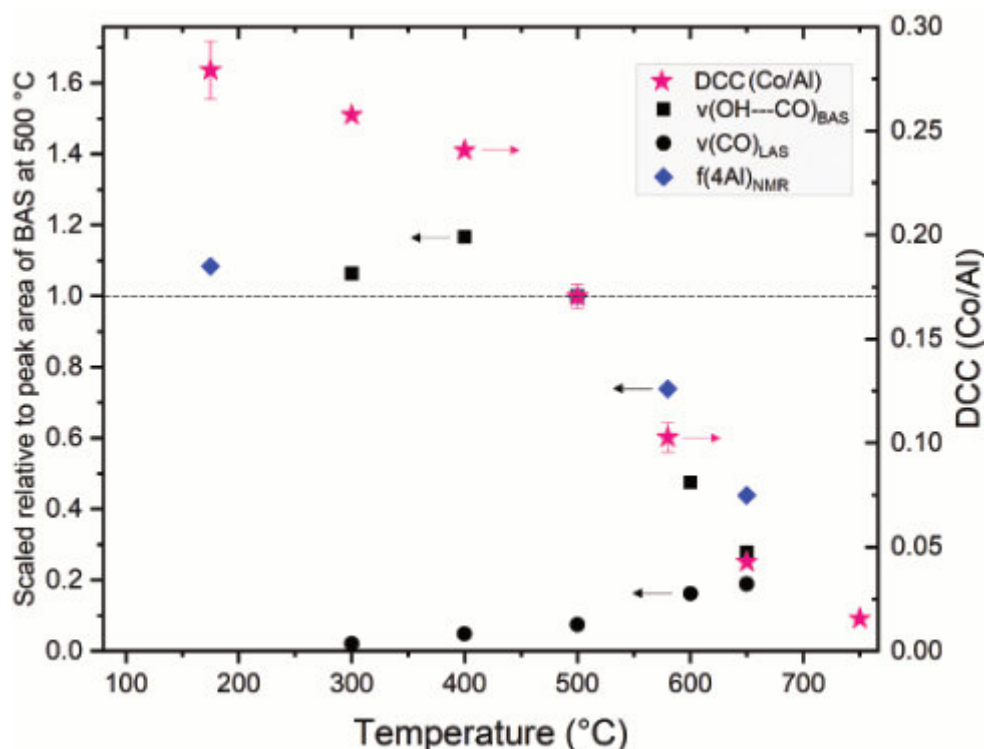


**Figure 1.** DCC (divalent cation capacity, from Co<sup>II</sup> exchange) in function of activation temperature of n-CHA[15] (pink stars; right axis). A variety of acid site quantification are referenced against pivotal values at 500 °C (left axis): FTIR (squares; v(OH---CO)<sub>BAS</sub> = quantified at 3300 cm<sup>-1</sup>; circles v(CO)<sub>LAS</sub> = quantified at 2200cm<sup>-1</sup> versus ) and from NMR (blue; 4Al at 56 ppm).

## CONCLUSIONS

The presented work [1] investigates the acidity upon heating of ozonated zeolites. We demonstrate that ozonation in combo with heating below 500 °C maintains the strong Brønsted acidity potential and produces virtually no Lewis acidity. In contrast, dealumination is unavoidable under conventional calcination conditions (≥550 °C), especially for small-crystals of SSZ-13.

Also thanks to ozonation, we can disentangle OSDA removal and thermal activation, enabling characterization such as CO-FTIR on OSDA-synthesized (high silica) zeolite activated at temperatures below 550 °C. This opens insight on the complex acidity evolution of zeolites in the low-temperature activation range (300-650 °C).

It seems that ozonation preserves the acidity features and Al distributions that stems from crystallization, hence it is informative regarding our knowledge of synthesis and to find synthesis–structure–activity relationships (we cover this topic in several ACS contributions).[2-3] Consideration of thermal activation could significant advance rational bottom-up design of zeolites (from synthesis to application).

Application potential was demonstrated via DCC, as well as via CO<sub>2</sub> hydrogenation to dimethyl ether.

## References

- [1] J. Devos , V. Sushkevich, I Khalil, S Robijns, R de Oliveira-Silva, D. Sakellariou, J. van Bokhoven, M.Dusselier, *J. Am. Chem. Soc.*, **X**, XXXXX-XXXXX 2024. *just accepted*,
- [2] J. Devos, M. L. Bols, D. Plessers, C. Van Goethem, J. W. Seo, S.-J. Hwang, B. F. Sels, M. Dusselier, *Chemistry of Materials*, **32**, 273-285 (2020).
- [3] J. Devos, S. Robijns, C. Van Goethem, I. Khalil, M. Dusselier, *Chemistry of Materials*, **33**, 2516–2531 (2021).
- [4] J. Devos, S. Robijns, G. Ivanushkin, I. Khalil, M. Dusselier. *Chemical Engineering Journal* **431**, 133862 (2022)
- [5] S. Lee, C. Nimlos, E. Kipp, Y. Wang, X. Gao, W. Schneider, M. Lusardi, V. Vattipalli, S. Prasad, A. Moini, R. Gounder, *Agents. Cryst Growth Des*, **22**, 6275–6295 (2022).

## Acknowledgments

J.D. acknowledges FWO (12E4623N).



## Carbon dioxide Methanation using Ni Catalysts Supported on Low-Cost Lynde Type A Zeolite Synthesized from Pretreated Iranian Coal Gangue

**Soheil Bahraminia, Mansoor Anbia**

*Research Laboratory of Nanoporous Materials, Faculty of Chemistry, Iran University of Science and Technology, P.O. Box 16846-13114, Tehran, Iran  
anbia@iust.ac.ir*

### Abstract

Coal gangue is solid waste generated from coal mining. Reducing carbon dioxide emissions is a challenge to mitigate the problems caused by global warming. In this work, zeolite LTA-5A is synthesized for the first time from the coal gangue of Iranian mines and used as catalyst support for preparing nickel catalysts for carbon dioxide methanation. These catalysts are characterized using XRD, FESEM, SEM, TEM, EDX, elemental mapping, H<sub>2</sub>-TPR, CO<sub>2</sub>-TPD, TGA, and low-temperature nitrogen adsorption. The methanation tests reveal that the 15%NiCGLTA-5A has the best catalytic performance among the catalysts, showing 73±2% CO<sub>2</sub> conversion and 91±2% CH<sub>4</sub> selectivity at 450 °C. The performance of these catalysts is comparable to those prepared from fly ash. Using coal gangue, an industrial waste with many environmental problems, as the primary source of silicon and aluminum can create a positive economic and ecological impact.

**Keywords:** Coal gangue, LTA zeolite, CO<sub>2</sub> methanation, Ni catalysts



## Optimizing the physiochemical properties of Ni-Pt/MFI zeolite catalysts for the hydrodeoxygenation of oleic acid

A. Alhendi<sup>1</sup>, A. Margellou<sup>2</sup>, S. Hinder<sup>3</sup>, M. Baker<sup>3</sup>, K. Triantafyllidis<sup>2</sup>, K. Polychronopoulou<sup>1</sup>, M. Khaleel<sup>1</sup>

<sup>1</sup> Khalifa University of Science and Technology, PO Box 127788, Abu Dhabi, United Arab Emirates.

<sup>2</sup> Aristotle University of Thessaloniki, University Campus, P.O. Box 116, GR-54124, Thessaloniki, Greece.

<sup>3</sup> University of Surrey, Guildford GU2 4DL, UK.

abdulla.alhendi@hotmail.com

### Introduction and Methodology

Bio-oils are upgraded by catalytic processes that target oxygen removal, such as hydrodeoxygenation (HDO), for enhancing their efficiency as fuels [1-2]. Zeolite-based catalysts provide valuable activity for HDO reactions due to the added functionality from zeolite supports; Al atoms act as Lewis acid sites for hydrogenation, while Brønsted acid sites in zeolites induce the removal of oxygen through dehydroxylation [3]. In particular, MFI zeolites are among the most used zeolite supports for HDO reactions due to their pore size and acidity. Conventional MFI is microporous, with a 0.56 nm pore size [4]. Whereas, hierarchical MFI zeolites are better suited for handling bulky molecules due to the presence of mesoporous (2-50 nm)/macroporous (>50 nm) channels in addition to the conventional micropores. Hierarchical MFI zeolites could be synthesized using organic structure directing agents (SDAs) to obtain self-pillared nanosheets of the zeolitic structure [5-6]. Ni-zeolite catalysts prepared using self-pillared MFI supports were less prone to deactivation than conventional MFI catalysts for the HDO of methyl stearate [7] and oleic acid [8]. Additionally, bi-metallic Ni-Pt conventional MFI catalysts demonstrated higher stability than analogues Ni-MFI catalysts when tested for the HDO of methyl stearate [9]. Therefore, this work aims at studying the influence of bi-metallic loading into self-pillared MFI supports for the HDO of oleic acid. Accordingly, Ni monometallic and Ni-Pt bimetallic catalysts were prepared using the incipient wetness impregnation (IWI) and ion-exchange (IE) techniques for both commercial MFI (ComMFI) and self-pillared MFI (SPP) supports. The prepared catalysts were characterized using various techniques including transmission electron microscopies (TEM), electron energy-loss spectroscopy (EELS), N<sub>2</sub>-physisorption, and temperature programmed desorption of ammonia (NH<sub>3</sub>-TPD). Whereas, the catalytic testing were conducted in a batch reactor at 250°C, 400 rpm, and 50 bar H<sub>2</sub>.

### Results and Discussion

The TEM images in Figure 1(a) clearly depict the differences in structures and sizes of both types of MFI supports (ComMFI and SPP) used for preparing the catalysts, which helped in diversifying the textural properties of the catalysts as illustrated by the N<sub>2</sub>-physisorption isotherms in Figures 1(d-e). Additionally, the TEM images displayed a higher concentration of metal particles for catalysts prepared by IWI compared to IE. Yet, IWI resulted in the formation of larger (> 30 nm) metal particles, especially for ComMFI catalysts. These large metal particles are too big to fit into the pores of the zeolites, so they are most likely collected on the external surfaces of the ComMFI zeolite particle and possibly blocking some pore entrances. This explains the drop in porosity observed for ComMFI-IWI catalysts in Figure 1(d) compared to the ComMFI-IE catalysts and pristine ComMFI, which was not observed for SPP-IWI catalysts in Figure 1(e) likely due to the enhanced metal dispersion exhibited by the SPP catalysts as shown in Figure 1(a). Still, the metal dispersion for ComMFI-IWI catalysts was enhanced with bimetallicity. Specifically, the size of metal particles decreased in ComMFI catalysts with higher Pt content. But, the same was not exactly true for the SPP-IWI catalysts. Instead, the 9.5-Ni-0.5-Pt-SPP-IWI catalysts (with highest Pt content) had the highest average metal particle size of all SPP-IWI catalysts possibly due to the formation of Ni-Pt clusters (Figure 1(c)), unlike the ComMFI catalyst (Figure 1(b)).

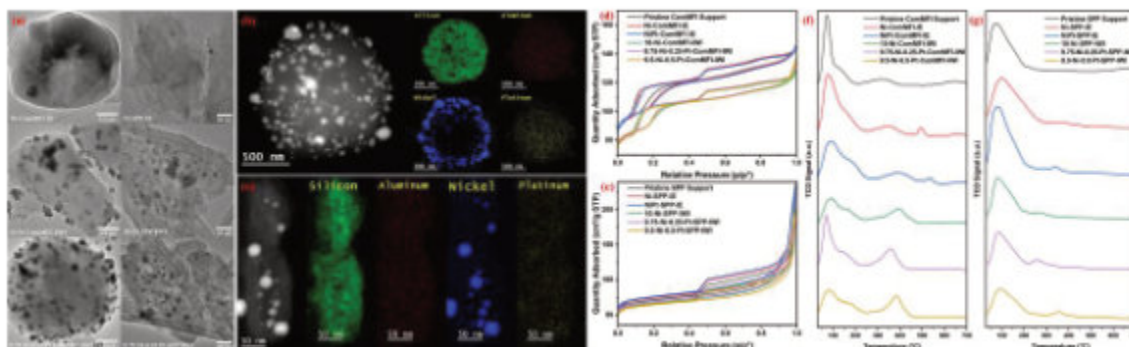


**Figure 1.** Characterization results of catalysts. (a) TEM images, STEM-EELS mapping results for (b) 9.5-Ni-0.5-Pt-ComMFI-IWI and (c) 9.5-Ni-0.5-Pt-SPP-IWI, (d-e) N<sub>2</sub>-physisorption isotherms, and (f-g) NH<sub>3</sub>-TPD profiles.



Moreover, the results in Figures 1(f-g) indicate that IE catalysts resulted in stronger acid sites than IWI (for both types of supports), despite their lower metal contents. The total quantity of acid sites was higher for ComMFI-IWI catalysts compared to ComMFI-IE. But with SPP catalysts, IE resulted in a higher quantity of total acid sites than IWI. And, the SPP catalysts generally contained weaker acid sites compared to the ComMFI catalysts.

In terms of catalytic results, all catalysts achieved 100% conversion of oleic acid during the 3 h reaction, except for the Ni-ComMFI-IE (48.7%) and NiPt-ComMFI-IE (33.3%) catalysts, both of which were prepared using IE resulting in very low Ni content (< 0.25 wt%). Additionally, these two catalysts had very low hydrodeoxygenation activity (resulting in low selectivity to alkanes as displayed in Figure 2(a)) and high cracking of alkanes (primarily producing alkanes shorter than C9 as shown in Figure 2(c)). Interestingly, the SPP-IE catalysts with slightly higher Ni content (> 0.8 wt%) achieved 100% conversion, with low cracking of alkanes (Figure 2(d)) and significant selectivity to alkanes (Figure 2(b)). Still, the IWI catalysts generally achieved higher selectivity to alkanes than IE catalysts for both types of supports, with the 9.5-Ni-0.5-Pt-SPP-IWI catalyst (containing Ni-Pt clusters) being the only exception. Accordingly, the highest selectivity to alkanes for SPP catalyst was achieved by the 9.75-Ni-0.25-Pt-SPP-IWI catalyst. While for the ComMFI-IWI catalysts, the selectivity to alkanes increased for higher Pt content. In fact, the 9.5-Ni-0.5-Pt-ComMFI-IWI catalyst was the only catalyst that achieved 100% selectivity to alkanes when tested for 3 h. Still, the stability testing results summarized in Figure 2(e) demonstrate that the 9.5-Ni-0.5-Pt-ComMFI-IWI and 10-Ni-ComMFI-IWI were less stable at long reaction durations (> 12 h) than the 9.75-Ni-0.25-Pt-SPP-IWI catalyst, with a significant decrease in selectivity to alkanes after 12 h of reaction likely due to the coke deposition on the active sites of the catalysts hence decreasing their HDO activity. This ultimately establishes the enhanced durability of the 9.75-Ni-0.25-Pt-SPP-IWI catalyst due to its hierarchical self-pillared morphology.

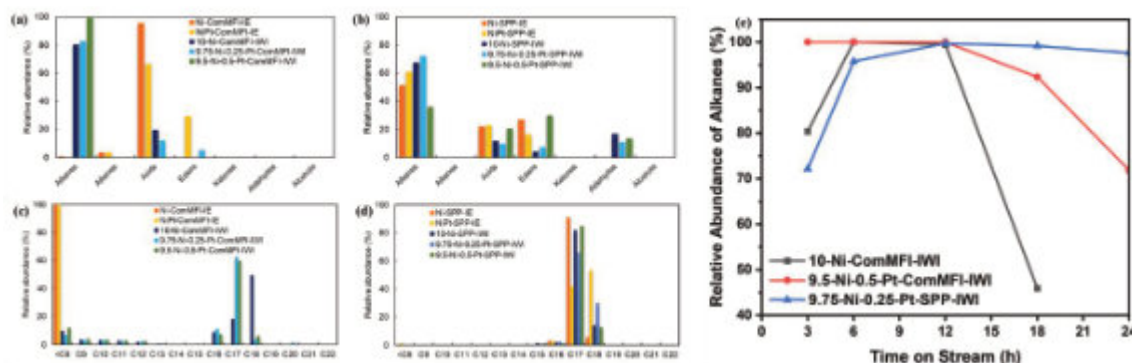


**Figure 2.** Catalytic HDO of oleic acid results conducted at 250°C; 400 rpm; 50 bar H<sub>2</sub>. (a-b) Product distribution after 3 h, (c-d) distribution of alkane products after 3 h, and (e) the relative abundance of alkanes produced during stability testing.

## Conclusions and Final Remarks

The physiochemical properties of catalysts played a significant role on the product selectivity. The stronger acid sites in ComMFI catalysts resulted in the cracking of alkanes while contributing to the high alkane selectivity for short reaction durations (< 12 h). Yet, the hierarchical morphology of SPP catalysts improved their stability in longer reactions (> 12 h), and their weaker acid sites minimized the cracking of alkane products.

## References

- [1] Q. Zhang, J. Chang, T. Wang, and Y. Xu, *Energy Conversion and Management*, **vol. 48**, pp. 87-92 (2007).
- [2] Y. Shi, E. Xing, K. Wu, J. Wang, M. Yang, and Y. Wu, *Catalysis Science & Technology*, **vol. 7**, pp. 2385-2415 (2017).
- [3] P. Yan et al., *Catalysis Science & Technology*, **vol. 10**, pp. 810-825 (2020).
- [4] C. McCusker, Database of Zeolite Structures, (1996).
- [5] F. Liu et al., *Journal of the American Chemical Society*, **vol. 134**, pp. 4557-4560 (2012).
- [6] X. Zhang et al., *Science*, **vol. 336**, p. 1684 (2012).
- [7] M. Schreiber, D. Rodriguez, O. Gutiérrez, and J. Lercher, *Catalysis Science & Technology*, **vol. 6**, pp. 7976-7984 (2016).
- [8] F. Feng, L. Wang, X. Zhang, and Q. Wang, *Industrial & Engineering Chemistry Research*, **vol. 58**, pp. 13112-13121 (2019).
- [9] X. Niu et al., *Industrial & Engineering Chemistry Research*, **vol. 59**, pp. 8601-8611 (2020).

## Acknowledgments

This work was financially supported by Khalifa University through the grants CIRA-2020-77, RC2-2018-024, and RC2-2019-007.





## Cu-oxo-exchanged mordenites prepared by activation under He or CO<sub>2</sub>: The nature of the Cu<sub>x</sub>O<sub>y</sub> species involved in the methane direct oxidation to methanol determined by *in situ* DRS-UV-Vis analyses

E. S. da Silva<sup>1</sup>, J. E. C. da Mata<sup>1</sup>, E. A. Urquieta-Gonzalez<sup>1</sup>

<sup>1</sup> Research Center on Advanced Materials and Energy (CPqMAE), Department of Chemical Engineering, Federal University of São Carlos, CEP 13565-905, São Carlos (SP), Brazil  
eliansoares@estudante.ufscar.br

**Abstract** - Cu-exchanged mordenites (Si/Al=10) were activated with He or CO<sub>2</sub> ([Cu<sub>x</sub>O<sub>y</sub>]-MOR samples), and then evaluated in the direct oxidation of methane to methanol (MTM). The nature and activity of the generated copper oxo-cations were studied by *in situ* DRS-UV-Vis analyses. The stepwise reaction of MTM involved: (i) activation of the Cu-exchanged mordenite with He or CO<sub>2</sub> at temperatures between 250 and 550 °C; (ii) MTM reaction with pure methane at 200°C, and (iii) off-line extraction of the formed methanol. The samples were characterized by XRD, H<sub>2</sub>-TPR, XRF, and *in situ* DRS UV-Vis analyses. Independently of the used activation agent, all the prepared [Cu<sub>x</sub>O<sub>y</sub>]-MOR were active to convert MTM, because of the generated copper oxocations having monomeric, dimeric or trimeric nature, as was verified by *in situ* DRS-UV-Vis. Moreover, after the MTM reaction, absorption bands at wave numbers greater than 30,000 cm<sup>-1</sup>, associated with the transfer charge from the ligand to the metal (O → Cu<sup>2+</sup>), showed greater loss of intensity, thus evidencing a significant participation as active species.

**Keywords:** Methane, Methanol, Cu-mordenite, Activation, Helium, Carbon Dioxide, Cu-oxocation, *In situ* DRS UV-Vis.

### Introduction

The selective oxidation of hydrocarbons such as methane, in oxygenated products, is a reaction that requires selective catalysts with high activity under mild conditions of temperature and pressure [1]. In this scenario, zeolites could play an important role, as they are microporous materials that stabilize copper oxocations [Cu<sub>x</sub>O<sub>y</sub>]<sup>2+</sup>, active in the direct conversion of methane to methanol [2]. The zeolite ion exchange with Cu<sup>2+</sup> with subsequent thermal activation, determines the nature of the generated Cu<sub>x</sub>O<sub>y</sub> oxocations in a particular zeolitic structure. Thus, knowing the importance of identifying the nature of these oxocations, the present study aimed to analyze the influence of He and CO<sub>2</sub> as activating agents on the formation of active [Cu<sub>x</sub>O<sub>y</sub>] species in mordenite zeolites exchanged with Cu<sup>2+</sup> and to verify their activity when applied to catalyze the methane direct oxidation to methanol.

### Experimental

Ion exchange of an ammonium mordenite (NH<sub>4</sub>MOR, Si/Al = 10) was performed using a solution of 0.05 mol L<sup>-1</sup> of copper acetate (AcCu) monohydrate (Sigma-Aldrich, 99%) performed from three procedures: (i) ion-exchange of the NH<sub>4</sub>MOR with AcCu at room temperature (sample Cu-NH<sub>4</sub>MOR(10)-Tamb); (ii) ion-exchange of the NH<sub>4</sub>MOR with AcCu at 60°C (sample Cu-NH<sub>4</sub>MOR(10)-60°C) and (iii) ion-exchange of a HMOR with AcCu at room temperature (Cu-HMOR(10)-Tamb). The ion exchanged proceeded under magnetic stirring for 24h, vacuum filtration, washing with distilled water and drying at 110°C. The Cu-NH<sub>4</sub>MOR(10)-Tamb, Cu-NH<sub>4</sub>MOR(10)-60°C and Cu-HMOR(10)-Tamb samples were characterized by H<sub>2</sub>-TPR, XRD and XRF. Among the obtained samples, that having the highest content of exchanged copper, besides it was evaluated in the catalytic tests, it was also used in the *in situ* DRS UV-Vis analyses that followed the methodology we used in a recent work [3]. Thus, the Cu-NH<sub>4</sub>MOR-60°C sample was activated with He or CO<sub>2</sub> at temperatures of 250, 350, 450 and 550 °C with the subsequent methane reaction at 200 °C under a flow of pure CH<sub>4</sub>. For the *in situ* DRS-UV-Vis analyses, it was used a Thermo- Scientific Evolution 300 UV-Vis Spectrophotometer equipped with a Harrick Praying Mantis accessory and a high-temperature reaction chamber (HVC-DRP-5), where the activation and reaction conditions were the same than those applied in the catalytic tests above described.

### Results and discussion

In the H<sub>2</sub>-TPR analysis (not shown), at temperatures up to 300 °C occurred a reduction of Cu<sup>2+</sup> to Cu<sup>+</sup> and between 500 and 700 °C the a reduction of from Cu<sup>+</sup> to Cu<sup>0</sup> [4]. The occurrence of two reduction regions indicates that the copper is in the zeolite exchange positions [3]. The CuNH<sub>4</sub>MOR(10)-60°C sample showed the highest hydrogen consumption and, therefore, the highest content of exchanged copper (3.02%). The X-ray diffractograms of the zeolites Cu-NH<sub>4</sub>MOR(10)-Tamb, Cu-NH<sub>4</sub>MOR(10)-60°C and Cu-HMOR(10)-Tamb (not shown), showed peaks referring to the MOR structure of the mordenite, since its crystal structure was not altered after ion exchange with copper. In addition, no peaks corresponding to the CuO phase were observed, evidencing its absence at detectable levels [5] and corroborating the H<sub>2</sub>-TPR results.

The MTM reaction was performed with the Cu-NH<sub>4</sub>MOR(10)-60°C sample, which among the three prepared catalysts presented the highest Cu content. The higher activity of Cu-MOR activated with He at 550 °C (6.03 μmol g<sub>cat</sub><sup>-1</sup>) or CO<sub>2</sub> at 450 °C (2.62 μmol g<sub>cat</sub><sup>-1</sup>) is attributed to the higher generation of active species, since their formation is kinetically or thermodynamically limited at a temperatures equal or greater than 450 °C, where a



higher fraction of Cu oxocations reaches a configuration capable of activating methane [6]. In this sense, to elucidate the behavior of the Cu-NH<sub>4</sub>MOR(10)-60°C sample when activated in He or CO<sub>2</sub>, *in situ* DRS UV-Vis analyses were performed (Figure 1), which allowed the identification of the nature of the generated oxocations [Cu<sub>x</sub>O<sub>y</sub>].

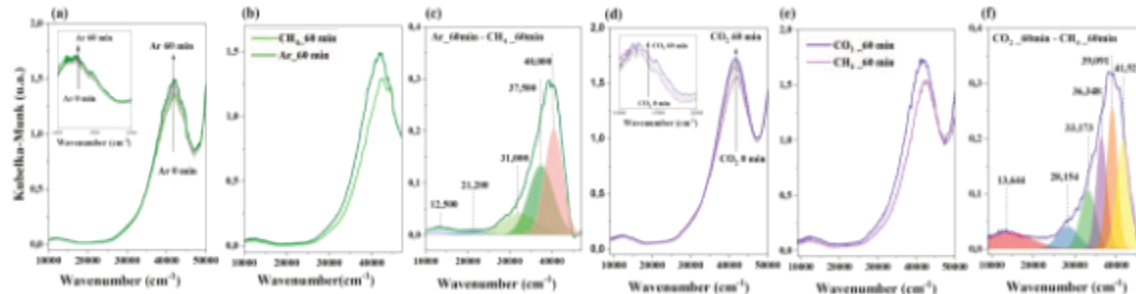


**Figure 1.** DRS-UV-Vis *in situ* spectra for CuNH<sub>4</sub>MOR(10)-60°C. (a) Air Activation; (b) comparison of the spectra of activation with Ar and reaction with CH<sub>4</sub> at 60 min; (c) difference between the activation spectra with Ar and reaction with CH<sub>4</sub> both at 60 min; (d) CO<sub>2</sub> activation; (e) comparison of the activation spectra with CO<sub>2</sub> and reaction with CH<sub>4</sub> at 60 min; (f) difference between the activation spectra with CO<sub>2</sub> and reaction with CH<sub>4</sub> both at 60 min.

In the activation with Ar (Figure 1a) and CO<sub>2</sub> (Figure 1d), it can be observed a tendency of the intensity of the spectrum to increase with the increase of the time, indicating the formation of active species. After activation, the *in situ* reaction with CH<sub>4</sub> at 200 °C was performed and the obtained activation and reaction spectra, both collected at 60 min, can be seen in Figure 1b for activation with inert gas: Ar and in Figure 1e for activation with CO<sub>2</sub>. Thus, it can be noted that after reaction with CH<sub>4</sub> there was a consumption of the active species due to the observed trend of the intensity reduction of the spectra in certain regions. In order to verify which species participated in the reaction, the difference between the activation and reaction spectra was made at 60 min, as shown in Figure 1c (Ar) and 1f (CO<sub>2</sub>). It should be noted that the shape of the curves is very similar for both activation agents, but they differ in the deconvolution profile in terms of species homogeneity.

As known, the bands between 12,000 and 20,000 cm<sup>-1</sup> refer to the d-d transitions of Cu<sup>2+</sup> and, the LMTC bands in the region of higher energy 20,000 to 30,000 cm<sup>-1</sup>, corresponding to charge transfer from extrastructural oxygens to copper (O<sub>ef</sub> → Cu<sup>2+</sup>) and those above of 30,000 cm<sup>-1</sup> correspond to charge transfer from structural oxygen to copper (O<sub>fw</sub> → Cu<sup>2+</sup>) [7,8]. As in this study, through theoretical and experimental calculations for Cu-oxo-MAZ zeolites activated with O<sub>2</sub> and CO<sub>2</sub> [9], we verified in the obtained UV-Vis spectra, the presence of absorption bands, corresponding to [Cu<sub>3</sub>O<sub>3</sub>]<sup>2+</sup> trimers in the region at about 30,000 to 38,000 cm<sup>-1</sup> and copper monohydroxide species (CuOH<sup>+</sup>) at about 40,000 cm<sup>-1</sup>. The presence of a copper trimer, related to the absorption band at 31,000 cm<sup>-1</sup> (Figure 1c and f), which corresponds to the region of charge transfer from structural oxygen to copper, evidences that during activation with an inert agent (Ar), the oxygen of the zeolite structure generates copper oxocations [8]. In addition, other authors [6] indicate that the thermal formation of highly mobile Cu<sup>+</sup> species by self-reduction of Cu<sup>2+</sup> under an inert gas atmosphere allows the reorganization of Cu cations into the MOR exchangeable sites, and this process is a necessary step for the formation of a reduced precursor of the [Cu<sub>3</sub>(μ-O)<sub>3</sub>]<sup>2+</sup> oxo-cation.

### Conclusions

By the *in situ* DRS-UV-Vis analyses, it was evidenced the formation of Cu<sub>x</sub>O<sub>y</sub> oxo-cations generated by the activation of the Cu<sup>2+</sup> exchanged cations with He or CO<sub>2</sub> and their subsequent consumption during the MTM reaction. Copper oxo-cations having dimeric, trimeric or (CuOH)<sup>+</sup> nature were identified. In the UV-Vis spectral region corresponding to structural or extrastructural oxygen transitions to Cu<sup>2+</sup>, occurred a greater loss of the intensity of the absorption bands, indicating that the associated species were more active.

### References

- [1] X. Guan, X. Zhanwei; D. Hong; L. Xiumei; Y. Peifang; G. Xinwen, *Catalysis Communications*, **163**, 2022.
- [2] P. Vanelderden, et al., *Journal Of The American Chemical Society*, **137**, 2015.
- [3] R. J. Passini, M. Picinini, J. M. C. Bueno, E. A. Urquieta Gonzalez, *Molecular Catalysis*, **530**, 2022.
- [4] H. Yousefzadeh, S. E. Bozbag, V. Sushkevich, J. A. Bokhoven, *Catalysis Communications*, **174**, 2023.
- [5] Asbrink, A. Waskowska, *Physics: Condensed Matter*, **42**, 1991.
- [6] T. Ikuno, S. Grundner, A. Jentys, G. Li, J. Pidko Fulton, J. A. Lercher, *Journal of Physical Chemistry C*, **123**, 2019.
- [7] Y. Kim; T. Y. Kim, H. Lee, J. Yi, *Chemical Communications*, **53**, 2017.
- [8] L. Bieseki, D.B. Ribeiro, E. V. Sobrinho, D. M. A. Melo, S. B. Pergher, *Cerâmica*, **59**, 2013.
- [9] T. C. Pereira, J. V. R. Vieira, C. H. F. Cunha, et al., *Applied Catalysis B: Environmental*, **342**, 2024.

### Acknowledgments

6<sup>th</sup> Euro-Asia Zeolite Conference. Alicante (Spain), January 19-22, 2025. EAZC-2025 Porous solids for the new societal challenges. The authors would like to thank ANP (PRH-39), FAPESP (Process 2018/01258-5) and CAPES (funding code 001) for their financial support. ESS thanks ANP (PRH-39) for the doctoral scholarship.



## Ultrafast dealumination of beta using a continuous-flow reactor

A. Minami<sup>1</sup>, M. Takemoto<sup>1</sup>, Y. Yonezawa<sup>1</sup>, Z. Liu<sup>1,2</sup>, Y. Yanaba<sup>3</sup>, A. Chokkalingam<sup>1</sup>, K. Iyoki<sup>1</sup>, T. Sano<sup>1</sup>, T. Okubo<sup>1</sup>, T. Wakihara<sup>1,2</sup>

<sup>1</sup> Department of Chemical System Engineering, The University of Tokyo, 7-3-1 Hongo, Bunkyo-ku, Tokyo 113-8656, Japan

<sup>2</sup> Institute of Engineering Innovation, The University of Tokyo, 2-11-16 Yayoi, Bunkyo-ku, Tokyo 113-8656, Japan

<sup>3</sup> Institute of Industrial Science, The University of Tokyo, 4-6-1 Komaba, Meguro-ku, Tokyo 153-8505, Japan

m\_takemoto@chemsys.t.u-tokyo.ac.jp

### Introduction

Zeolites are used as catalysts in various industrial fields, and zeolite catalysts are exposed to high temperature water vapor. Zeolites are known to be structurally degraded in such environments, and post-treatment is applied to synthetic zeolites to improve their hydrothermal stability. Dealumination is a typical method to improve the hydrothermal stability of zeolite, and various dealumination methods such as acid treatment[1, 2] and microwave[3] have been proposed. However, conventional dealumination requires several hours of treatment time, and it is desirable to establish a shorter treatment time for practical use. It is known that dealumination of zeolite is accelerated under high temperature conditions, and autoclave reactors are generally used. The method using autoclave reactor requires more than one hour to reach the target temperature and is a batch-type method, which requires a lot of time.

Recently, our group reported the ultrafast synthesis of zeolites using a stainless steel tubular reactor [4]. Owing to the faster heat transfer of the stainless steel tubular reactors for the reactants than that of batch-style autoclave, it takes a few seconds to minutes to reach the target temperature utilizing in the preheated oil bath. Based on the fast heat transfer of the stainless steel tubular reactor, we developed a tubular continuous-flow reactor for the ultrafast and continuous synthesis of zeolites [5, 6]. Furthermore, ultrafast post-synthetic treatments of the order of minutes have been realized for the introduction of core-shell structure [7] and mesoporosity [8]. In this study, based on the knowledge, a continuous and rapid dealumination of zeolite was performed.

### Experiment

Beta zeolite (Beta, HSZ-930NHA, Tosoh, Si/Al = 12.2) was dispersed in a sulfuric acid solution to obtain a uniform slurry. Dealumination of zeolite was carried out using a homemade reactor as shown in **Figure 1**. The heating and cooling sections were double-tubed, consisting of a stainless steel tube and a Teflon tube. Heated water was circulated through the Teflon tube, and the pressure was kept constant by a back pressure regulator. The pump pressure was adjusted to set the residence time in the heating section to 1-5 min. The collected slurry was centrifuged, washed, and dried at 80 °C to obtain samples. Dealuminated samples were also prepared by sealing the slurry in an autoclave reactor at 200 °C and by dealumination in a polypropylene container at room temperature.

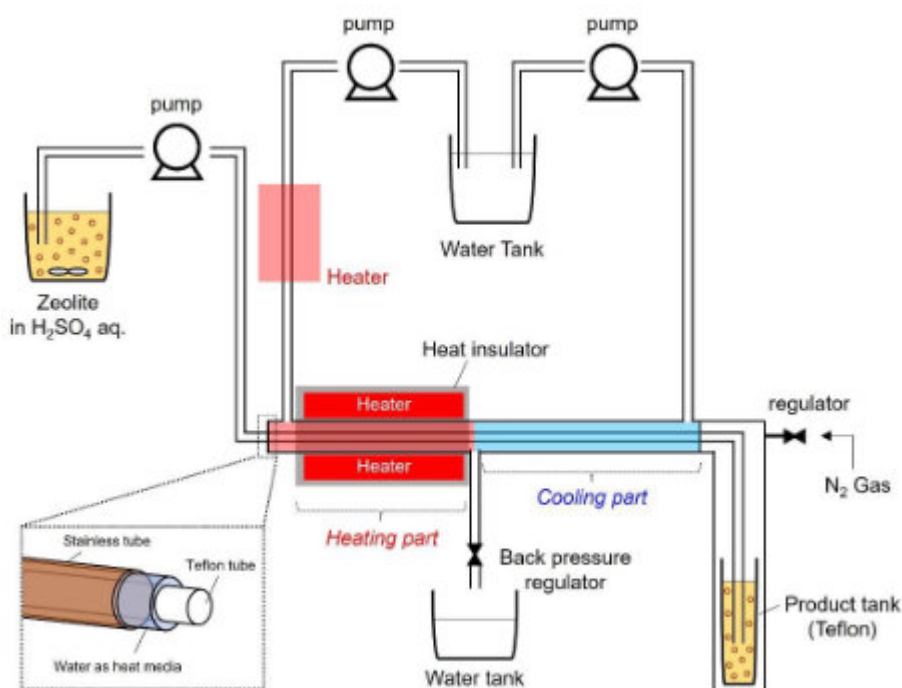


**Figure 1.** Schematics of the continuous-flow reactor.



**Figure 2** shows the Si/Al ratios for beta used as starting material and for the samples after dealumination. An increase in the Si/Al ratio was observed in all dealuminated samples. While the Si/Al ratio of the samples dealuminated at room temperature was about 25, the samples dealuminated under high temperature conditions using autoclave and flow reactor showed high Si/Al ratios (40~75). This is because dealumination was accelerated under high temperature conditions. When using an autoclave reactor, it takes at least several tens of minutes for the temperature of the contents to rise sufficiently. Therefore, the reason why the dealumination progressed better in the flow system than in the autoclave reactor is that the reactants were heated quickly due to the high heat transfer in the flow system. Powderly X-ray diffraction of the dealuminated beta samples confirmed that crystalline structure of beta retained after the dealumination at 200 °C, and the morphologies of the dealuminated beta did not change. It can be summarized that the present flow system enables ultrafast dealumination to be continuously performed under severe conditions. The hydrothermal stability of parent and dealuminated beta zeolites will be discussed on the presentation.

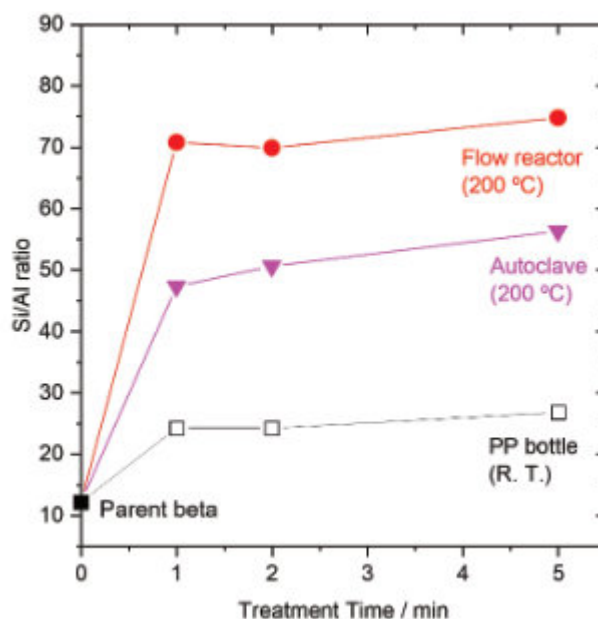


**Figure 2.** Si/Al ratios of the parent and dealuminated beta zeolites in various reactors as a function of treatment times.

## References

- [1] P. Matias, J. M. Lopes, P. Ayrault, S. Laforge, P. Magnoux, M. Guisnet, F.R. Ribeiro, *Appl. Catal. A*, **365**, 207-213 (2009).
- [2] S. Inagaki, S. Shinoda, Y. Kaneko, K. Takechi, R. Komatsu, Y. Tsuboi, H. Yamazaki, J.N. Kondo, Y. Kubota, *ACS Catal.*, **3**, 74-78 (2012).
- [3] M.D. González, Y. Cesteros, P. Salagre, *Microporous Mesoporous Mater.*, **144**, 162-170 (2011).
- [4] Z. Liu, J. Zhu, T. Wakihara, T. Okubo, *Inorg. Chem. Front.*, **6**, 14-31 (2019).
- [5] Z. Liu, T. Wakihara, N. Nomura, T. Matsuo, C. Anand, S. P. Elangovan, Y. Yanaba, T. Yoshikawa, T. Okubo, *Chem. Mater.*, **28**, 4840-4847 (2016).
- [6] Z. Liu, T. Wakihara, K. Oshima, D. Nishioka, Y. Hotta, S.P. Elangovan, Y. Yanaba, T. Yoshikawa, W. Chaikittisilp, T. Matsuo, T. Takewaki, T. Okubo, *Angew. Chem. Int. Ed.*, **127**, 5683-5779 (2015).
- [7] C. Peng, Z. Liu, Y. Yonezawa, Y. Yanaba, N. Katada, I. Murayama, S. Segoshi, T. Okubo, T. Wakihara, *Microporous Mesoporous Mater.*, **277**, 197-202 (2019).
- [8] C. Peng, Z. Liu, Y. Yonezawa, N. Linares, Y. Yanaba, C.A. Trujillo, T. Okubo, T. Matsumoto, J. García-Martínez, T. Wakihara, *J. Mater. Chem. A*, **8**, 735-742 (2020).

## Acknowledgments

This work was partially supported by Ministry of Education, Culture, Sports, Science and Technology (MEXT) "Establish Process Science toward Commercialization of Materials (Materialize)" Project (JPMX0219192801), Development Program, Japan Society for the Promotion of Science (JSPS) Grants-in-Aid for Scientific Research (KAKENHI) Grant-in-Aid for Transformative Research Areas (A) (JP20A206/20H05880) and New Energy and Industrial Technology Development Organization (NEDO), Japan Moonshot Research.



## Low-silica Cu-CHA Zeolite Enriched with Al Pairs Transcribed from Silicoaluminophosphate Seed: Synthesis and Ammonia Selective Catalytic Reduction Performance

Y. Wang<sup>1</sup>, J. Han<sup>1</sup>, M. Chen<sup>1</sup>, W. Lv<sup>2</sup>, P. Meng<sup>3</sup>, W. Gao<sup>4</sup>, X. Meng<sup>5</sup>, W. Fan<sup>3</sup>, J. Xu<sup>4\*</sup>, W. Yan<sup>1\*</sup>, and J. Yu<sup>1,6\*</sup>

<sup>1</sup> State Key Laboratory of Inorganic Synthesis and Preparative Chemistry, College of Chemistry, Jilin University, Changchun, P. R. China.

<sup>2</sup> Shanxi Normal University, Taiyuan, P. R. China.

<sup>3</sup> State Key Laboratory of Coal Conversion, Institute of Coal Chemistry, Chinese Academy of Sciences, Taiyuan, P. R. China

<sup>4</sup> National Centre for Magnetic Resonance in Wuhan, State Key Laboratory of Magnetic Resonance and Atomic and Molecular Physics, Innovation Academy for Precision Measurement Science and Technology, Chinese Academy of Sciences, Wuhan, P. R. China

<sup>5</sup> Key Lab of Applied Chemistry of Zhejiang Province, Department of Chemistry, Zhejiang University, Hangzhou, P. R. China

<sup>6</sup> International Center of Future Science, Jilin University, Changchun, P. R. China

E-mail: [yanw@jlu.edu.cn](mailto:yanw@jlu.edu.cn)

Cu-exchanged low-silica **CHA** zeolites ( $\text{Si}/\text{Al} \leq 4$ ) synthesized without organic templates are promising candidate catalysts for ammonia selective catalytic reduction of nitrogen oxides ( $\text{NH}_3\text{-SCR}$ ), but their practical application is restricted due to the low hydrothermal stability [1,2]. Here, inspired by the transcription from duplex DNA to RNA, we synthesized Al pairs enriched low-silica **CHA** zeolite (CHA-SPAEl,  $\text{Si}/\text{Al} = 3.7$ ) by using silicoaluminophosphate (SAPO) featured by strict alternation of  $-\text{Al}-\text{O}-\text{P}(\text{Si})-\text{O}-\text{Al}-\text{O}-$  tetrahedra as seed. The proportion of Al pairs in CHA-SPAEl is 78%, which is much higher than that in the conventional low-silica **CHA** (CHA-LS, 52%). After hydrothermal ageing at 800 °C for 6 h, Cu-exchanged CHA-SPAEl shows NO conversion above 90% within 225-500 °C under a gas hourly space velocity of 200,000  $\text{h}^{-1}$ , which is much better than that of Cu-exchanged CHA-LS. The spatial close proximity of Al pairs in CHA-SPAEl is confirmed by the  $^{27}\text{Al}$  double-quantum single-quantum two-dimensional NMR analyses. The strict  $-\text{P}(\text{Si})-\text{O}-\text{Al}-\text{O}-\text{P}(\text{Si})-\text{O}-$  sequence in the fragments from the dissolution of SAPO seed promotes the Al pairs with the  $-\text{Al}-\text{O}-\text{Si}-\text{O}-\text{Al}-\text{O}-$  sequence via a transcription process. The utilization of aluminophosphate-based zeolites as seeds opens up a new avenue for the regulation of the Al distribution in zeolites.

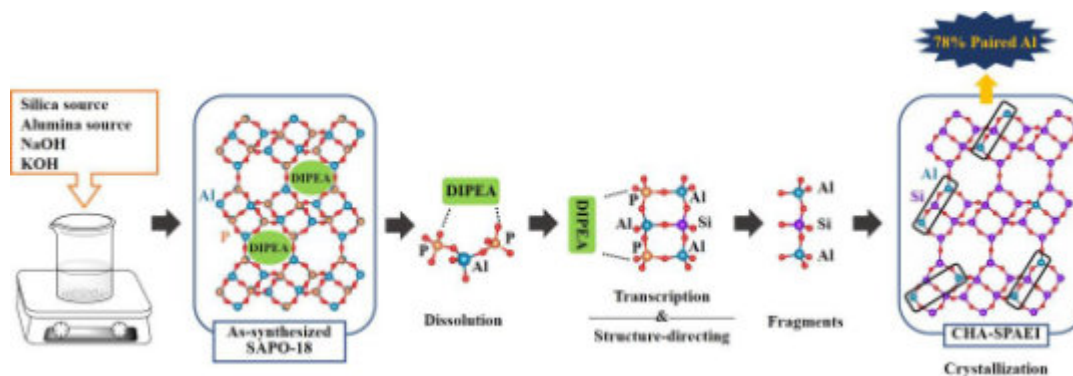


**Figure 1.** Proposed mechanism of the structure-directing and Al regulating process of SAPO-18-DIPEA seed. The  $(-\text{P}-\text{O}-\text{Al}-\text{O}-\text{P}-\text{O}-)_{\text{n}} \cdots \text{DIPEA}$  complex generated from the dissolution of the as-synthesized SAPO-18 seed induces the formation of  $-\text{Al}-\text{O}-\text{Si}-\text{O}-\text{Al}-$  fragments from the initial mixture through a transcription process, leading to the enrichment of Al pairs in the resultant CHA-SPAEl.

### References

- [1] R. Xu, W. Pang, J. Yu, Q. Huo, J. Chen, *Chemistry of Zeolites and Related Porous Materials: Synthesis and Structure*, John Wiley & Sons (Asia) Pte Ltd., Singapore, **2009**  
 [2] R. Y. Shan, J. Du, Y. Zhang, W. Shan, X. Shi, Y. Yu, R. Zhang, X. Meng, F.-S. Xiao, H. He, *Natl. Sci. Rev.* **2021**, *8*, nwab010

### Acknowledgments

We acknowledge the financial support from the National Natural Science Foundation of China (22288101), the National Key Research and Development Program of China (2021YFA1500401), National Engineering Laboratory for Mobile Source Emission Control Technology (NELMS2020A01), and the “111 Center” (B17020) for supporting this work.



## Understanding the Influence of Aging Treatments on Properties of Amorphous Precursors towards Rational Synthesis of CHA-type Zeolite

Y. Okada<sup>1</sup>, Y. Sada<sup>1,2</sup>, S. Miyagi<sup>1</sup>, H. Yamada<sup>2,3</sup>, K. Ohara<sup>2,3</sup>, Y. Yanaba<sup>1</sup>, M. Yoshioka<sup>4</sup>, T. Ishikawa<sup>4</sup>, Y. Naraki<sup>4</sup>, T. Sano<sup>1</sup>, T. Okubo<sup>1</sup>, R. Simancas<sup>1,\*</sup>, T. Wakihara<sup>1,\*\*</sup>

<sup>1</sup> The University of Tokyo, 7-3-1 Hongo, Bunkyo-ku, Tokyo, 113-8656, Japan

<sup>2</sup> Japan Synchrotron Radiation Research Institute / SPring-8, 1-1-1, Koto, Sayo-cho, Sayo-gun, Hyogo, 679-5198, Japan

<sup>3</sup> Shimane University, 1060, Nishikawatsu-cho, Matsue, Shimane, 690-8504, Japan

<sup>4</sup> Tosoh Corporation, 4560, Kaisei-cho, Shunan, Yamaguchi, 746-8501, Japan

\*rsimancas@chemsys.t.u-tokyo.ac.jp, \*\*wakihara@chemsys.t.u-tokyo.ac.jp

The influence of aging conditions on the properties of aluminosilicates is investigated and the crystallization process afterward is compared using amorphous aluminosilicate precursors with the same Si/Al ratio (SAR) but with different Al coordination and ring structures. When the aging temperature is raised, alkalinity is enhanced or aging time is extended, the SAR of the obtained amorphous precursor decreases. A detailed investigation is conducted on three amorphous precursors with the same SAR. It is revealed that aging under low temperatures or for a short aging time leads to the formation of aluminosilicate precursors with high ratio of tetrahedral Al and small rings. The three amorphous precursors were used for the synthesis of CHA-type zeolite (CHA) to investigate how those properties influence its crystallization behavior. Two of the three precursors result in shorter synthesis time compared with the conventional synthesis without aging.

### 1. Introduction

The crystallization rate and crystallinity of zeolites are largely influenced by the aging conditions of the synthesis mixture just before hydrothermal treatment [1–5]. It is reported that the physicochemical properties of the amorphous aluminosilicate precursors formed during aging influence the following nucleation and crystal growth steps [6]. For example, as for CHA-type zeolite (CHA), Minami *et al.* have proposed a mechanism for the amorphous aluminosilicate precursors to crystalline transformation during the CHA crystallization by *in-situ* HEXTS measurement, which revealed that ordered four-membered ring (4R) are formed during the induction period, then the significant increase of six- (6R) and eight-membered ring (8R) was observed in the following crystal growth stage [7]. This result could help us to understand the reported influence of aging conditions, suggesting that aluminosilicate precursors enriched in 4R could promote CHA crystallization. In this study, therefore, we first prepared aluminosilicate precursors under varied aging conditions and investigated the influence of the aging conditions on their physicochemical properties. Then, we used the obtained precursors in the synthesis of CHA zeolites to examine the influence of precursors' properties on the zeolite crystallization process.

### 2. Experimental

#### 2.1 Preparation of aluminosilicate precursors

NaOH aq., NaAlO<sub>2</sub>, colloidal silica and distilled water were mixed. The chemical composition was 1.0 SiO<sub>2</sub> : 0.10 Al<sub>2</sub>O<sub>3</sub> : x NaOH : 15 H<sub>2</sub>O (x = 0.4, 0.6, 0.9, 1.2). The mixture was aged under T [°C] (T = 5, 15, 25, 35) for t [h] (t = 2, 5, 8, 24, 72). The obtained solids were recovered by centrifugation, and referred to as Amor[T/x/t].

#### 2.2 Synthesis of CHA zeolites

CHA zeolite was synthesized according to a previously reported recipe with minor modification [8]. TMAOH aq., Si & Al sources, NaOH aq. and distilled water were mixed, where the chemical composition was 1.0 SiO<sub>2</sub> : 0.032–0.038 Al<sub>2</sub>O<sub>3</sub> : 0.25 NaOH : 0.25 TMAOH : 44 H<sub>2</sub>O. As Si & Al sources, aluminosilicate precursors with the SAR of 13 (Amor[5/1.2/24], Amor[15/0.4/24] and Amor[15/1.2/5], details shown in 3.1) were used. Conventional sources (colloidal silica and NaAlO<sub>2</sub>) were also used for comparison. The final mixture was heated to 160 °C for 1–5 days, and the solid products were recovered by filtration.

### 3. Results and Discussion

#### 3.1 Characterization of aluminosilicate precursors

All obtained aluminosilicates presented a broad signal in the XRD pattern, which is a characteristic of amorphous solids. SAR of the precursors are shown in Fig. 1. The SAR of the aluminosilicate precursors decreased with increasing NaOH/SiO<sub>2</sub> ratio or temperature. Similarly, long aging time also led to a decrease in the SAR. The results of these experiments suggest that it is possible to control the SAR to some extent by choosing the appropriate aging conditions.

Three samples having similar SAR were chosen as representative solids to be studied in more detail. Fig. 2(a) shows <sup>27</sup>Al MAS NMR spectra of the three amorphous aluminosilicates with a SAR of 13 (Amor[15/0.4/24],

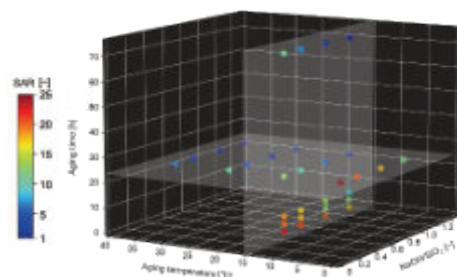
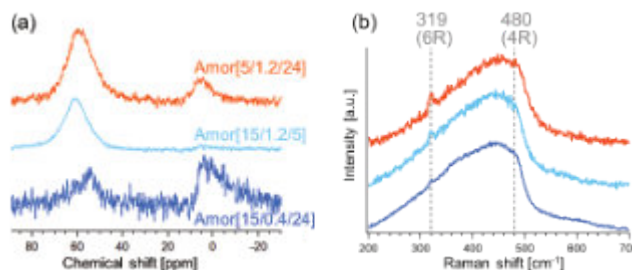


Fig. 1 SAR of aluminosilicate precursors prepared under varied aging conditions



Amor[5/1.2/24] and Amor[15/1.2/5]). The ratio of tetrahedral Al increased in the order of Amor[15/0.4/24] < Amor[5/1.2/24] < Amor[15/1.2/5]. The results indicate that incorporation of Al into the framework tend not to proceed under low alkalinity. UV-Raman spectra of the three samples are shown in Fig. 2(b). For Amor[5/1.2/24], peaks were observed at *ca.* 319 and 480 cm<sup>-1</sup>, associated with 6R and 4R, respectively [7]. Smaller peaks were observed for Amor[15/1.2/5] and peaks were almost indistinguishable for Amor[15/0.4/24]. It was found that Amor[5/1.2/24] and Amor[15/1.2/5] have higher ratio of 4R.



**Fig. 2** (a) <sup>27</sup>Al MAS NMR spectra and (b) UV-Raman spectra of Amor[5/1.2/24], Amor[15/1.2/5] and Amor[15/0.4/24]

### 3.2 Influence on CHA synthesis

The crystallization curves are shown in Fig. 3. Synthesis time could be shortened when using Amor[5/1.2/24] and Amor[15/1.2/5] as the starting materials. Synthesis time needed was largely the same when using Amor[15/0.4/24] or conventional sources. These results strongly indicate that the use of aluminosilicate precursors whose local structures are partially organized (Amor[5/1.2/24] and Amor[15/1.2/5]) could shorten the time needed for the nucleation.

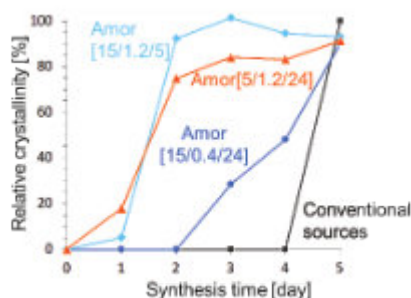


**Fig. 3** Crystallization curves when using different Si & Al sources  
(The relative crystallinity of obtained CHA zeolites was calculated from the XRD peak areas based on the

### 4. Conclusion

The effects of aging temperature, alkalinity and time on aluminosilicate precursors for synthesis of CHA-type zeolite (CHA) were studied. Higher aging temperature, higher alkalinity or longer aging time led to a decrease in the Si/Al ratio (SAR). <sup>27</sup>Al MAS NMR, UV-Raman and HEXTS measurements revealed that aging treatment under low temperature or for a short aging time led to the formation of aluminosilicate precursors with high ratio of tetrahedral Al and small rings. Using three of the samples with the same SAR and different properties in ring structures and Al coordination, the crystallization behavior of CHA was investigated. When aluminosilicate precursors with the higher ratio of incorporated Al and ordered ring structures were used as the starting material, the synthesis was shortened compared with the conventional synthesis.

### References

- [1] M. Ogura *et al.*, *Chem. Mater.*, **15**, 2661 (2003). [2] H. J. K orođlu *et al.*, *J. Cryst. Growth.*, **241**, 481 (2002). [3] R. Osuga *et al.*, *Chem. Commun.*, **58**, 11583 (2022). [4] Y. Lv *et al.*, *Microporous Mesoporous Mater.*, **293**, 109812 (2020). [5] Y. Joichi *et al.*, *Cryst. Growth Des.*, **18**, 5652 (2018). [6] C. S. Cundy *et al.*, *Microporous Mesoporous Mater.*, **82**, 1 (2005). [7] A. Minami *et al.*, *J. Am. Chem. Soc.*, **144**, 23313 (2022). [8] S. Lee *et al.*, *Cryst. Growth Des.*, **22**, 6275 (2022).

### Acknowledgments

HEXTS measurements conducted at beam line BL04B2 in SPring-8 were approved by the Japan Synchrotron Radiation Research Institute under proposal numbers 2022A1210 and 2023A1367.



## Metal exchanged zeolites for noble gas concentration

C. Courtney<sup>1</sup>, G. Couchaux<sup>1</sup>, B. Siberchicot<sup>1</sup>, F. Hauquier<sup>2</sup>, A. Tuel<sup>3</sup>, D. Farrusseng<sup>3</sup>, S. Topin<sup>1,2</sup>

<sup>1</sup> CEA, DAM, CEA-DIF, Bruyères-le-Châtel, F-91297 Arpajon, France

<sup>2</sup> Conservatoire National des Arts et Métiers, Analyse Chimique et Bioanalyse, EPN7, 292 Rue Saint-Martin, 75003 Paris, France

<sup>3</sup> Université de Lyon, Institut de Recherches sur la Catalyse et l'Environnement de Lyon, IRCELYON, UMR CNRS 5256, Université Lyon 1, 2 av. Einstein, 69626 Villeurbanne Cedex, France

[gabriel.couchaux@cea.fr](mailto:gabriel.couchaux@cea.fr), [sylvain.topin@cea.fr](mailto:sylvain.topin@cea.fr), [bruno.siberchicot@cea.fr](mailto:bruno.siberchicot@cea.fr)

In the context of the Comprehensive Nuclear-Test-Ban Treaty (CTBT), CEA develops system that are able to measure the radioactive noble gas isotopes at very low level. Indeed, some krypton and xenon radio-isotopes are fission products widely generated after a nuclear explosion. These markers can be then detected at thousands of kilometres from the nuclear test site. In order to measure it at very low concentration (< mBq/m<sup>3</sup>), it is essential to use a specific gas process that is able to concentrate the xenon into a sample (concentration of about 6 order of magnitude). In that purpose, CEA developed several years ago the SPALAX-NG (*Systèmes de prélèvement automatique en ligne avec l'analyse du xenon – New Generation*) which is particularly based on the use of specific adsorbent materials. Among them, silver-exchanged zeolites are the most efficient for Xe extraction. Before the use of a material in processes, it is crucial to ensure about its performance, especially when use in systems operating 24/7. Ag-ZSM-5 (one of the studied exchanged zeolite) is an efficient candidate to enrich Xe, but long-term stability seems to remain a topic.

In our study, we assay to elucidate the relation between the structure of the material (Ag-ZSM-5 from different suppliers and synthesis) and the property (xenon uptake and deactivation). We especially investigated structure parameters that influence the properties. This work is based on two approaches: 1/ the use of experimental technics for deep characterisation (liste) [1], 2/ the use of simulation by Density Functional Theory (DFT) [2].

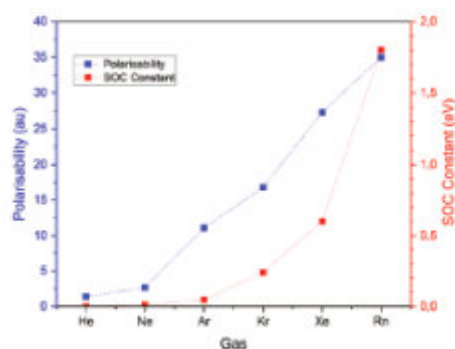


**Figure 1.** Nature of the interaction between Ag and Noble Gas [2].

### References

- [1] C Courtney, A Millet, G Couchaux, A Gossard, A Tuel, N Bonnet, S Topin, D Farrusseng, *Industrial & Engineering Chemistry Research*, **62**, 11939 (2023).  
[2] C Courtney, B Siberchicot, *Phys. Chem. Chem. Phys.*, **25**, 23929 (2023).





## Effect of the recrystallization process in the catalytic performance of micro-mesoporous zeolites on the isomerization of methyl oleate

J. F. Sierra-Cantor<sup>1</sup>, O. Gimello<sup>2</sup>, L. Bernardi<sup>3,4</sup>, C. A. Guerrero-Fajardo<sup>5</sup>, F. Di Renzo<sup>2</sup>, N. Tanchoux<sup>2</sup>, C. Gérardin<sup>2</sup>

<sup>1</sup> Institut de Chimie des Milieux et Matériaux de Poitiers, 86000 Poitiers, France

<sup>2</sup> Institut Charles Gerhardt de Montpellier, 34293 Montpellier, France

<sup>3</sup> Dip. Industrial Chemistry Toso Montanari, Alma Mater Studiorum Università di Bologna, 40136 Bologna, Italy

<sup>4</sup> C<sup>3</sup> Center for Chemical Catalysis, Alma Mater Studiorum Università di Bologna, 40126 Bologna, Italy

<sup>5</sup> Departamento de Química, Universidad Nacional de Colombia, 111321 Bogotá, Colombia

[francesco.di-renzo@umontpellier.fr](mailto:francesco.di-renzo@umontpellier.fr)

Considering the significance of micro-mesoporous materials in the utilization of biomass, recently, it was observed that the use of micro-mesoporous ferrierite as catalyst in the methyl oleate isomerization reaction has led to higher yields and better stability against deactivation [1-2]. In this study, to understand the effect of the mesopores on the catalytic performance in zeolitic materials, a secondary mesoporous system was generated by a well-controlled recrystallization process in two different zeolites, ferrierite [3] and zeolite Y [4].

They were obtained by treatment with a base and Cetyl Trimethyl Ammonium Bromide (CTAB), followed by a calcination at 550 °C in air for 8h. These micro-mesoporous materials from ferrierite (H-FER-REC) and zeolite Y (H-Y-REC) were deeply characterized by XRD, TEM, NH<sub>3</sub>-TPD, N<sub>2</sub> sorption, and FT-IR with acetonitrile as probe molecule. Moreover, their catalytic performance in methyl oleate isomerization to branched fatty acid methyl esters (brFAME) was evaluated along with their parent H-form (H-FER-PAR & H-Y-PAR) in a batch reactor (cat. loading: 5% wt., time: 8h, Temp.: 285°C, P: 2.0 MPa).

**Table 1.** Properties and catalytic performance of micro-mesoporous zeolites. 285 °C, WHSV 3.5 h<sup>-1</sup>, 8h.

Zeolite	Si/Al	V <sub>pore</sub> (cm <sup>3</sup> /g)		Acidity (μmol/g)	Yield in branched C <sub>18</sub> FAME
		V <sub>micro</sub>	V <sub>meso</sub>		
H-FER-PAR	9.7	0.13	0.07	1050	55.5
H-FER-REC	6.6	0.10	0.18	720	62.0
H-Y-PAR	30.2	0.17	0.28	254	36.8
H-Y-REC	24.4	0.10	0.48	239	39.1

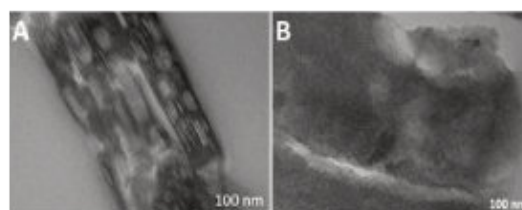


**Figure 1.** TEM micrographs: H-FER-REC (A) and H-Y-REC (B).

The properties of micro-mesoporous zeolites are summarized in Table 1. It is possible to see the new mesoporous systems created through the recrystallization process in the TEM micrographs shown in Figure 1. In the case of the ferrierite, parallelepipedal mesopores were formed. N<sub>2</sub> isotherms indicate that H-FER-REC mesopores are only accessible through channels smaller than 4 nm. The recrystallization led to an increase in the mesopore volume leaving a micropore volume similar to that of the parent material. It also leads to a nearly 30 % loss of silica content and total acidity value. On the other hand, the recrystallized zeolite Y showed a vermicular mesoporous structure inside the crystals of the microporous faujasite structure, creating a hierarchical micro-mesoporous zeolitic material, leading to an increase in the mesopore volume. Nearly 20 % silica was lost while the acidity remained unchanged.

The catalytic performance of both micro-mesoporous materials, ferrierite and zeolite Y, showed that the presence of mesopores led to higher yields in branched C<sub>18</sub> methyl esters. The best yield value, 62.0%, was found using the recrystallized ferrierite, 12 % higher than the 55% obtained with the parent one. In the case of the less selective zeolite Y, the recrystallized material led to a yield (39.1%) 6 % higher than the parent one (36.8%). It was observed that the main active sites were the strong acidic ones present in the microporous zeolitic structure. The main effect of the introduction of the secondary mesoporous system was the improvement of the availability of active sites. Other structures, such as the extra-framework aluminum sites (EFAL), played a significative role in the selectivity of by-products. All these results will be discussed during the conference.

### References

- [1] J. F. Sierra-Cantor, *et al*, *Applied Catalysis B: Environment and Energy*, **344**, 123602 (2024)
- [2] A. Bolshakov, *et al*, *Applied Catalysis B: Environment and Energy*, **263**, 118356 (2020)
- [3] X. Cheng, *et al*, *Microporous Mesoporous Materials*, **260**, 132, (2018)
- [4] R. Chal, *et al*. *Chemical Communications*, **46**, 7840, (2010)



## Synthesis of large-pore pure silica zeolites using phenyl-containing diquat OSDAs

A.V. Hilário<sup>1</sup>, K. Bernardo-Gusmão<sup>1</sup>, C.W. Lopes<sup>1,2</sup>

<sup>1</sup> Laboratory of Reactivity and Catalysis (LRC), Federal University of Rio Grande do Sul, Brazil

<sup>2</sup> Laboratory of Catalysis and Characterization of Materials (LC2M), Federal University of Paraná, Brazil.

christianwittee@ufpr.br

For over 50 years, zeolites have been widely used as catalysts in the most important industrial processes, with an estimated annual consumption of approximately 250,000 metric tons per year. For example, they are utilized in hydrocarbon conversion (alkylation, cracking, hydrocracking, isomerization, etc.) and are well-known for their efficient structural properties in capturing gases like CO<sub>2</sub>. Characteristics such as high acidity, well-defined structure, and excellent hydrothermal stability enable the broad demand for these microporous crystalline materials. They are commonly prepared from aluminosilicate gels in the presence of structure-directing agents (SDAs) – which can be inorganic and/or organic cations (OSDAs) – in basic or fluoride media under hydrothermal conditions [1-2]. The introduction of organic molecules into zeolite synthesis gels led to a surge in the number of new zeolitic structures obtained. The choice of OSDAs is of fundamental importance in the synthesis of a zeolite, as they play a role in directing the structure of a specific zeolite, which would not form in their absence. Moreover, they can exhibit a templating effect, allowing the configuration of the structure to be obtained based on its relationship with the size and shape of the OSDA employed [3]. In this work, organic ammonium and imidazolium cations (**Figure 1**) were used as OSDAs in zeolite synthesis. Purely siliceous materials were synthesized employing diquat OSDAs containing phenyl groups as spacer lengths between the OSDA charges.

The first step of the synthesis involved the exchange of the bromide anion (Br<sup>-</sup>) of both cations for hydroxyl anions (OH<sup>-</sup>). The exchange was carried out by dissolving the OSDAs in 50 mL of water and stirring with an ion exchange resin (Amberlite® IRN78 OH) for 24 hours. After this period, the resin was separated by filtration under reduced pressure. The solutions were then subjected to acid-base titration to quantify OH<sup>-</sup>, followed by concentration by rotary evaporation, and finally, they were titrated again. The second step involved mixing the aqueous solutions of the OSDAs obtained in the first step with the SiO<sub>2</sub> source, which in this case was tetraethyl orthosilicate (TEOS). The reaction mixture was kept under stirring at room temperature for water (H<sub>2</sub>O) evaporation to achieve the desired concentrations of the synthesis gels. At the end, hydrofluoric acid (HF 40%) was added, and the gel was homogenized. The syntheses followed the molar ratios: **1 SiO<sub>2</sub> : 0.2 OSDA(OH)<sub>2</sub> : 0.4 HF : xH<sub>2</sub>O**, where **x** represents the molar ratios 5, 10, and 15. The synthesis gels were divided into two stainless steel autoclaves lined with Teflon and kept in an oven with stirring at 40 rpm at 150 °C, one for 7 days and the other for 11 days. The resulting solids were then washed with 500 mL of water at 80 °C and 30 mL of acetone p.a., filtered under vacuum, and dried in an oven at 60 °C for 24 hours.

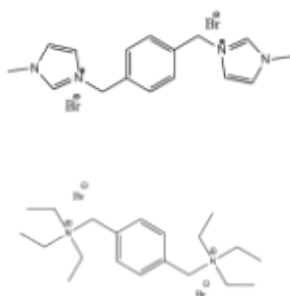


**Table 1.** Zeolite synthesis outputs from the employment of the OSDAs 1 and 2.

OSDA	H <sub>2</sub> O/Si=5	H <sub>2</sub> O/Si=10	H <sub>2</sub> O/Si=15
1	MTW	amorphous	amorphous
2	*STO	*STO	*STO

**Figure 1.** Organic structure-directing agents studied in this work.

**Table 1** presents the results obtained for each of the syntheses performed with OSDA1 and OSDA2. It is possible to observe the formation of only the MTW phase in the syntheses carried out with different H<sub>2</sub>O/Si ratios using the OSDA based on the imidazolium cation. As can be seen, the diffraction patterns (**Figure 2a**) when using an H<sub>2</sub>O/Si ratio of 5 correspond to the theoretical pattern of the large-pore MTW zeolite in its purely siliceous form. Increasing the H<sub>2</sub>O/Si ratio to 10 and 15 results in a predominantly amorphous solid with only a few reflections between 20-25° (2θ), indicating the initial formation of the MTW phase. The MTW topology is formed by unidirectional channels and has previously been obtained using a series of imidazolium cations [4-5]. The formation of a unidirectional material is not surprising due to the shape of OSDA1, which favors its accommodation in channels. The formation of a large-pore zeolite was also expected due to the geometric constraints of the directing molecule.



**Table 1** also presents the results of the tests conducted using OSDA2. The formation of the SSZ-31 zeolite with \*STO topology can be observed in various synthesis gel compositions. The \*STO topology belongs to the group of disordered zeolites. Like Beta zeolite, SSZ-31 has different polymorphs, which significantly affect the X-ray diffraction patterns [6]. **Figure 2b** shows the X-ray diffraction patterns of the large-pore zeolites with \*STO topology obtained with H<sub>2</sub>O/Si ratios of 5, 10, and 15. For the ratios of 5 and 15, it was found that the materials do not exhibit all the characteristic reflections of the \*STO phase due to being less crystalline compared to the sample obtained with an H<sub>2</sub>O/Si ratio of 10 or having a considerably smaller particle size. Furthermore, the peaks between 3-10° (2θ) in the zeolite obtained with an H<sub>2</sub>O/Si ratio of 10 are overlapped in the diffractogram, whereas in other samples, they are separated. This is a strong indication of the presence of different proportions of \*STO polymorphs. The use of OSDA2 was reported by Zones and collaborators in the synthesis of SSZ-43 zeolite, which strongly competes with the \*STO phase when other structure-directing agents are used and in different synthesis gel compositions [7]. In the present work, OSDA2 proved to be quite selective for the \*STO phase in fluoride media.

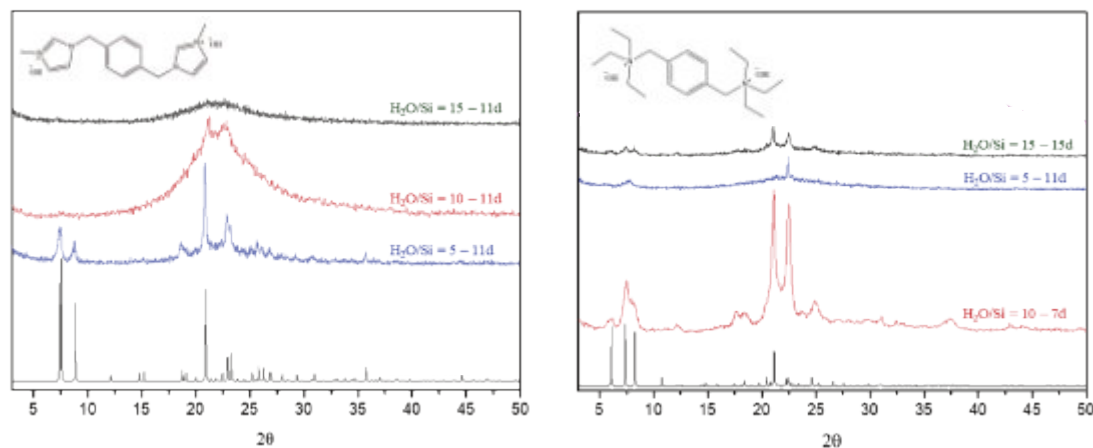


**Figure 2.** X-ray diffractograms of the pure silica zeolites obtained in fluoride media using OSDA1 (a) and OSDA2 (b).

The zeolites and OSDAs were subjected to solid-state <sup>13</sup>C NMR, and the results are consistent with the N<sub>2</sub> adsorption/desorption isotherms, as it was possible to confirm that OSDA1 and OSDA2 remain intact within the pores of the zeolites. Elemental analyses show that the C/N ratios were slightly higher in the zeolitic materials immediately after synthesis compared to the OSDAs, suggesting that the cations are intact within the pores of the zeolites, but with the presence of additional organic matter. The scanning electron microscopy (SEM) analyses of the MTW and \*STO zeolites confirmed that the zeolites exhibit rod-like morphology, which is characteristic of their topologies. Additionally, the transmission electron microscopy (TEM) images reveal its characteristic unidirectional channels.

These findings underscore the significant role of OSDAs in tailoring the structural and morphological properties of zeolites, offering insights into the design of advanced materials for catalytic applications. By carefully selecting and optimizing the OSDAs, it is possible to influence not only the crystallinity and pore architecture but also the overall performance of the zeolite in specific catalytic reactions.

## References

- [1] M. J. Mendoza-Castro, E. Oliveira-Jardim, N. T. Ramírez-Marquez, C. A. Trujillo, N. Linares, J. García-Martínez, *J. Am. Chem. Soc.*, **144**, 5163-5171 (2022).
- [2] M. Stöcker. *Micropor. Mesopor. Mater.*, **82**, 257–292 (2005).
- [3] L. G. Hortigüela e M. A. Cambor, Introduction to the Zeolite Structure-Directing Phenomenon by Organic Species: General Aspects. In: Insights into the Chemistry of Organic Structure-Directing Agents in the Synthesis of Zeolitic Materials. Structure and Bonding, Springer, Cham (2017).
- [4] A. Rojas, M. L. San-Roman, C. M. Zicovich-Wilson, M. A. Cambor, *Chem. Mater.*, **25**, 729-738 (2013).
- [5] A. Rojas, L. Gómez-Hortigüela, M. A. Cambor, *Dalton Trans.*, **42**, 2562 (2013).
- [6] H. V. Koningsveld, R. F. Lobo, *J. Phys. Chem. B*, **107**, 10983-10989 (2003).
- [7] M. Roslova, V. J. Cybulskis, M. E. Davis, S. I. Zones, X. Zou, D. Xie, *Angew. Chem. Int.*, **61**, e202115087 (2022).

## Acknowledgments

The authors thank the PRH 50.1 (PPGQ/UFRGS) and the National Agency of Petroleum, Natural Gas and Biofuels (ANP) for supporting this project.



## Enhancing nucleation to synthesize Al-rich CHA zeolites under ultra-low OSDA contents

E. Bello-Jurado<sup>1</sup>, I. Millet<sup>1</sup>, L. Van Tendeloo<sup>2</sup>, F-W. Schütze<sup>3</sup>, P. N. R. Vennestrøm<sup>4</sup>, A. Corma<sup>1</sup>, M. Moliner<sup>1</sup>

<sup>1</sup> Instituto de Tecnología Química, Universitat Politècnica de València-Consejo Superior de Investigaciones Científicas, Avenida de los Naranjos s/n, 46022 València, Spain

<sup>2</sup> Umicore N.V., Watertorenstraat 33, 2250 Olen, Belgium

<sup>3</sup> Umicore AG & Co. KG, Hanau 63457, Germany

<sup>4</sup> Umicore Denmark ApS, Kogle Allé 1, 2970 Hørsholm, Denmark  
esbelju@itq.upv.es

Cu-containing high-silica CHA zeolites were first reported 15 years ago as highly active, selective and most importantly hydrothermally stable catalysts for the selective catalytic reduction (SCR) of NO<sub>x</sub> using ammonia as reducing agent [1]. The preferred organic structure directing agent (OSDA) to synthesize CHA is the expensive and complex N,N,N-trimethyladamantammonium (TMAda) cation [2,3]. Among the different low-cost OSDA molecules reported for the synthesis of CHA, the use of simple tetraalkylammonium cations, such as tetraethylammonium (TEA) or methyltriethylammonium (MTEA) can be a very cost-attractive synthesis approach, particularly when attempting the preparation of Al-rich CHA materials with Si/Al~5 [4]. However, the preferred conditions to synthesize these Al-rich often require the use of pre-crystallized FAU zeolites as Al-source and MTEA (or TEA)/Si molar ratios above 0.15. In this work we rationalize the preparation in a more efficient way to reduce the synthesis cost and maximize the SCR performance, requiring FAU-free synthesis conditions and ultra-low MTEA/Si molar ratios.

We propose a synthesis route that involve the control of the nucleation step by preparing and introducing active CHA seeds in the preparative gels to facilitate the crystallization of the Al-rich CHA zeolites with reduced MTEA/Si molar ratios, avoiding the use of pre-crystallized FAU zeolites as Si and/or Al sources. The active CHA seeds have been introduced as “gel-type” precursor to maximize the dispersion/suspension of the formed CHA crystallites and to reduce the number of synthesis steps, such as filtration, separation and waste removal/treatments.

The first proposed step in our synthesis route involves the “in-situ” preparation of an amorphous silicoaluminate (ASA) precursor (see Figure 1 (a)), resulting in large agglomerates formed by very small nanosized primary ASA particles. The following step includes the “in-situ” deposition of nano-sized CHA particles from the “gel-type” seeds on the external surface of the ASA aggregates during the gel preparation (see yellow arrows in Figure 1 (b)). Once the prepared gel was introduced under hydrothermal conditions to carry out the MTEA-mediated CHA crystallization, a clear contraction and densification of the former ASA particles was observed at short times (see Figure 1(c)), and the crystallization appears to be initially occurring at the external surface of the contracted/densified ASA particles, with a clear crystallization/rearrangement from the external surface of the particles over time (see Figure 1 (d) and (e)).



**Figure 1.** FESEM images of the solids achieved and proposed crystallization mechanism at different synthesis steps.

The crystallization of Al-rich CHA zeolites with low MTEA/Si molar ratios and without using pre-crystallized FAU zeolites as Si and/or Al sources has been accomplished by controlling the nucleation step thanks to introducing active CHA nanoseeds in the preparative gels, making this synthetic route cost-competitive with commercial preparation descriptions for CHA. The optimized Al-rich CHA material performs as a very active and stable catalyst for heavy-duty NH<sub>3</sub>-SCR of NO<sub>x</sub> applications after post-synthetically incorporating extra-framework copper cations (see Figure 2) [5].

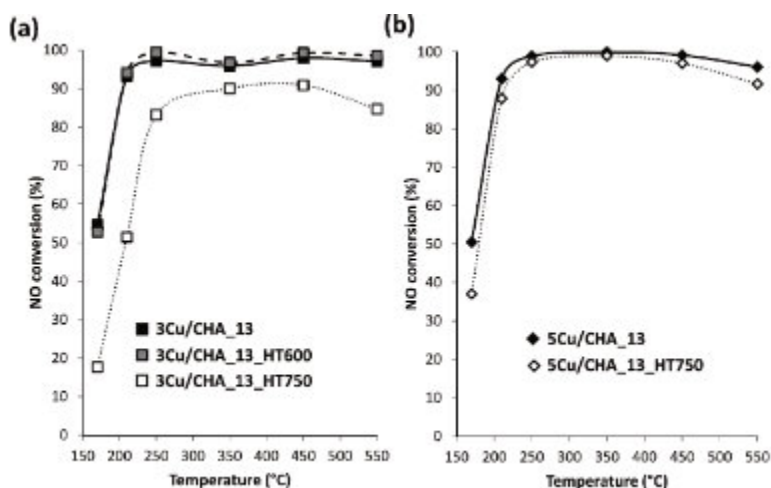


**Figure 2.** Catalytic performance for the  $\text{NH}_3$ -SCR of  $\text{NO}_x$  reaction using 3 wt% (a) and 5 wt% (b) Cu-containing CHA catalysts in their fresh and aged (steam at 600°C and/or 750°C for 16h) forms.

### References

- [1] I. Bull, S. Boorse, W.M. Jaglowski, G.S. Koermer, A. Moini, J.A. Patchett, W.-M. Xue, P. Burk, J.C. Dettling, M.T. Caudle, Copper CHA zeolite Catalysts, US7601662, 2009.
- [2] S.I. Zones, Zeolite SSZ-13 and its method of preparation, US4544538, 1985.
- [3] S.I. Zones, *J. Chem. Soc. Faraday Trans*, **87**, 3709-3716 (1991).
- [4] E. Bello, P. Ferri, M. Nero, T. Willhammar, I. Millet, F.W. Schütze, L. Van Tendeloo, P.N.R. Vennestr, M. Boronat, A. Corma, M. Moliner, *Applied Catalysis B: Environmental*, **303**, (2022).
- [5] E. Bello-Jurado, I. Millet, L. Van Tendeloo, F. Schütze, P.N.R. Vennestrom, A. Corma, M. Moliner, *Microporous and Mesoporous Materials*, **371**, (2024).

### Acknowledgments

The authors acknowledge financial support by Umicore, by the Spanish Government through PID2021-122755OB-I00 funded by MCIN/AEI/10.13039/501100011033 and TED2021-130739B-I00 funded by MCIN/AEI/10.13039/501100011033/EU/PRTR, and by Generalitat Valenciana through AICO/2021/201. The authors are also thankful for the Severo Ochoa financial support by the Spanish Ministry of Science and Innovation (CEX2021-001230-S/funding by MCIN/AEI/10.13039/ 501100011033). E.B.-J. acknowledges the Spanish Government for a FPI scholarship (PRE2019-088360). The Electron Microscopy Service of the UPV is also acknowledged for their help in sample characterization.



## Seed-Assisted Synthesis of Nanosized Zeolite P for Improved CO<sub>2</sub> Capture Kinetics

J. Al Atrach<sup>1</sup>, A. Aitblal<sup>1</sup>, A. Amedlous<sup>1</sup>, Y. Xiong<sup>1</sup>, R. Guillet-Nicolas<sup>1</sup>, and V. Valtchev<sup>1\*</sup>

<sup>1</sup> Normandie Université, ENSICAEN, UNICAEN, CNRS, Laboratoire Catalyse et Spectrochimie (LCS), 14000 Caen, France.

jaouad.al-atrach@ensicaen.fr

Slow adsorption rates in zeolites pose a significant challenge for industrial applications. One promising solution involves downsizing zeolite crystals to enhance gas adsorption and separation by increasing surface area and reducing diffusion pathways [1, 2]. This work presents a template-free synthesis of pure nanocrystalline P zeolite with Gismondine (GIS-type) framework using a relatively small amount of seeds, lower temperatures, and shorter synthesis times. The nanosized zeolite demonstrated superior CO<sub>2</sub> adsorption and separation as well as improved CO<sub>2</sub> adsorption kinetics compared to its micron-sized counterpart, as validated by breakthrough curve analysis, highlighting its enhanced diffusion properties and performance [3].

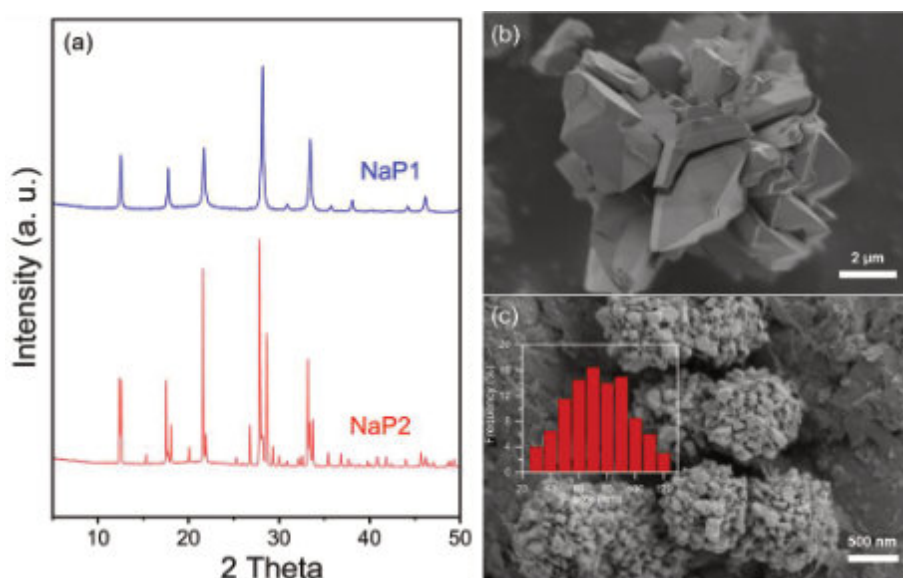


**Figure 1.** XRD patterns of as-synthesized zeolites (a) and SEM images of micron-sized NaP2 (b) and nanosized NaP1 (c).

Compared to the conventional synthesis method for zeolite P2, which typically produces micron-sized zeolite NaP2, the seed-assisted approach using pre-synthesized NaP2 as seeds successfully yielded highly pure and stable nanocrystalline zeolite P1 isotype (Figure 1a). The introduction of NaP2 crystal seeds accelerates nucleation kinetics and shifts the inter-zeolite transformations (IZTs) from NaX-to-NaP2 to NaP2-to-NaP1, resulting in a pure NaP1 phase within just 24 h at 100 °C. This method not only reduces synthesis time and temperature but also ensures phase purity. Additionally, substituting NaP2 seeds with NaP1 seeds in the process resulted in NaP1 (2<sup>nd</sup> Gen) phase, indicating that the type of NaP seed used does not significantly influence the final product.

During the conventional synthesis of micron-sized P2 zeolite, the crystals formed were diamond-shaped with sharp edges, indicating high crystallinity, and measured between 5–10 μm in size (Figure 1b). However, adding NaP2 seeds to the synthesis led to NaP1 zeolite forming as spherical agglomerates, with individual particles ranging from 30–120 nm and clusters measuring 500–800 nm (Figure 1c). This suggests that the NaP2 seeds partially dissolve during synthesis, facilitating heterogeneous nucleation and accelerating crystal growth, resulting in the formation of NaP1 nanoaggregates. The seeds effectively bypass the slow nucleation stage, directly promoting faster crystallization.

Potassium-exchanged P zeolites demonstrated significantly higher CO<sub>2</sub> adsorption compared to their sodium counterparts, with uptakes of 1.6 mmol/g for micron-sized KP2 and 1.9 mmol/g for nanosized KP1. These adsorbents showed negligible adsorption of N<sub>2</sub> and CH<sub>4</sub>, resulting in exceptionally high CO<sub>2</sub> selectivity. The enhanced selectivity is attributed to the small pore size and the exhibited trapdoor effect of the K-exchanged zeolites. The "molecular trapdoor effect" allows CO<sub>2</sub> to enter the pores by temporarily displacing K<sup>+</sup> cations, a mechanism not accessible to N<sub>2</sub> and CH<sub>4</sub>.



In addition to higher CO<sub>2</sub> uptake, nanosized zeolite KP1 demonstrated significantly faster adsorption kinetics compared to its micron-sized counterpart, KP2. KP1 reached equilibrium 93 times faster, indicated by a steeper adsorption curve, suggesting more uniform CO<sub>2</sub> diffusion through its smaller particles (Figure 2a). In contrast, KP2 exhibited a slower approach to equilibrium, attributed to its larger particle size and thus longer diffusion pathways (Figure 2b). Kinetics analysis supported by fitting results revealed that while KP2's diffusion was mainly limited by surface barrier resistance, KP1 benefited from a combination of intra-crystalline and surface barrier resistance mechanisms, enhancing overall diffusion rates. These findings highlight that reducing crystal size can significantly accelerate the adsorption rate in K-exchanged zeolites.

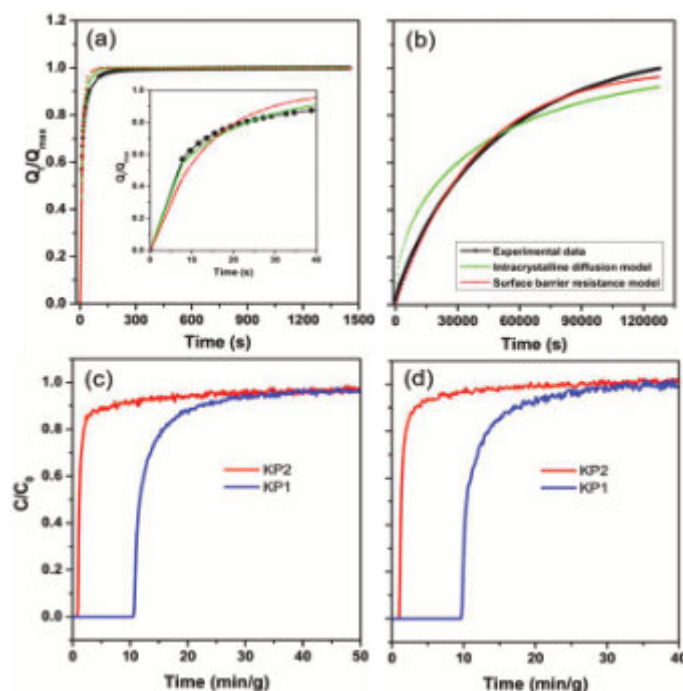


**Figure 2.** Fractional uptake curves and the fitting results of intra-crystalline diffusion and surface barrier resistance models for KP1 (a) and KP2 (b) samples at 0.05 bar and 25 °C. And CO<sub>2</sub> breakthrough curves at 25 °C obtained from competitive dynamic adsorption experiments, CO<sub>2</sub>/N<sub>2</sub>/He, 5/25/70 (c) and CO<sub>2</sub>/CH<sub>4</sub>/He, 10/15/75 (d).

Consistent with the equilibrium adsorption and kinetic results, breakthrough curve analysis confirmed these findings as fast and efficient CO<sub>2</sub>/N<sub>2</sub> and CO<sub>2</sub>/CH<sub>4</sub> separations recorded for the nanosized sample. The results showed a remarkably enhanced breakthrough time for KP2 vs KP1 in CO<sub>2</sub>/N<sub>2</sub> (1.0 vs 10.9 min) and CO<sub>2</sub>/CH<sub>4</sub> (1.1 vs 9.9 min) mixtures, along with much higher adsorption capacity for CO<sub>2</sub>/N<sub>2</sub> (0.18 vs 1.33 mmol/g) and CO<sub>2</sub>/CH<sub>4</sub> (0.18 vs 1.21 mmol/g) mixtures (Figure 2c and d). The reduced breakthrough time and adsorption capacity in KP2 results from a rapid saturation of the zeolite crystal surface adsorption sites and the absence of transport through the KP2 channel system. The set of experimental data demonstrates the importance of zeolite crystal engineering for improving the gas separation performance of processes involving CO<sub>2</sub>, N<sub>2</sub>, and CH<sub>4</sub>.

## References

- [1] Mintova, S.; Gilson, J.-P.; Valtchev, V. *Nanoscale*, 5 (15), 6693–6703 (2013).
- [2] Tosheva, L.; Valtchev, V. P. *Chem. Mater.*, 17 (10), 2494–2513 (2005).
- [3] Al Atrach, J.; Aitblal, A.; Amedlous, A.; Xiong, Y.; Desmurs, M.; Raux, V.; Guillet-Nicolas, R.; Valtchev, V. *ACS Appl. Mater. Interfaces*, 16 (29), 38006–38016 (2024).

## Seed-Assisted Synthesis of LEV Zeolite: Exploring a Novel Adsorbent for CO<sub>2</sub> Capture and Gas Separation

J. Al Atrach<sup>1</sup>, A. Amedlous<sup>1</sup>, Y. Xiong<sup>1</sup>, D Honorato-Piva<sup>1</sup>, R. Guillet-Nicolas<sup>1</sup>, and V. Valtchev<sup>1\*</sup>

<sup>1</sup> Normandie Université, ENSICAEN, UNICAEN, CNRS, Laboratoire Catalyse et Spectrochimie (LCS), 6 boulevard Marechal Juin, 14000 Caen, France.

jaouad.al-atrach@ensicaen.fr

The urgent need to mitigate carbon emissions has driven research into cost-effective small-pore zeolites with tunable Si/Al ratios for efficient CO<sub>2</sub> capture, offering a promising alternative to traditional energy-intensive amine-based separation methods [1-3]. Unlike other well-studied small-pore zeolites such as CHA, LTA, and RHO, Levynite (LEV-type) zeolite has rarely been utilized in CO<sub>2</sub> adsorption due to its typically higher Si/Al ratio and challenging synthesis. This study aims to address this gap by exploring Levynite's potential in CO<sub>2</sub> separation, highlighting the critical role of synthesis in optimizing the Si/Al ratio to enhance adsorption properties. The synthesis and morphology of nano-sized and micron-sized LEV zeolite were investigated using a seed-assisted method, both with and without an organic template, and the adsorption performances of the resulting materials were compared. Using different seeding protocols resulted in two distinct LEV-type zeolites with varying crystal sizes, morphologies and chemical compositions. The application of seeds enhanced the purity and reduced the synthesis time of the LEV samples (Figure 1a). Nanosized LEV was synthesized using a DMP template with pre-synthesized impure LEV seeds, while micron-sized LEV was obtained using nanosized seeds in a template-free synthesis (Figure 1c and d).

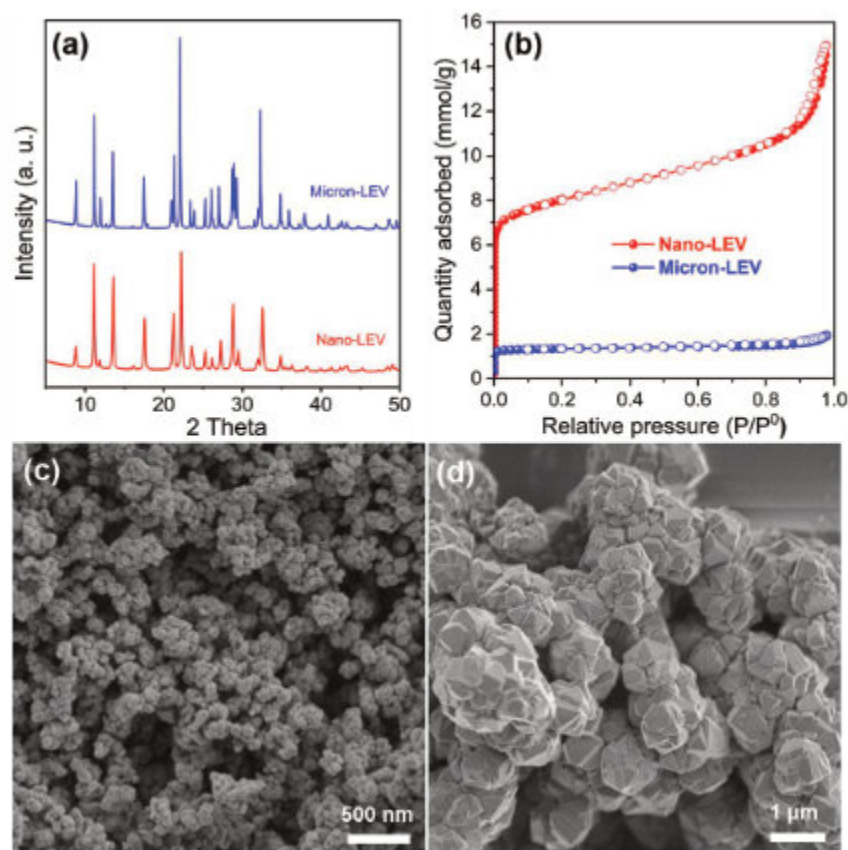


**Figure 1.** XRD patterns (a) N<sub>2</sub> adsorption-desorption at -196 °C (b) and SEM images of nanosized (c) and micron-sized LEV (d).

The synthesis of nanosized LEV zeolite involved a "sacrificial seeding" approach, where seeds fully dissolved within the first 24 hours of hydrothermal treatment, forming new nanocrystals after 48 hours. Our interpretation is that the dissolution of seed crystals is breeding structure fragments that serve as viable nuclei and promote nanocrystals formation. Conversely, micron-sized LEV was synthesized through a "seed preservation" method, where seeds remained partially intact, serving as stable sites for crystal growth. This resulted in larger crystals with distinct growth patterns and chemical compositions. These synthesis strategies highlight the influence of seeding techniques on the crystal morphology and composition of LEV zeolites.





These differences arose from the varying synthesis conditions, leading to two LEV materials with distinct crystal sizes and chemical compositions (Table 1). N<sub>2</sub> adsorption-desorption isotherms at cryogenic temperatures confirmed these differences, revealing that the nanosized LEV exhibited 6 times higher surface area and 14 times higher mesoporosity than its micron-sized counterpart (Figure 1b and Table 1). The microporosity was also found to be higher in the nanosized sample, likely due to the higher Na<sup>+</sup> content in the micron-sized LEV. The negligible micropore volume of micron-sized LEV suggests that in full occupation of ion exchange sites by sodium, the micropore volume is not accessible for nitrogen. These adsorption properties are crucial for understanding subsequent gas adsorption measurements.

Table 1: Chemical composition and porosity of as-prepared LEV adsorbents.

Material	Chemical composition	Si/Al ratio	Na <sup>+</sup> /Al ratio	S <sub>BET</sub> (m <sup>2</sup> /g)	V <sub>mic</sub> (cm <sup>3</sup> /g)	V <sub>t</sub> (cm <sup>3</sup> /g)
Nano-LEV	Na <sub>2.4</sub> H <sub>4.7</sub> Al <sub>7.1</sub> Si <sub>46.9</sub> O <sub>108</sub>	6.6	0.34	674	0.194	0.519
Micron-LEV	Na <sub>10.9</sub> Al <sub>11.2</sub> Si <sub>41.8</sub> O <sub>108</sub>	3.4	0.97	120	0.041	0.064

The CO<sub>2</sub> adsorption performance of sodium-containing nano- and micron-sized LEV adsorbents was evaluated through CO<sub>2</sub> adsorption isotherms measured at 0 to 50 °C and up to 1 bar. Micron-sized LEV demonstrated a higher CO<sub>2</sub> uptake (5.81 mmol/g at 0 °C) compared to Na-nanosized LEV (4.60 mmol/g), with the difference attributed to the Si/Al ratio (Figure 2a and b). The lower Si/Al ratio in micron-sized LEV (3.4) provided more Al sites and Na<sup>+</sup> cations, enhancing electrostatic interactions with CO<sub>2</sub> and resulting in a 22% greater adsorption capacity. Conversely, nanosized LEV (Si/Al = 6.6) exhibited weaker CO<sub>2</sub> interactions due to fewer charge sites. Both samples showed a decrease in CO<sub>2</sub> uptake with increasing temperature, while the distinct plateau in micron-sized LEV isotherms indicated full occupation of adsorption sites at high pressures, unlike nanosized LEV.

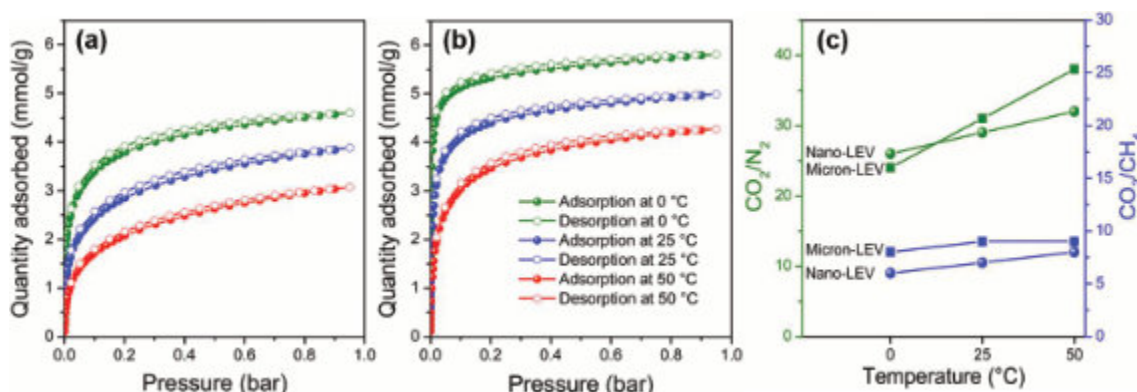


Figure 2. CO<sub>2</sub> adsorption-desorption isotherms at 0, 25, and 50 °C of: (a) nano-sized LEV and (b) micron-sized LEV, and (c) their CO<sub>2</sub>/N<sub>2</sub> (15/85, v/v) and CO<sub>2</sub>/CH<sub>4</sub> (40/60, v/v) selectivities varies with temperature.

CO<sub>2</sub> selectivity over N<sub>2</sub> and CH<sub>4</sub> was higher for the micron-sized LEV due to its superior CO<sub>2</sub> uptake at low pressure (Figure 2c). The CO<sub>2</sub>-over-N<sub>2</sub> selectivity increased with temperature under post-combustion conditions, while CO<sub>2</sub>/CH<sub>4</sub> selectivity remained stable under biogas conditions. The micron-sized LEV consistently showed higher selectivity compared to the nano-sized sample, emphasizing its potential for practical gas separation applications.

## References

- [1] M. Bui et al., *Energy Environ. Sci.*, vol. 11, no 5, p. 1062-1176 (2018).
- [2] F. Meng, Y. Meng, T. Ju, S. Han, L. Lin, J. Jiang, *Renewable and Sustainable Energy Reviews*, vol. 168, p. 112902 (2022).
- [3] R. L. Siegelman, E. J. Kim, et J. R. Long, *Nat. Mater.*, vol. 20, no 8, p. 1060-1072 (2021).



## Solvent-Free Synthesis of Ti isomorphously Substituted Beta Zeolite

K. Yomthong<sup>1</sup>, S. Klinyod<sup>1</sup>, S. Ittisanronnchai<sup>2</sup>, C. Wattanakit<sup>1</sup>

<sup>1</sup>School of Energy Science and Engineering, Vidyasirimedhi Institute of Science and Technology, Rayong 21210, Thailand

<sup>2</sup>Frontier Research Center, Vidyasirimedhi Institute of Science and Technology, Rayong 21210, Thailand  
Krissanapat.y\_s22@vistec.ac.th

To date, zeolites substituted with heteroatom at tetrahedral locations in their frameworks or encapsulated with the ultra-small metal clusters inside porous architectures demonstrated an advantage over the other non-porous metal oxides due to the influence of the pore confinement effect stabilized metal species. In particular, the crystalline titanosilicate with BEA topology described benefits and is widely used for many catalytic reactions, such as phenol hydroxylation, alkene epoxidation, and green epoxidation reactions with hydrogen peroxide [1,2]. However, its design still requires appropriate tuning of desirable properties such as textural properties, active site, and surface acidity to enhance an efficient catalytic activity. In this work, we demonstrate the use of a solvent-free approach for synthesizing highly dispersed Ti isomorphously substituted beta zeolite. The solvent-free synthesis approach overcomes some limitations, for example the requirement of large amounts of solvent, eventually leads to environmental concerns [3]. Moreover, to avoid low dispersion of Ti active species, Ti-aluminosilicate nanobead (Ti-SiAl-NB) is aimed to be used as a starting solid material for Ti-beta zeolite synthesis because nanobeads benefit the highly dispersed heteroatom in the starting silica [4,5]. To summarize, the design of highly dispersed Ti active species using a solvent-free approach is our challenge goal. The isomorphously Ti-substituted beta zeolite will be prepared using Ti-SiAl-NB as the starting titano-aluminosilicate source. Moreover, the Ti-beta zeolite will be further used as the epoxidation catalyst in catalytic biomass upgrading.

Obviously, the PXRD patterns of nanobeads confirmed the amorphous characteristic behavior. In addition, the nanobeads formed a spherical shape using a low amount of Ti content. Unfortunately, the non-spherical particle was obtained when the Ti content was increased. This is related to the fact that a high amount of Ti disturbs the formation of nanobeads. Subsequently, the Ti-SiAl-NB was used as the dual Ti and Si sources for the synthesis of the Ti-beta zeolite. The PXRD patterns, UV-Vis spectra, and morphology are illustrated in Figure 1. The sharp PXRD pattern confirms the formation of a crystalline BEA framework; however, the absence of a TiO<sub>2</sub> peak might be due to the low amount of Ti loading. For the UV-Vis spectra, the responded signal at around 210 nm was obtained with samples of low amount of Ti content (0.0001, 0.0003, and 0.0005 molar of Ti), indicating that the Ti could be incorporated into a tetrahedral framework. However, the highest content of Ti (0.0007-Ti-beta) exhibited two UV-Vis responded peaks, indicating that two Ti species were incorporated in the beta zeolite. The peaks of around 210 nm indicate a tetrahedral framework, and the peak of approximately ~270 to 300 nm indicates an extra-framework of Ti [6]. Unfortunately, the particle size of Ti-beta zeolite increased with an increase in the amount of Ti and promoted the non-homogeneous particle size distribution. It should be noted that the 0.0007-Ti-SiAl-NB was not fully utilized to form Ti-beta zeolite. The high amount of Ti might have disturbed the migration of the starting precursor to form the beta zeolite effect, which has affected the difficulty of Ti isomorphous insertion corresponding to the presence of spherical nanobead attached to the zeolite particle. In conclusion, this work opens a new perspective for catalyst design. In addition, the Ti-beta zeolite has potentially been applied in many catalytic reactions, for example, fatty acid methyl ester epoxidation.

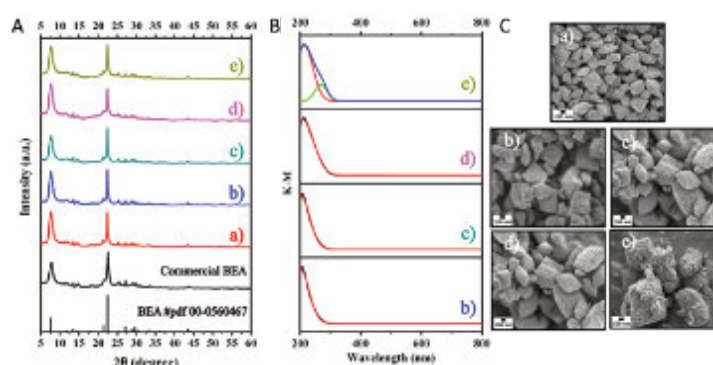


Figure 1. Illustration of (A) PXRD patterns, (B) UV-Vis spectra, and (C) FESEM images of Ti-beta zeolite, while a) – e) is the Ti loading of 0, 0.0001, 0.0003, 0.0005, and 0.0007 molar ratio

### References

- [1] L. Yuying, *Green Chemistry*, 2020, 22(5), 1681-1697.
- [2] Z. Zhongyao, *ACS Catalysis*, 2022, 12(2), 1481-1496.
- [3] W. Qinming, *Accounts of chemical research*, 2018, 51(6), 1396-1403
- [4] S. Kachaporn, *ACS Applied Nano Materials*, 2021, 4(11), 11661-11673
- [5] S. Kachaporn, *ACS Applied Nano Materials*, 2020, 3(4), 3252-3263.
- [6] Y. Guoju, *Inorganic Chemistry*, 2022, 61(12), 4887-4894.



## In-situ EPR study of the effect of sulfur poisoning and regeneration on Cu-CHA catalysts

T.K.Rønne-Nielsen<sup>1</sup>, Q.Gao<sup>1</sup>, T.V.W.Janssens<sup>2</sup>, F.Wen<sup>3</sup>, P.N.R.Vennestrøm<sup>2</sup>, S.Mossin<sup>1</sup>

<sup>1</sup>Technical University of Denmark, Kemitorvet 207, 2800 Kgs. Lyngby, Denmark

<sup>2</sup>Umicore Denmark Aps, Kogle Allé 1, 2970 Hørsholm, Denmark.

<sup>3</sup>Umicore AG & Co. KG – Hanau, Rodenbacher Ch 4, 63457 Hanau, Germany.

thkroi@dtu.dk

Zeolite-supported copper catalysts (Cu-CHA) are efficient catalysts for NO<sub>x</sub> removal from vehicle exhaust via NH<sub>3</sub>-Selective Catalytic Reduction. NO<sub>x</sub> emissions are harmful to the environment due to the formation of smog and acid rain, and international legislation keeps pushing to reduce emissions of NO<sub>x</sub>, which especially challenges the transportation industry. In particular, diesel-powered vehicles used for long-range transportation emit considerable amounts of NO<sub>x</sub>, thus there is a need for improved catalysts. The most extensive issue regarding the Cu-CHA as exhaust cleaning catalysts is the trace amounts of sulfur present in the exhaust gas, which deactivates the catalysts over time forcing the need for catalyst regeneration [1,2,3,4].

In this collaboration, sulfur deactivation and regeneration of a series of Cu-CHA catalysts (Si/Al = 7, 1 – 5 wt% CuO) were investigated. The investigation was carried out by ex-situ and in-situ Electron Paramagnetic Resonance (EPR) spectroscopy. The oxidation state of copper can be followed by EPR due to the paramagnetism of Cu<sup>2+</sup> [1] which gives an identifiable spectroscopic fingerprint for each individual copper species present.

The focus of this investigation was to quantify the impact of sulfur deactivation and regeneration procedures on the copper species, along with a quantification of the copper distribution between these different species.

The investigation proved that sulfur strongly influences the amount of redox active copper and the distribution between species [2,3,4] while also influencing rates of both reduction and oxidation. The sulfated copper species were proved to be caught in the oxidized (+2) state and thus could not enter the reduction half cycle of the SCR reaction. It was only partly reclaimed during the regeneration procedure [1,3]. Figure 1 summarizes the main conclusions: The amount of copper in the samples that are able to enter the redox cycle (light blue in Figure 1) has decreased significantly from the fresh to the sulfated catalyst and has only been partially reclaimed after a regeneration procedure. The effect is more pronounced on the high-Cu content sample, where a large amount of Cu is caught in the +2 oxidation state.

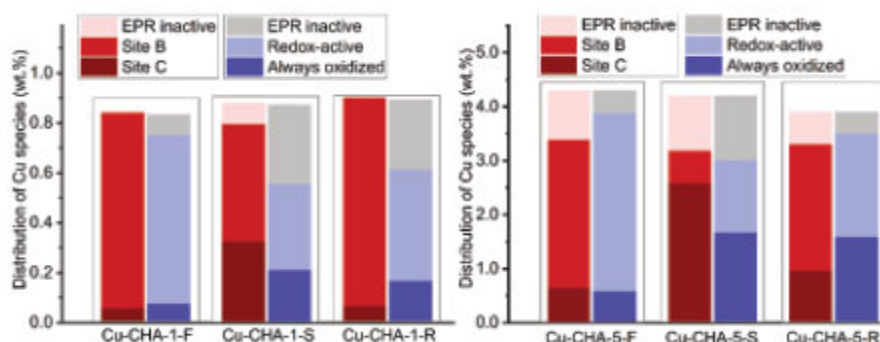


**Figure 1.** The distribution of Cu species after thermal activation (columns in red nuances) compared to the distribution of Cu according to the behaviour after reduction in NO+NH<sub>3</sub> and oxidation in NO+O<sub>2</sub> (columns in blue nuances) for fresh (F), sulfated (S), and regenerated (R) samples of a dilute Cu-CHA-1 (left) and of a concentrated Cu-CHA-5 (right).

### References

- [1] Q. Gao, T.K. Rønne-Nielsen, T.V.W. Janssens, F. Wen, P.N.R. Vennestrøm, S. Mossin (*In progress*)
- [2] S.L. Berman, S. Dahlin, V.V. Mesilov, Y. Xiao, J. Englund, S. Xi, C. Tang, M. Skoglundh, L.J. Pettersson, S.L. Bernasek, *Applied Catalysis B: Environmental*, 269, 118722 (2020)
- [3] V. Mesilov, S. Dahlin, S.L. Bergman, S. Xi, J. Han, L. Olsson, L.J. Pettersson, S.L. Bernasek, *Applied Catalysis B: Environmental*, 299, 120626 (2021)
- [4] A.Y. Molokova, R.K. Abasabadi, E. Borfecchia, O. Mathon, S. Bordiga, F. Wen, G. Berlier, T.V.W. Janssens, K.A. Lomachenko, *Chem. Sci.*, 14, 11521 (2023)



## Ru-MOFs as catalysts for the hydrogenation of dimethylurea to methane

I. Arnaiz, C. Márquez-Álvarez, E. Álvarez-Catalá, M. Zubimendi, J. Pérez-Pariente, M. Sánchez-Sánchez

Instituto de Catálisis y Petroleoquímica (ICP), CSIC, Madrid, Spain  
manuel.sanchez@icp.csic.es

### Motivation

In just over two decades, metal-organic materials (MOFs) have revolutionized the world of nanoporous materials and their applications [1]. In this context, thousands of different MOF materials have been described. However, MOFs based on ruthenium (Ru) are rather rare. Among the noble metals, Ru is the most abundant, the cheapest, and the one with the widest variety of oxidation states. As a consequence, this metal has been widely used in homogeneous and heterogeneous catalysis. In fact, the very few known Ru-MOFs have been studied as heterogeneous catalysts in different reactions [2,3]. Ru-HKUST-1 material is of particular interest. Also known as MOF-199, HKUST-1 is one of the most versatile MOFs in composition with a  $\text{Me}_3(\text{BTC})_2$  stoichiometry, where BTC is the acronym for the organic ligand trimesate (Benzene-1,3,5-TriCarboxylate). This stoichiometry is only broken by two metals, Fe and Ru, which can give a HKUST-1 with a mixture of oxidation states 2+ and 3+. In the case of Ru-HKUST-1, the stoichiometry is  $\text{Ru}^{\text{II}}_{1.5}\text{Ru}^{\text{III}}_{1.5}(\text{BTC})_2\text{Cl}_{1.5}$ , where  $\text{Cl}^-$  ions compensate for the electronic charge deficiency caused by replacing half of Ru(II) with Ru(III).

This work presents the new semiamorphous MOF Ru-BTC. Unlike a nanocrystalline MOF, a semiamorphous MOF refers to a MOF material that, while having a short- and medium-range crystalline order, does not possess any long-range order. Ru-BTC is prepared with the same metal and the same organic ligand as the MOF Ru-HKUST-1, so they could provide key information to understand the catalytic behaviour of Ru incorporated in MOFs. These two Ru-trimesate-based MOFs have been tested in this work in the hydrogenation of dimethylurea to methane. Urea and its derivatives can be considered as a solid source of  $\text{CO}_2$ , since the formation of urea from  $\text{CO}_2$  and ammonia (amines for dialkylureas) is a well-known and industrially exploited process [4]. The methylamine released in the hydrogenation of dimethylurea can react with fresh  $\text{CO}_2$ , and the whole process can be then considered an indirect way to convert  $\text{CO}_2$  in methane *via* dimethylurea under mild conditions. To the best of our knowledge, this is the first work addressing the catalytic capability of Ru-MOFs in the significant challenge of  $\text{CO}_2$  transformation to mitigate climate change.

### Experimental

The synthesis of Ru-HKUST-1 was carried out according to the recipe described elsewhere [5]. Ru-BTC samples were synthesized starting from a mixture with the following molar composition: 3.0  $\text{RuCl}_3 \cdot x\text{H}_2\text{O}$ : 2.0  $\text{H}_3\text{BTC}$  : 5.0  $\text{CH}_3\text{COOH}$  : 925  $\text{H}_2\text{O}$ , which was treated under hydrothermal conditions at 160 °C for 7 days. The resultant solid was filtered and washed with abundant distilled water and then with ethanol.

The reaction tests were carried out in a stirred batch reactor at 150 °C for 48 hours, using THF as the solvent (55 ml), dimethylurea (2,50 g) and  $\text{H}_2$  (20-40 bar) as reactants, dodecane as chromatographic internal standard, and Ru-HKUST-1 or Ru-BTC as catalyst, in the amount required to have 1 wt% of metal with respect to dimethylurea.

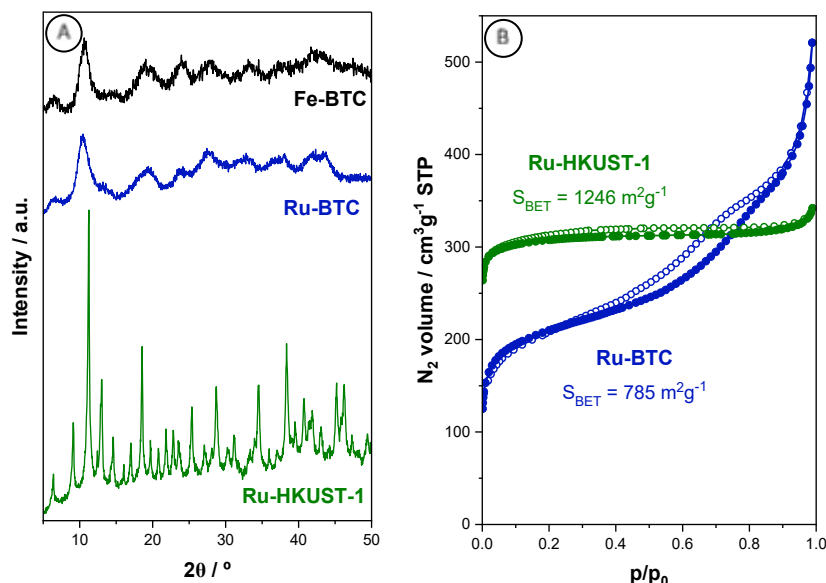
### Results and discussion

Figure 1A shows the XRD patterns of both Ru-HKUST-1 and semiamorphous Ru-BTC, and that of Fe-BTC for comparison purposes. The position and the relative intensity of the peaks of the XRD pattern of Ru-HKUST-1 perfectly match with the simulated XRD pattern of this material (not shown). However, the XRD pattern of sample Ru-BTC cannot be compared with any simulated pattern because of its condition of semiamorphous. This pattern exhibits low intense and broad XRD bands rather than well-defined peaks, which are typical for crystalline materials. However, the comparison with the experimental XRD pattern of a semiamorphous Fe-BTC, which is related to MIL-100(Fe) material but without long-range order [6], suggests that both materials have quite similar structural features. It is remarkable that Ru is, together with Fe, the only trivalent metal able to form this semiamorphous Me-BTC, in spite of some others like Cr, Al, Sc or In can form its long-range-ordered counterpart MIL-100(Me).

Figure 1B shows the  $\text{N}_2$  adsorption/desorption isotherms at -196 °C of both Ru-MOFs. Ru-HKUST-1 has higher specific surface area ( $1246 \text{ m}^2\text{g}^{-1}$ ), similar to those found by other authors for this material. However, the  $785 \text{ m}^2\text{g}^{-1}$  specific surface area of the semiamorphous Ru-BTC is a relatively high value for this type of semiamorphous material. Furthermore, the isotherm of the Ru-BTC sample exhibits a hysteresis loop, probably as a consequence of the agglomeration of its nanodomains into larger particles, which leave interparticle mesoporosity with a diameter of about 7 nm (mesopore distribution not shown). In fact, of the total specific surface area estimated for this MOF,  $528 \text{ m}^2\text{g}^{-1}$  correspond to microporous surface while the remaining  $257 \text{ m}^2\text{g}^{-1}$  are due to external surface. The same feature



was already described for the MOF Fe-BTC [6]. Thanks to the contribution of this intercrystalline mesoporosity, the total pore volume of the Ru-BTC sample ( $0.73 \text{ cm}^3\text{g}^{-1}$ ) exceeds that of the Ru-HKUST-1 sample ( $0.52 \text{ cm}^3\text{g}^{-1}$ ).



**Figure 1.** (A) XRD patterns of the MOFs Ru-HKUST-1, Ru-BTC and Fe-BTC (the latter for comparison purposes). (B)  $\text{N}_2$  adsorption/desorption isotherms at  $-196^\circ\text{C}$  of Ru-HKUST-1 and semiamorphous Ru-BTC.

The Ru-MOFs samples were also characterized by means of diffuse reflectance UV-vis, infrared and XPS spectroscopies and by means of thermogravimetric analysis. Among some other relevant information, the most significant difference found between them is that Ru-HKUST-1 indeed have Ru in both oxidation states, 2+ and 3+, whereas Ru-BTC only contains Ru in oxidation state 3+.

Table 1 shows the catalytic results of the hydrogenation of dimethylurea by both Ru-MOFs. The reaction in the absence of any catalyst does not take place at all. Adding any Ru-MOF under any tested conditions leads to certain conversion of dimethylurea. The conversion is generally higher when Ru-BTC is the catalyst. The best  $\text{H}_2$  pressure for this catalyst was found at 30 bar, with dimethylurea conversion close to 70 %, and with a selectivity to methane as high as 92 % (96 % for the sum of conversions of  $\text{CH}_4$  plus CO). These results become very competitive to the ones so far reported in the methanation of  $\text{CO}_2$  using other types of Ru-based catalysts.

**Table 1.** Hydrogenation of dimethylurea catalysed by Ru-MOFs.


## References

- [1] R. Freund, O. Zaremba, G. Arnauts, R. Ameloot, G. Skorupskii, M. Dincă, A. Bavykina, J. Gascon, A. Ejsmont, J. Goscińska, M. Kalmutzki, U. Lächelt, E. Ploetz, C.S. Diercks, S. Wuttke, *Angewandte Chemie International Edition*, **60** 23975 (2021).
- [2] C.H. Wang, W.Y. Gao, D.C. Powers, *Journal of the American Chemical Society*, **141**, 19203 (2019).
- [3] I. Agirrezabal-Telleria, I. Luz, M.A. Ortuño, M. Oregui-Bengoechea, I. Gandarias, N. López, M.A. Lail, M. Soukri, *Nature Communications*, **10**, 2076 (2019).
- [4] D. Sun, J. Ye, Y. Fang, Z. Chao, *Industrial & Engineering Chemistry Research*, **55**, 64 (2016).
- [5] G.R. Lorzing, K.P. Balto, A.M. Antonio, B.A. Trump, C.M. Brown, E.D. Bloch, *Chemistry of Materials*, **32** 7710 (2020).
- [6] M. Sánchez-Sánchez, I. de Asua, D. Ruano, K. Díaz, *Crystal Growth & Design*, **15**, 4498 (2015).

## Acknowledgments

Authors acknowledge MCIN/AEI and European Union "NextGenerationEU"/PRTR the funding through the projects TED2021-131143B-I00 and PID2022-136321OB-C21. E. Álvarez-Catalá thanks SECAT for the grant Ayuda 'Intro'-2024.



## Emerging co-synthesis of dimethyl oxalate and dimethyl carbonate using Pd/silicalite-1 catalyst with synergistic interactions of Pd and silanols

C. Wang<sup>1,2\*</sup>, R. Mei<sup>1</sup>, M. Li<sup>1</sup>, H. Guo<sup>1</sup>, S. Mintova<sup>1,2\*</sup>

<sup>1</sup> State Key Laboratory of Heavy Oil Processing, College of Chemistry and Chemical Engineering, China University of Petroleum (East China), Qingdao 266580, Shandong, China

<sup>2</sup> Laboratoire Catalyse et Spectrochimie (LCS), Normandie Université, ENSICAEN, UNICAEN, CNRS, 6 boulevard Maréchal Juin, Caen 14050, France

czwang@upc.edu.cn; svetlana.mintova@ensicaen.fr

### Introduction

Zeolites with adjustable acid-base sites, unique structures, and well-defined pores and cages are extensively used as catalysts and supports. In addition, silanols (Si–OH) are located in the internal and external surface of zeolites that can vary as types and amount depending on the properties of the zeolites [1]. The formation of zeolite silanols originates from the crystallization process, different nature and purity of chemical reagents, and post-synthesis treatment. The strategies employed to engineer silanol defects included the synthesis of layered zeolite, formation of mesopore, creation of defects by water intrusion, and the reduction of zeolite size. In contrast, several methods are available to heal the silanol defects, such as heat treatment, radical-assisted approach, silane-modified method, blocking defects and incorporation of metal heteroatoms [1]. The zeolite silanol defects play an imperative role in setting the catalytic activity. Therefore, tuning the silanols of zeolites and understanding the interactions between silanols and metal species are of great interest in the field of catalysis.

To reduce the dependence on fossil resources, considerable research efforts were devoted to developing sustainable technologies for the catalytic conversion of one-carbon molecules (CO, CO<sub>2</sub>, CH<sub>4</sub> and CH<sub>3</sub>OH) into fuels and chemicals. Dimethyl oxalate (DMO), (CH<sub>3</sub>OCO)<sub>2</sub> and dimethyl carbonate (DMC), (CH<sub>3</sub>O)<sub>2</sub>CO are industrial chemical intermediates with versatile properties. The Pd/ $\alpha$ -Al<sub>2</sub>O<sub>3</sub> catalyst has been successfully commercialized in the indirect oxidative carbonylation of CH<sub>3</sub>OH to DMO [2,3]. However, the chlorine-free Pd-based catalyst for single DMC synthesis could not be applied in the industry due to the unsatisfied stability [4]. Herein, we present a novel process for indirect oxidative carbonylation of CH<sub>3</sub>OH to co-synthesis of DMO and DMC. The process combined the advantages of the two separate routes of DMO and DMC syntheses [5]. The palladium containing silicalite-1 (Pd/S-1) catalyst was first used and showed to be highly active and stable for the co-synthesis of DMO and DMC (Figure 1).

### Materials and Methods

The pure-silica silicalite-1 (S-1) zeolite was purchased from Nankai Catalyst Factory (China). The Pd/S-1 catalyst was prepared by a vacuum-assisted method. 0.0106 g palladium acetate (Pd(CH<sub>3</sub>COO)<sub>2</sub>, 47.0 wt% Pd, Sinopharm Chemical Reagent Co., Ltd., China) was dissolved in 1.2 g toluene (C<sub>6</sub>H<sub>5</sub>CH<sub>3</sub>). 1.0 g S-1 zeolite was further pre-treated under vacuum for 2 h. Then, the resulting Pd(CH<sub>3</sub>COO)<sub>2</sub> solution was added dropwise into the pre-treated S-1 zeolite. After stirring for 2 h, the sample was dried at 60 °C for 8 h, and calcined for 2 h.

### Results and Discussion

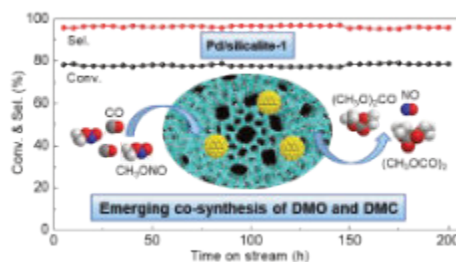


**Figure 1.** Schematic presentation of an emerging synthetic route for the co-synthesis of dimethyl oxalate and dimethyl carbonate.

The Pd/S-1@200 and Pd/S-1@300 showed the low apparent activation energy of 51 and 52 kJ mol<sup>-1</sup>, while the Pd/S-1@400 and Pd/S-1@500 were 89 and 101 kJ mol<sup>-1</sup>. The big difference among the apparent activation energies suggested that the reaction pathway and rate-controlling step were possibly different [6]. The TOF of Pd/S-1@200 and Pd/S-1@300 was two times larger than Pd/S-1@400 and Pd/S-1@500 (0.18 vs. 0.06 s<sup>-1</sup>). The apparent activation energy and the TOF confirmed that catalyst calcination temperature played a critical role in the activity.

The HAADF-STEM and elemental mapping of Si, O and Pd further verified the high dispersion of Pd (Figure 2). The DRIFTS spectra of CO adsorption and CO pulse chemisorption indicated that the adsorbed CO on the Pd/S-1@200 and Pd/S-1@300 catalysts was much larger than the Pd/S-1@400 and Pd/S-1@500 catalysts (Figure 3). This was in line with the catalytic performance: high TOF of Pd/S-1@200, Pd/S-1@300 vs. low TOF of Pd/S-1@400, Pd/S-1@500. The



adsorption of CO reactant is essential for formation of DMO and DMC following the Langmuir-Hinshelwood mechanism. Thus, enhanced adsorption of CO reactant can be considered as a critical descriptor of the high activity.

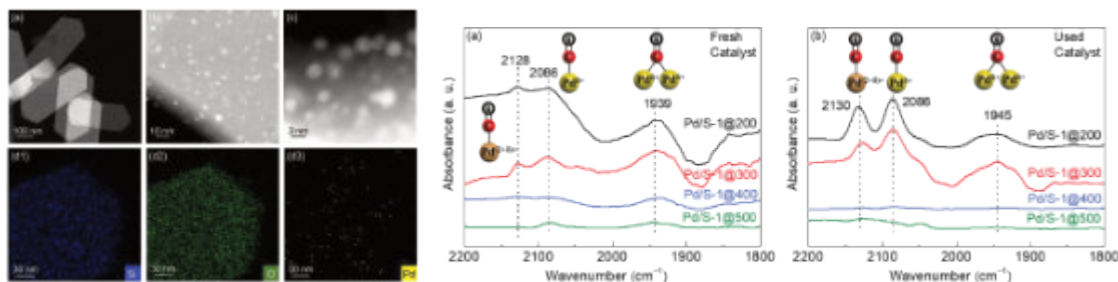


**Figure 2 (Left).** (a–c) aberration-corrected HAADF-STEM images and (d1–d3) HAADF-STEM-EDS elemental mapping on the used Pd/S-1@300 catalyst. **Figure 3 (Right).** DRIFTS spectra of CO adsorbed on (a) fresh and (b) used catalysts at 35 °C.

The FTIR spectra in the OH-stretch region are shown in Figure 4. The bands at 3736 cm<sup>-1</sup> and 3720 cm<sup>-1</sup> were assigned to the external and internal isolated silanols; the bands at 3682 cm<sup>-1</sup> and 3475 cm<sup>-1</sup> corresponded to vicinal silanols and silanol nests, respectively. With increasing the calcination temperature for the catalyst, the external and internal isolated silanols remained stable; the silanol nests gradually decreased while the vicinal silanols increased (Figure 4). Besides, the evolution of silanols was studied by <sup>29</sup>Si NMR spectroscopy (Figure 5). The resonance peak at -113 ppm was assigned to Q<sup>4</sup> [(OSi)<sub>4</sub>], while the peaks at -106 ppm and -102 ppm corresponded to Q<sup>3</sup> [HO-Si(OSi)<sub>3</sub>]. The intensity of the resonance peaks at -106 ppm and -102 ppm was considerably enhanced on the <sup>29</sup>Si CP MAS NMR spectra. The resonance peak of Q<sup>3</sup> species at -106 ppm on the Pd/S-1@300 catalyst was higher than the counterpart on the Pd/S-1@400. This confirmed that the silanols were partially healed at the high calcination temperature, which was in accordance with the FTIR results.

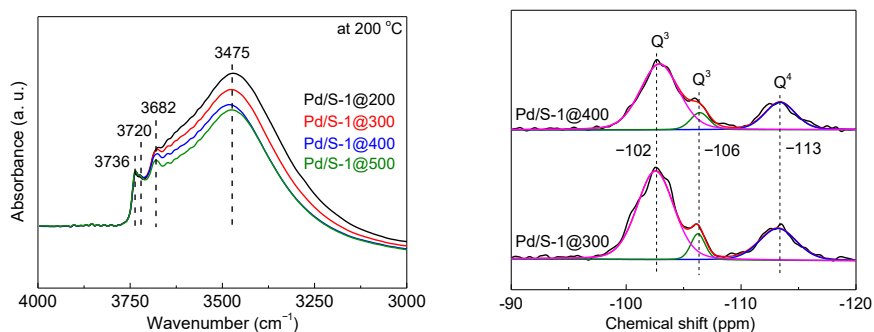


**Figure 4 (Left).** FTIR spectra in the OH-stretch region of the used catalysts outgassed under vacuum at the appointed temperature and measured at 200 °C. **Figure 5 (Right).** Solid-state <sup>29</sup>Si CP MAS NMR spectra of the used Pd/S-1@300 and Pd/S-1@400 catalysts.

In summary, the indirect oxidative carbonylation of CH<sub>3</sub>OH to co-synthesis DMO and DMC using Pd/S-1 catalyst is a new promising route due to its high activity and excellent stability. The Pd/S-1 catalyst with abundant silanols exhibited a higher turnover frequency (TOF) of 0.18 s<sup>-1</sup> and a lower apparent activation energy of 51 kJ mol<sup>-1</sup> in comparison to the catalyst with low silanol sites (0.06 s<sup>-1</sup> and 101 kJ mol<sup>-1</sup>). The optimal catalyst with 0.48 wt% Pd showed 78% CO conversion and 96% DMO+DMC selectivity, and excellent stability during the continuous test of 200 h. It was found that the catalytic performance strongly depended on the catalyst activation, as the heat treatment could tune the silanols around the Pd species on the S-1 zeolite. Furthermore, the existence of synergistic interactions between silanols and Pd was confirmed by a series of in situ infrared experiments, and the enhanced interactions could improve the adsorption of CO reactant on the Pd species. Finally, the newly designed Pd/S-1 catalyst with high activity on the co-synthesis of DMO and DMC by understanding the Pd-silanol synergistic interactions was reported.

## References

- [1] I.C. Medeiros-Costa, E. Dib, N. Nesterenko, J.P. Dath, J.P. Gilson, S. Mintova, *Chem. Soc. Rev.* **50**, 11156-11179 (2021).
- [2] K. Huang, S. Yuan, R. Mei, G. Yang, P. Bai, H. Guo, C. Wang, and S. Mintova, *Chin. J. Catal.*, **60**, 327-336 (2024).
- [3] C. Wang, X. Li, S. Yuan, L. Sun, P. Bai, L. Ling, H. Guo, and S. Mintova, *Catal. Rev.*, DOI: 10.1080/01614940.2024.2320165 (2024).
- [4] C. Wang, N. Xu, T. Liu, W. Xu, H. Guo, Y. Li, P. Bai, X. Wu, X. Gong, X. Liu, and S. Mintova, *J. Catal.*, **396** 269-280 (2021).
- [5] C. Wang, N. Xu, K. Huang, B. Liu, P. Zhang, G. Yang, H. Guo, P. Bai, and S. Mintova, *Chem. Eng. J.*, **466** 143136 (2023).
- [6] C. Wang, B. Liu, P. Liu, K. Huang, N. Xu, H. Guo, P. Bai, L. Ling, X. Liu, and S. Mintova, *J. Catal.*, **412** 30-41 (2022).

## Acknowledgments

This work was co-funded by European Union (ERC, ZEOLIGHT, 101054004), National Natural Science Foundation of China (22472204), National Key R&D Program of China (2022YFE0116000), and Sino-French International Research Network (IRN) "Zeolites".

# Tuning the Adsorptive Characteristics of MOFs through Trans-metalation: a Successful Strategy for Designing Selective Adsorbents for Aguas and Gas-Phase Applications

Fatemeh Nouroozi<sup>1,2</sup>, Hossein Kazemian<sup>1,2,3,4</sup>

<sup>1</sup>*Materials Technology & Environmental Research lab, University of Northern British Columbia, Prince George, BC, Canada*

<sup>2</sup>*Natural Resources & Environmental Studies Institute, University of Northern British Columbia, Prince George, BC, Canada*

<sup>3</sup>*Northern Analytical Lab Services (Northern BC's Environment & Climate Solutions Innovation Hub), University of Northern British Columbia, Prince George, BC, Canada*

<sup>4</sup>*Environmental Sciences Program, Faculty of Environment, University of Northern British Columbia, Prince George, British Columbia V2N4Z9, Canada*

Metal-organic frameworks (MOFs), particularly zirconium-based MOFs, have garnered significant attention due to their structural robustness, chemical stability, and high tunability for various applications, ranging from catalysis to adsorption. Zr-MOFs, characterized by their  $Zr_6O_4(OH)_4$  nodes and a variety of node morphologies connected by organic linkers, [1] providing large mesoporous cavities ideal for adsorption applications. Post-synthetic modification (PSM) of MOFs has predominantly focused on altering linkers to incorporate both organic and metallic center to the framework[2,3]. Although recent advances highlight the potential of modifying each individual nodes through metal incorporation to the node to improve adsorption performance[4], the number of reports about direct transmetalation which is due to exchange of metal from the node with a desired metal are significantly low.

In this study, the transmetalation of two different Zr-MOFs has been explored by incorporating divalent metal ions ( $M^{2+}$ ) into its Zr nodes. The presence of  $M^{2+}$  in the node was confirmed through X-ray photoelectron spectroscopy (XPS) and inductively coupled plasma (ICP) analysis. The modified frameworks remain structurally stable post-transmetalation with maintaining their porous structure (Specific surface area >1000  $m^2/g$ ) and exhibits enhanced adsorptive characteristics, particularly for semi-volatile organic compounds (SVOCs) in both aqueous and gas-phase environments. The modified MOFs demonstrated a 91% removal efficiency for ethyl cinnamate, a model compound representing UV filters used in skin care products found in water sources, compared to 55% removal efficiency of the parent MOFs. These results highlight an improved adsorption capacity ranging from 35% to 65% across various structures, effectively addressing environmental concerns related to persistent emerging contaminants. This research highlights the critical role of node engineering in tuning the physicochemical properties of MOFs, paving the way for more efficient adsorbents in water and air purification.

## References:

- [1] H. Furukawa, F. Gándara, Y.-B. Zhang, J. Jiang, W.L. Queen, M.R. Hudson, O.M. Yaghi, J. Am. Chem. Soc. 136 (2014) 4369–4381.
- [2] M. Allahbakhshi, M. Mosafieri, N.M. Mahmoodi, H. Kazemian, H. Aslani, Korean J. Chem. Eng. 40 (2023) 2892–2905.
- [3] M. Giménez-Marqués, A. Santiago-Portillo, S. Navalón, M. Álvaro, V. Briois, F. Nouar, H. Garcia, C. Serre, , J. Mater. Chem. A 7 (2019) 20285–20292.
- [4] M.G. Radhika, B. Gopalakrishna, K. Chaitra, L.K.G. Bhatta, K. Venkatesh, M.K. Sudha Kamath, N. Kathyayini, Mater. Res. Express 7 (2020) 054003.





## Hierarchical zeolites enable the design of multifunctional catalysts for fatty acids hydrodeoxygenation to alkanes

Shengzhe Ding<sup>1</sup>, Christopher M. A. Parlett<sup>1</sup> and Xiaolei Fan<sup>1,\*</sup>

<sup>1</sup> Department of Chemical Engineering, The University of Manchester, Manchester, M13 9PL, United Kingdom

[xiaolei.fan@manchester.ac.uk](mailto:xiaolei.fan@manchester.ac.uk)

Hierarchical zeolites, characterized by their multi-level pore structures, are important framework materials for improving conventional catalysis, as evidenced by the cases in catalytic cracking [1]. In the new era of sustainable development, they offer a powerful approach for developing new sustainable catalysis. This work [2] employs hierarchical ZSM-5 to achieve spatial segregation of metal (Pd nanoparticles, NPs) and acidic sites, and in the bifunctional catalysts active site location is governed by size exclusion effect, with acid sites selectively extracted from the mesopores and replaced with preformed Pd metal NPs, whilst Brønsted acidity is retained solely within the micropores of ZSM-5 (**Figure 1**). The spatial segregation of these two distinct catalytic active species shows profound benefit for the one-pot cascade hydrodeoxygenation (HDO) of the lauric acid to C12 alkanes, a model reaction for catalytic HDO fatty acid upgrading to sustainable aviation fuels (SAFs). This design strategy represents a generic platform for multifunctional materials, particularly for producing those in which spatial separation of different chemical functionalities is desired.

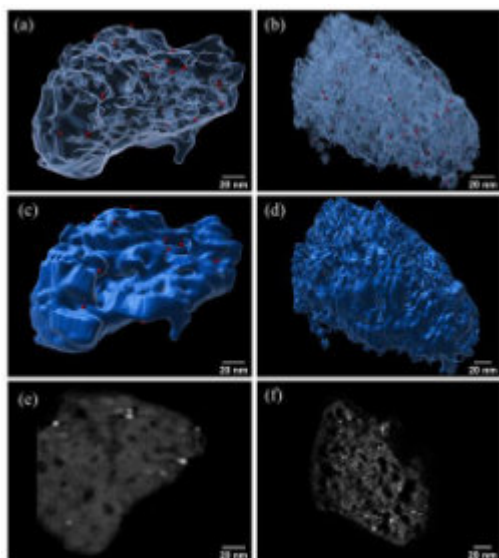


**Figure 1.** STEM tomogram reconstructions. (a) and (c) PdNP/H-MZSM5 and (b) and (d) Pd<sub>imp</sub>/H-MZSM5, with the Zeolite set as semi-transparent in (a, b) and non-transparent in (c, d). Cross-section slices from the centre of the catalyst are presented in (e) PdNP/H-MZSM5 and (f) Pd<sub>imp</sub>/H-MZSM5.

Mesopores (~8.6 nm) in hierarchical ZSM-5 was exploited for selective deposition of Pd NPs (4.6 ± 1.3 nm) solely within them through size exclusion (**Figure 1a**, PdNP/H-MZSM5). Conversely, conventional impregnation and thermal processing of a Pd salt (Pd<sub>imp</sub>/H-MZSM5) cannot achieve this active site spatial separation (**Figure 1b**). Further evidence of the difference in Pd distribution within the two catalysts is afforded through the combination of inductively coupled plasma (ICP) (Supplementary Table 2), X-ray photoelectron spectroscopy (XPS) and hard X-ray photoelectron spectroscopy (HAXPES). The spatial segregation within the systems here was beneficial to a cascade HDO that proceeds stepwise including reduction (carboxylic acid to alcohol) in the mesopores over Pd, dehydration (alcohol to alkene) in the micropores over acid sites, and finally hydrogenation (alkene to alkane) over Pd in the mesopores, with the alkane product diffusing to the bulk reaction media. In HDO of lauric acid PdNP/H-MZSM5 yielded a significant enhancement (**Table 1**), with dodecane (C12) yield increasing by ~20% and a 7-fold increase in production rate, a direct consequence of dictating the reaction sequence of the cascade. Thus, this study should inspire future HDO catalyst development while also highlighting the potential of spatial separation of active species within multifunctional materials for one-pot cascade reactions

### References

- [1] M.J. Mendoza-Castro, et. al., *Nature Communications*, **14**, 1256 (2023).  
[2] S. Ding, et. al., *Nature Communications*, **15**, 7718 (2024).

### Acknowledgments

This project has received funding from the European Union's Horizon 2020 research and innovation program under grant agreement No 872102.

**Table 1.** Lauric acid HDO performance over conventional prepared and spatial compartmentalised catalysts.<sup>a</sup>

Catalysts	Acid Conv., %	C <sub>12</sub> Sel., %	C <sub>11</sub> Sel., %	TON
H-MZSM5	0	0	0	0
PdNP/Na-MZSM5	2.2	27.3 (alcohol)	0 <sup>d</sup>	29
H-MZSM5 + PdNP/Na-MZSM5	20.6	28.1	2.1	278
PdNP/H-MZSM5	51.0	51.8	9.9	689
Pd <sub>imp</sub> /H-MZSM5	31.2	38.4	20.5	187
PdNP/H-MZSM5-DA	94.1	64.9	12.6	1272
Pd <sub>imp</sub> /H-MZSM5-DA	70.9	39.9	18.2	426
PdNP <sub>small</sub> /H-MZSM5	50.9	40.4	14.9	688
PdNP <sub>small</sub> /H-MZSM5-DA <sup>f</sup>	71.5	59.3	24.4	1205

<sup>a</sup> Reaction conditions: 100 mg 1 wt.% Pd-doped catalyst, 300 mg lauric acid, 0.1 cm<sup>3</sup> of nonane as the internal standard, 40 cm<sup>3</sup> of hexane as the solvent, at 200 °C, 30 bar and 1000 rpm for 6 h.



## Highly stable subnanometric Pt clusters in all silica K-doped zeolites: implications for the CO oxidation reaction

**B. Bohigues<sup>1</sup>, I. Millet<sup>1</sup>, P. Concepción<sup>1</sup>, A. Corma<sup>1</sup>, M. Moliner<sup>1\*</sup> & P. Serna<sup>1\*</sup>**

*1 Instituto de Tecnología Química, Universitat Politècnica de València-Consejo Superior de Investigaciones Científicas, Avenida de los Naranjos s/n, 46022 València, Spain  
bbohboh@itq.upv.es*

Supported Pt catalysts have been intensively studied for elemental steps in industrially-relevant applications, such as CO oxidation to CO<sub>2</sub> and water-gas-shift reactions. Pt clusters and small nanoparticles are highly active species for the CO oxidation reaction due to the effective activation of both CO and O<sub>2</sub> at moderate temperatures.[1]

Pt on ceria, in particular, has received wide attention in the last years thanks to the redox versatility of this support. It is believed that surface oxygen vacancies on ceria can activate O<sub>2</sub> readily, allowing a concerted activation mechanism between CO adsorbed on the Pt, and O<sub>2</sub> activated at the metal-support interface, that offers superior CO oxidation performance.[2] However, Pt/CeO<sub>2</sub> catalysts consisted in small Pt nanoparticles have an important limitation for the CO oxidation reaction ascribable to a drastically deactivation in O<sub>2</sub>-rich atmospheres, at moderate-to-high temperatures, following an oxidative fragmentation, process that yields Pt atoms (less active) strongly trapped by the support via SMSI (strong metal support interactions).[3]

On the other hand, typical non-reducible supports interact with Pt clusters too weakly to stabilize the dispersed species when the reaction conditions are harsh (e.g. high temperature in presence of reducing or oxidizing gases), contributing to a deactivation by Oswaldt-ripening sintering.[4] Moreover, the lack of the redox functionality of the non-reducible supports results in a non-efficient O<sub>2</sub> activation and, consequently, a negative impact on the catalytic activity. Nevertheless, certain non-reducible supports, such as zeolites, are highly tunable to modify the chemical environment of metals inside their micropores following rules that can be rationalized.[4,5]

In our group in the last decade, significant progress has been made to develop noble metal catalysts with outstanding stability in various atmospheres that include O<sub>2</sub>, H<sub>2</sub>, CO and H<sub>2</sub>O. For example, Al-rich small-pore CHA zeolites (Si/Al<10) are capable to trap single Pt atoms formed under oxidative atmospheres at high temperatures, thanks to the stabilizing role of Al-pairs; however, under CO oxidation conditions, this zeolite yields metallic Pt nanoparticles, even with an O<sub>2</sub>-rich feed.[4,6,7] Whereas Pt/CeO<sub>2</sub> systems undergoes re-dispersion into single metal atoms, Pt/CHA systems deactivate by sintering mechanisms.[3,7]

Recently, we developed a new K-Pt@MFI catalyst with outstanding redox stability assignable to the presence of K which has been proven to enhance the stability of single Pt atoms, even under typical Ostwald-ripening sintering conditions (e.g. in O<sub>2</sub> at high temperature).[8] An underlying premise of the present work is that, under CO oxidation conditions, the particular Pt speciation (electron-promotion) in K-Pt@MFI could improve Pt@Al-MFI and Pt/CeO<sub>2</sub> systems in terms of activity/stability.

To investigate the effect of K as an electronic modifier, we prepared a variety of Pt@MFI type materials with different content on K and/or Al with high crystallinity and a particle size distribution of 200-300nm (determined by PXRD patterns and FESEM images, respectively). The homogeneous formation of ~1 nm Pt particles in all materials is obtained after specific calcination-reduction treatments and observed by STEM images; moreover, through FTIR spectroscopy of reduced samples, and using CO as probe molecule, a blue-shift in the obtained spectra was determined in our series once K was incorporated (**Table 1**). These results are consistent with the role previously given to K<sup>+</sup> as a weak Lewis acid that increases the electron density of Pt nanoparticles upon back-donation to molecular orbitals with 2π\* character.

We then evaluated the CO oxidation performance of the reduced K<sub>0</sub>-Pt@MFI, K<sub>0.3</sub>-Pt@MFI, K<sub>0.6</sub>-Pt@MFI and H-Pt@MFI through light-off activity experiments under O<sub>2</sub>-rich conditions (O<sub>2</sub>/CO=6.3), because these are most challenging with state-of-the-art Pt/CeO<sub>2</sub> catalysis. Activity, measured as the TOF at 200°C (**Table 1, Figure 1a**), follows the order K<sub>0.6</sub>-Pt@MFI > K<sub>0.3</sub>-Pt@MFI > K<sub>0</sub>-Pt@MFI > H-Pt@MFI. This trend correlates well with the trend observed by CO-IR (**Figure 1b**), confirming that the CO oxidation activity of Pt clusters increases as the metal electron-density increases via support-to-metal charge transfer. Moreover, whereas the K<sub>0.6</sub>-Pt@MFI sample retains structural integrity at high temperature in CO, H<sub>2</sub> and O<sub>2</sub>, drastic deactivation by metal sintering is observed with low Si/Al ratio zeolites, as demonstrated in subsequent experiments.

To further test the resilience of the most active K<sub>0.6</sub>-Pt@MFI catalyst against oxidative fragmentation, we performed new light-off experiments, and set the final reaction temperature to 500°C. Subsequently, we followed the conversion vs temperature curve through a second light-off cycle, starting at room temperature, without any additional activation treatment in between. The reduced K<sub>0.6</sub>-Pt@MFI maintained its CO conversion profile almost unaltered at increasing temperatures for the two light-off catalysis cycles, as Pt nanoparticles of virtually invariable size were also retained. Under identical conditions, a highly active Pt/CeO<sub>2</sub> catalyst made in our labs, activated in CO at 300°C prior



to catalysis, underwent drastic deactivation, consistent with literature that demonstrate the redispersion of Pt nanoparticles into single atoms in the excess of O<sub>2</sub>. Thus, the activity of Pt/CeO<sub>2</sub> is magnificent in the first light-off reaching 75°C to achieve 50% of CO conversion, but in the second light-off the activity drops drastically to T<sub>50%</sub> of 275 °C. These results highlight the excellent resistance of the K<sub>0.6</sub>-Pt@MFI against drastic deactivation that typically occurs on reducible supports, leading to superior performance under practical reaction conditions.

To further evaluate the stability of materials under harsh conditions, we developed a strenuous test that subjects the materials to 50 oxidation-reduction cycles at high temperature (redox stress at 600°C) consisting on: a) flowing air; b) flowing N<sub>2</sub>; and c) flowing pure H<sub>2</sub>; all the steps are run for 30 min at 600°C, without cooling off in between. The treatments were applied to the K<sub>0.6</sub>-Pt@MFI, K<sub>0.3</sub>-Pt@MFI and H-Pt@MFI samples and the aged materials were characterized by FESEM and STEM microscopies. The formation of Pt aggregates larger than 50 nm was clearly observed in the FESEM images of the K-free H-Pt@MFI sample and, also, to a lesser extent, in the K<sub>0.3</sub>-Pt@MFI sample. Remarkably, FESEM and STEM images of the sample K<sub>0.6</sub>-Pt@MFI, show negligible formation of large nanoparticles after the 50 consecutive redox treatments at 600°C and the virtual exclusive presence of subnanometric Pt clusters inside the zeolite. We also evaluated the aged samples directly in the CO oxidation reaction. As expected, the aged K<sub>0.6</sub>-Pt@MFI offered the best catalytic activity in this series, showing an overwhelming 90°C temperature drop to reach ~50% conversion of CO relative to the aged K<sub>0.3</sub>-Pt@MFI sample and ~180 °C relative to the aged H-Pt@MFI.

**Table 1.** Characterization features and catalytic performance for the O<sub>2</sub>-rich CO oxidation reaction using different Pt-containing MFI materials

Pt/MFI	IR-CO Linear Pt-CO (cm <sup>-1</sup> )	Activity TOF 190°C [s <sup>-1</sup> ]	STEM <sup>b</sup> Average particle size (nm)
K <sub>0.6</sub> -Pt/MFI_H <sub>2</sub>	2081	0.073	1.1
K <sub>0.3</sub> -Pt/MFI_H <sub>2</sub>	n.d. <sup>a</sup>	0.054	1.2
K <sub>0</sub> -Pt/MFI_H <sub>2</sub>	2087	0.023	1.2
H-Pt/MFI_H <sub>2</sub>	2093	0.021	1.2

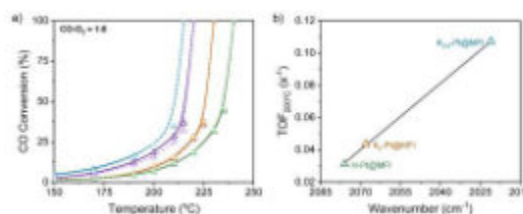


**Figure 1.** Catalytic activity and CO-IR spectra correlation for Pt@MFIs. a) CO conversion in O<sub>2</sub>-rich conditions for K<sub>0.6</sub>-Pt@MFI (blue), K<sub>0.3</sub>-Pt@MFI (purple), K<sub>0</sub> Pt@MFI (orange) and H-Pt@MFI (green). b) Correlation between TOF at 200°C and  $\nu_{CO}$  of the Pt nanoparticles from the catalysts (lower  $\nu_{CO}$  frequency indicates that the Pt nanoparticles are more electron-rich).

In this work, we have rationalized the preparation of highly active/highly stable CO oxidation catalysts using K-MFI zeolites. The incorporation of K as a counter cation of highly defective, pure silica MFI allows to support and retain Pt clusters smaller than 1 nm under harsh reaction conditions. These highly dispersed species resist, on the one hand, oxidative fragmentation in excess of O<sub>2</sub> (including O<sub>2</sub>-rich CO oxidation conditions), which causes state-of-the-art Pt/CeO<sub>2</sub> catalysts to deactivate; on the other hand, they also resist Ostwald-ripening sintering when exposed to severe redox stress at high temperature, in contrast to other supported catalysts based on non-reducible supports, thus, avoiding deactivation by agglomeration into low surface area metal particles. In addition to outstanding stability, a key to the high activity is the effective electron promotion of these small Pt species by K inside the MFI pores, leading to improved electron-rich metal clusters. Electronic promotion allows to compensate particle size effects, by which the smallest Pt clusters in some of these catalysts (< 0.9 nm) would not be so active if charge donation from the support was not substantial, as demonstrated by a combination of microscopy, FTIR and kinetic experiments. K in our sample plays, therefore, a dual role in K-Pt@MFI samples, as a metal-electron density modifier and as a stabilization agent, resulting in an outstanding catalytic performance for the CO oxidation.

## References

- [1] K. Ding et al., *Science*, **350** (6257), 189-192 (2015).
- [2] Y. Lu et al., *ChemCatChem*, **12** (6), 1726-1733 (2020).
- [3] Z. Zhang et al., *Nat Commun*, **14** (1), 2664 (2023).
- [4] M. Moliner et al., *J Am Chem Soc*, **138** (48), 15743-15750 (2016).
- [5] B.C. Gates, *Chem Rev* **95** (3), 511-522 (1995).
- [6] M. Moliner et al., *ACS Catal* **8** (10), 9520-9528 (2018).
- [7] P. Serna et al., *Angew Chem Int Ed* **60** (29), 15954-15962 (2021).
- [8] L. Liu et al., *Nat Mater* **18** (28), 866-873 (2019).

## Acknowledgments

This work has been supported by the Spanish Government through PID2021-122755OB I00 funded by MCIN/AEI/10.13039/501100011033 and TED2021-130739B-I00 funded by MCIN/AEI/10.13039/501100011033/EU/PRTR. The authors are also thankful for the Severo Ochoa financial support by the Spanish Ministry of Science and Innovation (CEX2021-001230-S/funding by MCIN/AEI/10.13039/501100011033). B.B. acknowledges the Spanish Government for a Severo Ochoa FPI scholarship (PRE2022 102555). The Electron Microscopy Service of the UPV is acknowledged for their help in sample characterization.



## Effect of defect-healing treatment on layered silicate precursors toward well-defined, cross-linked frameworks

Y. Ito<sup>1</sup>, K. Nayuki<sup>2</sup>, Y. Sasaki<sup>3</sup>, T. Wakihara<sup>1,4</sup>, T. Okubo<sup>1</sup>, and Kenta Iyoki<sup>1,5,6</sup>

<sup>1</sup> Department of Chemical System Engineering, The University of Tokyo, 7-3-1 Hongo, Bunkyo-ku, Tokyo 113-8656, Japan.

<sup>2</sup> JEOL Ltd., Solution Promotion Department, 3-1-2 Musashino, Akishima, Tokyo 196-8558, Japan

<sup>3</sup> Japan Fine Ceramics Center, 2-4-1 Mutsuno, Atsuta-ku, Nagoya 456-8587, Japan.

<sup>4</sup> Institute of Engineering Innovation, The University of Tokyo, 2-11-16 Yayoi, Bunkyo-ku, Tokyo 113-8656, Japan

<sup>5</sup> Department of Environment Systems, The University of Tokyo, 5-1-5 Kashiwanoha, Kashiwa-shi, Chiba 277-8563, Japan

<sup>6</sup> Precursory Research for Embryonic Science and Technology (PRESTO), Japan Science and Technology Agency (JST), Kawaguchi, Saitama 332-0012, Japan

ito\_y@chemsys.t.u-tokyo.ac.jp

### Introduction

Thin two-dimensional zeolite nanosheets with a single unit cell or near-single unit cell thickness (2–3 nm) can be synthesized [1, 2]. In recent years, the synthesis of three-dimensional zeolite frameworks from two-dimensional zeolite nanosheets using bonding layers has been actively pursued. Particularly, metal species such as iron and tin [3] bridging the layers are of particular interest because they can generate new catalytically active sites that differ from those in three-dimensional zeolite frameworks. However, the sites and their distribution of the metal species in the interlayers have not been precisely controlled. Two main problems have been reported: 1) insertion of metal species into the framework of layers and 2) cross-linkage by silicate species, which migrate from the layer frameworks. This causes the metal species in the layers and silicate species in the interlayers to have a random distribution. On the other hand, we recently reported a simple liquid-mediated, defect-healing method via self-defect-healing process [4] that can remove most defects in high-silica zeolites and realize extremely stable zeolites. Fluoride compounds that break siloxane bonds and promote the reconstruction of zeolite frameworks and organic pore fillers, which can stabilize the frameworks and prevent from structural collapse, worked cooperatively during the treatment. Although this method has only been adopted for zeolitic three-dimensional frameworks, it is also expected to be applicable to two-dimensional zeolite nanosheets. Defect-free zeolite nanosheets prepared using this method can be ideal precursors for interlayer linkages.

### Experimental

#### Synthesis of PREFER

PREFER—a layered precursor of FER-type zeolites—was synthesized as described in a previous study [5].

#### Defect-healing treatment of PREFER

In accordance with our previous report [4],  $\text{NH}_4\text{F}$  was dissolved in a dilute solution of tetraethylammonium hydroxide to prepare a solution with a molar composition of 0.1 TEAOH:0.1  $\text{NH}_4\text{F}$ :15  $\text{H}_2\text{O}$ . The synthesized PREFER powder was slowly added to this solution at a solid-to-liquid weight ratio of 1:2. The resulting mixture was heated in an autoclave at 170 °C for 24 h. The solid product was collected via filtration, washed with distilled water, and dried at 80 °C overnight. The product obtained after the defect-healing treatment is denoted as PREFER\_healed. The samples before and after the defect-healing treatment were calcined at 550 °C for 6 h and are denoted as PREFER\_calcined and PREFER\_healed\_calcined, respectively.

#### Crosslinking layers of PREFER with iron atoms

Referring to a previous paper [3] on interlayer expansion using metal-linker units, Crosslinking layers of PREFER with iron atoms was conducted.

### Results & Discussion

#### Synthesis of PREFER

The XRD patterns of the obtained PREFER matched the previously reported diffraction pattern of PREFER. The SEM images also confirmed that the products had layered structures, which are characteristic of the PREFER.

#### Defect-healing treatment of PREFER

No differences in the XRD patterns due to the defect-healing treatment were observed, indicating that no structural changes occurred during the treatment. Notably, the layers did not condense and maintained the interlayer distance during the defect healing treatment, judging from the  $d$  values of the first peaks. For the following discussion, the types of silanol species are categorized into intralayer silanol defects and interlayer silanol groups (Figure. 1). The  $^{29}\text{Si}$  DD MAS NMR spectra shown in Figure 2 indicate that the integrated intensity of the  $\text{Q}^3$  ( $\text{Si}(\text{OH})(\text{OSi})_3$ ) signals, interlayer silanol groups and silanol defects, were reduced after the defect-healing treatment compared with those that of the  $\text{Q}^4$  ( $\text{Si}(\text{OSi})_4$ ) signals in the frameworks. The presence of a certain amount of the  $\text{Q}^3$  signal after the defect-healing treatment suggests that the intralayer silanol defects were healed while the interlayer silanol groups in PREFER were maintained. This is because the interlayer silanol groups were separated from each other and stabilized by the OSDA by balancing the charges. DRIFT spectra measured at 550 °C are shown in Figures 3. The spectra were normalized to the bending vibrations of the Si-O bonds. As shown, the intensities of the absorption peaks



corresponding to the stretching vibration of silanol groups observed in the region of 3750–3690  $\text{cm}^{-1}$  were reduced by the defect-healing treatment. According to the previous studies [6,7], the peaks at 3691 and 3724  $\text{cm}^{-1}$  can be assigned to interlayer and intralayer silanol groups, respectively, because interlayer silanol groups form strong hydrogen bonds, and their stretching vibrations are considered to shift to lower frequencies [8]. The spectra indicated that the number of intralayer silanol groups was significantly reduced by the defect-healing treatment, while the interlayer silanol groups were maintained. These assignments were confirmed by comparing with DRIFT spectra obtained at different temperatures. The intensity of the absorption peak assigned to the interlayer silanol groups observed at 3691  $\text{cm}^{-1}$  started to decrease as the temperature increased owing to interlayer condensation, whereas that of the peak assigned to intralayer silanol groups at 3724  $\text{cm}^{-1}$  was maintained even after heating.

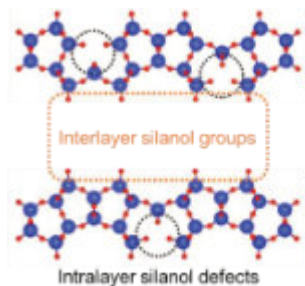


Figure 1. Types of silanol species

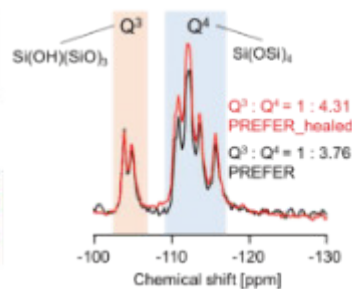


Figure 2.  $^{29}\text{Si}$  DD MAS NMR spectra of PREFER and PREFER\_healed.

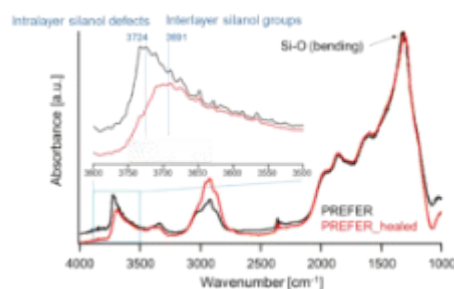


Figure 3. DRIFT spectra of PREFER and PREFER\_healed at 550 °C.

#### Crosslinking layers of PREFER with iron atoms

The first diffraction peaks of the crosslinked samples were shifted to a high angle (low  $d$  value) relative to those of PREFER, indicating that the interlayer distance of the crosslinked sample calculated from the  $d$  value was shorter than that of PREFER but longer than that of the FER-type zeolite, indicating that the condensed interlayer distances were increased by the insertion of iron atoms. The TEM images indicated that the interlayer distance has increased relative to FER structure in both PREFER and PREFER\_healed due to interlayer crosslinking, which is consistent with the  $d$  values calculated from the XRD patterns. The UV-Vis spectra of the samples crosslinked with iron atoms are shown in Figures 4. The UV-Vis spectra showed differences in the 200–300-nm peak depending on whether the starting material was defect-healed or not. This indicates that the numbers of isolated framework Fe(III) ions with tetrahedral coordination and isolated Fe(III) ions with octahedral coordination were reduced [9] in the defect-healed samples, which is thought to suppress the reaction of iron atoms outside the interlayer. Thus, the defect-healing treatment on the precursor suppressed the migration of silicate species, and more iron atoms were inserted between the layers of PREFER in homogeneous environment after the defect-healing treatment.

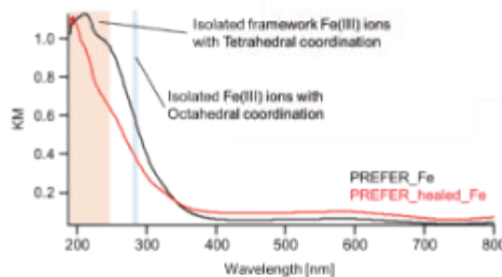


Figure 4. UV-Vis spectra of PREFER\_Fe and PREFER\_healed\_Fe.

#### Conclusion

Defect-healing treatment was applied to PREFER—a layered precursor of FER-type zeolite—which was subjected to interlayer crosslinking using iron atoms. The number of intralayer silanol defects was significantly reduced by the treatment, whereas the interlayer silanol groups were maintained. The UV-vis spectra of the crosslinked samples showed that the iron atoms were in different states depending on the treatment. The sample from the defect-healed precursor exhibited enhanced iron atom insertion in more homogeneous environments compared to the untreated precursor. The results demonstrate the possibility of controlling the atomic environment in layered materials. This study provides a new way to synthesize well-defined, crosslinked three-dimensional frameworks.

#### References

- [1] K. Iyoki et al., *Microporous Mesoporous Mater.* 2014, 189, 22–30. [2] M. E. Davis, *Nature* 2002, 417, 813–821.
- [3] H. Gies et al., *Microporous Mesoporous Mater.* 2016, 222, 235–240. [4] K. Iyoki et al., *J. Am. Chem. Soc.* 2020, 142, 3931–3938. [5] J. Ruan et al., *Chem. Mater.* 2009, 21, 2904–2911. [6] Y. Asakura et al., *Chem. Mater.* 2014, 26, 3796–3803. [7] I. C. Medeiros-Costa et al., *Chem. Soc. Rev.* 2021, 50, 11156–11179. [8] A. Erigoni et al., *Chem. Cat. Chem.* 2016, 8, 3161–3169. [9] J. Zhang et al., *Appl. Catal. A Gen.* 2022, 630, 118467.

#### Acknowledgments

This work was financially supported by the Japan Science and Technology Agency (JST) through Precursory Research for Embryonic Science and Technology (PRESTO, grant No. JPMJPR21N3) and the Strategic International Collaborative Research Program (SICORP) EIG CONCERT-Japan (grant No. JPMJSC22C5).

## Ultrafast Laser Synthesis of Silicalite-1 and Titanium Silicalite-1

Mehdi Hagverdiyev<sup>1</sup>, Meryem Merve Dogan<sup>1</sup>, Serim Kayacan Ilday<sup>2</sup>, Sezin Galioglu Ozaltug<sup>1</sup>

<sup>1</sup> UNAM-National Nanotechnology Research Center & Institute of Materials Science and Nanotechnology,  
Bilkent University, Ankara, 06800, Türkiye

<sup>2</sup> Faculty of Electrical Engineering and Information Technology, Ruhr University Bochum, 44801, Germany

In recent years, rapid synthesis methods for zeolites have gathered significant interest. Researchers aim to reduce the induction period and shorten reaction times to just a few hours, while maintaining high yield, crystallinity, and catalytic performance. However, current energy delivery methods lack the subtlety required to control silica polymerization and depolymerization processes at femto- and picosecond timescales, thereby limiting the precision of directed synthesis. To address this challenge, we propose an ultrafast laser synthesis technique that provides energy delivery with precise spatiotemporal control at these timescales and eliminating the need for external heating. By employing the unique regime of ultrafast lasers, multiphoton absorption of laser light within a localized region of the precursor suspension creates a microreactor. In the absorption zone, smaller oligomers grow as they absorb laser energy, while laser-induced convective flows continuously distribute newly formed clusters throughout the suspension. Utilizing this approach, we elucidated the entire nucleation and growth pathway of laser-synthesized TPA-silicate-1 zeolites, from the initial formation of oligomers to the development of fully crystalline crystals. The trials on the synthesis of Silicalite-1 zeolite have demonstrated success, with full characterization showing superior product quality and a comparable yield to hydrothermal methods, but with a reduction in reaction time from 24 hours to 3 hours. The synthesis method was tested in terms of reproducibility and more than 250 independent syntheses were carried out. Future perspectives are focused on more complex multi-functional Ti substituted silicalite-1 (TS-1) and zeolite A synthesis and enhancement of their photocatalytic and gas adsorption capacities. The precise spatiotemporal control offered by this technique opens up new possibilities for steering reaction pathways and investigating the extensive configurational space of zeolites.



## Structural modifications of pure silica MEL zeolite studied by in-situ X-Ray diffraction during adsorption of propane

A. Barros, S. Martí, M. Palomino, J. L. Jordá, S. Valencia, F. Rey

Instituto de Tecnología Química, Universitat Politècnica de València – Consejo Superior de Investigaciones Científicas (UPV-CSIC), 46022 Valencia (Spain).  
svalenci@itq.upv.es

Structural deformations of zeolites during adsorption processes have been reported previously for MFI [1], RHO [2] and many AlPO-zeotypes [3,4] among others. These structural modifications generally imply an increment of the adsorption capacity above certain pressure, evidenced by the presence of sharp increments in the adsorption isotherm profiles. This is accompanied by the appearance/disappearance of X-Ray diffraction (XRD) peaks indicating the occurrence of the phase transition without changes in the atomic connectivity (i.e. symmetry change). Additionally, it has been found that this phase transition does not depend solely on the gas pressure, but also on the nature of the adsorbate. For instance, CO<sub>2</sub> when adsorbed on a zeolite RHO of Si/Al ratio close to 5 induces a phase transition at a pressure around 2 bar, while CH<sub>4</sub> does not. This peculiarity provides of very high CO<sub>2</sub>/CH<sub>4</sub> selectivity to zeolite RHO for this relevant gas separation [2].

The Ar adsorption isotherm of pure silica ZSM-11 (MEL structure) shows an abrupt increase at 0.002 P/P<sub>0</sub>. Molecular simulation studies have attributed this sharp step in the isotherm to structural modifications of the tetragonal symmetry of MEL structure [5].

In this work, we have studied the structural modifications of the pure silica MEL zeolite upon adsorption of propane by in-situ X-Ray diffraction techniques compared to its adsorption isotherm.

### Experimental

Synthesis of pure silica MEL zeolite was carried out following methods reported previously [6]. The calcined material was outgassed at 400°C under high vacuum for 12 hours prior to any adsorption measurement. The Ar adsorption isotherms were measured at 77, 87, 92 and 97 K in an ASAP-2020 (from Micromeritics) equipped with a Cryotune attachment (from 3P analytics) that allows an accurate control of the temperature between 77 to 300 K. The propane adsorption isotherm on pure silica MEL sample was measured using a BELSORP Max-II instrument at 298 K. The pure-silica MEL sample was calcined in situ under inert atmosphere at 873 K for 8 h and subsequently cooled down at 303 K in an Anton-Paar XRK-900 reaction chamber attached to an Empyrean X-Ray diffractometer. Then, mixtures of propane/helium at different proportions were fluxed through the sample while X-Ray diffractions patterns were collected for four eight hours each. The X-Ray diffraction patterns obtained at the same partial pressure were carefully examined and those that are identical were added (assuming that equilibrium was reached), while those that showed dissimilarities were discarded.

### Results and Discussion

The Ar adsorption isotherms collected at different temperatures are shown in Figure 1. There, it is observed that the pure-silica MEL zeolite shows a very sharp step in the isotherms, being this step shifted to higher pressures as the temperature increases. When these isotherms are plotted versus partial pressure of propane, the abrupt adsorption step appear at the same P/P<sub>0</sub> values in all isotherms.

Attempts to fit the Ar isotherms by applying different models were unsuccessful and thus, the heat of adsorption in the whole range of loading were not calculated.

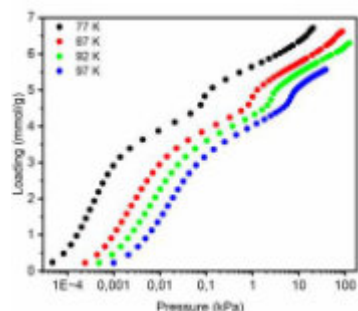


Figure 1: Ar adsorption isotherms on pure-silica MEL at different temperatures

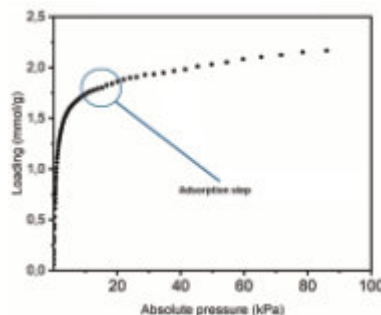


Figure 2: Propane adsorption isotherm at 298 K on pure silica MEL.

The heat of adsorption at propane loading below the abrupt step of the isotherms (i.e. below 3 mmol/g) gives a value of approximately 12 kJ/mol, which is of the order of values reported in literature for Ar adsorbed on non-polar surfaces.

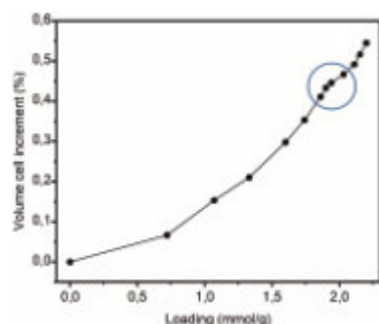
The propane adsorption isotherm on pure silica MEL at 298 K is shown in

Figure 2, where a subtle step is observed at 20 kPa of pressure. The step also precludes the fitting of the experimental isotherm by applying Langmuir based models (Toth, Dual Site, etc). The presence of this step may indicate that a phase transformation takes place at 20 kPa of pressure of propane in pure silica MEL, as was suggested to occur with Ar.



The heat of adsorption at propane loading below the abrupt step of the isotherms (i.e. below 3 mmol/g) gives a value of approximately 12 kJ/mol, which is of the order of values reported in literature for Ar adsorbed on non-polar surfaces.

The propane adsorption isotherm on pure silica MEL at 298 K is shown in Figure 2, where a subtle step is observed at 20 kPa of pressure. The step also precludes the fitting of the experimental isotherm by applying Langmuir based models (Toth, Dual Site, etc). The presence of this step may indicate that a phase transformation takes place at 20 kPa of pressure of propane in pure silica MEL, as was suggested to occur with Ar.



**Figure 3:** Variation of the tetragonal unit cell volume of MEL structure with the propane loading.

Thus, we performed an in-situ structural study by submitting the sample to different partial pressures of propane in He while recording the XRD patterns. All patterns of the pure silica MEL recorded at different propane pressures can be indexed in the same tetragonal symmetry. However, the unit cell volume increases with the propane loading as it is shown in Figure 3. Thus, these results indicate that there is no phase transition as occurs in other zeolites, such as MFI or RHO. However, the unit cell expansion is not linear with the propane uptake and there is an inflection point in the expansion curve at approximately 1.8 mmol/g of adsorbed propane on ZSM-11, which approximately corresponds to the sharp step observed in the adsorption isotherm of propane.

Consequently, the increase observed in the propane uptake at 20 kPa must be attributed to an abrupt expansion of the tetragonal unit cell rather than to a phase transition, since there is no symmetry change along the whole range of propane pressure studied here.

## References

- [1] E. García-Pérez, J.B. Parra, C.O. Ania, D. Dubbeldam, T.J.H. Vlugt, J.M. Castillo, P.J. Merklings, S. Calero, *J. Phys. Chem. C*, **112**, 9976 (2008).
- [2] M. Palomino, A. Corma, J.L. Jordá, F. Rey and S. Valencia, *Chem. Commun.*, **48**, 215 (2012).
- [3] A. Krajnc, J. Varlec, M. Mazaj, A. Ristic, N. Zabukovec Logar and G. Mali, *Adv. Energy Mater.*, **7**, 1601815 (2017).
- [4] J. Varlec, A. Krajnc, M. Mazaj, A. Ristic, K. Vanatalu, A. Oss, A. Samoson, V. Kaucic and G. Mali, *New J. Chem.*, **40**, 4178 (2016).
- [5] V. Sánchez-Gil, E.G. Noya, J.M. Guil, E. Lomba, S. Valencia, I. da Silva, L. Pusztai and L. Temleitner, *J. Phys. Chem. C*, **120**, 2260 (2016).
- [6] O. Terasaki, T. Ohsuna, H. Sakuma, D. Watanabe, Y. Nakagawa and R.C. Medrud, *Chem. Mater.*, **8**, 463 (1996).

## Acknowledgments

Financial support by the Spanish Ministry of Science and Innovation (CEX2021-001230-S and PID2022-136934OB-100 grants funded by MCIN/AEI/10.13039/501100011033 funded by "ERDF A way of making Europe" and TED2021-130191B-C41 grant funded by the European Union NextGenerationEU/PRTR) are gratefully acknowledged. Authors thank also the financial support by the Generalitat Valenciana (Prometeo 2021/077). This study forms part of the Advanced Materials programme and was supported by MCIN with partial funding from European Union Next Generation EU (PRTR-C17. I1) and by Generalitat Valenciana (MFA/2022/012 and MFA/2022/047). A. B. thanks to Generalitat Valenciana for grant PROMETEO/2021/077-02.



## Machine Learning and High-Throughput Simulation Methods to Design Organic Structure-Directing Agents for Zeolites

K. Muraoka<sup>1</sup>, K. Oishi<sup>1</sup>, S. Ito<sup>1</sup>, A. Nakayama<sup>1</sup>

<sup>1</sup> Department of Chemical System Engineering, The University of Tokyo, Japan

muraok\_k@chemsys.t.u-tokyo.ac.jp, nakayama@chemsys.t.u-tokyo.ac.jp

For the controlled synthesis of zeolites with targeted properties, the design of organic structure-directing agents (OSDAs) is a fundamental technique. While the complexity of the molecular design often necessitates costly trial-and-error experiments, various de novo molecular design methodologies have been developed to do it computationally [1–4]. These studies have provided insights into OSDAs that interact with zeolites through atomistic simulations and contributed to the development of methods for identifying the optimal point within the vast expanse of chemical space.

In this presentation, we report our recent efforts to use machine-learning and high-throughput simulation methods to design OSDAs. In the first part, we report the potential for human-machine collaboration in OSDA design using large language models (LLMs). In the second part, we introduce the use of neural network potential to get insights on Al-site directing ability of OSDAs for zeolites.

LLMs are machine learning models that have been trained on a diverse range of internet text. They are proficient in generating human-like text based on the given text. Because LLMs allow users to interact easily via natural language, it is natural to assume that they have the potential to become a great platform for realizing human-machine collaboration for designing targeted molecules.

We asked GPT-4—a leading-edge LLM created by OpenAI—to generate new OSDAs from the basic OSDA, tetraethylammonium (TMA) using natural language and SMILES notation (Figure 1). GPT-4 responded by generating SMILES string representing TMA derivative, adorned with additional functional groups, thereby demonstrating its potential as a tool for molecular generation. To further explore how we can guide the LLM to the desired direction of the molecular design, we instructed GPT-4 to incorporate a carbon ring into its outputs. In response, GPT-4 provided a candidate with carbon ring. This confirmed that GPT-4 can not only generate molecular structures but also refine them based on guidance provided via natural-language dialogue, showcasing its value in human-machine collaborative efforts in molecular design.

Figure 2 provides the overview of the de novo molecular design workflow, which incorporates elements such as GPT-4, prescreening filters, atomistic simulation, and a database. The data stored within the database encompasses the SMILES notation for the molecule and the corresponding affinity score for

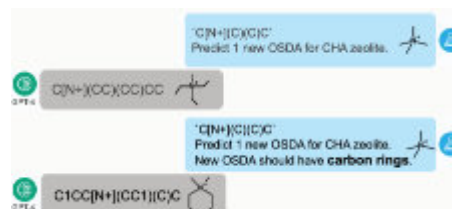


Figure 1: Generation of SMILES for OSDAs by GPT-4.

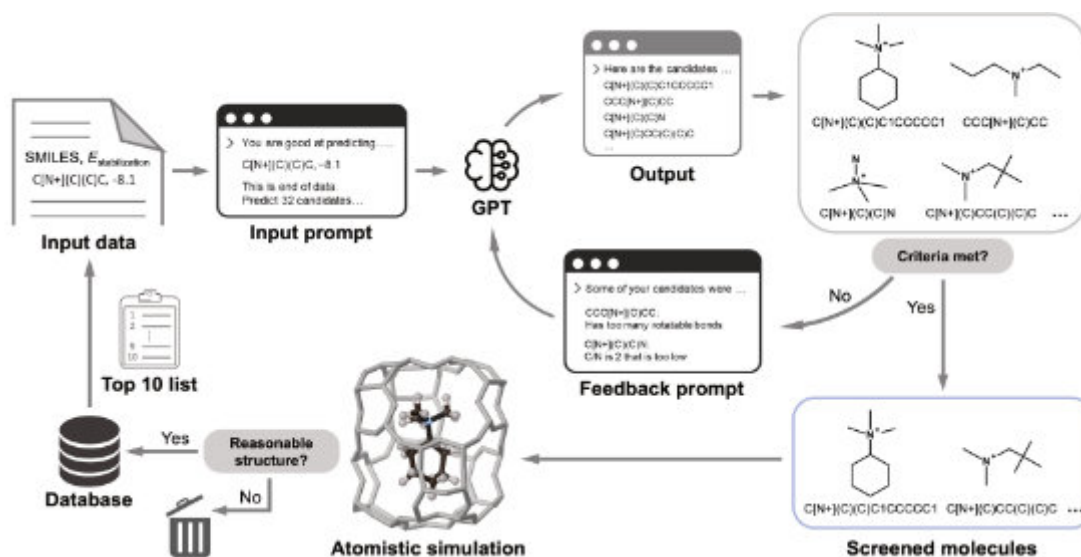


Figure 2: Schematic illustration of the computational workflow.

a specific zeolite. The algorithm retrieves the top 10 entries among 100 recent records from the database and formulates a text to instruct GPT-4 to generate potential molecules.

GPT-4 generates SMILES-like strings as requested. These strings are parsed and subjected to a series of empirical filtering to eliminate candidates unsuitable as OSDAs. The criteria check rigidity/flexibility, stability, and hydrophobicity/hydrophilicity. The rejected entries along with the reasons for the rejection are sent back to GPT-4. Molecules that meet the prescreening undergo atomistic simulation to assess their affinity against the targeted zeolite.

Our de novo molecular design methodology was applied to three cage-type zeolites, CHA, AEI, and ITE, which are frequently used structures to demonstrate de novo molecular design for OSDAs [5].

While generative models such as LLMs can be “foundational models” for general-purpose inference, neural network potentials can also be foundational models in chemistry and material science.

Several studies [6] have demonstrated that zeolite catalysts with varying aluminum distributions can exhibit different catalytic behaviors. In zeolites, the negative charges provided by the aluminum atoms are considered to influence the active sites, which typically consist of positively charged guest species introduced into the pores of the zeolites. An intuitive strategy to control the location of Al is through the utilization of OSDAs. Although a general agreement is that the positive charge introduced by OSDAs is close to Al in zeolites, a comprehensive understanding of factors contributing to the strength of this Al site-directing ability for different OSDAs is still lacking.

We tried to quantify the Al site-directing ability of different zeolite–OSDA complexes by atomistic simulations employing a neural network potential. We then calculated the probability that an Al is introduced to a specific T site, assuming the Boltzmann distribution.

Pinar et al. [6] assumed Al is at the tetrahedral (T) site closest to N in PYRR. To investigate whether this assumption holds, we plotted the relative energy of various PYRR–FER complexes against Al...N distance (Figure 3c). Our calculations revealed that the complex with the shortest Al...N distance contained Al at T3, which is in accordance with the previous study. However, our results show that Al at T1 site is more stable than Al at T3 site by 12 kJ/mol (Figure 3a) and that T3 is the least favorable site even when different computational levels are employed. This indicates that simple Al...N distance is not a perfect descriptor for predicting the stable Al sites.

For comparison, we performed an identical procedure for TMA–FER complexes. As shown in Figure 3b, TMA is confined in the center of the cage in the most stable structures of TMA–FER, and the shortest Al...N distance of the TMA–FER complexes was much longer than the case of PYRR–FER. It starkly contrasts with PYRR–FER, where OSDA could move and rotate to bring N closer to Al in optimization. Owing to this feature, the distribution of Al...N distances for TMA–FER was not as broad as PYRR–FER (Figure 3c). Moreover, the effects of O(–Al)...H interaction in the TMA–FER could be weaker than those in PYRR–FER, considering the weaker positive charge on terminal H and the longer O(–Al)...H distance in the most stable TMA–FER. These features likely result in a relatively narrow energy distribution of TMA–FER (Figure 3c). These results show that N–H moieties can enhance the Al site-directing ability [7].

In summary, LLMs and neural network potentials, two foundational models were successfully applied to design OSDAs for zeolites [5,7]. These findings will contribute to the future design of OSDAs for the controlled synthesis of zeolites with specific Al distribution while using chemical knowledge across various domains documented in diverse texts.

## References

- [1] D. W. Lewis, D. J. Willock, C. R. A. Catlow, J. M. Thomas, G. J. Hutchings, *Nature*, **382**, 604–606 (1996).
- [2] R. Pophale, F. Daeyaert, M. W. Deem, *J. Mater. Chem. A*, **1**, 6750–6760 (2013).
- [3] K. Muraoka, W. Chaikittisilp, T. Okubo, *Chem. Sci.*, **11**, 8214–8223 (2020).
- [4] L. Xu, X. Peng, Z. Xi, Z. Yuan, W. Zhong, *Chem. Eng. Sci.*, **282**, 119188 (2023).
- [5] S. Ito, K. Muraoka, A. Nakayama, *ChemRxiv* (2024). 10.26434/chemrxiv-2024-wqx17.
- [6] A. B. Pinar, L. Gómez-Hortigüela, L. B. McCusker, J. Pérez-Pariente, *Chem. Mater.*, **25**, 3654–3661 (2013).
- [7] K. Oishi, K. Muraoka, A. Nakayama, *Chem. Commun.*, **59**, 8953–8956 (2023).

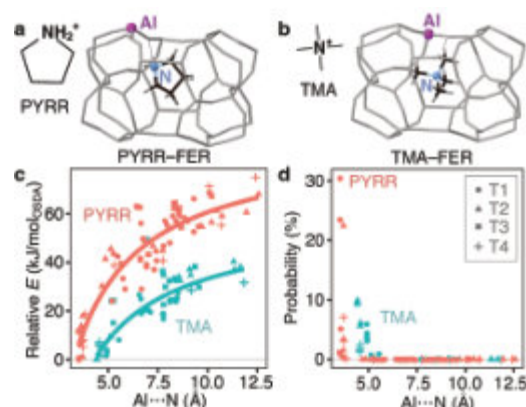


**Figure 3:** Most stable structures of (a) PYRR–FER and (b) TMA–FER complexes. Purple spheres represent Al, grey rods indicate the silicate framework, light blue spheres represent N, and black and white rods signify C and H, respectively. (c) Relationship between relative energy and Al...N distance. (d) Relationship between the probability of the configuration and Al...N distance.



## End-of-life PV panels as a circular economy products in synthesis of micro/mesoporous materials

**D.Czarna-Juskiewicz<sup>1</sup>, P.Kunecki<sup>1</sup>, Ł.Osuchowski<sup>2</sup>, T.Głowienko<sup>3</sup>, M.Wdowin<sup>1</sup>**

<sup>1</sup> Mineral and Energy Economy Research Institute, Polish Academy of Sciences, Wybickiego 7A, 31-261 Kraków, [dczarna@meeri.pl](mailto:dczarna@meeri.pl)

<sup>2</sup> Military University of Technology, gen. Sylwestra Kaliskiego 2, 00-98 Warsaw 46

<sup>3</sup> Geminus Sp. z o.o.

In this study, the potential use of waste materials such as used photovoltaic panels, for the synthesis of zeolites was investigated. The primary waste material was a silicon-rich fraction obtained as a by-product of the thermolytic decomposition of end-of-life photovoltaic panels. A simple hydrothermal synthesis process was employed to obtain the zeolite material, carried out at a temperature of 60°C for a duration of 6 days. During the synthesis, a 2.5 M NaOH solution was used, and the effect of the Si/Al molar ratio on the type of crystallized structure was examined. The samples were characterized using X-Ray Diffraction (XRD), Scanning Electron Microscopy (SEM). Additionally, the specific surface area was determined.

The conducted studies showed that it is possible to obtain zeolite A and NaP1 under the specified conditions. However, the phase composition is strictly dependent on the Si/Al molar ratio. At a Si/Al molar ratio of approximately 2, well-formed zeolite A with a small with a small percentage share of NaP1 was obtained. A decreasing share of aluminum in the reaction resulted in a reduction of the proportion of zeolite A in favour of NaP1. At the lowest Si/Al molar ratio (below 0.3), a high content of the amorphous phase was observed.

### **Acknowledgments**

The researches were realized within frame of statutory works of Mineral and Energy Economy Research Institute, Polish Academy of Sciences



## Rapid Synthesis of Cu-Encapsulated Nanoparticles in ZSM-5 Zeolite for Enhanced Catalytic Conversion of CO<sub>2</sub> to Methanol

R. Simancas<sup>1</sup>, S. Yamaguchi<sup>1</sup>, R. Kanomata<sup>2</sup>, K. Awano<sup>2</sup>, K. Kimura<sup>2</sup>, S. Yasuda<sup>3</sup>, H. Fujitsuka<sup>4</sup>, T. Tago<sup>2</sup>, T. Yokoi<sup>3</sup>, T. Okubo<sup>1</sup>, T. Wakihara<sup>1,5\*</sup>

<sup>1</sup>Department of Chemical System Engineering, The University of Tokyo, 7-3-1 Hongo, Bunkyo-ku, Tokyo 113-8656, Japan, <sup>2</sup>Department of Chemical Science and Engineering, School of Materials and Chemical Technology, Tokyo Institute of Technology, 2-12-1, Ookayama, Meguro-ku, Tokyo, 152-8552, Japan, <sup>3</sup>Nanospace Catalysis Unit, Institute of Innovative Research, Tokyo Institute of Technology, 4259 Nagatsuta, Midori-ku, Yokohama 226-8503, Japan, <sup>4</sup>Department of Chemical Engineering, Graduate School of Engineering, Kyoto University, Nishikyo-ku, Kyoto, 615-8510, Japan, <sup>5</sup>Institute of Engineering Innovation, The University of Tokyo, 2-11-16 Yayoi, Bunkyo-ku, Tokyo 113-8656, Japan. \*Corresponding author, wakihara@chemsys.t.u-tokyo.ac.jp

This study explores the encapsulation of Cu nanoparticles within ZSM-5 zeolite. Three different synthesis methods, slow, medium, and fast hydrothermal encapsulation, were applied to embed Cu nanoparticles within the zeolite. The fast encapsulation, performed in just 5 minutes, resulted in smaller and more uniformly distributed Cu nanoparticles compared to the medium and slow methods, which took several hours. This sample also showed an improvement in the CO<sub>2</sub> hydrogenation to methanol and resistance against agglomeration of Cu nanoparticles during reaction.

### Introduction

Metal nanoparticles offer promising catalytic potential due to their high surface-to-volume ratio enhancing the number of active surface sites compared with the bulk materials [1]. However, metal nanoparticles are thermodynamically unstable and tend to sinter at high reaction temperatures and in the presence of water, usually resulting in a decrease in catalytic activity. Cu-based catalysts play an important role in many industrial processes, such as the water-gas shift reaction, hydrogenation of CO<sub>2</sub> to methanol, partial oxidation of methanol, and selective hydrogenation of oils. Methanol obtained from CO<sub>2</sub> hydrogenation is one of the promising methods to contribute to carbon neutrality and mitigate the greenhouse effect. In this sense, CO<sub>2</sub> has great potential as feedstock for chemicals and renewable fuels. The commercial catalyst used in the process is Cu/ZnO/Al<sub>2</sub>O<sub>3</sub> which suffers deactivation due to the presence of water that is formed during the reduction of CO<sub>2</sub>.

Enhancing the stability of these materials against water is crucial to slow down the deactivation of the catalysts. Encapsulation of metal nanoparticles in zeolites allowed to combine the enhancement in the hydrothermal stability with the shape selectivity of the zeolites [2,3]. Direct incorporation of metal cations during zeolite crystallization is highly desirable to introduce the metal with a uniform distribution in the solid. However, the synthesis of zeolites usually requires high temperatures under alkaline media that causes the precipitation of metal oxides and hydroxides outside zeolite particles.

Previously, our group reported the preparation of Pt/Sn nanoparticles encapsulated in ZSM-5 zeolite by using standard metal precursors [4]. The key to avoiding precipitation of the metal was the acceleration of the zeolite crystallization. The Pt/Sn-encapsulated ZSM-5 zeolite was obtained in only 5 min of hydrothermal synthesis which allowed the concerted formation of nanoclusters of 1 nm. In this work, the encapsulation of Cu nanoparticles within ZSM-5 zeolite using the fast synthesis strategy was applied to prepare active catalysts for the CO<sub>2</sub> hydrogenation to methanol. Highly dispersed Cu-encapsulated ZSM-5 has been obtained in only 5 min of hydrothermal synthesis.

### Experimental part

Cu-containing ZSM-5 solids were prepared by the following methods:

*Cu/ZSM-5 coprecipitation (Coprecip):* the sample was prepared by oxalate gel precipitation. Calcined ZSM-5 obtained as previously reported [5] was added to a solution of Cu(NO<sub>3</sub>)<sub>2</sub> in ethanol under vigorous stirring. After the addition of oxalic acid, the slurry was stirred at room temperature for 1 h. The obtained solid was recovered by filtration and calcined under air at 550°C for 5 h.

*Cu@ZSM-5 encapsulation\_slow (Encap\_slow):* In a typical synthesis, LUDOX AS-40 was added to a mixture of Al(OH)<sub>3</sub>, TPAOH and NaOH. After 2 h of stirring at room temperature, Cu(acetate)<sub>2</sub> was added to the mixture that was stirred and ultrasonicated. The synthesis mixture with the following composition 25 Na<sub>2</sub>O : Al<sub>2</sub>O<sub>3</sub> : 300 SiO<sub>2</sub> : 20 TPAOH : 6 Cu(acetate)<sub>2</sub> : 3000 H<sub>2</sub>O was transferred to a Teflon<sup>®</sup>-lined stainless-steel autoclaves and heated at 150°C in static conditions for 4 – 21 h. The solid was recovered by centrifugation, washed with distilled water, dried at 80°C overnight, and calcined in air at 550°C for 5 h.

*Cu@ZSM-5 encapsulation\_medium and fast (Encap\_medium and Encap\_fast):* these samples were prepared following the Encap\_slow method, but in this case, an aging step at 90°C for 15 h was performed before the addition of Cu(acetate)<sub>2</sub>. The synthesis mixture was transferred to a stainless-steel tube and heated at 150°C for 0.25 – 5 h for the Encap\_medium, and 190°C for 2 - 15 min for the Encap\_fast synthesis.



## Results and discussion

Highly crystalline ZSM-5 zeolites were obtained after only 5 min of heating in the case of the Encap\_fast, while 2 h and 12 h of hydrothermal treatment were required for the Encap\_medium and Encap\_slow, respectively. After calcination at 550°C for 5 h, the absence of diffraction peaks corresponding to CuO species suggests the formation of small and well-dispersed nanoparticles in the zeolites prepared by encapsulation, while CuO was observed in the coprecipitated sample (Coprecip). The incorporation and size of metal nanoparticles was confirmed by TEM. In Figure 1, visible nanoclusters larger than 15 nm can be observed in Coprecip. All the samples prepared by encapsulation present smaller Cu nanoclusters of less than 5 nm. However, the particles shown in Encap\_fast appear more homogeneously distributed in the crystals, while in the case of Encap\_slow, the nanoparticles seem to be located on the surface of the crystals. In all cases the particle size of metal particles is larger than the channels of the ZSM-5 zeolite which indicates that most of these nanoparticles are fixed in the zeolite crystals.

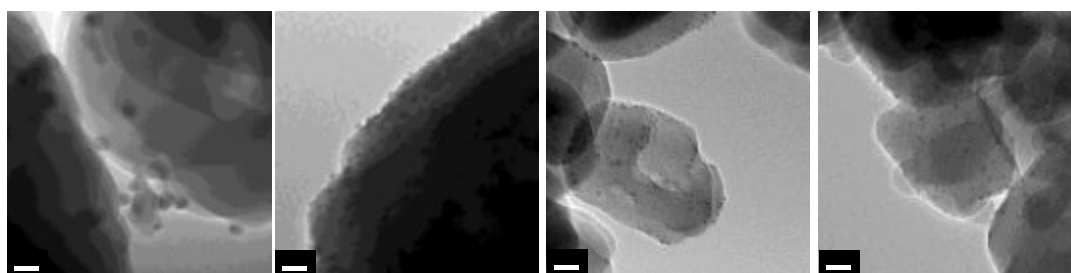


**Figure 1.** TEM images of the samples prepared by coprecipitation and encapsulation slow, medium and fast methods after calcination at 550°C for 5 hours.

Absorption bands associated with the presence of isolated  $\text{Cu}^{2+}$  cations together with CuO nanoparticles, and large CuO particles only in Coprecip sample, were observed in the UV-Vis spectra.  $\text{H}_2$ -TPR profiles showed reduction peaks between 200 and 400°C which are attributed to the reduction of Cu oxide. However, the maximum reduction peaks of all the Cu encapsulated ZSM-5 zeolites appear at a higher temperature than that of the Coprecip sample, which indicates the encapsulated Cu species are hardly reduced due to the confinement effect.

Catalytic tests in the  $\text{CO}_2$  hydrogenation to methanol at 250°C and 2 MPa (Figure 2) using the reduced Encap\_fast and Encap\_medium zeolites show a moderate  $\text{CO}_2$  conversion of 10% with a methanol selectivity higher than 10%. On the contrary,  $\text{CO}_2$  conversion and methanol selectivity decreases to 4.0% and 0.14%, respectively, for Encap\_slow, whereas 1.5% of  $\text{CO}_2$  conversion with negligible formation of methanol was obtained for Coprecip sample. The addition of Zn together with Cu species in the Encap\_fast sample preparation, allowed to obtain Cu and Zn encapsulated materials which show more than double of methanol selectivity, higher than 20% in both cases, but slightly lower  $\text{CO}_2$  conversion of around 7%.

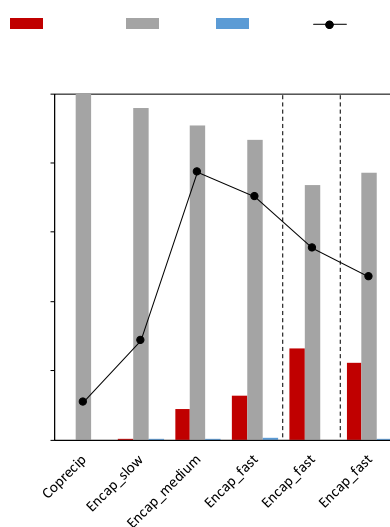


**Figure 2.** Product selectivity and  $\text{CO}_2$  conversion for  $\text{CO}_2$  hydrogenation performed at 250°C, 2 MPa at 3 h of reaction using the samples prepared by Coprecip, Encap\_slow, Encap\_medium, Encap\_fast with 2wt% of Cu and Encap\_fast with 2wt% Cu and 1 and 2 wt% of Zn.

## Conclusions

The fast encapsulation method for Cu nanoparticles within ZSM-5 zeolite offers significant advantages over slower methods, resulting in better nanoparticle dispersion, smaller particle sizes, and enhanced catalytic performance in  $\text{CO}_2$  hydrogenation to methanol. This fast synthesis approach, which accelerates the crystallization process to just 5 minutes, presents a promising pathway for the development of stable and efficient Cu-based catalysts, highlighting its potential for scalable industrial applications.

## References

- [1] C. Gao et al., *Chem. Rev.* **121** 34–881 (2021). [2] H. Wang et al., *ACS Cent. Sci.* **6** 1685–1697 (2020). [3] R. Kanomata et al. *J. Chem. Eng.* **485** (2024) 149896. [4] J. Zhu et al., *Angew. Chemie Int. Ed.* **59** 19669–19674 (2020). [5] M. Deguchi et al. *Microporous Mesoporous Mater.* **270** (2018) 200–203.



## Synthesis and asymmetric catalytic activity of the chiral zeolite GTM-4 prepared from benzylated ephedrine derivatives

**Jaime Jurado-Sánchez, Ramón de la Serna, Carlos Márquez-Álvarez, Joaquín Pérez-Pariente, Luis Gómez-Hortigüela.**  
*Instituto de Catálisis y Petroleoquímica (ICP-CSIC), Calle Marie Curie, 2, 28049, Madrid, España.*  
jaime.jurado@csic.es

Chirality is the property of an object of not being superimposable on its mirror image. In chemistry, these two different images of a molecule are called enantiomers. In the pharmaceutical industry, most drugs are chiral, and in most cases an enantiomer has a greater therapeutic effect on the body than its mirror image. Such differences in activity can be lethal to humans, so the development of chiral heterogeneous catalysts that promote the synthesis of one enantiomer over the other represents one of the most difficult and exciting challenges in current scientific research.

Zeolites are among the most suitable candidates for this task due to their perfectly ordered three-dimensional structure, which provides very interesting confinement properties for their use as heterogeneous catalysts.

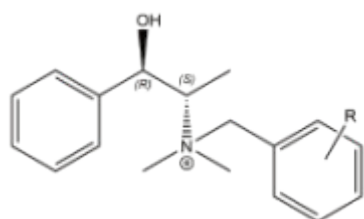


**Figure 1.** Derivatives of (1*R*,2*S*)-ephedrine with which the study was conducted, where R = H, CH<sub>3</sub> or F.

In this context, the -ITV type is among the most intriguing zeolitic frameworks, as it combines the presence of extra-large and chiral pores. This type of zeolite, discovered in 2009 at the Instituto de Tecnología Química (ITQ-37) [1], was not enriched in any of the two enantiomeric polymorphs of the zeolite as it was prepared from an achiral structure-directing agent (SDA), and therefore was not able to develop enantioselective discrimination processes. Years later, our group developed two zeolitic materials with the -ITV structure called GTM-3 and GTM-4. Both materials are enriched in one of the two polymorphs of the -ITV structure, so they are able to carry out asymmetric catalytic processes, reaching enantiomeric excesses of up to 60%. [2,3]

In the present work we study how the crystallisation of the -ITV structure is affected by the use of benzyl-containing derivatives of the alkaloid (1*R*,2*S*)-ephedrine as structure-directing agents (SDAs). The compounds studied included benzyl substituents (benzylmethylephedrinium derivatives, BnMEph), with methyl and fluorine groups at each of the different positions of the aromatic benzyl ring (*Figure 1*). Different variables were studied in relation to the composition of the zeolite synthesis gels, including the Si/Ge ratio, the concentrations of the SDA and mineralizing agent, as well as the crystallisation temperature and time.

As can be seen in *Table 1*, the benzyl-containing SDAs without additional groups (BnMEph, R = H in *Figure 1*) was not very efficient for the production of the -ITV phase. However, by adding both the methyl group and especially the fluorine group, the crystallisation of the -ITV phase was greatly improved (*Table 1*). With them, pure -ITV phase was obtained in all cases for a Si/Ge ratio of 2 and at 80 °C. At higher temperatures, the formation of the achiral structure BEC (polymorph C of the beta zeolite) was observed. For SDAs with methyl groups (R = CH<sub>3</sub>), pure -ITV phase was obtained only with the *o*-methylbenzyl derivative (*o*-MBnMEph) at 100 °C, as in this case the formation of BEC was inhibited.

In addition to the mentioned study, this work will also show how the asymmetric catalytic properties of the GTM-4 material are improved in the opening reaction of trans-stilbene oxide with 1-butanol, a chiral test reaction. In this reaction, the enantiomeric excess of the main chiral products with inversion of configuration (S<sub>N</sub>2 mechanism) is increased to reach values of 60%, the highest values obtained so far, when using *o*-MBnMEph as SDA in the synthesis of GTM-4. It is also observed that the enantiomeric excesses obtained vary significantly depending on the SDA used in the synthesis of the catalyst, which suggests a different

**Table 1.** Conditions and crystalline phases obtained using the different structure-directing agents (SDAs).

SDA	Si/Ge	T(°C)	Crystalline phase
BnMEph	3	100	BEC
BnMEph	3	80	ITV + BEC
BnMEph	2	100	BEC
BnMEph	2	80	BEC
<i>o</i> -MBnMEph	3	100	Amorfo
<i>o</i> -MBnMEph	3	80	Amorfo
<b><i>o</i>-MBnMEph</b>	<b>2</b>	<b>100</b>	<b>-ITV</b>
<i>o</i> -MBnMEph	2	80	Amorfo + -ITV
<i>m</i> -MBnMEph	3	100	Amorfo
<i>m</i> -MBnMEph	3	80	-ITV + Amorfo
<i>m</i> -MBnMEph	2	100	Amorfo
<i>m</i> -MBnMEph	2	80	-ITV + BEC
<i>p</i> -MBnMEph	3	100	BEC
<i>p</i> -MBnMEph	3	80	Amorfo
<i>p</i> -MBnMEph	2	100	BEC
<i>p</i> -MBnMEph	2	80	Amorfo + -ITV
<i>o</i> -FBnMEph	3	100	BEC
<b><i>o</i>-FBnMEph</b>	<b>3</b>	<b>80</b>	<b>-ITV</b>
<i>o</i> -FBnMEph	2	100	-ITV + BEC
<b><i>o</i>-FBnMEph</b>	<b>2</b>	<b>80</b>	<b>-ITV</b>
<i>m</i> -FBnMEph	3	100	BEC
<i>m</i> -FBnMEph	3	80	-ITV + Amorfo
<i>m</i> -FBnMEph	2	100	-ITV + BEC
<b><i>m</i>-FBnMEph</b>	<b>2</b>	<b>80</b>	<b>-ITV</b>
<i>p</i> -FBnMEph	3	100	BEC
<b><i>p</i>-FBnMEph</b>	<b>3</b>	<b>80</b>	<b>-ITV</b>
<i>p</i> -FBnMEph	2	100	-ITV + BEC
<b><i>p</i>-FBnMEph</b>	<b>2</b>	<b>80</b>	<b>-ITV</b>



enantiomeric enrichment in one of the polymorphs of the -ITV phase depending on the substituent of the benzyl group attached. These differences in catalyst enrichment could be due to both the different sizes and electronic properties of the benzyl substituent, as well as the different hydrophobicity provided to the SDA by the methyl and fluorine groups. [4]

These results highlight the relevance of the GTM-4 material as a chiral zeolitic catalyst capable of performing enantioselective discrimination processes during an asymmetric reaction. This opens a new path in the development of asymmetric heterogeneous catalysis, where extra-large pore chiral zeolites can play a leading role.

## References

- [1] Sun, J., Bonneau, C., Ángel Cantín, Corma, A., Díaz-Cabañas, M. J., Moliner, M., Zhang, D., Li, M., & Zou, X. *Nature*, **458**, 1154–1157 (2009).
- [2] De la Serna, R., Nieto, D., Sainz, R., Bernardo-Maestro, B., Mayoral, Á., Márquez-Álvarez, C., Pérez-Pariente, J., & Gómez-Hortigüela, L. *Journal of the American Chemical Society*, **144**, 8249–8256 (2022).
- [3] De la Serna, R., Arnaiz, I., Márquez-Álvarez, C., Pérez-Pariente, J., & Gómez-Hortigüela, L. *Chemical Communications*, **58**, 13083–13086 (2022).
- [4] De la Serna, R., Jurado-Sánchez, J., Márquez-Álvarez, C., Pérez-Pariente, J., & Gómez-Hortigüela, L. *Microporous and Mesoporous Materials*, **371**, 113083 (2024).

## Acknowledgments

The authors would like to thank the State Research Agency, the Ministry of Science, Innovation and Universities, and the European Regional Development Fund for funding the projects PID2019-107968RB-I00 and PID2022-138481NB-I00, as well as the European Union NextGenerationEU/PRTR for the project PDC2022-138481NB-I00.



## Synthesis of zeolites coated 1D TiO<sub>2</sub> nanotubes arrays

R. Passalacqua<sup>1</sup>, A. Aloise<sup>2</sup>, A. Marino<sup>2</sup>, N. Di Nicola<sup>2</sup>, S. Perathoner<sup>1</sup>, G. Centi<sup>1</sup>

<sup>1</sup> Department of Chemical, Biological, Pharmaceutical and Environmental Sciences (ChiBioFarAm) & INSTM CASPE (Lab. of Catalysis for Sustainable Production & Energy) - University of Messina Viale F. Stagno d'Alcontres, 31 - 98166 Messina, Italy

<sup>2</sup> Department of Physical and Chemical Sciences, via Vetoio, Coppito 2 - 67100 L'Aquila, Italy  
rpassalacqua@unime.it

In this work, we report the preparation of a nanozeolite/TiO<sub>2</sub> composite obtained using an innovative synthesis approach in which nanocrystals of Silicalite-1 zeolite were growth directly on TiO<sub>2</sub> nanotubes [1] by modified Steam Assisted Crystallisation (SAC) [2] method, leading to the incorporation of the zeolite inside the titania nanotube's structure (Fig. 1). The resulting composite was denoted as nano-Sil1/TiO<sub>2</sub>NTs. A novel coating technique in two steps was used for the composite preparation consisting of a dip-coating procedure followed by a hydrothermal synthesis. For the coating step, a zeolite synthesis gel, typically consisting of a source of silica (tetraethylortosilicate, TEOS), a templating agent (tetrapropylammonium hydroxide, TPAOH), and water, was homogeneously dispersed on top of TiO<sub>2</sub> substrate. The so treated substrate was transferred into a supported-Teflon covered steel autoclave, then heated up to 170 °C and the temperature was kept for 24 hours. This process facilitates the crystallization of the Silicalite-1 on the walls of the titanium nanotubes without affecting (clogging) the tubular structure.

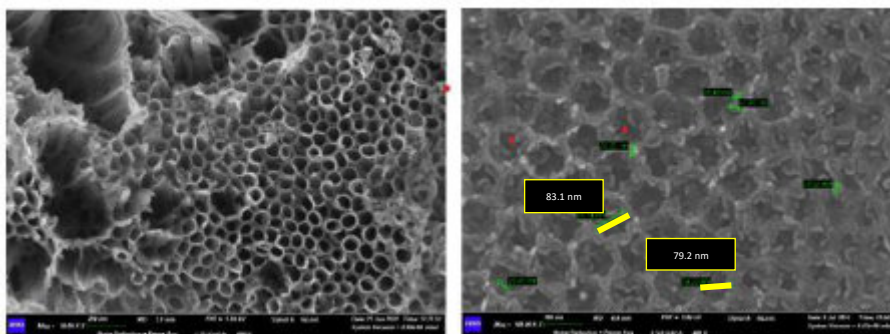


**Figure 1.** SEM image of the top of TiO<sub>2</sub> nanotubes (left) and of nano-Sil1/TiO<sub>2</sub>NTs composite (right).

The following step involves the calcination of the composite in static air at 450 °C for 8 hours, to remove the organic template, without affecting the anatase titania phase. The composite was characterized by XRD, SEM, TEM, and N<sub>2</sub> physisorption [3], in order to evaluate the physicochemical and structural properties, as well as the nanocrystals distribution on titania nanotubes.

The synthesized composite represents a promising new heterogeneous catalyst in which selectivity can be modulated by modifying the properties of the nanozeolites confined in an ordered structure with a controlled geometry, as titania nanotubes. The composite is under consideration for further testing in reactions of industrial interest.

### References

- [1] R. Passalacqua, S. Perathoner, G. Centi, *Catalysis Today*, **251**, 121 (2015).
- [2] H. Yang, P. Yang, X. Liu, Y. Wang, *Chemical Engineering Journal*, **299**, 112 (2016).
- [3] I. Paramasivam, A. Avhale, A. Inayat, A. Bösmann, P. Schmuki, and W. Schwieger, *Nanotechnology*, **20**, 225607 (2009).





## Gold nanoclusters prepared from an eighteenth century two-phases procedure supported on chiral zeolitic material GTM-4 for liquid phase oxidation of cyclohexene with molecular oxygen

P. Sánchez-Morena<sup>1</sup>, A. Mayoral<sup>2</sup>, L. Gomez-Hortigüela<sup>1</sup>, J. Pérez-Pariente<sup>1</sup>

<sup>1</sup> Instituto de Catálisis y Petroleoquímica (CSIC), Marie Curie, 2, 28049 Cantoblanco, Madrid, Spain

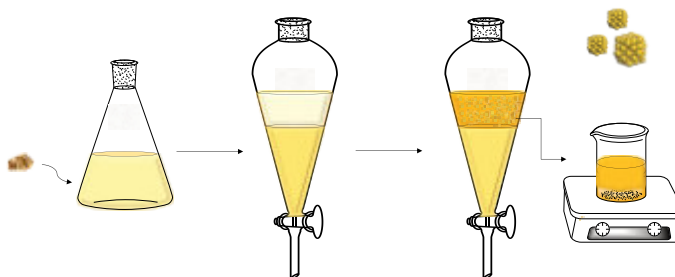
<sup>2</sup> Instituto de Nanociencia y Materiales de Aragón (INMA), CSIC-Universidad de Zaragoza, Zaragoza 50009, Spain  
p.sanchez@icp.csic.es

Gold nanoparticles have received significant attention in recent years due to their unique size-dependent properties, which have led to their extensive application in materials science, catalysis, and biomedicine. The chemical and catalytic reactivity of gold nanoparticles is influenced by various factors, including their size and shape. When these nanoparticles are supported on a solid material, the specific properties of the support play a crucial role as well. These properties not only govern the metal-support interaction, but also affect the diffusion and adsorption/desorption of reagents and products under real reaction conditions. In this context, preparing stable gold nanoparticles with controlled size and shape is a significant challenge, and several methods have been developed along the time to meet this objective. In this work, we have prepared gold nano-entities using a two-liquid phase system method reported in the mid-eighteenth century [1]. This method involves the contact between an organic phase composed of an essential oil and a gold solution in *aqua regia*. After prolonged contact, the gold is spontaneously reduced and transferred to the organic phase, which turns red in color and was called “potable gold of Mademoiselle Grimaldi”. This phase contains Au nanoparticles, (AuNPs), small Au clusters (AuNCs) and even isolated gold atoms [2].

One of the emerging areas of research in catalysis is the use of zeolites to immobilize active metal nanoparticles within their porous structure, controlling the growth process and preventing them from agglomeration and leaching. Based on this background, we report the method of immobilization of gold nanoclusters produced by this eighteenth century recipe on the extra-large pore chiral zeolitic material GTM-4 [3] and the use of the resulting gold-containing materials as catalysts for the oxidation of cyclohexene in liquid phase by using molecular oxygen as oxidant. This is a preliminary study whose final purpose is to prepare Au-catalysts for enantioselective oxidations of pro-chiral substrates by using molecular oxygen.

### Experimental part

Following the methodology outlined in Scheme 1, gold nanoclusters were prepared using a two-liquid phase system inspired from [1]. A gold lump was dissolved under gentle stirring in *aqua regia* (a 4:1 w/w mixture of nitric acid and ammonium chloride). This solution had a gold-to-*aqua regia* weight ratio of 1:320. The resulting golden-yellow solution was transferred to a separatory funnel, and rosemary essential oil was gently added, forming a top layer over the gold solution. 1 day (L1d) and 4 days (L4d) after the addition of rosemary oil, the organic layer was mixed with butanol. The extracted GTM-4 material was then added to the resulting solution, and the mixture was stirred at room temperature for 4 hours (/4h) or 8 (/8h) hours. Afterwards, the solid was separated by centrifugation and washed with butanol. The samples were denoted as L4d/4h, L4d/8h, and L1d/4h.



Scheme 1. Method for preparing gold nanoparticles using a two-phase liquid

### Results

The stability of the catalyst was studied using X-ray diffraction (XRD), which showed the same pattern as the original gold-free zeolitic GTM-4 after the impregnation protocol. The absorption spectra of the catalysts in the UV–vis region generally showed bands in the ~250-400 nm range, attributed to Au nanoclusters, and in some samples also a low intensity surface plasmon resonance band at ~520 nm, characteristic of Au nanoparticles. Techniques such as scanning transmission electron microscopy (STEM), X-ray photoelectron spectroscopy (XPS), and total reflection X-ray fluorescence (TXRF) have been also used to characterize the Au-materials.



In the oxidation of cyclohexene, molecular oxygen was used as the oxidant at atmospheric pressure, with toluene as solvent, a small amount of TBHP (tert-Butyl hydroperoxide, 5 wt.% referred to cyclohexene) as the radical initiator, and  $T = 65^{\circ}\text{C}$ . The ratio of catalyst to cyclohexene was 0.5 wt %. The three catalysts were active in this reaction (Figure 1). However, the L4d/8h catalyst, which had a longer phase contact and impregnation time, showed higher conversion. Notably, the amount of TBHP initiator in the reaction mixture is much lower than the observed conversion, which clearly indicates that the oxidation of cyclohexene involves the participation of molecular oxygen, being the presence of TBHP strictly necessary to start the reaction. No changes appear in the UV-vis absorption spectra of the catalyst recovered after reaction.

Four main reaction products were identified, one of them resulting from the addition of oxygen to the cyclohexene double bond, namely cyclohexene epoxide, and the other three coming from the allylic oxidation of the cyclohexene ring: 2-cyclohexen-1-ol, 2-cyclohexen-1-one and 2-cyclohexenyl hydroperoxide. The selectivity to these four products was more than 90% (Table 1), being the allylic oxidation pathway dominant. 2-Cyclohexenyl hydroperoxide was the first product to appear in the reaction. Subsequently, the other products began to form, while the selectivity of 2-cyclohexenyl hydroperoxide tend to decrease as the conversion increased, while that of the enone and enol increased with conversion. The enone/enol ratio increased with conversion from 1.4 to 1.6.

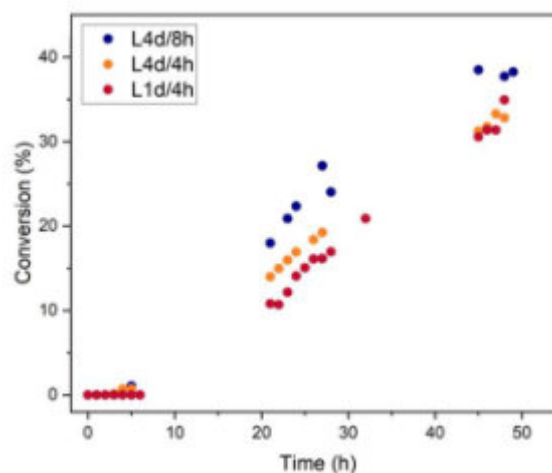


**Figure 1.** Conversion as a function of time for catalysts L4d/8h (blue); L4d/4h (orange); L1d/4h (red)

**Table 1.** Conversion and selectivity for selected catalyst

Catalyst	Conversion 24 h (%)	Conversion 48 h (%)	Selectivity 24h				Selectivity 48h			
			OOH	OH	O	Epoxide	OOH	OH	O	Epoxide
L4d/8h	20.9	37.7	59.6	11.8	16.7	6.4	44.9	15.0	24.3	7.9
L4d/4h	16.9	32.8	64.1	9.7	14.3	6.3	46.8	13.9	21.9	9.0
L1d/4h	14.1	35.0	64.4	9.4	12.2	4.6	48.0	13.6	22.0	6.6

## Conclusions

Gold nanoclusters can be conveniently prepared using a two-phase liquid system from a gold solution in aqua regia, with rosemary oil serving as the organic phase and reducing agent, following a technique reported in the eighteenth century. These gold entities can be immobilized on the chiral zeolitic material GTM-4, by varying different synthetic time parameters, and the zeolite structure is preserved in the resulting Au-materials. Generally, these catalysts exhibit gold nanoclusters rather than gold nanoparticles. These gold-containing materials act as active catalysts for the liquid-phase oxidation of cyclohexene with molecular oxygen at mild conditions, producing four major products with a selectivity more than 90%. Moreover, the Au nanoentities immobilized in the zeolite are stable during reaction.

## References

- [1] N. Lémery, *Cours de chimie: contenant la manière de faire les opérations qui sont en usage dans la Médecine par une Méthode facile*, Laurent-Charles d'Houry, Paris (1757).
- [2] A. Mayoral, J. Agúndez, I.M. Pascual-Valderrama, and J. Pérez-Pariente, *Gold Bull.*, **47**, 161–165 (2014).
- [3] R. de la Serna, I. Arnaiz, C. Márquez-Álvarez, J. Pérez-Pariente and L. Gómez-Hortigüela, *Chem. Commun.*, **58**, 13083 (2022)

## Acknowledgments

The authors would like to thank the State Research Agency, Ministry of Science and Innovation, and the European Regional Development Fund for funding the project PID2022-138481NB-I00.



## Capturing Different Intermediate Phases during Zeolite Synthesis

Jinjin Zeng,<sup>1</sup> German Sastre,<sup>2</sup> and Suk Bong Hong<sup>1,\*</sup>

<sup>1</sup> Center for Ordered Nanoporous Materials Synthesis, Division of Environmental Science and Engineering, POSTECH, Pohang 37673, Korea.

<sup>2</sup> Instituto de Tecnología Química (UPV-CSIC), Universidad Politécnica de Valencia, Av. Naranjos s/n, Valencia 46022, Spain.

Email: sbhong@postech.ac.kr

Zeolites are crystalline microporous aluminosilicates with commercial uses in catalysis, ion exchange, adsorption, and separation. Nevertheless, the rational design and synthesis of zeolites with finely tuned physicochemical properties for particular applications are still far from reality, primarily due to the lack of a solid understanding of the mechanisms involved in their crystallization. Here, we investigate whether and how the nucleation and/or transformation pathways in the crystallization process of zeolites with a particular framework topology can be controlled in the formation of intermediate and final zeolite phases.

We revisited the synthesis of the high-silica medium-pore zeolite TNU-9 (framework type TUN), because a disordered MCM-22 (MWW) precursor (MCM-22(P)) is first formed over narrow ranges of gel Si/Al and Na/Al ratios in the presence of diquateryary 1,4-bis(*N*-methylpyrrolidinium)butane (1,4-MPB<sup>2+</sup>) ions [1,2]. To intentionally induce the formation of intermediate phases other than MCM-22(P) before TNU-9 crystallization, we applied the multiple inorganic cation approach that has been shown to be effective in promoting a synergy between different types of inorganic SDAs in the search for novel zeolite structures. As shown in Figure 1, a high-silica (Si/Al ~ 11) BIK-type zeolite was found to be a new intermediate phase after heating an aluminosilicate gel with Si/Al = 50, Na/Al = 17.5, and Na/Cs = 7 at 150 °C for 4 days. To identify whether all TNU-9 samples purely synthesized here have intermediate phases other than this small-pore zeolite, we analyzed a series of solid products isolated as a function of time after heating synthesis gels with different Na/Al and Cs/Al ratios at 150 °C using powder X-ray diffraction (PXRD). We were able to isolate analcine (ANA) as another new intermediate at gel Na/Al and Na/Cs ratios of 22.5 and 15, respectively (middle diagram in Figure 1). We also observed MCM-22(P) at a higher Na/Cs ratio of 20 (right diagram in Figure 1). These results indicate that the structure type of intermediates formed during TNU-9 synthesis in the presence of 1,4-MPB<sup>2+</sup> is strongly dependent on the gel Na/Cs ratio. Of particular interest is that the transformation pathway of intermediates during TNU-9 synthesis is dependent on their structure type. The force field simulation results suggest that the nucleation of different intermediate phases is not thermodynamically but kinetically controlled.

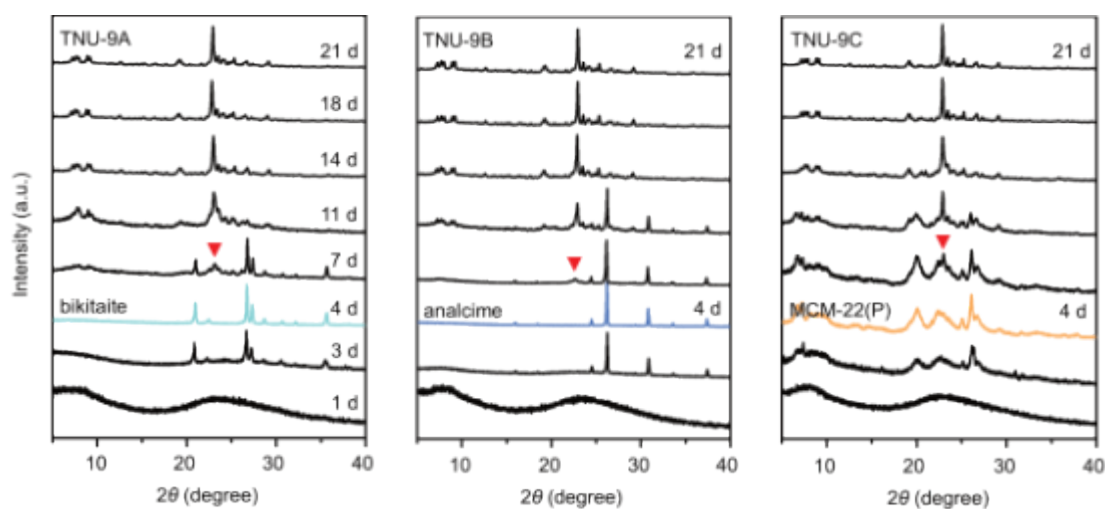


**Figure 1.** PXRD patterns of a series of solid products isolated as a function of time during TNU-9 synthesis under static conditions at 150 °C, using aluminosilicate gels with the same Si/Al ratio (50) but different Na/Al and Cs/Al ratios: 0.75(1,4-MPB)O·5.25Na<sub>2</sub>O·0.75Cs<sub>2</sub>O·0.3Al<sub>2</sub>O<sub>3</sub>·30SiO<sub>2</sub>·300H<sub>2</sub>O (left), 0.75(1,4-MPB)O·6.75Na<sub>2</sub>O·0.45Cs<sub>2</sub>O·0.3Al<sub>2</sub>O<sub>3</sub>·30SiO<sub>2</sub>·300H<sub>2</sub>O (middle), and 0.75(1,4-MPB)O·6.00Na<sub>2</sub>O·0.30Cs<sub>2</sub>O·0.3Al<sub>2</sub>O<sub>3</sub>·30SiO<sub>2</sub>·300H<sub>2</sub>O (right). The X-ray peak around  $2\theta = 22.9^\circ$  due to the TUN 151 reflection is marked by an inverted triangle.

In summary, we found two new intermediate zeolites (i.e., high-silica BIK- and ANA-type phases) during the synthesis of medium-pore TNU-9 zeolite by controlling the extent of cooperation between the structure-forming Na<sup>+</sup> and structure-breaking Cs<sup>+</sup> ions, i.e., the Na/Cs ratio of synthesis gels, in the presence of 1,4-MPB<sup>2+</sup> ions as an unselective SDA. We also found that 1,4-MPB<sup>2+</sup> play a role as a ‘structure-spectating’ agent rather than as an SDA in the nucleation and growth of these two intermediates. This study provides valuable insights into how the nucleation and growth pathways in zeolite crystallization can be controlled and will inspire future efforts aimed at the rational synthesis of novel zeolite structures and/or compositions.



**6<sup>th</sup> Euro-Asia Zeolite Conference**  
Alicante (Spain), January 19-22, 2025



## References

- [1] Hong, S. B.; Min, H.-K.; Shin, C.-H.; Cox, P. A.; Warrender, S. J.; Wright, P. A. *J. Am. Chem. Soc.*, **129**, 10870-10885 (2007).
- [2] Gramm, F.; Baerlocher, C.; McCusker, L. B.; Warrender, S. J.; Wright, P. A.; Han, B.; Hong, S. B.; Liu, Z. Ohsuna, T.; Terasaki, O. *Nature*, **444**, 79-81 (2006).

## Acknowledgments

We acknowledge financial support from the National Research Foundation of Korea (2021R1A3A-3088711), GVA (PROMETEO/2021/077), MCIN (Severo Ochoa CEX-2021-001230-S), ASIC-UPV, and SGAI-CSIC for the use of computational facilities.



## Synthesis, characterization and structural determination by 3D electron diffraction of the extra-large pore zeolite ITQ-70

J. I. Tirado<sup>1</sup>, A. Sala<sup>1</sup>, A. Bordes<sup>1</sup>, P. Pratim Das<sup>2</sup>, L. Palatinus<sup>3</sup>, S. Nicolopoulos<sup>2</sup>, J. L. Jordá<sup>1</sup>, A. Vidal-Moya<sup>1</sup>, T. Blasco<sup>1</sup>, G. Sastre<sup>1</sup>, S. Valencia<sup>1</sup>, F. Rey<sup>1</sup>

<sup>1</sup> Instituto de Tecnología Química (UPV-CSIC), Universitat Politècnica de València-Consejo Superior de Investigaciones Científicas, Avenida de los Naranjos s/n, 46022, Valencia, Spain

<sup>2</sup> NanoMEGAS SPRL, Rue Émile Claus 49 bte 9, B-1080, Brussels, Belgium

<sup>3</sup> Institute of Physics of the Czech Academy of Sciences, v.v.i.Na Slovance 2, Prague 8 182 00, Czechia.  
jjorda@itq.upv.es

Zeolites with large and extra large pores are attracting a significant interest from scientific and industrial points of view due to their multiple uses as catalysts and in separation and ion exchange processes, as well as many other new applications. Their properties, and therefore their applications, strongly depends on the framework topology of each material. Then, the determination of their zeolitic structure is key in order to optimize their applicability. In the case of zeolites, the use of common techniques as single crystal x-ray diffraction (SCXRD) is in many cases precluded by the unavailability of crystals large enough for the analysis, while the severe peak overlapping in powder x-ray diffraction (PXRD) due to the large unit cells makes the use of this technique extremely challenging. So, these limitations led to the use of 3D electron diffraction tomography (3D-EDT) for these studies, as it enables the collection of single-crystal diffraction data from nanosized crystallites. [1]

In this study, the use of tetrakis(diethylamino)phosphonium (TDAP) hydroxide as organic structure directing agent (OSDA) has allowed obtaining a new pure silica zeolitic structure, that has been named ITQ-70. The elemental and chemical analysis of the as-made material, as well as its <sup>13</sup>C and <sup>31</sup>P-MAS-NMR spectra indicate that TDAP remains intact within the pores of the zeolite after the synthesis. The large amount of OSDA detected by these analysis, as well as the results from the thermogravimetric study of the material, suggest that ITQ-70 presents large pores and void volumes in its framework.

The PXRD pattern of ITQ-70 does not seem to correspond to any other zeolite previously described, suggesting that this is a novel material. Moreover, it can be indexed with a hexagonal unit cell with cell parameters  $a=b=19.343 \text{ \AA}$  and  $c=19.597 \text{ \AA}$ , while the systematic extinctions indicate the extinction symbol  $P6_2 -$ , corresponding to the pairs of enantiomorphic space groups  $P6_2$  (#171) and  $P6_4$  (#172) or  $P6_222$  (#180) and  $P6_422$  (#181). Attempts to determine the structure of the as-made material using the PXRD data did not give acceptable results.

The zeolite ITQ-70 was calcined under a continuous flow of dry air. Its new PXRD pattern suggests that the structure was retained upon calcination, as evidenced by the presence of intense low angle diffraction peaks, but becomes clearly distorted, as only a few peaks at low angles remain clearly observable, thus preventing the determination of the structure of the calcined sample by PXRD. However, N<sub>2</sub> and Ar volumetric adsorption isotherms, at 77 K and 87 K respectively, indicate that the microporous structure is retained after calcination.

So, 3D-EDT was applied for determining the structure of the non-calcined zeolite ITQ-70. The spot positions and systematic extinctions observed by 3D-EDT are in good agreement with the hexagonal unit cell and space groups obtained by PXRD, confirming these values and that the selected crystals corresponded to the main phase. After extracting and merging the intensities of the reflections corresponding to ten selected nanocrystals, the ab-initio determination of the framework structure solution was carried out by applying the charge flipping algorithm with the program Superflip [2]. The space group  $P6_222$  was first attempted over  $P6_2$  due to its higher symmetry and therefore lower number of parameters to be determined. In these conditions, all the 63 silicon and 138 oxygen positions within the unit cell were readily located, with 6 Si and 12 O atoms in the asymmetric unit. It is of special interest that two of the T-sites correspond to non-fully connected Q<sup>3</sup> sites (i.e. T-sites not surrounded by other 4 T-sites, but only by 3).

The framework of ITQ-70 can be described as series of helicoidal chains interconnected to each other conforming a gyroidal structure with 18-ring channels in the  $ab$  plane, having a pore diameter of  $10.8 \text{ \AA}$ , and another set of 18-ring openings along the  $c$  axis, with a diameter of  $11.0 \text{ \AA}$ . These channels intersect one to each other, creating large empty spaces within the structure. This makes the structure of zeolite ITQ-70, with a framework density of  $10.0 \text{ T}/1000 \text{ \AA}^3$ , the zeolite containing oxygen connecting T-atoms with the lowest density ever reported, to the best of our knowledge.

The location of the 6 OSDA molecules estimated from the elemental and thermogravimetric analysis within the zeolite ITQ-70 was determined from the 3D-EDT data using a simulated annealing algorithm [3]. After that, the obtained positions were confirmed and optimized through a Rietveld refinement of the entire structure using the PXRD data of the as-made zeolite, obtaining a good agreement between the calculated and observed patterns, as well as good residual values ( $R_{wp} = 19.4$ ,  $R_{exp} = 8.48$ ,  $R_B = 9.80$  and  $R_F = 5.50$ ). The structure of ITQ-70 view along the  $c$  axis is shown in Figure 1.

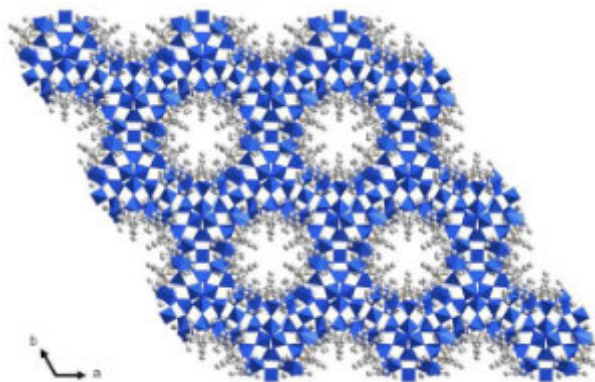


**Figure 1.** Structure of as-made ITQ-70 refined using PXRD data views along the c axis. Blue tetrahedra: zeolitic framework; gray. OSDA.

In addition, the bidimensional (2D) Double Quantum-Single Quantum (DQ-SQ)  $^{29}\text{Si}$  MAS NMR spectrum of the material was recorded. The comparison of the results obtained with the Si-Si connections derived from the diffraction techniques allowed assigning each of the six  $^{29}\text{Si}$  NMR signals to their corresponding T-sites of the framework including the two  $\text{Q}^3$  sites.

To learn more about the distribution of silanol groups in the two  $\text{Q}^3$  sites,  $^1\text{H}$ -NMR experiments were conducted. Two broad peaks at 8 ppm and 16 ppm, with a relative intensity of 2:1, are attributed to hydrogens of SiOH groups. The zeolite ITQ-70 contains two different  $\text{Q}^3$  sites, with identical multiplicities corresponding to 12 Si atoms per unit cell each one. This result indicates, then, that one of the  $\text{Q}^3$  sites contains 12 SiOH groups while the other contains 6 SiOH and 6 SiO, i.e., there is a preferential location of the H groups in the  $\text{Q}^3$  sites. However, although these sites are formally Si-O $^-$  and Si-OH, the short O-O distance and strong hydrogen bonding suggest that the H and the negative charge are shared by both atoms, rather than being localized on each one, forming a SiO $^{\delta-}$ -H-O $^{\delta-}$ Si group, which is supported by the high  $^1\text{H}$  NMR chemical shift.

As a conclusion, commercial TDAP was employed as OSDA for the synthesis of a new zeolite called ITQ-70. This zeolite features 18-ring channels, structured around a building unit containing highly strained silicon atoms. Notably, the as-synthesized ITQ-70 exhibits 38% of its silicon atoms as underconnected  $\text{Q}^3$  silanol or siloxy groups, achieving the lowest framework density observed among known zeolites containing oxygen connecting the T-atoms. Comprehensive structural characterization have provided a clear description of the zeolite, including the inorganic silica framework, the location of the OSDA molecules, and the identification of the siloxy and silanol groups.

## References

- [1] Z. Huang, T. Willhammar, X. Zou, *Chem. Sci.*, **12**, 1206A (2021)
- [2] L. Palatinus, G. J. Chapuis, *Appl. Crystallogr.*, **40**, 786 (2007)
- [3] M. C. Burla, R. Caliendo, B. Carrozzini, G. L. Cascarano, C. Cuocci, C. Giacovazzo, M. Mallamo, A. Mazzone, G. Polidori, *J. Appl. Cryst.*, **48**, 306 (2015)

## Acknowledgments

We thank CTI-CSIC and ASIC-UPV for computational facilities. Financial support by the Spanish Ministry of Science and Innovation (CEX2021-001230-S and PID2022-136934OB-100 grants funded by MCIN/AEI/10.13039/501100011033 funded by "ERDF A way of making Europe" and TED2021-130191B-C41 grant funded by the European Union NextGenerationEU/PRTR) are gratefully acknowledged. Authors thank also the financial support by the Generalitat Valenciana (Prometeo 2021/077). A.S. thanks for the grant BES-2016-078684 and J.I.T. thanks financial support from Severo Ochoa Program PRE2018-083623. This study forms part of the Advanced Materials programme and was supported by MCIN with partial funding from European Union Next Generation EU (PRTR-C17. I1) and by Generalitat Valenciana (MFA/2022/012 and MFA/2022/047). The authors acknowledge the Electron Microscopy Service of the Polytechnique University of Valencia (UPV) for assistance in electron microscopy characterization. Authors thank Antonio L. Llamas-Saiz from the Unidad de Rayos X (Área Infraestructuras e Investigación) of the Universidad de Santiago de Compostela for structural elucidation of the OSDA.



## Zeolites and MOFs as easily-tunable macroligands of metal catalysts for organic reactions

A. Leyva-Pérez<sup>1</sup>, J. Oliver-Meseguer<sup>1</sup>.

<sup>1</sup> Instituto de Tecnología-Química UPV-CSIC (Valencia, Spain).

anleyva@itq.upv.es

Nanostructured solids have been traditionally used in fields somewhat away of organic synthesis, such as petrochemistry and water treatment, since spatial restrictions have been viewed as an unsurmountable issue when dealing with relatively big molecules; however, we will show here that this view can be incorrect, and that zeolites and MOFs can be used as suitable supports for a variety of complex organic reactions.[1] Indeed, the microporous frameworks act as macroligands for the catalytic metal species, for instance for single metal atoms and clusters, to catalyze relatively complex organic reactions with extremely high turnovers, >1 million in some cases. The electronics of the zeolite and the MOF can be easily modulated with exchanging counterbalancing cations, which translates into the catalytic metal site electronics, thus ultimately controlling the organic reaction itself. This catalytic approach is very convenient for industrial purposes, where the amount of expensive metal catalysts must be minimized and allows easy recovery, reuse and implementation in continuous processes.

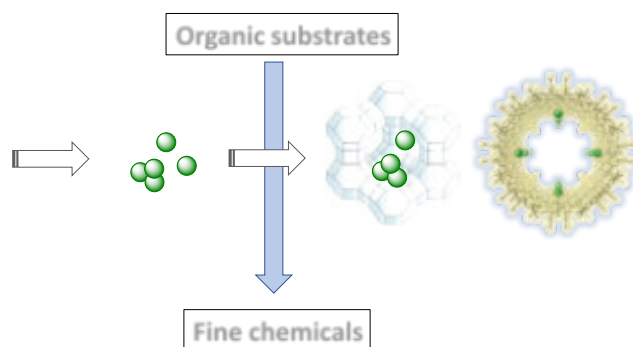


**Figure 1.** Sub-nanometric metal species in solution and supported in zeolites or MOFs as catalysts for organic reactions.

Key industrial reactions such as the Mizoroki-Heck carbon-carbon cross-coupling reaction,[2] the hydrosilylation of alkenes and alkynes,[3] the oxidation of alcohols,[4] the isomerization of alkenes [5], the carbene insertion reaction [6] and the semi-hydrogenation of acetylene in ethylene streams [7] will be shown. Besides, the (supported) single metal atoms and clusters enable striking changes in product selectivity [2, 3, 6], and the design of in-flow processes [2] and one-pot reactions.[5]

### References

- [1] J. Oliver-Meseguer, and A. Leyva-Pérez, *ChemCatChem*, e202201681 (2023); b) M. Viciano-Chumillas, X. Liu, A. Leyva-Pérez, D. Armentano, J. Ferrando-Soria, and E. Pardo, *Coord. Chem. Rev.*, **451**, 214273 (2022).
- [2] F. Garnes-Portolés, R. Greco, J. Oliver-Meseguer, J. Castellanos-Soriano, M. Consuelo Jiménez, M. López-Haro, J. C. Hernández-Garrido, M. Boronat, R. Pérez-Ruiz, and A. Leyva-Pérez, *Nat. Catal.*, **4**, 293 (2021).
- [3] M. Angel Rivero-Crespo, J. Oliver-Meseguer, K. Kapłńska, P. Kuśtrowski, E. Pardo, J. P. Cerón-Carrasco, and A. Leyva-Pérez, *Chem. Sci.*, **11**, 8113 (2020).
- [4] E. Tiburcio, R. Greco, M. Mon, J. Ballesteros-Soberanas, J. Ferrando-Soria, M. López-Haro, J. C. Hernández-Garrido, J. Oliver-Meseguer, C. Marini, M. Boronat, D. Armentano, A. Leyva-Pérez, and E. Pardo, *J. Am. Chem. Soc.*, **143**, 2581 (2021).
- [5] S. Sanz-Navarro, M. Mon, A. Doménech-Carbó, R. Greco, J. Sánchez-Quesada, E. Espinós-Ferri, and A. Leyva-Pérez, *Nat Commun*, **13**, 2831 (2022).
- [6] Y. Zheng, A. Vidal-Moya, J. C. Hernández-Garrido, M. Mon, and A. Leyva-Pérez, *J. Am. Chem. Soc.*, **145**, 24736 (2023).
- [7] J. Ballesteros-Soberanas, N. Martín, M. Bacic, E. Tiburcio, M. Mon, J. C. Hernández-Garrido, C. Marini, M. Boronat, J. Ferrando-Soria, D. Armentano, E. Pardo, and A. Leyva-Pérez. *Nat. Catal.*, **7**, 452 (2024).

# Phase Selection and Framework Composition in Mixed-Cations Zeolite Synthesis Utilizing Hydrated Silicate Ionic Liquids (HSILs)

Anjul Rais<sup>1</sup>, Dries Vandenaabeele<sup>1</sup>, Nikolaus Doppelhammer<sup>1</sup>, Christine Kirschhock<sup>1</sup>, Eric Breynaert<sup>1,2\*</sup>

1. Centre for Surface Chemistry and Catalysis Characterisation and Application Team (COK-KAT), KU Leuven, Leuven 3001, Belgium.
2. NMRCoRe-NMR-X-Ray platform for Convergence Research, KU Leuven, Leuven 3001, Belgium.

\*[eric.breynaert@kuleuven.be](mailto:eric.breynaert@kuleuven.be)

Despite over 70 years of research, our fundamental understanding of how zeolite form remains largely constrained by general heuristics. This limitation arises, in part, from the complexity of conventional synthesis methods, which typically begin with a gel(-like) system. The inherent heterogeneity of the gel-based syntheses hinders a consistent study of individual parameters. For instance, if the alkalinity increases, so does the solubility and dissolution rate of aluminosilicates so that also the aging time should be adjusted if one wants to study the influence hereof. Hydrated Silicate Ionic Liquids (HSILs)[1] offer an elegant avenue to reduce the complexity. HSILs are low-viscosity[2], homogeneous liquids composed of charge-stabilized liquid-born aluminosilicate oligomers and can be envisioned as a molten alkali silicate salt. The liquids are “activated” by addition of aluminates, forming a wide range of zeolite topologies. In previous work, we have shown that HSILs allow the systematic variation of individual parameters.[3], [4] Known correlations between cation type and topology were confirmed, while other new heuristics, for instances between alkalinity and framework composition, were proposed and validated beyond the HSIL domain.

This study builds on previous findings, aiming to assess their robustness in mixed-cation systems. It examines how multiple cation systems affect phase selection and framework composition over a range of synthesis compositions. Specifically, zeolites were synthesized. Zeolites were synthesized using formulation  $0.5 \text{ Si(OH)}_4 - 0.03\text{Al(OH)}_3 - x\text{MOH} - y\text{H}_2\text{O}$ , maintaining  $\text{Si(OH)}_4/\text{Al(OH)}_3$  ratio of 16.67. The synthesis conditions explored span a  $\text{SiO}_2/\text{OH}^-$  (batch alkalinity) ratio between 0.125 and 1 and an  $\text{H}_2\text{O}/\text{OH}^-$  (cation hydration) ratio between 4 and 100, with a focus on three distinct relative molar ratios for the explored cations, -1:1 (50-50%), 3:1 (75-25%), and 9:1 (90-10%) for binary combinations of Na, K, and Cs. Additionally, an equimolar mixture of all three cations was synthesized to investigate their collective influence on zeolite formation.

Our results reveal that, in mixed-cation systems, the cation with the highest affinity for ion pairing, dictates the resulting structure. The framework composition follows suit accordingly. Moreover, we found that the heuristics established for single-cation systems—specifically, those regarding the effects of water content[3], [4], [5] and alkalinity - are equally applicable in mixed systems. Notably, no synergistic cation effects were observed within the recipes tested in this study. Our findings validate the previously described links between synthesis liquid composition and framework composition for mixed cation systems and highlight the importance of kinetic drivers in gel-based crystallization.

## References

- [1] M. Haouas, L. Lakiss, C. Martineau, J. El Fallah, V. Valtchev, and F. Taulelle, “Silicate ionic liquid synthesis of zeolite merlinoite: Crystal size control from crystalline nanoaggregates to micron-sized single-crystals,” *Microporous and Mesoporous Materials*, vol. 198, pp. 35–44, Nov. 2014, doi: 10.1016/j.micromeso.2014.07.011.
- [2] J. Vekeman *et al.*, “Simple Molecular Model for Hydrated Silicate Ionic Liquids, a Realistic Zeolite Precursor,” *Chem. Mater.*, vol. 36, no. 8, pp. 3886–3897, Apr. 2024, doi: 10.1021/acs.chemmater.4c00285.
- [3] K. Asselman *et al.*, “Ion-Pairs in Aluminosilicate-Alkali Synthesis Liquids Determine the Aluminum Content and Topology of Crystallizing Zeolites,” *Chem. Mater.*, vol. 34, no. 16, pp. 7150–7158, Aug. 2022, doi: 10.1021/acs.chemmater.2c00773.
- [4] K. Asselman, D. Vandenaabeele, N. Pellens, N. Doppelhammer, C. E. A. Kirschhock, and E. Breynaert, “Structural Aspects Affecting Phase Selection in Inorganic Zeolite Synthesis,” *Chem. Mater.*, vol. 34, no. 24, pp. 11081–11092, Dec. 2022, doi: 10.1021/acs.chemmater.2c03204.
- [5] K. Asselman *et al.*, “Does Water Enable Porosity in Aluminosilicate Zeolites? Porous Frameworks versus Dense Minerals,” *Crystal Growth & Design*, vol. 23, no. 5, pp. 3338–3348, May 2023, doi: 10.1021/acs.cgd.2c01476.





## Mechanism of N<sub>2</sub>O decomposition catalysed by Cu-exchanged zeolites

**M. Ródenas<sup>1\*</sup>, M. Boronat<sup>1</sup>, R. Millán<sup>1</sup>**

<sup>1</sup> Instituto de Tecnología Química, Universitat Politècnica de València - Consejo Superior de Investigaciones Científicas, Avenida de los Naranjos s/n, 46022 Valencia, Spain  
miroses1@itq.upv.es

Cu-exchanged zeolites are promising catalysts for the decomposition of N<sub>2</sub>O, a compound with a global warming potential ~300 times larger than CO<sub>2</sub> and whose emissions will increase significantly if the maritime industry substitutes oil-based fuels by ammonia-based fuels [1-2].

The reaction, 2N<sub>2</sub>O → 2N<sub>2</sub> + O<sub>2</sub>, follows a redox catalytic cycle in which Cu<sup>+</sup> and Cu<sup>2+</sup> interconvert, with the possibility of generating NO as an undesired by-product. Although binuclear and isolated Cu<sup>+</sup> sites have been proposed as possible active sites [3, 4] the mechanism in Cu-CHA has not been thoroughly investigated. Therefore, identifying the possible active sites is crucial for the understanding and optimisation of the catalytic cycle [5, 6]. In this contribution, we apply periodic DFT calculations and *ab initio* molecular dynamics (AIMD) simulations to investigate the key elementary steps of the mechanism of N<sub>2</sub>O decomposition on Cu-CHA models containing binuclear Cu<sup>+</sup> sites and isolated Cu<sup>+</sup> sites located in different environments of the CHA crystallographic structure [7]. The objective is to find the optimum catalyst composition and reaction conditions for this challenging process.

Calculations were carried out at the PBE+D3 and HSE06 level of theory (LOT), using the VASP code for the static DFT calculations and the CP2K software for the AIMD simulations. The reaction and activation free energies were corrected using a deep learning model trained on energies and forces at the HSE06 LOT using as initial reference the minimum and TS structures optimized at PBE+D3 LOT. The acquisition of training data was performed using an iterative active learning (AL) approach in which every iteration consisted of a NEB calculation, followed by single points HSE06 evaluations and final training of the deep learning model. Several microkinetic models, one per proposed active site, were developed for the determination of the apparent activation energies. The rate constants used in these models were obtained from Transition-state Theory (TST) and non-adiabatic Transition-state Theory (NA-TST).

In the proposed mechanism we considered minimum energy crossing points (MECPs) for the transitions between adiabatic potential energy surfaces (PES) which is relevant to account for the difference of multiplicity between the reactant (<sup>1</sup>N<sub>2</sub>O) and the product (<sup>3</sup>O<sub>2</sub>). Key elementary steps in the mechanism follow Eley-Rideal or Langmuir-Hinshelwood mechanisms.

The mechanistic study shows possible routes for the formation of O<sub>2</sub>, NO and N<sub>2</sub> as well as spectroscopically observed intermediate structures (Cu<sup>2+</sup>-NO<sub>3</sub><sup>-</sup>) [8]. Microkinetic models predict a higher activity for the dimeric Cu<sup>+</sup> active sites than for the isolated Cu<sup>+</sup> active sites. Calculated activation energies of the order of 40 kcal/mol (Fig. 1) show the N<sub>2</sub>O decomposition is feasible for Cu-CHA under typical experimental conditions (T ≈ 350 °C, P ≈ 1 atm).

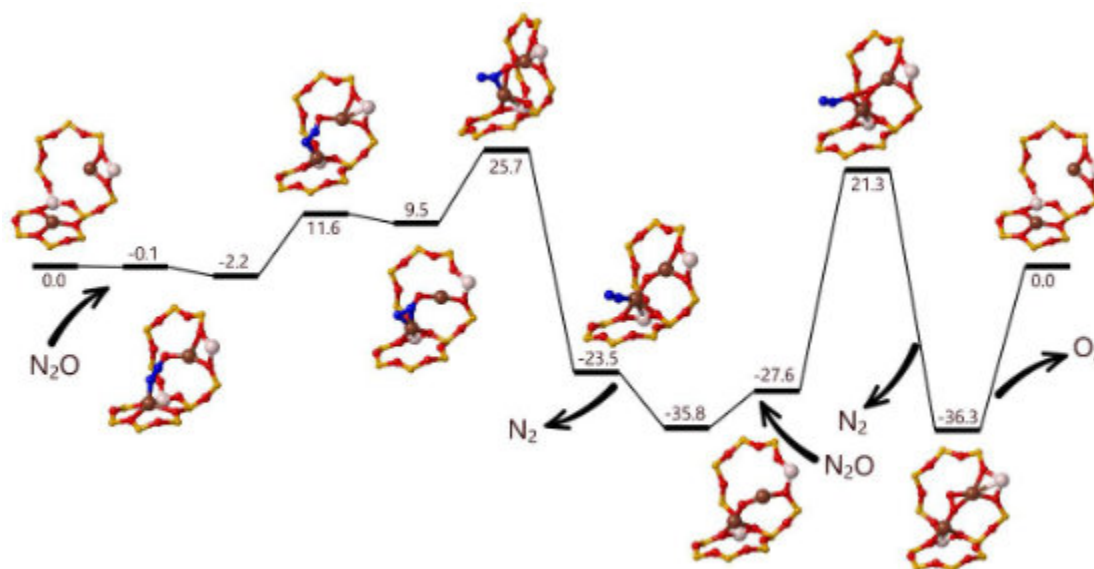


**Figure 1.** Free energy profile of the decomposition of  $\text{N}_2\text{O}$  on dimeric  $\text{Cu}^+$  sites on Cu-CHA. Calculations are done at 673.15 K with an accessible volume correction according to CHA framework. Free energies are given in kcal/mol.

#### References

- [1] W. Winiwarter, L. Höglund-Isaksson, Z. Klimont, W. Schöpp, M. Amann, *Environ. Res. Lett.*, **13**, 014011 (2018)
- [2] P. Ciambelli, A. Di Benedetto, E. Garufi, R. Pirone, G. Russo, *J. Catal.*, **2**, 161 (1998)
- [3] T. Beutel, J. Sárkány, G.-D. Lei, J. Y. Yan, W. M. H. Sachtler, *J. Phys. Chem* **100**, 845 (1996)
- [4] X. Liu, Z. Yang, R. Zhang, Q. Li, Y. Li, *J. Phys. Chem C*, **116**, 20262 (2012)
- [5] R. Millan, P. Cnudde, V. van Speybroeck, M. Boronat, *JACS Au* **1**, 1778 (2021)
- [6] R. Millan, E. Bello-Jurado, M. Moliner, M. Boronat, R. Gómez-Bombarelli, *ACS Central Science* **9**, 2044 (2023)
- [7] E. Borfecchia, P. Beato, S. Svelle, U. Olsbye, C. Lamberti, S. Bordiga, *Chem. Soc. Rev.*, **47**, 8097 (2018)
- [8] M. V. Konduru, S. S. C. Chuang, *J. Catal.* **196**, 271 (2000)

#### Acknowledgments

This work has been supported by Spanish Ministry of Science and Innovation MCIN/AEI/10.13039/501100011033 through CEX2021-001230-S, PID2020-112590GB-C21 and TED2021-130739B-I00 (MCIN/AEI/FEDER, UE/PRTR), and Generalitat Valenciana through Prometeo CIPROM/2023/034. M.R. thanks the FSE+ as part of the scholarship PRE2022-101971. Red Española de Supercomputación (RES) is acknowledged for computational resources and technical support.



## POST-SYNTHETIC STRUCTURAL CONSOLIDATION OF Sn-β: ENHANCING STABILITY IN THE CONTINUOUS PRODUCTION OF METHYL LACTATE

J.M Jimenez-Martin<sup>1</sup>, S.H Lima<sup>1</sup>, A. Garcia<sup>1</sup>, J. Iglesias<sup>1,2</sup>

<sup>1</sup> Chemical & Environmental Engineering Group. Universidad Rey Juan Carlos. C/ Tulipan S/N. Mostoles. 28933. Madrid. Spain

<sup>2</sup> Instituto de Tecnologías para la Sostenibilidad. Universidad Rey Juan Carlos. C/ Tulipan S/N. Mostoles. 28933. Madrid. Spain

[jose.iglesias@urjc.es](mailto:jose.iglesias@urjc.es)

### Abstract

K-exchanged Sn-functionalized β zeolite ([K]Sn-β) prepared through post-synthetic metalation exhibits high activity and selectivity in the transformation of glucose into methyl lactate under batch reaction conditions. However, this catalyst shows a significant decline in catalytic activity when operating under continuous flow operation conditions, due to structural damage, as evidenced by X-ray diffraction. The inclusion of silicon atoms into aluminum vacancies created during dealumination through silylation with trimethylsilyl chloride allows the structural consolidation of the zeolite, providing great stability for long time-on-stream periods. Thus, the activity of silylated material lasted for at least 170 hours in the transformation of glucose into methyl lactate.

### Introduction

Lewis acid Sn-functionalized zeolites have demonstrated a great activity in several transformations, including isomerization of aldoses and/or aldol condensation and retroaldol cleavage of carbohydrates [1]. However, the hydrothermal preparation of tin containing zeolites, such as Sn-β, conventionally requires long crystallization times to accommodate Sn in the zeolite structure. As alternative to hydrothermal crystallization, post-synthetic metalation synthesis procedures are simpler and easier to implement. These methods require generating vacancies in the zeolite framework –either by dealumination or desilication– to which attach the metal species. This methodology allows incorporating higher metal contents as compared to hydrothermal crystallization, though at the expense of weakening the zeolite structure. Nevertheless, recent studies on the grafting of organosilanes in zeolites, and subsequent calcination, have demonstrated to stabilize dealuminated zeolites [2]. Within this context, we have applied this procedure to enhance the stability of a Sn-functionalized β zeolite prepared through a post-synthetic metalation method. The prepared material has demonstrated excellent catalytic activity in the transformation of glucose methanolic solutions yielding methyl lactate as main product, and showing very high stability under continuous flow conditions in a fixed bed reactor operating for more than 150h.

### Experimental

A commercial β zeolite material (CP814C\*; Si:Al = 19, Zeolyst) was dealuminated in a nitric acid solution ([HNO<sub>3</sub>]=10M) for 1h. Afterwards, the solid was recovered by centrifugation and washed with deionized water until neutral pH, and the material was dried at 110°C overnight. The entire dealumination process was repeated twice to ensure complete removal of aluminum. Afterwards tin was incorporated by contacting the dealuminated zeolite with a SnCl<sub>4</sub> solution in CH<sub>2</sub>Cl<sub>2</sub> (0.17 mmol·g<sub>zeolite</sub><sup>-1</sup>; 40 mL·g<sub>zeolite</sub><sup>-1</sup>) under reflux conditions. The material was then recovered by filtration and calcined in air at 550°C. Ion exchange with an aqueous KCl solution ([KCl]=0.5M; 100 mL·g<sub>zeolite</sub><sup>-1</sup>) at 50°C for 2h allows removing most of the Brønsted acidity. The material was finally calcined, following the same procedure (550°C), denoting the obtained material as [K]Sn-β.

The zeolite structure consolidation was carried out using trimethylsilyl chloride (TMCS) as silylating agent, letting the system to stir for 5h to allow an intimate contact of the organosilane with the zeolite. Afterwards, the zeolite was separated by filtration and dried at ambient conditions, washed with hexane under reflux conditions for 30 minutes to remove unreacted TMCS, and recovered by filtration. The final material was calcined at 550°C, denoting the obtained material as [K]Sn-β-sil-ca.

The prepared materials have been thoroughly characterized by means of different technics (Ar adsorption-desorption isotherms, XRD, FTIR, DR-UV-Vis, and SS-NMR). The catalytic performance of the transformation of prepared catalysts was assessed in the transformation of glucose to methyl lactate in a fixed bed reactor, using 0.5 g of catalyst loading, feeding a methanolic solution (4wt% water) of glucose (0.26 mol·L<sup>-1</sup>) at 0.05 mL·min<sup>-1</sup>. The reactor was operated at 150 °C and 13 bar (N<sub>2</sub> pressurized). Samples were periodically collected and analysed by means of GC.

### Results and discussion

[K]Sn-β has demonstrated high activity in the transformation of glucose towards methyl lactate in batch conditions when the reaction media contains small amounts of water (4wt%) [3], providing methyl lactate and methyl vinyl glycolate as main products, with a total combined yield over 90%. This transformation involves the retro-aldol



cleavage of the starting glucose into minor sugars –glycolaldehyde, dihydroxyacetone, erythrose–, which are subsequently converted on the Sn Lewis acid sites to the corresponding  $\alpha$ -hydroxyesters. However, under continuous operation in fixed bed reactors, despite showing a good initial catalytic performance, the [K]Sn- $\beta$  zeolite undergoes fast deactivation (Figure 1A, front results). The recovered catalyst after 170 hours of time-on-stream evidenced the loss of crystallinity, as determined by XRD, pointing to the destruction of the zeolite structure as the main cause of deactivation. [K]Sn- $\beta$ -sil-ca prepared by silylation using TMCS was analysed by <sup>29</sup>Si MAS SS NMR, whose results revealed the decreasing of the contributions of Q2 & Q3 silicon species to the spectrum, and the increase of Q4 silicon species abundance, indicating the removal of silanol species by creation of new siloxane bonds. [K]Sn- $\beta$ -sil-ca catalyst was also evaluated in the transformation of glucose into methyl lactate in a fixed bed reactor using the very same reaction conditions applied for [K]Sn- $\beta$ . The results obtained in the stability tests (Figure 1A, back results), performed for over 170 hours reflected the high stability of [K]Sn- $\beta$ -sil-ca. This catalyst demonstrates a remarkable stability without variations of product distribution for over 170 hours of time-on-stream. XRD after reaction (Figure 1B, back) shows a well preserved crystalline structure of the  $\beta$  zeolite, demonstrating the beneficial effect of defects silylation over structure preservation of the catalyst and catalytic stability.

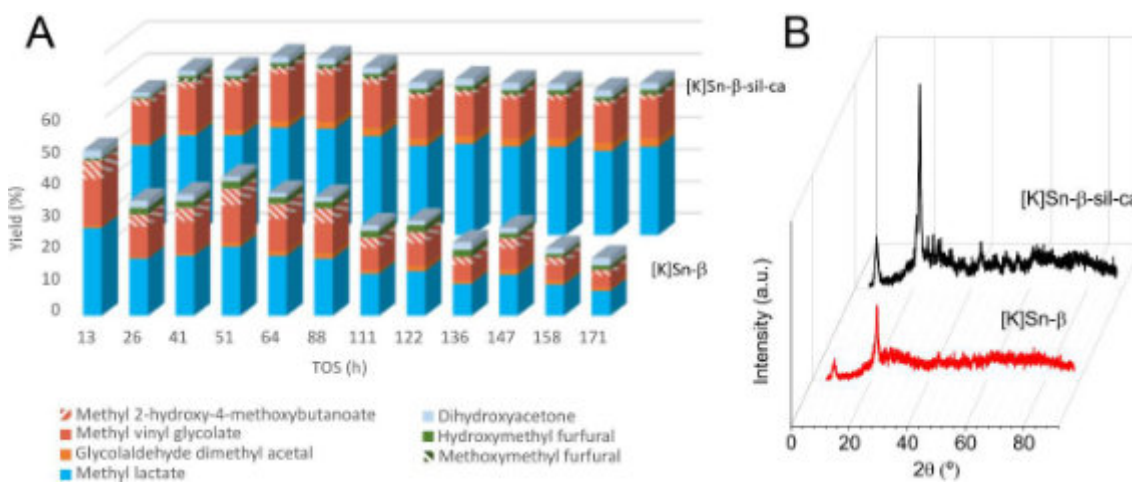


**Figure 1.** A) Comparison of the catalytic performance of [K]Sn- $\beta$  and [K]Sn- $\beta$ -sil-ca catalysts over time on stream under continuous operation (excluding sugars). Conditions: 0.5 g catalyst; 0.05 mL·min<sup>-1</sup>; 0.26 mol·L<sup>-1</sup> glucose; methanol:water (96:4); 150°C; B) XRD patterns for post-reaction catalyst.

## Conclusions

Tin containing zeolite [K]Sn- $\beta$  is an excellent catalyst for monosaccharides valorization towards methyl lactate attending to its catalytic activity and selectivity, however the performance at long reaction times, as required for industrial applications, lacks on stability. The defect healing by incorporation of silicon by silylating agent (trimethylsilane chloride) to unoccupied vacancies generated during dealumination consolidates the zeolite structure, providing to the catalyst a great stability, thus allowing to this [K]Sn- $\beta$ -sil-ca catalyst to perform the transformation of glucose into methyl lactate for over 170 hours with no alteration on catalytic performance or product distribution.

## References

- [1] M. Moliner, Y. Roman-Leshkov, M. Davis, Proceedings of the National Academy of Sciences of the United States of America, 107 (2010) 6164-6168.
- [2] S. Prodingler, M.A. Derewinski, A. Vjunov, S. D. Burton, I. Arslan, J.A. Lercher, Journal of the American Chemical Society, 138 (2016) 4408-4415.
- [3] J.M. Jimenez-Martin, M.E. Tawil-Lucas, M. Montaña, M. Linares, A. Osatiashtiani, F. Vila, D. M. Alonso, J. Moreno, A. García, J. Iglesias, ACS Sustainable Chemistry&Engineering, 12 (2024) 2771-2782.

## Acknowledgments

This project has received funding from the Bio Based Industries Joint Undertaking (JU) under the European Union's Horizon 2020 research and innovation program under grant agreement No 101023202, and from the Spanish Ministry of Science and Innovation through project PID2021-122736OB-C44 being funded by MCIN/AEI/10.13039/501100011033/FEDER, UE.

## Mechanism of selective oxidation of methane to methanol over a pair of $\alpha$ -oxygens formed by dioxygen splitting. DFT study

J. Dedecek<sup>1,2</sup>, S. Sklenak<sup>1</sup>, M. Lemishka<sup>1</sup>, H. Jirglova<sup>1</sup>

<sup>1</sup>J. Heyrovský Institute of Physical Chemistry of the CAS, Dolejškova 3, CZ 18200 Prague, Czech Republic

<sup>2</sup>METTOC, Nyklickova 40, CZ 15800 Prague, Czech Republic

jiri.dedecek@jh-inst.cas.cz, jiri.dedecek@mettoc.com

Selective oxidation of methane to methanol represents one of the possibilities for minimizing the emissions of methane, which is a greenhouse gas with high global warming potential. Further, this reaction is one of the key steps in the transformation of CO<sub>2</sub> and hydrogen into synthetic fuels. Recently developed systems based on binuclear transition metal ions sites capable of splitting molecular oxygen and forming highly active  $\alpha$ -oxygen species ( $[M^{4+}=O_2]^{2+}$ , M = Fe, Co, Mn, Ni) [1,2]. These binuclear sites can be prepared in zeolite matrices of various topologies (FER, \*BEA, MOR) containing local structure and Al organization allowing the formation of binuclear sites [3,4]. There are two unique properties of these sites: (a) they are able to oxidize methane to methanol even at room temperature, (b) methanol is released from the zeolite without any effluent. This opens the possibility of producing progressive catalytic material for efficient methane oxidation.

For the theoretical study of the behavior of isolated and paired  $\alpha$ -oxygen  $[Fe^{4+}=O_2]^{2+}$  periodic DFT calculations were performed by employing the Vienna Ab initio Simulation Package (VASP) code. The high-spin electron configuration  $d_5\uparrow d_1\downarrow$  was used for the Fe species accommodated in the zeolite. A plane-wave cutoff of 600 eV and the density-dependent energy correction (dDsC) dispersion correction were used for the geometry optimizations, and a smaller cutoff of 400 eV and the DFT-D2 method were used for the molecular dynamics (MD) simulations. The MD computations used the exact Hellmann-Feynman forces acting on atoms and applied the statistics of a canonical ensemble to the motion of the atomic nuclei by using the Verlet velocity algorithm to integrate Newton's equations of motion. The collected snapshots were optimized. The most stable structure for each of the seven investigated models was then used for the subsequent calculations of all the complexes, transition states, and products. For details see [1,3,5].

DFT calculations allowed the analysis of the energetics of all steps of the activation of molecular oxygen and the interaction of methane with  $\alpha$ -oxygen. It was found that there is a significant difference in the interaction of methanol with isolated and paired  $\alpha$ -oxygen. Moreover, the oxygen activation depends on the conditions of the reaction conditions including subsequent treatment in an inert atmosphere. This is in sound agreement with in-situ FTIR spectroscopy studies and reaction tests [1,-4].

### References

- [1] Tabor E., Dedecek J., Mlekodaj K., Sobalik Z., Andrikopoulos P.C., Sklenak S., *Sci. Adv.* **2020**, 6, eaaz9776.
- [2] Mlekodaj K., Lemishka M., Sklenak S., Dedecek J., Tabor E., *Chem. Commun.* **2021**, 57, 3472-3475.
- [3] Tabor E., Lemishka M., Olszowka J. E., Mlekodaj K., Dedecek J., Andrikopoulos P. C., Sklenak S., *ACS Catal.* **2021**, 11, 2340-2355.
- [4] Kornas A., Tabor E., Wierzbicki D. K., Olszowka J. E., Pilar R., Dedecek J., Sliwa M., Jirglova H., Sklenak S., Rutkowska-Zbik D., Mlekodaj K. *Appl. Cat.B* **2023**, 335, 122912.
- [5] Sklenak S., Andrikopoulos P.C., Boekfa B., Jansang B., Novakova J., Benco L., Bucko T., Hafner J., Dedecek J., Sobalik Z. *J. Catal.* **2010**, 272, 262-274.



## On the thermodynamics of adsorption based contaminant removal: Pharmaceuticals and hydrophobic zeolites

J. Brauer<sup>1,2</sup>, M. Fischer<sup>1,2</sup>

<sup>1</sup> *Crystalline Microporous Materials, Crystallography and Geomaterial Research, Faculty of Geosciences, University of Bremen, Klagenfurter Straße 2-4, 28359 Bremen, Germany*

<sup>2</sup> *Bremen Center for Computational Material Science and MAPEX Center for Materials and Processes, University of Bremen*

jabr@uni-bremen.de

Pollution of water resources by pharmaceuticals and agents of personal care products (PPCPs) poses an ever-rising environmental issue. The pathways of contamination range from production facilities over landfills and livestock farming to urban and hospital waste waters [1]. The unfitness of conventional waste water treatment plants to remove certain pollutants makes the developments of innovative water treatment processes necessary. Hydrophobic zeolites could be utilized in adsorption-based processes, where zeolites could have significant advantages over activated carbon materials in terms of their selectivity and regenerability [2].

The large number of possible PPCP-zeolite combinations allows experimental investigation only for case studies. Computational modelling can guide the selection of promising PPCP-zeolite combinations that exhibit a strong interaction [3]. To make an informed choice which zeolite framework is most fit to remove the PPCPs of interest from water, the interaction energy of the pollutant molecule and the zeolite framework can only serve as a first indicator. To describe the competition between adsorption and solvation for pollutant molecules, entropy losses have to be considered to evaluate the free energy of adsorption resp. hydration. While the free energy of adsorption is governed by the attractive interaction between the framework and the molecule and the entropy loss upon confinement in the pore, the free solvation energy takes into account the interactions between water molecules and the pollutant and the work of forming a cavity in the bulk liquid.

Obtaining free energies for a system of interest can be done by means of several approaches. *Ab initio* frequency calculation profit from the more accurate treatment of the system, but are computationally demanding and in some cases not straightforward to evaluate. Forcefield-based free energy perturbation (FEP) simulations are a well-developed method to calculate free energies of interaction but they rely on classical forcefield parameters to describe the molecules and the zeolite framework/water molecules. Also, empirical corrections to the OK-interaction energy can be applied, reducing the computational cost, but relying on empirically fitted parameter.

In this work we study a set of environmentally relevant PPCPs and all-silica zeolite frameworks with respect to their interactions on various levels of theory. By clustering the contaminants into their drug classes, frameworks with an enhanced affinity towards certain PPCPs of interest can be identified. We compare the free energies of transfer from solution into the adsorbed state (obtained by FEP simulations) with experimental values derived from adsorption isotherms published by De Ridder *et al.* [4] and report a semi-quantitative agreement with experimental values on the forcefield level of theory. An empirical formula by Dauenhauer *et al.*, developed for alkanes and noble gases [5], is applied to the chemically more diverse set of PPCPs in different zeolites, showing a surprising reliability. By representing the zeolite pores beyond their accessible volume, the empirical formula is refined and the agreement between the simulated and the empirically corrected values is improved. As a complementary pathway which provides a more complete description of the systems of interest, *ab initio* frequency calculation on the density functional level of theory are employed to obtain adsorption free energies. Several theoretical approaches to evaluate the adsorption free energy and adsorption entropy are investigated by means of the toolkit TAMkin[6]. A critical evaluation of the *ab initio* free adsorption energies allows for a more efficient setup of the computationally demanding frequency calculation by eliminating insignificant degrees of freedom.

### References

- [1] D. J. Lapworth, N. Baran, M. E. Stuart, R. S. Ward, *Environmental Pollution* **163**, 287 (2012).
- [2] N. Jiang, R. Shang, S. G. J. Heijman, and L. C. Rietveld, *Water Res.* **144**, 145 (2018).
- [3] J. Brauer, M. Fischer, *ChemPhysChem* e202400347 (2024).
- [4] De Ridder *et al. Sep. Pur. Tech.* **89**, 71 (2012).
- [5] P. J. Dauenhauer, O. A. Abdelrahman, *ACS Cent. Sci.* **4**, 1235 (2018).
- [6] A. Ghysels, *et al, J. Chem. Inf. Model.* **50**, 1736 (2010).

### Acknowledgments

Funding by the Deutsche Forschungsgemeinschaft (German Research Foundation, DFG), project IDs 455871835 and 492604837, is gratefully acknowledged.



## TS-1@Co-PDA: A Bifunctional Catalyst for Synergistic Hydrogen Peroxide Generation and Oxidation of Organic Molecules

H. S. Tabatabaeizadeh<sup>1</sup>, F. Rosso<sup>1</sup>, F. Bonino<sup>1</sup>, S. Bordiga<sup>1</sup>, V. Crocellà<sup>1</sup>, M. Signorile<sup>1</sup>

<sup>1</sup> Department of Chemistry, NIS and INSTM Reference Centre, Università di Torino, Via G. Quarello 15, 10135 and Via P. Giuria 7, 10125, Torino, Italy.

hediehsadat.tabatabaeizadeh@unito.it

TS-1 (Titanium Silicalite-1) is a widely studied and highly effective catalyst, primarily known for its ability to catalyze selective oxidation reactions using hydrogen peroxide ( $H_2O_2$ ) as an oxidant. It consists of a microporous zeolite structure (MFI framework) with titanium atoms substituted into the silica framework. One of the key advantages of TS-1 is its high selectivity, which allows it to carry out specific oxidation reactions without over-oxidizing the substrate. This selective oxidation capability is attributed to its unique microporous structure and the isolated Ti centers within the silicalite framework. Additionally, TS-1 can efficiently activate  $H_2O_2$  without the formation of harmful byproducts, making it highly suitable for green chemistry applications. Hydrogen peroxide is a clean, high-efficiency oxidant which currently the primary method of  $H_2O_2$  production remains the energy-intensive oxidation anthraquinone process [1], that poses challenges for advancing sustainable and green chemistry practices. For instance, the concentration of commercial  $H_2O_2$  greatly exceeds that required by organic reagent oxidation processes which causes energy waste in the dilution steps. In recent years, the electrocatalytic two-electron oxygen reduction reaction ( $2e^-$  ORR) has gained attention as a promising alternative, offering on-site and on-demand  $H_2O_2$  production under mild conditions, powered by renewable energy [2].

In this work, TS-1@Co-PDA, a novel bifunctional catalyst inspired by recent literature, is under investigation. This material is able to integrate the unique catalytic properties of both its core and shell components for enhanced reactivity in electrochemical and organic oxidation reactions [3]. The core, TS-1, exhibits high catalytic efficiency in the oxidation of organic reagents due to its ability to activate hydrogen peroxide in selective oxidation processes. Surrounding the TS-1 core is a cobalt-doped polydopamine (Co-PDA) shell, which serves as an active site for the electrochemical oxygen reduction reaction (ORR) to generate  $H_2O_2$  via a two-electron pathway. When TS-1@Co-PDA is used as a cathode in organic solution with blowing  $O_2$ , OOH species will first be generated via the  $2e^-$  ORR at the Co-PDA active sites, which then transport inward to be captured by the inner  $Ti^{4+}$  sites, as shown in Fig.1 a. The formed intermediate species, supposing Ti-OOH, have a high oxidation activity and can selectively oxidize organic substrates into value-added products. Therefore, this bifunctional catalyst facilitates the in-situ generation and utilization of  $H_2O_2$  at a single electrode, resulting in minimizing equipment needs and lowering operating costs.

TS-1 catalyst was hydrothermally synthesized using a Design of Experiment (DOE) approach to find the most optimized synthesis pathway [4]. After successfully synthesizing TS-1, the TS-1@Co-PDA catalyst was synthesized by thermally pyrolyzing polydopamine and cobalt acetate outside of TS-1 crystals. The characterization techniques such as TGA, TEM, EDX, ICP, BET specific surface area, XRD -as shown in Fig.1 b, Raman, ATR, and UV-Vis spectroscopy were used to deeply understand the position of Ti species in the framework and Co-PDA shell. Furthermore, the ORR performance via a rotating ring disk electrode (RRDE) using a standard three-electrode system was performed to evaluate the electrochemical performance of the catalyst. As a modification and further steps, iron and copper species are being investigated as alternatives to cobalt for their different electrochemical responses [5]. Further studies will be carried on the effect of changing the nitrogen-carbon layer and using large and extra-large Ti-zeolites such as ZEO, MWW and Beta zeolites instead of TS-1 for the oxidation of bulky molecules.

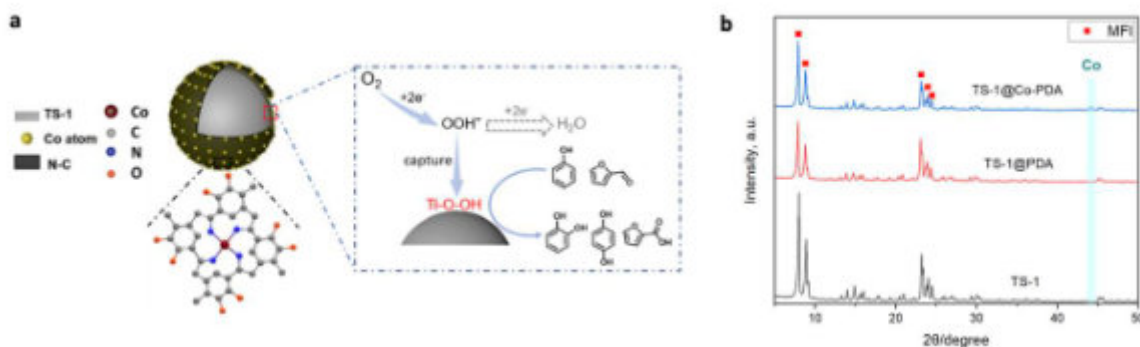


Figure 1. a) The catalytic reaction schematic for the TS-1@Co-N-C catalyst, adapted from [3], and b) XRD analysis of the three samples, TS-1, TS-1@PDA, and TS-1@Co-PDA.



**6<sup>th</sup> Euro-Asia Zeolite Conference**  
Alicante (Spain), January 19-22, 2025



## References

- [1] Sprauer, J. W. Production of Hydrogen Peroxide, US2657980A, (1953).
- [2] Jiang, Y., Ni, P., Chen, C., Lu, Y., Yang, P., Kong, B., . . . , Wang, X., *Advanced Energy Materials*, **8**, 1801909 (2018).
- [3] S. Wu, H. Zhang, X. Huang, Z. Wei, *Chem. Commun.*, **58**, 8942 (2022).
- [4] F. Rosso, A. Rizzetto, A. Airi, K. Khoma, M. Signorelle, V. Crocellà, S. Bordiga, S. Galliano, C. Barolo, E. Alladio, F. Bonino, *Inorg. Chem. Front.*, **9**, 3372 (2022).
- [5] Y. Zhang, X. Gao, Y. Ye, Y. Shen, *Analyst*, **147**, 956 (2022).

## Acknowledgments

The authors acknowledge support from the Project CH4.0 under the MUR program “Dipartimenti di Eccellenza 2023–2027”.





## Insertion of Active Sites in ZEO-3 Matrix: A Promising Catalyst for Partial Oxidation of Bulky Molecules

H. S. Tabatabaeizadeh<sup>1</sup>, F. Rosso<sup>1</sup>, F. Bonino<sup>1</sup>, S. Bordiga<sup>1</sup>, V. Crocellà<sup>1</sup>, M. Signorile<sup>1</sup>

<sup>1</sup> Department of Chemistry, NIS and INSTM Reference Centre, Università di Torino, Via G. Quarello 15, 10135 and Via P. Giuria 7, 10125, Torino, Italy.

hediehsadat.tabatabaeizadeh@unito.it

Zeolites are microporous silicates with a large variety of applications as catalysts, adsorbents, molecular sieves, and cation exchangers. Stable silica-based zeolites with extra-large pores are actively studied because they allow adsorption and processing of large molecules. Still, their synthesis procedures are usually challenging. In this work, a novel highly stable pure silica zeolite called ZEO-3 (IZA code: JZT) is being investigated [1]. This material has a multidimensional, interconnected system of extra-large pores open through windows made by 16 and 14 silicate tetrahedra, as shown in Fig.1 a, and is the least dense crystalline polymorph of silica, with a specific surface area of more than 1000 m<sup>2</sup>/g.

In preliminary synthetic attempts, by analysing the NMR data of various samples, it was realized that the purity of tricyclohexylphosphine (PCy<sub>3</sub>), as the main reagent to synthesize the organic structure directing agent (OSDA), is crucial due to its high sensitivity to air. When exposed to oxygen, PCy<sub>3</sub> rapidly oxidizes, forming tricyclohexylphosphine oxide (PCy<sub>3</sub>=O) and phosphonic acid esters as by-products. This oxidative degradation not only decreases the reagent's efficacy but can also interfere with reactions, leading to unwanted side products and reduced yields and crystallinity of the catalyst.

Furthermore, it was found that with higher amount of OSDA, namely tricyclohexyl-methyl-phosphine hydroxide [2,3], i.e. OSDA/SiO<sub>2</sub> = 0.82 compared to the reference molar ratio of 0.5, the structure is obtained along with higher crystallinity, even though the amorphous fraction increases upon calcination, as shown in Fig.1 b. Based on these preliminary results, further studies to correlate the effect of different concentration of OSDA (0.5 < OSDA/SiO<sub>2</sub> < 1) with the quality of the final material are ongoing. Next investigations will involve the insertion of metals such as Ti in the framework, to be exploited as catalytic active centres for partial oxidation of bulky molecules along with H<sub>2</sub>O<sub>2</sub>, a better understanding of the crystallization process, the advanced characterization of the synthesized materials, and the effect of different factors such as change in temperature, pressure and concentration of the gel components on the final catalyst, by using the design of experiment (DOE).

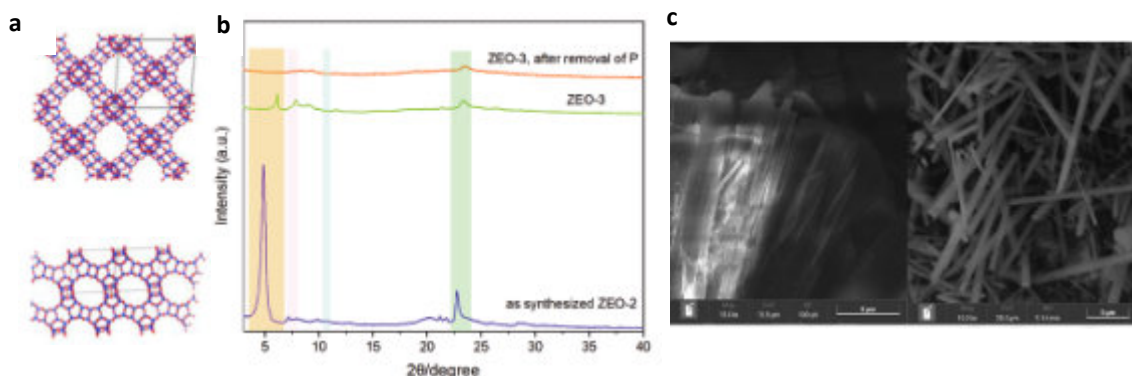


**Figure 1.** a) Representation of (up)16- and (down)14-member ring windows of ZEO-3 framework, adopted from [1], b) Effect of calcination on ZEO-3, OSDA/SiO<sub>2</sub> = 0.82, analysed by PXRD, and c) SEM images of the (left) not calcined ZEO-3, namely ZEO-2 and (right) the calcined ZEO-3.

### References

- [1] Li, J., Gao, Z. R., Lin, Q. F., Liu, C., Gao, F., Lin, C., Zhang, S., Deng, H., Mayoral, A., Fan, W., Luo, S., Chen, X., He, H., Cambor, M. A., Chen, F. J., & Yu, J., *Science (New York, N.Y.)*, **379**, 283–287, (2023).
- [2] Lin, Q. F., Gao, Z. R., Lin, C., Zhang, S., Chen, J., Li, Z., Liu, X., Fan, W., Li, J., Chen, X., Cambor, M. A., & Chen, F. J., *Science (New York, N.Y.)*, **374**, 1605–1608, (2021).
- [3] H. Darmandeh, T. Scherpf, K.S. Feichtner, C. Schwarz, V.H. Gessner, *Z Anorg Allg Chem*, **646**, 835-841, (2020).

### Acknowledgments

The authors acknowledge support from the Project CH4.0 under the MUR program “Dipartimenti di Eccellenza 2023–2027”.



## Comparison of Physisorption and Chemosorption Integrated with Silica Gel for Direct air capture in harsh atmosphere like Qatar

Y. Abdellatif,<sup>1,2</sup> R. Surkatti,<sup>1</sup> R. Muhammad,<sup>1</sup> A. Sodiq,<sup>1</sup> O. Alrebei,<sup>1</sup> T. Al-Ansari,<sup>1,2</sup> and A. I. Amhamed\*<sup>1</sup>

<sup>1</sup>Qatar Environment and Energy Research Institute (QEERI), Hamad Bin Khalifa University, Qatar Foundation, Doha, Qatar

<sup>2</sup>College of Science and Engineering, Hamad Bin Khalifa University, Qatar Foundation, Doha, Qatar

\*Corresponding author's email: aamhamed@hbku.edu.qa

Direct air capture (DAC) faces significant energy challenges due to the low concentration of CO<sub>2</sub> in the atmosphere, around 400 ppm. The presence of water, especially in humid environments, further increases the energy penalty required for effective CO<sub>2</sub> separation. This study tackles the energy challenges of DAC in humid environments by comparing four cases. Two benchmark materials, a physisorption-based material (MOF) and a chemisorption-based material (Lewatit), will be evaluated individually and in combination with a silica gel dehumidifier. The comparisons will include: physisorption vs. chemisorption, physisorption with silica gel vs. chemisorption with silica gel. Each case will be assessed under Qatar's atmospheric conditions throughout the year, aiming to reduce the energy penalty associated with humidity. The key findings of this study reveal that integrating silica gel into DAC systems enhances efficiency in humid environments by effectively removing moisture before CO<sub>2</sub> reaches the adsorbent. In systems combining silica gel with Lewatit (chemisorption), efficiency increased by up to 7% compared to Lewatit alone, at lower temperatures and higher humidity. When paired with NbOFFIVE (physisorption), silica gel improved efficiency by 19%, for different ambient conditions whereas NbOFFIVE alone performed poorly under the same conditions. The results demonstrate that silica gel can significantly improve the performance of DAC systems, particularly when integrated with HVAC where humidity and temperature are controlled.

In this study, three materials silica gel, Lewatit, and NbOFFIVE-1-Ni—were selected for evaluation under DAC conditions. Silica gel was experimentally tested at 25°C to assess its ability to adsorb CO<sub>2</sub> and water, and to desorb water. Lewatit's CO<sub>2</sub> adsorption equilibrium was modeled using the temperature-dependent Toth isotherm, while water adsorption was described using the Guggenheim-Anderson-de Boer (GAB) model [1]. To account for the influence of water on CO<sub>2</sub> adsorption, the Mechanistic Co-adsorption model was applied. For NbOFFIVE-1-Ni, the CO<sub>2</sub> adsorption isotherms were modeled using the Toth isotherm, and water adsorption followed the GAB model, with binary CO<sub>2</sub>-H<sub>2</sub>O sorption modeled using the Modified Toth equation [2]. We will compare four cases under DAC conditions: (1) using Lewatit alone, (2) using a bed of NbOFFIVE-1-Ni, (3) using a bed of silica gel followed by Lewatit, and (4) using silica gel followed by NbOFFIVE-1-Ni. The purpose of positioning the silica gel before the main CO<sub>2</sub> adsorbent is to remove water, thereby reducing energy consumption. These four cases will be compared in terms of energy requirements for DAC. The electrical and thermal energy required for the temperature-vacuum swing adsorption (TVSA) cycle for each adsorbent was calculated based on established references [3], with thermal properties of Lewatit and NbOFFIVE-1-Ni sourced from [1] and [2], respectively.

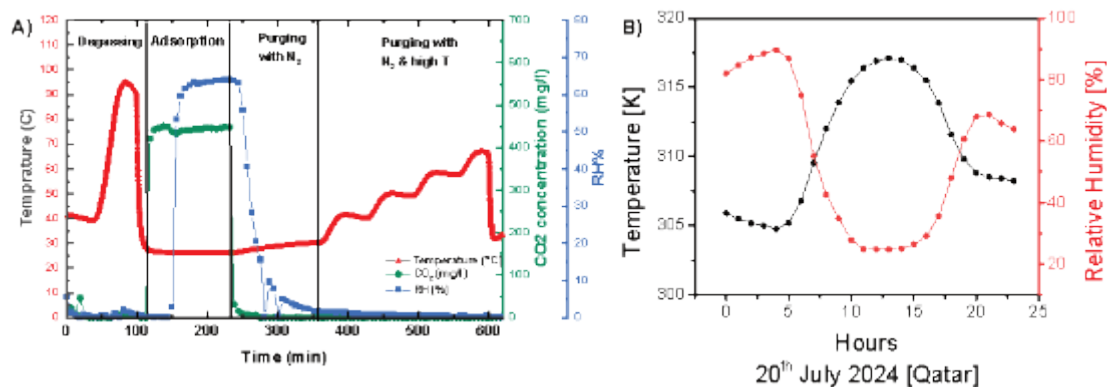


Figure 1: A) CO<sub>2</sub> and water adsorption performance of Silica gel B) Temperature and humidity variation throughout 20<sup>th</sup> July In Qatar

The experiment, based on Figure 1, investigated the adsorption and regeneration of water and CO<sub>2</sub> under Direct Air Capture (DAC) conditions, focusing on minimizing thermal energy consumption during regeneration. Starting with 60% relative humidity and 400 mg/L CO<sub>2</sub>, the procedure included degassing at 100°C, adsorption of CO<sub>2</sub> and water vapor, and regeneration in two stages: nitrogen purging at room temperature, followed by purging while increasing the temperature to 70°C. The results demonstrated that silica gel adsorbed only water, not CO<sub>2</sub>, making it a viable



humidifier in DAC systems. Importantly, the water was fully regenerated using nitrogen purging without any need for heating, showing that silica gel does not contribute to the system's thermal energy demand. This setup enables the DAC adsorbent to function efficiently in humid conditions, matching its performance in dry conditions. Additionally, Figure 2 presents humidity and temperature data from one of the hottest days in Qatar (20/7/2022), highlighting the main uncontrolled variables impacting the system's efficiency across the four studied cases. These environmental factors, especially high humidity and temperatures, will directly influence adsorption behaviour and regeneration efficiency, underscoring the importance of designing DAC systems to adapt to such conditions.

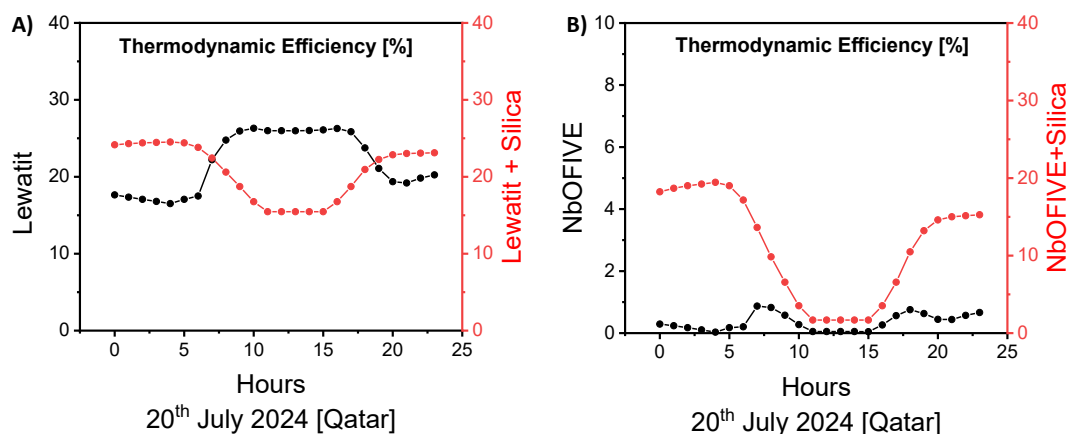


Figure 2 : thermodynamic efficiency Comparison between four cases A) lewatit only compared to silica gel + lewatit B) NbOFFIVE only compared to silica gel + NbOFFIVE

Figure 3 compares the efficiency of two systems tested over time, with humidity and temperature values corresponding to those presented in Figure 2. The second case uses a dual-bed system with silica gel followed by Lewatit, where the silica gel removes nearly all humidity before air reaches the Lewatit, leaving temperature as the sole factor affecting efficiency. As temperature increases, the system's efficiency decreases. In contrast, in the first case where silica gel is absent, efficiency improves with higher temperatures, indicating that humidity is the dominant factor—lower humidity enhances performance. The system with silica gel performs better under conditions of higher humidity and lower temperatures, which are common in HVAC systems, making it a more suitable option for such environments. In figure 4, we replace Lewatit, a chemisorption material, with NOFFIVE, which falls under the physisorption category. The data reveal that when using NOFFIVE alone, the efficiency drops significantly, underscoring how sensitive this material is to humidity—even when the humidity isn't at its peak. However, with the addition of silica gel, the system's efficiency improves considerably, reaching around 19% at certain temperatures and dropping to about 1.5% at higher temperatures. This highlights the substantial effect of temperature on the performance of the silica gel + NOFFIVE system, reinforcing the importance of using HVAC conditions as an optimal environment. By utilizing silica gel, NOFFIVE's efficiency becomes comparable to Lewatit, with NOFFIVE achieving a maximum of approximately 19%, while Lewatit reaches around 24%. In colder environments like HVAC systems, the performance of the silica gel + NOFFIVE system could potentially surpass that of the silica gel + Lewatit setup, further optimizing the system's efficiency.

## References

- [1] Y.M. Abdullatif, A. Sodiq, T. Al-Ansari, N.N. Nassar, and A.I. Amhamed, *Energy Conversion and Management*, 291, 117280 (2023).
- [2] B.M. Balasubramaniam, P.-T. Thierry, S. Lethier, V. Pignet, P. Llewellyn, and A. Rajendran, *Chemical Engineering Journal*, 485, 149568 (2024).
- [3] R. Surkatti, Y.M. Abdullatif, R. Muhammad, A. Sodiq, K. Mroue, T. Al-Ansari, et al., *Separation and Purification Technology*, 354, 128641 (2025).



## Development of zeolite adsorbent with low water sensitivity for CO<sub>2</sub> capture

P. Hu<sup>1,2</sup>, R. Oishi<sup>2</sup>, H. Ya<sup>2</sup>, Y. Yonezawa<sup>1</sup>, M. Matsukura<sup>1</sup>, K. Iyoki<sup>2,3</sup>, T. Okubo<sup>2</sup>, T. Wakihara<sup>1,2</sup>

<sup>1</sup> Institute of Engineering Innovation, The University of Tokyo, 2-11-16 Yayoi, Bunkyo-ku, Tokyo 113-8656, Japan

<sup>2</sup> Department of Chemical System Engineering, The University of Tokyo, 7-3-1 Hongo, Bunkyo-ku, Tokyo 113-8656, Japan

<sup>3</sup> Department of Environment Systems, Graduate School of Frontier Sciences, The University of Tokyo, 5-1-5 Kashiwanoha, Kashiwa, Chiba 277-8563, Japan

hu\_pd@chemsys.t.u-tokyo.ac.jp

### Introduction

Carbon dioxide (CO<sub>2</sub>) is the most important greenhouse gas resulting from the human activities, and the development of efficient CO<sub>2</sub> capture technology is in high demand. Pressure swing adsorption (PSA) is an advanced gas separation technology that is realized based on the difference of the adsorption characteristics of the gas components on the solid materials and the change of the adsorption capacity regulated by the pressure [1]. PSA has already been applied to the pre-combustion and post-combustion CO<sub>2</sub> capture in thermal power plants.

Zeolites are widely used as adsorbents for PSA systems taking advantages of their high adsorption capacity and selectivity, and excellent stability and durability. In the current PSA systems for the CO<sub>2</sub> capture, zeolite 5A (Ca<sup>2+</sup>-exchanged zeolite A, LTA-type) and zeolite 13X (Na<sup>+</sup>-exchanged zeolite X, FAU-type) are commonly utilized because of their high CO<sub>2</sub> adsorption capacity. However, the competitive adsorption caused by water vapor is an intractable problem that significantly impairs the CO<sub>2</sub> adsorption efficiency of the PSA systems [2]. This issue will no longer be a problem if adsorbents with low water sensitivity are applicable. In addition to the working capacity, the adsorption speed of the bulk adsorbent pellets is another key factor that determines the efficiency of the PSA systems.

In this study, we evaluated the CO<sub>2</sub> adsorption performance (capacity and speed) of two typical zeolite adsorbents, FAU- and MFI-type zeolites, with different Si/Al ratios and extra-framework cations (H<sup>+</sup>, Na<sup>+</sup>) under the dry and humid conditions using a homemade single bed simulator (SBS). Among the tested commercial samples, H-MFI-type zeolite with a Si/Al ratio of 940 (MFI\_H\_940) showed a higher hydrophobicity and a superior CO<sub>2</sub> adsorption capacity at a relative humidity of 75%. After the defect-healing treatment developed by our group [3], the MFI\_H\_940\_healed sample exhibited the best CO<sub>2</sub> adsorption performance that hardly changed under the dry and humid conditions.

### Experimental

#### Materials

The zeolite samples were obtained commercially, and are basically denoted as “Topology\_Cation\_Si/Al”. The liquid-mediated defect-healing treatment of MFI\_H\_940 was conducted according to our previous paper [3], and the final sample is denoted as MFI\_H\_940\_healed.

#### CO<sub>2</sub> adsorption/desorption experiments using single bed simulator (SBS)

The illustration of the SBS used in this study is shown in Figure 1a. Before the experiments, the powdered zeolites were first compacted into self-supporting pellets and pretreated at 250 °C under vacuum for 3 h, and then cooled down to 25 °C. The brief illustration of the experimental procedure of the simulated operation of CO<sub>2</sub> PSA is shown in Figure 1b. Saturated NaCl solutions were introduced into each tank to realize a relative humidity of 75% (75%RH). The amount of CO<sub>2</sub> was calculated from the measured pressure based on the van der Waal's equation.

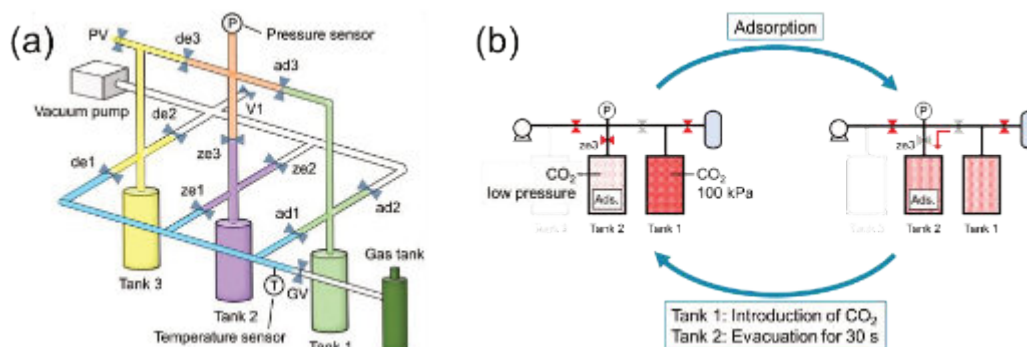


**Figure 1.** (a) Illustration of SBS used in this study. (b) Illustration of experimental procedure of simulated operation of CO<sub>2</sub> PSA.



## Results and discussion

### Static adsorption

For both types of zeolites, the zeolites with H<sup>+</sup> and Si-rich composition exhibit lower CO<sub>2</sub> adsorption amount at the equivalent pressure according to the CO<sub>2</sub> adsorption isotherms (Figure 2a). Stronger physical and chemical adsorption of CO<sub>2</sub> occurs inside the zeolites with Na<sup>+</sup> and more Na<sup>+</sup> (i.e., lower Si/Al ratio) leads to a larger adsorption capacity. It is noted that the detriment derived from H<sup>+</sup> to the adsorption capacity is more noticeable for the FAU-type zeolite. The equilibrium uptake of CO<sub>2</sub> at 20 kPa, for example, on FAU\_H\_3.0 is only 0.37 mmol g<sup>-1</sup>, approximately 10% of that on FAU\_Na\_2.9 (3.5 mmol g<sup>-1</sup>), and even much lower than that on MFI\_H\_12 (1.2 mmol g<sup>-1</sup>). In contrast, the high-silica MFI\_H\_940 still demonstrates an equilibrium CO<sub>2</sub> uptake as high as 0.64 mmol g<sup>-1</sup> at 20 kPa.

The hydrophilicity/hydrophobicity of the various samples was evaluated by the static water vapor adsorption at 25 °C, and the adsorption amount at 75%RH is focused (Figure 2b). Basically, the affinity for water of the zeolites decreases as their framework Al content goes down. For the FAU-type zeolite, a slightly larger water vapor adsorption capacity is observed on the zeolite containing extra-framework Na<sup>+</sup>, the same trend as that in the CO<sub>2</sub> adsorption. On the contrary, MFI\_Na\_12 (12.9 wt%) and MFI\_H\_12 (14.0 wt%) exhibit similar water vapor adsorption capacity.

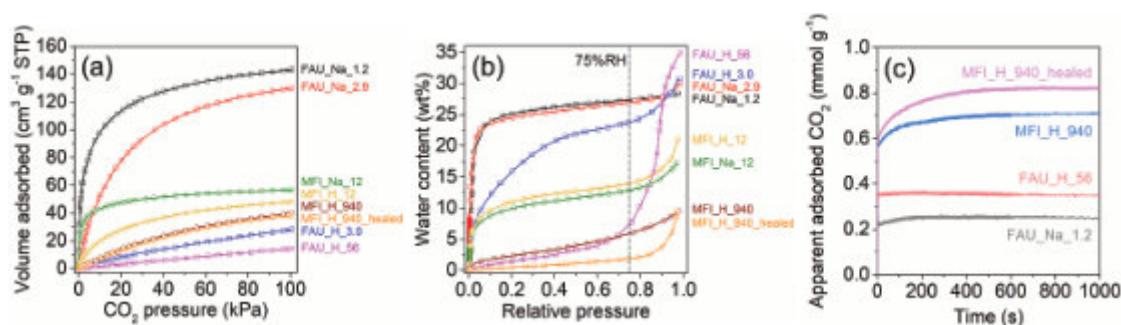


**Figure 2.** Adsorption isotherms of (a) CO<sub>2</sub> and (b) water vapor on various zeolites at 25 °C. (c) Apparent adsorption amount of CO<sub>2</sub> on various zeolite pellets under humid condition during the adsorption process in a steady CO<sub>2</sub> PSA cycle using SBS.

### Operation of CO<sub>2</sub> PSA by SBS

FAU\_Na\_1.2, FAU\_H\_56, MFI\_H\_940 and MFI\_H\_940\_healed were tested under the humid condition and the apparent adsorption amount of CO<sub>2</sub> during the adsorption process after the steady CO<sub>2</sub> PSA was achieved is shown in Figure 2c. As expected, FAU\_Na\_1.2, which displays the best CO<sub>2</sub> adsorption performance under the dry condition (Figure 2a), exhibits the lowest CO<sub>2</sub> working capacity of 0.25 mmol g<sup>-1</sup> due to the loss of a large number of effective adsorption sites to capture CO<sub>2</sub>, where H<sub>2</sub>O molecules are preferentially adsorbed. Although the CO<sub>2</sub> adsorption capacity of FAU\_H\_56 in the absence of water vapor is much lower than that of FAU\_Na\_1.2 (Figure 2a), its improved hydrophobicity greatly helps alleviate the competitive adsorption of H<sub>2</sub>O, consequently leading to a superior CO<sub>2</sub> PSA performance (0.35 mmol g<sup>-1</sup>) compared with that of FAU\_Na\_1.2.

On the other hand, the high-silica MFI\_H\_940 outperforms the high-silica FAU\_H\_56 under both dry and humid conditions because of the stronger dispersive interactions with the CO<sub>2</sub> molecules in the narrower pores of MFI-type zeolites and the higher hydrophobicity (Figure 2b). In a steady CO<sub>2</sub> PSA cycle containing water vapor, the working capacity of MFI\_H\_940 can reach 0.71 mmol g<sup>-1</sup>, double that of FAU\_H\_56. Furthermore, by performing the defect-healing treatment on MFI\_H\_940, the hydrophilic silanol groups can be eliminated so that the adverse effect of H<sub>2</sub>O can be minimized. As a result, MFI\_H\_940\_healed possesses an overwhelming CO<sub>2</sub> working capacity of 0.82 mmol g<sup>-1</sup>. Furthermore, 75% of the working capacity (0.61 mmol g<sup>-1</sup>) can be achieved within 10 s.

## Conclusion

By defect-healing treatment of the high silica MFI-type zeolite, a water-resistant zeolite adsorbent for CO<sub>2</sub> capture is obtained. The CO<sub>2</sub> working capacity can reach 0.82 mmol g<sup>-1</sup> under the humid condition (75%RH) in a simulated PSA process, and 75% of the working capacity can be achieved within 10 s.

## References

- [1] S. Sircar, *Ind. Eng. Chem. Res.*, **41**, 1389-1392 (2002).
- [2] Y. Wang, and M.D. LeVan, *J. Chem. Eng. Data*, **55**, 3189-3195 (2010).
- [3] K. Iyoki, K. Kikumasa, T. Onishi, Y. Yonezawa, A. Chokkalingam, Y. Yanaba, T. Matsumoto, R. Osuga, S.P. Elangovan, J.N. Kondo, A. Endo, T. Okubo, and T. Wakihara, *J. Am. Chem. Soc.*, **142**, 3931-3938 (2020).



## SYNTHESIS OF HIGH-SILICA ERI BY MACHINE LEARNING ASSISTED OSDA DESIGN

Y. Semante-Esquivel<sup>1</sup>, M. Xie<sup>2</sup>, D. Schwalbe-Koda<sup>2,3</sup>, E. Bello-Jurado<sup>1</sup>, A. Hoffman<sup>2</sup>, C. Paris<sup>1</sup>, M. Moliner<sup>\*1</sup>, R. Gómez-Bombarelli<sup>\*2</sup>

<sup>1</sup> Instituto de Tecnología Química, Universitat Politècnica de Valencia – Consejo Superior de Investigaciones Científicas, Avenida de los Naranjos s/n, 46022, Valencia, España.

<sup>2</sup> Department of Materials Science and Engineering Massachusetts Institute of Technology, Cambridge, MA 02139, USA.

<sup>3</sup> Department of Materials Science and Engineering, University of California Los Angeles, CA 90095-1595, USA.

yosees@itq.upv.es

The rational design of zeolites focuses on the synthesis of new or existing zeolitic frameworks where the chemical properties and crystal morphology of the material can be fine-tuned for a specific reaction or chemical process. In this sense, the development of new organic structure-directing agents (OSDAs) will be key not only for the synthesis of new zeolites but also for the optimization of the physicochemical properties of the existing ones.<sup>1</sup> In the last decade, the incorporation of new informatic tools triggered the prediction of new OSDAs for the synthesis of 'on-demand zeolites' with specific properties. However, some of the of the resulting chemical structures for OSDAs were not feasible from the synthetic point of view, or required many synthetic steps.

With the assistance of machine learning (ML), an extensive library of OSDA-like molecules was created, using mathematical models and experimental validation. Using this novel methodology, the interactions between the zeolite framework and the organic molecules (binding energies, BE) were calculated for the synthesis of the small-pore Erionite (ERI) zeolite, selecting those chemical structures with the greatest affinity for ERI. In addition, phase competition between different zeolite structures and OSDAs were also considered. Moreover, filters were applied to discard expensive, poorly soluble or difficult-to-synthesize OSDAs.<sup>2</sup> The synthesis of ERI-type zeolites is traditionally made using diquateryary OSDAs and potassium (K<sup>+</sup>) cations, limiting the Si/Al ratio to 5-6 and thus, mostly affecting their chemical stability under harsh conditions.<sup>3</sup> To enhance the Si/Al ratio and improve the stability, we propose the use of monoquateryary OSDAs with the aim of significantly reduce the number of positive charges incorporated by the OSDA molecules trapped within the *eri* cavities. Here, we showcase an experimentally validated study using a "de novo OSDA screening workflow" to select OSDA candidates for templating high-silica ERI, with new chemical compositions that break their current synthesis limitations. We evaluated monoquateryary molecules for synthesizing high silica ERI and chose two promising candidates: Mol-ERI-1 and Mol-ERI-4 (Fig 1-A). In both cases, it was possible to achieve erionite with higher Si/Al ratios (12.3 for ERI(Mol1) and 7.7 for ERI(Mol4), respectively) than traditional methods, confirming the computational model's predictions. Testing Cu-exchanged ERI zeolites for selective catalytic reduction (SCR) applications showed that Cu/ERI(Mol-1) had better resistance to deactivation under harsh conditions (severe ageing treatments) compared to traditional Cu/ERI(OSDA-1) in Fig. 1-C.<sup>4</sup> This novel approach for the synthesis of small-pore zeolites opens the possibility to extend the methodology to other materials with relevant industrial applications.

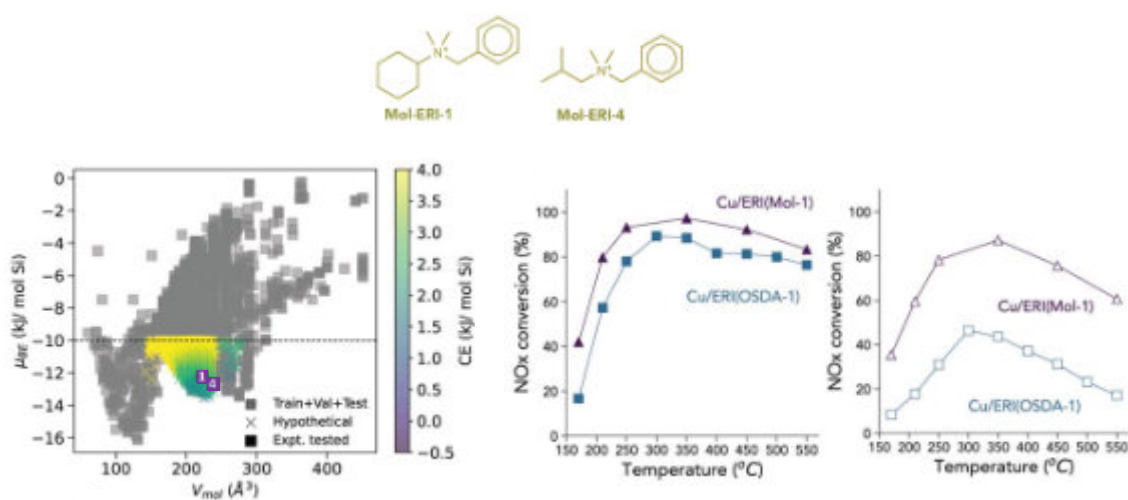


**Figure 1.** A) Selected OSDAs molecules for synthesizing erionite. B) Diagram for CE and  $V_{mol}$  parameters with hypothetical monoquateryary OSDA and screening of the most competent molecules for ERI. C) NO conversion in the NH<sub>3</sub>-SCR reaction using two catalysts: designed Cu/ERI(Mol-1) (purple triangles) and standard Cu/ERI(OSDA-1) (blue squares), in their fresh form (filled symbols) and steam-aged at 750°C (empty symbols).



**6<sup>th</sup> Euro-Asia Zeolite Conference**  
Alicante (Spain), January 19-22, 2025



## References

- [1] M. Moliner, F. Rey, and A. Corma, *Angew. Chem. Int. Ed.*, **52**, 13880–13889 (2013).
- [2] D. Schwalbe-Koda, S. Kwon, C. Paris, *et al.*, *Science*, **374**, 308–315 (2021).
- [3] M. Moliner, C. Martinez and A. Corma, *Chem. Mater.*, **26**, 246–258 (2014).
- [4] N. Martín, C. Paris, P. Vennestrøm, *et al.*, *Appl. Catal. B Environ.*, **217**, 125–136 (2017).

## Acknowledgments

This work has been supported by the Spanish Government-MINECO through “Severo Ochoa” (SER-2016-0683). M.S.E acknowledges the Spanish Government-MCIU for a FPI scholarship (PRE2020-092319). Computer calculations executed at the Massachusetts Green High-Performance Computing Center with support from MIT Research Computing. The Electron Microscopy Service of UPV is acknowledged for its help in sample characterization. Financial support by Severo Ochoa centre of excellence program (CEX2021-001230-S) is gratefully acknowledged.



## Alcohol-Assisted Synthesis of ZSM-5 Zeolites Contributes to Enhanced BTX Production from Methanol

Q. Li<sup>1</sup>, L. Zhao<sup>1</sup>, Y. Wang<sup>1,2</sup>, P. Xiao<sup>1</sup>, Y. Sun<sup>1</sup>, T. Yokoi<sup>1,2</sup>

<sup>1</sup> Institute of Innovative Research, Tokyo Institute of Technology, 4259 Nagatsuta, Midori-ku, Yokohama 226-8501, Japan

<sup>2</sup> iPEACE223 Inc., Konwa Building, Tsukiji, Chuo-ku, Tokyo, 1-12-22, Japan

li.q.ak@m.titech.ac.jp

### Abstract

The methanol-to-aromatics (MTA) reaction is emerging as an important process for producing benzene, toluene, and xylene (BTX) products, with ZSM-5 serving as a key acid catalyst. In this study, a series of ZSM-5 zeolites were synthesized with the assistance of alcohol, and their ability to produce BTX products in the MTA reaction was investigated. Two different silica sources, SiO<sub>2</sub> and TEOS, were employed, with a focus on exploring the effects of methanol on the crystallization and Al distribution in the ZSM-5 framework. When SiO<sub>2</sub> was used as the silicon source, the addition of methanol into the mother gel significantly altered the morphology of the zeolite, resulting in smaller particles. However, methanol did not produce a noticeable reduction in particle size when TEOS was used as the silicon source. Moreover, methanol led to the formation of distorted tetrahedral Al sites (Al(IV)-2) in both types of ZSM-5, which contributed significantly to BTX production, increasing selectivity by up to 13% (WHSV = 2 h<sup>-1</sup>). However, the amount of methanol added must not be too high; when the methanol/Si ratio exceeds 0.25, the selectivity for BTX decreases. This is attributed to the excessively high electrostatic potential caused by the excess methanol, which disrupts the crystallization process of ZSM-5. To further investigate the mechanism of the effect of methanol addition, as a control, silicalite-1 was synthesized in the presence of methanol. This study provides valuable insights for enhancing the catalytic performance of ZSM-5 in the MTA reaction and offers broad potential applications.

### Introduction

Aromatic compounds are essential for the production of products in industries such as plastics, agriculture, and pharmaceuticals, and are currently derived exclusively from non-renewable petroleum resources. In recent years, methanol has been explored as a feedstock for producing BTX (benzene, toluene, and xylene) using zeolite catalysts [1]. Among them, 10-membered ring (10-MR) zeolites like ZSM-5 offer the optimal confinement effect necessary for aromatization during the conversion process, making the effective design and synthesis of ZSM-5 crucial for BTX production. This design involves controlling both morphology and acid sites. Alcohols are commonly used as solvents and structure-directing agents (SDAs) in zeolite synthesis. Previous studies have shown that alcohol co-solvents can significantly influence the axis length of Si-MFI crystals during microwave heating [2], and that bulky alcohol molecules leads to the unique Al distribution in the ZSM-5 framework [3]. Therefore, the presence of alcohols can greatly affect the morphology or Al distribution of zeolites under specific conditions. In light of this, the present work aims to explore the influence of methanol on the crystallization of MFI zeolites, with a focus on its impact on the structure and catalytic performance for BTX production.

### Experimental section

The ratio of raw material to synthesize ZSM-5 is 1SiO<sub>2</sub>:0.02Al<sub>2</sub>O<sub>3</sub>: TPAOH: NaOH: xCH<sub>3</sub>OH. The specific synthesis method is to successively add water, NaOH, Al(NO<sub>3</sub>)<sub>3</sub>·9H<sub>2</sub>O and TPAOH into the Teflon reaction dish, and the mixture must be mixed evenly before each raw material is added. After finishing, TEOS or colloidal silica was slowly added to the mixture, sealed and heated in an oven at 80 °C for 5h for aging test. After the aging experiment, the mixture was placed at room temperature, methanol was added and transferred to the reactor, and the hydrothermal synthesis experiment was carried out at 170 °C for 24 hours. Hydrothermal synthesis was followed by filtration to obtain as-made samples. Calcined samples were obtained by calcining the as-made samples at 550 °C for 9h. Put the calcined samples in the polymer bottle and stirred in 2.5mol/L ammonium nitrate solution for 6h for ion exchange, and then filtered and calcined again to obtain H-type ZSM5. The ZSM-5 zeolites synthesized from TEOS and SiO<sub>2</sub> with or without methanol were named T-Z5 and T-Z5-M, S-Z5 and S-Z5-M, respectively.

### Results and discussion

Two different silica sources (SiO<sub>2</sub> and TEOS) were used to synthesize ZSM-5 zeolites with distinct morphologies. ZSM-5 synthesized from SiO<sub>2</sub> (S-Z5) exhibited an aggregated large-particle morphology formed by the aggregation of smaller particles, while the TEOS-derived ZSM-5 (T-Z5) displayed a coffin-like crystal shape. Upon the addition of methanol, S-Z5 showed significantly smaller particle sizes with aggregation, whereas T-Z5's particle size remained largely unchanged. Moreover, the specific surface areas of both zeolites increased significantly **due to the presence of methanol**. The NMR results indicated that, after the addition of methanol, the peak corresponding to tetrahedrally coordinated Al around 55 ppm was shifted towards the downfield, and a noticeable hump appeared in the chemical shift range of 45–50 ppm, which was attributed to the formation of distorted tetrahedral Al (Al(IV)-2).





The catalytic performance of thus prepared zeolites in MTA reaction was evaluated (Figures 1 (a) and (c)). Both T-Z5 and T-Z5-M exhibited a stable conversion of 100 % along with TOS. Note that there was a significant difference in the product distributions; T-Z5-M gave a higher BTX selectivity than T-Z5. These results indicate that the presence of these distorted Al sites promoted the aromatization process. However, it is noteworthy that when the methanol content exceeded 0.25, the BTX yield began to decrease. To further investigate the effect of methanol, as-made samples synthesized using TEOS were analysed. The TG results revealed that the presence of methanol enhanced the proportion of compensated type of TPA<sup>+</sup>, which means more Al sites connected to TPA ions [4]. This results demonstrated the structure-directing effect of TPA<sup>+</sup> was enhanced and contributed to the formation of distorted Al(IV)-2, leading to a greater distribution of Al at larger intersection positions, which further facilitated BTX production.

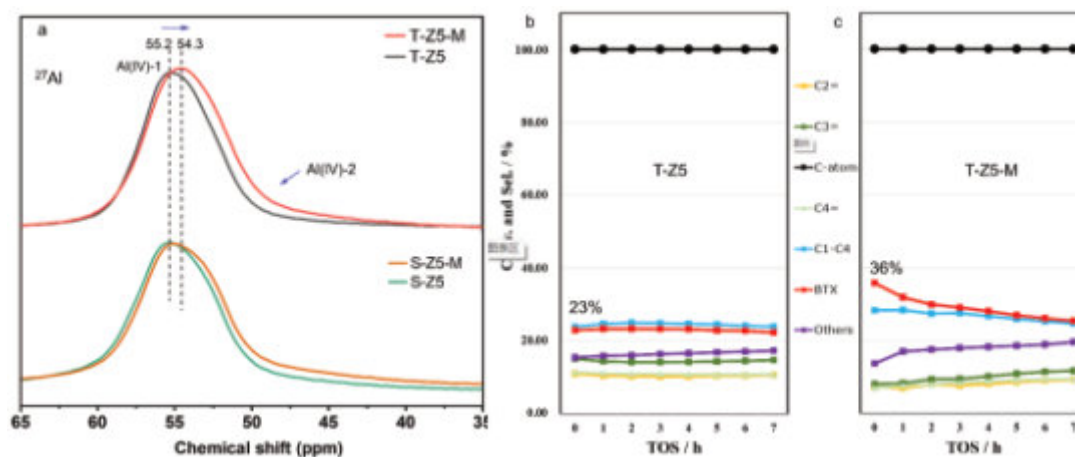


Figure 1. (a) <sup>27</sup>Al NMR results for the various samples and MTA results for T-Z5 (b) and T-Z5-M (c). Reaction conditions: 50 mg catalyst, W/F<sub>MeOH</sub>: 15.98 g·h·mol<sup>-1</sup>, WHSV: 2.0 h<sup>-1</sup>, 450 °C.

## Conclusion

In this study, the influence of methanol on the crystallization, morphology, and catalytic performance of ZSM-5 zeolites synthesized from different silicon sources (SiO<sub>2</sub> and TEOS) was systematically investigated. The addition of methanol altered the zeolite morphology, reduced particle size, and increased surface area, particularly in SiO<sub>2</sub>-derived ZSM-5 (S-Z5). Furthermore, methanol induced the formation of distorted tetrahedral Al sites (Al(IV)-2) in both types of ZSM-5, which significantly improved BTX selectivity during the methanol-to-aromatics (MTA) reaction. However, excessive methanol (methanol/Si ratio > 0.25) led to a decline in BTX yield, likely due to its disruptive effect on the ZSM-5 crystallization process. These findings demonstrate the crucial role of methanol in modulating the structural properties of ZSM-5 and optimizing its catalytic performance for BTX production. This study provides valuable insights into the design of zeolite catalysts for aromatic hydrocarbon production and highlights the potential of methanol as a key factor in tailoring zeolite properties for enhanced catalytic activity.

## References

- [1] Li et al. *Chem. Soc. Rev.*, **44**, 7112 (2015)
- [2] Chen. et. al. *Micropor. Mesopor. Mater.* **23**, 296-304 (2007)
- [3] Biligetü et. al. *J. Catal.*, **353**, 1-10 (2017)
- [4] Zhao et al. *ACS Appl. Mater. Interfaces* **16**, 17701–17714 (2024)



## Synthesis of ZSM-5 from natural mordenite from Spain

*Itziar Arnaiz<sup>1</sup>, Yaregal Awoke<sup>2</sup>, Manuel Sánchez-Sánchez<sup>1</sup>, Isabel Diaz<sup>1</sup>*

*1 Instituto de Catálisis y Petroleoquímica, ICP-CSIC. C/Marie Curie 2, 28049 Madrid, Spain*

*2 Chemistry Department, Addis Ababa University, Arat Kilo Campus, Addis Ababa, Ethiopia*

*itziar.arnaiz@csic.es*

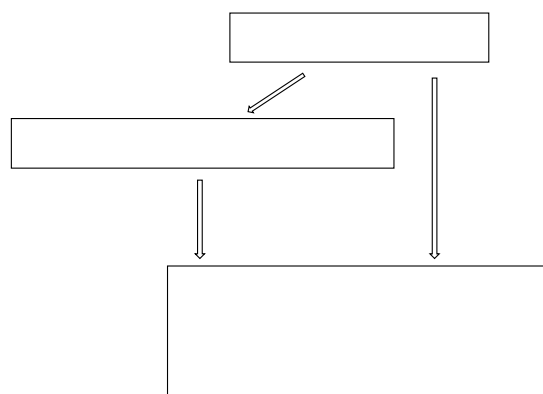
### Introduction

ZSM-5 zeolite is one of the most important heterogeneous catalyst, widely utilized in numerous petrochemical processes, including cracking, isomerization, aromatization, and alkylation. It is used in various catalytic reactions, such the MTO (methanol-to-olefins) and MTH (methanol-to-hydrocarbons) reactions [1]. With rising industrial demand, many research studies have addressed the synthesis of ZSM-5 zeolite to meet the significant market need for this material, specially focusing on reducing the synthesis cost [2]. Synthesis has been attempted using natural aluminosilicate materials like rice husk ash, kaolin, rectorite, perlite, and diatomite, which serve as silica and alumina precursors. These natural materials are easily available and cost-effective compared to chemical sources of silica or alumina [3]. However, all these methods imply a previous step of activation or amorphization using calcination. What we propose is an inter-zeolite transformation between a natural zeolite to yield a synthetic ZSM-5 [4]. In this study, we identify the optimal method for increasing the Si/Al ratio and removing natural inorganic oxide impurities from natural mordenite from Spain [5]. Additionally, we investigate the effects of various parameters, including synthesis methods (starting from dealuminated zeolite or adding extra silica source to reach the desired Si/Al ratio), growth solution composition, synthesis time, and temperature, on the transformation of natural mordenite into ZSM-5 in the presence of an organic structure-directing agent (TPAOH).

### Experimental Section

The raw natural mordenite (N-MOR) sample used in this study was collected from the southeast of Spain [5] and used as it is without any further treatment. The main parameter to be adjusted is the Si/Al ratio from 5 to approximately 20. This adjustment has been attempted following two approaches: i) dealumination or ii) adding extra silica source. The exact dealumination process optimized in this work involved stirring a suspension of the natural mordenite in 20 ml of 8 M HCl solution per gram of solid in a reflux-attached round bottom flask at 100 °C for 24 hours. After treatment, the solid was filtered and washed with distilled water repeatedly until all chloride was removed (indicated by the pH of the solution matching the pH of distilled water), and then the solid was dried. The acid-treated (dealuminated) samples were labelled as "D" and characterized by XRD, SEM, and ICP-OES. In the second approach, the Si/Al ratio of the synthesis gel is adjusted by simply adding a silica source without dealumination, the samples prepared though this method are called "R" from Raw. The entire experimental design is depicted in Scheme 1.

For the characterization of the samples Powder X-ray diffraction (XRD) patterns were collected with a Philips X'PERT diffractometer equipped with an X'Celerator detector and using Cu K $\alpha$  radiation. The percentage of crystallinity of the synthesized zeolite ZSM-5 was calculated by comparing the sum of peak areas of five intense and non-overlapped peaks of the synthesized zeolite ZSM-5 and the commercial zeolite ZSM-5 (CBV3024E) which was used as standard (100% crystalline) in this work [6]. Inductively Coupled Plasma Optical Emission Spectrometry, (ICP-OES) (Optima 3300 DV model) was used to determine the composition. The morphology was studied by Scanning Electron Microscopy using FEI, Verios 460, without coating. Thermogravimetric analyses were carried out under air flow, with a Perkin-Elmer TGA 7 instrument in the temperature range of 30-900 °C in the heating rate of 20 °C/min.



**Scheme 1.** Designed experiments for the two hydrothermal synthesis approaches: on the left, using previously-dealuminated natural mordenite (D samples); and, on the right, adding SiO<sub>2</sub> source to the untreated natural mordenite N-MOR (R samples).



## Results and Discussion

Zeolite ZSM-5 has been synthesized using natural mordenite from San José-Los Escullós deposit in southeast Spain. The final pure ZSM-5 was achieved without the need for calcination of the natural mordenite and without gelation or aging prior to crystallization. The Si/Al ratio of the natural mordenite was modified through two main methods: (i) dealumination under acidic conditions (D samples) and (ii) the addition of an extra silica source (R samples). The optimization of both synthesis approaches involved varying the alkalinity source, NaOH concentration, TPAOH concentration, and adjusting the synthesis temperature and time as indicated in Scheme 1. As shown in the XRD patterns in Figure 1-left, ZSM-5 with over 100 % crystallinity compared to commercial ZSM-5 with similar Si/Al ratio (CBV3024E) was produced under hydrothermal synthesis conditions at 190 °C for 48 hours using either liquid ammonia or NaOH as the alkalinity sources. The crystal morphology and particle size distributions appear more homogeneous systematically in the synthesis prepared with liquid ammonium, as compared with those prepared with NaOH that yield a more heterogeneous distribution of sizes and shapes, with a clear presence of other phases. Comparing the two approaches in the case of NH<sub>3</sub>, both dealuminated (D) (Figure 1-right) and adding silica (R) show very interesting and promising particle size distribution and crystal size to be evaluated in catalysis. Both show coffin shaped crystals with sizes in the range of 200 to 400 nm. The route involving the addition of extra silica, shows higher density of crystals with the typical MFI twinning.

In summary, highly-crystalline ZSM-5 with relatively small crystals size and Si/Al ratio near 20 can be obtained from natural mordenite from Spain under the following synthesis conditions: crystallization temperature and time 190 °C for 48 h, or 120 °C for 5 days; the choice of temperature/time for a more sustainable transformation would be established upon coming quantification studies of the energy consumption of the overall process would be conducted. In the case of NaOH, TPAOH: SiO<sub>2</sub> ratio of 0.25 is the optimum while when the source of alkalinity is liquid ammonia the required SiO<sub>2</sub>:TPAOH ratio is 10. Furthermore, we have demonstrated the feasibility of reproducible dealumination of the raw natural mordenite to adjust the Si/Al ratio of the starting material and to minimize metal oxide impurities. This approach to ZSM-5 synthesis is more sustainable compared to other reported methods using raw sources, as it eliminates the need for calcination (amorphization) of natural mordenite, resulting in energy saving, and avoids the aging process.

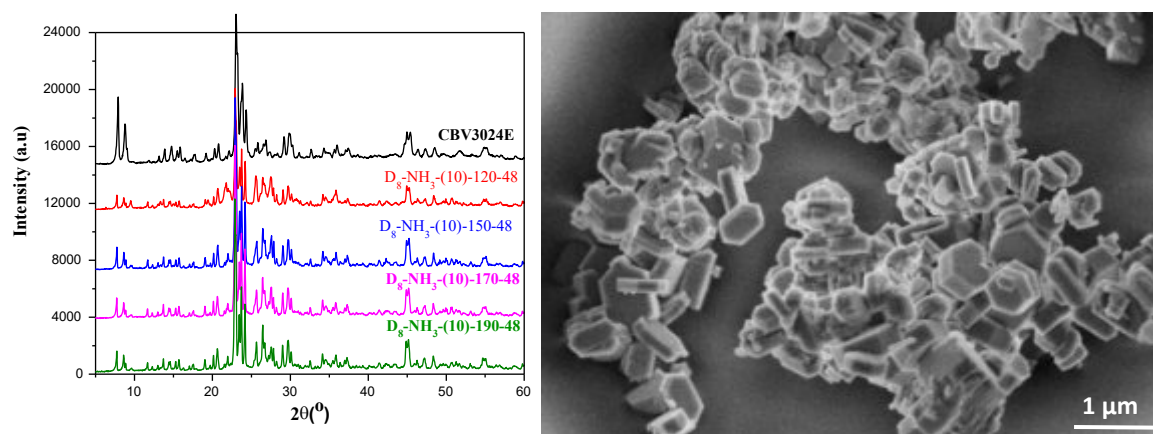


**Figure 1.** On the left, XRD diffraction patterns of ZSM-5 synthesized from raw natural mordenite dealuminated by hydrothermal synthesis method using ammonia at different temperature. On the right, SEM image of sample D-NH<sub>3</sub>-190-48h after calcination at 550 °C for 6 h.

## References

- [1] Q. Zhang, J. Yu, A. Corma *Adv. Mater.*, **32**, 2002927 (2020).
- [2] S. Gao, H. Peng, B. Song, J. Zhang, W. Wu, J. Vaughan, P. Zardo, J. Vogrin, S. Tulloch, Z. Zhu, *J. Environ. Chem. Eng.* **11**, 108995 (2023).
- [3] I. El Bojaddayni, M. Emin Küçük, Y. El Ouardi, I. Jilal, S. El Barkany, K. Moradi, E. Repo, K. Laatikainen, A. Ouammou, *Miner. Eng.*, **198**, 108086 (2023).
- [4] Li C, Moliner M, Corma A. *Angew Chem Int Ed Engl.* **57**, 15330 (2018).
- [5] L. Presa, J.L. Costafreda, D.A. Martín, I. Díaz, *Molecules*, **25**, 1(2020).
- [6] L. Ayele, J. Pérez-Pariente, Y. Chebude, I. Díaz, *Microporous Mesoporous Mater.*, **215**, 29 (2015).

## Acknowledgments

The authors acknowledge funding from MCIN/AEI grant code: PID2022-1363210B-C21/ AEI/10.13039/501100011033/ FEDER, UE. CSIC is also acknowledged through an iCOOP call i-COOPB22002. We acknowledge the service from the MiNa Laboratory at IMN, and funding from CM (project S2018/NMT-4291 TEC2SPACE), MINECO (project CSIC13-4E-1794) and EU (FEDER, FSE)



## Crystallization kinetics of ITQ-13: A solid-state NMR study

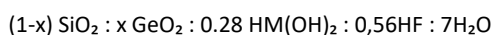
M. Tarchi<sup>1</sup>, J. A. Vidal-Moya<sup>1</sup>, F. Rey<sup>1</sup> and T. Blasco<sup>1</sup>

<sup>1</sup>Instituto de Tecnología Química, Universitat Politècnica de València – Agencia Estatal del Consejo Superior de Investigaciones Científicas (UPV-CSIC), Avda. de los Naranjos s.n., 46022-Valencia, Spain  
mtarchi@itq.upv.es

Zeolite ITQ-13 possesses the ITH type structure with three sets of intercrossed medium-pore channels (9 Å x 10 Å x 10 Å) with orthorhombic unit cell and contains *d4r*, *stf*, *lau* and *mel* cages.[1] When zeolites are synthesized using gels with HF as mineralizing agent, fluoride is usually incorporated into the smallest cages of the structure compensating the OSDA cations. Moreover, incorporating Ge during synthesis is known to stabilize *d4r* by replacing Si in these cages.

In this work, we investigate the crystallization process of pure silica and Ge-containing ITQ-13 zeolite synthesized in fluoride medium using hexamethonium as organic structure directing agent (OSDA). The main objective is to determine the role played by the fluoride anions and by Ge during the crystallization, mainly using solid-state NMR in combination with XRD. Special attention will be paid to the distribution of fluoride in the different cages of the ITH structure at varying crystallization times.

Pure silica and Ge-containing (Si/Ge = 6) gels were synthesized with the following composition:



And then heating at 175 °C in Teflon lined stainless-steel autoclaves at its autogenous pressure under tumbling (60 rpm) for times ranging from 1 to 17 days (also 2h, 5h, 8h, 12h for the sample containing Germanium). <sup>19</sup>F solid state-(ss) NMR spectra of the resulting materials were recorded with Bruker Avance III HD 400 MHz spectrometer. Powder X-ray diffraction patterns (PXRD) were obtained at room temperature (25 °C) using a PANalytical CUBIX diffractometer with Cu Kα radiation.

### Results

Figure 1 shows the XRD patterns of the pure silica and Ge-containing samples at selected time of synthesis. At short synthesis time (up to 2 days for pure silica and 5 days for the Ge-containing samples) the diffractograms show broad background around 2θ values of 20-25 degrees indicating the formation of an amorphous phase. The diffractogram of the pure silica sample obtained after 4 days shows that there is an intergrowth of two phases, ITR and ITH [2]. At longer crystallization times (6, 10 and 17 days) ITH phase is the majority component in the intergrowth, although there still some ITR domains. Figure 1B shows the diffractograms of the Ge-containing samples. After 5 hours of synthesis, the XRD patterns shows a series of reflections corresponding to the BEC topology superimposed to a broad background of amorphous phase, which practically disappears after 8 hours. As the synthesis time increases between to 1 and 5 days, a mixture of phases corresponding to the ITQ-34 zeolite (ITR topology) and BEC zeolites is observed although we cannot rule out the presence of ITH. For synthesis time longer than 5 days, the target ITQ-13 as intergrowth of ITH and ITR is clearly identified as the majority phase, although the XRD patterns suggest the presence of some ITR phase and the occurrence of BEC cannot be excluded.

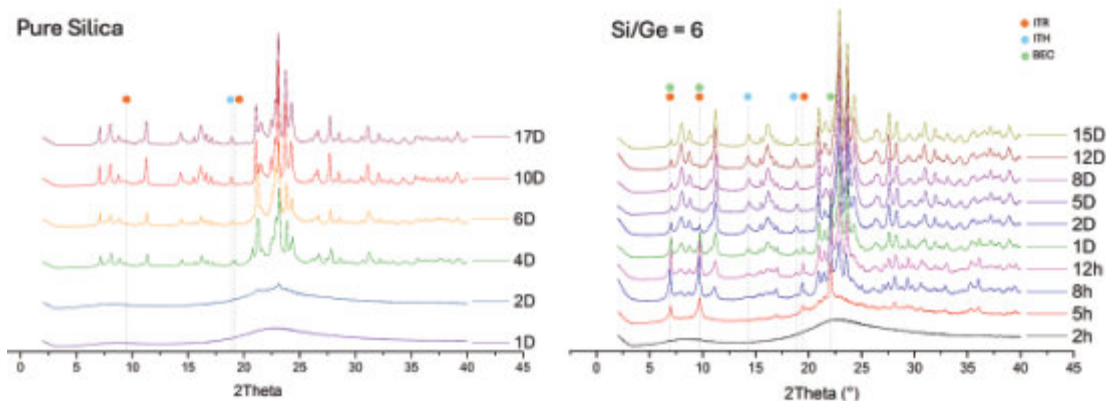


**Figure 1.** XRD analysis of Pure silica samples on the left and Ge-containing samples on the right at different synthesis time. Each sample is labelled with the “h” corresponding to the time in hours or “D” for the time in days. Dotted line indicates different principal reflexes of different phase, green for BEC phase, blue for ITH and orange for ITR.

<sup>19</sup>F NMR spectroscopy has been used to follow the fluoride environment during the crystallisation throughout the entire process. The <sup>19</sup>F NMR spectra of the pure silica samples, displayed in Figure 2, shows two signals at -38 and -66



ppm, corresponding to fluoride anions in the *d4r* and *mel* cages respectively[3]. The  $^{19}\text{F}$  NMR spectra of the Ge-containing samples shows, besides these two resonances, additional signals at -8 and -20 ppm indicating the presence of fluoride within the *d4r* cage with 4 and 1Ge atoms respectively, and another resonance at -55 ppm related to the *mel* cage with 1 atom of germanium [4,5].

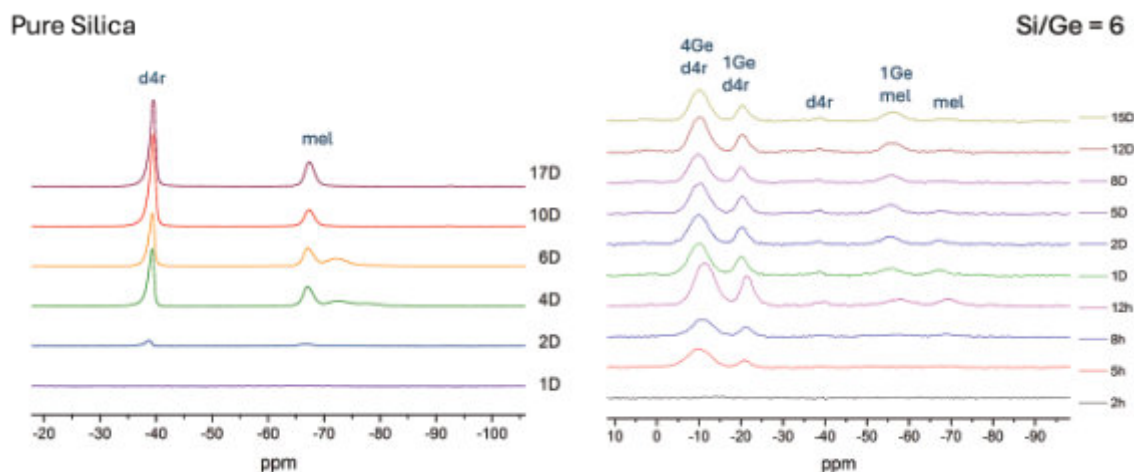


**Figure 2.**  $^{19}\text{F}$  NMR of pure silica samples on the left and Ge-containing samples on the right at different synthesis time. Each sample is labelled with the “h” corresponding to the time in hours or “D” for the time in days. Relevant peaks are marked with the name of the cage where fluoride ions are placed.

Comparison of the  $^{19}\text{F}$  NMR spectra indicates that as the zeolite crystallization proceeds, more fluoride anions are incorporated in pure silica ITQ-13 zeolite. For Ge-containing samples there is an initial increase in the amount of fluoride (from 2h to 12h) and then it does not sensitively change at longer time of synthesis. Analysis of the relative intensity of the  $^{19}\text{F}$  NMR resonances suggests that the incorporation of germanium in the zeolite starts in the *d4r* and then in *mel* cage. As far as XRD concern, various phases have been observed during the crystallisation, and especially the ITR and ITH intergrowth are presents in both pure silica and Ge-containing samples, but also BEC is observed in Ge-containing samples. ITR and BEC structures have been detected mostly in the early stages of the synthesis and ITH mostly at longer time. A transformation of one phase into another following an ADOR process has been proposed[6]. However, further studies are needed to support this conclusion.

#### Reference

- [1] A. Corma, M. Puche, F. Rey, *Angewandte Chemie*, vol. **115**, no. 10, pp. 1188–1191, Mar. 2003,
- [2] A. Corma, M. J. Diaz-Cabanas, J. L. Jorda, *Journal of Physical Chemistry C*, vol. **113**, pp. 9305–9308, May 2009,
- [3] M. Fischer, C. Bornes, L. Mafra, J. Rocha, *Chem. Eur. J.* 2022, **28**, e202104298
- [4] A. Pulido, G. Sastre, and A. Corma, *ChemPhysChem*, vol. **7**, no. 5, pp. 1092–1099, May 2006,
- [5] J. A. Vidal-Moya, T. Blasco, F. Rey, A. Corma, *Chemistry of Materials*, vol. 15, no. 21, pp. 3961–3963, Oct. 2003
- [6] M. Shamzhy *et al* *Chemistry of Materials*, vol. 26, no. 19, pp. 5789–5798, Oct. 2014



## Ordered mesoporous carbons as promising electrocatalysts for the selective oxidation of lignin-derived molecules

P. Squillaci \*, D. Chillè, G. Papanikolaou, S. Perathoner, G. Centi and P. Lanzafame

Department of Chemical, Biological, Pharmaceutical and Environmental Sciences (ChiBioFarAm) – University of Messina, ERIC aisbl and CASPE/INSTM, V.le F. Stagno d'Alcontres 31, 98166 Messina, Italy.  
paolo.squillaci@unime.it

Ordered Mesoporous Carbons (OMCs) represent a sophisticated class of materials that exhibit significant potential for catalytic applications. Their highly organized mesoporous structure, combined with a large surface area and excellent thermal and chemical stability, makes them ideal candidates for catalytic applications [1].

In recent years OMCs have been identified as promising materials for electrocatalytic applications due to their well design structure which facilitates ions and electrons transfer. However, their poor hydrophilicity and low electrical conductivity could be improved by the incorporation of different heteroatoms leading to a more defective structure having additional active sites [2]. Among the various carbon replicas, those derived from SBA-15 are particularly noteworthy due to their uniform mesopores distribution which enhances accessibility to active sites. For this purpose, a carbon replica of the ordered mesoporous silica SBA-15 was synthesized, and its structure was subsequently modified by doping with various heteroatoms, including boron (B@OMC), nitrogen (N@OMC) and phosphorus (P@OMC). All materials were in depth characterized for investigating the textural and morfological properties using different techniques as N<sub>2</sub> adsorption, X ray diffractions (XRD), Raman spectroscopy and SEM/EDS analysis. The characterization results evidenced a good replication degree of silica frameworks presenting a prevalent mesoporous structure with high surface area (up to 1000 m<sup>2</sup>/g).

The synthesized materials were employed in the fabrication of electrocatalysts, and their electrocatalytic performance were investigated in the selective oxidation of lignin-derived molecules, with phenolic monomers being the most prominent class. Valorizing these phenolic monomers could yield chemicals with significant potential for use in various industries, including pharmaceuticals and plastic manufacturing [3].

The electrocatalytic activity of OMC based materials was studied in a commercial flow cell in a three electrodes configuration and compared with the results obtained using commercial boron doped diamond (BDD) and boron doped graphene (BDG) used as benchmark electrocatalysts (Figure 1).

The results pointed out that all OMCs are active in the selective oxidation of phenol to benzoquinone (BQ), a high added value product. In particular the best electrocatalytic performances were obtained when phosphorous was incorporated into the structure leading a phenol conversion up to 50% and BQ selectivity higher than 40%.

These findings highlight the potential of OMCs as electrocatalysts for the electrochemical valorization of lignin-derived molecules, offering a promising alternative to the critical raw materials traditionally used in these reactions.

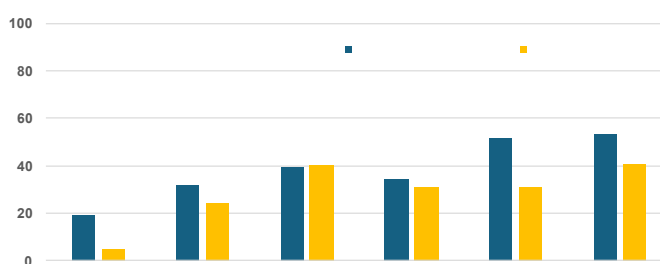


Figure 1. Phenol conversion and BQ selectivity of benchmarks and synthesized OMC based electrodes.

### References

- [1] A. Eftekhari and Z. Fan, *Mater. Chem. Front.*, **1**, 1001-1027 (2017).
- [2] Y. Gao, Q. Wang, G. Ji, A. Li and J. Niu, *RSC Advance*, **11**, 5361 (2021).
- [3] A. Di Tinno, R. Cancelliere, P. Mantegazza, et al., *Nanomater.*, **12**, 1779-1793 (2022).

### Acknowledgments

This work was realized in the frame of the activities of the EU project EPOCH (Electrocatalytic Production of liquid Organic hydrogen carrier and CHemicals from lignin; No. 101070976).

P.S. thank sthe Ministry of University and Research (MUR) for the grant received in the frame of the project D.M. 352 co-financed Versalis S.p.A(CUP J94D22000730009)

Corresponding author: Paolo Squillaci (paolo.squillaci@studenti.unime.it)



## Design of bi-functional Ni-zeolites for ethylene oligomerization: Controlling zeolite properties by one-pot and post-synthetic Ni incorporation

A. Martínez Gómez-Aldaraví, Christos Kanteler, C. Paris, M. Moliner, C. Martínez

Instituto de Tecnología Química, Universitat Politècnica de València-Consejo Superior de Investigaciones Científicas, Avenida de los Naranjos s/n, 46022 València, Spain

[ckantel@itq.upv.es](mailto:ckantel@itq.upv.es)

Light olefins ( $C_2^=$ - $C_6^=$ ) are considered to be important intermediates for the synthesis of various organic product, fuels, and solvents. More specifically, the oligomerization of light olefins has drawn an industrial interest due to the flexibility of selecting the starting material as well as the range of the molecular weight of the final product [1]. Acid zeolites have been extensively employed as efficient heterogeneous oligomerization catalysts when using propylene or higher olefins but, in the case of ethylene, the incorporation of transition metals enables the activation and conversion of the olefin under moderate temperature conditions [2]. Nickel is the most studied metal and traditionally post-synthesis ion-exchange, or impregnation methods are used for its addition to the zeolite-based support.

Here we present the rational design of a set of Ni-containing zeolites based on two crystalline structures, BEA and MFI, where the chemical composition (Si/Al ratios from 10 to 40) and Ni incorporation (by conventional post-synthesis impregnation and by one-pot synthesis employing N-ligands) were studied [3]. The samples have been thoroughly characterized and their catalytic behavior has been compared with that of commercial MFI and BEA with comparable Ni loadings in the oligomerization of ethylene to heavier olefins. Catalytic tests have been performed in a fixed-bed reactor under two different condition sets: 2.5 bar, 180°C, 16.3 h<sup>-1</sup> and 2.5 vol% C<sub>2</sub>H<sub>4</sub> and 35 bar, 200°C, 2.1 h<sup>-1</sup> and 15 vol% C<sub>2</sub>H<sub>4</sub>.

According to the characterization results obtained for the different Ni-zeolites prepared, the formation of NiO nanoclusters inside the zeolitic pores is favored by the one-pot synthesis of nanocrystalline Ni-zeolites, while nickel incorporation by post-synthesis impregnation lead to higher contents of cationic Ni<sup>2+</sup> in ion exchange positions, species that are better stabilized for zeolites with higher Al contents.

Regarding the catalytic behavior of these samples, when working under near ambient pressure, low partial pressure and high space velocity, crystal size does not play a decisive role, and catalysts prepared by post-synthesis methods are more active due to the higher amount of Ni<sup>2+</sup> species. When reaction is performed under higher pressures and higher ethylene/catalyst ratios, more representative of industrial operation, other factors besides Ni speciation play an important role in the catalytic behavior of the bifunctional Ni-catalysts. Thus, the nano-sized zeolites are more active and more stable towards deactivation than the commercial-based catalysts with larger crystals (see Figure 1) and present a higher selectivity to C<sub>5+</sub> hydrocarbons and one-pot Ni incorporation increases even more the yields to heavier oligomers.

### References

- [1] C. Martínez, A. Corma, *Coord. Chem. Rev.*, **255**, 1550-1558, (2011)
- [2] C.P. Nicholas, *Appl. Catal. A Gen.*, **543**, 82, (2017)
- [3] A. Martínez Gómez-Aldaraví, C. Paris, M. Moliner, C. Martínez, *Journal of Catalysis*, **426**, 140, (2023)
- [4] E.M. Gallego, C. Paris, M.R. Díaz-Rey, M.E. Martínez-Armero, J. Martínez-Triguero, C. Martínez, M. Moliner, A. Corma, *Chem. Sci.*, **8**, 8138, (2017)

### Acknowledgments

This work has been supported by Spanish Government through PID2021-122755OB-I00 funded by MCIN/AEI/10.13039/501100011033 and TED2021-130739B-I00 funded by MCIN/AEI/10.13039/501100011033/EU/PRTR). Financial support by Severo Ochoa centre of excellence program (CEX2021-001230-S) is also gratefully acknowledged. AMGA acknowledges the Spanish Government for a Severo Ochoa FPI scholarship (PRE2019-088361). CK acknowledges the Spanish government for a FPI scholarship (PRE2022-10366).



## LEU-2: a new pure silica zeolite with 10-ring channels

J. Bae<sup>1</sup>, D. Plessers<sup>1</sup>, L. B. McCusker<sup>2</sup>, M. Dusselier<sup>1</sup>

<sup>1</sup> Center for Sustainable Catalysis and Engineering (CSCE), KU Leuven, Celestijnenlaan 200F, 3001 Leuven, Belgium.

<sup>2</sup> Department of Materials, ETH Zurich, 8093 Zurich, Switzerland (retired).

Juna.bae@kuleuven.be

The introduction of amines and quaternary ammonium cations as organic structure-directing agents (OSDAs) in zeolite synthesis has facilitated the formation of new ordered domains in (semi)crystalline networks, leading to the extensive discovery of new zeolites and related materials [1,2]. This has led to attempts to design new types of compounds suitable for use as SDAs. Supramolecules offer unique conformations that are not found in common organic molecules. The use of supramolecular SDAs in zeolite synthesis was first reported in 1990, when high-silica faujasite (framework type **FAU**) and its hexagonal analog (framework type **EMT**) were crystallized using crown ether complexes with Na<sup>+</sup> ions [3]. Since then, the use of metal-organic complexes, typically in the form of 0-dimensional clusters, has allowed several new framework types (e.g., **DON**, **JST**, **JSR**) to be found, and transition metals (e.g., Ni, Cu) to be loaded directly into cage-based, small-pore molecular sieves (e.g., **AEI**-, **CHA**- and **SAV**-type materials).

Understanding the preferred coordination geometries of metal centers together with appropriately selected (or designed) organic ligands has enabled the formation of diverse coordination compounds with extended dimensions. To our knowledge, however, there are few examples where high-dimensional coordination polymers have been utilized as SDAs or templates in the crystallization of 3D open-framework inorganic oxide-based materials. Among these are an aluminoborate, [Zn(DAP)<sub>2</sub>][AlB<sub>5</sub>O<sub>10</sub>] (DAP = 1,3-diaminopropane), interpenetrated with a 2D Zn-DAP coordination polymer with square lattice topology [4], and two isostructural borates, M(DAP)[B<sub>4</sub>O<sub>7</sub>] (M = Co and Zn), where the transition metal in a helical M-DAP chain is directing the structure of the borate walls [5,6]. In particular, this approach has not yet been applied to silica-based zeolitic systems. Here, we report the synthesis and structure of LEU-2, a novel pure silica zeolite with 10-membered rings that was made via a similar but unique process (with post-synthetic steps) combined with the use of interzeolite conversion [7]. The details of the structure direction process will be a part of the presentation as will be further information on the novel topology. LEU-2 crystallizes as thin plates (Figure 1a) and contains a 1D channel system consisting of straight 10-ring channels along the b-axis (Figure 1b). This zeolite has a framework density of 20.1 T-atoms per 1000 Å<sup>3</sup>, which is relatively high when compared with other medium-pore materials, partly accounting for the low micropore volume (0.04 cm<sup>3</sup> g<sup>-1</sup>) measured by N<sub>2</sub> adsorption.

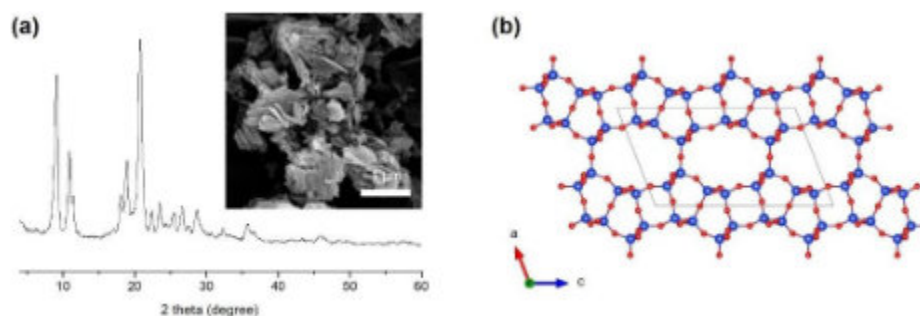


**Figure 1.** (a) Powder XRD pattern and SEM image of LEU-2. (b) Structure of LEU-2 viewed along the b-axis.

### References

- [1] L. Gómez-Hortigüela and M. A. Camblor, *Insights into the chemistry of organic structure-directing agents* Ch. 1, Springer (2018).
- [2] C. Baerlocher and L. B. McCusker, *Database of Zeolite Structures* (Structure Commission of the International Zeolite Association, accessed in July 2024); <http://www.iza-structure.org/databases/>.
- [3] F. Delprato, L. Delmotte, J. L. Guth and L. Huve, *Zeolites*, **10**, 546-552 (1990).
- [4] L. Wei, Q. Wei, Z. -E. Lin, Q. Meng, H. He, B. -F. Yang and G. -Y. Yang, *Angew. Chem. Int. Ed.*, **53**, 7188-7191 (2014).
- [5] C. -Y. Pan, L. -J. Zhong, F. -H. Zhao, H. -M. Yang and J. Zhou, *Chem. Commun.*, **51**, 753-756 (2015).
- [6] S. -C. Zhi, Y. -L. Wang, L. Sun, J. -W. Cheng and G. -Y. Yang, *Inorg. Chem.*, **57**, 1350-1355 (2018).
- [7] J. Devos, M. A. Shah and M. Dusselier, *RSC. Adv.*, **11**, 26188-26210 (2021).

### Acknowledgments

This work was performed with the financial support of the Research Foundation Flanders (FWO Vlaanderen) for personal postdoc funding (12E6923N to J.B.).





## Zeolite-Catalyzed 1,2-Dibromination of Cinnamates: A Green and Efficient Approach to $\alpha,\beta$ -Dibromohydrocinnamates

M. Jurin<sup>1,2</sup>, A. Palčić<sup>1\*</sup>

<sup>1</sup> Ruđer Bošković Institute, Bijenička cesta 54, 10000 Zagreb, Croatia

<sup>2</sup> Institute for Anthropological Research, Ljudevita Gaja 32, 10 000 Zagreb, Croatia

ana.palcic@irb.hr

Organobromine compounds, also known as organobromides, are a diverse group of chemical substances that include both naturally occurring and synthetic substances with a wide range of biological and chemical properties. These compounds are characterized by the presence of one or more bromine atoms attached to an organic framework [1]. Organobromides serve as important synthetic intermediates in the production of various derivatives of natural products, pharmaceuticals, agrochemicals, and other fine chemicals [2]. They are extremely valuable building blocks for a number of fundamental chemical transformations, including Grignard reactions, cross-coupling reactions, and nucleophilic substitutions [3]. Zeolites are a special class of inorganic microporous crystalline aluminosilicates [4] that have a wide range of applications in numerous large-scale industries. These include use as catalysts, materials for ion exchange and adsorbents for organic compounds (5). In addition, zeolites have been developed into advanced functional materials used in other fields, including luminescence, electrical engineering, magnetism, medicine and microelectronics [6].

In the present research, the  $\alpha,\beta$ -dibromohydrocinnamate derivatives were synthesized by 1,2-dibromination of a various *trans*-cinnamates in the presence of 1,3-dibromo-5,5-dimethylhydantoin (DBDMH) as a bromine source, and a zeolite (beta (Si/Al = 12), Y (Si/Al = 26) or ZSM-5 (Si/Al = 24)) as a catalyst in diethyl ether at room temperature. The reusability of the zeolites H $\beta$ , HY and HZSM-5 as catalysts for the bromination of methyl *trans*-cinnamate to  $\alpha,\beta$ -dibromo-3-phenylpropanoate was also investigated. The catalysts were successfully recovered after reaction by centrifugation, washing, and then calcination at 550 °C. This process was repeated for two further cycles, demonstrating the catalysts' high stability and activity with no significant loss of performance. The recovered catalysts were analyzed using IR, UV-Vis, PXRD, SEM and TG.

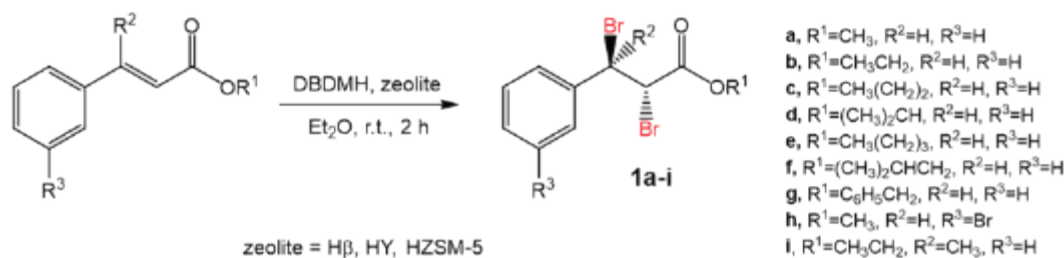


**Figure 1.** Zeolite-catalyzed bromination of various cinnamates.

The results showed that the conversion of cinnamate exceeded 67% with both zeolite beta and Y. ZSM-5 is not as effective a catalyst as the other two. The catalyst-free reactions resulted in lower conversions compared to the zeolite-catalyzed reactions. The results of the <sup>1</sup>H NMR analysis indicated that the 1,2-dibromination proceeded with *anti*-stereoselectivity in all cases, and gave the 1,2-dibromide compounds. It was also found that the catalysts can be recycled three times without significant loss of catalytic activity. The TG analysis of catalysts showed differences after each cycle.

This study shows the significant influence of zeolite pore architecture on the reaction outcome, with the H $\beta$  zeolite showing the highest catalytic activity. It also highlights the advantages of using zeolites as catalysts for this transformation, including mild reaction conditions, high conversions, short reaction times, and a wide range of cinnamate substrates. The reusability of the zeolites has also demonstrated, highlighting their potential for environmentally and sustainable chemical synthesis.

### References

- [1] G.W. Gribble, *Environ Sci Pollut Res Int.*, **7**, 37-47 (2000).
- [2] H. Xue, H. Tan, D. Wei, Y. Wei, S. Lin, F. Liang, B. Zhao, *RSC Adv.*, **3**, 5382–5385 (2013)
- [3] L. Wang, L. Zhai, J. Chen, Y. Gong, P. Wang, H. Li, X. She, *J. Org. Chem.*, **87**, 3177–3183 (2022)
- [4] S. Gaber, D. Gaber, I. Ismail, S. Alhassan, M. Khaleel, *CrystEngComm*, **21**, 1685–1690 (2019)
- [5] Y. Li, J. Yu, *Nature Reviews Materials*, **6**, 1156–1174 (2021)
- [6] J. Li, A. Corma, J. Yu, *Chem. Soc. Rev.*, **44**, 7112–7127 (2015)

### Acknowledgments

The authors would like to thank the Croatian Science Foundation for funding this research (Project ID: UIP-2019-04-4977).



## Enhanced Hydrodeoxygenation of m-Cresol via Pt/HY Catalysts in Microwave-Assisted Systems: A Pathway to Efficient Bio-Oil Upgrading

C.B. Souza<sup>1</sup>, J.M.A.R. de Almeida<sup>2</sup>, J. Garcia-Martinez<sup>3</sup>, P.N. Romano<sup>4</sup>

<sup>1</sup> EPQB/EQ, Universidade Federal do Rio de Janeiro, Av. Athos da Silveira Ramos, 149, Rio de Janeiro, Brazil 21941-909

<sup>2</sup> Instituto de Química, Universidade Federal do Rio de Janeiro, Av. Athos da Silveira Ramos, 149, Rio de Janeiro, Brazil 21941-909

<sup>3</sup> Laboratorio de Nanotecnología Molecular, Departamento de Química Inorgánica, Universidad de Alicante, 03690, Alicante, Spain

<sup>4</sup> Campus Duque de Caxias, Universidade Federal do Rio de Janeiro, Rodovia Washington Luiz, 19593, Rio de Janeiro, Brazil, 25240-005.

pedro.romano@caxias.ufrj.br

### Motivation

The increasing demand for energy solutions has shifted attention toward lignocellulosic biomass as a renewable source for producing eco-friendly fuels and chemicals. Hydrodeoxygenation (HDO) of lignin-derived compounds, such as m-cresol, is a key process in converting biomass into high-energy hydrocarbons by removing oxygen atoms. However, the C-O bond dissociation in phenolic compounds presents a challenge, typically requiring harsh reaction conditions ( $T > 300^{\circ}\text{C}$ ,  $P \sim 30$  bar) [1,2]. To address this, the development of bifunctional catalysts that combine metal and acid properties has emerged as a promising strategy to enhance HDO efficiency by facilitating cooperative interactions between active sites [3]. In this sense, it is widely believed that the metal sites are responsible for saturating the phenolic ring, reducing the stability of the OH group, followed by an acid catalyzed dehydration step.

On the other hand, microwave-assisted reactions are gaining traction as an electrification strategy for chemical processes, offering rapid and uniform heating that can enhance reaction rates while reducing energy consumption [4]. In this work, we report for the first time the use of microwave (MW) heating for hydrodeoxygenation (HDO) under mild conditions ( $150^{\circ}\text{C}$  and 10 bar of  $\text{H}_2$ ), using m-cresol as a model compound for pyrolysis oil. Additionally, we compared the performance of conventional and MW heating systems using Pt/ $\text{Al}_2\text{O}_3$  and Pt/HY catalysts, highlighting the critical role of bifunctional properties and zeolite acidity in achieving efficient HDO conversion.

### Results and Discussion

The performance of Pt/ $\text{Al}_2\text{O}_3$  and Pt/HY catalysts under microwave (MW) heating are markedly different as shown in Figure 1 (a, b) and Table 1. The Pt/ $\text{Al}_2\text{O}_3$  catalyst showed poor deoxygenation activity under the mild conditions ( $175^{\circ}\text{C}$ , 10 bar  $\text{H}_2$ ), producing mainly methylcyclohexanol and methylcyclohexanone products of ring hydrogenation catalysed by metal sites, followed by tautomerisation. Complete conversion was achieved after 90 minutes, but the yield for methylcyclohexane was only 2.5%, with no formation of toluene, a major HDO product. The inability of Pt/ $\text{Al}_2\text{O}_3$  to completely hydrodeoxygenate m-cresol can be attributed to its weak acidity. In stark contrast, Pt/HY showed full conversion with 100% yield for methylcyclohexane in only 10 minutes, demonstrating its exceptional HDO activity. The m-cresol conversion rate for Pt/HY was  $2.5 \text{ mmol.gcat}^{-1}.\text{min}^{-1}$ , almost three times higher than that of Pt/ $\text{Al}_2\text{O}_3$ . In addition, the rate of HDO product formation was significantly higher,  $2.50 \text{ mmol.gcat}^{-1}.\text{min}^{-1}$  for Pt/HY compared to only  $0.02 \text{ mmol.gcat}^{-1}.\text{min}^{-1}$  for Pt/ $\text{Al}_2\text{O}_3$ . This remarkable difference in performance highlights the critical role of the synergy between metal and acid sites. This is further supported by the turnover frequency (TOF) values, with Pt/HY exhibiting a TOF of  $12.5 \text{ s}^{-1}$ , almost a four-fold increase over the  $3.3 \text{ s}^{-1}$  observed for Pt/ $\text{Al}_2\text{O}_3$ .

**Table 1:** Methylcyclohexane yields, reaction rates and TOF for the Pt/ $\text{Al}_2\text{O}_3$  and Pt/HY catalysts.

Catalyst	Methylcyclohexane yield (%) <sup>a</sup>	m-cresol conversion rate (mmol.gcat <sup>-1</sup> .min <sup>-1</sup> )	Methylcyclohexane production rate (mmol.gcat <sup>-1</sup> .min <sup>-1</sup> )	TOF (s <sup>-1</sup> )
1%Pt/ $\text{Al}_2\text{O}_3$	2.5%	0.86	0.02	3.3
1%Pt/HY	100%	2.50	2.50	12.5

<sup>a</sup>Reaction conditions:  $175^{\circ}\text{C}$ , 10 bar  $\text{H}_2$ , 600 rpm, 0.1 M m-cresol in dodecane.

Given the high activity of the Pt/HY catalyst, achieving full conversion within just 10 minutes, we decided to further reduce the reaction temperature to  $150^{\circ}\text{C}$  and increase the concentration of the m-cresol solution by a factor of five. The results, shown in Figure 1d, indicate that even with a lower temperature and a higher m-cresol/catalyst ratio, full conversion was achieved within 15 minutes, with 86% selectivity for methylcyclohexane, the desired HDO product. Complete conversion to methylcyclohexane was observed after 90 minutes. To evaluate the specific influence of microwave (MW) heating on the catalyst's remarkable performance under mild conditions, we compared the MW system with a conventional reactor. The results of the reaction using conventional heating at  $150^{\circ}\text{C}$  and 10 bar with the Pt/HY catalyst are shown in Figure 1c. In this case, full conversion of m-cresol occurred only after 120 minutes,

with intermediates such as toluene, methylcyclohexanol, and methylcyclohexanone detected. These findings suggest that MW heating plays a significant role in accelerating the reaction rate. The rate of methylcyclohexane formation under MW heating ( $8.3 \text{ mmol.gcat}^{-1}.\text{min}^{-1}$ ) was 2.5 times higher than that achieved in the conventional reactor ( $3.4 \text{ mmol.gcat}^{-1}.\text{min}^{-1}$ ). Moreover, the presence of methylcyclohexanol and methylcyclohexanone during the early stages of the conventional reaction indicates that the process likely begins with ring hydrogenation catalyzed by the Pt metal sites, followed by an acid-catalyzed dehydration step.

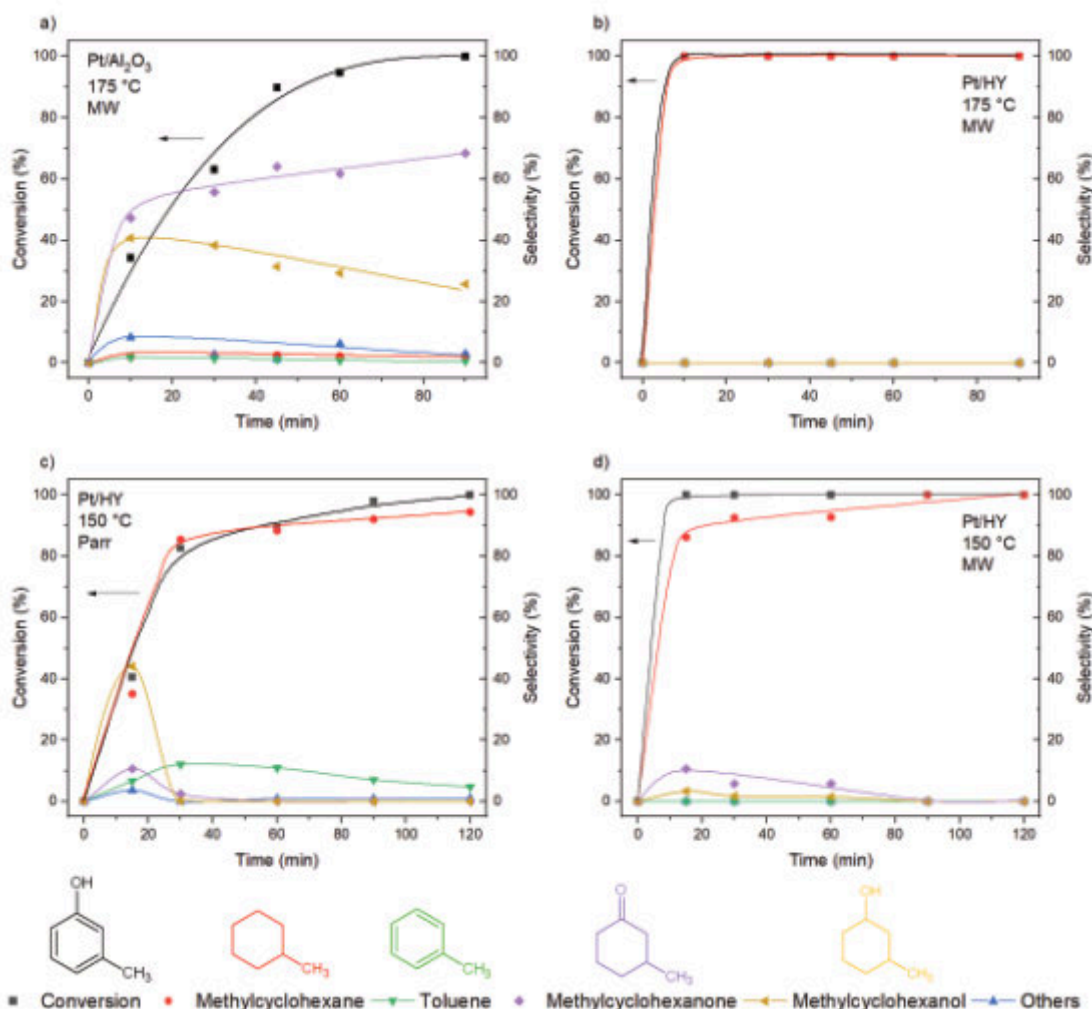


**Figure 1.** m-cresol HDO reactions using **a)** Pt/Al<sub>2</sub>O<sub>3</sub>, MW heating at 175 °C, 10 bar H<sub>2</sub>, 600 rpm, 0.1 M m-cresol in dodecane. **b)** Pt/HY, MW heating at 175 °C, 10 bar H<sub>2</sub>, 600 rpm, 0.1 M m-cresol in dodecane. **c)** Pt/HY, Parr reactor at 150 °C, 10 bar H<sub>2</sub>, 600 rpm, 0.5 M m-cresol in dodecane. **d)** Pt/HY, MW heating at 150 °C, 10 bar H<sub>2</sub>, 600 rpm, 0.5 M m-cresol in dodecane.

## Conclusions

In conclusion, the Pt/HY catalyst demonstrated markedly superior performance in the microwave-assisted hydrodeoxygenation (HDO) of m-cresol under mild conditions, compared to the Pt/Al<sub>2</sub>O<sub>3</sub> catalyst. The synergy between the metal and acid sites on Pt/HY enabled complete conversion and high selectivity toward methylcyclohexane in a remarkably short reaction time, emphasizing the value of bifunctional catalytic properties. Moreover, microwave heating proved instrumental in significantly accelerating reaction rates and boosting efficiency compared to conventional heating. More specifically, under conventional heating at 150 °C, full conversion of m-cresol took 2 hours. In contrast, microwave heating at the same temperature reduced the reaction time to just 20 minutes. These findings highlight the potential of combining bifunctional catalysts with microwave-assisted processes for more efficient bio-oil upgrading, contributing to the advancement of sustainable and electrified chemical processes.

## References

- [1] Huang, R., Kwon, O., Lin, C. & Gorte, R. J., *Journal of Catalysis* **398**, 102–108 (2021).
- [2] Sosa, L. F. *et al.*, *Applied Catalysis B: Environmental* **331**, 122720 (2023).
- [3] Hunns, J. A. *et al.*, *ACS Catal.* **14**, 7052–7061 (2024).
- [4] Romano, P. N. *et al.*, *ChemSusChem* **9**, 3387–3392 (2016).



## Crystal size and morphology control of SAPO-40 zeolite

Jie Du<sup>1</sup>, Yao Lu<sup>1</sup>, Yin Liu<sup>1</sup>, Yong Wang<sup>1</sup>, Peipei Xiao<sup>1</sup>, Toshiyuki Yokoi<sup>1,\*</sup>

*1. Institute of Innovative Research, Tokyo Institute of Technology, 4259 Nagatsuta-cho, Yokohama, 226-8503 Japan*

*\*Corresponding author, yokoi@cat.res.titech.ac.jp*

In this study, SAPO-40 zeolites with different crystal sizes and morphologies were synthesized by adjusting the amount of organic structure-directing agent (OSDA) and adding cetrimonium bromide (CTAB). The crystal size was decreased with a low amount of OSDA. Introduction of CTAB resulted in the formation of a new hexahedral stone morphology crystal. The characterization results demonstrated that the changes in the amount of OSDA and/or the addition of CTAB not only affected the crystal size and morphology but also influenced the acidity as well as hydrophilicity/hydrophobicity.

### Introduction

SAPO-40 is a 2-dimensional silicoaluminophosphate AFR-type zeolite with 12-ring channels and intersected 8-ring channels, and it exhibits highly stable toward thermal and hydrothermal treatments. The high stability is essential for the dehydration of glycerol to acrolein, as the reaction takes place at high temperatures and in the presence of water. Fernandes et al. [1] used tetrapropylammonium hydroxide (TPAOH) and [3-(trimethoxysilyl)propyl]-octadecyldimethyl-ammonium chloride (TPOAC) as mixture templates to prepare hierarchical SAPO-40. Compared with conventional SAPO-40, the hierarchical SAPO-40 exhibited higher acrolein selectivity and a significantly longer catalytic lifetime in the dehydration of glycerol to acrolein reaction. Recently, Zhou et al. [2] reported that the morphology of SAPO-34 varied from a cubic stacked structure to a spherical shape by increasing the amount of CTAB. CTAB acts as a cationic surfactant and is able to combine with anionic species (such as silicate, aluminate, phosphate, etc.) through electrostatic interaction in the precursor of SAPO-34 zeolite. Therefore, the crystal nucleus would be agglomerated and contribute to different morphologies. Taking inspiration from this, in this research, the morphology of SAPO-40 was controlled by varying the OSDA amount and/or the addition of CTAB.

### Experimental

The SAPO-40 zeolites were synthesized according to the published paper [1]. Briefly, pseudoboehmite, water, and ortho-phosphoric acid were mixed and stirred for 3 h. Then a mixture solution of TPAOH and fumed silica was added, and the gel was stirred for another 3 h. After that, the seed was added into the mixture. The final gel with a molar composition of 1 Al<sub>2</sub>O<sub>3</sub>: 1.04 P<sub>2</sub>O<sub>5</sub>: 0.2 SiO<sub>2</sub>: 2.0 TPA: 60 H<sub>2</sub>O was crystallized at 200 °C for 120 h under static condition. The as-synthesized product was obtained after washing, filtering, and drying. The as-synthesized product was subsequently calcined at 550 °C for 6 h in air, and thus obtained sample was named SAPO-40-2.0TPA.[1] SAPO-40-1.1TPA was synthesized using the same method but with a reduced TPA/Al<sub>2</sub>O<sub>3</sub> ratio of 1.1. In addition, SAPO-40-1.1TPA-0.2CTAB was obtained by adding 0.2 molar ratio of CTAB/Al<sub>2</sub>O<sub>3</sub> to the synthesis gel, similar to SAPO-40-1.1TPA.

### Results and Discussion

Figure 1A shows the XRD patterns, indicating the formation of the AFR structure for the three samples. In the cases of SAPO-40-1.1TPA and SAPO-40-1.1TPA-0.2CTAB, the intensity of peak (110) increased, while that of peak (200)

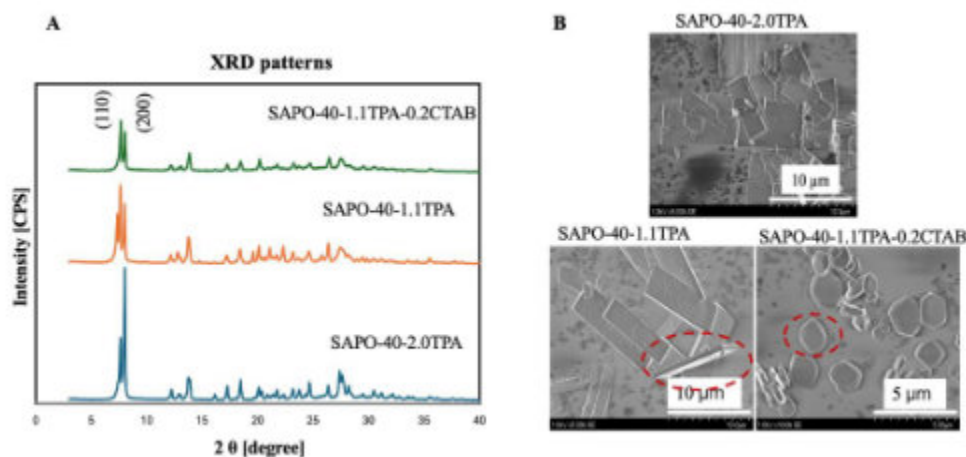


Figure 1 A: XRD patterns and B: SEM images of SAPO-40 zeolites.



decreased, which possibly due to the change of crystal morphology. The assumptions can be verified by the SEM images in Figure 1B. SAPO-40-2.0TPA was a rectangular sheet with a thickness of 0.1-0.2  $\mu\text{m}$ , but the thickness of SAPO-40-1.1TPA was 0.4-0.6  $\mu\text{m}$ . After adding CTAB, the morphology was changed from a thin sheet to a hexagonal stone with a size of 2-3  $\mu\text{m}$ .

Table1. The chemical and physical properties of the prepared samples

Samples	$S_{\text{BET}}$ [ $\text{m}^2\text{g}^{-1}$ ] <sup>a</sup>	$V_{\text{micro}}$ [ $\text{cm}^3\text{g}^{-1}$ ] <sup>b</sup>	$V_{\text{meso}}$ [ $\text{cm}^3\text{g}^{-1}$ ] <sup>c</sup>	$V_{\text{total}}$ [ $\text{cm}^3\text{g}^{-1}$ ] <sup>a</sup>	Acid amount (mmol/g) <sup>d</sup>		
					Weak	Medium	Strong
SAPO-40-2.0TPA	747	0.31	0.106	0.411	0.42	0.21	0.51
SAPO-40-1.1TPA	745	0.30	0.103	0.404	0.31	0.11	0.13
SAPO-40-1.1TPA-0.2CTAB	510	0.18	0.230	0.406	1.04	0.38	0.25

<sup>a</sup> Based on the Brunauer-Emmett-Teller (BET) equation.

<sup>b</sup> Calculated by the t-plot method.

<sup>c</sup> Calculated by the BJH method.

<sup>d</sup> Determined by  $\text{NH}_3$ -TPD; fitting curves of the weak, medium, and strong acid amount were calculated at approximately 150, 250, and 320  $^\circ\text{C}$ , respectively.

Table 1 listed the porosity and acidic data of the prepared zeolites. The BET surface area of SAPO-40-1.1TPA is similar with that of SAPO-40-2.0TPA. However, the BET surface area of SAPO-40-1.1TPA-0.2CTAB is relatively smaller than that of SAPO-40-1.1TPA, mainly due to the morphology change by adding CTAB.

The strong acidity exhibited by SAPO-type materials results from the isomorphous incorporation of Si into the structure and it is dependent both on the amount of Si incorporated and on the mechanism of Si incorporation, being the formation of silica islands (from heterogeneous SM3 or homogeneous SM2 + SM3 mechanisms) responsible for the generation of the strongest acid sites [3]. Compared with SAPO-40-2.0TPA, the decrease of TPA content in SAPO-40-1.1TPA resulted in the reduction of the binding of silicon atoms in the form of silica islands and the reduction of strong acid sites. However, the strong acid site of SAPO-40-1.1TPA-0.2 CTAB increased after adding CTAB.

## Conclusion

SAPO-40 zeolites with different morphologies were synthesized by adjusting the amount of OSDA and/or adding CTAB. The changed morphology influenced the acidity and adsorption ability, possibly expanding the application in catalytic reaction and adsorption separation in the future.

## References

- [1] A. Fernandes, M. F. Ribeiro, J.P. Lourenço, Catal. Commun., 95 (2017) 16-20.
- [2] Z. Zhou, X. Wang, R. Jiang, Adv. Powder Technol., 33 (2022) 103414.
- [3] J.P. Lourenço, A. Fernandes, R.A. Bertolo, M.F. Ribeiro, RSC Adv., 5 (2015) 10667-10674.



## Neutron total scattering unravels pre-zeolite structures in amorphous aluminosilicate gels

L. Gigli<sup>1</sup>, A. Morsli<sup>2</sup>, D. T. Bowron<sup>3</sup>, S. Imberti<sup>3,\*</sup>, S. Quartieri<sup>4</sup>, A. Bengueddach<sup>5</sup>, F. Di Renzo<sup>6</sup>, R. Arletti<sup>4</sup>

<sup>1</sup> Elettra-Sincrotrone Trieste, Basovizza, Trieste, Italy

<sup>2</sup> Laboratory of Engineering of Environmental Processes, University of Science and Technologies of Oran "M. Boudiaf", Oran, Algeria

<sup>3</sup> ISIS Rutherford Appleton Laboratory, Didcot, United Kingdom

<sup>4</sup> Department of Chemical and Geological Sciences, University of Modena and Reggio Emilia, Italy

<sup>5</sup> Oran, Algeria

<sup>6</sup> ICGM, University of Montpellier-CNRS-ENSCM, Montpellier, France

\*Current address: ACS Publications, ACS International Ltd., Oxford, United Kingdom

Francesco.di-renzo@umontpellier.fr

Amorphous aluminosilicate hydrogels find important applications as glazers, binders and concrete additives, often under the name of geopolymers. They are also intermediates in the hydrothermal synthesis of most zeolites, ordered microporous materials produced at million-ton scale for ion exchange, catalysis and adsorption applications. The structure of the amorphous precursors has always been considered as having a paramount influence in the nucleation and growth of zeolites, especially as a controlling factor in the selectivity of phase formation. The amorphous nature of the phases that take part in the molecular processes occurring during evolution of aluminosilicate hydrogels has made nanoscale research challenging. Here, we investigated the local structure of sodium-aluminosilicate hydrogels with different chemistry by means of total scattering neutron diffraction. The data have been modeled using **EPSR (empirical potential structure refinement) [1,2] to provide a consistent and detailed structural model in terms of network forming elements (Si, Al) and network modifier elements (Na, OH, H<sub>2</sub>O).** These structural information can improve the knowledge on the nucleation of the microporous materials and the factors that control the properties of geopolymers.

### Materials

A series of sodium aluminosilicate hydrogels with Si/Al ratios from 1.5 to 24, representing the precursors of zeolites from Na-X to Na-ZSM-5, have been prepared by mild hydrothermal synthesis. Equilibrated gels have been formed by keeping reaction mixtures at the synthesis temperature of each zeolite for a duration significantly shorter than the crystallization time of the zeolite. The Al-richest precursor gels of zeolite X have been formed at 80°C for 4 h. The Si-richest precursors of ZSM-5 have been formed at 170°C for 4 h.

### Multi-technique characterization

Lab **powder XRD** (Cu K $\alpha$  radiation) confirmed the amorphous nature of the materials. The position of the main XRD hump typical of amorphous silicates was correlated to the composition of the gel. Its position as a function of the Al content of the gel is shifted from about 23° 2 $\theta$  (3.9 Å) for the silica-richest gels to 30° 2 $\theta$  (3 Å) for the aluminum-richest gels. If the 3.9 Å parameter is classical for silica gels or glasses, lower characteristic distances in the presence of Al have not yet been satisfactorily explained. <sup>27</sup>Al and <sup>29</sup>Si **MAS-NMR** indicated that all aluminum and silicon were in tetrahedral coordination. The distribution of Q4 and Q3 peaks of <sup>29</sup>Si NMR allowed to determine the distribution of lattice Al and silanol defects.

For the **total scattering neutron diffraction** experiments, the samples have been deuterated and dried at 80°C under N<sub>2</sub> flow. Neutron diffraction data have been collected at SANDALS beamline at ISIS Rutherford Appleton Laboratory. The structural characterization of two samples with Al/(Si+Al) 0.05 and 0.22 (henceforth named Al05 and Al22, respectively) is presented in this communication. EPSR start as a standard Monte Carlo simulation, where both samples have been described by a cubic box with periodic boundary condition containing 13830 or 10316 atoms for the sample Al05 or Al22, respectively. After this first step, the structure factors of the model are calculated and compared with the experimental data. The difference between them is used to generate a set of empirical potential perturbation functions with the aim to drive the model towards the experimental coordination determined by <sup>29</sup>Si NMR.

### Results

The model obtained by EPSR reproduces successfully the experimental data for both samples. The analyses of the partial  $g(r)$  of T-O, Na-Ow and O-Na provide bond lengths and distributions of coordination number, reported in table 1, that are a clear indication of the topology of the materials (Fig. 1). The neutron diffusion data confirm the <sup>27</sup>Al MAS-NMR information about the tetrahedral coordination of Al, as expected by the favoured formation of aluminate anions in the alkaline conditions in which the materials have been formed. The degree of condensation of the tetrahedra is correlated to the amount of Al, the number of interruptions of the framework being significantly higher in the Si-rich sample. This is consistent with the well-known effect of aluminate as condensing agents for silicates in alkaline conditions, where silica alone would be highly soluble. The incorporation in the network of aluminate anions



requires the presence of charge compensating cations. From this point of view, the degree of coordination of Na with the oxygens of the aluminosilicate framework is extremely relevant. Na is coordinated to more than 5 network oxygens in the Al-rich sample and to 2-3 network oxygens in the Si-rich sample. The different environment of sodium in the two samples is critical to the understanding of their topology.

**In the Si-rich sample Al05**, Na is coordinated to  $2.3 \pm 0.2$  network oxygens and  $7.5 \pm 0.7$  H<sub>2</sub>O molecules. In effect, Na essentially stabilizes water clusters at the surface of the silicate, accounting for the significant retention of water in the sample. XRD hump near 4 Å is typical of silica gels or glasses and traditionally attributed to a disordered cristobalite-like structure. It is remarkable that sample Al05 presents an XRD characteristic distance of 3.9 Å, despite its extremely interrupted network. It can be observed that also the most intense diffraction peak of silica-rich MFI is at 3.85 Å.

**In the Al-richer sample Al22**, the charge compensation of the network anions is at the basis of a structure-directing role of Na. The coordination of the Na cation is nearly saturated by  $5.4 \pm 0.4$  network oxygens and  $2.1 \pm 0.2$  H<sub>2</sub>O molecules, a configuration reminiscent of the organization of zeolite tetrahedra around structuring cations, for instance Na in site I of faujasite. Each water molecule is coordinated to  $1.1 \pm 0.2$  Na and  $1.9 \pm 0.2$  other water molecules, themselves coordinated to another Na each. This configuration is compatible with a continuous network of water molecules alternating with sodium cations, itself surrounded by partially condensed aluminosilicate rings. It seems reasonable that this amorphous zeolite-like structure can easily evolve to a periodic zeolite network.

**Table 1.** Composition of samples Al05 and Al22 and coordinations obtained by EPSR in  $g(r)$ : Tet is Si+Al. Si-O is the number of lattice oxygen coordinated to the average Si; Na-OW is the number of water molecules coordinated to the average Na.

	Al05	Al22
Al/tet	0.05	0.22
H <sub>2</sub> O/tet	3.22	0.71
Si-O	3.20	3.62
Si-OH	0.34	0.17
Si-OW	0.41	0.14
Total Si coordination	3.95	3.92
Al-O	2.50	3.30
Al-OH	0.24	0.15
Al-OW	1.20	0.34
Total Al coordination	3.95	3.90
Na-O	2.33	5.38
Na-OW	7.52	2.05
OW-Na	0.06	1.06
OW-OW	5.0	1.9

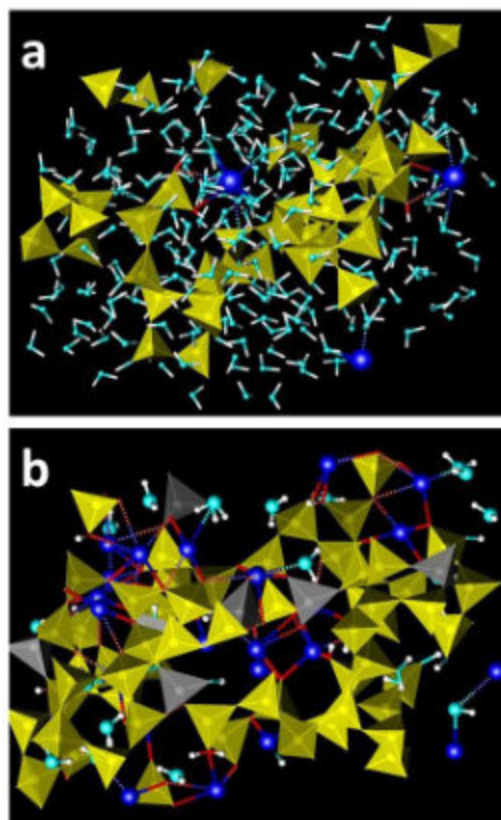


**Figure 1.** Local structures of Al05 (a) and Al22 (b) samples obtained by EPSR. Yellow Si tetrahedra, grey Al tetrahedra, deep blue Na cations, light blue oxygen and white hydrogen atoms of H<sub>2</sub>O.

## References

- [1] A. Soper, *EPSR shell: A User's Guide*, ISIS Disordered Materials Group, Didcot, U.K. (2010).
- [2] D. S. Sivia, *Elementary Scattering Theory for X-ray and Neutron User*, Oxford University Press, Oxford, U.K. (2012).



## Assessing the effect of zeolites structure into ethanol to butanol selective conversion by Guerbet reaction

E. Cocco<sup>1</sup>, A. Marino<sup>1</sup>, R. Passalacqua<sup>2</sup>, A. Carlone<sup>1</sup>, M. Crucianelli<sup>1</sup>, A. Aloise<sup>1</sup>

<sup>1</sup> Department of Physical and Chemical Sciences, University of L'Aquila, via Vetoio, Coppito 2 - 67100 L'Aquila, Italy

<sup>2</sup> Department of Chemical, Biological, Pharmaceutical and Environmental Sciences (ChiBioFarAm) & INSTM CASPE (Lab. of Catalysis for Sustainable Production & Energy) - University of Messina Viale F. Stagno d'Alcontres, 31 - 98166 Messina, Italy  
alessia.marino3@univaq.it

As part of energy transition, production of higher alcohols from sustainable sources is becoming focus of research interest, since they can be used as intermediates in a wide range of applications, such as in the production of biofuels, surfactants, and lubricants. In this context, Guerbet reaction is a key process for converting bioethanol into higher alcohols through a multi-step mechanism, which sequentially involves dehydrogenation, aldol condensation, dehydration and hydrogenation (Figure 1A) [1]. Although homogeneous Guerbet catalytic systems are recognized as suitable approaches both in terms of selectivity and reaction conditions, heterogeneous catalysis offers different advantages, simplifying separation and recyclability processes, and then favouring the industrial scale transition [2]. Among the others, zeolites represent promising catalysts since their properties can be modulated not only in terms of intrinsic physicochemical features, such as acidity and pores size, but also by combining them with basic functionality to obtain multifunctional catalysts able to simultaneously catalyse dehydration and condensation in the multi-step Guerbet reaction.

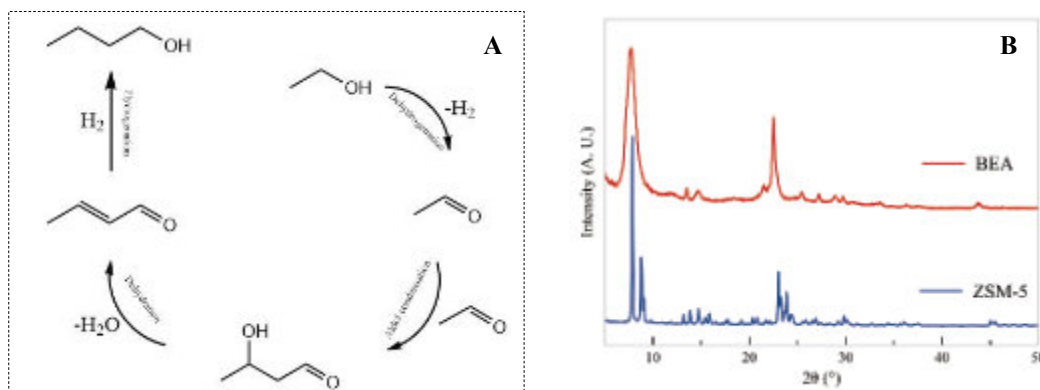


Figure 1 – A) Schematic representation of Guerbet reaction pathway. B) XRD pattern of ZSM-5 and BEA zeolites.

In this work, zeolites with different structures (BEA, MFI, among the others) were prepared with the aim of studying the influence of either topology or pore size on catalytic performances in ethanol to butanol conversion by Guerbet reaction. All catalysts were synthesised by hydrothermal method, calcined to remove the organic template, ion-exchanged with  $\text{NH}_4^+$ , and further calcined to be converted into the active  $\text{H}^+$  form [3]. The structural and morphological features of the prepared zeolites were then investigated by XRD,  $\text{N}_2$ -physisorption, and SEM, while the acidic properties were studied by FT-IR and  $\text{NH}_3$ -TPD. Finally, the catalysts were tested into the target reaction in batch reactor, in the temperature range 220 - 250 °C and at autogenic pressure, and then the products were analysed by GC-FID.

The physicochemical characterisation shows that the prepared samples exhibit good crystallinity and high purity (figure 1B). In addition, the preliminary catalytic tests reveal that the different textural and morphological properties affect the butanol selectivity, in the target reaction, since the largest-pore 3D framework zeolite (BEA) facilitates the access of bulkier molecules, compared to MFI structure, featuring smaller pores framework.

Therefore, the tested catalysts have proved to be a good starting point in the study of the correlation between selectivity toward butanol and structural properties of selected zeolites in Guerbet reaction. Finally, the influence of either the reaction parameters, the acidity of zeolites and the catalyst deactivation will be also deeply investigated in the further course of this work.

### References

- [1] S. Xie, Z. Li, S. Luo, and W. Zhang, *Renewable and Sustainable Energy Reviews*, **192**, 114240 (2024).
- [2] J. T. Kozłowski, and R. J. Davis, *ACS Catalysis*, **3**, 1588 (2013).
- [3] A. Marino, A. Aloise, H. Hernando, J. Feroso, D. Cozza, E. Giglio, M. Migliori, P. Pizarro, G. Giordano, D. P. and Serrano, *Catalysis Today*, **390**, 210 (2022).



## Mobility of solvated Cu cations in Cu-CHA predicted by machine learning accelerated molecular dynamics

R. Millán<sup>1</sup>, M. Boronat<sup>1</sup>

<sup>1</sup> Institute of Chemical Technology, Universitat Politècnica de València, 46022, Valencia, Spain  
 reimilca@itq.upv.es

Cu-exchanged zeolites play a crucial role in the chemical industry as redox catalysts, for instance, in the abatement of NO<sub>x</sub> emissions with the selective catalytic reduction (SCR) using NH<sub>3</sub> as reductant.[1] These materials rely on mobile solvated Cu<sup>+</sup> cations for their catalytic activity, but the effect of the framework composition (e.g Si/Al ratio) and the nature of the ligands (NH<sub>3</sub>, H<sub>2</sub>O, etc) in diffusion is not fully understood. [2-4] Ab initio molecular dynamics simulations can provide quantitative atomistic insight but are too computationally expensive to explore large length and time scales or diverse compositions. We report a machine-learning interatomic potential that accurately reproduces ab initio results allowing multianosecond simulations and diverse chemical compositions.

The training of Neural Network potentials (NNP) was based on the PaiNN architecture which uses equivariant message-passing for the ground truth prediction. The acquisition of training data was performed using active learning (AL) with a query-by-committee approach with an ensemble of four potentials. The final dataset contains 70k geometries with Si/Al ratios ranging from 5 to 50 for CHA framework and different Cu cationic species. The trained NNP is capable of prediction energies and forces with a mean absolute error of 1 kcal/mol (Figure 1).

Simulations at several temperatures in the NVT ensemble show that while two ammonia molecules are sufficient to mobilize Cu<sup>+</sup>, a higher water concentration is needed to fully detach Cu<sup>+</sup> from the framework. Aluminum pairs in 8R windows lower the free energy barrier for diffusion and stabilize the product configuration with two [Cu(NH<sub>3</sub>)<sub>2</sub>]<sup>+</sup> cations in the same cage. The mobility of [Cu(NH<sub>3</sub>)<sub>2</sub>]<sup>+</sup> is increased by NH<sub>3</sub> up to 3 molecules per cavity while the mobility of Cu<sup>+</sup> and Cu<sup>2+</sup> complexes increase with water content(Figure 2a). In general, the mobility of Cu<sup>2+</sup> species is lower compared with Cu<sup>+</sup>(Figure 2a). Regular MD simulations show that Cu complexes can diffuse as far as ~30 Å in the nanosecond scale (Figure 2b). Our results demonstrate the power of combining high-throughput DFT calculations, machine learning, and molecular dynamics simulations for simulating transport in nanoporous catalysts.

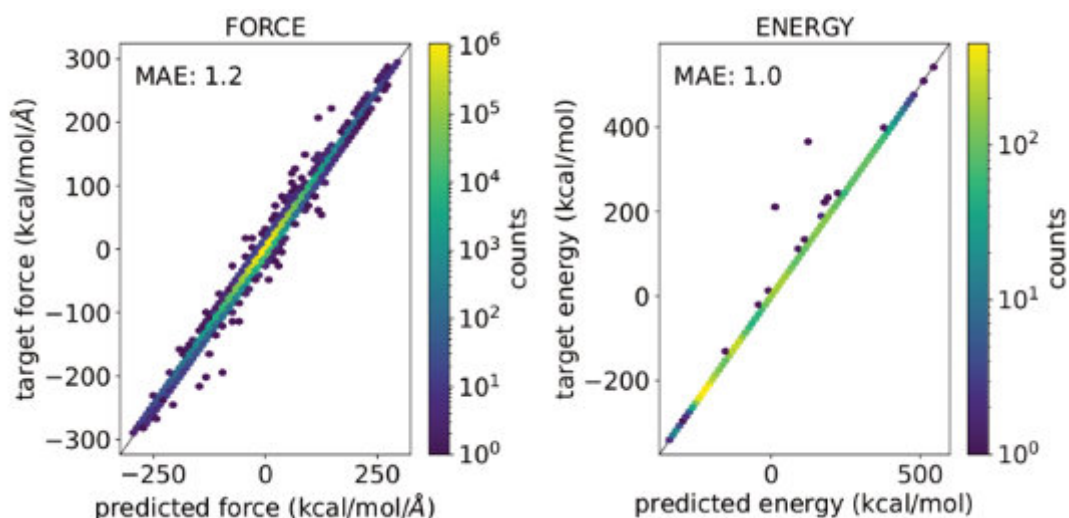


**Figure 1.** Metrics of the final trained Neural Network Potential. Mean absolute errors in the prediction of forces (left) and energies (right). Energies are given in kcal/mol and forces in kcal/mol/Å.

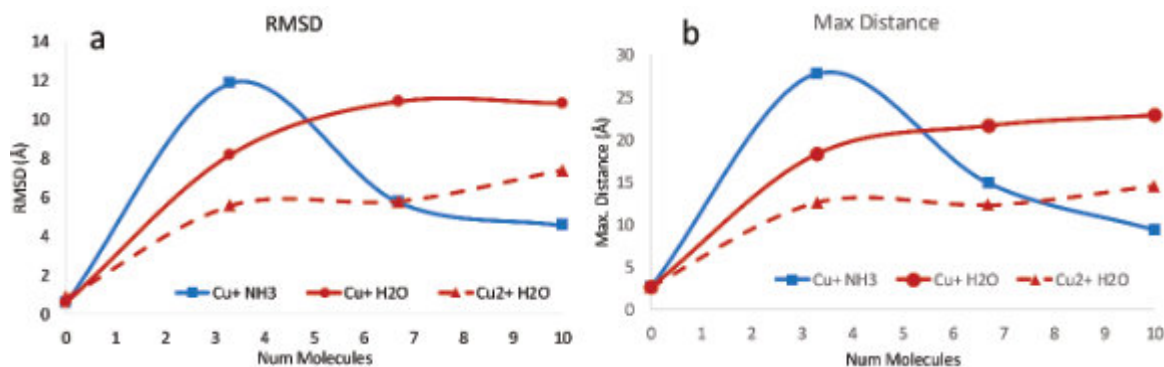


**Figure 2.** Effect of the number of ligand molecules (blue for ammonia and red for water) on the mobility of Cu cations (solid line for Cu<sup>+</sup> and dashed line for Cu<sup>2+</sup>). (a) Root mean squared displacements (RMSD) of Cu cations during the simulation. (b) Maximum distance travelled by the Cu cations during the simulation.

### References

- [1] C. Peden, *Journal of Catalysis*, **373**, 384 (2019).
- [2] R. Millan, E. Bello-Jurado, M. Moliner, M. Boronat, R. Gomez-Bombarelli, *ACS Central Science*, **9**, 2040-2056 (2023).
- [3] M. Signorile et al. *Chem. Sci.* **13**, 10238 (2022).
- [4] C. Paolucci et al. *Science* **357**, 898 (2017).

### Acknowledgments

This work was supported by the Margarita Salas grant funded by the European Union-Next Generation EU and Spanish government through PID2020-112590GB-C21, and TED2021-130739B-I00 (MCIN/AEI/FEDER, UE).



## Application of Zr-MOF and Ionic Liquids in SPEEK Membranes

**Katiúscia M. N. Borba<sup>1</sup>, Caroline A. Troglío Ibañez<sup>1</sup>, Letícia Zanchet<sup>1</sup>, Leticia Trindade<sup>1</sup>, Fernando Rey<sup>2</sup>, Urbano Díaz<sup>2</sup>, Katia Bernardo-Gusmão<sup>1</sup>.**

<sup>1</sup>Laboratório de Reatividade e Catálise - Universidade Federal do Rio Grande do Sul, Av. Bento Gonçalves, 9500, P.O. Box 15003, Porto Alegre 91501-970, Brazil

<sup>2</sup>Universidad Politécnica de Valencia, Institute of Chemical Technology (ITQ), 46022 Valencia, Spain  
katiusciamn@gmail.com

### Introduction

Metal-organic frameworks (MOFs) are a new class of porous materials, typically composed of metal ions connected to organic ligands through coordination bonds. Among the many applications of MOFs, the most promising are gas storage and separation. UiO-66, a zirconium-based MOF, stands out for its high surface area, stability, and low electrical conductivity, which are advantageous characteristics for use in fuel cells. Recent studies have demonstrated that the incorporation of MOFs into hybrid membranes can significantly increase proton conductivity [1]. This work presents the encapsulation of ionic liquids into a UiO-66 (Zr-MOF) framework and their insertion into SPEEK membranes for the fabrication of proton exchange membranes (PEM). The modified particles and membranes are characterized in terms of structure and morphology and compared with pristine SPEEK membranes in terms of swelling, water uptake, oxidative stability, and proton conductivity.

### Experimental

The SPEEK membrane [2] and the ionic liquids 3-triethylammonium propane sulfonic acid hydrogen sulfate (TEA-PS.HSO<sub>4</sub>), 1-butylimidazole hydrogen sulfate (Blm.HSO<sub>4</sub>) and 1-butyl-3-methylimidazolium hydrogen sulfate (BMI.HSO<sub>4</sub>) were prepared according to the literature. The synthesis of the UiO-66 (Zr-MOF) framework was performed by combining the reactants, terephthalic acid and zirconium chloride (IV) (ZrCl<sub>4</sub>), with 1:1 ratio. The synthesis was performed in DMF as described in the literature [3]. Proportional amounts of SPEEK and Zr-MOF were mixed in DMA at 80 °C under constant stirring for 8 h. The homogeneous mixture was poured onto a petri dish and dried in a vacuum oven at 80 °C for 24 h. After evaluating the structure of these composite membranes SPEEK/Zr-MOF by ATR-FTIR and TG analysis and evaluating their proton conductivity in conditions of controlled relative humidity at 25 and 80 °C, the membrane with 7.5 wt.% of Zr-MOF was chosen for addition of ionic liquid, because it had the highest proton conductivity among the samples studied. The ionic liquids employed in the Zr-MOF were TEA-PS.HSO<sub>4</sub> (TEA), Blm.HSO<sub>4</sub> (BH) and BMI.HSO<sub>4</sub> (BM). These composite membranes were prepared using 2.5 or 5 wt.% of IL encapsulated in Zr-MOF.

### Results and Discussion

The results for SPEEK/MOF membranes with concentrations 2.5, 5, 7.5 and 10 wt.% Zr-MOF (Table 1) show that an increase in Zr-MOF concentration causes an improvement in membrane conductivity, with a limit value reached when 7.5 wt.% Zr-MOF in the polymer was used. The conductivity of the SMOF10 sample undergoes a drastic decrease in its value when compared to the SMOF7.5 membrane. Through thermal analysis it is evident that the increase in Zr-MOF concentration from 7.5 wt.% to 10 wt.% is also accompanied by loss of thermal stability in the material, since the SMOF10 sample decomposes at a lower temperature when compared to the other samples. Considering these results, the amount of Zr-MOF to be placed on the SPEEK membrane was set at 7.5 wt.%. SPEEK/MOF composite membranes with 7.5 wt.% of Zr-MOF exhibit high conductivity.

**Table 1.** Proton conductivity ( $\sigma$ ) and relative humidity (RH) of SPEEK/MOF composite membranes with different amounts of Zr-MOF at 25 °C and 80 °C. SMOF<sub>x</sub> indicate SPEEK/MOF membrane with x wt.% Zr-MOF.

Sample	$\sigma$ (mS cm <sup>-1</sup> )	
	25 °C (100% RH)	80 °C (60% RH)
S0 (pristine SPEEK)	77	126
SMOF2.5	84	141
SMOF5	96	146
SMOF7.5	104	172
SMOF10	85	129

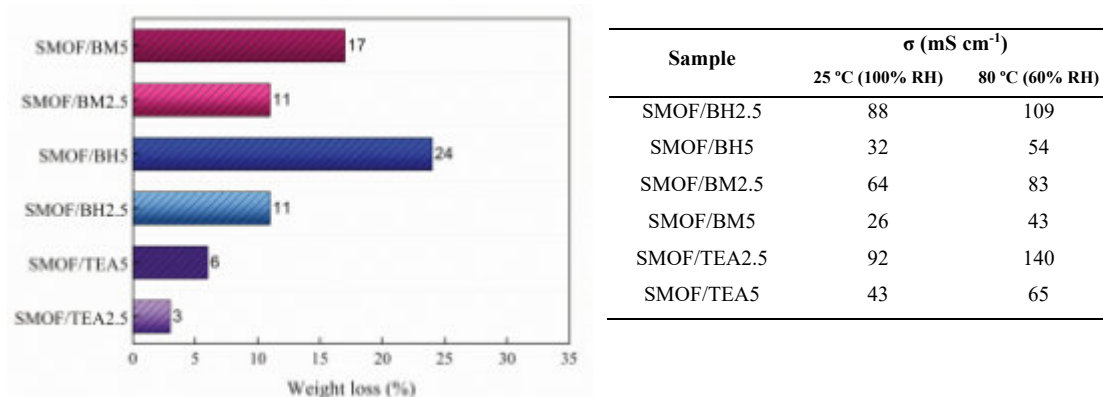
The pore sizes of the MOF facilitate the aggregation of water molecules, which are fixed within the pores by hydrogen bonds. This increases conductivity, but also the degree of swelling, which causes MOF dissolution when in prolonged contact with water. In order to increase thermal and chemical stability of the membrane, BlmH.HSO<sub>4</sub>, BMI.HSO<sub>4</sub> and TEA-PS.HSO<sub>4</sub> ILs were encapsulated at 2.5 wt% and 5 wt% by wet impregnation method. Figure 1 shows the ability of the ionic liquid to exit the membrane in aqueous medium. The samples show the same leaching tendency, that is, with an increase in the amount of IL encapsulated in the Zr-MOF, the leaching is increased. We can relate the pattern



of leaching of the composite membranes with the interaction force of IL cations with the sulfonic group of SPEEK. The increase in leaching follows the order  $\text{BIm}^+ > \text{BMI}^+ > \text{TEA-PS}^+$ , indicating that the higher the cation, the greater the interaction of IL with Zr-MOF and SPEEK (Figure 1).

The oxidative stability test was performed to evaluate whether the pure Zr-MOF or the MOF/IL particles accelerate the chemical degradation of the SPEEK membrane. During PEMFC operation, reactive oxygen radicals ( $\bullet\text{OH}$ ,  $\bullet\text{OOH}$ ) can be generated by a chemical or electrochemical reaction between hydrogen and oxygen in the Pt catalyst [46]. The results show that the addition of 7.5 wt.% Zr-MOF to SPEEK increases membrane degradation by 26%. However, when IL is encapsulated in the Zr-MOF particles, the tendency of chemical degradation of the polymer is reduced for all concentrations.

The conductivity and the water uptake properties of the composite membranes follow the same order:  $\text{SMOF7.5} > \text{SMOF/TEA} > \text{SMOF/BH} > \text{SMOF/BM}$ . The conductivity of the SMOF7.5 membrane is higher in both conditions studied, since the Zr-MOF can form hydrogen bonds between the neighbouring water molecules with the 1,4-benzoldicarboxylic acid binder [4]. On the other hand, when the ionic liquid is encapsulated in the Zr-MOF pore, it prevents the water from entering, reducing the formation of hydrogen bonds decreased thus the proton conductivity. The results show that the ideal amount of ionic liquid encapsulated for increasing the conductivity in both studied temperatures (25 and 80 °C) is 2.5 wt.%, for the three ionic liquids used. The increase in the amount of encapsulated IL to 5 wt.% significantly decreases all conductivity values. This reduction in proton conductivity may be related to the increase of particle agglomerations inside in the polymer channel, which can block the membrane channels preventing water retention [5]. The SMOF/TEA2.5 composite membrane presented the highest conductivity values among membranes modified with MOF/IL particles. This behaviour can be attributed to the fact that the TEA-PS.HSO<sub>4</sub> IL has a SO<sub>3</sub>H group in the cation and a SO<sub>4</sub>H group in the anion. These groups are protonic and their dissociation produce more H<sup>+</sup>, thus contributing to the increase of proton conductivity.



Sample	$\sigma$ (mS cm <sup>-1</sup> )	
	25 °C (100% RH)	80 °C (60% RH)
SMOF/BH2.5	88	109
SMOF/BH5	32	54
SMOF/BM2.5	64	83
SMOF/BM5	26	43
SMOF/TEA2.5	92	140
SMOF/TEA5	43	65

**Figure 1.** Leaching out of SMOF/TEA2.5, SMOF/TEA5, SMOF/BH2.5, SMOF/BH5, SMOF/BM2.5 and SMOF/BM5 and proton conductivity ( $\sigma$ ) and relative humidity (RH) of same composite membranes at 25°C and 80 °C.

## Conclusion

Among the three ionic liquids tested in the SPEEK/Zr-MOF membranes, the composite membrane with 2.5wt.% by mass of TEA-PS.HSO<sub>4</sub> encapsulated in the Zr-MOF (SMOF/TEA2.5 sample) showed higher water retention capacity and the best proton conductivity result between the studied SPEEK/MOF-IL composite membranes. This high conductivity is attributed to the fact that the TEA-PS.HSO<sub>4</sub> IL has a SO<sub>3</sub>H group in the cation and a SO<sub>4</sub>H group in the anion. These groups are protonic and their dissociation produces more H<sup>+</sup>, thus contributing to the increase of proton conductivity. The proton conductivity measured at 80 °C is approximately 111% greater than the pure SPEEK membrane (126 mS cm<sup>-1</sup>) at the same temperature; this demonstrates that SMOF/TEA2.5 may be a promising membrane for use in PEMFC-type fuel cells.

## References

- [1] B. Zhangab, Y. Cao, Z. Li, *Electrochim. Acta* 240 (2017) 186-194.
- [2] L.G. da Trindade, E.C. Pereira, *Eur. J. Inorg. Chem.* 2017 (2017).
- [3] J.B. De Coste, T.J. Demasky, M.J. Katz, *New J. Chem.* 39 (2015) 2396-2399.
- [4] H. Furukawa, F. Gándara, Y.-B. Zhang, *J. Am. Chem. Soc.* 136 (2014) 4369-4381.
- [5] J.H. Chun, S.G. Kim, J.Y. Lee, D.H. Hyeon, *Renew. Energ.* 51 (2013) 22-28.

## Acknowledgments

The authors acknowledge the financial support from ANP - PR50.



## Metal-doped hierarchical ZSM-5 zeolites towards more stable catalysts in the aromatization of paraffins and olefins in plastic pyrolysis liquids

R.S. Dias<sup>1</sup>, P.R. Frigols<sup>1</sup>, A. Fernández-Arroyo<sup>1</sup>, M.E. Domine\*<sup>1</sup>

<sup>1</sup> Instituto de Tecnología Química (ITQ, UPV – CSIC). Universitat Politècnica de València. Consejo Superior de Investigaciones Científicas. Avda. Los Naranjos s/n, 46022, Valencia, Spain.

[mdomine@itq.upv.es](mailto:mdomine@itq.upv.es)

### Introduction

In 2020, only 35% of the 29.5Mt of post-consumer plastics waste was sent to recycling, whereas 42% was underexploited through energy recovery (incineration) and 23% was directly landfilled in Europe [1]. Therefore, the development of new chemical recycling technologies is crucial to deal with complex plastic waste streams, which cannot be mechanical recycled and would otherwise end in incineration or landfills. In this regard, more than €8 billion are foreseen to be invested in Europe to construct chemical recycling facilities to produce 2.8Mt of recycled plastics by 2030, wherein 80% of these planned investments focus on pyrolysis and gasification plants dealing with mixed plastic waste [2]. Interestingly, thermal pyrolysis of plastic mixtures (i.e., LHDPE, PP, PS) yields liquids containing high amount of paraffins (C<sub>6</sub>-C<sub>20</sub>+ alkanes), olefins (C<sub>6</sub>-C<sub>20</sub> alkenes) and a lower amount of aromatics [3], which can be catalytically upgraded into high-added value chemicals. More specifically, the direct production of BTXs (benzene, toluene and xylenes) via aromatization becomes an environmentally friendlier strategy compared to the traditional catalytic reforming of naphtha and lighter fractions currently used in petrochemical industry. In this regard, aromatization or dehydro-aromatization of light hydrocarbons is a complex acid-catalyzed reaction involving several steps: alkane dehydrogenation to alkenes, alkene oligomerization and cyclization to obtain the desired products. Moreover, other reactions like cracking and trans-alkylation can also take place when higher alkanes or olefins are processed. H-ZSM-5 zeolite with an MFI structure has been widely used as light hydrocarbons aromatization catalyst due to its excellent thermal stability and shape selectivity towards BTXs [4-5]. Nevertheless, these specific micropore and acid properties also translate into a large formation of gases and a rapid deactivation by coke formation. For this reason, several metals have been investigated as H-ZSM-5 promoters for the catalytic aromatization of light hydrocarbons. Both, Ga and Zn stand out based on their paraffin dehydrogenation and olefin oligomerization promoting effect, respectively [6-7]. Nevertheless, most of this research focuses on single paraffin/olefin conversion with monoatomic-doped zeolite catalysts. In this work, commercially available H-ZSM-5 zeolites co-doped with Ga, Zn and additional transition metals have been evaluated in the aromatization of mixtures of hydrocarbons and olefins simulating liquids derived from plastic pyrolysis. Moreover, several post-synthesis strategies conducive to optimize acid properties and limit mass transport limitations by using hierarchical zeolites have been also assessed in order to overcome major disadvantages reported in previous studies. Most promising catalysts have finally been essayed with prolonged reaction times and in the upgrading of a real pyrolysis oil.

### Experimental Procedure

Metal-doped and co-doped catalysts were prepared by wetness impregnation of commercial H-ZSM-5 zeolites (with different Si/Al ratios) purchased from Zeolyst. Desilication towards hierarchical zeolites and Brønsted acid sites partial blocking by Na were performed following the procedures reported in literature [8-9]. Catalysts were characterized by ICP, XRD, AE, TG, N<sub>2</sub> adsorption isotherms, pyridine-FTIR and different microscopy techniques, among others. All samples were calcined in air at 500 °C before use; and a continuous flow fixed-bed catalytic reactor system (ITQ design) was employed for studying catalytic aromatization of a mixture of alkanes and olefins. The system is composed by a HPLC pump (for liquid feeding), a pressurized recipient for liquids or gases injection into the reactor, a pre-heating stage before reactor, a stainless-steel tubular reactor with the catalyst placed in a fixed bed with internal and external temperature controls, an electric furnace with temperature control, a pressure regulation valve, different manometers and the recovering of liquids and gases at the outlet of the reactor for further analysis (GC-TCD and GC-FID). A liquid model mixture composed by hydrocarbons (H = n-octane + n-decane) and olefins (O = 1-hexene + 1-octene) with a H/O molar ratio = 3, representative of pyrolysis liquids was used as a feed. Moreover, all reactions were performed at 400 °C, 10 bar, 1g of catalyst (W/F: 0.12 h<sup>-1</sup>) and a N<sub>2</sub> flow of 50NmL/min during 5.5 to 30h.

### Results and Discussion

The aromatization reaction of hydrocarbons and olefins mixture (simulating the major components of the pyrolysis liquids of plastics) was firstly evaluated by employing Ga- and Zn-doped ZSM-5 as catalysts. Preliminary tests showed that Ga offers a superior selectivity towards BTXs attributed to the high dehydrogenation activity from these Lewis acid sites and based on the higher content of paraffins in the feed. Zn- and Ga-Zn/ZSM-5 catalysts showed lower selectivity and no synergetic effect was observed. The Si/Al molar ratio in ZSM-5 materials was found to be crucial to reach full conversion of olefins and paraffins. In this regard, 0.60Ga/Z11 (Si/Al = 11) with a higher acidity only reached 47% conversion of paraffins and a low BTXs yield was obtained (*Table 1*). Higher Si/Al ratios with similar Ga loadings led to higher BTXs selectivity (51-53%), where Z25 (Si/Al = 25) was the optimum support

towards maximizing BTXs yield. Moreover, different Ga loadings were studied on this Z25 zeolite, wherein nice Ga nanoparticle distributions were achieved (measured by HR-STEM). Similar BTXs selectivity was obtained regardless of Ga content, although 0.85Ga/Z25 catalyst offered a slight advantage in terms of BTX yield (*Table 1*). It is worth noticing that these results were completely reproducible and have been correlated to the acid properties (acid sites density and Brønsted/Lewis acid sites ratio) of these materials. Additionally, different post-synthesis strategies have been assessed. On one hand, desilication procedures performed on Z25 zeolite resulted in a slight modification of Si/Al ratios of this material, together with the formation of mesopores. C<sub>3</sub>/C<sub>4</sub> ratio in the gas phase was altered as an effect of the different acid properties and cracking activity of the new catalysts, but unfortunately, these changes barely affected the overall liquid and BTXs yield. On the other hand, Brønsted acid sites partial blocking by Na did result in a better performance in terms of liquid and BTXs yields. *Table 1* highlights that when specific NaOH concentrations were used during post-synthesis, Brønsted/Lewis acid sites ratio could be fine-tuned and a new catalyst was obtained, which outperformed our previous reference material. Finally, co-doping strategies were investigated, where Mo was the most suitable co-dopant compared to other metals (i.e., W, Re) in order to achieve good catalytic results. In spite of the fact that initial results at 5.5h did not show an improvement (*Table 1*), longer reaction times revealed the superior stability of 0.24Mo-0.81Ga/Z25 catalyst compared to 0.85Ga/Z25. Particularly, co-doping strategy allowed maintaining higher paraffins conversion than Ga-only catalysts, and higher BTXs yields were obtained for a longer time. Nevertheless, this co-doped catalyst still showed significant deactivation as measured by elemental analysis and HR-TEM.

**Table 1.** Catalytic performance of different catalysts in the aromatization reaction of a liquid model mixture (H/O = 3) during 5.5h.

Catalyst	Conversion (mol%)		BTXs selectivity (mol%)	Yield (wt%)			Mass balance (wt%)
	Olefins	Paraffins		Gas	Liquid	BTX	
0.60Ga/Z11	96	47	21	43	39	7	83
0.66Ga/Z25	96	98	51	58	39	19	98
0.64Ga/Z40	97	98	53	63	34	17	97
0.85Ga/Z25	99	98	63	55	35	20	90
0.82Ga/1NaZ25	97	97	53	47	46	23	93
0.24Mo-0.81Ga/Z25	99	98	59	61	35	19	96

Finally, 0.24Mo-0.81Ga/Z25 catalyst was tested in the aromatization reaction of a real pyrolysis oil. This material showed a high production (52%) of mono-aromatics (mainly BTXs) as measured by GCxGC (*Figure 1*) after 1.5h. Samples collected at longer reaction times (5.5h) indicated a strong catalyst deactivation mainly caused by coke formation. In conclusion, an adequate acidity of zeolites is crucial for obtaining high yields of aromatics, whereas co-doping strategy and acid properties optimization have resulted in more active and specially, stable catalysts in the production of BTXs. Further research towards the stabilization of these catalytic systems must be developed in order to become a viable alternative for the production of aromatics from real pyrolysis liquids.

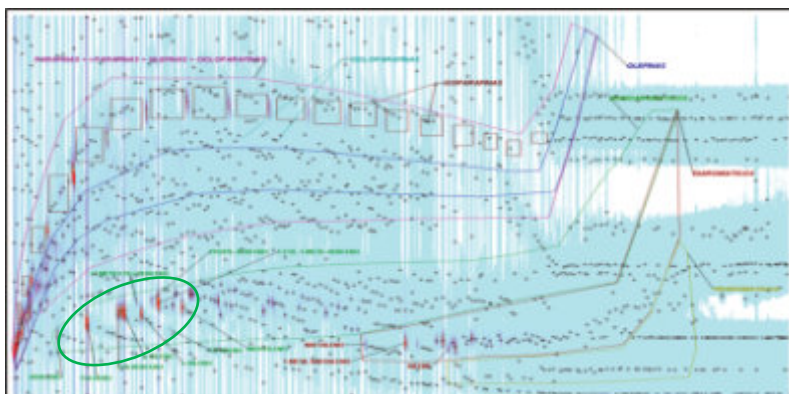


**Figure 1.** GCxGC (2D GC) showing production of mono-aromatics with 0.24Mo-0.81Ga/Z25 after 1.5h from a real pyrolysis oil.

## References

- [1] <https://plasticseurope.org/knowledge-hub/plastics-the-facts-2022-2/>
- [2] <https://plasticseurope.org/sustainability/circularity/recycling/chemical-recycling/>
- [3] B. Kunwar, H.N. Cheng, S.R. Chandrashekar, B.K. Sharma, *Renew. Sustain. Energy Rev.*, **54**, 421-428 (2016).
- [4] C. Zhang, G. Kwak, H.-G. Park, K.-W. Jun, Y.-J. Lee, S.C. Kang, et al., *Microp. Mesop. Mater.*, **276**, 292-301 (2019).
- [5] X. Cui, H. Lyu, Y. Chai, B. Liu, D. Zhao, C. Liu, *Sep. Purif. Tech.* **349**, 127881 (2024).
- [6] T.E. Thsabalala and M.S. Scurrrell. *Catal. Commun.* **72**, 49-52 (2015).
- [7] X. Su, W. Zan, X. Bai, G. Wang, W. Wu, *Catal. Sci. Technol.* **7**, 9, 1943-1952 (2017)
- [8] D. Murindababisha, A. Yusuf, Y. Sun, C. Wang, Y. Ren, J. Lv, H. Xiao, G. Chen, J. He, *Environ. Sci. Pollut. Res.* **28**, 62030-62060 (2021).
- [9] Y. Bai, D. Liu, L. Zhao, J. Gao, C. Xu, H. Pang, X. Gao, *Ind. Eng. Chem. Res.* **61**, 43, 15842-15855 (2022).

## Binuclear vanadium species in ferrierite zeolite and their reactivity

**Mariia Lemishka<sup>1\*</sup>, Jiri Dedecek<sup>1</sup>, Kinga Mlekodaj<sup>1</sup>, Dalibor Kaucky<sup>1</sup>, Agnieszka Kornas<sup>1</sup>, Edyta Tabor<sup>1</sup>**

<sup>1</sup>J. Heyrovský Institute of Physical Chemistry of the CAS, Dolejškova 3/2155, 182 23 Prague, Czech Republic

Corresponding author: [mariia.lemishka@jh-inst.cas.cz](mailto:mariia.lemishka@jh-inst.cas.cz)

Transition metal ion (TMI) species stabilized within zeolite frameworks can be used in various catalytic processes, including the selective oxidation of methane to methanol.<sup>1,2</sup> In this case, methane is oxidized by small molecules, such as O<sub>2</sub>, previously activated over TMI-based zeolites. Recently, it has been shown that two cooperating bare Fe(II) ions located in adjacent cationic β positions (binuclear species) in ferrierite (FER) zeolite can split O<sub>2</sub> at room temperature (RT).<sup>1,3</sup> Two α-oxygen [Fe(IV)=O]<sup>2+</sup> species are formed and oxidize methane to methanol. Furthermore, the spontaneous desorption of methanol to the gas phase at low temperatures renders binuclear Fe(II) species highly promising systems for the utilization of natural gas by direct oxidation with O<sub>2</sub>. Up to now, the possibility of creating binuclear cationic species active in O<sub>2</sub> splitting has been reported for zeolites of FER topology – Fe(II), Co(II), Mn(II), and Ni(II) cations.<sup>4</sup> The tunability of the binuclear cationic species represents a significant challenge for the potential redox systems that may be employed for methane oxidation by O<sub>2</sub>. The use of vanadium-containing catalysts in hydrocarbon transformations is well-established.<sup>5</sup> This suggests the potential for expanding the group of promising cations that may participate in the formation of binuclear species. This contribution aims to explore the possibility of creating binuclear V(II) species in the FER matrix and investigate their properties for O<sub>2</sub>/CH<sub>4</sub> activation.

The commercially available Na, K-FER (Tosoh Corporation) with Si/Al 8.6 was employed as the parent material to obtain V-FERs with varying amounts of vanadium extra-framework species. All steps of the preparation procedure were conducted under a protective N<sub>2</sub> atmosphere. Initially, Na, K-FER was ion exchanged to NH<sub>4</sub>-form of FER. Then, the NH<sub>4</sub>-FER was mixed with the solution of VCl<sub>2</sub> in degassed distilled water and stirred at 60°C for two hours. Subsequently, the sample was washed with degassed distilled water and dried overnight at RT. Several techniques, including in-situ FTIR, UV-Vis spectroscopy, and XRD, were employed to study and analyze vanadium species in the FER matrix. The XRD results confirmed that the introduction of vanadium as an extra-framework species into FER topology does not affect zeolite structure. Furthermore, analysis of XRD patterns of prepared samples revealed the formation of V(III) and V(V) bulk oxides. These findings are consistent with those obtained from UV-Vis spectroscopy measurements. In-situ FTIR spectra of V-FERs evacuated at 450 °C exhibited bands around 890, 913, and 930 cm<sup>-1</sup> (Fig. 1A), which attributed to the antisymmetric T-O-T vibrations of FER rings perturbed by the ligation of bare metal V(II) ions<sup>6,7</sup>. The interaction of V-FER with O<sub>2</sub> at RT results in the disappearance of the bands attributed to V(II) bare cations and the formation of a new band at around 878 cm<sup>-1</sup> (Fig.2B). The band around 878 cm<sup>-1</sup> was suggested as a benchmark of the divalent oxo-cationic species (α-oxygen).<sup>1-4</sup> Moreover, the band at 878 cm<sup>-1</sup> is stable at 200°C and after desorption of O<sub>2</sub> at RT. Subsequent interaction of methane with O<sub>2</sub>-oxidized V-FERs resulted in the disappearance of the band at 878 cm<sup>-1</sup>, accompanied by the reappearance of the band characteristic of V(II) in β positions (Fig.1C). V-FERs, which contained divalent vanadium cationic species located in β positions, were successfully prepared. This study opens the possibility of developing vanadium-based zeolite catalysts with the potential for hydrocarbon oxidation by O<sub>2</sub>.

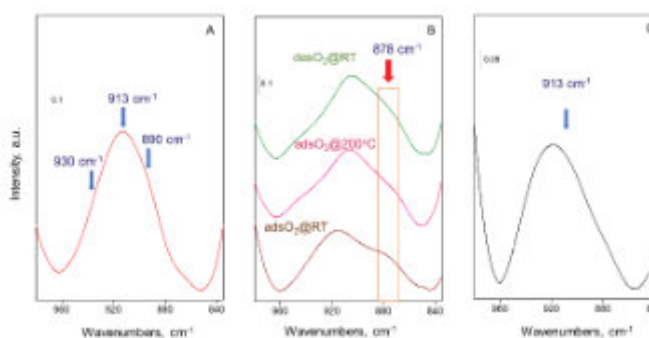


Figure 1. In-situ FTIR study of V-FER.

### References

- [1] E. Tabor, J. Dedecek, K. Mlekodaj, Z. Sobalik, P.C. Andrikopoulos and S. Sklenak, *Sci. Adv.* **6**, eaaz9776, (2020).
- [2] G. I. Panov, V. I. Sobolev and A. S. Kharitonov, *J. Mol. Cat.*, **61**, 85-97, (1990).
- [3] K. Mlekodaj et al., *ACS Catal.*, **13**, 3345-3355, (2023).
- [4] K. Mlekodaj, M. Lemishka, S. Sklenak, J. Dedecek and E. Tabor, *Chem. Commun.*, **57**, 3472-3475, (2023).
- [5] B. Guo, L. Zhu, X. Hu, Q. Zhang, D. Tong, G. Li and C. Hu, *Catal. Sci. Technol.*, **1**, 1060-1067, (2011).
- [6] M. Lemishka, K. Mlekodaj, Z. Sobalik, E. Tabor and J. Dedecek, *Pure Appl. Chem.*, **91**, 1721-1732, (2019).
- [7] Z. Sobalik, Z. Tvaruzkova and B. Wichterlova, *J. Phys. Chem. B*, **102**, 1077-1085, (1998).

## CHIRALITY IN CONFINED SPACES. STUDY OF THE ASYMMETRIC CATALYTIC REACTION OF GTM-4 WITH PROCHIRAL CIS-STILBENE OXIDE.

Ramón de la Serna, Jaime Jurado-Sánchez, Joaquín Pérez-Pariente, Luis Gómez-Hortigüela

Instituto de Catálisis y Petroleoquímica (ICP-CSIC), Calle Marie Curie, 2, 28049, Madrid, Madrid

ramon.serna@csic.es

Chirality, formally described as the property of any object not to be superimposable with its mirror image, has proven to be a determining attribute for pharmaceutical chemistry since most drugs are chiral molecules, and generally each enantiomer has different therapeutic properties. In the pharmaceutical industry, homogeneous chiral catalysts are currently used almost exclusively, with their well-known limitations that force the evolution to new heterogeneous catalysts. Transferring this spatial property into a three-dimensional heterogeneous system while maintaining the high enantioselectivity of homogeneous catalysts is, in most cases, a highly challenging task that is rarely achieved. Among many other candidates we find supported enzymes, MOFs and, in the current case, zeolites.

Zeolites are crystalline materials, with highly ordered pores in the three-dimensional space, which can contain catalytic centres. Among the over 260 zeolites known today, only 8 have a chiral structure, although they have traditionally been obtained in racemic form (50 % mixture of enantiomeric polymorphs). The first chiral zeolite where polymorph enantiomeric enrichment was demonstrated was the STW structure, which has limitations such as its small pore size of 6 Å and the enantiomeric excesses obtained in test reactions of around 10 % [1]. More recently, our group has obtained the materials GTM-3 and GTM-4 [2,3], with the -ITV extra-large pore (19.2 Å) chiral structure, synthesised for the first time in its racemic form at the Institute of Chemical Technology (ITQ-37) [4]. These materials have been shown to be highly selective in the catalytic opening reaction of trans-stilbene oxide with alcohols, showing enantiomeric excesses up to ±60% [5]. Though this value is very promising, these materials still require fundamental and systematic studies of their asymmetric catalytic properties in order to improve their enantioselectivity. The ring-opening reaction of trans-stilbene oxide with 1-butanol, using the GTM-4 material as catalyst, has shown good enantiomeric excess, reaching values up to 60%. Nevertheless, this reaction, although it has an exceptional host-guest fit, has the disadvantage of being a kinetic resolution. In this type of reaction, a chiral substrate starts in its racemic form, where products reach their maximum enantiomeric excess at the beginning of the reaction and gradually decrease until one of the two enantiomers of the reactants is consumed, then abruptly decay to zero. Such reactions tend to be avoided because of their limited application potential, preferring to start from a non-chiral reactant to give a chiral product. Trans-stilbene oxide has its cis-isomer which, since it is a *meso*-compound, is achiral (R,S-configuration). Thus, the motivation of this work is the study of the ring-opening reaction of cis-stilbene oxide (CSO) with four alcohols of different chain length by using the chiral zeolite GTM-4 as catalyst to evaluate its enantioselective performance (Figure 1).

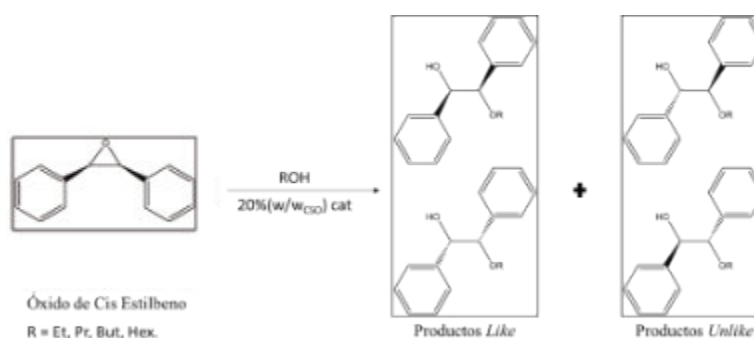


**Figure 1.** Opening reaction of cis-stilbene oxide with four different alcohols using GTM-4 as catalyst. The columns represent the enantiomers of the molecules.

The experiments were carried out using GTM-4 (obtained using (1R,2S)-2-methylbenzylmethyl-ephedrinium as structure-directing agent) as catalyst (20% in proportion to CSO) and 4 alcohols (ethanol, 1-propanol, 1-butanol and 1-hexanol) at a CSO concentration of 1mg/mL, at room temperature; reaction products were analysed by chiral HPLC. Moreover, the influence of the reaction conditions has been analysed in the case of the alcohol that shows the best enantioselectivity for the epoxide opening, performing it at 3 different temperatures, with the aim of maximising the enantiomeric excess and evaluating the effect of temperature on the system.

The results showed that the GTM-4 catalyst is active in the reaction, but the reaction proceeds slower than with trans-stilbene oxide and shows higher enantioselectivity towards the S<sub>N</sub>2 products (with inversion of configuration, *like* products in Figure 1 with R,R or S,S configuration) showing a maximum in propanol, reaching a value close to 45% (Figure 2).



In contrast, the values obtained for the  $S_N1$  ring-opening reaction (*unlike* products, right in Figure 1) showed a small enantiomeric excess at the beginning of the reaction, which practically disappears at the end of the reaction. The *like/unlike* ratio decreases as the size of the alcohol increased.

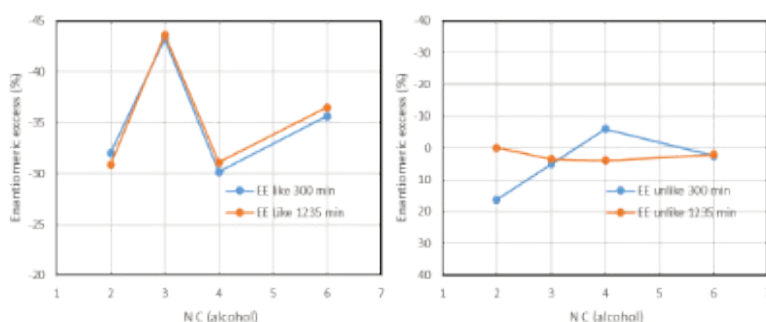


**Figure 2.** Enantiomeric excess of *Like* (left) and *Unlike* (right) products. Analyses performed after 300 min (blue) and 1235 min (orange) reaction times.

Observing that the largest enantiomeric excess of the ring-opening reaction of CSO to the *like* product corresponds to 1-propanol, the experiment was repeated at 50°C and at -20°C. A slight temperature dependence of the enantiomeric excess can be observed, with a maximum at low conversions and -20°C of 60% (Figure 3). The highest temperature dependence is observed in the *like/unlike* ratio, which increases significantly the temperature decreases.

The *like/unlike* ratios decrease as the chain length of the alcohol increases, reaching values close to 0 in the case of 1-hexanol, which implies a 'deactivation' of the main (and most enantioselective) route of the reaction. As the temperature decreases, a slight increase in the enantiomeric excess of the  $S_N2$  products of the ring-opening reaction with 1-propanol is observed, reaching a maximum of 60%, which decreases over time. After analysing the *like/unlike* ratios, it is observed that, as the temperature decreases, the  $S_N2$  route gains importance, reaching four times increase comparing the reaction at 50°C and at -20°C, which indicates that the  $S_N1$  route has a higher activation barrier.

In conclusion, the enantiomerically enriched catalyst GTM-4 is active in the ring-opening reaction of cis-stilbene oxide with linear alcohols. Of the alcohols used, the most selective, in terms of enantiomeric excess, is 1-propanol which gives a maximum of about 60%, indicating the best chiral host-guest match for -ITV and CSO/1-propanol system.

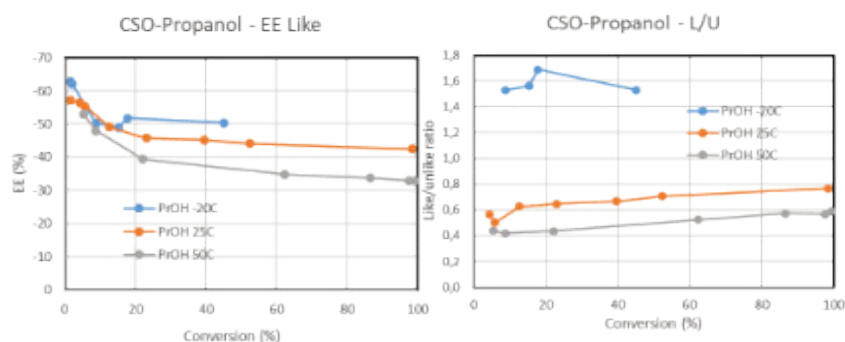


**Figure 3.** Enantiomeric excess *like* (top) and *like/unlike* ratio vs. conversion (bottom) of reactions performed with 1-propanol at 50°C (green), 25°C (orange) and -20°C (blue).

## Bibliography

- [1] S. Brand, J. Schmidt, M. Deem, F. Daeyaert, Y. Ma, O. Terasaki, M. Orazov, and M. Davis, PNAS, **114** (20) 5101-5106 (2017).
- [2] R. de la Serna, D. Nieto, R. Sainz, B. Bernardo-Maestro, A. Mayoral, C. Márquez-Álvarez, J. Pérez-Pariente and L. Gómez-Hortigüela, JACS, **144**, 7951-8400 (2022)
- R. de la Serna, I. Arnaiz, C. Márquez-Álvarez, J. Pérez-Pariente and Luis Gómez-Hortigüela, Chem. Commun., **58**, 13083 (2022)
- [4] J. Sun, C. Bonneau, A. Cantín, A. Corma, M. Díaz-Cabañas, M. Moliner, D. Zhang, M. Li, X. Zou, Nature, **458**, 1154–1157 (2009).
- [5] R. de la Serna, J. Jurado-Sánchez, C. Márquez-Álvarez, J. Pérez-Pariente, L. Gómez-Hortigüela, Microporous Mesoporous Materials, **371**, 113083(2024)

## Acknowledgments

The authors would like to thank the Spanish Ministry of Science, Innovation and Universities for funding the project (PID2019-107968RB-I00 and PID2022-138481NB-I00). RSV thanks the Spanish Ministry of Science, Innovation and Universities for funding its pre-doctoral contract (PRE2020-095946).

## FT-IR and UV-vis spectroscopies supported with MCR-ALS analysis for active species identification in alcohol-to-hydrocarbons processes

K. A. Tarach, A. Kordek, A. Walczyk, A. Olszewska, K. Góra-Marek

Faculty of Chemistry, Jagiellonian University in Kraków, Gronostajowa 2, 30-387 Krakow, Poland

[karolina.tarach@uj.edu.pl](mailto:karolina.tarach@uj.edu.pl)

FT-IR spectroscopy has played a major role in identifying reaction intermediates in catalytic processes since the first detection of surface-adsorbed species. In this study, methanol and ethanol conversion process was carried out over protonic chabazite (Si/Al = 8) zeolite. Advanced FT-IR operando spectroscopic techniques were employed, along with simultaneous mass spectrometry and gas chromatography analysis of products. The identical experimental conditions were applied during UV-vis spectroscopic studies.

The spectroscopic investigation provided information about the species formed on the surface of catalysts. Mass spectrometry and gas chromatography methods were used to identify the desorbed products. The studies were also supported by spectroscopic, chromatographic, and thermogravimetric analyses of the coke species formed on the catalyst's surface during alcohol conversion. The experimental spectroscopic data was analysed using Multivariate Curve Resolution by Alternating Least Squares (MCR-ALS) algorithms. This allowed for identifying concentration profiles for specific species found in complex spectra.

The FT-IR spectra (Figure 1) registered during ethanol conversion showed the extensive formation of species involved in HCP in chabazite cages. This is confirmed by the rapid formation of propylene and C<sub>4+</sub> hydrocarbons upon contact with the SSZ-13 catalyst and ethanol. The bands at 1602 and 1617 cm<sup>-1</sup> can tentatively be attributed to aromatic compounds as highly methylated (ethylated) benzenium cations. The m/z = 70 fragmentation ion observed may come from the ethylketene formed over the acid sites of SSZ-13 in trace amounts during the first 25 minutes of the reaction. The band observed at 1505 cm<sup>-1</sup> was identified in the methanol-to-hydrocarbon process as alkyl-substituted cyclopentenyl cations.

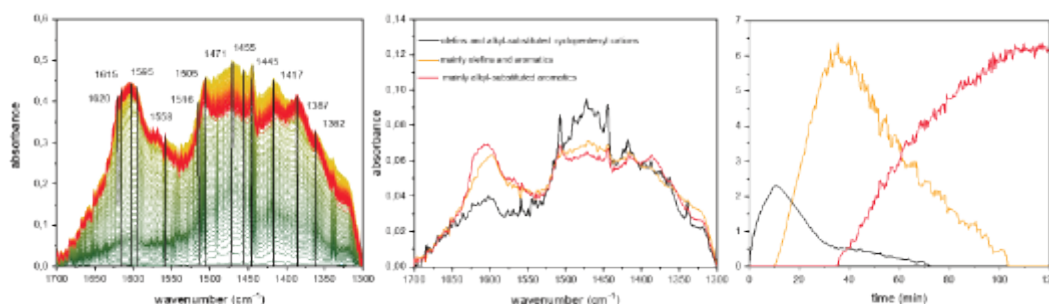


**Figure 1.** (Left) Top-down projection of FT-IR spectra, (middle) mass spectrometry results and (right) gas chromatography selectivities and conversions collected during ethanol conversion over HSSZ-13.

Spectroscopic results obtained by both methods indicate the presence of various chemical compounds. MCR-ALS analysis separated the spectra of different components and showed their changes in time. MCR-ALS of the obtained results helped identify three distinct species formed during ethanol dehydration over SSZ-13 zeolite. The concentration profiles provided information on the timing of their formation. Species A (black curve), represented by bands specific for alkyl-substituted cyclopentenyl cations (band at 1505 cm<sup>-1</sup>), was identified as the one formed at the beginning of ethanol conversion. Species B (yellow curve) and C (red curve) were formed in the later stages of the reaction. Species B (yellow curve) is expected to be olefinic products formed only in part of the reaction and then prone to oligomerise to aromatics represented by species C (red curve).

Overall, the MCR-ALS allows for the resolution of complex spectra of a mixture of species into pure-component contributions. At the same time, the component profiles are constrained by physical or chemical objectives (for instance, non-negativity and unimodality).

### References

1. M.J. Wulfers, F.C. Jentoft, *ACS Catalysis*, 4 (2014) 3521-3532.
2. S. Zeng, W. Zhang, J. Li, S. Lin, S. Xu, Y. Wei, Z. Liu, *Journal of Catalysis*, 413 (2022) 517-526.
3. E.D. Hernandez, F.C. Jentoft, *ACS Catalysis*, 10 (2020) 5764-5782

**Acknowledgement** The National Science Centre, Poland, supported the work within Grant No. 2023/49/B/ST4/02340.



## Mixed interzeolite conversion enabling fast AEI synthesis

**E. Brozzi<sup>1</sup>, R. Simancas<sup>2</sup>, T. Wakihara<sup>2,3</sup>, M. Dusselier<sup>4</sup>, S. Kuhn<sup>1</sup>**

1. Department of Chemical Engineering, KU Leuven, Celestijnenlaan 200F, 3001 Leuven, Belgium

2. Department of Chemical System Engineering, The University of Tokyo, 7-3-1 Hongo, Bunkyo-ku, Tokyo 113-8656, Japan

3. Institute of Engineering Innovation, The University of Tokyo, 2-11-16 Yayoi, Bunkyo-ku, Tokyo 113-8656, Japan

4. Centre for Sustainable Catalysis and Engineering (CSCE), KU Leuven, Celestijnenlaan 200F, 3001 Leuven, Belgium

[elena.brozzi@kuleuven.be](mailto:elena.brozzi@kuleuven.be)

### Introduction

SSZ-39, with AEI-type framework, belongs to the family of small pores zeolites, which are promising candidates as the catalyst of the future for the methanol-to-olefin (MTO) reaction, selective catalytic reduction of NO<sub>x</sub> with NH<sub>3</sub> (NH<sub>3</sub>-SCR), methane to methanol reaction, etc. [1]. However, the synthesis of this zeolite requires long synthesis times, and its pure phase can be obtained only in a very narrow reactant composition window. A fast synthesis of AEI zeolite was achieved by Hu *et al.* in 80 minutes by using amorphous reactants, with a final Si/Al ratio of the product in the range 6-7 [2]. In this work, a mixture of commercial FAU zeolites is employed as source to achieve complete synthesis of AEI in 30 minutes with a final Si/Al ratio of 11. The use of a combination of two zeolitic sources – mixed interzeolite conversion (IZC) - enables fast dissolution and potentially means to control the Si/Al ratio of this framework and simultaneously substantially speed up AEI crystallization.

### Materials and Methods

Two different FAU zeolites (Tosoh HSZ373HUA, Si/Al ratio 15, and Tosoh HSZ390HUA, Si/Al ratio 385) used as Si and Al source are mixed in different proportions to obtain a nominal final Si/Al ratio of 25. Tetramethylpyperidinium hydroxide (SACHEM, 35wt%) is used as OSDA, NaOH (50wt%) is used as mineralizing agent. The composition of the synthesis mixture for both seed preparation and fast synthesis is the following: 1 SiO<sub>2</sub> : 25<sup>-1</sup> Al: 0.25 TPA<sup>+</sup> : 0.25 Na<sup>+</sup> : 0.5 OH<sup>-</sup> : 10.5 H<sub>2</sub>O. This recipe, using a Teflon-lined stainless steel autoclave at 170 °C for 5 days in a rotating oven at 30 rpm, yielded pure AEI zeolite that is subsequently used as seeds for the fast synthesis. As-made seeds are subsequently ball milled using ZrO<sub>2</sub> balls (mixer machine Thinky Mixer ARE-310) to retain partial crystallinity and decrease their particle size. 2wt% on a Si basis of milled seeds are used in the fast synthesis, which is achieved in a tubular batch reactor made of stainless steel, at 210 °C in an oil bath under static conditions.

### Results

The traditional hydrothermal synthesis in the autoclave results in a solid net yield above 40%, a Si/Al ratio of 11, a particle size distribution in the range 2-3 μm, and typical cubic morphology, as shown in Fig. 1A. To achieve faster synthesis, the kinetics of the system is sped up by progressively increasing the temperature until 210 °C and by making use of this product as seeds.

Seeding as-made AEI zeolite has no effect on the synthesis kinetics; only partial milling allows ‘seed activation’, probably thanks to a much smaller particle size distribution, see Fig. 1B. Furthermore, Raman spectroscopy will be performed on the seeds subjected to different milling strengths and times to characterize the effect of exerting mechanical forces on the zeolite microstructure.

A combination of milled seeds and high temperatures allows the synthesis to reach completion in times as low as 30 minutes in a tubular batch reactor (as shown in Fig. 2A), achieving net solid yields around 45%, a Si/Al ratio of 11, and an average particle size around 500 nm (see Fig. 1C). Only 2wt% of seeds on a Si basis is revealed sufficient to speed up the synthesis. As evident from Fig. 2B, the synthesis does not go through an amorphous intermediate, but a continuous transformation from FAU to AEI seems to take place in crystalline form, with the solid yield remaining almost unchanged. Interestingly, it is the synergy between a fast-dissolving FAU source and a Al-rich FAU source, namely mixed IZC, that allows completion of the synthesis in a short time. The use of a single FAU source or a Si-rich amorphous source is incapable of synthesizing pure AEI in such short batch times and high yield as evidenced from control experiments.

### Conclusions

SSZ-39 zeolite, with AEI-type framework, could be synthesized in 30 minutes in a tubular batch reactor at 210 °C, obtaining solid yields above 40%, thanks to the simultaneous use of two FAU zeolites of different Si/Al ratio as chemical source in the preparation mixture. The product presents a typical cubic morphology with an average crystal size of 500 nm. This fast synthesis not only allowed the preparation of SSZ-39 suitable for catalytic application in less than 30 min of hydrothermal treatment, but also shows potential for further tuning of the Si/Al ratio.

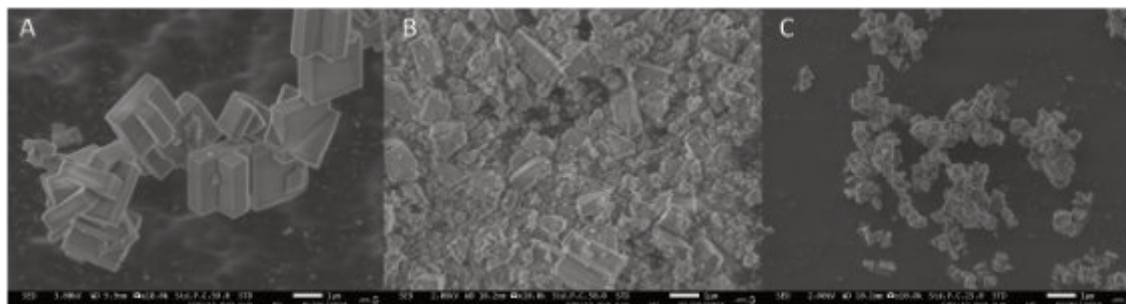


**Figure 1.** A) SEM of as-made AEI zeolite synthesized in the autoclave (seeds); B) SEM of the milled seeds; C) SEM of the tubular reactor product.

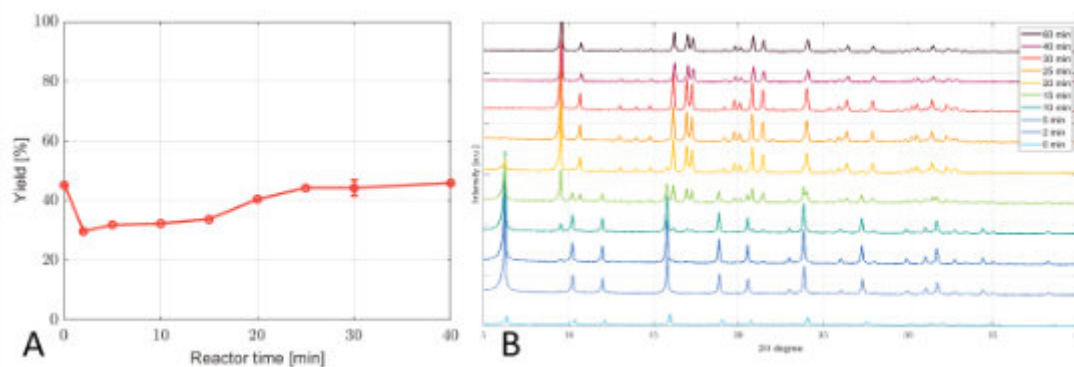


**Figure 2.** A) Evolution of the solid yield over time for AEI synthesis in a tubular batch reactor at 210 °C; B) Evolution of the XRD pattern from 0 to 60 min synthesis time in a tubular batch reactor at 210 °C.

## References

- [1] M. Dusselier and M. E. Davis, "Small-Pore Zeolites: Synthesis and Catalysis," *Chem. Rev.*, vol. 118, no. 11, pp. 5265–5329, 2018, doi: 10.1021/acs.chemrev.7b00738.
- [2] P. Hu *et al.*, "Broadening synthetic scope of SSZ-39 zeolite for NH<sub>3</sub>-SCR: A fast and direct route from amorphous starting materials," *Microporous Mesoporous Mater.*, vol. 330, no. November 2021, p. 111583, 2022, doi: 10.1016/j.micromeso.2021.111583.

## Finetuning the adsorption behavior of SSZ-13 by the addition of Li during and after synthesis

S. Robijns<sup>1</sup>, N. De Witte<sup>2</sup>, J. Devos<sup>1</sup>, T. R. C. Van Assche<sup>2</sup> and M. Dusselier<sup>1</sup>.

<sup>1</sup> Center for Sustainable Catalysis and Engineering (CSCE), KU Leuven, B-3001 Leuven, Belgium

<sup>2</sup> Department of Chemical Engineering, Vrije Universiteit Brussel (VUB), Pleinlaan 2, B-1050 Brussels, Belgium.

svn.robijns@kuleuven.be

In recent years, focus in zeolite synthesis has shifted from controlling parameters such as Si/Al-ratio, particle morphology and crystal size towards the incorporation of hetero-atoms, creation of mesopores and a precise control over the aluminium distribution inside the crystal. The latter of which can be split up between aluminium zoning, which is an inhomogeneous aluminium distribution on the scale of a crystal, and aluminium siting, which tries to look at the crystallographic positions occupied by the aluminium. When two aluminium atoms are only separated by one (Next Nearest Neighbour) or two (Next Next Nearest Neighbour) silicon atoms and are in the same accessible cavity, an Al pair is created.[1] The presence of these paired Al sites have already been shown to have a profound impact on catalysis. Firstly, in acid catalysis, these nearby protons can cause synergistic effects, and secondly, paired Al is capable of stabilizing divalent (transition metal) cations, these are often the active sites in redox catalysis. Control over the amount of paired Al inside of a zeolite, as probed by an aqueous cobalt exchange and expressed as a Co/Al ratio or the Divalent Cation Capacity (DCC), has mainly been thermodynamic in nature. The use of both organic and inorganic SDA's could result in an increased DCC, if the sites of both SDA's inside the framework were sufficiently close to stabilize the negative charges of an Al pair. [1] [2] However, recent advances showed the viability of a kinetic route, namely Interzeolite Conversion or IZC (sometimes called interzeolite transformation), to steer the DCC to never obtained heights. This way, Devos et al. were able to produce SSZ-13 (Si/Al=35) zeolites with up to 70% paired Al (DCC~0.35).[3]

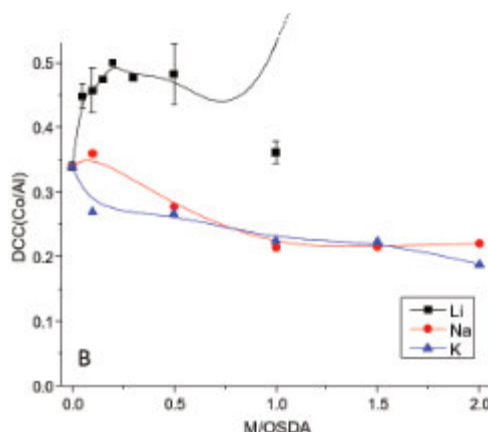


**Figure 1:** DCC of syntheses with different concentrations of alkali cations, where M is either Lithium, Sodium or potassium. The batch composition of the syntheses was 1 SiO<sub>2</sub>:0.025 AlO<sub>2</sub>:0.35-X OSDA<sup>+</sup>:X M<sup>+</sup>: 0,35 OH<sup>-</sup>: 16.5 H<sub>2</sub>O.

The goal of this research which was already published in crystal growth and design [4] was to combine both the thermodynamic and kinetic routes by adding different alkali metals (Li<sup>+</sup>, Na<sup>+</sup> and K<sup>+</sup>) to a FAU to CHA IZC system similar to the one reported by Devos et al.[3] To assure no interference by other factors, the total hydroxide concentration was kept constant between trials, whilst varying the M<sup>+</sup>/OSDA-ratio.

The DCC displayed in figure 1, indicate similar trends for the Na<sup>+</sup> and K<sup>+</sup> systems, showing a clear decrease in DCC as the alkali concentration increases. This is surprising for two reasons, first of all, in syntheses starting from amorphous sources, Na<sup>+</sup>-ions have a positive effect on the DCC.[2] And second of all, there is no increase in K<sup>+</sup> which is retained in the zeolite as the batch concentration increases indicating the role of K<sup>+</sup> ions during dissolution and crystal growth must be equally important in controlling Al distributions in the resulting SSZ-13 zeolite. Finally, the Li<sup>+</sup> series shows by far most interesting results. Even at low concentrations, a sharp increase in DCC is observed all the way to a value of 0.5, which indicates 100% of the Al is in a paired state. This plateau is held over a range of M<sup>+</sup>/OSDA from 0,15 to 0,5 after which it drops again. The observation that the DCC remains constant over a range of Li<sup>+</sup> concentrations, shows great confidence towards paired alumina being responsible for the Co<sup>2+</sup>-uptake of this sample, as the amount of lithium inside of the formed zeolite was also observed to be increasing over this range, excluding defects from

stabilizing  $\text{Co}^{2+}$ . This beneficial effect of lithium has already been observed in syntheses from amorphous sources, where it resulted in SSZ-13 with a DCC of 0.20, which is among the highest non-IZC values mentioned in literature. Lithium's effect was appointed to its low polarizability and high charge density.[5]

Interestingly, when these Li samples were exchanged for  $\text{Na}^+$  and tested for alkene adsorption using inverse gas chromatography, it was noticed that, unlike their commercial  $\text{Na}$ -exchanged counterparts, no cracking took place during the measurement (see figure 2) Allowing for the determination of the Henry constants of linear alkenes on SSZ-13 for the first time. This effect was found to be independent of the DCC and seemed to be caused by the presence of residual Li in the zeolite structure. FTIR measurements (figure 2) showed that samples that contained Li (introduced through synthesis or post synthetically) showed a less intense signal of internal silanols and silanol nests. This passivation of weakly acidic silanols might be an explanation as to why no cracking was observed.

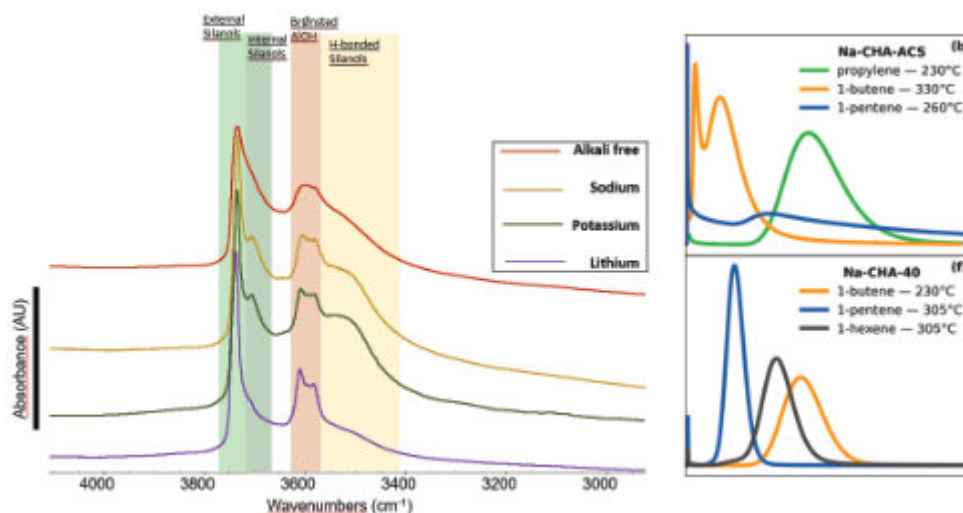


**Figure 2:** Left) FTIR spectra (150°C) of the OH region of different SSZ-13 zeolites synthesized in the presence of different alkali cations. As can be seen the sample synthesized in the presence of Li shows a lower signal in the silanol and silanol nest region. Right) Inverse gas chromatography plots of different alkenes. The commercial sample displays cracking as multiple peaks appear or the curve is not gaussian.

In conclusion, we would like to apply for a talk during EAZC 2024 in order to further elucidate the role of Li when in steering Al distributions and defect passivation.

## References

- [1] E. E. Bickel, C. T. Nimlos and R. Gounder, *J. Cat.*, 399, 75-85 (2021).
- [2] J. R. Di Iorio, S. Li, C. B. Jones, C. T. Nimlos, Y. Wang, E. Kunkes, V. Vattipalli, S. Prasad, A. Moini, W. F. Schneider, and R. Gounder, *J. Am. Chem. Soc.*, 142, 4807-4819 (2020).
- [3] J. Devos, M. L. Bols, D. Plessers, C. Van Goethem, J. W. Seo, S.-J. Hwang, B. F. Sels, and M. Dusselier, *Chem. Mater.*, 32 (1), 273-285 (2020).
- [4] S. Robijns, J. Devos, T. Donckels, R. De Oliveira-silva, N. De Witte, T. R. C. Van Assche and M. Dusselier, *Cryst. Growth Des.* 23 (1), 289-299 (2022)
- [5] W. Lv, S. Wanga, P. Wang, Y. Liu, Z. Huang, J. Li, M. Dong, J. Wang, W. Fan., *J. Cat.*, 393, 190-201 (2021).

## Acknowledgments

S.R., N. D.W, T. V. A., and M.D. thank the Research Foundation—Flanders (FWO Vlaanderen) for funding (Grants G085220N and G0A0D24N to M.D.). The authors are grateful to the Hercules Foundation for financing the TEM (AKUL/13/19).

## *In-situ* investigation of water harvesting by CAU-10-OH MOF: a 2-steps process

G. Nénert<sup>1</sup>, M. van der Veen<sup>2</sup>, D. Rega<sup>2</sup>

<sup>1</sup> Malvern Panalytical B. V. Lelyweg 1, 7601 EA Almelo, The Netherlands

<sup>2</sup> Catalysis Engineering Department of Chemical Engineering TU Delft, Delft 2628, The Netherlands  
gwilherm.nenert@malvernpanalytical.com

MOFs exhibits interesting harvesting water capabilities from the air or as heat pumps as they demonstrate a steep increase in water uptake in the range 10-30 RH% [1]. Optimal water isotherms are represented by an alternation of moderately hydrophilic and hydrophobic sites. However even within MOFs exhibiting such alternation, the required steep uptake of water relevant for real applications is quite scarcely met [2]. Recently, we have studied the CAU-10-X (H = H, CH<sub>3</sub>) members and unravelled the materials' structural deformation and water ordering during absorption [3]. We have shown that the steric hindrance of the -CH<sub>3</sub> group lowers the number of average hydrogen bonds from 3.3 to 2.3 explaining the difference in the water uptake behaviour.

Among the various members of the CAU-10-X family, X = OH is particularly interesting as this is the only composition where a steep 2-step process is taking place within the isotherm [2]. Aiming to determine a conceptual understanding of the mechanism resulting from this water absorption to design "de novo" water harvesting materials, we have investigated the members X = OH using *in-situ* relative humidity powder diffraction. We present in Fig. 1 our results for X = OH. These results demonstrate for the first time the existence of an intermediate phase.

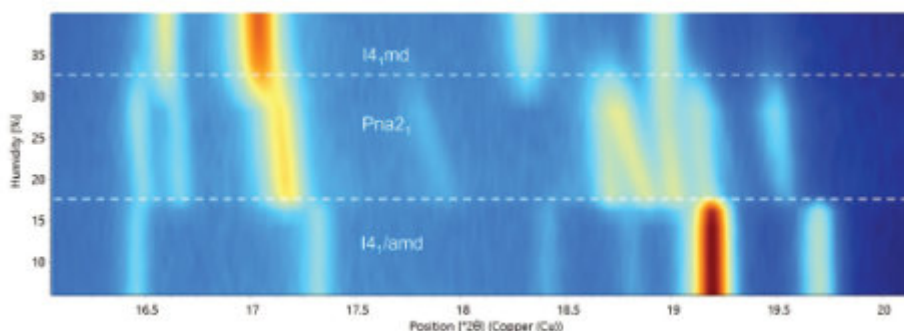


**Figure 1:** *In-situ* relative humidity study of CAU-10-OH carried out at T = 60°C.

The existence of this intermediate phase stabilized under temperature and moderate RH shed some new light in our understanding and call for further investigation of the water uptake mechanism. The possibility to stabilize and study an intermediate phase enables us to have further understanding of the water uptake mechanism.

### References

- [1] Kalmutzki, M.J., Diercks, C.S., Yaghi, O.M. (2018) *Adv. Mater.* **30**, 1
- [2] Reinsch, H. van der Veen, M.A. *et al.*, (2013) *Chem. Mater.* **25**, 17
- [3] van der Veen, M. *et al.*, (2024) *Adv. Materials*, **36**, 2210050



## Adsorption of small molecules on zeolite SSZ-45

**A.Barros<sup>1</sup>, J.Valero<sup>1</sup>, S.Valencia<sup>1</sup>, F.Rey<sup>1</sup>**

*Instituto de Tecnología Química, Universitat Politècnica de València – Consejo Superior de Investigaciones Científicas (UPV-CSIC), 46022 Valencia (Spain)  
abarpar@itq.upv.es*

**Introduction** – The increasing global demand for energy, driven by technological advancements and population growth, poses a significant challenge. According to the Energy Information Administration (EIA) in 2007, there is a projected 57 % increase in energy demand from 2004 to 2030 [1]. A substantial portion of the world's energy consumption, ranging from 10 to 15%, is attributed to separation processes of various chemical compounds. These separations involve processes such as cryogenic distillations, amine scrubbing or extraction-evaporation-distillation that could be replaced by separation units based on the use of porous materials as selective adsorbents. Crystalline porous materials have been extensively studied as exceptional adsorbents for selective gas separation due to their high versatility in pore engineering [2].

Small-pore zeolites are of particular interest for molecules separations due to their large pore volume and preferential guest molecule size exclusion [3]. In particular, high-silica small-pore zeolites combine fine molecular sieving and high thermal stability resulting in appropriate candidates for small molecules separations.

This study is focused on the high silica zeolite SSZ-45 that belongs to this category and consists of a one-dimensional pore system of 8R channels with large side pockets [4]. In the present work, the adsorption properties of zeolite SSZ-45 have been studied by single component adsorption isotherms of small molecules to evaluate its capability for different separations.

**Experimental** - Zeolite SSZ-45 was synthesized according to a reported recipe [4] and characterized by using different techniques, such as powder X-ray diffraction (XRD), scanning electron microscopy (SEM), solid state NMR, and determination of textural properties by N<sub>2</sub> and CO<sub>2</sub> adsorption. The adsorption capacities of different gases (CO<sub>2</sub>, CH<sub>4</sub>, C<sub>2</sub>H<sub>6</sub> and C<sub>2</sub>H<sub>4</sub>) were measured in a volumetric adsorption instrument (iSorb HP, Quantachrome) at high pressure and different temperatures for studying the adsorption behaviour by means of the corresponding thermodynamic and kinetic parameters.

**Results and Discussion** - The zeolite SSZ-45 was successfully synthesized as confirmed by its characterization using XRD, SEM and textural properties determination. The high pressure adsorption measurements revealed that CO<sub>2</sub> exhibits the highest uptake, followed by C<sub>2</sub>H<sub>4</sub> and C<sub>2</sub>H<sub>6</sub>, with CH<sub>4</sub> showing the lowest below 200 kPa (Figure 1). Above this pressure, C<sub>2</sub>H<sub>6</sub> is the least adsorbed molecule, which may be related to the nature of SSZ-45 being a small pore zeolite with a narrow aperture and the limitations for molecules whose size and shape prevent entry into the cavities can lead to diffusional restrictions.

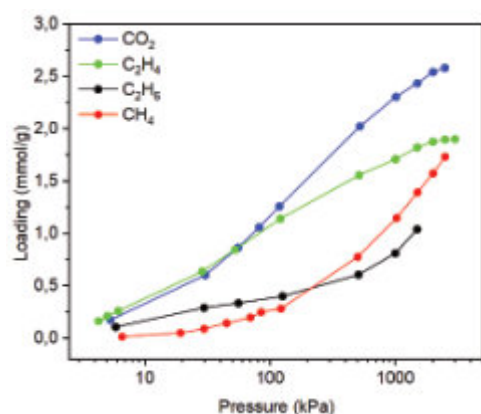


**Figure 1.** Adsorption Isotherms of different adsorbates on zeolite SSZ-45 at 298 K.

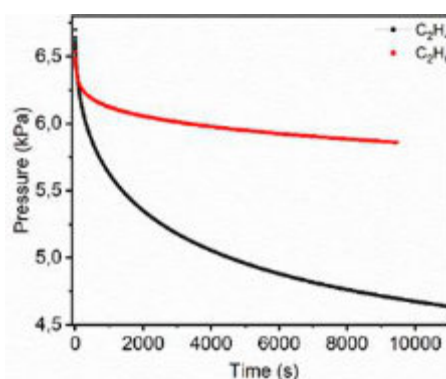


**Figure 2.** Kinetic study of C<sub>2</sub>H<sub>4</sub> (black) and C<sub>2</sub>H<sub>6</sub> (red) adsorption on SSZ-45 at 298 K.

As can be seen in Figure 1, CH<sub>4</sub> adsorption follows a type I isotherm tendency, but less squared than CO<sub>2</sub>, which means that CH<sub>4</sub> molecules interact less strongly than CO<sub>2</sub> ones with the solid. This suggests that CO<sub>2</sub> and CH<sub>4</sub> could be thermodynamically separated using this zeolite.

Only C<sub>2</sub>H<sub>4</sub>, CH<sub>4</sub> and CO<sub>2</sub> reached thermodynamic equilibrium, confirming the diffusional restrictions for C<sub>2</sub>H<sub>6</sub>. In the case of the adsorption of the C<sub>2</sub>H<sub>6</sub> and C<sub>2</sub>H<sub>4</sub>, the difference in the diffusion rates between the olefin (C<sub>2</sub>H<sub>4</sub>) and the





paraffin ( $C_2H_6$ ) could be the reason for the different adsorption behaviour, allowing a possible kinetic separation of both adsorbates. Figure 2 shows the pressure drop in the measuring cell caused by the adsorption of the  $C_2H_6$  and  $C_2H_4$  by the zeolite. As deeper is the pressure drop, higher is the diffusion of this component within zeolite micropores. Therefore, it is clearly seen that  $C_2H_4$  is the fastest adsorbed molecule instead of its corresponding paraffin. Thus, zeolite SSZ-45 shows a promising kinetic separation mechanism, wherein the olefin exhibits greater adsorption compared to the paraffin. This suggests the potential for a less energy-intensive process to selectively separate one over the other based on SSZ-45's distinctive kinetic separation properties.

The calculation of isosteric heats of adsorption of the different adsorbates studied is shown in Figure 3. As can be seen in the figure,  $CH_4$  is the molecule less strongly adsorbed on SSZ-45 zeolite with significant difference from  $CO_2$ , which interacts much more strongly, allowing a possible thermodynamic separation of  $CO_2$  from  $CH_4$  with this zeolite, as was also suggested by the isotherms shown in Figure 1.

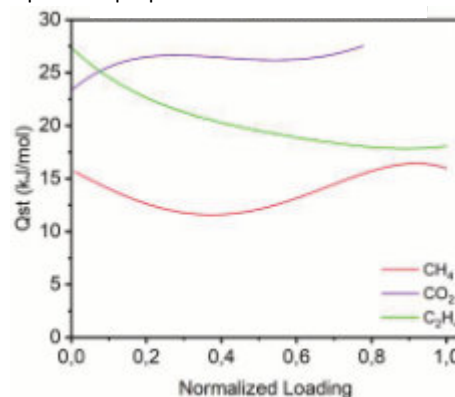


**Figure 3.** Isosteric heat of adsorption of  $CH_4$  (red),  $CO_2$  (blue), and  $C_2H_4$  (green) on zeolite SSZ-45.

**Conclusions** - Zeolite SSZ-45 shows a promising kinetic separation mechanism, wherein the olefin exhibits greater adsorption compared to the paraffin. This suggests the potential for a less energy-intensive process to selectively separate one over the other based on SSZ-45's distinctive separation properties.

#### References

- [1] H. Yang, Z. Xu, M. Fan, R. Gupta, R.B. Slimane, A.E. Bland, I. Wright, J. Environ. Sci. 20 (2008), 14–27.
- [2] M. Dusselier, M.E. Davis, Chem. Rev. 118 (2018), 5265–5329.
- [3] E. Pérez-Botella, S. Valencia, F. Rey, Chem. Rev. 122 (2022), 17647–17695.
- [4] S. Smeets, D. Xie, L. B. McCusker, Chem. Mater. 26 (2014), 3909–3913.



## Influence of Al distribution in transition-metal-free aluminosilicate Ferrierite zeolite on the performance of methane oxidation

P. Xiao<sup>1</sup>, H. Toyoda<sup>1</sup>, K. Nakamura<sup>1</sup>, Y. Wang<sup>1</sup>, T. Yokoi<sup>\*1,2</sup>

<sup>1</sup> Institute of Innovative Research, Tokyo Institute of Technology, 4259 Nagatsuta, Midori-ku, Yokohama 226-8503, Japan

<sup>2</sup> iPEACE223 Inc., Konwa Building, 1-12-22 Tsukiji, Chuo-ku, Tokyo, 104-0045, Japan

E-mail: yokoi@cat.res.titech.ac.jp

Direct activation of methane highly depended on the transition- or noble-metal-loading catalysts in the past decades. In our recent work, the commercial transition-metal-free aluminosilicate Ferrierite (FER) zeolite from Zeolyst (CP914C) has been reported to catalyze methane and N<sub>2</sub>O to methanol effectively. A possible reaction pathway similar to the Fe-containing zeolites was advocated. As a source of active sites, the environment of Al atoms in FER zeolite was found to influence the reaction performance in methane oxidation reaction significantly. Herein, FER zeolites with different Al locations and arrangements have been synthesized by adjusting the organic structure directing agent (OSDA) or pore filling agent. The activity of Al species from different T sites in methane to methanol reaction was studied at 250 °C. The Al arrangement affecting the tandem reaction of methanol to hydrocarbon was investigated at 350 °C. This work further verified our recent work and guided the preparation of active zeolite for methane oxidation.

### Introduction

Reduction and utilization of greenhouse gases, such as methane, nitrous oxide, and carbon dioxide, are important and urgent issues to be resolved.<sup>[1]</sup> Direct conversion of methane into liquid chemicals suitable for transportation and storage, such as methanol, is a major subject with significant economic and environmental value.<sup>[2]</sup> In the past decades, the catalysts were merely focused on precious metals such as Pt and Au,<sup>[3]</sup> and transition metals such as Cu, Co, and Fe as catalytically active species.<sup>[2]</sup> Particularly, the transition-metal-exchanged zeolites have widely been used in gas and liquid-phase reaction systems.<sup>[2]</sup> However, the aluminosilicate zeolites directly catalyze methane to methanol has seldom been reported. In our recent work, aluminosilicate FER zeolite was found effective in the activation of methane and N<sub>2</sub>O to methanol.<sup>[3]</sup> As the source of active sites, the environment of Al atoms in FER zeolite deserves further and comprehensive study. FER is a 2-dimensional zeolite with 8-ring channels and intersected 10-ring channels. A cavity that is only accessible through the 8-ring windows is formed, and known as the FER cage. FER zeolite is considerably stable towards thermal, hydrothermal, and chemical treatments.<sup>[3]</sup>

### Experimental

The aluminosilicate FER zeolites were synthesized using 1,4-dioxane as the pore-filling agent or pyrrolidine as OSDA referring to literature.<sup>[4]</sup> Specifically, a basic solution with the composition of SiO<sub>2</sub>: 0.05Al<sub>2</sub>O<sub>3</sub>: 0.0625Na<sub>2</sub>O: 1 dioxane or pyrrolidine: 20H<sub>2</sub>O was first obtained by dissolving dioxane or pyrrolidine, NaOH, and NaAlO<sub>2</sub> in deionized water, and then colloidal silica was added to the liquid and vigorously stirred at room temperature for 1 h. Finally, the obtained gel was transferred into an autoclave and subjected to crystallization in a tumbling oven at 165 °C for 7 days. The solid product was collected by centrifugation, washed, and dried overnight at 100 °C. The as-synthesized samples using 1,4-dioxane and pyrrolidine were named as-FER(Diox) and as-FER(Pyrr), respectively. 1,4-Dioxane and pyrrolidine in as-synthesized samples were removed by calcination at 550 °C for 10 h. H-FER(Diox) and H-FER(Pyrr) were prepared by using calcined samples to exchange with 2.5 mol·L<sup>-1</sup> NH<sub>4</sub>NO<sub>3</sub> at 80 °C for 3 h and followed by calcination in air at 550 °C for 5 h.

The continuous oxidation of methane to methanol reaction was carried out in the online-reaction-analysis system. In a typical test, 100 mg of catalyst with a granular form (particle size 500–1000 μm) was charged into a quartz tube (inner diameter 4 mm), which was placed in an electric tube furnace. The catalyst was pretreated at 500 °C for 1 h before reaction at 250 or 350 °C in a flowing gas mixture of CH<sub>4</sub>, N<sub>2</sub>O, H<sub>2</sub>O, and Ar with flow rates of 10, 10, 2, and 3 mL·min<sup>-1</sup>.

### Results and Discussion

The narrow <sup>27</sup>Al MAS NMR spectra of as-FER(Diox) and as-FER(Pyrr) suggested that Al atoms were in the framework as a tetra-coordination state (Al<sub>IV</sub>) (Figure 1a). Al location at different T sites was further confirmed based on the <sup>27</sup>Al MQMAS NMR spectra. Specifically, 60% Al atoms of as-FER(Diox) were at T4 sites, where T4 sites were on the 8-ring channels and shared a 6 MR with T2 sites (Figure 1b). In the case of as-FER(Pyrr), 54% Al atoms occupied T3 sites, where T3 sites were on the 10-ring channels and shared a 10 MR with T1 and T2 sites (Figure 1b). The <sup>27</sup>Al MAS NMR spectra of H-FER(Diox) and H-FER(Pyrr) almost overlapped (Figure 1a). The proportion of normal tetra-coordination Al (Al<sub>IV-1</sub>), distorted tetra-coordination Al (Al<sub>IV-2</sub>), penta-coordination Al (Al<sub>V</sub>), and hexa-coordination Al (Al<sub>VI</sub>) for H-FER(Diox) and H-FER(Pyrr) was identical. However, 45 and 36 % Al atoms were located at T4 and T3 for H-FER(Diox) and H-FER(Pyrr) among the total Al content, respectively. The NH<sub>3</sub>-TPD profiles of H-FER(Diox) and H-FER(Pyrr) almost corresponded due to the similar Si/Al ratio and similar proportion of framework Al (Figure 1c).

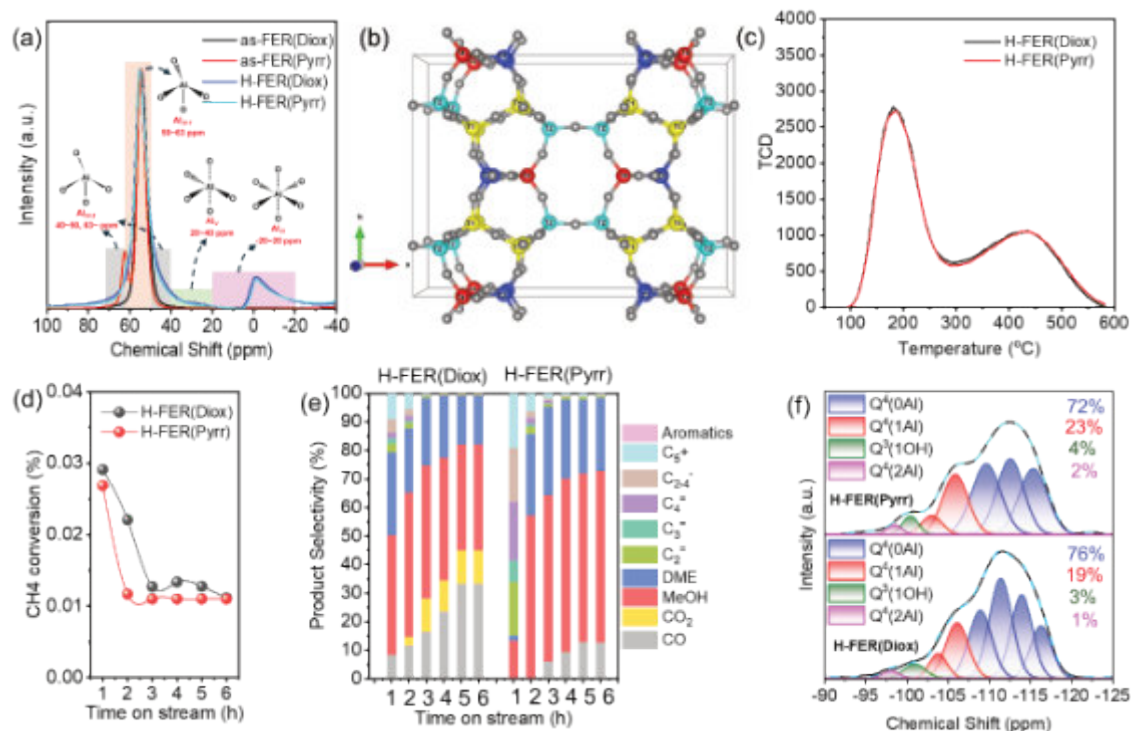


**Figure 1.** (a) <sup>27</sup>Al MAS NMR spectra of as-synthesized and H-type FER(Diox) and FER(Pyrr) zeolites. (b) Location of four T sites in FER zeolite. (c) NH<sub>3</sub>-TPD profiles of H-FER(Diox) and H-FER(Pyrr). (d) Compare CH<sub>4</sub> conversion of H-FER(Diox) and H-FER(Pyrr) zeolites at 250 °C. (e) Compare product distribution of H-FER(Diox) and H-FER(Pyrr) zeolites at 350 °C. Reaction conditions: 100 mg catalyst, CH<sub>4</sub>/N<sub>2</sub>O/H<sub>2</sub>O/Ar=10/10/2/3 ml·min<sup>-1</sup>. (f) Deconvolution <sup>29</sup>Si MAS NMR spectra for H-FER(Diox) and H-FER(Pyrr).

Firstly, the activity of methane to methanol (MTM) was investigated at 250 °C, and methanol was the main product for both H-FER(Diox) and H-FER(Pyrr). H-FER(Diox) achieved higher CH<sub>4</sub> conversion than H-FER(Pyrr), indicating the more active feature of Al species for H-FER(Diox) (Figure 1d). The newly formed Al<sub>IV-2</sub>, Al<sub>V</sub>, and Al<sub>VI</sub> derived from the dealumination of framework Al at T4 and T3 sites for H-FER(Diox) and H-FER(Pyrr), respectively. Therefore, we concluded that Al species originating from T4 were more active than those from T3 sites. Secondly, the tandem reaction of methanol to hydrocarbon (MTH) was studied at 350 °C. The initial hydrocarbon selectivity of H-FER(Pyrr) was up to 90%, which was much higher than that of H-FER(Diox) under the premise of a similar acid amount (Figure 1e). As emphasized in our recent work,<sup>[5]</sup> except for the acid amount, the distance between the oxidative site and the acid site, and the propagation path of methanol also influenced the production of hydrocarbon. We ascribed hydrocarbon formation on H-FER(Pyrr) to the higher proportion of Al pairs, which can be proved by <sup>29</sup>Si MAS NMR spectra (Figure 1f) and Co<sup>2+</sup>-exchanged results.

## Conclusion

In summary, the significance of Al distribution and arrangement in FER zeolite on methane oxidation has been clarified. FER zeolites with different Al distributions were prepared using 1,4-dioxane as the pore-filling agent or pyrrolidine as the OSDA. Framework Al atoms for FER(Diox) and FER(Pyrr) were mainly located at T4 and T3 sites, respectively. The higher methane conversion of H-FER(Diox) than H-FER(Pyrr) at 250 °C certified the more active feature of Al species from T4 sites. Additionally, the higher hydrocarbon selectivity of H-FER(Pyrr) indicated that Al pairs contributed to the tandem reaction of methanol to hydrocarbons. This work highlighted the significance of the distribution and arrangement of Al atoms in FER zeolite for methane oxidation and guided the preparation of active zeolite for methane oxidation.

## References-

- [1] E. D. Schulze, S. Luysaert, P. Ciaias, A. Freibauer, I. A. Janssens, *et al.*, *Nat. Geosci.* **2**, 842 (2009).
- [2] N. F. Dummer, *et al.*, *Chem. Rev.*, **12**, 6359 (2023).
- [3] P. Xiao, Y. Wang, Y. Lu, K. Nakamura, N. Ozawa, M. Kubo, H. Gies, T. Yokoi, *J. Am. Chem. Soc.*, **146**, 10014 (2024).
- [4] P. Xiao, Y. Wang, L. Wang, H. Toyoda, K. Nakamura, S. Bekhti, Y. Lu, J. Huang, H. Gies, T. Yokoi, *Nat. Commun.* **15**, 2718 (2024).
- [5] Z. Xiong, G. Qi, L. Bai, E. Zhan, Y. Chu, J. Xu, N. Ta, A. Hao, F. Deng, W. Shen, *Catal. Sci. Technol.*, **12**, 4993 (2022).

# Hierarchical MEL Type Materials with Intracrystalline Macropores: Syntheses and Characterization

T. Weissenberger,<sup>1</sup> A. Machoke,<sup>1</sup> B. Apeleo Zubiri,<sup>2</sup> D. Drobek,<sup>2</sup> E. Spiecker,<sup>2</sup> M. Hartmann<sup>3</sup> and W. Schwieger<sup>1,3,\*</sup>

<sup>1</sup> Institute of Chemical Reaction Engineering, University of Erlangen-Nuremberg, Germany

<sup>2</sup> Institute of Micro- and Nanostructure Research (IMN) & Center for Nanoanalysis and Electron Microscopy (CENEM), University of Erlangen-Nuremberg, Germany

<sup>3</sup> Erlangen Catalysis Resource Center (ECRC), University of Erlangen-Nuremberg, Erlangen, Germany

\*Corresponding author: [wilhelm.schwieger@fau.de](mailto:wilhelm.schwieger@fau.de)

## 1. Introduction

In recent years, major progress has been made preparing of highly ordered porous materials with tailored porosities, different structures, controlled surface functionality and their structure related applications. In particular, advances have been made in the synthesis and structural characterization of so-called hierarchical zeolites, which combine porosity features of different scale lengths like the intrinsic zeolitic micropores and a second pore system, mostly additional mesopores, in one zeolite crystal. Such approaches can be based on direct or post-synthetic methods.<sup>1</sup>

Here, this contribution will focus on MEL-type zeolites with additional, embedded macropores to provide materials with an interconnected microporous/macroporous system. Thus, the contribution will highlight the generation of an additional porosity by an implementation of a macropore system in an MEL-type zeolite. A special emphasis will be laid on the characterization of this additional pore system by advanced imaging techniques, like electron tomography and ptychographic X-ray tomography.

## 2. Experimental

The synthesis of macroporous zeolite crystals was carried out following a similar approach as reported in our previous work.<sup>2</sup> The mesoporous silica particles (MSPs) were impregnated with the structure-directing agent (TBAOH). The impregnated and dried MSPs were then converted to micro/macroporous zeolites by steam-assisted crystallization at different conditions (temperature; time). The products were washed, dried (348 K; overnight) and calcined (823 K; 10h). Selected area electron diffraction (SAED), high-angle annular dark-field (HAADF) scanning transmission electron microscopy (STEM) and electron tomography (ET) of ZSM-11 particles (180 °C, 7 d, 0.05 M NaAlO<sub>2</sub>) were performed on a double aberration-corrected FEI Titan Themis<sup>3</sup> 300 operated at 300 kV.

## 3. Results and Discussion

As an example for prepared final products, the characterization of the macroporous MEL type zeolites is shown in this abstract. In the upcoming contribution, the impact of the variation of the

different content of the heteroatoms will be discussed in detail, also with respect to their preparation pathway. The XRD pattern of the sample after SAC indicates a typical MEL-type crystal (not shown here). The transmission electron microscopy investigation in figure 1 unravels important structural and morphological features of the resulting porous particulate product. The STEM image and electron tomography volume reconstruction (Figure 1a and 1c) prove the presence of large spherical macropores within the MEL-type crystal, which appear to be well interconnected to each other. Figure 1b shows that the electron diffraction pattern is consistent with the MEL crystal structure viewed along [100] zone axis.

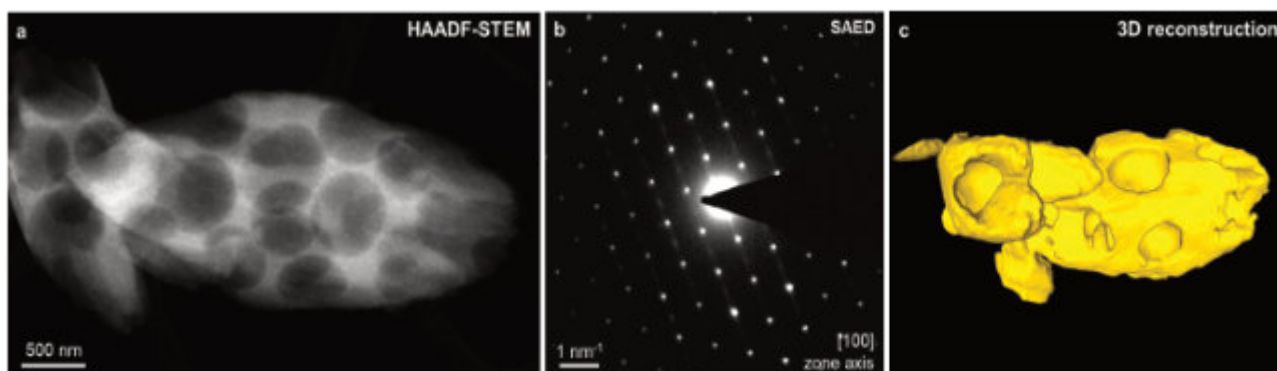


Figure 1: Characterization of the macroporous MEL-type zeolite: a) Scanning transmission electron microscopy (STEM) image, b) selected area electron diffraction (SAED) pattern, c) surface rendering of 3D electron tomographic reconstruction.

#### 4. Conclusions

After the earlier reported macroporous MFI-type crystals, now we could successfully prepare MEL-type zeolites with additional intracrystalline macropores by a similar approach, the steam-assisted crystallization of mesoporous silica spheres in presence of the TBA-cation as a template. 3D tomographic imaging by ET and PXCT proved to be valuable tools for visualizing the hierarchical zeolites, i.e. the existence of a macropore system within the microporous MEL type crystal. As already shown for the MFI-type zeolites earlier, the macropores of the prepared MEL crystal are very well embedded within the crystal and interconnected to each other forming a system, which can be accessed from the outer surface of the crystal directly.

#### References

1. W. Schwieger, A. G. Machoke, T. Weissenberger, A. Inayat, T. Selvam, M. Klumpp, & A. Inayat, *Chem. Soc. Rev.*, 45(12), 3353-3376 (2016).
2. A.G. Machoke, A.M. Beltran, A. Inayat, B. Winter, T. Weissenberger, N. Kruse, R. Güttel, E. Spiecker, W. Schwieger, *Adv. Mater.* 27(6), 1066-1070 (2015).



## Chlorate control in water phase by Pt-based zeolite catalysts

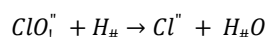
**N. Benmebirouk-Pareja<sup>1</sup>, A. Plá-Hernández<sup>1</sup>, A.E. Palomares<sup>1</sup>**

*1 Instituto de Tecnología Química, Universitat Politècnica de València – Consejo Superior de Investigaciones Científicas (UPV-CSIC), Valencia, Spain*  
[nbenpar@itq.upv.es](mailto:nbenpar@itq.upv.es)

### Introduction

Water is an essential resource for life and it is necessary to ensure its availability and quality, mainly when is used human consumption<sup>[1]</sup>. An emerging pollutant affecting water quality is the chlorate ion and its control is a significant challenge in the European Union. Chlorates are by-products that may be generated during the disinfection treatment of natural water using oxidizing agents, such as chlorine dioxide or ozone. They are produced by the oxidation of natural chloride ions that use to be present in natural water. Chlorates are highly toxic and potent oxidizers. This makes them harmful to health, as they can oxidize haemoglobin, leading to haemolytic anaemia. Additionally, some research has shown that chlorates can interfere with iodine uptake by the thyroid gland and negatively impact both the quantity and quality of sperm. Due to these health risks, the World Health Organization (WHO) has set a provisional limit of 0.7 mg/L for chlorates in drinking water<sup>[2]</sup>.

As a result of this, there is a necessity of sustainable methods able to remove this contaminant from water. Catalytic hydrogenation has been suggested as a potential solution for treating this pollutant as it can be reduced to innocuous chloride according to:



The main knowledge gaps, lessons learned and new opportunities for the catalytic reduction of water pollutants have been reviewed recently by Liu *et al.*<sup>[3]</sup>. However, in these reactions, the use of zeolitic materials as catalysts is not common, even though zeolites are potential catalysts or catalyst supports due to their high surface area, ion exchange properties and topology<sup>[4]</sup>. Hereby, we study the performance of different mono and bimetallic Pt catalysts supported on zeolites for the hydrogenation of chlorate at room temperature and atmospheric pressure and evaluate the influence of the zeolite characteristics on the final activity. The optimized catalyst has been tested for the simultaneous removal of chlorate, chlorite and bromate ions in the water phase and different strategies are proposed to reduce the Pt content in the final catalyst.

### Experimental

Catalysts were prepared using commercial FAU, MFI and MOR zeolites supplied by Zeolyst, commercial BEA zeolite supplied by PQ Zeolites B.V and ITQ-2 zeolite prepared in the laboratory. Different aqueous solutions of a platinum precursor (PtCl<sub>4</sub>) were added by the wet impregnation method to obtain the desired platinum content in the final catalyst. After impregnation, catalysts were calcined at 350°C for 3 h and cooled down to room temperature. Another Pt-catalyst was prepared by ion exchange with an aqueous solution containing PtCl<sub>4</sub> with adequate concentration to achieve the desired amount of metal on the zeolite and with a solid/liquid ratio of 1/40. The metal exchange was made at room temperature. After 24 h under mechanical stirring, the solutions were washed, filtered, dried at 100°C and calcined at 350°C for 3 h. All the catalysts were activated with hydrogen at 200°C for 4 h. Bimetallic catalysts were prepared by the same method but in this case, two impregnation and calcination stages were carried out at different temperatures (500 and 350°C). For this purpose, different aqueous solutions of a vanadium precursor (VOSO<sub>4</sub>·xH<sub>2</sub>O) and platinum precursor (PtCl<sub>4</sub>) were added to obtain the desired content in the final catalyst. After impregnation and calcination, all the catalysts were activated with hydrogen at 200°C for 4 h.

The polluted water was prepared by dissolving NaClO<sub>3</sub> in Milli-Q water. The experiments were conducted at room temperature and atmospheric pressure in a stirred batch reactor containing 0.6 L of water with 50 ppm of chlorate. The stirring velocity was 900 rpm. In specific experiments, 50 ppm of chlorite or bromate ions were added to the water. The experiments were made using 1 g of catalyst and before each test the polluted water was hydrogenated for 2 h with a gas flow of 200 mL·min<sup>-1</sup>. The same hydrogen flow was maintained throughout the reaction. Reactants and products were determined by an ionic chromatograph 883 Basic IC Plus (Metrohm®) equipped with a conductivity detector and a chemical suppressor. The anions were separated in a Metrosep A Supp 5–150/4.0 column.

### Results and discussion

Previous studies determined the most adequate conditions for the preparation of Pt-catalysts that will be active in this reaction. These conditions<sup>[5]</sup> were used for the preparation of the Pt catalysts supported on different microporous supports. Initially, the influence of the zeolite structure on the catalytic activity was evaluated, concluding that the structure plays a secondary role, being necessary the presence of acid sites for the catalytic reduction. This was proved by studying the influence on the catalytic activity of the Si/Al ratio of the zeolite. The Brønsted and Lewis acidity of the parent zeolites was determined by adsorbing pyridine and desorbing it at increasing temperatures. The results

are presented in Table 1, where it is observed that an increase in the aluminium content, i.e. a decrease of the Si/Al ratio, results in an increase in the number of acid sites. It was observed that this is related with the catalyst activity as the best activity was obtained with the catalysts with lower Si/Al ratio (Figure 1A). These results clearly indicate that the presence of these sites is an important issue for this reaction. The influence of acidity on the final activity was also checked by exchanging the Brønsted acid sites (this is the protons) with Na<sup>+</sup>. It was observed that according to the previous results, when the sodium content in the zeolite increases, the activity decreases, due to the substitution of the Brønsted acid sites by Na<sup>+</sup> in the zeolite.

**Table 1.** The acidity of parent zeolites as determined by FT-IR combined with pyridine adsorption and desorption at increasing temperatures.

Supports	Concentration of acid sites ( $\mu\text{molPy g}^{-1}$ )					
	Brønsted			Lewis		
	T <sub>1</sub> =150°C	T <sub>2</sub> =250°C	T <sub>3</sub> =350°C	T <sub>1</sub> =150°C	T <sub>2</sub> =250°C	T <sub>3</sub> =350°C
FAU – Si/Al = 2.6	367	287	160	170	128	96
FAU – Si/Al = 6	210	167	95	78	58	45
FAU – Si/Al = 40	130	120	55	30	22	35

Finally the influence of the method used for the incorporation of Pt to the zeolite was studied. It was observed that when the catalyst was prepared by the ion exchange procedure, the activity of the catalyst increases. As it can be seen in Figure 1B the catalyst containing 1 wt% of Pt but prepared by ion-exchange presents a similar activity than the catalyst with 5 wt% of Pt prepared by wet impregnation. This has been related to a better dispersion of the platinum in the catalyst prepared by ion exchange, as the analysis of the Pt crystallites by electronic microscopy suggests. It was observed that in the catalyst prepared by ion exchange the distribution of the Pt crystallites is centred around 5–15 nm, whilst in the catalyst with the same platinum content but prepared by wet impregnation it is centred around 30–40 nm.

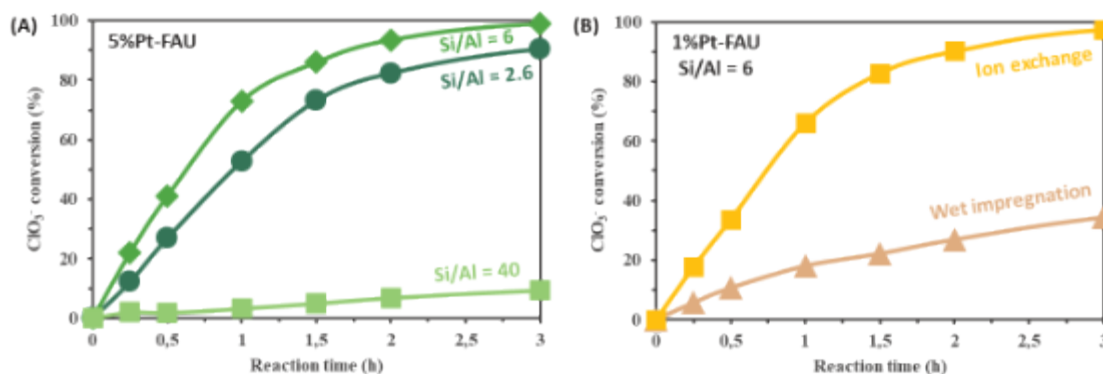


**Figure 1.** The activity of Pt catalysts supported on FAU zeolite with different (A) Si/Al ratios and (B) prepared by different methods.

From this study was concluded that one of the key factors in the catalytic activity of the Pt-zeolites for the hydrogenation of chlorates is the presence of acid sites in the support together with a good dispersion of the noble metal on the catalyst surface. The presence of acid sites favours the interaction of the catalyst with the anion that will be reduced by the hydrogen activated in the well-dispersed Pt active sites. The use of the ion exchange procedure for the catalysts preparation results in an improved activity of the Pt-zeolite allowing an important decrease of the noble metal content. In this way, catalysts with even lower Pt content supported on different zeolites prepared by ion exchange are being studied and characterized for their use in this reaction. This strategy is combined with the incorporation of a second non-noble metal in the zeolite, improving in this way the final activity of the material and significantly increasing the reaction rate.

## References

- [1] European Commission, *Directive (EU) 2020/2184 of the European Parliament and of the Council of 16 December 2020 on the quality of water intended for human consumption (recast)*, EUR-Lex, Belgium (2020).
- [2] *Guidelines for drinking-water quality: 4th edition incorporating the first and second addenda*, World Health Organization, Geneva (2022).
- [3] J. Liu and J. Gao, *Frontiers of Environmental Science & Engineering*, **17**, 26 (2023).
- [4] A. Plá-Hernández, F. Rey and A.E. Palomares, *Catalysis Today*, **429**, 114461 (2024).
- [5] A. Plá-Hernández, J.L. Cerillo, F. Rey and A.E. Palomares, *Catalysis Today*, **424**, 114294 (2023).

## Morphological and Textural Changes in the Synthesis of Nanostructured ZSM-11 Zeolites

A. López Albero<sup>1</sup>, M. Alonso-Doncel<sup>1</sup> and D.P. Serrano<sup>1,2</sup>

<sup>1</sup> Thermochemical Processes Unit, IMDEA Energy Institute, 28935 Móstoles, Madrid, Spain.

<sup>2</sup> Chemical and Environmental Engineering Group, Rey Juan Carlos University, 28933, Móstoles, Madrid, Spain.

Conventional zeolites face obstacles processing large molecules due to a combination of steric and diffusional hindrances caused by the small size of their micropores. To address this issue, several strategies have been developed in order to enhance the external surface area of the zeolitic materials, including the synthesis of nanocrystalline, lamellar, and hierarchical zeolites [1]. Adding to these efforts, our research group has reported recently the synthesis of ZSM-5 zeolite showing a dendritic nanoarchitecture, which is characterized by a branched arrangement of zeolitic nanounits in a radial orientation. This unique morphology confers these materials with an unprecedented level of interconnectivity between the natural microporosity of zeolites, and the meso- and macroporosity derived from their dendritic conformation [2]. The objective of the current work is to assess whether the synthesis strategy developed for dendritic ZSM-5 (d-ZSM-5) can be utilized to modify the morphology of ZSM-11 zeolite (MEL structure). Although ZSM-11 exhibits comparable framework density and micropore size to ZSM-5, it displays a distinctive channel architecture. Thus, ZSM-5 is characterized by the presence of intersecting straight and sinusoidal channels, whereas ZSM-11 exhibits exclusively straight channels. This distinction may impact significantly their catalytic and adsorption characteristics, underscoring the importance of investigating the viability of synthesizing MEL structure with different crystal conformations [3].

In this study, several ZSM-11 zeolite samples were synthesized using a procedure adapted from the literature for the preparation of d-ZSM-5 zeolites [4]. In a first approach, the effect of adding a 5 mol% of an amphiphilic organosilane (TP) to a synthesis gel with a Si/Al ratio of 50 was evaluated, this liquid gel was then subjected to hydrothermal crystallization at 170 °C for 4 days.

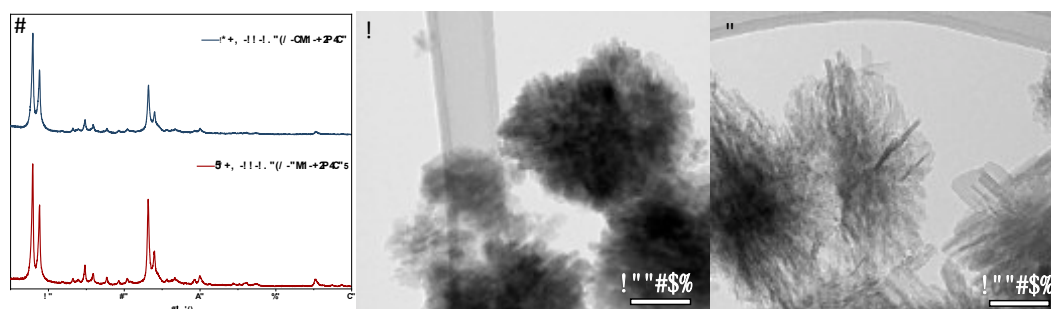


**Figure 1.** XRD (a), TEM images of the ZSM-11-170°C-0TP-SiAl50 (b), and ZSM-11-170°C-5TP-SiAl50 (c).

Despite both samples obtained by the silanized liquid gel crystallization procedure show an X-ray pattern corresponding with a well crystallized MEL structure (Fig. 1a), significant differences can be observed in the morphological conformation of the resulting crystals. The sample obtained omitting the organosilane incorporation is formed by rectangular nanocrystals between c.a. 25 x 10 nm arranged in globular-like particles (Fig. 1b). In contrast, the sample obtained from the silanized synthesis gel displays a singular nanoarchitecture characterized by a nanosheet house-of-cards arrangement (Fig. 1c). This crystal conformation produces a highly accessible sample with a BET surface area of 547 m<sup>2</sup>/g and a total pore volume of 0.88 cm<sup>3</sup>/g, with an external volume share of 70%.

A further investigation was conducted to unveil the impact of modifying the conventional procedure to obtain accessible ZSM-11 from highly concentrated gels (CG). For this, the effect of the presence of the amphiphilic organosilane (7 mol%) employed as silanization agent (0TP – 7TP), and the silicon-to-aluminum ratio (SiAl<sub>30</sub>, SiAl<sub>50</sub>, SiAl<sub>∞</sub>) in the synthesis gel were evaluated. Samples were designated according to their synthesis parameters. Although liquid and concentrated gel methodologies share the majority of the steps, the hydrothermal crystallization was reduced to 24 h in the CG procedure.

The characterization results of the samples obtained using the CG method show X-ray patterns that correspond to the MEL structure in all cases (Figs. 2a-e). However, important conclusions can be drawn from the differences in crystal morphologies based on the variables studied. In this way, the sample prepared without both aluminum and organosilane (CG-ZSM-11-170°C-0TP-SiAl<sub>∞</sub>) forms cubic nanocrystal aggregates with no significant intergrowth. This intergrowth becomes noticeable when aluminum is added to the sample (CG-ZSM-11-170°C-0TP-SiAl<sub>50</sub>), resulting as well in a reduction of the crystal size.



Additionally, introducing the organosilane into an aluminum-free synthesis gel (CG-ZSM-11-170°C-7TP-SiAl $\infty$ ) appears to inhibit the crystal growth, resulting in an arrangement of nanosheets with minimal intergrowth (Fig. 2c). Moreover, combining the aluminum incorporation with the organosilane favors the nanosheets intergrowth leading to a "house-of-cards" morphology in the CG-ZSM-11-170°C-7TP-SiAl50 sample. Interestingly, a further increase of the Al content provokes the generation of a dendrite-like nanostructure (CG-ZSM-11-170°C-7TP-SiAl30 sample).

Moreover, a noticeable reduction in XRD intensity is observed as the aluminum content in the initial synthesis gel increases in the TP containing samples (Figs. 2c-e), which correlates with the decreasing size of the constituent nanocrystals. In addition, Argon (87K) isotherms of the calcined samples shows that the non-silanized samples exhibit microporosity and interparticle porosity, whereas the silanized samples display a trimodal pore size distribution comprising micro-, meso-, and macropores. The CG-ZSM-11-170°C-7TP-SiAl50 exhibits similar textural properties to its liquid gel sample counterpart, with a BET surface area of 547 m<sup>2</sup>/g, a total pore volume of 0.88 cm<sup>3</sup>/g, and an external volume contribution of 70%. Nevertheless, the CG gel method achieved a synthesis yield of 95%, a notable improvement over the 79% yield of the liquid gel method. Combined with the reduction in crystallization time from 4 days to just 1 day, this has a substantial impact on the overall sustainability of the synthesis process.

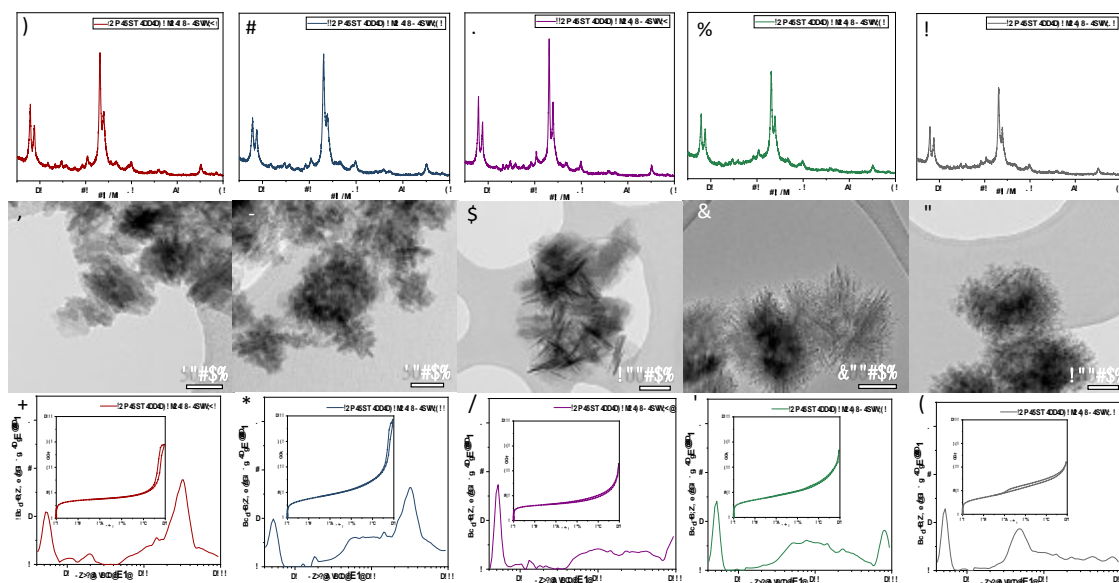


**Figure 2.** XRD (a-e), TEM images (f-j), and Ar (87K) isotherms (k-o) of the CG-ZSM-11-170°C-0TP-SiAl $\infty$ , CG-ZSM-11-170°C-0TP-SiAl50, CG-ZSM-11-170°C-7TP-SiAl $\infty$ , CG-ZSM-11-170°C-7TP-SiAl50 and CG-ZSM-11-170°C-7TP-SiAl30, respectively.

In summary, two synthesis methodologies have been employed to obtain highly accessible ZSM-11 zeolites, along with a study of the synthesis variables in both procedures. Characterization results of the samples indicate that highly crystalline MEL nanostructures can be successfully synthesized using both methods when hydrothermal crystallization is performed at 170 °C. Nevertheless, a significant reduction in synthesis time is achieved with the concentrated gel crystallization method while simultaneously enhancing the synthesis yield. Additionally, the presence of an amphiphilic organosilane in the synthesis medium promotes the formation of nanosheet-like morphology, which arranges into a dendritic structure when the cooperative effect of both aluminum and silanization agent is present. At low Al concentrations, it favors the intergrowth among constituent nanocrystals, while at higher concentrations, it promotes the nanounits branching. This demonstrates the possibility to produce dendritic ZSM-11 samples through a high-yield dry gel crystallization process, which also significantly reduces the synthesis time of the final zeolite.

## References

- [1] J. Přeck, P. Pizarro, D. P. Serrano and J. Čejka. *Chem. Soc. Rev.*, 47. (2018), 8263-8306
- [2] M. Alonso-Doncel, E.A. Giner, D. de la Calle, J. Cueto, P. Horcajada, R.A. García-Muñoz, and D. Serrano. *Cryst. Growth Des.* 23(8), (2023), 5658–5670.
- [3] Th.L.M. Maesen, M. Schenk, T.J.H. Vlugt, and B. Smit. *J. Catal.* 203. (2001) 281–291.
- [4] D.P. Serrano, J. Aguado, J.M. Rodríguez and A. Peral. *Stud. Surf. Sci. Catal.* 170 (2007), 282-28

## Acknowledgements

This work has been financed by the European Research Council (TODENZE project, grant agreement n<sup>o</sup> 101021502).



## ITQ-35: A new microporous germanate zeolite

J. I. Tirado<sup>1</sup>, J. Valero<sup>1</sup>, P. Pratim Das<sup>2</sup>, L. Palatinus<sup>3</sup>, S. Nicolopoulos<sup>2</sup>, J. L. Jordá<sup>1</sup>, G. Sastre<sup>1</sup>, A. Cantín<sup>1</sup>, S. Valencia<sup>1</sup>, F. Rey<sup>1</sup>

<sup>1</sup> Instituto de Tecnología Química, Universitat Politècnica de València – Consejo Superior de Investigaciones Científicas (UPV-CSIC), 46022 Valencia, Spain

<sup>2</sup> NanoMEGAS SPRL, Rue Émile Claus 49 bte 9, B-1080, Brussels, Belgium

<sup>3</sup> Institute of Physics of the Czech Academy of Sciences, v.v.i. Na Slovance 2, Prague 8 182 00, Czechia  
Jovaji2@upvnet.upv.es

Zeolites are microporous materials widely used as catalysts and adsorbents in industry due to their uniform porosity, stability and possibility of generating active sites. These materials consist of frameworks built from the linkage of TO<sub>4</sub> tetrahedra, where T represents typically Si and Al, but other heteroatoms can be also present. In recent years, the inclusion of germanium and the use of fluoride anions as mobilizing agent in the synthesis compositions have led to the formation of new zeolite frameworks with multidirectional large and extra-large channels [1]. This is related to the flexibility of T-O-T bond angles in the presence of Ge, which frequently direct the formation of small units such as double four ring (D4R) [2], and the presence of this type of small cages enables the formation of low framework density materials.

In this work, we describe a new pure open-framework germanate zeolitic material, denoted as ITQ-35, and its structural elucidation by applying precession electron diffraction tomography (PEDT) and standard powder X-ray diffraction (PXRD) methods. The organic structure directing agent (OSDA) utilized for the synthesis has been prepared by a photochemically induced [2+2] cycloaddition reaction [3].

Zeolite ITQ-35 was synthesized at 175°C in fluoride medium as germanate and silicogermanate with high Ge content using the dicationic organic molecule 2,2,3a,3b,5,5,6a,6b-octamethyldecahydrocyclobuta[1,2-c:3,4-c']dipyrrole-2,5-dium as OSDA [3]. The characterization of the material indicated that the organic molecules were incorporated intact within the porosity of the zeolite, which accounts for around 17%, and its X-ray diffraction pattern was not coincident with any of the XRD patterns compiled in the database of zeolite structures [4]. Besides that, the zeolite contains fluoride anions located in germanium-rich D4R cages, as revealed by <sup>19</sup>F-MAS-NMR spectroscopy.

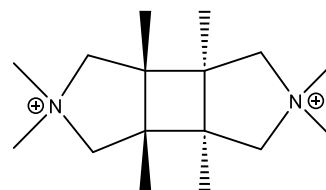


Figure 1. Organic structure directing agent used for the synthesis of zeolite ITQ-35.

Due to the high Ge content, the calcination of ITQ-35 material yielded to amorphization and precluded performing further characterization in the absence of organic inside the pores, making impossible the crystalline structure resolution of the OSDA-free zeolite. Indeed, zeolite ITQ-35 was first synthesized several years ago, but its structure remained unknown until now due to these instability problems of the sample. In fact, one of the main challenges when new zeolite materials are obtained is their structure determination, being this even more difficult when attempting to solve the organic-containing zeolite. On this regard, 3D electron diffraction (3DED) techniques have emerged in the latest years as a very powerful tool for elucidation of crystalline structures [5]. Thus, 3DED technique was applied for structural determination of the as-synthesized zeolite ITQ-35 with a pure germanate composition.

The general procedure in 3DED consists of collecting a series of non-oriented diffraction patterns using a camera installed in the TEM while a selected crystal is tilting around an arbitrary axis. To improve the quality of the data, beam precession is combined during the data acquisition and this technique, known as Precession Electron Diffraction Tomography (PEDT), was used in this case. The inorganic part of the zeolite framework was derived from the structure solution attempted and it was kinematically refined against 3DED data. This crystalline structure was found to crystallize in the space group *Im-3m* with the following unit cell parameters as obtained from 3DED data:  $a = b = c = 17.7548 \text{ \AA}$ ;  $\alpha = \beta = \gamma = 90^\circ$ ,  $V_{c.u.} = 5596.9 \text{ \AA}^3$ . This framework presents structural unconnected T sites (Q<sup>3</sup> species) which are associated to germanol groups (GeOH) or negatively charged germanates (GeO<sup>-</sup>). The unit cell exhibits 16 unconnected oxygen atoms that are highlighted in red in Figure 2, making a total of 16 Q<sup>3</sup> species per unit cell.

Given the unsuccessful efforts to determine of the OSDA structure, it was attempted through the application of theoretical molecular dynamics methods based on Monte Carlo simulations, in particular, the software *zeoTsd* was used to calculate the optimal configuration and the number of OSDA molecules within the cavities [6]. The calculations resulted in a structure model with 6 OSDA molecules per unit cell, accounting for a sum of 12 positive charges that were, in part, counterbalanced by six fluoride anions (according to <sup>19</sup>F MAS-NMR), while the remaining positive charges should be balanced by 6 Q<sup>3</sup> defects in the form of GeO<sup>-</sup>, and 10 GeOH will complete the 16 Q<sup>3</sup> species. Therefore, the chemical composition of the material can be described by the formula: Ge<sub>64</sub> O<sub>120</sub> (OH)<sub>10</sub> (O<sup>-</sup>)<sub>6</sub> (F<sup>-</sup>)<sub>6</sub> · 6(N<sub>2</sub>C<sub>16</sub>H<sub>32</sub>)<sup>2+</sup>.

Considering these calculations, the complete hybrid inorganic and organic structure of the as-made ITQ-35 retrieved from Rietveld refinement against PXRD data crystallizes in the space group  $Im-3m$  with the following unit cell parameters:  $a = b = c = 17.1677(5) \text{ \AA}$ ;  $\alpha = \beta = \gamma = 90^\circ$ ,  $V_{u.c.} = 5059.9(2) \text{ \AA}^3$ .

The as-made ITQ-35 presents pore apertures of 12 and 8 rings forming a tri-directional channel system of  $12 \times 12 \times 12$  and  $8 \times 8 \times 8$ -ring, respectively. Zeolite ITQ-35 exhibits a relatively low framework density of 12.6 T atoms per 1000  $\text{\AA}^3$  representing the lowest density of a pure germanate zeolite.

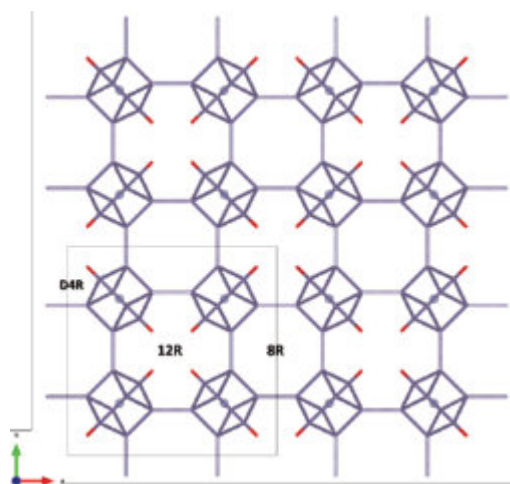


**Figure 2.** The 3D framework structure of ITQ-35 viewed along [001] direction. The 8 and 12-ring channels are formed along [100], [010] and [001] directions. T-T bonds (T=Ge) are represented in purple sticks, fluoride anions in blue and terminal OH/O<sup>-</sup> groups are highlighted in red for clarity.

In conclusion, a new zeolite framework with three-directional 8R pores connected by 12R channels and containing D4R units, named ITQ-35, synthesized as pure germanate and silicogermanate with an OSDA obtained by a photochemically induced [2+2] cycloaddition reaction, has been determined by precession electron diffraction tomography. The framework presents structural unconnected T-O-H and T-O<sup>-</sup> and results the lowest framework density material reported until now for germanate zeolites.

## References

- [1] J. Jiang, J. Yu, A. Corma, *Angew. Chem. Int. Ed.*, **49**, 3120 (2010).
- [2] J. Li, A. Corma, J. Yu, *Chem. Soc. Rev.*, **44**, 7112 (2015).
- [3] A. Cantín, S. Leiva, J. L. Jordá, S. Valencia, F. Rey, A. Corma, *Stud. Surf. Sci. Catal.*, **170**, 330 (2007).
- [4] C. Baerlocher, L. McCusker, Database of Zeolite Structures, <http://www.iza-structure.org/databases/>.
- [5] Z. Huang, T. Willhammar, X. Zou, *Chem. Sci.*, **12**, 1206 (2021).
- [6] M. Gálvez-Llompart, A. Cantín, F. Rey, G. Sastre, *Z. Kristallogr.*, **234**, 451 (2019).

## Acknowledgments

Financial support by the Spanish Ministry of Science and Innovation (CEX2021-001230-S and PID2022-136934OB-100 grants funded by MCIN/AEI/10.13039/501100011033 funded by "ERDF A way of making Europe" and TED2021-130191B-C41 grant funded by the European Union NextGenerationEU/PRTR) are gratefully acknowledged. Authors thank also the financial support by the Generalitat Valenciana (Prometeo 2021/077). This study forms part of the Advanced Materials programme and was supported by MCIN with partial funding from European Union Next Generation EU (PRTR-C17. I1) and by Generalitat Valenciana (MFA/2022/012 and MFA/2022/047). The authors acknowledge the Electron Microscopy Service of the Polytechnique University of Valencia (UPV) for assistance in electron microscopy characterization. J.I.T. and J.V. thank financial support from Severo Ochoa Program (PRE2018-083623J) and Generalitat Valenciana (PROMETEO/2021/077-01), respectively. We thank CTI-CSIC and ASIC-UPV for computational facilities.



## Ni-based MOFs as CO<sub>2</sub> adsorbent in biogas: Effect of linker and its modification with ethylenediamine

Y. K. Krisnandi<sup>1,2</sup>, M. R. Ramdani<sup>1,2</sup>, P. Andini<sup>1,2</sup>, Rizkiyah<sup>1,2</sup>, I. Abdullah<sup>1,2</sup>

<sup>1</sup> Department of Chemistry, Faculty of Mathematics and Natural Sciences, Universitas Indonesia, Kampus UI Depok, Depok 16424, Indonesia

<sup>2</sup> Solid Inorganic Framework Laboratory, Department of Chemistry, Faculty of Mathematics and Natural Sciences, Universitas Indonesia, Kampus UI Depok, Depok 16424, Indonesia

E-mail: yuni.krisnandi@sci.ui.ac.id

### 1. Introduction

Biogas is a sustainable energy source substitute for fossil fuels. However, biogas possesses a relatively high carbon dioxide content (CO<sub>2</sub>) to methane (CH<sub>4</sub>), which is undesirable as it can damage the engine through corrosion and deposition. Adsorption techniques have been widely employed to extract CO<sub>2</sub> from biogas using Metal-Organic Frameworks (MOFs), which made up of metals connected by organic linker compounds [1]. It is widely recognised that the addition of polar groups, such as amines, to MOFs can increase their capacity for CO<sub>2</sub> adsorption [2]. Hence, this study aims to investigate how ethylenediamine (EDA) modification affects the CO<sub>2</sub> adsorption performance of Ni-based MOFs with a variation of organic linkers.

### 2. Methodology

The synthesis of Ni-based MOFs was carried out using the modified procedure reported by Asgharnejad *et al.* [3], through heating a homogeneous mixture consisting of Ni precursor (Ni(NO<sub>3</sub>)<sub>2</sub>·6H<sub>2</sub>O, linker, and DMF at 120 °C for 24 h in a Teflon-lined autoclave. The resulting product was then cooled to room temperature, filtered, washed with DMF several times, and dried at room temperature overnight. Furthermore, the modification of MOFs with ethylenediamine (EDA) (15% w/w) was prepared following the modified procedure from Ashgar *et al.* [4], by adding a certain amount of 1.5 M EDA and ethanol to MOF 170 °C under reflux condition. The MOFs were synthesised using three types of linkers, including terephthalic acid (BDC), aminoterephthalic acid (NH<sub>2</sub>-BDC), and 2,5-dihydroxyterephthalic acid (DOBDC), which were then denoted as Ni-BDC, Ni-BDC-NH<sub>2</sub>, and Ni-DOBDC, respectively. While the modified MOFs were then denoted as Ni-BDC/EDA, Ni-BDC-NH<sub>2</sub>/EDA, and Ni-DOBDC/EDA.

CO<sub>2</sub> adsorption test was carried out following the procedure by Serna-Guerrero *et al.* [5]. Prior to adsorption test, 0.1 g adsorbent was activated at 60 °C for 1 h. Adsorbent was then placed in a tubular column which is then fed with CO<sub>2</sub>/CH<sub>4</sub> mixture gas. The adsorption capacity of each adsorbent was analysed using a Shimadzu TCD-8A Gas Chromatography (GC) instrument equipped with PorapakQ column and thermal conductivity detector at 100 °C with a flow rate of 20 mL min<sup>-1</sup> using Ar as carrier gas.

### 3. Results

In this work, Ni-MOFs were synthesised using three types of organic linkers (insert in Fig. 1) : (1) terephthalic acid (BDC), (2) 2-aminoterephthalic acid (NH<sub>2</sub>-BDC), which is the modification of BDC linker with an amino group at position 2 of the benzene ring, and (3) 2,5-dihydroxy terephthalic acid (DOBDC), also known as hydroxylated BDC which undergo modification with the addition of two hydroxyl groups at position 2 and 5 of the benzene ring. The modification of BDC into NH<sub>2</sub>-BDC and DOBDC resulted to more unsaturated metal centres with capacity to adsorb and bind CO<sub>2</sub>. XRD patterns in Fig. 1a show different structures of the synthesised Ni-MOFs as a result of their Ni bonding with different organic ligands. XRD results of all three Ni-MOFs show similar patterns to study from Cheng *et al.* [6]. The as-synthesised materials were then modified with EDA and tested as adsorbent of CO<sub>2</sub> in biogas model of CO<sub>2</sub>/CH<sub>4</sub> mixture gas.

The  $S_{\text{BET}}$  of Ni-MOFs adsorbent (Table 1) with BDC linker (13 m<sup>2</sup> g<sup>-1</sup>) increased after amine modification in NH<sub>2</sub>-BDC (21 m<sup>2</sup> g<sup>-1</sup>) and more significantly increased using hydroxylated BDC of DOBDC (681 m<sup>2</sup> g<sup>-1</sup>). However, the modification with EDA decreased also decreased the  $S_{\text{BET}}$  significantly, which described the possibility of EDA position in the pores or covering the porosity. Ni-DOBDC also shows the highest basicity (1.5644 mmol g<sup>-1</sup>) compared to Ni-NH<sub>2</sub>-BDC (0.1601 mmol g<sup>-1</sup>) and Ni-BDC (0.1934 mmol g<sup>-1</sup>), which is due to enhanced coordinative unsaturated properties of Ni metal centre and the addition of amines polar group. Furthermore, the basicity of Ni-NH<sub>2</sub>-BDC and Ni-DOBDC were increased significantly after the modification with EDA, while the Ni-BDC shows otherwise. Despite of the lower  $S_{\text{BET}}$  and basicity to Ni-DOBDC, Ni-BDC and Ni-NH<sub>2</sub>-BDC show better CO<sub>2</sub> adsorption capacity, indicative of the importance of proper number of active sites to capacitate CO<sub>2</sub> in biogas mixture (Fig. 1b).

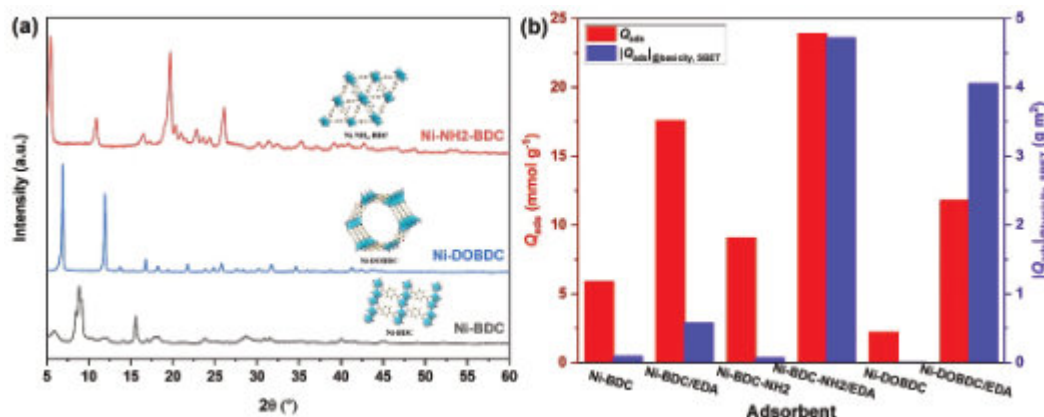


Figure 1. (a) XRD patterns of the as-prepared Ni-MOFs and (b) The  $Q_{ads}$  and  $|Q_{ads}|_{@basicity, S_{BET}}$  value of Ni-MOFs adsorbents.

Table 1. Physicochemical properties and adsorption capacity of Ni-MOFs.

Adsorbent	$S_{BET}$ [m <sup>2</sup> g <sup>-1</sup> ] <sup>a</sup>	Basicity [mmol g <sup>-1</sup> ] <sup>b</sup>	$Q_{ads}$ [mmol g <sup>-1</sup> ] <sup>c</sup>
Ni-BDC	13	0.1934	5.8880
Ni-BDC/EDA	3	0.0986	17.5680
Ni-BDC-NH <sub>2</sub>	21	0.1601	9.0500 <sup>d</sup>
Ni-BDC-NH <sub>2</sub> /EDA	8	1.5767	23.9100
Ni-DOBDC	681	1.5644	2.1940 <sup>d</sup>
Ni-DOBDC/EDA	17	5.8383	11.792

<sup>a</sup> Determined using BET method from N<sub>2</sub>-physisorption.

<sup>b</sup> Determined using CO<sub>2</sub>-TPD.

<sup>c</sup> Determined using GC-TCD with CO<sub>2</sub> gas at maximum  $T = 70$  °C.

<sup>d</sup> Determined using GC-TCD with CO<sub>2</sub> gas at  $T = 25$  °C.

#### 4. Conclusion

Ni-MOFs prepared with modified BDC linker resulted to different structure and were efficient to increase the total surface area ( $S_{BET}$ ) and basicity due to the additional functional groups. However, in the application of CO<sub>2</sub> adsorption, proper number of active sites to capacitate CO<sub>2</sub> in biogas mixture is necessary as higher basicity and surface area of Ni-DOBDC exhibited lower adsorption capacity ( $Q_{ads}$ ) compared to Ni-BDC and Ni-NH<sub>2</sub>-BDC.

#### References

- [1] M.J. Uddin, R.E. Ampiauw, W. Lee, Adsorptive removal of dyes from wastewater using a metal-organic framework: A review, *Chemosphere* 284 (2021) 131314. <https://doi.org/10.1016/J.CHEMOSPHERE.2021.131314>.
- [2] J. Lee, O.K. Farha, J. Roberts, K.A. Scheidt, S.T. Nguyen, J.T. Hupp, Metal-organic framework materials as catalysts, *Chem Soc Rev* 38 (2009) 1450–1459. <https://doi.org/10.1039/b807080f>.
- [3] L. Asgharnejad, A. Abbasi, A. Shakeri, Ni-based metal-organic framework/GO nanocomposites as selective adsorbent for CO<sub>2</sub> over N<sub>2</sub>, *Microporous and Mesoporous Materials* 262 (2018) 227–234. <https://doi.org/10.1016/J.MICROMESO.2017.11.038>.
- [4] A. Asghar, N. Iqbal, L. Aftab, T. Noor, B.M. Kariuki, L. Kidwell, T.L. Easun, Ethylenediamine loading into a manganese-based metal-organic framework enhances water stability and carbon dioxide uptake of the framework, *R Soc Open Sci* 7 (2020). <https://doi.org/10.1098/RSOS.191934>.
- [5] R. Serna-Guerrero, Y. Belmabkhout, A. Sayari, Further investigations of CO<sub>2</sub> capture using triamine-grafted pore-expanded mesoporous silica, *Chemical Engineering Journal* 158 (2010) 513–519. <https://doi.org/10.1016/J.CEJ.2010.01.041>.
- [6] J. Cheng, Y. Shao, H. Guo, Z. Zhang, Y. Mao, L. Qian, K. Xin, W. Yang, Ni-based metal-organic frameworks prepared with terephthalic acid hydroxylation converted methyl palmitate into jet-fuel range hydrocarbons in CO<sub>2</sub> atmosphere, *Fuel* 318 (2022) 123679. <https://doi.org/10.1016/J.FUEL.2022.123679>.

#### Acknowledgments

This work was supported by Universitas Indonesia through Hibah Publikasi Terindeks Internasional (PUTI) Q2 Research Grant No. NKB-781/UN2.RST/HKP.05.00/2023 and Indonesian Ministry of Research, Technology and Higher Education (Menristekdikti) through Bantuan Operasional Perguruan Tinggi Negeri (BOPTN) Research Grant No. NKB-906/UN2.RST/HKP.05.00/2024.



## Investigation of Co behaviour encapsulated within the lamellar structure of hierarchical ZSM-5 zeolite

I. Khatrin<sup>1,2</sup>, I. Abdullah<sup>1,2</sup>, A. J. McCue<sup>3</sup>, Y. K. Krisnandi<sup>1,2</sup>

<sup>1</sup> Department of Chemistry, Faculty of Mathematics and Natural Sciences, Universitas Indonesia, Kampus UI Depok, Depok 16424, Indonesia

<sup>2</sup> Solid Inorganic Framework Laboratory, Department of Chemistry, Faculty of Mathematics and Natural Sciences, Universitas Indonesia, Kampus UI Depok, Depok 16424, Indonesia

<sup>3</sup> Advanced Centre for Energy and Sustainability (ACES), Department of Chemistry, School of Natural and Computing Sciences, University of Aberdeen, Aberdeen AB24 3UE, UK

E-mail: irena.khatrin@sci.ui.ac.id

### 1. Introduction

Engineering of crystal morphology affects the catalytic and adsorption properties of zeolitic materials. Considering the anisotropic diffusion of molecules derived from its topological features and the dispersion of active sites, metal oxide nanoparticles have been incorporated into zeolite architectures to increase the dispersion of metal active sites in the porous system [1]. The functionalization of zeolites with metal oxide led to the creation of bifunctional catalysts with different physicochemical properties compared to their respective starting materials. In this work,  $\text{Co}_3\text{O}_4$  were enclosed in the sheet-like hierarchical ZSM-5 structure *via* one-pot synthesis and post-synthetic method with the aim of altering the morphology and physicochemical structure of ZSM-5 zeolite.

### 2. Methodology

The synthesis of hierarchical sheet-like ZSM-5 was modified based on the method by Liu et al. using urea as a *b*-axis growth inhibitor agent [2]. The molar ratio of the synthesis gel was  $1.00 \text{ Al}_2\text{O}_3 : 64.35 \text{ SiO}_2 : 10.08 (\text{TPA})_2\text{O} : 3571.66 \text{ H}_2\text{O} : 128.7 \text{ Urea}$ , with ZSM-5 denoted as ZS64-2.0, as indicative of the Si/Al ratio of 64 and Urea/ $\text{SiO}_2$  ratio of 2.0. The one-pot synthesis method includes the addition of N-[3-(trimethoxy silyl)propyl]ethylenediamine (TPE) as a ligand to protect the cobalt ion, with the as-synthesised material being denoted as CoA@ZS64-2.0. While the post-synthetic method includes the modification of as-impregnated ZSM-5 ( $\text{Co}_3\text{O}_4/\text{ZSM-5}$ ) through the addition of 0.3 M TPAOH, with the as-synthesised material being denoted as CoB@ZS64-2.0.

### 3. Results

Two types of encapsulation method were carried out to synthesise  $\text{Co}_3\text{O}_4$  enclosed in sheet-like hierarchical ZSM-5 zeolites with a reduced *b*-axis length (Fig. 1). These methods include: (a) one-pot technique with the presence of low-cost directing agent urea as the low-cost directing agent to reduce the length of the *b*-axis and produce the sheet-like structure of ZSM-5 [3], as well as ligand-protected metal cations N-[3-(trimethoxy silyl)propyl]ethylenediamine (TPE) that work to preclude the precipitation of metal precursors in alkaline synthesis gels and form covalent linkages with nucleating zeolite precursors to enforce metal uptake into crystallised solid [4]. Also (b) the post-synthetic approach which involves the re-crystallisation of  $\text{Co}_3\text{O}_4$  impregnated on hierarchical ZSM-5 in the presence of a template to generate the extra-framework, which leads to the insertion of metal oxide nanoparticles on the framework of ZSM-5 zeolite [5]. A series of instrumentations, including XRD, FT-IR, XRF,  $\text{N}_2$ -physisorption, SEM, and  $\text{H}_2$ -TPR, were utilised to study the physicochemical characteristics of the as-synthesised ZSM-5. Urea effectively aided the formation of the sheet-like crystal ZSM-5, as revealed by electron microscopy and IR spectroscopy analysis. XRD result showed no peak indicative of Co from one-pot synthesis method, which might be due to the location of Co inside the zeolite framework, or the small size of Co resulted (Fig. 1). Furthermore, different reducibility of Co particles by different encapsulation method were also observed by  $\text{H}_2$ -TPR (Fig. 1). These developed strategies may be effective in improving the adsorption and catalytic properties of ZSM-5 zeolite.

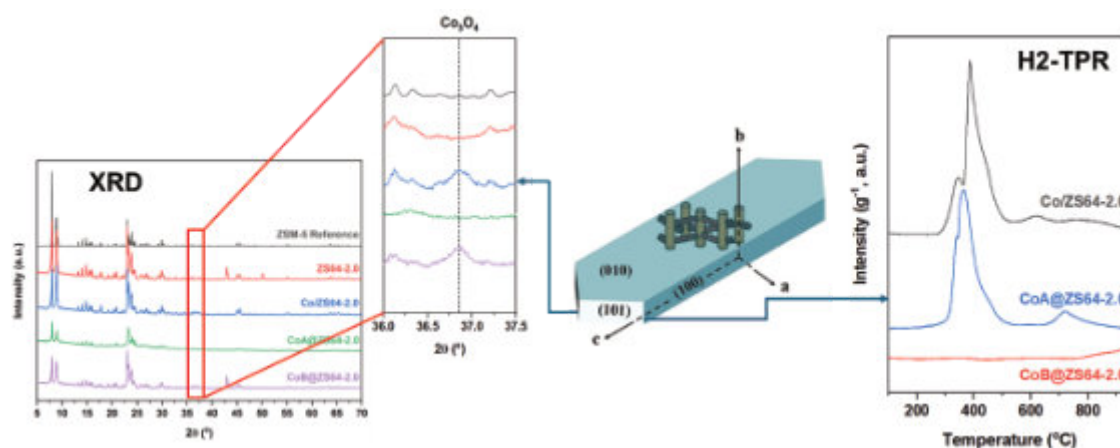


Figure 1. Graphical abstract of sheet-like ZSM-5 with the XRD patterns and H<sub>2</sub>-TPR results.

## Conclusion

The synthesis of sheet-like hierarchical ZSM-5 with lamellar structure has been successfully carried out with the addition of urea as the inhibitor of *b*-axis growth. Characterisation results observed that one-pot synthesis and post-synthetic method generated different types of Co-oxide in terms of its position in the ZSM-5 framework and its reducibility as shown by H<sub>2</sub>-TPR results. These results indicate that both encapsulation method lead to ZSM-5 with different physicochemical features which will be useful for its application as a catalyst.

## References

- [1] P. Peng, X.H. Gao, Z.F. Yan, S. Mintova, Diffusion and catalyst efficiency in hierarchical zeolite catalysts, *Natl Sci Rev* 7 (2020) 1726–1742. <https://doi.org/10.1093/NSR/NWAA184>.
- [2] Y. Liu, X. Zhou, X. Pang, Y. Jin, X. Meng, X. Zheng, X. Gao, F.S. Xiao, Improved para-Xylene Selectivity in meta-Xylene Isomerization Over ZSM-5 Crystals with Relatively Long *b*-Axis Length, *ChemCatChem* 5 (2013) 1517–1523. <https://doi.org/10.1002/CCTC.201200691>.
- [3] Q. Yue, C. Liu, H. Zhao, H. Liu, P. Ruterana, J. Zhao, Z. Qin, S. Mintova, Urea-assisted morphological engineering of MFI nanosheets with tunable *b*-thickness, *Nano Res* (2023) 1–11. <https://doi.org/10.1007/S12274-023-5749-0/METRICS>.
- [4] T. Otto, S.I. Zones, E. Iglesia, Synthetic strategies for the encapsulation of nanoparticles of Ni, Co, and Fe oxides within crystalline microporous aluminosilicates, *Microporous and Mesoporous Materials* 270 (2018) 10–23. <https://doi.org/10.1016/J.MICROMESO.2018.04.045>.
- [5] Z. Hong, Z. Wang, D. Chen, Q. Sun, X. Li, Hollow ZSM-5 encapsulated Pt nanoparticles for selective catalytic reduction of NO by hydrogen, *Appl Surf Sci* 440 (2018) 1037–1046. <https://doi.org/10.1016/J.APSUSC.2018.01.239>.

## Acknowledgments

This work was supported by Indonesian Ministry of Research, Technology and Higher Education (Menristekdikti) through Pendidikan Magister menuju Doktor untuk Sarjana Unggul (PMDSU) Research Grant No. NKB-798/UN2.RST/HKP.05.00/2024.



## Enhancement of oil properties from plastic waste pyrolysis through zeolite-based (MCM and TNU) catalytic upgrading

A. Pinto<sup>1,2</sup>, L. Amodio<sup>1,2</sup>, M. Kubů<sup>3</sup>, J. Cueto<sup>1</sup>, P. Eliášová<sup>3</sup>, P. Pizarro<sup>1,2</sup>, J. Čejka<sup>3</sup>, D. P. Serrano<sup>1,2</sup>

<sup>1</sup> Thermochemical Processes Unit, IMDEA Energy, Avda. Ramón de la Sagra 3, 28935, Móstoles, Madrid, Spain

<sup>2</sup> Chemical and Environmental Engineering Group, Rey Juan Carlos University, Móstoles, Madrid, Spain

<sup>3</sup> Department of Physical and Macromolecular Chemistry, Faculty of Science, Charles University, Hlavova 8, Prague, Czech Republic

[alberto.pinto@imdea.org](mailto:alberto.pinto@imdea.org)

The rapid increase in plastic consumption and its short life cycle have led to a significant rise in plastic waste generation. Despite substantial efforts to increase recycling and reuse rates, these remain very low due to the diversity of plastics present in the same waste stream (e.g., PC, PP, PVC...) and the presence of undesired halogenated compounds, such as chlorine or bromine [1]. However, significant efforts are being made to develop new pathways to convert plastic waste into high-quality fuels or valuable chemicals efficiently. Pyrolysis is a promising alternative due to its simplicity and flexibility in processing a wide range of raw materials. Although obtaining a refined oil with direct industrial application from the pyrolysis of real plastic waste is challenging, post-catalytic treatment needs to be performed to improve its characteristics, increasing the light hydrocarbon yield and reducing halogen content [2].

In this context, zeolites represent an important group of porous crystalline materials with unique properties that make them one of the most attractive materials in waste valorization. They had been known as 3D frameworks until the formation of MCM-22 via the layered precursor [3]. So-called layered or lamellar solids have opened new possibilities for the formation of novel porous structures and materials. Thus MCM-22, MCM-49, MCM-56, MCM-36 and ITQ-2 have been discovered and identified [4, 5]. These structures differ in the stacking arrangement of MCM-22 monolayers. The layered precursor MCM-22P possesses layers stacked in vertical alignment with separation 0.2 nm longer (2.7 nm) than in the complete 3D framework (2.5 nm) formed during calcination. MCM-49 represents the product of the direct synthetic path to the 3D MWW structure with connectivity identical to the calcined material (2.5 nm). The delaminated MCM-56 zeolite is an intermediate in the synthesis of MCM-49 zeolite with disordered arrangement of individual monolayers [5].

Further advancing the field, TNU-9 is a high silica zeolite with a very complex framework with a projection like that of ZSM-5 or ZSM-11 perpendicular to y-axis, but with quite different connections between the layers. There are two different types of straight 10-ring channels running parallel to the y-axis with the dimensions of 0.52x0.60 and 0.51x0.55 nm. The channels perpendicular to y-axis join these straight channels to form a 3D 10-ring channel system [6].

The present contribution focuses on improving the properties of an oil derived from the pyrolysis of real plastic waste by investigating how the use of different zeolites (TNU-9, MCM-22, MCM-48 and MCM-56) affects the dehalogenation process and the production of aromatic compounds in the treated oil.

The starting oil was characterized using various analytical techniques, as described in a previous study [7], to determine its elemental and molecular composition and chlorine concentration (see Table 1). It can be observed that this oil presents a relatively high chlorine concentration (290 ppm) and is enriched in aliphatic compounds, with a notable amount of paraffins, and a smaller proportion of olefinic, naphthenic, and aromatic hydrocarbons. It is also worth mentioning that it contains a high proportion of heavy compounds that cannot be detected by GC-MS (43.5 wt%). A fixed-bed catalytic reactor with a 3/4" diameter was used, where the oil was fed through an HPLC pump. The zeolites prepared according to [8], whose properties are listed in Table 1, were placed in the centre of the reactor. At the reaction system outlet, a liquid sample condensation system was set up to collect samples at different reaction times, which were analyzed using the same techniques as the starting oil. The gases were collected with the help of a totalizer, and their composition was determined using  $\mu$ -GC. The reaction temperature used was 450 °C, operating at WHSV of 5 h<sup>-1</sup>.

**Table 1.** Characterization of the oil and zeolites. <sup>1</sup>: CHNS-O, <sup>2</sup>: AOD-IC, <sup>3</sup>: GC-MS, <sup>4</sup>: ICP-OES, <sup>5</sup>: N<sub>2</sub> adsorption (77 K).

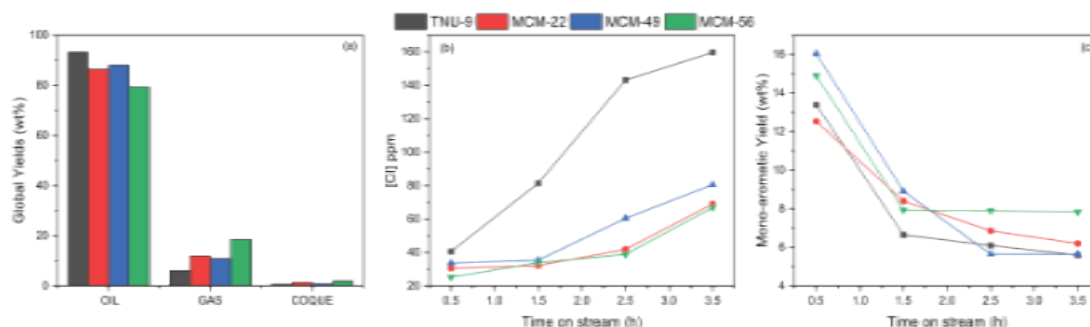
Oil elemental composition (wt%)		Oil molecular composition (wt%) <sup>3</sup>		Zeolite characterization				
				Sample	Si/Al <sup>4</sup>	S <sub>BET</sub> (m <sup>2</sup> /g) <sup>5</sup>	V <sub>mic</sub> (cm <sup>3</sup> /g) <sup>5</sup>	V <sub>total</sub> (cm <sup>3</sup> /g) <sup>5</sup>
C <sup>1</sup>	85.52	Mono-aromatics	5.5	TNU-9	29.5	524	0.19	0.21
		Naphthenes	7.2	MCM-22	31.2	541	0.19	0.31
H <sup>1</sup>	14.45	Olefins	8.2	MCM-49	10.4	460	0.16	0.29
Cl <sup>2</sup>	0.029	Paraffins	35.6	MCM-56	9.3	406	0.12	0.48



Figure 1 displays the main results obtained in the oil catalytic upgrading over the different zeolites. As can be observed in Figure 1 (a), MCM-56 exhibits the highest cracking capacity, resulting in the greatest gas yield (18.56 wt%), the lowest oil yield (79.36 wt%) and slightly higher coke formation (2.08 wt%). This finding is congruent with the higher total pore volume and better accessibility of this zeolite. In contrast, TNU-9 demonstrates the opposite behavior, with minimal oil cracking and a gas yield of 6.1 wt%. MCM-22 and MCM-49 display similar and intermediate performance. In all cases, the produced gases represent a valuable stream, predominantly composed of olefins and paraffins with 3 and 4 carbon atoms.

On the other hand, Figure 1 (b and c) shows the temporal evolution of two key parameters used to assess the improvement in oil quality: chlorine concentration and mono-aromatics production. Eliminating chlorine from pyrolysis oil is essential to ensure industrial equipment durability, reduce environmental pollution, improve product quality, enhance catalyst performance, and meet regulatory requirements. It plays a key role in transforming pyrolysis oil into a safer and more valuable resource for sustainable fuel and chemical production. It can be seen in Figure 1 (b) that the upgraded oil Cl content during the initial half hour of reaction shows little differences among the four zeolites studied. However, these trends change noticeably over time. TNU-9 exhibits the poorest performance, becoming rapidly deactivated and in terms of dehalogenation performance, starting from a Cl content of 40.6 ppm at 0.5 hours and increasing up to 159.7 ppm at 4 hours. In contrast, the other zeolites demonstrate more stable dehalogenation activity, with MCM-22 and MCM-56 displaying similar variations over time in the Cl content.

On the other hand, the production of monoaromatics from green resources is vital for building a more sustainable, resilient, and environmentally responsible chemical industry. Through the valorization of pyrolysis oil, all the zeolites tested increased significantly the yield of mono-aromatics (Figure 2 (c)). However, all of them suffered from rapid deactivation, leading to a fast decline in mono-aromatic production as the reaction time progressed. The MCM-56 and MCM-49 materials exhibit the highest monoaromatics initial yields (15 and 16 wt%, respectively). Moreover, MCM-56 proves to be the most stable after the first hour of reaction, maintaining a consistent monoaromatic yield of 8 wt%. Also, TNU-9 seems to have a constant profile after initial 0.5 h with an average yield of 6 wt%.



**Figure 1.** (a) Global mass yields of the different fractions, (b) Temporal evolution of chlorine concentration and (c) Mono-aromatics production as a function of the reaction time on stream. Operation conditions: 450 °C and 5 h<sup>-1</sup>.

In summary, the performance of various zeolitic materials in upgrading pyrolysis oil has been assessed. Among them, MCM-56 stands out as the most promising catalyst, demonstrating excellent performance for dehalogenation and aromatization of the initial oil.

## References

- [1] P. Das, J-C. P. Gabriel, C. Y. Tay, J-M. Lee, *Chemosphere*, **269**, 129409 (2021).
- [2] A. Lopez-Urionabarrenechea, I. Marco, B. Caballero, M. Laresgoiti, A. Adrados, *Fuel Process. Technol.*, **137**, 229-239 (2015).
- [3] M. K. Rubin, P. Chu, US Patent 4, 954, 325 (1990).
- [4] W. J. Roth, *Stud. Surf. Sci. Catal.* 158 (ed. J. Čejka, N. Žilková, P. Nachtigall), Elsevier, Amsterdam (2005).
- [5] W. J. Roth, D. L. Dorset, G. J. Kennedy, *Microporous Mesoporous Mater.*, **142**, 168-177 (2011).
- [6] F. Gramm, Ch. Baerlocher, L. B. McCusker, S. J. Warrender, P. A. Wright, B. Han, S. B. Hong, Z. Liu, T. Ohsuna, O. Terasaki, *Nature*, **444**, 79-81 (2006).
- [7] L. Amodio, J. López, A. Souza, J. Cueto, H. Hernando, P. Pizarro, D. P. Serrano, *J. Hazard. Mater.*, **465**, 133357 (2024).
- [8] M. Shamzhy, B. Gil, M. Opanasenko, W. L. Roth, J. Čejka, *ACS Catal.*, **11**, 2366-2396 (2021).

## Acknowledgments

This work is part of the action PCI2023-143433, funded by MCIN/AEI/10.13039/501100011033 and by the European Union. The authors also acknowledge the EIG Concert Japan program (Nr. 8123003).



## Bifunctional catalysts CuAl<sub>2</sub>O<sub>4</sub>/SAPO-34 for CO<sub>2</sub> hydrogenation to olefins

Abdelhakim Elmhamdi<sup>1,2</sup>, Khaleel<sup>1</sup> Maryam<sup>2</sup>

<sup>1</sup> Department of Chemical and Petroleum Engineering, Khalifa University, P.O. Box 127788, Abu Dhabi, United Arab Emirates  
abdelhakim.elmhamdi@ku.ac.ae

<sup>2</sup> Research and Innovation Center in CO<sub>2</sub> and H<sub>2</sub> (RICH), Khalifa University, P.O. Box 127788, Abu Dhabi, United Arab Emirates  
maryam.khaleel@ku.ac.ae

### Abstract

CO<sub>2</sub> hydrogenation is a promising strategy for CO<sub>2</sub> conversion and valorisation due to its sustainability. This process can produce various hydrocarbon products, including methanol, methane, dimethyl ether (DME), olefins, and aromatics. Among these, the hydrogenation of CO<sub>2</sub> into olefins is particularly attractive due to the critical role of olefins in producing numerous petrochemical products. There are two main routes for CO<sub>2</sub> hydrogenation to olefins: the CO intermediate route via the Modified-Fischer Tropsch pathway, where olefin selectivity is constrained by the Anderson-Schulz-Flory (ASF) distribution, and the methanol intermediate route using bifunctional catalysts (metal oxide + zeolite), which breaks the ASF distribution.

In this study, we present the preparation of a novel bifunctional catalyst composed of CuAl<sub>2</sub>O<sub>4</sub> and SAPO-34, featuring a spinel oxide CuAl<sub>2</sub>O<sub>4</sub> hollow structure, for CO<sub>2</sub> hydrogenation into olefins. To the best of our knowledge, this is the first report in the literature where a tandem catalyst combining a spinel oxide hollow structure with SAPO-34 has been designed and utilized for CO<sub>2</sub> hydrogenation to olefins. The catalysts were extensively characterized using XRD, TEM, XPS, and TPD techniques, and their catalytic activity was evaluated under various reaction conditions.

**KEYWORDS:** CO<sub>2</sub> hydrogenation, olefins, spinel oxide-based catalysts, bifunctional catalysts, zeolite.



## Bifunctional catalysts CuAl<sub>2</sub>O<sub>4</sub>/SAPO-34 for CO<sub>2</sub> hydrogenation to olefins

Abdelhakim Elmhamdi<sup>1,2</sup>, Khaleel<sup>1</sup> Maryam<sup>2</sup>

1 Department of Chemical and Petroleum Engineering, Khalifa University, P.O. Box 127788, Abu Dhabi, United Arab Emirates  
abdelhakim.elmhamdi@ku.ac.ae

2 Research and Innovation Center in CO<sub>2</sub> and H<sub>2</sub> (RICH), Khalifa University, P.O. Box 127788, Abu Dhabi, United Arab Emirates  
maryam.khaleel@ku.ac.ae

### Abstract

CO<sub>2</sub> hydrogenation is a promising strategy for CO<sub>2</sub> conversion and valorisation due to its sustainability. This process can produce various hydrocarbon products, including methanol, methane, dimethyl ether (DME), olefins, and aromatics. Among these, the hydrogenation of CO<sub>2</sub> into olefins is particularly attractive due to the critical role of olefins in producing numerous petrochemical products. There are two main routes for CO<sub>2</sub> hydrogenation to olefins: the CO intermediate route via the Modified-Fischer Tropsch pathway, where olefin selectivity is constrained by the Anderson-Schulz-Flory (ASF) distribution, and the methanol intermediate route using bifunctional catalysts (metal oxide + zeolite), which breaks the ASF distribution.

In this study, we present the preparation of a novel bifunctional catalyst composed of CuAl<sub>2</sub>O<sub>4</sub> and SAPO-34, featuring a spinel oxide CuAl<sub>2</sub>O<sub>4</sub> hollow structure, for CO<sub>2</sub> hydrogenation into olefins. To the best of our knowledge, this is the first report in the literature where a tandem catalyst combining a spinel oxide hollow structure with SAPO-34 has been designed and utilized for CO<sub>2</sub> hydrogenation to olefins. The catalysts were extensively characterized using XRD, TEM, XPS, and TPD techniques, and their catalytic activity was evaluated under various reaction conditions.

**KEYWORDS:** CO<sub>2</sub> hydrogenation, olefins, spinel oxide-based catalysts, bifunctional catalysts, zeolite.



## Production of jet fuel-ranged aromatic hydrocarbons through catalytic pyrolysis of lignocellulosic waste over metal-loaded HZSM-5

Haneul Shim<sup>1</sup>, Bo Sung Kang<sup>1</sup>, Jihyeon Seo<sup>1</sup>, Yong Jun Choi<sup>1</sup>, Hoesuk Yim<sup>2</sup>, Sumin Pyo<sup>3</sup>, Young-Kwon Park<sup>1,\*</sup>

*1 School of Environmental Engineering, University of Seoul, Seoul 02504, Republic of Korea,*

*2 School of Chemical and Biological Engineering, Seoul National University, Seoul 08826, Republic of Korea,*

*3 Department of Chemical and Biomolecular Engineering, KAIST, Daejeon 34141, Republic of Korea*

*catalica@uos.ac.kr*

### Introduction

The ever-increasing need for transportation has led to wide consumption of jet fuel (typically C<sub>8</sub>-C<sub>12</sub> hydrocarbons) or aviation turbine fuel. The common route for jet fuel production mainly relied on petroleum-derived fuels which are costly, pollutive, and non-renewable. In this context, the production of renewable jet fuel has been the main focus of numerous studies, owing to being the most viable and sustainable energy solution for the aviation industry. The conversion of lignocellulosic waste to jet fuel via the pyrolysis-to-jet approach stands out for its simplicity in operation, enabling parameter control, minimal pollutant emissions, and adaptability to the current energy and chemical infrastructure. However, the resulting bio-oil possesses high viscosity, high water content, high oxygenated compounds, and reduced thermal stability.

Catalytic pyrolysis could be a reliable approach, enhancing bio-oil quality by triggering deoxygenation reactions such as decarbonylation, decarboxylation, and hydrodeoxygenation during pyrolysis, making it suitable for use as jet fuel. However, the use of catalysts has several obstacles including their rapid deactivation due to excessive coke formation and a decrease in the high-quality-bio-oil yield during the catalytic pyrolysis. Therefore, an effective target-based design of the catalytic pyrolysis is required to increase the activity and number of active sites of the catalyst and control the distribution of the products of the catalytic pyrolysis. Generally, the metal-loaded zeolites, particularly the transition metal-loaded ones, enhance the conversion of bio-oil into jet fuel-range hydrocarbons due to the dual benefit of the metal centers (enhancing the dehydrogenation/hydrogenation reaction of the conversion) and the zeolite centers (enhancing the dehydration/hydrolysis reaction of the conversion) of these catalysts. The current study offers insight into the production of jet fuel range hydrocarbons via catalytic pyrolysis of lignocellulosic biomass using Fe and Mo modified HZSM-5(38) in a single and bimetallic form. As a matter of fact, the bimetallic catalysts were designed to enhance the organic phase of oil and jet fuel range hydrocarbons subsequently.

Hence, the performance of monometal (1 wt. % Fe or Mo)-loaded HZSM-5(38) and bimetal (0.5 wt. % Fe-0.5 wt. % Mo or 1 wt. % Fe-1 wt. % Mo)-loaded HZSM-5(38) were evaluated for the enhanced production of jet fuel-range hydrocarbons generation via catalytic pyrolysis of lignocellulosic biomass.

### Experimental

In the current investigation, the commercial HZSM-5 (SiO<sub>2</sub>/Al<sub>2</sub>O<sub>3</sub>: 38) was used as the catalyst precursor which was purchased from Zeolyst International–USA. Furthermore, iron (III) nitrate nonahydrate (Fe(NO<sub>3</sub>)<sub>3</sub>·9H<sub>2</sub>O) and molybdenum oxide (MoO<sub>3</sub>) were used as metal precursors in the synthesis. The metal(s) of different fractions (1 wt. % Fe, 1 wt. % Mo, 1 wt. % Fe-1 wt. % Mo, and 0.5 wt. % Fe-0.5 wt. % Mo) were impregnated onto the HZSM-5(38) support from the respective metal precursors using the incipient wetness impregnation method followed by dried for 8 h at 110 °C and the calcination under air at 550 °C for 3 h to obtain the corresponding catalysts. The pyrolysis experiments were conducted using a two-section reactor system, wherein the upper reactor accommodated the feedstock for thermal conversion, followed by catalytic upgrading in the lower reactor. The reactors were fixed using clamps, while a thermocouple was placed inside each reactor to monitor the internal temperature of each reactor. Typically, a ratio of 3:1 for feedstock and catalyst was applied in all experiments while a constant N<sub>2</sub> flow (50 mL/min) was introduced into the reactors. The cut-off temperature of the pyrolytic and catalytic reactors was set to 550 and 500 °C. The reaction was initiated by lowering the upper furnace once the desired temperature was reached in both reactors and the reaction duration was determined at 30 min. Finally, the condensable materials were collected and stored as bio-oil, while the gaseous product (non-condensable) was gathered in a Tedlar bag. The product composition was quantified using GC-TCD, GC-FID, and GC-MS.

### Results and Discussions

Catalytic pyrolysis of lignocellulosic waste were conducted to evaluate the use of HZSM-5 (38) and metal loaded HZSM-5 (e.g., 1%Mo, 1%Fe, 0.5%Fe0.5%Mo, 1%Fe0.1%Mo) on the production of jet fuel-range aromatic hydrocarbons. The product distribution of non-catalytic and different catalytic lignocellulosic waste shows distinct impact of employed catalysts (Fig. 1a). Compared to non-catalytic pyrolysis, catalytic pyrolysis generated a lesser amount of bio-oil due to the further cracking of its bio-oil intermediates into medium or smaller gas compounds. Meanwhile, the bio-oil yield under the 0.5 wt. % Fe-0.5 wt. % Mo/HZSM-5(38) and 1 wt. % Fe-1 wt. % Mo/HZSM-5(38) catalysts were similar (46.87 and 46.66% %) due to the suppression of excessive cracking of the bio-oil. The highest organic-phase bio-oil yield of the pyrolysis was under the 1 wt. % Fe-1 wt. % Mo/HZSM-5(38) catalyst (20.74 %) probably due to the synergistic effect of the Fe and Mo resulting in optimum acidity (Table 1). In addition, the pyrolysis



under the bimetal-loaded HZSM-5(38) (1 wt.% Fe-1 wt.% Mo/HZSM-5(38)) catalysts resulted in minimum coke formation (0.60%) compared to the coke formation during the pyrolysis under the 1 wt. % Mo/HZSM-5(38) (1.27%) and 1 wt.% Fe/HZSM-5(38) (0.93%) catalysts, probably due to well-balanced acidity (Table 1). In particular, these Fe-Mo/HZSM-5(38) catalysts probably inhibited the polycondensation reactions of macromolecular oxygen-containing compounds mainly responsible for coke formation during the pyrolysis [1]. However, the char content in the product was the same under no catalyst/ different catalysts due to the pyrolysis being ex-situ.

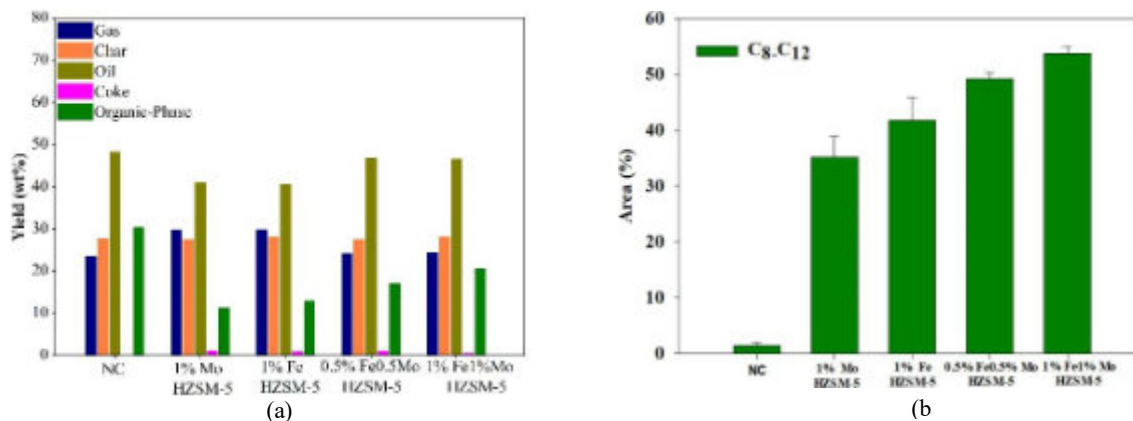


**Figure 1.** The experimental procedure of current study (a) and the jet fuel-range hydrocarbons obtained from the pyrolysis of lignocellulosic biomass under no catalyst and different catalysts.

The non-catalytic (NC) run mainly produced oxygenated compounds (e.g., acid, ketone, aldehydes) (Fig. 1b). However, the use of metal-loaded HZSM-5 significantly increased the proportion of jet fuel range hydrocarbons due to enhancement of hydrogenation and hydrodeoxygenation reactions during the pyrolysis [2]. In particular, hydrocarbon generation from the 1 wt. % Fe/HZSM-5(38) catalytic pyrolysis was higher than that from the 1 wt. % Mo/HZSM-5(38) catalytic pyrolysis possibility due to the higher stability and acidity of the 1 wt. % Fe/HZSM-5(38) catalyst (Table 1). Furthermore, use of bimetal further enhanced the hydrocarbon generation, and the 1 wt. % Fe-1 wt. % Mo/HZSM-5(38) catalyst exhibited the highest hydrocarbon generation due to the synergistic effect of Fe and Mo, which probably promoted the conversion of furans to ketones and aldehydes, increasing the hydrocarbons generation via decarbonylation and decarboxylation reactions during the pyrolysis. Furthermore, the 0.5 wt. % Fe-0.5 wt. % Mo/HZSM-5(38) and 1 wt. % Fe-1 wt. % Mo/HZSM-5(38) catalyst have the higher yield of organic-phase bio-oil compared to the monometal-loaded HZSM-5(38) (Fig. 1a), highlighting the benefit of dual enhancement of the organic phase bio-oil yield and the hydrocarbon yield by the bimetal loading.

**Table 1.** Textural characteristics of the employed catalysts.

Catalyst	BET surface area (m <sup>2</sup> /g)	Pore volume (cm <sup>3</sup> /g)	NH <sub>3</sub> desorbed (mmol/g)
HZSM-5(38)	310.9	0.289	0.473
1 wt. % Mo/HZSM-5(38)	296.2	0.282	0.359
1 wt. % Fe/HZSM-5(38)	284.7	0.265	0.417
1 wt. % Fe-1 wt. % Mo/HZSM-5(38)	278.0	0.268	0.402
0.5 wt. % Fe-0.5 wt. % Mo/HZSM-5(38)	298.4	0.265	0.365

## Conclusion

The possibility of enhancing jet fuel-range hydrocarbons generation and inhibiting coke formation during the catalytic pyrolysis of lignocellulosic waste with the use of Fe and Mo-loaded HZSM-5(38) catalysts was investigated in this study. The addition of Fe and Mo in comparison with the addition of Fe or Mo into the HZSM-5(38) resulted in a higher organic-phase bio-oil yield in the corresponding catalytic pyrolysis by preventing excessive cracking and dehydration of the bio-oil intermediates via its well-balanced acidity. 1 wt. % Fe-1 wt. % Mo/HZSM-5(38) catalyst also generated lesser coke compared to those at under other catalysts. This study will open new avenues for the development of target-based catalysts for obtaining both above-mentioned objectives.

## References

- Cheng, S., et al., Hydrocarbon bio-oil production from pyrolysis bio-oil using non-sulfide Ni-Zn/Al<sub>2</sub>O<sub>3</sub> catalyst. Fuel Processing Technology, 2017. **162**: p. 78-86.
- Cheng, S., et al., Upgrading pyrolysis bio-oil to hydrocarbon enriched biofuel over bifunctional Fe-Ni/HZSM-5 catalyst in supercritical methanol. Fuel Processing Technology, 2017. **167**: p. 117-126.

## Acknowledgments

This research was financially supported by the National Research Foundation of Korea (RS-2024 -00341143, RS-2024-00416414). Also, this work was supported by the Ministry of Environment's waste resource energy recycling professional training project (YL-WE-22-001).



## Visualizing the Superiority of Binder-free Zeolite Catalyst for the Alkylation of Benzene with Ethylene

Duozheng Ma<sup>1,2</sup>, Eelco T. C. Vogt<sup>2</sup>, Zhendong Wang<sup>1,\*</sup>, Bert M. Weckhuysen<sup>2,\*</sup>, Weimin Yang<sup>1,\*</sup>

<sup>1</sup> State Key Laboratory of Green Chemical Engineering and Industrial Catalysis, Sinopec Shanghai Research Institute of Petrochemical Technology Co., Ltd. Shanghai, 201208, PR China.

<sup>2</sup> Inorganic Chemistry and Catalysis group, Debye Institute for Nanomaterials Science, Utrecht University, Universiteitsweg 99, 3854 CG Utrecht, the Netherlands.

\*Email: yangwm.sshy@sinopec.com (Weimin Yang); B.M.Weckhuysen@uu.nl (Bert M. Weckhuysen), wangzd.sshy@sinopec.com (Zhendong Wang)

Industrial catalysts for the alkylation of benzene with ethylene to ethylbenzene typically contain active zeolites and binders. Binders are designed to provide strength and access to the active materials but can also dilute the active phase and block access to the acid sites. Therefore, binder-containing catalysts are needed to transform into binder-free catalysts. Unfortunately, there is no visual measurements available on the accessibility, distribution and efficiency of acid sites in binder-free shaped catalysts. Here, the binder-free shaped catalyst (M-25S) was prepared via Hexamethylene Imine (HMI) -assisted hydrothermal re-crystallization from binder-containing extrudates (M-15 and M-25). By employing advanced fluorescence microscopy approach and fast-response fluorescent nanoprobe reactions, we distinguished the pore accessibility and acid sites distribution of binder-free/containing single extrudate body. Further chemical imaging and time-resolved spectral studies showed that catalytic efficiency benefited from moderate-to-high strength acid sites, and large-sized coke species were mainly caused by polymerization of ethanol/ethylene at weak acid sites during alkylation. Our deep understanding of the superiority of industrial-grade binder-free zeolite catalysts can lead to enhanced design of shaped zeolite materials, which can improve porosity diffusion and acid efficiency in a vast range of catalytic processes.

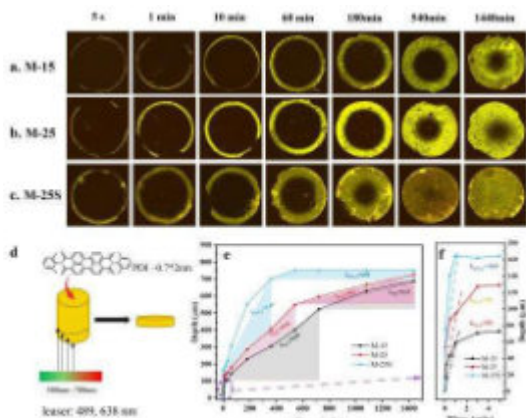


**Figure 1 (left).** Visualizing the diffusion effect in binder-containing and binder-free extrudates.

### Preparation of Catalyst

The MCM-22 fresh zeolite powder was synthesized from our previous work [1]. The binder (including SiO<sub>2</sub>, NaAlO<sub>2</sub> and sesbania powder) was mixed with fresh zeolite extruded into M-15 (15% of binder) and M-25 (25% of binder) catalyst bodies. Binder-free M-25S is derived from the secondary crystallization of M-25 extrudates in an OSDA-containing gel at 160°C hydrothermal treatment.

### Results and Discussion

The ~2 nm PDI (**Figure 1**) probe molecule has a high photostability and a fluorescence quantum yield close to unity, so it was used to study the network and diffusion behavior of extrudates [2]. The confocal fluorescence images of M-15, M-25 and M-25S were completely recorded. Due to the increase in binders, the diffusion rate of M-25 ( $k_{25,2}=0.78$ ) is slightly higher than that of M-15 ( $k_{15,2}=0.59$ ). The diffusion rate of M-25S ( $k_{25S,2}=1.49$ ) is much higher than that of M-25 ( $k_{25,2}=0.78$ ), indicating that the interparticle macropores created by secondary crystallization accelerate the migration of PDI molecules.

Coke deposition of M-25S is significantly less than that of M-25 after 24h alkylation reaction (**Figure 2a, e**). This is mainly due to the abundant macropores of M-25S. As the reaction time increased from 0h to 72h, the bodies of M-25S catalyst gradually changed from light green to dark reddish brown. It is worth noting that in the early stage of the reaction, carbon deposits gradually spread from the outer edge towards the center of the catalyst. Subsequently, the catalyst center uniformly deposits carbon, but the fluorescence intensity at the outer edge decreases (**Figure 2b, d, c, f**). This is because the edge region is more prone to diffusion, causing the coking macromolecules to undergo cracking [3]. After 72 hours, the catalyst has accumulated deep carbon deposits entire bodies, with no difference between the center and edge.

The contribution of acid sites in different temperature ranges of M-25S catalyst to the reaction is different. Weak acid sites below 350°C can only catalyze less ethylene conversion, while strong acid sites above 400°C can convert over 85% of ethylene (**Figure 3a, b**). The acid sites in the T350-400 range have the highest contribution to the reaction ( $\eta=5.9$ , **Table 1**). Time resolved in-situ diffuse reflectance UV-vis spectra indicates that weak acid sites are the main cause of carbon deposition at 680nm wavelength (**Figure 3c, d**). This further explains why M-25S is less prone to



carbon deposition compared to M-15 and M-25, as the former does not contain binders, thereby reducing the production of more weak acid sites.

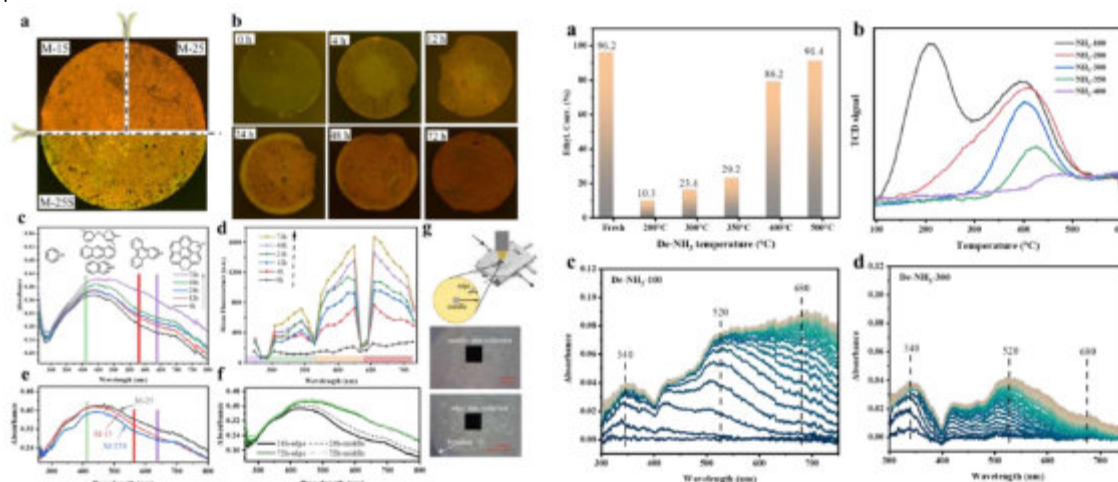


**Figure 2 (left).** Visualizing carbon deposition phenomena at different stages of alkylation reaction. (a, b): CFM images; (d) is fluorescence intensity of CFM images at different reaction time; (c, e, f) schematic representations of the type and location of molecules observed on extrudates of alkylation reaction.

**Figure 3 (right).** (a) Ethylene conversion rate of M-25S catalyst desorption at different temperatures after being poisoned by ammonia; (b) M-25S acidity curves in different temperature ranges (NH<sub>3</sub>-TPD); (c, d) Time-resolved in-situ diffuse reflectance UV-vis spectra during the alkylation of ethanol and ethylene on M-25S adsorb ammonia at 100°C and 300°C.

**Table 1.** The acid content of M-25S in different temperature ranges corresponds to the ethylene conversion rate and contribution factor of alkylation reactions.

Temperature range	Δ Acid sites	Δ Conversion	Contribution (η)
T100-200	55.4%	10.3%	0.19
T200-300	14.9%	6.3%	0.42
T300-350	16.4%	12.6%	0.77
T350-400	9.7%	57%	5.9
T400-600	3.6%	5.2%	1.4

## Conclusion

We have demonstrated the binder-free M-25S has better diffusion properties and alkylation reactivity, as well as less carbon deposition based on advanced spectroscopic characterization. The zeolite catalyst produced by secondary crystallization not only maintains a certain mechanical strength, but also generates abundant macropores, which has good industrial application prospects.

## References

- [1] Wang, Z.; Cichocka, M. O.; Luo, Y.; Zhang, B.; Sun, H.; Tang, Y.; Yang, W. *Chinese J Catal*, 2020, 41 (7), 1062-1066.
- [2] Hendriks, F. C.; Meirer, F.; Kubarev, A. V.; Ristanovic, Z.; Roeffaers, M. B. J.; Vogt, E. T. C.; Bruijninx, P. C. A.; Weckhuysen, B. M. *J. Am. Chem. Soc*, 2017, 139 (39), 13632-13635.
- [3] Whiting, G. T.; Nikolopoulos, N.; Nikolopoulos, I.; Chowdhury, A. D.; Weckhuysen, B. M. *Nat Chem*, 2019, 11 (1), 23-31.



## Continuous flow CO<sub>2</sub>/CH<sub>4</sub> separation using MMU-1 and CHA zeolites

**B. Tapping, L. Tosheva, A. M. Doyle**

Department of Natural Sciences, Manchester Metropolitan University, Chester St., Manchester, M1 5GD, UK  
Robert.S.Tapping@stu.mmu.ac.uk

In recent years, significant research efforts have been directed towards advancing carbon dioxide capture technologies globally, with the aim of addressing the escalating challenge of climate change emerging from industrial emissions and waste. Conventional CO<sub>2</sub>/CH<sub>4</sub> separation methods heavily rely on treatment via harsh alkanolamine scrubbing, which is hindered by high regeneration costs, equipment corrosion, and large volumes of hazardous waste [1]. Selective separation using a solid adsorbent is an attractive alternative to amine scrubbing due to the ease of recovery/regeneration of the captured gas/adsorbent, respectively.

Owing to their high adsorption capacity and high selectivity, low silica small pore zeolites are excellent candidates for the selective adsorption of CO<sub>2</sub>. We have recently reported the template-free synthesis of novel zeolite MMU-1, a Cs,Na-modified EDI-type small pore zeolite [2]. Alterations to the molar composition of the precursor gel synthesized Cs,Na-Chabazite (CHA), a well-known candidate in the CO<sub>2</sub>/CH<sub>4</sub> separation [3], which served as a comparable reference in this study. The aim of this work is to evaluate the suitability of as-made MMU-1 and MMU-1 zeolites prepared by ion exchange with K (K,Cs,Na-MMU-1) to selectively adsorb CO<sub>2</sub> using a continuous flow method and compare the results with similarly prepared CHA samples.

The dynamic adsorption was studied at ambient temperature in a quartz fixed-bed reactor placed inside a temperature-controlled furnace. A feed mixture of 10 ml min<sup>-1</sup> comprising CO<sub>2</sub>:CH<sub>4</sub>:Ar equal to 1:1:8 was used in all tests. 2.0 g of 900-1000 μm MMU-1 or CHA pellets was pretreated in 15 ml min<sup>-1</sup> He at 300 °C for 3 h, 5 °C min<sup>-1</sup> ramp. After cooling to ambient temperature, adsorption measurements were recorded at 3 min intervals (minimum interval possible) until saturation. Gas concentrations were monitored using a gas chromatograph-thermal conductivity detector (GC-TCD).

The breakthrough profiles for CO<sub>2</sub>/CH<sub>4</sub> over Cs,Na-MMU-1 and Cs,Na-CHA (Figure 1a) demonstrate that both MMU-1 and CHA selectively adsorb CO<sub>2</sub> over CH<sub>4</sub> on a continuous flow basis. CH<sub>4</sub> is initially adsorbed but is displaced due to competitive adsorption resulting in an overshoot of the CH<sub>4</sub> concentration. The capacity for CO<sub>2</sub> decreased in the order K,Cs-CHA > K,Cs,Na-MMU-1 > Cs,Na-CHA > Cs,Na-MMU-1. Exchanging with K<sup>+</sup> ions improved the capacity for CO<sub>2</sub> in both zeolites (Figure 1b), notably for K,Cs,Na-MMU-1 which increased by a factor of five. Overall, the results confirm that MMU-1 and CHA are viable zeolites capable of separating CO<sub>2</sub> from CH<sub>4</sub> under the continuous flow conditions. A full set of results will be presented at the conference.

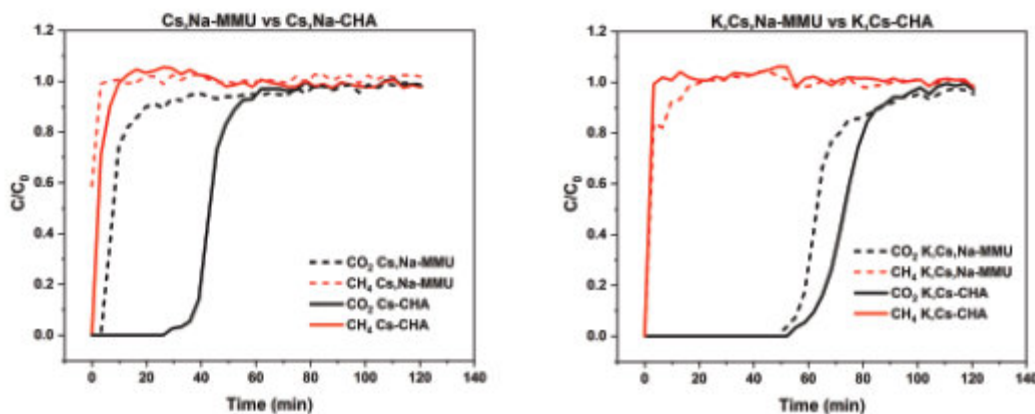


**Figure 1.** a) Breakthrough profiles of Cs,Na-MMU-1 and Cs,Na-CHA b) breakthrough profiles of K,Cs,Na-MMU-1 and K,Cs-CHA.

### References

- 1- Wang, T. Hovland, J. Jens, K. J. Amine reclaiming technologies in post-combustion carbon dioxide capture, *Journal of Environmental Sciences*. **27**, 276-289 (2015).
- 2- Tosheva, L. Garbev, K. Miller, G.J. Mihailova, B. Toward the synthesis of new zeolite structures in the presence of cesium: zeolite MMU-1, *Crystal Growth & Design*. **23**, 3834-3844 (2023).
- 3- Ghojavand, S. Coasne, B. Clatworthy, E.B. Alkali Metal Cations Influence the CO<sub>2</sub> Adsorption Capacity of Nanosized Chabazite: Modeling vs Experiment. *ACS Applied Nano Materials*. **5**, 5578-5588 (2022).



## SAPO Precursor and Multiple Template-Assisted Synthesis of Highly Acidic SAPO Molecular Sieves with Excellent NH<sub>3</sub>-SCR Activity of Their Cu-Exchanged Form

M. Yang, Y. Wang, P. Tian and Z. Liu

National Engineering Research Center of Lower-Carbon Catalysis Technology, Dalian National Laboratory for Clean Energy, Dalian Institute of Chemical Physics, Chinese Academy of Sciences, Dalian 116023, China  
[yangmiao@dicp.ac.cn](mailto:yangmiao@dicp.ac.cn), [liuzm@dicp.ac.cn](mailto:liuzm@dicp.ac.cn)

Ammonia selective catalytic reduction of NO<sub>x</sub> (NH<sub>3</sub>-SCR) is one of the most effective technologies to eliminate NO<sub>x</sub> emissions of heavy-duty diesel vehicles, where Cu-SSZ-13 with a Si/Al ratio of around 10 has been implemented as the state-of-the-art catalyst. Although the catalyst exhibits superior activity and hydrothermal durability, it is still highly desirable to further improve the activity and stability of the NH<sub>3</sub>-SCR catalysts for better adaption of the complex operating conditions of diesel vehicle, and meeting the continuously enhanced standards for NO<sub>x</sub> emission. There has been a long-time intense searching for new zeolite catalyst candidates. A series of small-pore zeolites with abundant 6-rings units have been synthesized and their corresponding Cu-exchanged samples show huge potential as the alternative NH<sub>3</sub>-SCR catalysts. However, the syntheses of these zeolites generally require the aid of complex and expensive organic structural directing agent (OSDA) and/or the assistance of fluoride media to enhance their Si/Al ratio and stability.

In contrast to zeolites, the synthesis of iso-structured SAPO materials is an alternative, cost-effective way to obtain catalyst supports, which reduces the ion exchange steps by avoiding use of alkali metal cations. Although the Cu-SAPO-34 with CHA structure has experienced perplexing failure as the commercial NH<sub>3</sub>-SCR catalyst, the atomic-level investigations show that optimizing the chemical compositions of SAPO materials (Si distribution etc.) may solve the problem. Unfortunately, how to rationally introduce silicon atoms and improve their distribution remains a major challenge in SAPO synthesis. A composite Cu-CHA<sub>DNL</sub> compound containing both microenvironments of SSZ-13 and SAPO-34 was synthesized bearing both advantages of the two, which behaves excellent NH<sub>3</sub>-SCR activity and robust high- and low-temperature hydrothermal stabilities.<sup>1</sup>

In this work, we show an effective SPMT strategy, i.e. using SAPO Precursors and Multiple Templates, to synthesize different SAPO materials with high silica content and uniform Si distribution. As shown in Figure 1, the SAPO precursor provides a rich set of Si containing active structural units to modulate the crystallization kinetics and optimize the Si distribution of the final product. The crystalline phase is simultaneously controlled by precursor and multiple templates, where the second template can play a decisive role when the zeolite has multiple cage structures. A series of high silica SAPO materials with strong acidity and special morphology have been synthesized through this method. In particular, the prepared copper-ion exchanged Cu-SAPO-17 exhibits an unexpectedly wide activity temperature window, with over 90% NO conversion from 175 to 700°C in the NH<sub>3</sub>-SCR reaction. This work not only provides an effective strategy for the synthesis of SAPO molecular sieves with strong acidity, but also opens up a new perspective for breaking through the range of the active temperature window for the NH<sub>3</sub>-SCR reaction.

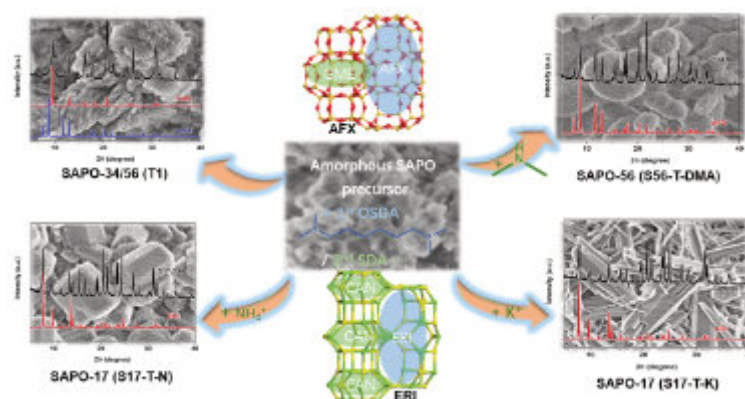


**Figure 1** The synthetic strategy and results of SAPO materials.

### References

[1] L. Sun, M. Yang, L. Cao, Y. Cao, S. Xu, D. Zhu, P. Tian, Z. Liu, *Microporous Mesoporous Mater.* **309** (2020) 110585.

### Acknowledgments

The authors thank the National Natural Science Foundation of China (Grant Nos. 22171259, 21991090, 21991091, 22288101, 22372020), and the AI S&T Program of Yulin Branch, Dalian National Laboratory for Clean Energy, CAS (Grant DNL-YL A202206).

## A waste of time? The synthesis of Mg-doped Aluminophosphates from a waste source of magnesium.

C. Crockett<sup>1</sup> and R. A. Taylor<sup>1\*</sup>

<sup>1</sup> Department of Chemistry, Durham University, Durham, DH1 3LE, UK  
[catherine.crockett@durham.ac.uk](mailto:catherine.crockett@durham.ac.uk), [russell.taylor@durham.ac.uk](mailto:russell.taylor@durham.ac.uk)

Aluminophosphates (AlPO) are a neutral oxide framework comprised of strictly alternating  $[\text{AlO}_4]^-$  and  $[\text{PO}_4]^+$  tetrahedra.[1] Similar to their zeolite counterparts, these small building units can form a plethora of different frameworks, each with varying ring sizes and channel dimensionality. The target framework for this work is AFI (AlPO-5) which comprises of 12, 6 and 4 membered rings, and unidimensional channels (**Figure 1**). The framework neutrality of AlPO's limits their catalytic potential, however, Brønsted acidity can be created by substituting framework atoms for those with different oxidation states. The charge imbalance created upon this substitution can be compensated for by a proton, which generates Brønsted acidity.[2] Here, magnesium is being substituted into the framework as a replacement for aluminium and can be accomplished using hydrothermal synthetic techniques. Ordinarily, the source of magnesium is a synthetic salt. In this work, a waste material, struvite ( $\text{MgNH}_4\text{PO}_4 \cdot 6\text{H}_2\text{O}$ ), is being used as an alternative and novel source of magnesium. Struvite precipitates from highly concentrated nutrient waste streams, causing pipe blockages.[3] It is costly to remove, and contains both Mg and P which are listed as critical raw materials by the EU, hence it would be beneficial from economic and environmental perspectives to find a use for struvite.[4]

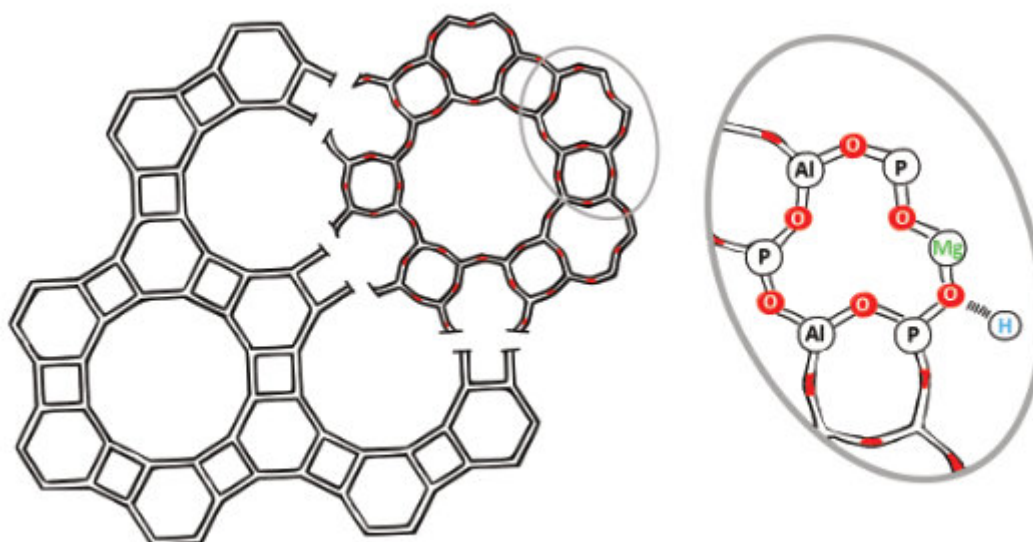


**Figure 1.** Diagram of the AFI (AlPO-5) framework, shown conventionally with T atoms only, and with oxygen atoms (top right). The formation of a Brønsted acidic proton upon the substitution of aluminium for magnesium is also shown. (enlarged, right).

To prepare these materials, D.I  $\text{H}_2\text{O}$  and  $\text{H}_3\text{PO}_4$  were added to a beaker. A portion of  $\text{Al}(\text{OH})_3 \cdot x\text{H}_2\text{O}$  was added and stirred for 10 min, followed by the magnesium source, and stirred for a further 10 min. Lastly, N,N-dicyclohexylmethylamine was added and stirred for 90 min. The final molar gel ratio was 0.97 Al: 1.50 P: 0.80 SDA: 40  $\text{H}_2\text{O}$ : 0.03 Mg. The gel was divided between six Teflon lined autoclaves with stirrer bars and placed in the oven at 180 °C. The autoclaves were removed after 2 h and cooled on ice for 30 min. Each mixture was then centrifuged, to separate the liquor and solid product. The remaining solid product was then washed with D.I.  $\text{H}_2\text{O}$  via centrifugation. The solid product was oven dried at 80 °C overnight and then calcined at 550 °C for 16 h. The MgAlPO-5 synthesised from magnesium acetate will be referred to as OAc-MgAlPO-5, and the MgAlPO-5 from struvite as S-MgAlPO-5 hereon in.

The powder x-ray diffraction patterns show that both the conventional OAc-MgAlPO-5 and S-MgAlPO-5 form the pure AFI framework after 2 h (**Figure 2**). An AlPO-5 without magnesium was synthesised for comparison.

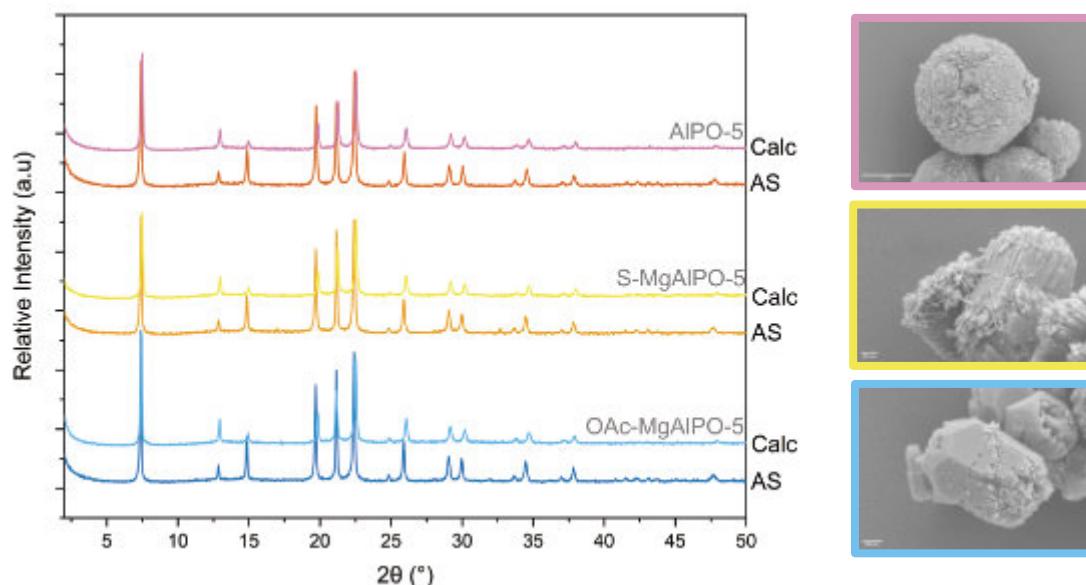


**Figure 2.** Powder x-ray diffraction patterns of MgAlPO's synthesised using Mg-acetate (bottom) and struvite (middle), and an AlPO without Mg (top). Both the as-synthesised (AS) and calcined (Calc) patterns are shown. SEM images corresponding to the calcined samples are shown (right)

Elemental analysis of OAc-MgAlPO-5 and S-MgAlPO-5 indicated similar levels of Mg incorporation, giving (Al+Mg)/P ratios of 0.97 and 0.95 respectively, suggesting similar values of Mg incorporation. To investigate the structure at a local level <sup>27</sup>Al and <sup>31</sup>P solid-state MAS NMR spectra have been obtained. The <sup>27</sup>Al spectra for both MgAlPO's is similar; a sharp intense peak at 38 ppm, and a further small peak at -13 ppm, indicating the presence of both tetrahedrally and octahedrally coordinated aluminium environments. The samples were not dehydrated prior to analysis so the octahedral environment is likely due to the coordination of water molecules to the aluminium environment. The <sup>31</sup>P spectra show a single broad asymmetric peak, matching previously reported MgAlPO-5 spectra.

The stability of the OAc-MgAlPO-5 and S-MgAlPO-5 samples was examined using thermogravimetric analysis. The calcined samples were heated from 30 – 800 °C under air. Both OAc-MgAlPO-5 and S-MgAlPO-5 had a similar total mass loss of 16 wt%, while the mass loss of the AlPO-5 was 9 wt%. The higher mass loss for the MgAlPO-5 is ascribed to higher levels of hydration caused by the presence of the Brønsted acid site.

Scanning electron microscopy (**Figure 2**) and transmission electron microscopy of both OAc-MgAlPO and S-MgAlPO show similar crystal morphologies however differences occur on the surface; the OAc-MgAlPO crystals are sparsely covered in small spheres (~10 nm) whereas the S-MgAlPO crystals are coated in needle-like growths (10's-100's nm in length) (**Figure 2**). This can be corroborated by TEM images. EDS-TEM will be needed to further elucidate the elemental composition of these structures.

To conclude, thus far, S-MgAlPO shows very few differences when compared to its more conventional OAc-MgAlPO counterpart. The bulk structure, elemental composition, thermal stability and local structure all prove alike. Further analysis such as N<sub>2</sub> adsorption is needed to analyse the internal surface of the materials, which may yield subtle differences in the pore structure and pore size distribution. Moreover, the functionality and acidic character of the two materials may show variation consequently affecting potential catalytic behaviour. Using probe molecules when collecting DRIFT's spectra or SS-NMR measurements will prove useful for further understanding of this unconventional source of magnesium in the synthesis of aluminophosphate materials.

## References

- [1] S T. Wilson, B M. Lok, C A. Messina, T R. Cannan, E M. Flanigen, *J. Am. Chem. Soc.*, **104**, 1146-1147 (1982)
- [2] H O. Pastore, S. Coluccia, L. Marchese, *Annu. Rev. Mater. Res.*, **35**, 351-395 (2005)
- [3] R. Kumar, P. Pal, *Environ. Sci. Pollut. Res. Int.*, **22**, 17453-17464 (2015)
- [4] European Commission. *Critical Raw Materials. European Commission – Single Market Economy*. [Accessed October 30, 2024] from [https://single-market-economy.ec.europa.eu/sectors/raw-materials/areas-specific-interest/critical-raw-materials\\_en](https://single-market-economy.ec.europa.eu/sectors/raw-materials/areas-specific-interest/critical-raw-materials_en).

## Acknowledgments

The EPSRC Centre for Doctoral Training in Renewable Energies Northeast Universities (ReNU, Grant No. EP/S023836/1) is thanked for the funding for this project, as well as the Chemistry Department analytical services. In addition, the Taylor group consisting of Russell, Jess and Phoebe.

## Formation of Nanostructured Cu and Ni Si-MFI Zeolites for Bioethanol Upgrading

J. Bedward<sup>1</sup>, R. Taylor<sup>1</sup>

<sup>1</sup> Durham University, Department of Chemistry, Durham, DH13LE, UK  
 jessica.r.bedward@durham.ac.uk

### Introduction

At present, the global chemical manufacturing industry relies primarily on fossil fuel-based feedstocks for the synthesis of chemicals and fuels. As such, there is an ever-increasing pressure to utilise renewable alternatives. Upgrading of biomass-derived bioethanol into bioacetaldehyde provides a route to many higher value chemicals such as butadiene, pyridine and butanol, with the latter having biofuel applications. Zeolites act as robust, versatile, and effective catalysts with tuneable structural properties, making them highly appropriate for this application. [1] Recent work by Pang et al. reports that Cu-MFI shows high selectivity (93%) and productivity (97%) for the non-oxidative dehydrogenation of ethanol to acetaldehyde. [2] Additionally, a series of Cu/NiAlO<sub>x</sub> catalysts have been studied for ethanol conversion by Li et al., who concluded that optimal ethanol conversion (~35%) and n-butanol selectivity (~45%) were achieved over 0.75% Cu/NiAlO<sub>x</sub> at 250 °C. [3] Consequently, we aim to complement these findings through the preparation of zeolite catalysts with extra framework Cu and Ni Lewis acid sites.

Herein, we have explored the synthesis of zeolite frameworks with reduced Brønsted acidity, namely Si-MFI. Controlling framework acidity can enhance butanol selectivity, by minimising undesired dehydration reactions that lead to the formation of ethylene or diethyl ether. [4] Conventionally, hydrothermal synthesis of Si-MFI is performed in the presence of F<sup>-</sup> ions, which act as an effective mineraliser, facilitating the synthesis of defect-free Si-MFI. [5] Despite providing a route to defect-free Si-MFI, the use of HF in such synthesis is not desirable due to safety and environmental concerns, and consequently there is a need for a fluoride free synthesis pathway. [5] This work aims to utilise the fluoride-free hydrothermal synthesis method proposed by Pang et al., to synthesise Si-MFI. [2] Different synthesis conditions have been investigated, namely gel stirring time and crystallisation time, in order to evaluate the impact they have on the homogeneity and presence of defects in the Si-MFI produced. Additionally, we report details of the incorporation of earth abundant, extra framework metal sites (Cu, Ni), onto siliceous MFI zeolite catalysts, for the application of bioethanol upgrading.

### Materials and Methods

Si-MFI was prepared via hydrothermal synthesis according to the protocol reported by Pang et al, with amended gel stirring times (3 vs 24 hr) and crystallisation times (24, 48, 72 hr). [2] Subsequently, mono-metallic (10% Cu/zeolite, 10% Ni/zeolite) and bimetallic (5% Cu, 5% Ni/zeolite) Si-MFI catalysts were prepared via incipient wetness impregnation according to the method proposed by Kumar et al. [6]

### Results and Discussion

Si-MFI samples follow the naming notation Si-MFI-a-b, where a denotes the gel stirring time, and b denotes the crystallisation time. pXRD analysis indicates all Si-MFI samples are highly crystalline with little amorphous character. [2] The diffraction patterns all exhibit the major reflections associated with the MFI framework such as the high intensity peaks at  $2\theta = 7 - 9^\circ$  and  $23 - 25^\circ$ , confirming they adopt MFI conformation, and no impurity phases are present. [2] <sup>29</sup>Si HPDEC and <sup>1</sup>H-<sup>29</sup>Si CPMASSs NMR spectroscopy experiments were carried out in order to assess the nature of the Si environments in the Si-MFI samples. When comparing across samples, it can be confirmed all the studied Si-MFI materials have a similar Q<sup>4</sup>Si(OSi)<sub>4</sub>/Q<sup>3</sup>Si(OSi)<sub>3</sub>(OH), ratio of 13-16, despite the different gel stirring and crystallisation times used in their synthesis. Such results indicate a degree of Si site homogeneity within the samples.

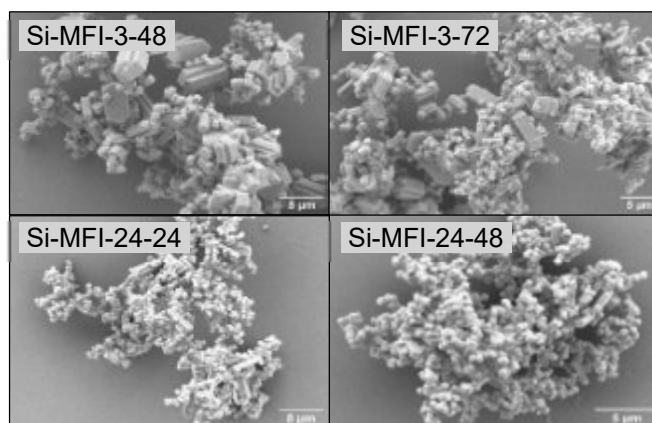


Figure 1: SEM images of Si-MFI samples coated in 35 nm Au. Images acquired at 5 Kv using a Sigma EVO SEM microscope.

As seen in Figure 1, clear morphological differences are observed in the Si-MFI sample depending upon the synthesis conditions used. A more homogeneous particle size and shape distribution is observed for Si-MFI samples which were stirred for 24 h (Si-MFI-24-24, Si-MFI-24-48) in comparison to those stirred for only 3 h (Si-MFI-3-48, Si-MFI-3-72). Samples stirred for 24 h are mostly comprised of ~0.5  $\mu\text{m}$  uniform hexagonal particles. In contrast, samples stirred for 3 h are a mixture of larger ~5  $\mu\text{m}$  coffin shaped particles in addition to the ~0.5  $\mu\text{m}$  hexagonal particles. Extended stirring facilitates better dispersion of TPAOH and TEOS, leading to more nucleation sites and subsequently smaller crystals as growth competition is evenly distributed. [7] The larger particles present in the Si-MFI samples which were stirred for only 3 h occur as the result of inhomogeneous supersaturation. [7] The longer gel stirring time can therefore be shown to help maintain a stable supersaturation level, in turn leading to a more controlled nucleation process, resulting in a more homogeneous particle shape distribution. [7]

Following Cu and Ni incipient wetness impregnation on Si-MFI-24-48 analysis of heteroatom content via ICP-OES revealed Cu concentrations of between 7.0 wt% and 9.1 wt% for mono-metallic Cu-Si-MFI, and Ni concentrations of between 8.0 wt% and 9.1 wt% for monometallic Ni-Si-MFI. For bimetallic catalysts, Cu loadings of between 4.2 wt% and 4.9 wt%, and Ni loadings of between 4.0 wt% and 4.8 wt% were achieved for Cu/Ni-Si-MFI.

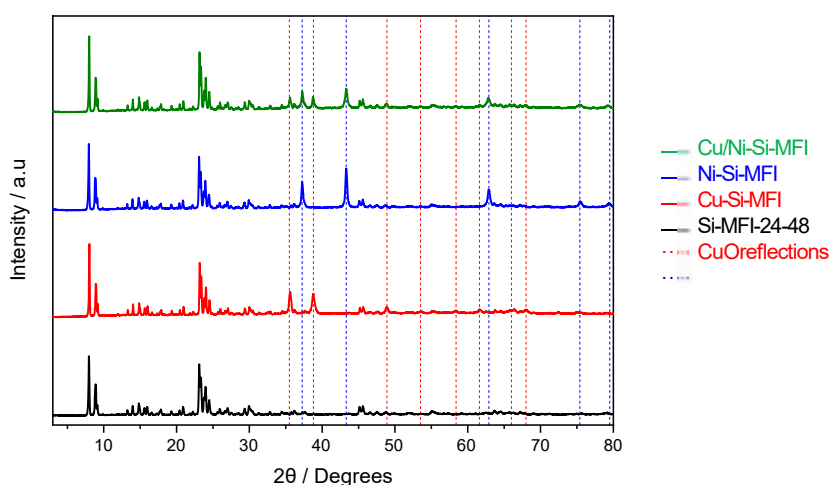


Figure 2: pXRD diffraction patterns of Si-MFI-24-48, Cu-Si-MFI, Ni-Si-MFI and Cu/Ni-Si-MFI, shown in black, red, blue and green, respectively. Data was collected using a Bruker D8 Advanced diffractometer ( $\lambda_{\text{K}\alpha} = 1.54184 \text{ \AA}$ ).

As shown in Figure 2, both mono- and bi-metallic Si-MFI show characteristic reflections for MFI, indicating a high degree of crystallinity and no change to the framework structure upon metal impregnation. [2] pXRD analysis also confirms that Cu and Ni are present in their oxide forms, CuO and NiO, for both mono- and bi-metallic Si-MFI. Cu-Si-MFI shows diffraction peaks at  $2\theta$  values of 35.5°, 38.5° and 48.9°, 53.5°, 61.6°, 66.0° and 68.0° which occur as the result of CuO present in the sample. [6] Furthermore, all mono-metallic Ni-zeolites show diffraction peaks at  $2\theta$  values of 37.3°, 43.3°, 62.9°, 75.4° and 79.5°, which can be attributed to NiO in the sample. [6] Bi-metallic samples show all the aforementioned diffraction peaks, but at a much lower intensity, indicating the presence of both CuO and NiO, in a lower concentration than in mono-metallic samples. [6]

#### Significance

Since 2015, global bioethanol production has exceeded 25 billion gallons per year, predominantly for use as a biofuel. [9] Consequently, the upgrading of bioethanol into higher value chemicals and fuels is of great interest and will provide a more sustainable route for chemical synthesis. Looking ahead, the bioethanol upgrading capability of all synthesised catalysts will be investigated using a flow reactor with online GC-MS-BID analysis.

#### References

- [1] S. J. Raynes, R. A. Taylor, *Sustain. Energy Fuels*, 5, 2136–2148 (2021).
- [2] J. Panget al., *ACS Catal.*, 10, 13624–13629 (2020)
- [3] J. Li et al., *ChemCatChem*, 14, e202200539 (2022).
- [4] J. Sun, Y. Wang, *ACS Catal.*, 4, 1078–1090 (2014).
- [5] K. Jiao et al., *Microporous and Mesoporous Mater.*, 225, 98–104 (2016).
- [6] R. Kumar et al., *Bioresour. Technol.*, 279, 404–409 (2019).
- [7] C. S. Cundy, P. A. Cox, *Microporous Mesoporous Mater.*, 82, 1–78 (2005).
- [9] Renewable Fuel Association: World Fuel Ethanol Production <https://ethanolrfa.org/markets-and-statistics/annual-ethanol-production> (04/11/2024).

#### Acknowledgments

XAS analysis was provided by the Durham X-ray Absorption Facility, supported by the Engineering and Physical Sciences Research Council [grant number EP/V029053/1]



## Tuning the Cu/ZSM-5 properties as catalyst in the conversion of 2,3-Butanediol to butenes

Patricia Pizarro<sup>1,2</sup>, Adriana Souza<sup>1</sup>, Sinay Turriziani<sup>1</sup>, Mar Alonso-Doncel and David P. Serrano<sup>1</sup>

<sup>1</sup> Thermochemical Processes Unit, IMDEA Energy Institute, Móstoles (Madrid), Spain.

<sup>2</sup> Chemical and Environmental Engineering Group, Rey Juan Carlos University, Móstoles (Madrid) Spain

patricia.pizarro@imdea.org

2,3-Butanediol (2,3-BDO) is a molecule derived from fermentation processes of organic waste that is receiving increasing attention as platform substrate to produce biofuels and bio-based chemicals [1]. Full dehydration of 2,3-BDO leads to butenes that can be further converted via oligomerization and hydrogenation into hydrocarbons suitable for fuels formulation. However, the production of butenes is quite challenging due to the highly favoured formation of intermediate dehydration products (methyl ethyl ketone (MEK) and methyl propanal (MPA)). Among the catalysts tested until now, those combining metal Cu active phases with acidic supports under H<sub>2</sub> atmosphere have shown promising results [2]. However, there is still room for improvement in the butenes yield and for understanding the role of the catalyst preparation method over its physico-chemical and catalytic properties.

In this work our goal was to explore the role of the method applied to disperse Cu nanoparticles onto a nanocrystalline MFI-type zeolite with a Si/Al ratio of 40 (n-ZSM-5(40)), on both the physicochemical properties of the resultant catalysts and on their activity in terms of conversion of 2,3-BDO, selectivity to butenes and stability in reaction. Three methods to disperse 10 wt.% of Cu were approached: 1: incipient wetness impregnation (IWI); 2: wet impregnation (WI) and 3: ammonia-driving deposition-precipitation (ADP). These samples were characterized by different techniques, including XRD, TEM, N<sub>2</sub> physisorption and Pyr/FTIR. The catalytic activity was tested in a fixed-bed reactor at 250 °C, 1 bar, with WHSV of 3 h<sup>-1</sup>, and H<sub>2</sub>/2,3-BDO molar ratio = 5/1. Prior to the reactions, the catalysts were pre-reduced in-situ at 400 °C with hydrogen. The vapours exiting the reactor passed through a condensation system where the less volatile components were collected as a liquid phase and analysed by GC-MS (molecular organic composition) and Karl-Fischer titration (water content). The fraction of gases not condensed was analysed in micro-GC.

The method for Cu dispersion was a key factor in the catalyst performance, with ADP being the unique giving 100% conversion of 2,3-BDO during the 4 h of reaction tested, where the others suffered progressive deactivation from the second hour (Figure 1). In terms of products distributions, both IWI and WI gave similar results with low C<sub>4</sub> olefins mass yields (below 10 wt.%), due to a partial 2,3-BDO dehydration that led to MEK as main product. On the other hand, a significant change was observed with ADP method, with a much higher yield of water and C<sub>4</sub> olefins (around 25 wt.%), at expense of MEK and other oxygenated compounds.

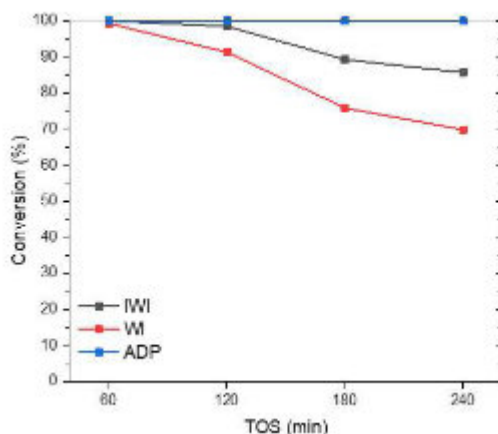


Figure 1. Conversion of 2,3-BDO over 10 wt.% CuO/n-ZSM-5(40) zeolite prepared with different impregnation methods.

The different catalytic performance of the three catalysts was correlated with their physico-chemical properties. XRD analyses revealed clear differences between them: diffraction signals corresponding to CuO (as-synthesized) and metal Cu<sup>0</sup> (reduced samples) were evident for IWI and WI methods, whereas they were absent in the ADP method. Since ICP-OES analysis demonstrated the presence of Cu in amounts matching with the theoretical loadings, the absence of XRD signals was attributed to a much better dispersion provided by ADP method. On the other hand, all catalysts exhibited the typical signals corresponding to the ZSM-5 zeolitic framework, corroborating their stability even after reduction treatment. TEM images were also taken of the three catalysts (Figure 2), clearly showing a much



better dispersion, with very homogeneous and smaller CuO nanoparticles observed in the catalysts prepared by the ADP method.

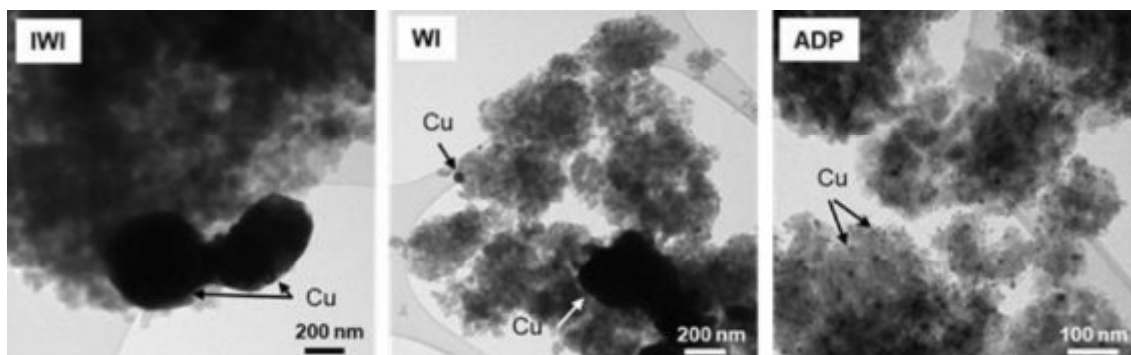


Figure 2. TEM images of 10 wt.% CuO/n-ZSM-5(40) catalysts prepared with different impregnation methods.

Acidic properties of the catalysts were measured by means of pyridine-adsorption coupled to FTIR analyses (Pyr/FTIR). It was revealed that the impregnation of copper led to a drastic reduction of Brønsted acid sites while some increase of Lewis-type ones. This indicates that Brønsted acid sites of ZSM-5 do not seem to play an important role in the conversion of 2,3-BDO to butenes, at least under the reaction conditions here employed.

In conclusion, a drastic increase of the Cu/n-ZSM-5 activity is attained when ammonia-driving deposition-precipitation method is used to disperse copper on the zeolite, this effect being attributed to a much better dispersion of Cu nanoparticles with a narrower size distribution.

#### References

- [1] N.T.T. Nguyen, F. Matei-Rutkowska, M. Huchede, K. Jaillardon, G. Qingyi, C. Michel, J.M.M. Millet., *Catalysis Today*, 323, 62-68 (2019).
- [2] Quanxing Zheng, Michael D. Wales, Michael G. Heidlage, Mary Rezac, Hongwang Wang, Stefan H. Bossmann, Keith L. Hohn, *Journal of Catalysis*, 330, 222-23 (2015).

#### Acknowledgments

The authors acknowledge the financial support of BIOCTANE project with Grant N° 101084336. Funded by the European Union. Views and opinions expressed are however those of the author(s) only and do not necessarily reflect those of the European Union or the European Climate, Infrastructure and Environment Agency (CINEA). Neither the European Union nor CINEA can be held responsible for them.

## Ethylene/ethane permeation behavior through Ag-Beta zeolite membrane

Y. Koshiishi<sup>1</sup>, M. Sakai<sup>1</sup>, M. Matsukata<sup>1,2,3,\*</sup>

<sup>1</sup> Department of Applied Chemistry, Faculty of Science and Engineering, Waseda University, Shinjuku 162-0041, Japan

<sup>2</sup> Research Organization for Nano & Life Innovation, Waseda University, Shinjuku 162-0041, Japan

<sup>3</sup> Research Institute for Science and Engineering, Shinjuku 169-8555, Japan

\*mmatsu@waseda.jp

Ag-exchanged zeolite beta membrane was synthesized, and its separation behavior for ethylene/ethane separation was examined. The membrane showed good separation performance even at low ethylene partial pressures, achieving highly pure ethylene in a single-stage membrane separation. The adsorption on Ag-beta membrane saturated with the partial pressure of ethylene between 0.25–0.5 kPa, resulting in a change of the permeation mechanism before and after the saturation.

### Introduction

Olefins are widely used in industry as raw materials for polymers. Given that olefins are produced simultaneously with paraffins, they must be purified to a high degree of purity. Cryogenic distillation is currently used for the separation of olefins and paraffins, which consumes a large amount of energy for the purification. These processes account for approximately 0.3% of the global energy consumption.[1] In light of this, membrane separation has drawn attention as an energy-efficient method for olefin purification.

Ag<sup>+</sup>-exchanged zeolites are effective for olefin purification. The strong interaction between Ag<sup>+</sup> and olefin provides high separation performance.[2] In particular, beta-type zeolite, with their large 12-membered ring pores, exhibit a high ethylene selectivity.[3]

The objective of this study was to examine ethylene/ethane separation behavior through Ag-beta zeolite membrane.

### Experimental method

Na-beta zeolite membrane was synthesized on an outer surface of tubular support by a secondary growth method. A porous  $\alpha$ -alumina tube with an outer diameter of 12 mm, an inner diameter of 9.0 mm, and a length of 30 mm was used as support. Seeded support prepared by a dip-coating method was hydrothermally treated at 403 K for 7 days in a synthesis solution having a molar composition of 1 SiO<sub>2</sub>:0.01 Al<sub>2</sub>O<sub>3</sub>: 0.3 Na<sub>2</sub>O:17 H<sub>2</sub>O.

Ag-beta membrane was obtained through ion exchange with Na-beta membrane. Na-Beta membrane was immersed in an AgNO<sub>3</sub> aqueous solution and degassed under reduced pressure using an aspirator for 1 h. Subsequently, the membrane was kept in the solution while stirring for 1 h and then washed thoroughly.

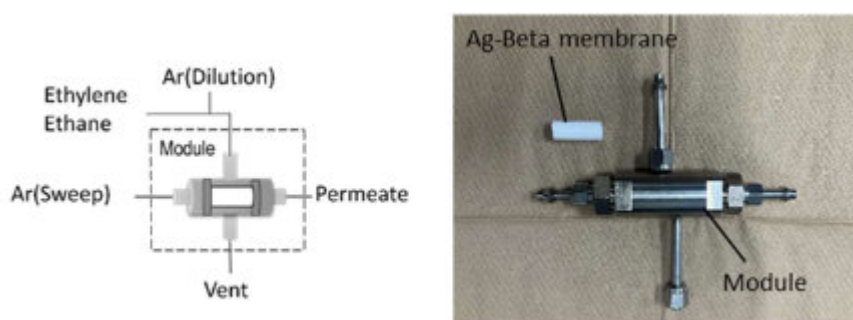


Figure 1. A schematic diagram of ethylene / ethane separation equipment.

Ethylene/ethane separation tests were performed to evaluate the performance of the synthesized Ag-beta membrane. Figure 1 shows a schematic diagram and a photo of the separation equipment. A mixture of ethylene and ethane were supplied as feed, and the permeated gases were analyzed for its composition using a gas chromatography with a flame ionization detector (GC-FID). Ar gas was supplied as a sweep gas at 300 mL min<sup>-1</sup>. CH<sub>4</sub> was used as internal standard for quantification. The partial pressure of ethylene in the feed gas was varied from 0 to 100 kPa, while maintaining the total pressure at 100 kPa with ethane on the feed side. The dependence of permeation and separation behavior on the partial pressures of ethylene and ethane was studied.



### Results and discussion

Figure 2 shows the results of ethylene/ethane separation tests at 393 K. In Fig. 2(a), the results with different ethylene partial pressures of 0-100 kPa were shown.

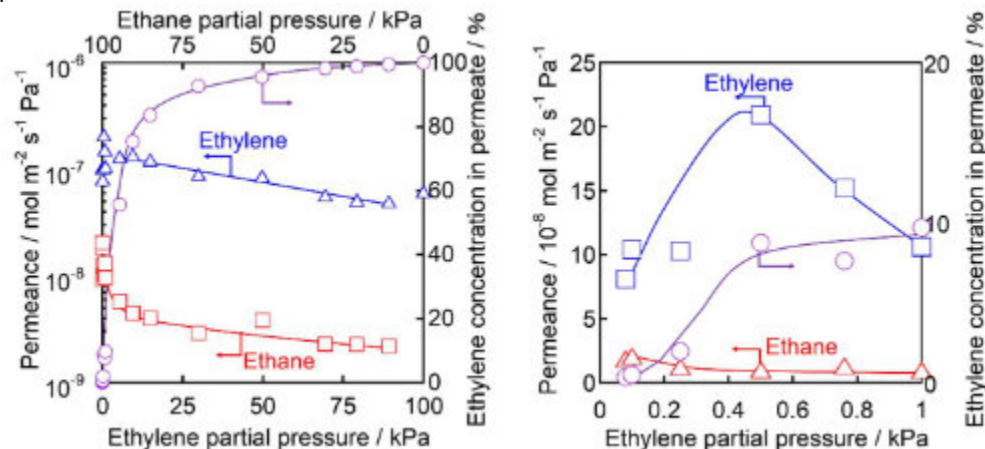


Figure 2. Permeances of ethylene and ethane at 393 K as a function of ethylene partial pressure. (a) 0-100 kPa. (b) Enlarged view of low ethylene partial pressure range (< 1 kPa).

The ethylene permeance was an order of magnitude higher than that of ethane, resulting in the superior ethylene selectivity. Separation performance was observed even at low ethylene partial pressures. Ethylene adsorption at low partial pressures was sufficient to inhibit the permeation of ethane. A feed containing 50% ethylene achieved an ethylene purity of 95.6% with Ag-beta membrane. Highly pure ethylene was obtained with a single-stage membrane separation.

The ethylene permeance sharply increased between 0.25 and 0.5 kPa of the ethylene partial pressure and reached a maximum, as shown in Fig. 2(b), suggesting that adsorbed amount of ethylene almost saturated with the ethylene partial pressure around 0.5 kPa. Within this range, the concentration of ethylene in the permeate increased significantly. For example, a feed with 1% ethylene was enriched to 10% in the permeate, achieving roughly a tenfold concentration.

### References

- [1] D. S. Sholl, R. P. Lively, *Nature*, 532, 435-437 (2016).
- [2] M. Sakai, N. Fujimaki, Y. Sasaki, N. Yasuda, M. Seshimo, M. Matsukata, *ACS Appl. Mater. Interfaces*, 12, 24086-24092 (2020).
- [3] M. Sakai, Y. Tsuzuki, N. Fujimaki, M. Matsukata, *Chem. An Asian J.*, 16, 1101-1105 (2021).



## The Synthesis of Nanosized LEV Zeolite

Wenhua. Fu<sup>1</sup>, Shengli. Zhao<sup>1</sup>, Tiezhu. Zhang<sup>1</sup>, Zhendong. Wang<sup>1</sup>

<sup>1</sup> State Key Laboratory of Green Chemical Engineering and Industrial Catalysis, Sinopec Shanghai Research Institute of Petrochemical Technology Co., Ltd., Shanghai 201208, China  
fuwh.sshy@sinopec.com

The synthesis of nanosized zeolite has attracted tremendous interest [1]. LEV zeolite is a small pore zeolite with 8-ring pore and large [4<sup>9</sup>6<sup>5</sup>8<sup>3</sup>] cavities. LEV zeolite can be prepared using different organic structure-directing agents (OSDA) [2]. Nevertheless, the synthesis of nanosized LEV zeolite remains challenging. The size of LEV zeolite crystals could be reduced to 30 nm *via* the so-called interzeolite conversion approach using deeply dealuminated USY zeolite as silicon and aluminum source [3]. In this communication, LEV zeolite with nanosized crystals in 50~100 nm range is synthesized by employing isopropyltrimethylammonium hydroxide (IPTMAOH) as OSDA.

LEV zeolite was prepared by heating the mixture of sodium aluminate, sodium hydroxide, IPTMAOH, colloidal silica and water at 160 °C for 72 h. The molar composition of the initial gel was 0.17 IPTMAOH: SiO<sub>2</sub>: 0.0067~0.05 Al<sub>2</sub>O<sub>3</sub>: 0.3~0.45 NaOH: 7 H<sub>2</sub>O. LEV zeolite could be obtained in a broad SiO<sub>2</sub>/Al<sub>2</sub>O<sub>3</sub> ratio range by the regulation of alkalinity. When the initial SiO<sub>2</sub>/Al<sub>2</sub>O<sub>3</sub> ratio was in the range of 20~40, pure LEV zeolite formed at a NaOH/Si ratio of 0.3. CDO zeolite impurity emerged at a higher SiO<sub>2</sub>/Al<sub>2</sub>O<sub>3</sub> ratio. Raising the SiO<sub>2</sub>/Al<sub>2</sub>O<sub>3</sub> ratio to 80 and 150, pure LEV zeolite yielded at elevated NaOH/Si ratio of 0.375 and 0.45, respectively. The XRD patterns and SEM images of LEV zeolites with various SiO<sub>2</sub>/Al<sub>2</sub>O<sub>3</sub> ratios are exhibited in **Figure 1** and **Figure 2**, respectively. All the samples display typical diffraction peaks corresponding to LEV zeolite structure without the appearance of any impurities. The crystal size is in the range of 50~100 nm, rendering the present study the first report on the rapid synthesis of nanosized LEV zeolite utilizing conventional silicon and aluminum sources.

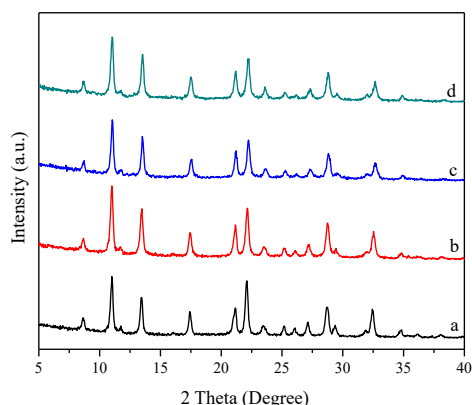


**Figure 1.** XRD patterns of LEV zeolites with different SiO<sub>2</sub>/Al<sub>2</sub>O<sub>3</sub> ratios: 20 (a), 40 (b), 80 (c) and 150 (d).

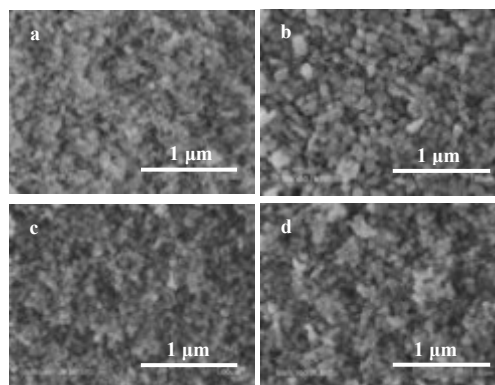


**Figure 2.** SEM images of LEV zeolites with different SiO<sub>2</sub>/Al<sub>2</sub>O<sub>3</sub> ratios: 20 (a), 40 (b), 80 (c) and 150 (d).

The SiO<sub>2</sub>/Al<sub>2</sub>O<sub>3</sub> ratios in the products were lower than those in the initial gels. All the samples exhibit two signals in the NH<sub>3</sub>-TPD profiles. The signal at *ca.* 200 °C is ascribed to weak acid sites, while the signal at 410~450 °C is attributed to strong acid sites. With the increasing of the SiO<sub>2</sub>/Al<sub>2</sub>O<sub>3</sub> ratio, the latter signal shifts to higher temperature, indicating the presence of stronger acidity. The N<sub>2</sub> adsorption-desorption isotherms depict type-I curve, characteristic of zeolitic microporous materials. The remarkable uptake of N<sub>2</sub> in the high pressure regime is caused by the inter-crystals voids, which is in line with the SEM images. The specific surface area and micropore volume of all the four samples are 500~700 m<sup>2</sup>/g and 0.20~0.26 cm<sup>3</sup>/g, respectively, suggesting the high crystallinity of the LEV zeolites. The total pore volume and mesopore volume increase with the rising of the SiO<sub>2</sub>/Al<sub>2</sub>O<sub>3</sub> ratio. The largest total pore volume reaches 1.09 cm<sup>3</sup>/g, significantly higher than that of conventional LEV zeolite reported previously.

### References

- [1] W. Schwieger, A.G. Machoke, T. Weissenberger, et. al., *Chem. Soc. Rev.*, **45**, 3353-3376 (2016).
- [2] M. Dusselier, M.E. Davis, *Chem. Rev.*, **118**, 5265-5329 (2018).
- [3] N. Funase, T. Tanigawa, Y. Yamasaki, et. al., *J. Mater. Chem. A*, **5**, 19245-19254 (2017).

### Acknowledgments

This work was supported by National Natural Science Foundation of China (22272201, 21802168), Shanghai Rising-Star Program (23QB1406300) and China Petrochemical Corporation (Sinopec Group).

## Operando Characterization of Zeolites via Reactive Neural Network Potentials

I. Saha<sup>1</sup>, D. Willmetz<sup>1</sup>, D. Brako-Amofo<sup>1</sup>, C. Bornes<sup>1</sup>, A. Erlebach<sup>1</sup>, L. Grajciar<sup>1</sup>, C.J.Heard<sup>1</sup>

<sup>1</sup> Department of Physical and Macromolecular Chemistry, Charles University in Prague. Hlavova 8, 12800, Prague 2, Czech Republic  
 heardc@natur.cuni.cz

The natural heterogeneity of zeolites demands precise spectroscopic and microscopic characterization in order to classify samples and rationalise performance. This is particularly important, given the diversity of heteroatom concentrations and distributions, framework acidity, and the presence and concentration of defects, internal water and charge-carriers. The location and the character of the aluminium within the zeolite framework is one of the important determinants of performance in industrial applications and is typically probed by <sup>27</sup>Al NMR spectroscopy. At sufficiently high field strengths, additional NMR-active nuclei, such as the common counterion <sup>23</sup>Na may also provide valuable information for determining the siting or distributions of Al. In addition to characterization of the zeolite framework, understanding of the intra-pore dynamics is important, as micro-confined water, bearing charge-carrying ions interacts, often destructively, with the framework, generating and reordering defects. To understand the motion of water and ions in the pore, methods such as quasi-elastic neutron scattering provide valuable information.

In this contribution, we deployed advanced machine learning-based methods to help bridge the time and model complexity scale by first utilizing neural network interatomic potentials to achieve significant speed-up in structure sampling compared to traditional density functional theory (DFT) approaches, [1] and second by training regression models to cost-effectively predict the <sup>27</sup>Al, <sup>29</sup>Si, and/or <sup>23</sup>Na chemical shifts of industrially relevant zeolites, including H-MFI, H-RTH and H/Na-CHA. This allowed us to comprehensively explore the effect of various conditions relevant to catalysis, including water loading, temperature, Al distribution and the aluminium concentration, on the solid-state NMR signals.

We demonstrate that both water content and temperature significantly affect the Al chemical shift and do so in a non-trivial way that is highly T-site dependent, highlighting a need for adoption of realistic, case-specific models. [2] With our approach, we were able to: i) tentatively assign the Al NMR peaks for all considered zeolites (see Fig 1. For H-MFI assignment), ii) identify underpopulated T sites through comparison between calculated and experimental Al-Si 2D correlation spectra, and iii) partially classify Al distributions in Na-CHA, via analysis of predicted <sup>23</sup>Na chemical shifts. [3]

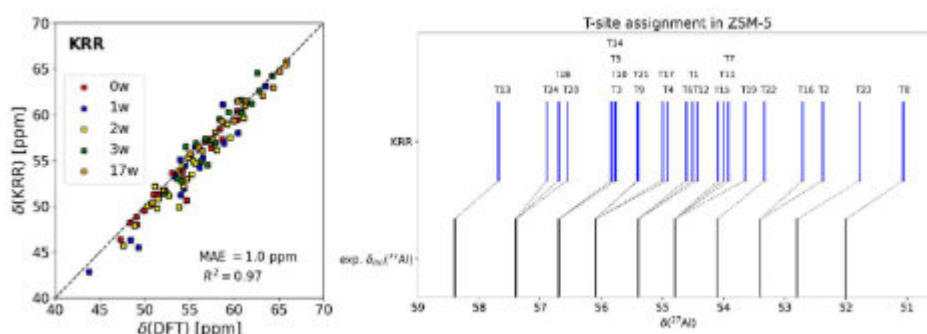


Figure 1. Left: KRR performance for Al chemical shifts in hydrated H-MFI. Right: Assignment of H-MFI Al peaks (top from this work [2], bottom from Holzinger et al. [4])

Subsequently, our neural network potentials were systematically improved to even higher reference level (hybrid density functional theory), to accurately reproduce water diffusivity and reaction energetics for hydrolytic defect formation, and then applied to predict QENS experimental observables, including water jump diffusion lengths, and site residence times.

We observe that these hybrid-level reactive NNPs are able to reproduce the QENS observables with improved accuracy over classical forcefields, owing to the inherently reactive nature of water-zeolite interactions that are captured by the potentials, and we demonstrate the significant role of hydrolytic defects in the confinement and hindrance of water motion in industrial samples of dealuminated zeolite Y (see Fig. 2).

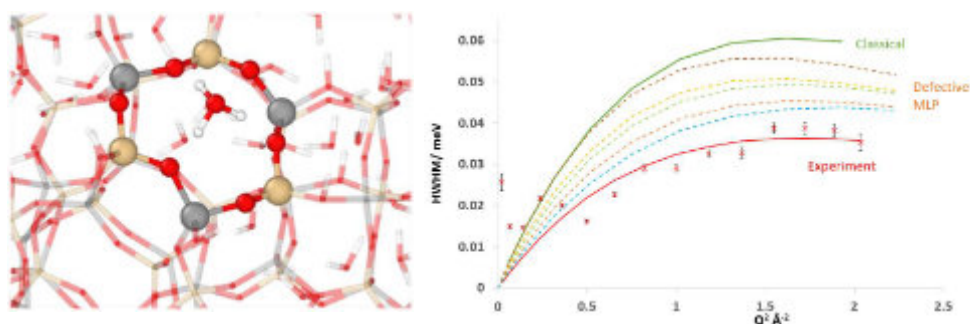


Figure 2. Left: Hydrated model of H-FAU showing a pinned H<sub>3</sub>O<sup>+</sup> configuration. Right comparison of QENS prediction with experiment.

## References

- [1] A. Erlebach, M. Šípka, I. Saha, P. Nachtigall, C.J. Heard and L. Grajciar, *Nat. Commun.*, 15, 4215 (2024).
- [2] D. Willmetz, A. Erlebach, C.J. Heard and L. Grajciar, *ChemRxiv*.doi:10.26434/chemrxiv-2024-x7qx6 (2024).
- [3] C. Lei, C. Bomes, O. Bengtsson, A. Erlebach, B. Slater, L. Grajciar and C.J. Heard, *Faraday Discuss.*, doi:10.1039/D4FD00100A (2024).
- [4] J. Holzinger, M. Nielsen, P. Beato, R.Y. Brogaard, C. Buono, M. Dyballa, H. Falsig, J. Skibsted and S. Svelle, *J. Phys. Chem. C.*, 123, 7831 (2018).

## Acknowledgments

The authors acknowledge support from Alex O'Malley and Alex Porter (Bath – QENS measurements and calculations), Teresa Blasco and Joaquin Martínez Ortigosa (synthesis and NMR of H-RTH), and Ben Slater and Oscar Bengtsson (UCL – calculations on Na-CHA). We acknowledge financial support from the Czech Science Foundation (GAČR standard project 23-07616S). Charles University Centre of Advanced Materials (CUCAM) (OP VVV Excellent Research Teams, project number CZ.02.1.01/0.0/0.0/15\_003/0000417) is acknowledged. This work was supported by the Ministry of Education, Youth and Sports of the Czech Republic through the e-INFRA CZ (ID: 90254) and ERC\_CZ project LL2104 (C.J.H.). C. acknowledges the funding from the European Union's Horizon Europe research and innovation program under the ERA-PF grant agreement No. 101180584.

## Exploring Zeolite Crystal Size Effects in Palladium-Encapsulated Catalysts for the Selective Hydrogenation Reaction of Phenylacetylene

F.J. Escobar-Bedia<sup>1</sup>, A. Martínez Gomez-Aldaravi<sup>1</sup>, C. Martínez<sup>1</sup>, M. Moliner<sup>1</sup>

<sup>1</sup> Instituto de Tecnología Química UPV-CISC, Avd. de los naranjos s/n, 46022, Valencia, Spain.

fraesbe5@itq.upv.es

### Introduction

Styrene (Sty) is a key chemical intermediate used in various industries, including rubber, pharmaceuticals, and agrochemicals [1]. Extracting styrene from cracked petroleum is a cost-effective method, but phenylacetylene (Pha), a harmful impurity, accumulates during extraction and poisons the polymerization catalyst [2,3]. To address this, selective hydrogenation (such as semi-hydrogenation) of phenylacetylene is employed before polymerization. However, over-hydrogenation can lead to unwanted byproducts like alkanes, making the development of catalysts with both high selectivity and activity crucial. This work proposes utilizing the zeolite crystal size to leverage diffusion mechanisms, enhancing both catalytic activity and selectivity for Pd.

### Experimental results

To examine the impact of zeolite crystal size, two distinct catalysts were synthesized adapting previous one-pot synthesis methodologies described in the literature [4,5]: 0.2Pd@nMFI, a nanocrystalline ZSM-5 zeolite with 0.2 wt% Pd, and 0.2Pd@ $\mu$ MFI, its microcrystalline counterpart. Both catalysts had similar palladium loadings of approximately 0.2%, as verified by ICP-AES analysis. HAADF-TEM analysis of the nanocrystalline and microcrystalline catalysts (Figure 1.A and 1.B, respectively) confirmed that Pd was encapsulated effectively and uniformly dispersed throughout the crystals, without large agglomerates. Additionally, both catalysts displayed a narrow particle size distribution, around 2.0 nm (Figure 1.C).

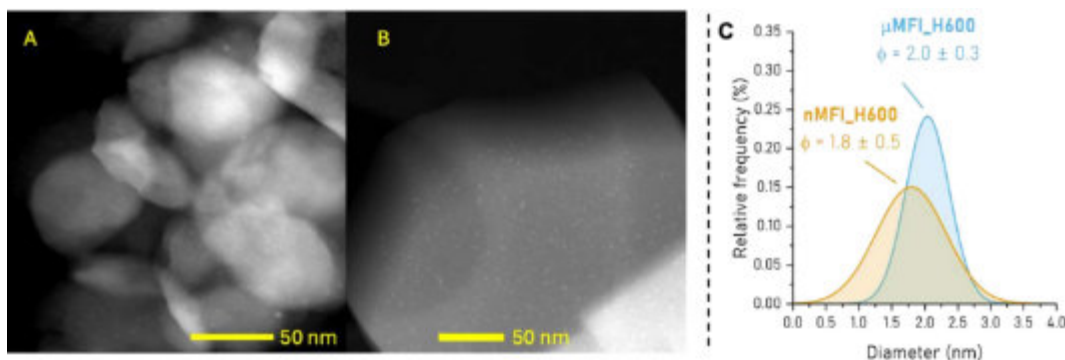


Figure 1. Left Panel: A) 0.2Pd@nMFI, B) 0.2Pd@ $\mu$ MFI and Right Panel: Particle size distribution for both materials.

Catalytic tests for the semi-hydrogenation of phenylacetylene were conducted in a stainless-steel autoclave with a TEFロン liner, operating at 30°C under 6 bar H<sub>2</sub> pressure with magnetic stirring. Alongside the zeolitic catalysts, a third catalyst, 0.5Pt/Al<sub>2</sub>O<sub>3</sub> from a commercial source, was selected as a baseline due to its lack of diffusional limitations. As anticipated from the perspective of diffusional limitations, the commercial Pt catalyst exhibited the highest reaction rate, followed by the nanocrystalline and, lastly, the microcrystalline material (Figure 2.A). Interestingly, significant differences in selectivity were observed (Figure 2.B); both the nanocrystalline and commercial catalysts maintained similar selectivity, even at high conversion levels. In contrast, the microcrystalline catalyst displayed a declining selectivity trend, attributed to the over hydrogenation of styrene to ethylbenzene.

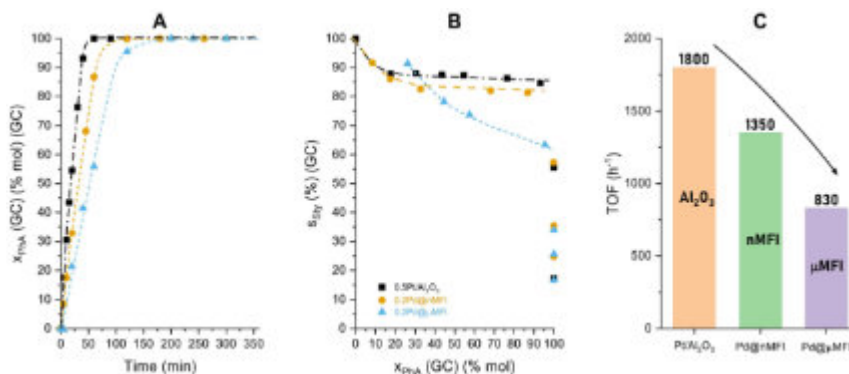
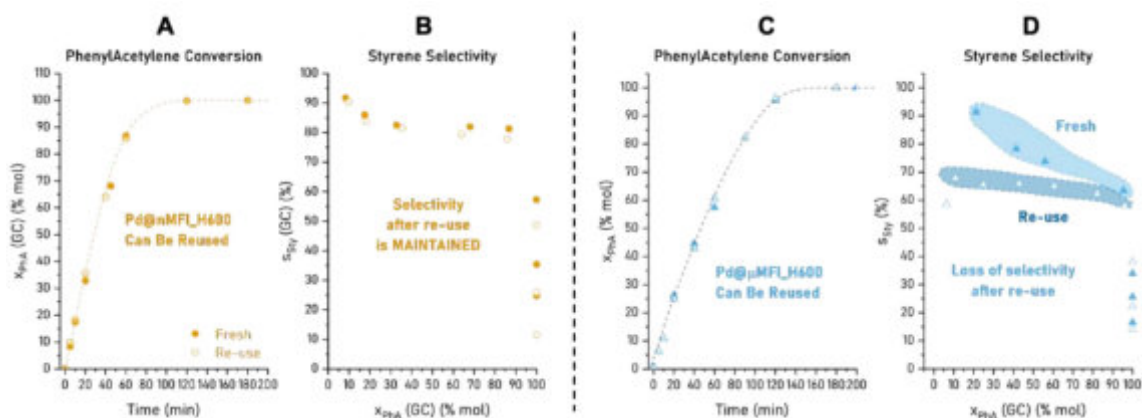


Figure 2. A: Evolution of Phenylacetylene conversion, B: Styrene selectivity at different conversions and C: Turn Over Frequency (TOF) for 0.5Pt/Al<sub>2</sub>O<sub>3</sub>, 0.2Pd@nMFI and 0.2Pd@ $\mu$ MFI.



To standardize the results of platinum- and palladium-based catalysts, turnover frequencies (TOFs) were calculated. The results demonstrated that, as previously mentioned, the 0.5Pt/Al<sub>2</sub>O<sub>3</sub> catalyst exhibited the highest activity with a TOF of 1618 h<sup>-1</sup>. This was followed by 0.2Pd@nMFI, which showed a slightly lower TOF of 1350 h<sup>-1</sup>, and then 0.2Pd@μMFI, which had a significantly lower TOF of 830 h<sup>-1</sup>. These findings further highlight the influence of crystal size on catalytic performance, with the nanocrystalline 0.2Pd@nMFI significantly outperforming the microcrystalline 0.2Pd@μMFI.

The analysis of the materials' reusability (Figure 3) showed that the nanocrystalline material maintained both activity and selectivity after reuse. In contrast, the microcrystalline material exhibited a notable decline in selectivity, especially at lower conversion levels. HAADF-TEM images and ICP-AES analyses of the reused materials revealed no significant changes in metal particle dispersion or content. However, further chemical composition analysis showed a slight potassium content decrease in the microcrystalline material, from 0.6 wt.% to 0.5 wt.%. This potassium loss could affect the metal environment's electronic properties, potentially explaining the observed selectivity decline. Further study is required to confirm this hypothesis.



**Figure 3.** Evolution of phenylacetylene conversion and styrene selectivity after re-use for: Left Panel (A, B). 0.2Pd@nMFI and Right Panel (C, D). 0.2Pd@μMFI

### Conclusions

This study underscores the advantages of nanocrystalline zeolite in overcoming diffusional limitations in catalysis. The 0.2Pd@nMFI nanocrystalline catalyst, with its small crystal size, showed catalytic performance and selectivity comparable to a commercial 0.5Pt/Al<sub>2</sub>O<sub>3</sub> catalyst, which has no diffusional constraints. This similarity highlights how reduced crystal size enables effective diffusion, enhancing reaction rates and maintaining high selectivity even at high conversion levels. In contrast, the microcrystalline counterpart, 0.2Pd@μMFI, displayed a significant drop in selectivity, likely due to diffusional barriers leading to over-hydrogenation. Additionally, the nanocrystalline catalyst demonstrated excellent reusability, retaining its activity and selectivity after repeated use. On the other hand, the microcrystalline catalyst experienced a decrease in selectivity upon reuse, potentially linked to a slight potassium leaching. Overall, this study shows that nanocrystalline zeolites are a promising strategy for overcoming diffusional limitations, offering high performance, stability, and reusability in catalytic applications.

### References

- [1] M. Crespo-Quesada, F. Cárdenas-Lizana, A.-L. Dessimoz, L. Kiwi-Minsker, *ACS Catal.* 2012, 2, 1773.
- [2] G. Vilé, D. Albani, N. Almora-Barrios, N. López, J. Pérez-Ramírez, *ChemCatChem* 2016, 8, 21.
- [3] L. Shao, X. Huang, D. Teschner, W. Zhang, *ACS Catal.* 2014, 4, 2369
- [4] N. Wang, Q. Sun, R. Bai, X. Li, G. Guo and J. Yu, *J. Am. Chem. Soc.*, 2016, 138, 7484-7487
- [5] L. Liu, M. Lopez-Haro, C. W. Lopes, C. Li, P. Concepcion, L. Simonelli, J.J. Calvino and A. Corma, *Nature Mater.*, 2019, 18, 866-873.

### Acknowledgments

This work has been supported by the Spanish Government through PID2021-122755OB I00 funded by MCIN/AEI/10.13039/501100011033 and by the Generalitat Valenciana through the Prometeo Program (CIPROM/2023/34). The authors are also thankful for the Severo Ochoa financial support by the Spanish Ministry of Science and Innovation (CEX2021-001230-S/funding by MCIN/AEI/10.13039/501100011033). AMG-A acknowledges the Spanish Government for a Severo Ochoa FPI scholarship (PRE2019-088361). The Electron Microscopy Service of the UPV is acknowledged for their help in sample characterization.



## Mixed Metal Oxide catalyst in tandem with zeolites as a highly selective Catalyst for CO<sub>2</sub> hydrogenation to Jet Fuel

P. Clayton<sup>1\*</sup>, R. Taylor<sup>1</sup>,

<sup>1</sup> Durham University, Department of Chemistry, Lower Mount Joy, South Road, Durham DH13LE

\*gls43@durham.ac.uk

### Introduction:

Atmospheric carbon dioxide (CO<sub>2</sub>) levels have been rising at an alarming rate, with projections estimating concentrations could reach 570 ppm by the end of this century. This increase in a greenhouse gas poses significant environmental challenges including worsening climate change. [1] CO<sub>2</sub> hydrogenation offers a promising approach to address these issues, providing a sustainable method to convert CO<sub>2</sub> into high-energy-density fuels like methanol. [2] Traditionally, methanol synthesis in industry relies on syngas processed with Cu/ZnO/Al<sub>2</sub>O<sub>3</sub> catalysts; however, these catalysts are not optimal for pure CO<sub>2</sub> streams due to selectivity limitations and vulnerability to water deactivation. [3]

Tandem catalytic systems made of mixed metal-oxide and zeolite catalysts offer a promising method for CO<sub>2</sub> hydrogenation to high-value hydrocarbons, such as jet fuel. Tandem catalysts leverage the synergy of multifunctional active sites to facilitate complex chemical transformations in a single reactor, minimising process steps and enhancing efficiency. Mixed metal oxides can hydrogenate CO<sub>2</sub> to intermediates such as methanol due to their redox properties and reducible oxygen vacancies. The acidic sites in zeolites can subsequently catalyse methanol-to-hydrocarbons (MTH) reaction, yielding jet fuel-range hydrocarbons with high selectivity.

There is increasing interest in the use of ZrO<sub>2</sub> as a support, promoter and active species for CO<sub>2</sub> upgrading due to its unique properties. [4] Many binary and ternary ZrO<sub>2</sub> systems have been investigated for use in CO<sub>2</sub> hydrogenation to methanol. [5] This project explores novel synthesis routes for various Cu/Zn/ZrO<sub>2</sub> catalysts, aiming to enhance the hydrogenation rate and improve methanol selectivity.

### Materials and Methods

A series of Cu/Zn/ZrO<sub>2</sub> metal catalysts were prepared via coprecipitation and hydrothermal synthesis.

The hydrothermal synthesis protocol is as follows: 0.5 M Cu/Zn-Zirconium nitrate precursor solutions and 5 M NaOH solutions were made using deionised water. The metal zirconium nitrate solution was stirred at 350 rpm while the NaOH solution was added via a dropping funnel over 30 minutes. The solution was then sonicated at room temperature for 30 minutes. The mixture was then divided into six Teflon-lined stainless-steel autoclaves and 2 mL of absolute ethanol was additionally added to each autoclave. The autoclaves were put in a Carbolite AX60 oven preheated to 200 °C for 24 hours. The resultant white solid was then washed with deionised water and absolute ethanol. In between each wash, the sample was centrifuged for 5 minutes in a Heraeus Megafuge 8 at 6000 rpm. The washed sample was dried overnight at 80 °C.

The prepared catalysts were characterized by BET surface area, XRD, XRF, STEM and in-situ DRIFTS.

### Results and Discussion

The XRD profiles confirm the successful hydrothermal synthesis of high-purity, high-crystallinity ZrO<sub>2</sub> in the monoclinic phase (m-ZrO<sub>2</sub>). In contrast, XRD patterns of CuZrOx catalysts synthesised via coprecipitation revealed peaks corresponding only to CuO, indicating an amorphous zirconia phase. However, CuZrOx catalysts produced via the hydrothermal protocol exhibited the m-ZrO<sub>2</sub> phase. Increasing Cu loading in these catalysts resulted in the emergence of multiple Cu phases, although CuO was not detected.

For ZnZrOx catalysts synthesised by coprecipitation, the XRD patterns showed the tetragonal phase (t-ZrO<sub>2</sub>) without observable ZnO peaks, suggesting the formation of a ZnZrO<sub>2</sub> solid solution. Similarly, hydrothermal synthesis of ZnZrOx led to a solid solution, with a phase transition of zirconium from monoclinic to tetragonal as Zn was increasingly incorporated. Elemental analysis revealed limited zinc incorporation within the solid solution unlike with Cu in CuZrO<sub>2</sub>.

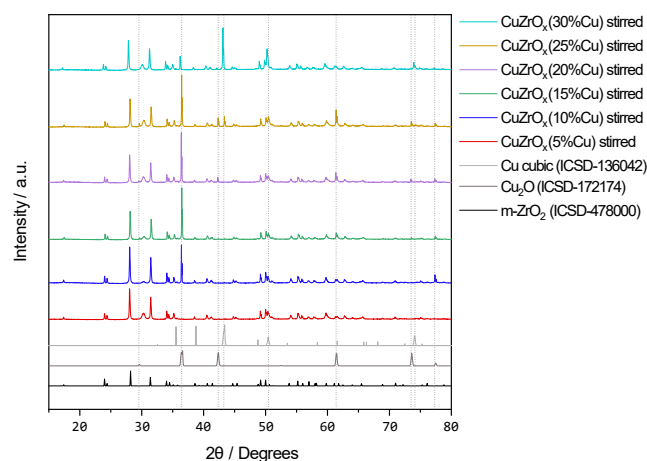


Figure 1 PXRD of hydrothermally synthesised  $\text{CuZrO}_x$  with different observed phases.

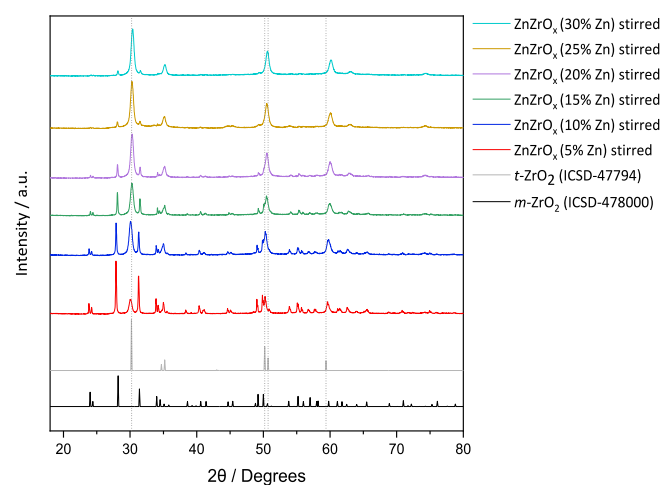


Figure 2. PXRD of hydrothermally synthesised  $\text{ZnZrO}_x$  with observed  $\text{ZrO}_2$  phase transition.

#### References:

- [1] W. Wang, S. Wang, X. Ma, and J. Gong, *Chem. Soc. Rev.*, 40, 3703-3727 (2011).
- [2] Wenhui Li, Haozhi Wang, *RSC Adv.*, 8, 7651 (2018).
- [3] R. Guil-López, N. Mota, J. Llorente, et al. *Materials (Basel)*, 2019, 12, 23
- [4] P. Gao, F. Li, N. Zhao, F. Xiao, W. Wei, L. Zhong, Y. Sun, *Appl Catal A Gen.*, 468 (2013).
- [5] P. Ticali, D. Salusso, R. Ahmad, C. Ahoba-Sam, A. Ramirez, G. Shterk, K. A. Lomachenko, E. Borfecchia, S. Morandi, L. Cavallo, J. Gascon, S. Bordiga, U. Olsbye, *Catal Sci Technol* 4, 11 (2021).

#### Acknowledgments

I want to thank ReNUCDT for funding my research project.





## Design and investigation of superalkalis for CO<sub>2</sub> and N<sub>2</sub> molecules activation: first-principles studies

N. Wiszowska<sup>1</sup>, N. Rogoża<sup>1</sup>, C. Sikorska<sup>1,2</sup>

<sup>1</sup> Faculty of Chemistry, University of Gdańsk, Fahrenheit Union of Universities in Gdańsk, 80-308 Gdańsk, Poland

<sup>2</sup> Department of Physics, The University of Auckland, 38 Princes Street, Auckland 1010, New Zealand

Celina.sikorska@ug.edu.pl

A superatom is a cluster of atoms that acts like a single atom. Superalkalis are a class of superatoms that mimic the chemistry of alkali atoms. The ionization energies of superalkalis are smaller than those of alkalis [3.89 eV (cesium atom)]. This contribution aims at designing novel superalkalis for redox applications, see Figure 1. These research studies not only describe new superalkalis but also verify the usefulness of computational chemistry methods to predict the stability and physicochemical properties of chemical compounds. According to our recent results, [2] a superalkali with smaller ionization energy should more easily transfer an electron to counterpart molecules (e.g., CO<sub>2</sub> or N<sub>2</sub>) compared to one with a larger ionization energy. We used a hybrid approach that combines *ab initio* computational techniques of quantum chemistry and a machine learning strategy to design and investigate BAe<sub>3</sub> (Ae=Be, Mg, Ca, Sr, Ba) molecular clusters with strong reducing abilities. [3] The studied molecular clusters feature low ionization energy values and highly delocalized singly occupied molecular orbital (SOMO). The BBa<sub>3</sub> has the lowest IE here (3.59 eV), which is smaller than that of any alkali. Moreover, we developed a mathematical model describing the dependence of ionization energy of superalkalis on their composition. The developed quantitative structure-property relationship (QSPR) model predicts the reducing ability of a superalkali, where a suitable alkaline earth metal decreases the ionization energy of the resulting superalkali cluster. Finally, we demonstrated that the BAe<sub>3</sub> electron donors can be used in the reduction of counterpart systems with low electron affinity (such as the carbon dioxide or nitrogen molecules). Our results emphasize how the structure and stability of the BAe<sub>3</sub>/Y systems (Y = CO<sub>2</sub>, N<sub>2</sub>) can be tuned upon single atom substitution and can be used to bond and remove toxic compounds from the environment.

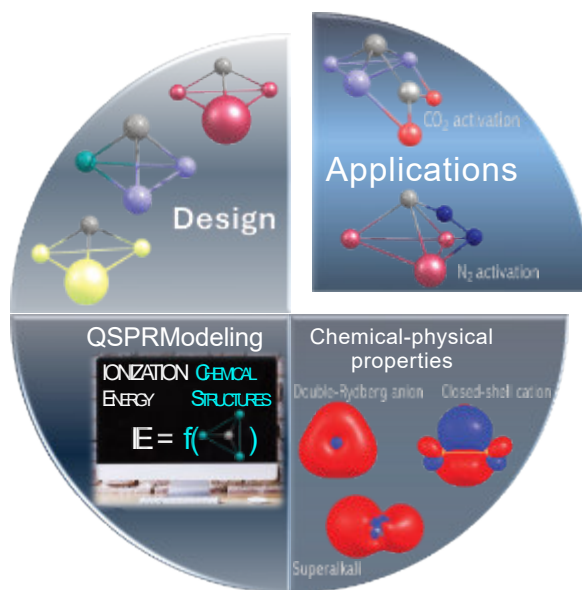


Figure 1. Scope of studies

### References

- [1] C. Sikorska, *Micromachines* **15**, 78 (2024).  
 [2] C. Sikorska, N. Gaston, *J Chem Phys* **153**, 144301 (2020).  
 [3] N. Wiszowska, N. Rogoża, C. Sikorska, *PCCP* (2025).

### Acknowledgments

This research is part of the project No. 2022/45/P/ST4/01907 co-funded by the National Science Centre and the European Union Framework Programme for Research and Innovation Horizon 2020 under the Marie Skłodowska-Curie grant agreement No. 945339. Calculations have been carried out in (a) the Wrocław Centre for Networking and Supercomputing, (b) the Centre of Informatics–Tricity Academic Supercomputer and Network (CI TASK) in Gdansk, and (c) the New Zealand eScience Infrastructure (NeSI) high-performance computing facilities.

## Design of Efficient Zeolite-Based Catalysts by Le Chatelier's Principle

Feng-Shou Xiao and Liang Wang

College of Chemical Engineering, Zhejiang University, Hangzhou 310030, China  
fsxiao@zju.edu.cn

It is well known that chemical reaction equilibrium is easily adjusted by reaction temperature and pressure due to Le Chatelier's Principle. Because many reactions are performed in the presence of catalysts, it is reasonably suggested that catalytic reactions could be adjusted by adsorbate species on the catalyst surface. In this talk, we have shown that enriching reactants and intermediates and fast transfer of products significantly enhance the catalytic activity and selectivity in a series of reactions over zeolite-based catalysts [1-3]. For example, after modification of the external surface of the zeolite with organosilanes as a molecular fence, it is achieved for enhanced methanol productivity in methane oxidation by in situ generated hydrogen peroxide at mild temperature. The silanes appear to allow diffusion of hydrogen, oxygen, and methane to the catalyst active sites, while confining the generated peroxide there to enhance its reaction probability. At 17.3% conversion of methane, methanol selectivity reached 92%, corresponding to methanol productivity up to 91.6 millimoles per gram of AuPd per hour [1].

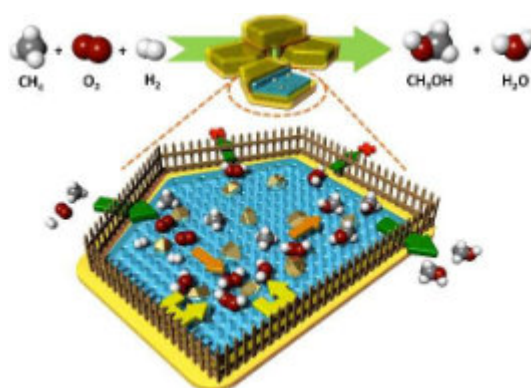


Figure 1. "Molecular fence" catalyst for low-temperature oxidation of methane into methanol in the presence of  $O_2$  and  $H_2$ , where the concentration of hydrogen peroxide as reaction intermediate was efficiently enhanced inside of zeolite crystals, leading to high conversion from methane to methanol.

### References

- [1] Z. Jin, L. Wang, E. Zuidema, K. Mondal, M. Zhang, J. Zhang, C. Wang, X. Meng, H. Yang, C. Mesters, F.-S. Xiao, Hydrophobic Zeolite Modification for in situ Peroxide Formation in Methane Oxidation to Methanol, *Science*, 367, 193-197 (2020).
- [2] H. Zhou, X. Yi, Y. Hui, L. Wang, W. Chen, Y. Qin, M. Wang, J. Ma, X. Chu, Y. Wang, X. Hong, Z. Chen, X. Meng, H. ang, Q. Zhu, L. Song, A. Zheng, F.-S. Xiao, Isolated boron in zeolite for oxidative dehydrogenation of propane, *Science*, 372, 76-80 (2021).
- [3] L. Liu, J. Lu, Y. Yang, W. Ruttinger, X. Gao, M. Wang, H. Lou, Z. Wang, Y. Liu, X. Tao, L. Li, Y. Wang, H. Li, H. Zhou, C. Wang, Q. Luo, H. Wu, K. Zhang, J. Ma, X. Cao, L. Wang, F.-S. Xiao, Dealuminated Beta zeolite reverses Ostwald ripening for durable copper nanoparticle catalysts, *Science*, 383, 94-101 (2024).